MECHANISMS OF MESENCHYMAL STEM CELL THERAPY FOR ENTERIC NEUROPATHY ASSOCIATED WITH COLITIS

RHIAN STAVELY

This thesis is submitted in total fulfilment of the requirements for the degree of Doctor of Philosophy

Principal Supervisor: Associate Professor Kulmira Nurgali
Co-Supervisor: Dr Samy Sakkal

College of Health and Biomedicine Victoria University,
Melbourne, Australia
December 2018

ABSTRACT

Due to the limited efficacy and high toxicity of current treatments, the development of novel therapies is crucial for inflammatory bowel disease (IBD). Mesenchymal stem cell (MSC) therapies have demonstrated positive outcomes in IBD patients that are refractory to conventional treatment options and produce fewer side-effects. To develop and optimise MSC therapies, their mechanism of action must be fully elucidated. This thesis aims to explore the mechanisms of MSC treatments in experimental intestinal inflammation with a focus on damage to the enteric nervous system (ENS).

The guinea-pig model of TNBS-induced colitis was utilised in proof of principle experiments to evaluate the neuroprotective potential of MSCs. Treatments with MSCs attenuated acute inflammation as well as neuronal and nerve fibre loss. MSCs suppressed leukocyte infiltration to the myenteric plexus (plexitis) and the production of superoxide by myenteric neurons. Furthermore, MSCs derived from the bone-marrow (BM-MSCs) were more efficacious than those isolated from adipose tissue (AT-MSCs) in ameliorating damage to the ENS.

For the first time, the effects of MSC treatments were explored in a model of spontaneous chronic colitis (*Winnie* mice). Using high-throughput RNA sequencing, *Winnie* mice were determined to closely replicate the transcriptome of human IBD with a high degree of accuracy not observed previously in models of chemically-induced colitis. Treatments with BM-MSCs decreased the disease activity of colitis and reduced leukocyte infiltration to the mucosa in *Winnie* mice. BM-MSCs were determined to reduce the expression of many proinflammatory factors in *Winnie* mice that contribute to IBD in human patients. The concordance of inflammatory gene expression in *Winnie* mice was highly representative of IBD. Thus, this model and *in vitro* organotypic cultures of longitudinal muscle-myenteric plexus were used to elucidate mechanisms of inflammation-associated enteric neuropathy.

The expression of many genes associated with the ENS and neurotransmission pathways were normalised by BM-MSC treatments in *Winnie* mice. BM-MSCs restored neuronal density and attenuated plexitis in *Winnie* mice to near control levels. This correlated with a reduction in the disease activity of colitis and may have contributed to their ability to normalise many neuronal and synapse-associated genes. In *Winnie* mice, myenteric neurons were sensitive to oxidative stress with a strong accumulation of oxidised DNA/RNA adducts and superoxide generation from the mitochondria. This was attenuated to control levels by BM-MSCs. In *in vitro* studies, oxidative stimuli caused neuronal loss which was inhibited by BM-MSCs in a paracrine manner and was mediated, at least in part, by superoxide dismutase 1. BM-MSC treatments also upregulated several genes associated with metabolism and antioxidant defences in *Winnie* mice that may contribute to the resolution of oxidative injury.

In vitro experiments provided evidence that cytoplasmic translocation of the damage associated molecular pattern, high-mobility group box 1 (HMGB1) protein, is induced by oxidative stress in myenteric neurons. HMGB1 was determined to be translocated in myenteric neurons of *Winnie* mice which correlated with neuronal loss. Treatment with BM-MSCs inhibited HMGB1 translocation in myenteric neurons of *Winnie* mice *in vivo* and organotypic cultures *in vitro*. Pharmacological inhibition of HMGB1 attenuated neuronal loss in *Winnie* mice without reducing plexitis and mitochondrial superoxide production. This suggests that BM-MSC treatments increased neuronal density by attenuating plexitis and oxidative stress which is upstream of HMGB1 translocation and myenteric neuronal death.

In these studies, we have defined potent neuroprotective properties elicited by BM-MSCs which ameliorate damage to the myenteric ganglia in experimental colitis. The use of high-throughput transcriptome sequencing illustrates the complex alterations to the nervous system in chronic experimental colitis and IBD patients. The results of this thesis may be utilised as a reference to provide future direction in the fields of MSC therapies and ENS pathophysiology in intestinal inflammation.

DECLARATION

I, Rhian Stavely, declare that the PhD thesis entitled " Mechanisms of Mesenchymal Stem Cell Therapy for Enteric Neuropathy Associated with Colitis" is no more than 100,000 words in length including quotes and exclusive of tables, figures, appendices, bibliography, references and footnotes. This thesis contains no material that has been submitted previously, in whole or in part, for the award of any other academic degree or diploma. Except where otherwise indicated, this thesis is my own work.

Rhian Stavely

December 2018

DECLARATION OF CONTRIBUTION TO WORK

The following people have made the stated contributions to this work:

Chapter 1

Assistance in preparing the manuscript for part of this chapter was provided by V Stojanovska, S Sakkal and K Nurgali.

Chapter 2

Technical assistance and training for MSC cell culture was provided by S Sakkal. Technical assistance and training with *in vivo* MSC-based treatments and immunohistochemical studies was provided by AM Robinson and S Miller. Training for microdissection was provided by S Carbone. Training for histological studies was provided by V Jovanovska. Assistance in preparing the manuscript for this chapter was provided by AM Robinson, R Boyd, S Sakkal and K Nurgali.

Chapter 3

Technical assistance and training for RNA isolation, quality control and bioinformatics was provided by S Fraser. Assistance in preparing the manuscript for this chapter was provided by K Nurgali and S Sakkal.

Chapter 4

Assistance in preparing the manuscript for this chapter was provided by K Nurgali and S Sakkal.

Chapter 5

Assistance in preparing the manuscript for this chapter was provided by K Nurgali and S Sakkal.

Chapter 6

Technical assistance for intraperitoneal injections was provided by R Filippone. Assistance in preparing the manuscript for this chapter was provided by K Nurgali and S Sakkal.

PUBLICATIONS

Publications from this Thesis

Stavely R., Robinson A.M., Miller S., Boyd R., Sakkal S. and Nurgali K., 2015. Human Adult Stem Cells Derived from Adipose Tissue and Bone Marrow Attenuate Enteric Neuropathy in the Guinea-pig Model of Acute Colitis. *Stem Cell Research & Therapy* 6(1):244.

Stavely R., Sakkal S., Stojanovska V. and Nurgali K., 2014. Mesenchymal stem cells for the treatment of inflammatory bowel disease: from experimental models to clinical application. *Inflammation and Regeneration* 34(4):184-197.

Other Related Publications

Stavely R., Sharma S., Fraser S., Rahman A.A., Stojanovska V., Sakkal S., Apostolopoulos V., Bertrand P. and Nurgali K., 2018. The Onset and Progression of Chronic Colitis Parallels Increased Mucosal Serotonin Release via Enterochromaffin Cell Hyperplasia and Downregulation of the Serotonin Reuptake Transporter. *Inflammatory Bowel Disease* 24(5):1021-1034.

Stavely R., Robinson A.M., Miller S., Boyd R., Sakkal S. and Nurgali K., 2015. Allogeneic Guinea-pig Mesenchymal Stem Cells Ameliorate Neurological Changes in Experimental Colitis. *Stem Cell Research & Therapy* 6(1):263.

Co-Authored Publications

Stojanovska V., McQuade R., Fraser **S.,** Prakash M., Gondalia S., **Stavely R**., Palombo E., Apostolopoulos V., Sakkal S., Nurgali K. 2018. Oxaliplatin-Induced Changes in Microbiota, TLR4+ Cells and Enhanced HMGB1 Expression Associated with Immunosuppression in the Colon. *PLoS One* 13(6): e0198359

Filippone R., Jovanovska V., Robinson A., **Stavely R.,** Apostolopoulos V., Bornstein J., Nurgali K., 2018. Targeting Eotaxin-1 and CCR3 Receptor Alleviates Enteric Neuropathy and Colonic Dysfunction in TNBS-Induced Colitis in Guinea-Pigs. *Neurogastroenterology & Motility* 30(11):e13391.

McQuade R.M., Stojanovska V., **Stavely R.,** Timpani C., Petersen A.C., Abalo R., Bornstein J.C., Rybalka E., Nurgali K. 2018. Oxaliplatin-Induced Enteric Neuronal Loss and Intestinal Dysfunction is Prevented by Co-Treatment with BGP-15. *British Journal of Pharmacology* 175(4):656-677.

Robinson AM, Rahman AA, Miller S, **Stavely R,** Sakkal S, Nurgali K. 2017. The Neuroprotective Effects of Human Bone Marrow Mesenchymal Stem Cells are Dose-Dependent in TNBS Colitis. *Stem Cell Research & Therapy* 18;8(1):87.

Media Releases

Allogeneic Guinea-pig Mesenchymal Stem Cells Ameliorate Neurological Changes in Experimental Colitis (2016). Mesenchymal Cell News: Vol 8.00, January 5, 2016.http://www.mesenchymalcellnews.com/issue/volume-8-00-jan-5/

PRESENTATIONS

Invited Presentations

Stavely R., Robinson A. M., Fraser S., Apostolopoulos V., Sakkal S., Nurgali K. 2018. Enteric Neuropathy Associated with Chronic Intestinal Inflammation: Benefits of Mesenchymal Stem Cell Therapy as an Anti-Inflammatory & Neuroprotective Treatment. Australian Gastroenterology Week. Brisbane. Oral presentation - Invited speaker.

Stavely R., Robinson AM, Miller S, Sakkal S, K Nurgali. 2016. Mesenchymal Stem Cells Derived from Bone Marrow and Adipose Tissue: Comparison in a Model of Intestinal Neuropathy. Health Research Symposium; Victoria University and the University of Texas El Paso. Oral presentation – Invited speaker.

Oral Presentations from Refereed Abstracts

Stavely R., Robinson A. M., Fraser S., Apostolopoulos V., Sakkal S., Nurgali K. 2018. Therapeutic Mechanisms of Mesenchymal Stem Cell Therapy in Chronic Colitis. International conference. Little Brain Big Brain, Kleve, Germany. Oral presentation.

Stavely R., Rahman A. A., Stojanovska V., Sakkal S., Bertrand P., Nurgali K. 2017. Mesenchymal stem cell therapy prevents the hypersecretion of mucosa derived serotonin associated with the onset and progression of chronic colitis by reducing enterochromaffin cell hyperplasia. Victoria University College of Health and Biomedicine Post-Graduate Research Conference. Oral presentation.

Stavely R., Rahman A. A., Stojanovska V., Sakkal S., Bertrand P., Nurgali K. 2016. Characterisation of Serotonin Release in Mice with Spontaneous Chronic Colitis after Mesenchymal Stem Cell Therapy. Victoria University Immunology Summit. Oral presentation.

Stavely R., Robinson A. M., Filippone R., Rahman A. A., Eri R., Sakkal S., Nurgali K. 2018. Mesenchymal stem cell treatment for colitis-associated enteric neuropathy. ENS 2018. Development of the Enteric Nervous System: Cells, Signals, Genes and Therapy, Boston, USA. Oral presentation.

Miller S., Robinson A. M., **Stavely R**., Eri E., Sakkal S., Nurgali K. 2015. Mesenchymal stem cells attenuate enteric neuropathy in acute and chronic models of colitis. Australian Society for Medical Research (ASMR) Victorian Student Research Symposium, Melbourne, Australia. Oral presentation.

Miller S., Robinson A. M., **Stavely R**., Eri E., Sakkal S., Nurgali K. 2015. Mesenchymal stem cells attenuate enteric neuropathy in acute and chronic models of colitis. Bugs, Bowels and Beyond: Innovations in Digestive Health and Disease

Research, Australian Society for Medical Research (ASMR) National Scientific Conference, Adelaide, Australia. Oral presentation.

Poster Presentations from Refereed Abstracts

Stavely R., Robinson A. M., Filippone R., Rahman A. A., Eri R., Sakkal S., Nurgali K. 2018. Mesenchymal Stem Cell Therapy in Chronic Colitis: Potential Therapeutic Mechanisms in Alleviating Oxidative Stress and Enteric Neuropathy. Federation of Neurogastroenterology and Motility. Amsterdam, Netherlands. Poster presentation.

Stavely R., Robinson A. M., Filippone R., Rahman A. A., Eri R., Sakkal S., Nurgali K. 2018. Enteric neuropathy associated with intestinal inflammation: Effects and potential mechanisms of mesenchymal stem cell therapy. International Society for Stem Cell Therapy. Annual meeting, Melbourne, Australia. Poster presentation.

Stavely R., Robinson A. M., Filippone R., Rahman A. A., Eri R., Sakkal S., Nurgali K. 2018. Neurogenic mechanisms of mesenchymal stem cell therapy in chronic colitis. Australian Students of Medical Research Symposium, Melbourne, Australia. Poster presentation.

Stavely R., Robinson A. M., Filippone R., Rahman A. A., Eri R., Sakkal S., Nurgali K. 2017. Mesenchymal stem cell treatment for enteric neuropathy associated with colitis. International Society of Autonomic Neuroscience (ISAN) Congress, Nagoya, Japan. Poster presentation.

Stavely R., Rahman A. A., Stojanovska V., Sakkal S., Bertrand P., Nurgali K. 2017. Characterisation of Serotonin Release in Mice with Spontaneous Chronic Colitis after Mesenchymal Stem Cell Therapy. Australasian Neurogastroenterology and Motility Association Scientific Meeting, Melbourne, Australia. Poster presentation.

Stavely R., Rahman A. A., Stojanovska V., Sakkal S., Bertrand P., Nurgali K. 2017. Characterisation of Serotonin Release in Mice with Spontaneous Chronic Colitis after Mesenchymal Stem Cell Therapy. Australian Students of Medical Research Symposium, Melbourne, Australia. Poster presentation.

Stavely R., Robinson A. M., Miller S., Sakkal S., Nurgali K. 2015. Efficacy of Bone Marrow and Adipose Tissue-Derived Allogeneic and Xenogeneic Mesenchymal Stem Cells for the Treatment of Intestinal Inflammation – Australian Students of Medical Research Symposium, Melbourne, Australia. Poster presentation.

ACKNOWLEDGEMENTS

The completion of this thesis and my PhD studies would not have been possible without the support and guidance of many people.

First, and foremost, I express my sincerest gratitude to **Associate Professor Kulmira Nurgali**. Your dedication to your students and your research is second to none. All my achievements thus far, and those to come, are yours. Thank you for pushing me out of my comfort zone and moulding me into the best researcher I could be. All I can try to do is pay forward what you have done for me to others. The first day we meet, I told you how excited I was to join your group. You said I would probably be sick of you by the end of my honours year. Four years later and still enjoying every day of our research together. Thank you.

I also owe my gratitude to **Dr Samy Sakkal**. You were my gateway to research and took me in under your wing. Not that you had a choice, I wanted to work with you and would have kept pestering you until you said yes. Your passion and curiosity inspired me to pursue a career in research. Your teachings go beyond what you have taught me in the lab. Thank you for educating me the practice of applying epistemological values (and fancy words) to my research and my everyday life.

Thank you to the molecular guru **Dr Sarah Fraser**. You have trained me and taught me everything I know about molecular biology since my undergraduate years. Thank you for being so kind and generous with your valuable time and being a such a great mentor throughout my studies.

Thank you to the MSC team. To **Ainsley Robinson**, thank you for all the time and training you put into me. Your skills and knowledge really allowed me to hit the ground running. You have been a delight to work with and always looked out for me which I am grateful for. To **Sarah Miller**, thank you for all your help and training at the start of the project and our good times together.

I have had many mentors, but I would like to specifically thank **Professor Vasso Apostolopoulos**, **Associate Professor Damian Myers**, **Dr Paul Bertrand** and **Dr Ahmed Rahman** for all your guidance during my studies.

I would also like to thank all other KN lab members, **Rachel**, **Vanesa**, **Elif**, **Adam**, **Rhiannon**, **Monica**, **Elizabeth**, **Abilasha** and **Nyanbol**. Thank you to the lab manager **Varsha**. I truly feel lucky to have shared the lab with so many people willing to help and support each other. Work has never felt tedious or melancholic when you were there.

To my family you have all contributed to my thesis and my studies. Thank you for believing in me. I hope to make you all proud.

To my mother **April**, I do not know anyone who has overcome as many obstacles as you in life. All with a smile on your face. You are the strongest person I know and if I inherit a fraction of your fighting spirit I should be fine. Never give up, never surrender. You always said I would be a humanitarian; although I do not see my contributions as majorly significant yet, I hope that day comes when I can bring some people happiness from my work.

To my father **Gordon**, thank you for empowering my curiosity and creativity growing up. Looking back, I had a lot of crazy ideas for home experiments: eel catching, worm farming, hook-less fishing and trying to build saw blade-wielding robots. My current research has taken me in another direction, but thanks for giving me that sense of wonder. Who knew you could make a career out of being curious.

To my grandparents **Carel** and **Bill**, you are two of the most positive influences on my life. So generous, caring and wise. You have always been there for me whether I needed a computer for school or just people to talk to. Thank you for always believing in me and teaching me the value of education and family.

To my parents in law **Jo** and **Ron**, thank you for helping us with everything. The support you have provided to me and Jordan with the kids is the only way we could have possibly managed. Thanks for letting me come over to overtake your office and reminding me to eat when I am deep in my own world of writing.

To my brothers **Kaine**, **Benjamin** and **Jarrod**, sister **Melissa**, my nieces **Charlee**, **Lilee** and **Ava**, and my best man **Scott**. Thanks for cheering me on and keeping my sanity. Your love and support has meant a lot to me.

Thank you to my wife **Jordan Leeanne Stavely** and daughters **Evangelina Skye**, **Bonnebelle Jaye** and **Gwendolyne Anne** to whom I dedicate this thesis.

DEDICATION

This thesis is written in dedication to my loving wife **Jordan Leeanne Stavely** and daughters **Evangelina Skye**, **Bonnebelle Jaye** and **Gwendolyne Anne**.

Dear Jordan, this achievement is as much yours as it is mine. Thank you for caring for the girls when I am absent. I know it can be difficult to understand why I put myself and us through what I do, and I am sorry for all the times that I have missed. Thank you for believing in me and my vision. I hope it will all pay off one day and we can show the girls how important it is to become educated and try to help others. I am so proud of your accomplishments as a mother and in your studies. When we were teenagers I never thought I would be finishing my PhD and have such a beautiful family so young. I have everything I want and every day I feel so lucky to have your love and support.

Dear Evangelina 'Pookie', your name means good news; and that is what I hear every day when I walk through that door and see your brimming smile. You have enough energy and optimism to share which can empower me through the worst of days. I started on this journey for you and I hope it makes you proud.

Dear Bonnebelle 'Baby Belle', you are such a thoughtful and inquisitive girl. I love how you question every detail and never conform to the status quo. You truly have a mind of your own and I hope that never changes. Your ideas to perform experiments at home bring me so much joy. Sharing this with your class was the most fun I have had all year. You have asked me if you can read this thesis as a bedtime story; all the while acknowledging that it may take a 'couple' of nights. Thanks for being interested in my work.

Dear Gwendolyne 'Goo', you have only known Daddy as a PhD student. Cuddling and reading to you at night is the highlight of my day. You have been such a good girl (and sleeper) which has made our lives much easier. We have both done a lot of growing over the last two years. Looking forward to taking our next step to grow together some more.

TABLE OF CONTENTS

CHAPTER TWO

CHAPTER FIVE

CHAPTER SIX

LIST OF FIGURES

CHAPTER ONE

CHAPTER TWO

CHAPTER THREE

CHAPTER FOUR

CHAPTER FIVE

CHAPTER SIX

CHAPTER SEVEN

LIST OF TABLES

CHAPTER ONE

CHAPTER TWO

CHAPTER THREE

CHAPTER FOUR

CHAPTER FIVE

CHAPTER SIX

LIST OF SUPPLEMENTARY DATA

LIST OF ABBREVIATIONS

•OH	hydroxyl radical
5-HT	5-hydroxytryptamine
5-HT4R	5-hydroxytryptamine receptor 4
8-OHdG	8-hydroxy-2'-deoxyguanosine
ACh	acetylcholine
APEX1/REF1	apurinic/apyrimidinic endodeoxyribonuclease 1
AT-MSC	adipose tissue-derived MSCs
BCL-2	B-cell lymphoma 2
BM-MSC	bone marrow-derived MSCs
Bregs	regulatory B-cells
CAT	catalase
CCR3	C-C chemokine receptor type 3
CD	Crohn’s disease
CDAI	Cohn’s disease activity index
CFU-f	colony forming unit-fibroblast
CGRP	calcitonin gene-related peptide
ChAT	choline acetyltransferase
CNS	central nervous system
COX	cyclooxygenase
CXCL12	C-X-C chemokine ligand 12
CXCR4	C-X-C chemokine receptor type 4
DAI	disease activity index
DAMP	damage-associated molecular pattern
DAPI	4',6-diamidino-2-phenylindole
DAVID	database for annotation, visualization and integrated discovery
DC	dendritic cells
DEG	differentially expressed genes
DMSO	dimethyl sulfoxide
DNBS	dinitrobenzenesulfonic acid
DRG	dorsal root ganglion

DSS	dextran sodium sulphate
DUOX	dual oxidases
ELAVL	embryonic lethal abnormal vision-like
ENS	enteric nervous system
ER	endoplasmic reticulum
ETC	electron transport chain
FBS	foetal bovine serum
FC	fold change
FMO	flavin-containing monooxygenase
FOXO3	forkhead box O3
FOXP3	forkhead box P3
GA	glycyrrhizic acid
GABA	γ-aminobutyric acid
GDNF	glial cell line-derived neurotrophic factor
GEO	Gene Expression Omnibus
GO	gene ontology
GPx	glutathione peroxidase
GSH	reduced glutathione
GSSG	oxidised glutathione
GST	glutathione S-transferases
H2O2	hydrogen peroxide
HGF	hepatocyte growth factor
HIF-1	hypoxia-inducible factor-1
HLA	human leukocyte antigen
HMGB1	high-mobility group box 1
HO-1	haem oxygenase 1
HSP70	heat-shock protein 70
IBD	inflammatory bowel disease
IDO	indoleamine 2,3-dioxygenase
IFN	interferon
Ig	immunoglobulin
IL	interleukin

iNOS	inducible NOS
iPSC	induced-pluripotent stem cells
KEGG	Kyoto Encyclopedia of Genes and Genomes
KLK	kallikreins
LGR5	leucine-rich repeat-containing G-protein coupled receptor 5
LMMP	longitudinal muscle and myenteric plexus
LOX	lipoxygenase
LPS	lipopolysaccharide
MAP2	microtubule-associated protein 2
MCP-1	monocyte chemoattractant protein-1
MGP	matrix Gla protein
MLN	mesenteric lymph nodes
MPO	myeloperoxidase
mPTP	mitochondrial permeability transition pore
MRC1; CD206	mannose receptor C-type 1
MSCs	mesenchymal stem cells
MUC2	mucin 2
Mφ	macrophages
Mφ1	type 1 pro-inflammatory macrophage
Mφ2	type 2 anti-inflammatory macrophage
NAC	N-acetyl cysteine
NDS	normal donkey serum
NFκB	nuclear factor kappa-light-chain-enhancer of activated B cells
NK	natural killer
NLRP3	NOD-like receptor protein 3
nNOS	neuronal nitric oxide synthase
NO	nitric oxide
NOD	nucleotide-binding oligomerization domain
NOD2	nucleotide-binding oligomerization domain-containing protein 2
NOS	nitric oxide synthase

NOX	nicotinamide adenine dinucleotide phosphate, reduced (NADPH)-oxidase
NPY	neuropeptide Y
NQO	ribosyldihydronicotinamide dehydrogenase, quinone
NRF2	nuclear factor erythroid 2–related factor 2
NSAIDs	nonsteroidal anti-inflammatory drugs
O_2^-	superoxide anion
OCT	optimal cutting temperature
PAMPs	pathogen-associated molecular patterns
PBS	phosphate buffered saline
PDL	population doubling level
PGP9.5	protein gene product 9.5
PMN	polymorphonucleated neutrophils
RAGE	receptor for advanced glycation end-products
redox	reduction-oxidation
REG3	regenerating islet-derived protein 3
RIN	RNA integrity number
RIP	receptor-interacting protein
RIP3	receptor interacting protein kinase 3
RNA-Seq	RNA-Sequencing
ROS	reactive oxygen species
S100B	S100 calcium-binding protein B
SEM	standard error of the mean
SIRT3	NAD-dependent deacetylase sirtuin-3, mitochondrial
SOD	superoxide dismutase
SOD1	superoxide dismutase 1
SPINK	serine protease inhibitor Kazal-type
STAT3	signal transducer and activator of transcription
TGF	transforming growth factor
T_h	T helper
Th	tyrosine hydroxylase
TJPs	tight junction proteins

TLR	toll-like receptors
TNBS	2,4,6-trinitrobenzenesulfonic acid
TNF	tumour necrosis factor
TRAIL	TNF-related apoptosis-inducing ligand
Tregs	regulatory T lymphocytes
TRX1	thioredoxin
TSG-6	TNF-stimulated gene 6 protein
TSP1	thrombospondin 1
UC	ulcerative colitis
UCP2	upregulate uncoupling protein 2
VAChT	vesicular acetylcholine transporter
VCAM-1	vascular cell adhesion protein-1
VEGF	vascular endothelial growth factor
β-CGRP	β-calcitonin gene-related peptide
Ψmito	mitochondrial membrane potential

CHAPTER ONE

LITERATURE REVIEW

STAVELY, R., SAKKAL, S., STOJANOVSKA, V. & NURGALI, K. 2014. Mesenchymal Stem Cells for the Treatment of Inflammatory Bowel Disease: From Experimental Models to Clinical Application. *Inflamm Regen*, 34, 184-197.

1.1. Inflammatory Bowel Disease (IBD)

Inflammatory Bowel Disease (IBD) is comprised of two mutually exclusive pathologies, Crohn's disease (CD) and ulcerative colitis (UC) which are characterised by the presentation of recurrent idiopathic intestinal inflammation. In CD, inflammation occurs transmurally and manifests as discontinuous skip lesions throughout the intestinal tract. Conversely, inflammation in UC is localised specifically in the colon and is more severe in the mucosa (Freeman, 2007, Singh et al., 2010, Baumgart and Sandborn, 2012). In addition, indeterminate colitis can be presented in approximately 10% of cases of IBD where the disease phenotype is unable to be defined (Tremaine, 2012). During the disease course, IBD patients alternate through periods of remission and active inflammation which results in severely debilitating symptoms and sequelae such as bloody stool, persistent diarrhoea or constipation, abdominal pain, cramps, the formation of ulcers, fistulae, strictures and peri-anal fissures (Strober et al., 2007). The mortality rate in IBD patients is escalated due to intestinal complications including perforation of the bowel, excessive bleeding from ulcerations and obstruction or scarring of the bowel. IBD further increases the risk of mortality by predisposing patients to surgical complications and the development of pulmonary disease, ischemic heart disease, infection and cancers including colorectal cancer and lymphoma (Landgren et al., 2011, Rungoe et al., 2013, de Ridder et al., 2014, Jussila et al., 2014).

The debilitating symptoms of IBD, and the potential stigma associated with them, can affect the psychology of patients leading to reduced workforce productivity and absenteeism (Lönnfors et al., 2014). Combined with medical cost, this results in a financial burden of $3 billion per year in Australia (Crohn's and Colitis Australia, 2013). IBD is highly prevalent in westernised society; however, increases in the incidence of IBD are bordering on epidemic proportions throughout Asia which have paralleled the industrialisation and westernisation of these societies (Gearry and Leong, 2013, Ng, 2014). It is predicted that the prevalence of IBD in Australia will reach 100,000 people by the year 2022 (Wilson et al., 2010, Crohn's and Colitis Australia, 2013). The pathogenesis of IBD remains unidentified; however

concordant twin studies have revealed that the development of IBD requires a multi-genetic predisposition and environmental perturbations (Mayer, 2010). Furthermore, CD and UC share numerous predisposing genes with an overlap of around 30% of identified loci associated with the diseases (Khor et al., 2011). Nevertheless, predicted genes and environmental stimuli that can contribute to the development and progression of IBD are highly diverse (Ananthakrishnan, 2015). This indicates that the disease is multi-faceted which is exemplified by the significant variance in the presentation of inflammation and the disease course between patients (Fiocchi, 2018). Despite this, common mechanisms that may contribute to the pathophysiology of IBD have been identified. This includes leukocyte dysregulation, antigenic responses to commensal bacteria, epithelial barrier permeably, damage to the enteric nervous system (ENS) and oxidative stress (Lakhan and Kirchgessner, 2010, Abraham and Medzhitov, 2011, Manichanh et al., 2012, Fries et al., 2013, Piechota-Polanczyk and Fichna, 2014, Pereira et al., 2016, Tian et al., 2017).

1.1.1. Current treatments

Current conventional therapies for IBD include anti-inflammatory drugs (aminosalicylates), corticosteroids, immunomodulators (thiopurines, methotrexate and cyclosporine) and biological agents (anti-tumour necrosis factor-α (TNF-α) antibodies) (Pithadia and Jain, 2011). While these treatments can be effective in improving quality of life, some of them are heavily toxic and fail to induce and maintain remission in a significant number of patients necessitating resection of the inflamed bowel in 70%–90% of cases (Chernajovsky and Robbins, 2011). The anti-inflammatory agents, aminosalicylates are a first-line maintenance therapy and are predominantly used in mild to moderate cases of colitis. Many patients do not respond to aminosalicylates or develop intolerance; treatment is further complicated by hypersensitivities and nephritis (Freeman, 2012). Corticosteroids are effective suppressants of inflammation but are not feasible for long-term treatment due to side-effects including opportunistic infections, diabetes mellitus, hypertension, hypothalamic-pituitary-adrenal axis suppression and psychiatric

complications (Curkovic et al., 2013). Immunomodulators often take 2–3 months to have an effect after the initiation of treatment. The most commonly used immunomodulators, thiopurines, are not tolerated in up to 28% of patients (Schwab et al., 2002). Frequent monitoring is essential for the use of thiopurines due to risks of hypersensitivity, bone-marrow suppression, non-Hodgkin's lymphoma and hepatotoxicity (Krishnareddy and Swaminath, 2014). The immunomodulators, methotrexate and cyclosporine, are also toxic with chronic use and associated with severe opportunistic infections (Hirten et al., 2015, Herfarth et al., 2016). Furthermore, methotrexate is teratogenic and cyclosporine can cause anaphylaxis, liver failure and seizures (Zenlea and Peppercorn, 2014). Recently developed biological therapies such as monoclonal antibodies targeting TNF-α have demonstrated efficacy, however they only elicit a therapeutic response in a subset of patients and are less effective in stricturing CD (Cottone and Criscuoli, 2010). Furthermore, side-effects of TNF-α blockers include an increased risk of serious infections due to immuno-suppression and high toxicity. TNF-α blockers are associated with an increased risk of developing cancer and recent reports have also suggested that anti-TNF-α agents are capable of causing a paradoxical autoimmune response and demyelinating disease in some patients (Seror et al., 2013, Fiorino et al., 2014). Antibiotics are also commonly prescribed for IBD treatment despite limited data to support its therapeutic effects; additionally, concern remains on the predisposition to developing *C. difficile* infection in the gut (Bernstein et al., 2010).

Current treatments for IBD often lose their therapeutic efficacy after repeated exposure and combination therapy with two of the most potent immune suppressants is only capable of prolonging steroid free remission in 56.8% of cases (Colombel et al., 2010). A combination of low efficacy, toxicity, side-effects and intolerance are critical limitations in current therapeutic strategies for IBD pateints. This highlights the need of further research and development into novel treatment options suited for all forms of IBD. The development of current treatments focuses solely on mitigating the immunological component of IBD and has failed to yield an all-encompassing, long-term treatment option; thus, alternative avenues for therapy should be investigated. Dysregulation in the epithelial barrier, ENS and

oxidative stress are also implicated in the pathophysiology of IBD and are viable therapeutic targets (Lakhan and Kirchgessner, 2010, Abraham and Medzhitov, 2011, Manichanh et al., 2012, Fries et al., 2013, Piechota-Polanczyk and Fichna, 2014, Pereira et al., 2016, Tian et al., 2017). Recently, mesenchymal stem cells (MSCs) have become a promising candidate therapy for IBD and could potentially target the various mechanisms of the disease pathophysiology (Singh et al., 2010, del Pilar Martínez-Montiel et al., 2014).

1.2. Mesenchymal Stem Cell Therapy for IBD

1.2.1. Mesenchymal stem cells

Friedenstein et al. (1966) first theorised the existence of osteogenic stem cells after observing the presence of highly proliferative spindle-shaped cells in cultures of murine bone marrow. Years later, fibroblast-like cells that are clonogenic and demonstrate osteogenic potential were isolated from guinea-pig bone marrow and spleen by Friedenstein et al. (1970). Although these cells could not be fully characterised by modern standards, the studies conducted by Friedenstein et al. have been accredited by the scientific community as the pioneering research of what are now known as mesenchymal stem cells, multipotent stromal cells or mesenchymal stromal cells (MSCs) (Bianco et al., 2008). In addition to osteogenesis, all MSCs universally exhibit adipogenic and chondrogenic differentiation potential (Qian et al., 2010, Perrier et al., 2011, Giuliani et al., 2013). Under certain conditions, MSCs can also differentiate into myoblasts, tenocytes, epithelial cells, endothelial cells, hepatocytes, cardiomyocytes and neuron-like cells; this suggests that MSCs can differentiate into cells of all three germ lineages (Gang et al., 2004, Ferrand et al., 2011, Guan et al., 2011, Piryaei et al., 2011, Schneider et al., 2011, Scuteri et al., 2011, Wang et al., 2013a). The International Society for Cellular Therapy (ISCT) recommends that bona-fide MSCs are defined *in vitro* by the following criteria: 1) their ability to differentiate into osteogenic, chondrogenic and adipogenic lineages; 2) clonogenicity; 3) adherence to plastic and 4) specific surface marker expression (Dominici et al., 2006). A typical surface marker phenotype includes positive

expression of CD29, CD44, CD73, and CD90 in addition to negligible expression of hematopoietic and endothelial markers, CD45 and CD34 (Dominici et al., 2006). It should be noted that there are additional surface markers that are used to identify MSCs and that there are some variations in the expression of these surface markers depending on the source tissue from which MSCs are derived (Lin et al., 2012b).

MSCs possess various unique properties that have led to interest in utilising them as a cell-based therapy for many diseases including IBD (Singh et al., 2010, Wang et al., 2012, Wei et al., 2013, Stavely et al., 2014). MSCs are present in vastly heterogeneous tissues distributed throughout the body and have been isolated from many tissue sources other than bone-marrow (Caplan, 1991, Gnecchi and Melo, 2009, Mosna et al., 2010) including adipose (Zuk et al., 2002, Mizuno et al., 2012), placenta (Semenov et al., 2010), peripheral blood (Chong et al., 2012), Wharton's jelly (Wang et al., 2004), umbilical cord (Tong et al., 2011), amnion (Manochantr et al., 2013) and dental pulp (Pierdomenico et al., 2005). Additionally, da Silva Meirelles et al. (2006) have demonstrated that MSCs can be isolated from almost every post-natal organ in mice. The two most studied sources of MSCs for disease therapy are from adult adipose tissue and bone marrow due to their relative ease of isolation for autologous therapies. The isolation and purification of MSCs by virtue of their adherence to plastic and proliferative nature is an affordable and reproducible process that can be performed in most labs globally (Caplan, 1991, Zuk et al., 2002, Mosna et al., 2010). Bone marrow derived MSCs are isolated by directly culturing bone marrow aspirate. MSCs derived from adipose tissue require digestion and are made into a single cell suspension before culturing. In both processes, MSCs adhere to plastic while contaminating cells are removed by subsequent washing of non-adherent cells. Passaging of MSC cultures ensures purity of the highly proliferative MSC population. Samples of these adult tissues are obtainable without damaging the host and MSCs can be expansively cultured to generate large numbers of cells for treatments (Caplan, 1991, Zuk et al., 2002, Mosna et al., 2010, Forbes et al., 2014, Garcia-Arranz et al., 2016). Multiple factors during the expansion process can influence the characteristics of MSCs which must be considered. This includes seeding densities and reagents used for cell culture.

Unlike many cancer cell lines, MSCs are expansive even at very low densities; seeding MSCs at low density increases their expansive potential (Dvorakova et al., 2008, Neuhuber et al., 2008). After expansion of MSCs through subsequent passaging, MSCs can develop from a spindle to a flat morphology with a loss of stemness and clonogenicity (Neuhuber et al., 2008). Seeding MSCs at a low density of 60 cells/cm^2 assists in maintaining the spindle morphology of MSCs (Dvorakova et al., 2008). MSC proliferation is dose-dependent with the concentration of FBS (Riekstina et al., 2008). The use of 16.5% FBS has been recommended for MSC expansion (Gang et al., 2007). Nevertheless, lot-to-lot differences in the quality of FBS makes standardising concentrations for MSC expansion difficult (Amiri et al., 2015). To overcome this, FBS pre-qualified to maintain MSC stemness and proliferation is regularly used for cell culture (Yamada et al., 2011, Han et al., 2014a, Höfig et al., 2016). The use of FBS is currently the most efficient method to expand MSCs (Russell et al., 2015). However, other methods of expanding clinical grade MSCs without FBS are sought to avert xenogeneic antigens being administered into patients (Oikonomopoulos et al., 2015). Recent studies have also demonstrated the viability of mass culture of clinical grade MSCs using an automated bioreactor which can improve the affordability of MSC production and provide financial feasibility for their use in the clinic (Russell et al., 2018).

Once administered, MSCs can home to, and engraft specifically to sites with active inflammation (Karp and Leng Teo, 2009, Sohni and Verfaillie, 2013). There, MSCs can elicit an array of therapeutic effects. MSCs promote trophic support and angiogenesis either directly by their secretome or via the induction of endogenous mechanisms that can repair damaged tissue (Wu et al., 2007, Chen et al., 2008, Sémont et al., 2013). Moreover, MSCs are receptive to environmental cues and respond by secreting various cytokines depending on the stimuli (Waterman et al., 2010). MSCs exposed to inflammatory conditions are immunomodulatory and suppress the pro-inflammatory immune response by secreting anti-inflammatory factors or promoting the generation of anti-inflammatory leukocyte populations (Ma et al., 2013). These therapeutic characteristics can be observed between individuals and species across the histocompatibility barrier (Li et al., 2012,

Ankrum et al., 2014). Due to these characteristics, MSCs have shown promise in a spectrum of pathologies including: autoimmune diseases (Ben-Ami et al., 2011), graft-versus-host disease (GvHD) (Kebriaei and Robinson, 2011), cartilage regeneration (Anderson et al., 2013a), tissue engineering (Martinez and Kofidis, 2011), neurodegenerative disease (Joyce et al., 2010), vehicles for drug delivery and cancer therapy (Porada and Almeida-Porada, 2010). Likewise, positive results continue to be reported in multiple studies using MSC therapy to treat intestinal inflammation in experimental models and in IBD patients (**Tables 1.1 and 1.2**).

In seminal studies, García-Olmo et al. (2005) and Onken et al. (2006) observed clinical responses to MSC treatments for CD-related fistulae and the inflammatory luminal pathology of CD in refractory patients, respectively. Considering that these patients were not previously responding to conventional therapy, MSC treatments demonstrated promise as an alternative therapeutic option. Shortly thereafter, investigations into the mechanism of MSCs in intestinal inflammation emerged with Hayashi et al. (2008), Ando et al. (2008) and Tanaka et al. (2008) demonstrating that MSCs could attenuate chemically-induced colitis in rats by offering trophic support and reducing inflammation. While the number of clinical studies has steadily grown since 2005, the number of studies in experimental colitis models has proliferated between 2014 and 2018 with 59 studies published out of the 81 in experimental models (**Figure 1.1A, Tables 1.1 and 1.2**). The enthusiasm in the field is largely driven by clinical trials like that conducted by Forbes et al. (2014) which have demonstrated favourable outcomes using MSC therapy to treat IBD. However, it is still necessary to elucidate mechanisms of MSC therapy to optimise treatments. Due to the complex and multi-faceted nature of intestinal inflammation, and MSCs themselves, novel findings continue to be published which are bringing MSC therapies closer to the clinic.

1.2.2. MSC heterogeneity: species

A multitude of experimental models and designs have been employed in MSC research with *in vivo* animal models studying MSCs from the same or alternative

host-donor species (**Figure 1.1B, Tables 1.1 and 1.2**). In these studies, syngeneic (minimal genetic variation), allogeneic (same species) or xenogeneic (different species) MSCs have been used. Each experimental design has benefits, but none can fully replicate clinical treatments. MSCs derived from inbred strains of murine species and applied into the same strain should be considered syngeneic due to their genetic similarity; this is most representative of autologous (same individual) MSC therapy. Allogeneic MSC therapy is achieved by administering MSCs from the same species that are genetically dissimilar such as those from outbred strains or across different strains of animals. Human MSCs are often used in xenogeneic models of experimental colitis. While this does not model the host-donor histocompatibility in the clinic, this experimental design is often favourable to study the mechanisms of human MSCs which function via different mechanisms to those from other species. For example, the suppression of T-cell mitogenesis is dependent on 2,3-dioxygenase (IDO) in human MSCs and inducible nitric oxide synthase (iNOS) in murine MSCs (Ren et al., 2009, Ghannam et al., 2010). Despite the genetic diversity between xenogeneic MSCs and animals used to model disease, the majority of literature has supported the application of human MSCs into animal models with evidence of engraftment and functionality across species barriers (Li et al., 2012, Lin et al., 2012a, Wang et al., 2017). MSCs secrete a number of paracrine factors; the sequence homology for many of these factors is similar in mammalian species; explaining the ability of MSCs to function across xenogeneic barriers. This is plausible considering that trophic proteins from foetal bovine serum are used to provide nourishment for other mammalian cells *in vitro* (Gstraunthaler, 2003). Furthermore, xenogeneic MSCs can exert their therapeutic action via antioxidant enzymes that metabolise and detoxify simple molecules in the recipient regardless of sequence homology between species (Ashour et al., 2016). In experimental models of colitis, administration of allogeneic and human xenogeneic MSCs yield similar results in mice, rats and guinea-pigs (**Table 1.2**). This is not a specific feature of human MSCs as xenogeneic canine MSCs can also attenuate colitis in mice (Song et al., 2018). Considering that xenogeneic MSCs are effective in animal models of colitis, and the therapeutic mechanisms of MSCs differ between species, studies have preferred to utilise human MSCs in models of

experimental colitis (**Figure 1.1B**). Favourable results from these studies demonstrate the immune evasive nature of MSCs which further highlights the practicability of using allogeneic MSCs as a cellular therapy in the clinic.

Allogeneic MSCs were commonly utilised for the treatment of UC and the luminal inflammatory pathology of CD (**Figure 1.1B**). The appeal of allogeneic MSCs is often predicated on the potential for dysfunction in the activity of MSCs derived from patients with pathological conditions. RNA-Sequencing (RNA-Seq) has revealed that AT-MSCs from CD patients and uninflamed controls exhibit differences in the expression of genes related to cell growth and proliferation (Hoffman et al., 2018). Nevertheless, it has been observed in experimental colitis that the conditioned medium of MSCs derived from CD patients is more effective than that derived from non-inflamed controls. Allogeneic MSCs are also favourable because they can be extensively expanded and subsequently stored, however it is well established that MSCs lose their characteristics over subsequent passages (Yang et al., 2018). This is illustrated in GvHD where MSCs have demonstrated a far greater efficacy after 1 to 2 passages as opposed to 3 to 4 (von Bahr et al., 2012). Thus, the development of expansive MSC cell lines may have limited efficacy. Evaluation of autologous or allogeneic MSC sources must be carefully deliberated and assess efficacy, accessibility of cells, costs of production and importantly, risk to the patient. To properly address these issues further studies are required.

Figure 1.1 ***Summary of studies using MSCs to treat intestinal inflammation***

A) Number (#) of articles in chronological order using MSC treatments in experimental models of colitis (blue) and clinical trials for IBD (red). **B)** Host-donor homology and **C)** the tissue of origin of MSCs used for treatments in experimental models of colitis (blue) and clinical trials for IBD (red). **D)** Routes of MSC administration and **E)** types of experimental models of colitis used to study MSC therapy.

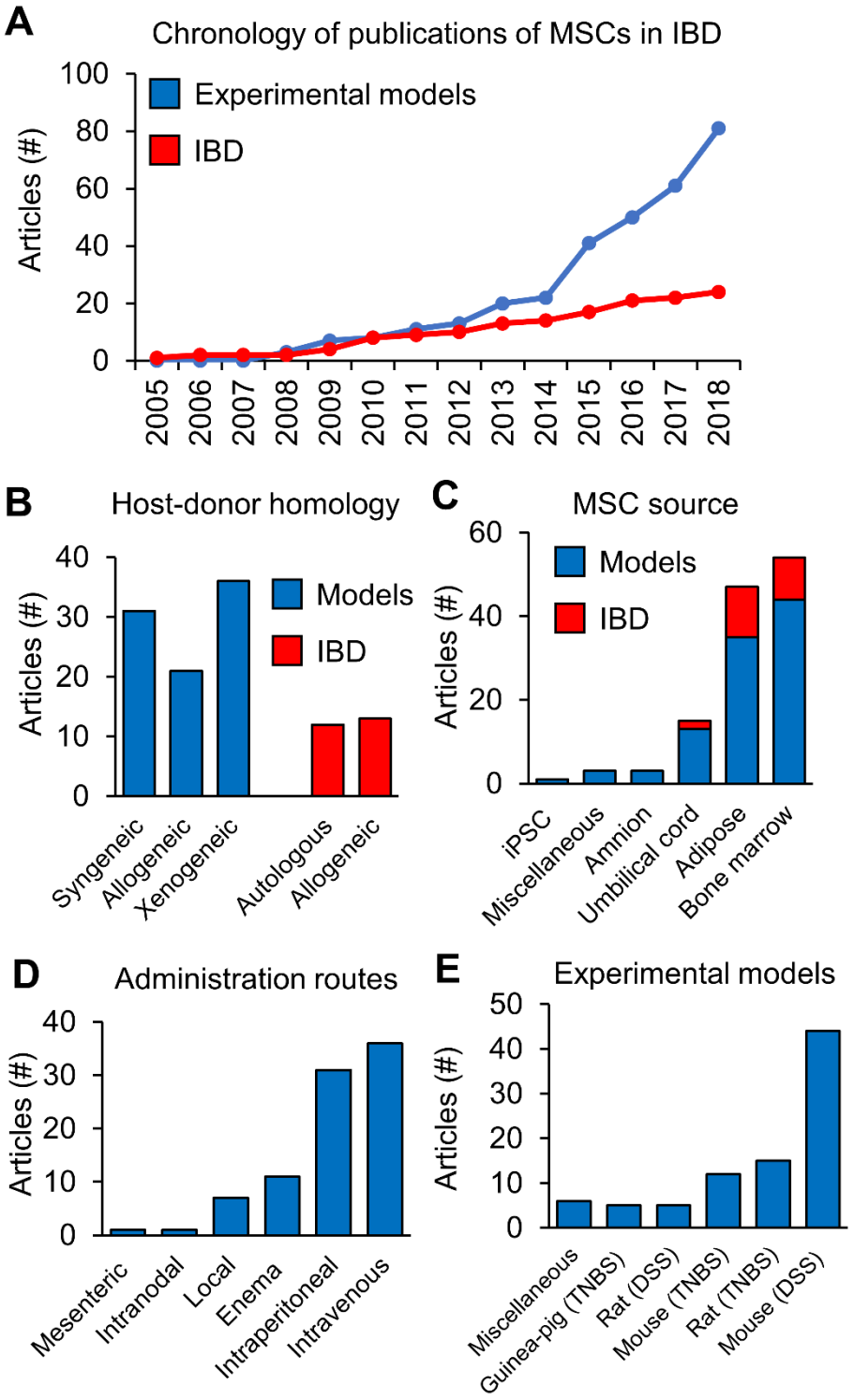
A
Chronology of publications of MSCs in IBD
Articles (#)
Experimental models
IBD
2005
2006
2007
2008
2009
2010
2011
2012
2013
2014
2015
2016
2017
2018
B
Host-donor homology
Models
IBD
Syngeneic
Allogeneic
Xenogeneic
Autologous
Allogeneic
C
MSC source
iPSC
Miscellaneous
Amnion
Umbilical cord
Adipose
Bone marrow
D
Administration routes
Mesenteric
Intranodal
Local
Enema
Intraperitoneal
Intravenous
E
Experimental models
Miscellaneous
Guinea-pig (TNBS)
Rat (DSS)
Mouse (TNBS)
Rat (TNBS)
Mouse (DSS)

Table 1.1 ***Clinical trials of mesenchymal stem cell therapy in IBD***

MSC Homology	MSC Source	MSC Delivery	Targeted Pathology	Therapeutic Outcome	Ref
Allogeneic	AT-MSC	Injection into fistulous tract wall	Crohn's disease-related complex perianal fistulae	• Complete closure of the treated complex perianal fistula in 9/16 subjects after 24 weeks	(de la Portilla et al., 2013)
Allogeneic	AT-MSC	Injection into fistulous tract wall	Crohn's disease-related complex perianal fistulae	• Expanded MSC cell line (Cx601) • Dosage of $120x10^6$ cells • Remission in 53/107 patients with intention to treat vs 36/105 with placebo • Remission in 53/103 patients with a modified intention to treat vs 36/101 with placebo • 18/103 patients experienced adverse events vs 30/103 with placebo • Nature of adverse events were similar between groups (anal abscess, proctalgia) • Increased remission by MSCs in patients with combined anti-TNF/immunomodulators, TNF alone or neither; but not immunomodulators on their own	(Panes et al., 2016)
Autologous	AT-MSC	Injection into fistulous tract wall and sealed with fibrin glue	Crohn's disease-related complex perianal fistulae	• Fistula closure in 5/7 subjects treated with AT-MSCs and fibrin glue • Positive response to fibrin glue alone in 1/7 subjects	(Garcia-Olmo et al., 2009a)
Autologous	AT-MSC	Injection into fistulous tract wall and sealed with cells suspended in fibrin glue	Crohn's disease-related entero-cutaneous fistulae	• Complete healing with re-epithelialisation of the fistula opening in 3/4 treated subjects Healing of the fistula with the stromal vascular fraction in 1/4 treated subjects	(Garcia-Olmo et al., 2009b)
Autologous	AT-MSC	Injection into fistulous tract wall and mucosa of the opening and sealed with fibrin glue	Crohn's disease-related fistulae	• Partial closure in 3/3 treated subjects with $1x10^7$ MSCs/mL • Complete healing in 2/3 treated subjects with 2 $x10^7$ MSCs/mL at week 8 after injection • Complete healing in 1/3 treated subjects with $4x10^7$ MSCs/mL	(Cho et al., 2013)

				• No fistulae re-occurrence 8 months after injection in 3/3 subjects with complete healing at 8 weeks	
Autologous	AT-MSC	Injection into fistulous tract wall or rectal mucosa	Crohn's disease-related fistulae	• Complete re-epithelialisation in 6/8 various types of fistulae 8 weeks after treatment	(García-Olmo et al., 2005)
Autologous	AT-MSC	Injection into fistulous tract wall and sealed with cells suspended in fibrin glue	Crohn's disease-related fistulae	• Complete closure of various fistulae in 27/33 subjects administered with autologous AT-MSCs and fibrin glue after 8 weeks • Sustained closure in a one year follow up in 23/26 patients with previously healed fistulae	(Lee et al., 2013)
Autologous	BM-MSC	Injection into fistulous tract wall and lumen	Crohn's disease-related fistulae and disease activity index	• Closure of fistulae in 7/10 subjects • Statistically significant decrease in Crohn's disease and perianal activity indexes • Significant increase in mucosal and peripheral Tregs • Tregs remained significantly elevated at 1 year follow up	(Ciccocioppo et al., 2011)
Allogeneic	BM-MSC	Injection into fistulous tract wall	Crohn's disease-related perianal fistulae	• Dose response with $1x10^7$, $3x10^7$ or $9x10^7$ MSCs • No adverse events • Healing in at week 24 in 4/5 after $1x10^7$, 4/5 after $3x10^7$ and 1/5 with $9x10^7$ compared to 2/6 with placebo • Individual fistulae healing at week 24 in 6/9 after $1x10^7$, 6/7 after $3x10^7$ and 2/7 with $9x10^7$ compared to 3/9 with placebo	(Molendijk et al., 2015)
Autologous	AT-MSC	Injection into fistulous tract wall and lumen with fibrin glue	Crohn's disease-related perianal fistulae	• Long term effects of MSCs on fistula closure determined from phase 2 trial • Complete closure in 21/26 after 24 months (patents selected per protocol; PP) • Closure at 8 weeks maintained to 24 months (20/24)	(Cho et al., 2015)
Autologous	AT-MSC	MSC-coated matrix fistula plug	Crohn's disease-related perianal fistulae	• Phase 1 trial of MSCs implanted on bio-absorbable matrix • No serious adverse events recorded • 9/12 patients with complete closure at 3 months • 10/12 patients with complete closure at 6 months	(Dietz et al., 2017)

Autologous	AT-MSC	Injection into fistulous tract wall	Crohn's disease-related perianal fistulae	• Fistula closure 1 year after treatment in 2/3 patients • The 2 patients with closure received MSCs with fibrin glue	(Garcia-Olmo et al., 2015)
Autologous Allogeneic	AT-MSC	Injection into fistulous tract wall	Crohn's disease-related rectovaginal fistulae	• Complete healing of rectovaginal fistulae in 3/4 women treated with AT-MSCs and fibrin glue • No healing in subjects treated with fibrin glue only • Only 4/8 women had fistulae resultant of Crohn's disease	(Garcia-Olmo et al., 2010)
Allogeneic	AT-MSC	Injection into fistulous tract wall	Crohn's disease-related rectovaginal fistulae	• Phase 1-2a trial - $20x10^6$ cells administered, additional 40 $x10^6$ cells if no healing occurred after 12 weeks • No serious adverse events recorded • 8/10 patients required follow up dose • Closure in 9/10 patients at some stage of the study. • Long term closure at 52 weeks in 3/5 patients • Trending decrease in IL-6 in 7/10 patents, 2/10 low before treatment.	(Garcia-Arranz et al., 2016)
Allogeneic	UC-MSC	Intravenous Injection	Moderate-severe Luminal Crohn's disease	• $1×10^6$ cells/kg once a week (four weeks) • Decreased CDAI, HBI, CD endoscopic index of severity and corticosteroid dosage after 12 months compared to control (n=41/group) • No patient achieved complete remission • Fever developed in 4 patients after infusion • No serious adverse events	(Zhang et al., 2018)
Allogeneic	UC-MSC	Intravenous Injection	Moderate-severe Ulcerative colitis	• Decrease Mayo and histology scores after MSC infusion (n=34) compared to control (n=36) until end of study at 24 months • Increase in IBDQ scores (quality of life) • 30/36 patients with clinical response to MSC infusion at 3 months according to mayo score • No change to serum levels of TNF-α, IL-6 and IFN-γ 3 months post-treatment • N.D. to CRP between groups	(Hu et al., 2016)
Allogeneic	BM-MSC	Intravenous Injection	Refractory luminal Crohn's disease	• Clinical response in 12/15 subjects after 4 weeks • Clinical remission achieved in 8/15 subjects after 4 weeks • Endoscopic improvement in 7/15 subjects	(Forbes et al., 2014)

				• 4x weekly $2x10^6$ cells/kg	
Allogeneic	BM-MSC	Intravenous injection	Refractory luminal Crohn's disease	• Two doses of $2x10^6$ or $8x10^6$ cells • Clinical response in 3/9 patients	(Onken et al., 2006)
Allogeneic	BM-MSC	Intravenous injection	Refractory luminal Crohn's disease	• Decrease in CDAI in 80% pf patients after 8 weeks (8/10 patents PP), dropped to 55.5% by week 12 (5/9 patents PP) • Clinical response at 2 weeks (36%) to 12 weeks (22.1%, PP) • 3 patients achieved clinical remission through study • Worsening of disease in 2 patients (no concomitant therapy) • MSC treatments increased proportion of NK and NKT-lymphocytes after 12 weeks • No change in Treg, naïve Th, memory Th, cytotoxic T lymphocyte, B lymphocytes or Ig levels after 12 weeks	(Gregoire et al., 2018)
Autologous	BM-MSC	Intravenous Injection	Refractory luminal Crohn's disease	• Phase 1 trial of dosages $2x10^6$, $5x10^6$ and $10x10^6$ cells/kg (n=4/group) • Clinical response at 2 weeks by CDAI scores observed in 50% ($2x10^6$ cells/kg), 25% ($5x10^6$ cells/kg) and 50% ($10x10^6$ cells/kg). • 7 adverse events recorded. 2 possibly related to MSC infusion, *C. difficil*e infection and appendicitis • 5 due to CD flare, despite positive responses observed in CDAI at 2 weeks • MSCs were fully characterised *in vitro* and inhibited T lymphocyte proliferation suggesting functional competency • Cells did not undergo cryopreservation	(Dhere et al., 2016)
Autologous	BM-MSC	Intravenous injection	Refractory luminal Crohn's disease	• Clinical response in 3/9 subjects after 6 weeks • Worsening of disease in 3/9 subjects • Reduced endoscopic severity in 2/9 subjects • Reduction in $CD4^+$ T lymphocytes	(Duijvestein et al., 2010)
Allogeneic	BM-MSC	Slow drip Intravenous injection	Ulcerative colitis	• Dosage of $1.5\text{-}2x10^8$ • Decreased clinical and morphological indices in 34/44 patients	(Lazebnik et al., 2010a)

Allogeneic	BM-MSC	Slow drip Intravenous injection	Ulcerative colitis	• MSC treatments compared with aminosalicylic acid and glucocorticoids • After 12 months, highest decrease in Rachmilewitz clinical activity index and Mayo scores after 3 weekly MSC infusions compared to singular injection and current treatments • Relative risk of UC decreased after 24 months in subjects with 3 weekly MSC infusions compared to singular injection and current treatments	(Lazebnik et al., 2012)
Allogeneic	BM-MSC	Intravenous injection	Ulcerative colitis and Crohn's disease	• Dosage of 1.5-2x10^8 • Remission in 31/39 UC and 9/11 CD patients • 4-8 month follow up	(Lazebnik et al., 2010b)

AT, adipose tissue; BM, bone marrow; CDAI, Crohn's disease activity score; CRP, C-reactive protein; HB1, Harvey-Bradshaw index; IFN-γ, interferon γ; Ig, immunoglobulin; IL, interleukin; MSC, mesenchymal stem cell; N.D., no difference; NK, natural killer cell; NKT, natural killer T lymphocyte; PP, per protocol cohort; Th, T helper cell; TNF-α, tumour necrosis factor α; Treg, regulatory T lymphocyte

Table 1.2 ***Mesenchymal stem cell treatment in experimental colitis models***

Model	MSC homology	MSC tissue source	MSC Administration	Major findings	Ref
Canine (fistulae)	Xenogeneic	Embryonic stem cell derived-MSCs (human)	Local Intra-lesional	• No adverse events • 6/6 fistula closure at 3 months. Relapse in 2/6 at 6 months. • ↓IL-2 ↓IL-6 in serum	(Ferrer et al., 2016)
Canine (IBD)	Allogeneic	AT-MSCs	i.v. Injection	• No adverse events • ↓ Endoscopic score in stomach, duodenum, ileum and colon • ↓ Histological score in stomach, duodenum, ileum and colon	(Perez-Merino et al., 2015)
Guinea-pig (TNBS)	Allogeneic	AT-MSCs BM-MSCs	Enema	• First study characterising and applying guinea-pig derived MSCs • ↓Histopathology • ↑Body weight with BM-MSCs only • ↓Leukocytes in submucosa and mucosa at 24 and 72h. ↑ with AT-MSCs than uninflamed controls at 24h • ↓Leukocyte infiltration to myenteric ganglia at 24 and 72h. ↑ with AT-MSCs than uninflamed controls and BM-MSCs at 24h • ↑ Myenteric neurons ↑ChAT neurons ↓nNOS neurons • MSCs secreted TGF-β1. Inhibition of TGF-β receptor 1 blocked neuroprotection by MSCs *in vitro*	(Stavely et al., 2015a)
Guinea-pig (TNBS)	Xenogeneic	AT-MSCs BM-MSCs (human)	Enema	• ↓Histopathology • ↑Body weight • ↓Leukocyte infiltration to myenteric ganglia • ↑Myenteric neurons. AT-MSCs ↓than uninflamed controls. • ↓nNOS neurons ↑ChAT neurons. ↓ChAT with AT-MSCs than uninflamed controls at 24h. • ↑CGRP ↑Th and ↑VAChT nerve fibres • MSCs detected in epithelial layer and near myenteric ganglia • MSCs chemoattracted to Myenteric cells stimulated with LPS *in vitro*	(Stavely et al., 2015b)
Guinea-pig (TNBS)	Xenogeneic	BM-MSCs	Enema	• MSC and MSC-CM • ↑Body weight ↓histopathology • ↑Nerve fibre innervation	(Robinson et al., 2014)

		BM-MSC conditioned medium (human)		• ↓Leukocytes in colon ↓leukocyte infiltration to myenteric ganglia • ↑Myenteric neurons ↑ChAT neurons ↓nNOS neurons • ↓Colon motility propagation speed ↑Number of contractions	
Guinea-pig (TNBS)	Xenogeneic	BM-MSCs BM-MSC conditioned medium (human)	Enema	• MSC and MSC-CM • MSCs detected in mucosa and submucosa until at least 72h • ↑Body weight ↓histopathology • ↓Leukocytes by 24h. N.D. at 6h • ↓Leukocyte infiltration to myenteric ganglia at 24h ↓to control levels by 72h • ↑Nerve fibre innervation by 24h. N.D. at 6h • ↑Myenteric neurons ↓nNOS neurons ↑ChAT neurons at 24h	(Robinson et al., 2015)
Guinea-pig (TNBS)	Xenogeneic	BM-MSCs (human)	Enema	• MSCs detected in mucosa, submucosa and muscle layers • ↓Leukocytes in mucosa and muscle • ↑Nerve fibre innervation in mucosa and muscle • ↑Myenteric neurons ↓nNOS neurons ↑ChAT neurons • All parameters dose dependent until $1x10^6$ cells	(Robinson et al., 2017b)
Mouse (azoxymethane + DSS)	Xenogeneic	UC-MSCs (human)	i.v. injection	• Mouse model of colitis-associated colorectal cancer • MSCs migrate to inflamed-colon. Also detected in lung. • ↓Disease activity ↓histopathology ↑Colon length • ↓IL-1α ↓IL-1β ↓IL-5 ↓IL-6 ↓IL-12p40 ↓*Il1b* ↓*Il5* ↓*Tnf* mRNA ↓phosporalated-P65 • ↑Treg • ↑FOXP3 in naïve $CD4^+$ T lymphocyte partially dependent on MSC-secreted TGFβ *in vitro* • ↑SMAD2 signalling by MSC-CM in immortalised T lymphocytes • ↓Tumours result of the suppression of colitis	(Tang et al., 2015a)
Mouse (DSS)	Allogeneic	AT-MSCs	i.v. injection	• ↓Histopathology and weight loss with AT-MSCs and iPSC-MSCs	(Soontarak et al., 2018)

		Induced-pluripotent stem cell (iPSC)-derived MSC		• MSCs detected in lung, liver and spleen. Few cells in the colon • ↑Ki67 ↑LGR5 in epithelial cells • ↑Vascularisation of epithelium • ↓Abundance of proteobacteria with AT-MSCs and iPSC-MSCs • ↑Bacterial diversity with iPSC-MSCs • ↑$FOXP3^+$ ↓$F4/80^+$ cells with AT-MSCs and iPSC-MSCs	
Mouse (DSS)	Allogeneic	BM-MSC (immortal)	i.v. injection	• VCAM-1 Ab-coated MSCs ↑homing to the colon ↑Tregs	(Ko et al., 2010)
Mouse (DSS)	Syngeneic	AT-MSC AT-MSC conditioned medium	i.p. Injection	• ↓Disease activity ↓histopathology ↑Colon length • ↑IL-10 ↓IL-17 in MLN, spleen and serum • ↑TGFβ in MLN for both, ↑ TGFβ in spleen and serum for MSC-CM • ↑Treg in MLN and spleen for both	(Heidari et al., 2018)
Mouse (DSS)	Syngeneic	AT-MSC Conditioned medium	i.p. injection	• ↓Disease activity ↓ histopathology • ↑Treg in MLN, N.D. in spleen	(Pouya et al., 2018)
Mouse (DSS)	Syngeneic	AT-MSC	i.v. injection	• ↓Disease activity ↓histopathology ↑Colon length • ↑GSH • ↑SOD activity, N.D. Catalase activity, N.D. GPx activity • No effect of MSCs on ↑ lipid oxidation	(da Costa Gonçalves et al., 2017)
Mouse (DSS)	Syngeneic	AT-MSCs	i.p. Injection	• ↓Disease activity ↑Colon length • ↑ZO-1 • ↓IFN-γ ↓TNF-α ↑IL-10 • ↓IL-6 ↓MCP1 • ↓ Mφ and DC in lamina propria N.D. in MLN • ↑ARG1	(de Aguiar et al., 2018)
Mouse (DSS)	Syngeneic	AT-MSCs	i.p. Injection	• ↓Histopathology ↑colon length • MSCs detected in spleen and MLN but not colon • ↑Treg in colon and MLN • N.D. CD103+ DC (promoters of Treg) • MSCs secrete little TGFβ • MSCs activate latent TGFβ by TSP1 • TSP1 KD MSCs do not ameliorate colitis or induce Treg *in vivo*	(Takeyama et al., 2017)

Mouse (DSS)	Syngeneic	AT-MSCs IL37b-AT-MSCs	i.p. injection	• *Il37b* expression via adenovirus vector • ↓Histopathology ↑colon length • ↑Treg and myeloid derived suppressor cells in spleen • ↑IL-2 ↓IFN-γ in $CD4^+$ T lymphocytes in spleen • *Il37b* expression enhanced all parameters	(Wang et al., 2015)
Mouse (DSS)	Syngeneic	AT-MSCs IL35-AT-MSCs	i.v. injection	• IL-35 transduced MSCs (IL35-MSC) • IL35-MSC ↓disease activity ↓Histopathology ↑colon length. • ↓TNF-α ↓IFN-γ ↓IL-17 ↑Treg • Normal MSC has no effect on these parameters	(Yan et al., 2018)
Mouse (DSS)	Syngeneic	BM-MSCs	Enema	• MSC-derived spheroids • ↓Disease activity ↑colon length, N.D. Endoscopy scores • ↓SAA serum ↓MPO colon • ↓IFN-γ ↓IL-6 ↓IL-2 ↓IL-4, N.D. TNF, IL-17A, IL-10	(Molendijk et al., 2016)
Mouse (DSS)	Syngeneic	BM-MSCs BM-MSC derived spheroids	i.p. injection Local (Endoscopic injection)	• MSCs and MSC spheroids detected in colon after endoscopic injection • ↓Disease activity ↓histopathology in MSCs and MSC spheroids • ↓SAA serum with MSC spheroids	(Barnhoorn et al., 2018)
Mouse (DSS)	Syngeneic	BM-MSCs	i.p. injection	• Limited immunomodulation • No change in disease activity	(Nam et al., 2015)
Mouse (DSS)	Syngeneic	BM-MSCs	i.p. injection	• <1% MSCs reached colon • MSCs formed aggregates in peritoneal cavity containing Mφ and B and T lymphocytes • Aggregates ↑FOXP3, ↑IL-10, ↑TGF-β, ↑Arginase type II, ↑CCL22, ↑HO-1 and ↑TSG6 • ↑TSG6 in serum • $TSG6^{-/-}$ MSCs ineffective • Recombinant TSG6 ↓ severity of colitis ↓ leukocytes ↑$FOXP3^+$ leukocytes	(Sala et al., 2015)
Mouse (DSS)	Syngeneic	BM-MSCs	i.p. injection	• ↓Disease activity ↓histopathology ↑Colon length • ↓TNF-α ↓IL-1β ↑TGFβ ↑IL-10 in serum (GAL3 inhibition in MSCs ↑IL-10)	(Simovic Markovic et al., 2016)

				• ↓ Mφ, mast cells, DCs and NKT-lymphocytes. • ↓ Mφ IL-1β$^+$ IL-12$^+$ ↑IL-10$^+$ ↑ Mφ2, GAL3 inhibition in MSCs ↑IL-10 ↑ Mφ2 • GAL3 inhibition ↑ Mφ2 polarisation *in vitro*	
Mouse (DSS)	Syngeneic	BM-MSCs	i.v. injection	• Long term DSS treatment (3 cycles over 33 days), MSCs administered on first cycle. • ↓Histopathology, N.D. colon length • ↑IL-10, N.D. TNF-α, TGFβ	(Lee et al., 2016)
Mouse (DSS)	Syngeneic	BM-MSCs	i.v. injection	• ↓Disease activity • ↓IL-6 ↓IL17A ↓IFN-γ ↓TNF-α • ↑TGF-β1 – major source from macrophages • ↓Therapeutic effect of MSC after macrophage ablation • Recombinant TGF-β1 replicated effect of MSCs	(Liu et al., 2015)
Mouse (DSS)	Syngeneic	BM-MSCs	i.v. Injection	• MSCs engrafted and proliferated until at least 21days • ↓Mucosal permeability: D-lactic acid and Diamine oxidase • ↓Histopathology • ↑ E-cadherin • ↓MDA ↑SOD	(Sun et al., 2015)
Mouse (DSS)	Syngeneic	BM-MSCs	i.v. injection i.p. injection Enema	• Most effective localisation to colon with i.p. and enema • Most entrapment of MSC in lung, liver and spleen after i.v. - least with enema • i.p. MSCs in epithelium, enema MSCs in lumen, few i.v. MSCs in lamina propria • ↑Colon length ↓MPO ↓histopathology ↓Collagen • ↓TNF-α ↑IL-10 • ↑FOXP3$^+$ cells • Improved efficacy of all parameters with i.p. injection • ↑TSG6 after i.p. • ↑Ki67$^+$ cells in crypts after i.p. and enema	(Wang et al., 2016)
Mouse (DSS)	Syngeneic	BM-MSCs	i.v. injection	• ↓Disease activity partly mediated by TGFβ1	(Wu et al., 2015)

				• miR21$^{-/-}$ MSCs ↑TGFβ1 secretion *in vitro* • miR21$^{-/-}$ MSCs enhance ↓Disease activity ↑Treg *in vivo* • miR21 targets PTEN ↑Akt activation ↑NFκB activation ↓TGFβ1 in MSCs	
Mouse (DSS)	Syngeneic	BM-MSCs	i.v. injection	• ↓Disease activity ↓histopathology of colitis • ↓Pro-inflammatory cytokines in the colon	(He et al., 2012)
Mouse (DSS)	Syngeneic	BM-MSCs	i.v. injection	• ↓Disease activity ↓histopathology of colitis • MSCs increased expression of phosphorylated TGF-βR1 and downstream target SMAD2 in colon • TGF-βR1 inhibition abrogated therapeutic effect of MSC • Mφ2 major source of TGF-β1 in colon	(Wang et al., 2014)
Mouse (DSS)	Syngeneic	BM-MSCs	i.p. injection	• ↓Disease activity ↓histopathology ↑Colon length • ↓IL-1β ↓IL-12 ↓IL-6 in serum • ↓IL-1β ↓IL-12 ↓TNF-α ↑GAL3 secretion in supernatants of DSS activated DCs *in vitro* transwell culture with MSCs • ↓IL-6 ↓TNF-α ↓CD86, ↓CD80, ↓MHC II expressing activated DCs *in vitro* transwell culture with MSCs • ↑GAL3 in serum • Adoptive transfer of DSS+MSC primed DCs ↓Disease activity ↓Histopathology of DSS-induced colitis compared to DSS-primed DCs	(Nikolic et al., 2018)
Mouse (DSS)	Syngeneic	Compact-bone MSCs	i.p. Injection	• ↓*Ifng* ↓*Tnf* ↓*Il6* ↑*Il10* ↑*tgfb* mRNA of naïve and LPS stimulated DCs in co culture *in vitro* • MSC primed DCs ↑FOXP3 in splenocytes *in vitro* • MSCs and MSC primed DCs ↓ histological severity ↑colon length • ↓Phosphorylated STAT3 ↑IL-10 ↑TGFβ after MSC or MSC primed DCs • ↑FOXP3^{+} cells after MSC or MSC primed DCs	(Jo et al., 2018)

Mouse (DSS)	Xenogeneic	Amniotic fluid MSCs conditioned medium (human)	i.p. injection	• ↓Histopathology • ↓*Tnf* ↓*Il1b* ↑*Il10* mRNA • ↓TNF-α ↓MMP2 ↑TGF-β1	(Legaki et al., 2016)
Mouse (DSS)	Xenogeneic	AT-MSCs Conditioned medium (human)	Enema	• Application of conditioned medium from MSCs derived from CD patients and uninflamed controls by enema • ↓Disease activity ↓histopathology only in CD MSC-CM • ↓*Il1b* ↓*Il6* ↓*Ccl2* mRNA colon only in CD MSC-CM • ↑Ki67^{+} cells in epithelium only in CD MSC-CM • Changes in cell growth and proliferation associated genes between CD and control MSCs detected by RNA-Seq • ↑*Il17a* ↑*Ccl23* ↑*Vegfa* mRNA, ↑Akt ↑GSK3B ↑P65 protein ↑Proliferation in epithelial cells *in vitro* with CD MSC-CM • ↑Lactoferrin (LTF) in CD-MSCs. Administration of LTF ↓Disease activity, ↑Colon length and ↑Ki67^{+} cells in epithelium.	(Hoffman et al., 2018)
Mouse (DSS)	Xenogeneic	AT-MSCs (canine)	i.p. injection	• MSCs detected in heart, lung, liver, spleen, kidney, and colon after 2h. No MSCs observed in the colon after 1d • ↓Disease activity ↓histopathology ↑Colon length • ↓TNF-α ↓IL-6 ↑IL-10 • ↓Cellular apoptosis • ↓iNOS ↓IL-6 ↑IL-10 ↑CD206 in PBMC-derived macrophages in transwell co-culture *in vitro* • ↓F4/80^{+} ↑CD206^{+} cells *in vivo* • ↓ *Nos2* (iNOS) ↑ *Mrc1* (CD206) ↑*Arg1* ↑*Fizz1* ↑*Ym1* mRNA *in vivo* • *Tnfaip6* (TSG6) siRNA KD MSCs had no effect on all parameters	(Song et al., 2018)
Mouse (DSS)	Xenogeneic	AT-MSCs (human)	Enema	• MSCs derived from CD patients • CD MSCs ↓disease activity ↓histological severity and ↓ weight loss • Effect of CD MSCs was increased by co-treatment with human umbilical cord blood-derived platelet lysate	(Forte et al., 2015)

				(CBPL) which had no effect on its own. • ↓IL-6 ↓TNF-α ↓IL-10 ↓IFN-γ in serum after CD MSC • ↓IL-6 ↓TNF-α ↓ IL-10 ↓IFN-γ ↓IL-1β ↓IL-17 in serum after CD MSC + CBPL • CD MSCs engrafted into colon ↑Engraftment with CBPL	
Mouse (DSS)	Xenogeneic Allogeneic Syngeneic	AT-MSCs (Human) AT-MSCs (mouse) AT-MSCs (mouse)	i.p. injection	• ↓Disease activity ↓histopathology • ↓Neutrophil infiltration in the colon • ↓Pro-inflammatory cytokines in the colon • ↓Pro-inflammatory cytokine production of mononuclear cells *in vitro* • MSC and monocytes or dendritic cell co-cultures progressively reduced T lymphocyte proliferation and IFN-γ secretion suggesting APCs may have a significant role in further suppressing pro-inflammatory T lymphocytes • IL-10 blockade partially reversed this effect • ↓Production of IFN-γ, ↑ IL-10 and no effect on IL-4 in *in vitro* stimulated MLNs • ↑Treg in *in vitro* MLN • Implantation of T lymphocytes isolated after MSC treatment ameliorated colitis mediated by Tregs • Abolishment of IL-10 and Tregs *in vivo* negated therapeutic effect of MSCs	(Gonzalez-Rey et al., 2009)
Mouse (DSS)	Xenogeneic	AT-MSCs (human)	i.p. injection	• ↓Disease activity ↓histopathology ↑Colon length • ↓TNF-α ↓IL-1β, ↓IFN-γ ↓IL-17 ↑IL-10 • ↑*Mrc1* (CD206) ↑*Arg1* ↑*Fizz1* ↑*Ym1* mRNA Mφ2 markers • ↓CD11b ↑CD206 Mφ2 polarisation • MSCs detected in heart, lung, liver, spleen, and kidney. Very low engraftment into the colon • TNF-α caused ↑TSG6 in MSCs *in vitro* • MSCs ↑Mφ2 polarisation in Mφ cell line in paracrine manner *in vitro.*	(Song et al., 2017c)

				Effects ↑ with TNF-α pre-treated MSCs • TSG6 siRNA KD in MSCs block Mφ2 polarisation *in vitro* • TSG6 siRNA KD in MSCs had no effect on disease activity, histopathology and colon length or Mφ2 polarisation	
Mouse (DSS)	Xenogeneic	AT-MSCs (human) AT-MSCs (canine) protein scaffold	i.v. injection i.p. injection	• MSCs implanted with CellSaics recombinant protein scaffold. • ↑Colon length ↓histopathology only with human MSCs on scaffold only • ↑Colon length with canine MSC on scaffold only	(Iwazawa et al., 2018)
Mouse (DSS)	Xenogeneic	Gingiva derived MSCs (human) BM-MSCs (human)	i.p. injection	• ↓Disease activity ↓histopathology • Suppress $CD4^+$ T lymphocyte infiltration • ↑FOXP3 expression • ↓Pro-inflammatory cytokines in colon • ↑Anti-inflammatory cytokines in colon	(Zhang et al., 2009b)
Mouse (DSS)	Xenogeneic	Tonsil derived MSCs (human)	i.p. injection	• ↓Disease activity ↓histopathology • ↓IL-1β ↓IL-6 • MSCs detected in colon	(Song et al., 2017a)
Mouse (DSS)	Xenogeneic	UC-MSC extracts (human)	i.p. injection	• ↓Disease activity ↓histopathology ↑Colon length • ↓MPO • ↓IL-17A ↑IL-10 ↑TGFβ1	(Song et al., 2017b)
Mouse (DSS)	Xenogeneic	UC-MSCs (human)	i.v. injection	• Study performed in NOD.CB17-Prkdc (SCID)/J – T and B lymphocyte deficient mice • ↓Disease activity ↓histopathology ↑Colon length • MSCs observed in lamina propria • ↓MPO activity • N.D to ↓catalase activity in serum • ↓MMP2 and 9 activities • ↓ER stress UPR pathway (↓BIP, ↓PDI)	(Banerjee et al., 2015)
Mouse (DSS)	Xenogeneic	UC-MSCs (human)	i.p. injection	• TLR-3 or TLR-4 primed MSCs • ↓Disease activity ↓histopathology ↑Colon length in TLR-3 primed MSCs • ↓Histopathology only in naïve MSCs	(Fuenzalida et al., 2016)

				• N.D. or worse outcomes with TLR-4 primed MSCs	
Mouse (DSS)	Xenogeneic	UC-MSCs (human)	i.p. injection	• Co-treatment of MSC and a micro-particle that activated NOD2 and TLR-9 signalling (MIS416) enhance the migration and therapeutic efficacy of MSCs	(Lee et al., 2018)
Mouse (DSS)	Xenogeneic	UC-MSCs (human) BM-MSCs (human)	i.p. injection	• UC-MSCs ameliorated DSS-induced colitis • UC-MSCs modulated Treg/T_h17 cells in the spleen and mesenteric lymph nodes • UC-MSCs inhibited LPMCs *in vitro*	(Li et al., 2013b)
Mouse (DSS)	Xenogeneic	UC-MSCs (human)	i.v. injection	• MSCs detected in colon • ↓Disease activity ↓histopathology ↑Colon length • ↓MPO • ↓IL-1β ↓TNF-α ↓IL-6 ↓IFN-γ	(Lin et al., 2015)
Mouse (DSS)	Xenogeneic	UC-MSCs (human)	i.v. injection	• MSC-derived exosomes detected in colon, spleen and liver • ↓weight loss ↓spleen size with MSCs and exosomes • ↓*Tnf* ↓*Il1b* ↓*Il6* ↑*Il10* mRNA in colon and spleen with exosomes • ↓IL-7 protein in colon and spleen with exosomes • ↓*Tnf* ↓*Il1b* ↓*Il6* ↑*Il10* ↓IL-7 in macrophages treated with exosomes *in vitro*	(Mao et al., 2017a)
Mouse (DSS)	Xenogeneic	UC-MSCs (human)	i.v. injection	• MSCs migrated and engrafted into colons and spleens • ↓*Tnf* ↓*Il1b* ↓*Cxcl10* (IP-10) ↓*Il6* ↑*Il10* mRNA in colon and spleen • ↓phosphorylated STAT3 ↓15-LOX-1 in colon and spleen • ↓phosphorylated STAT3 ↓15-LOX-1 protein ↓*Tnf* ↓*Il1b* ↓*Cxcl10* (IP-10) ↓*Il6* ↑*Il10* mRNA in macrophages co cultured with MSC *in vitro*	(Mao et al., 2017b)
Mouse (TNBS and DSS)	Syngeneic xenogeneic	AT-MSCs (mouse) AT-MSCs (human)	i.p. injection	• Mouse MSCs ↓disease activity ↓Histopathology • Human MSC co-cultured with Mφ ↑Mφ2 • Human MSC induced Mφ2 ↑TGF-β1, ↑IL-10 and ↓IL-12	(Anderson et al., 2013b)

				• Human MSC stimulated macrophages ↓splenocyte proliferation *in vitro* • Effect was diminished in IL-10 knockouts • Human MSC stimulated Mφ ↓Disease activity ↓histopathology	
Mouse (TNBS and DSS)	Xenogeneic Syngeneic	BM-MSCs (human) BM-MSCs (mouse)	i.p. injection	• IFN-γ stimulated MSCs • ↓Disease activity • ↓Histopathology	(Duijveste in et al., 2011)
Mouse (TNBS and DSS)	Xenogeneic	Cord-blood derived MSCs (human)	i.p. injection	• CB-MSCs reduced colitis severity • Higher anti-inflammatory properties in NOD2 stimulated CB-MSCs	(Kim et al., 2013a)
Mouse (TNBS)	Allogeneic	BM-MSCs	i.v. injection	• Green fluorescent protein labelled MSCs homed to the inflamed colon • ↓Disease activity ↓histopathology • ↓Colonic expression of T_h1 and T_h17 related cytokines. • ↓Colonic expression of T_h1 and T_h17 markers *Tbx21* (T-bet) and *Rorc* (RORγt) • ↑Colonic expression of T_h2 and Treg related cytokines. • ↑ Colonic expression of T_h2 and Treg marker *Gata3* and *Foxp3* • ↑Proliferation of intestinal epithelial cells • ↑Differentiation of intestinal stem cells	(Chen et al., 2013)
Mouse (TNBS)	Syngeneic	BM-MSCs	i.p. injection	• MGP KD by shRNA in MSC • ↓Proliferation of $CD3^+$, $CD4^+$ and $CD8^+$ T lymphocytes in *in vitro* co-culture; partial role of MGP • ↓TNF-α and IFN-γ in $CD4^+$ and $CD8^+$ T lymphocytes in *in vitro* co-culture; MGP required for inhibiting TNF-α • ↓Disease activity ↓histopathology ↑colon length; MGP KD ↓ effect on disease activity, Required for ↓histopathology and ↑colon length. • ↓Number of $CD3^+$, $CD4^+$ and $CD8^+$ T lymphocytes in colon; MGP required • MGP required for ↓*Tnf* ↓*Ifng* ↓*Il1b* ↓*Il6* ↓*Il17* and ↑*Il10* mRNA in colon	(Feng et al., 2018)

				• ↓Number of $CD3^+$, $CD4^+$ and $CD8^+$ T lymphocytes in intraperitoneal lavage; MGP required for $CD4^+$, $CD8^+$ and partially for $CD3^+$ T lymphocytes • MGP required for ↓*Tnf* ↓*Il1b* ↓*Il6* ↓*Il17* and ↑*Il10*, N.D. in *Ifng* mRNA in intraperitoneal lavage • Note: not all MSC cell lines have high expression of MGP	
Mouse (TNBS)	Syngeneic	BM-MSCs	i.v. injection	• *Cxcr4* overexpression in MSCs • MSCs with and without ↑CXCR4 ↓Disease severity • ↑CXCR4 ↑Homing to the colon	(Chen et al., 2018b)
Mouse (TNBS)	Xenogeneic Allogeneic Syngeneic	AT-MSCs (human) AT-MSCs (mouse) AT-MSCs (mouse)	i.v. injection	• ↓Clinical and histopathology of colitis • ↓Pro-inflammatory cytokines ↑IL-10 in the colon • ↓TNF-α in LPMCs isolated from MSC treated mice • Co-cultures of MSCs or conditioned media with colitic macrophages significantly ↓TNF-α and IL-12 production • *In vitro* mesenteric lymph nodes co-cultured with MSCs or conditioned media ↓IL-2/IFN-γ and ↑IL-10 secreting T lymphocytes • ↑Treg in MLN of MSC treated colitic mice • Isolated T lymphocytes from MSC treated mice ameliorate experimental colitis	(González et al., 2009)
Mouse (TNBS)	Xenogeneic	AT-MSCs (human)	Intranodal (intralymphatic) Injection	• MSCs injected into inguinal lymph nodes • ↓Weight loss in over half of mice	(Lopez-Santalla et al., 2017)
Mouse (TNBS)	Xenogeneic	AT-MSCs (human)	i.p. injection	• ↓Disease activity • MSCs detected predominantly in liver, spleen and intestine. Lower numbers detected in lung, heart, blood and various lymph nodes. • Mice that responded to treatment had better migration of MSCs to intestine.	(Lopez-Santalla et al., 2018)
Mouse (TNBS)	Xenogeneic	UC-MSCs (human)	i.p. injection	• ↓Disease activity ↓histopathology ↑Colon length • ↓ MPO activity • MSC detected in abdomens until at least day 5	(Chao et al., 2016)

				• ↑Tregs, ↓Th1 and ↓Th17 in spleen and MLN • ↓TNF-α ↓IL-12 ↓IL-6 ↓IL-23 and ↓IL-21, N.D. IL-17A ↑IL-10 ↑TGFβ1 • ↑$CD5^+$ B-cell in spleen and MLN • MSCs ↑ $CD5^+$ B lymphocytes in splenic lymphocytes *in vitro* • Adoptive transfer of B lymphocytes ↓colitis • B lymphocytes ↓T lymphocytes differentiation *in vitro*	
Mouse (TNBS)	Xenogeneic	UC-MSCs (human)	i.p. injection	• Enhanced effects after TLR-3 stimulation	(Qiu et al., 2016)
Mouse (TNBS)	Xenogeneic	UC-MSCs (human)	i.v. injection	• ↓Disease activity ↓histopathology • ↓Neutrophil infiltration in the colon • ↓Pro-inflammatory cytokines in the colon • ↓ Th17 marker RORγt in the colon • Transwell MSC co-culture with LPMCs ↓IFN-γ and ↓IL-17 suggesting immune suppression of T_h1 and T_h17 in paracrine fashion	(Liang et al., 2011)
Rat (acetic acid)	Allogeneic	BM-MSCs	i.v. injection	• ↓ Histopathology of colitis • ↑Mucin secreting cells	(Fawzy et al., 2013)
Rat (DNBS and electrocoagulation ulcer)	Allogeneic	BM-MSC AT-MSC	Local (Endoscopic transplant)	• Transplanted MSC sheets • ↓ Ulcer size AT-MSC>BM-MSC • Both MSCs improved endoscopic scores	(Pak et al., 2018)
Rat (DSS and DSS +BM hypoplasia)	Allogeneic	BM-MSCs	i.v. injection	• Poor MSC migration to colon in DSS colitis • No therapeutic effect in DSS colitis • ↑Tight junction proteins, claudin 2, 12 and 15 in DSS bone marrow hypoplasia model	(Yabana et al., 2009)
Rat (DSS)	Allogeneic	BM-MSCs	i.v. injection	• IL-25 primed MSCs • ↓Disease activity ↓histopathology ↑colon length (Il-25 and wildtype) • Enhanced efficacy in IL-25 primed MSCs compared to wildtype • $CD4^+$ cells: ↓IFN-γ^+ ↑$IL\text{-}4^+$ ↓$IL\text{-}17A^+$ ↑$FOXP3^+$ (IL-25 > wildtype MSCs for T_h17/Treg axis)	(Cheng et al., 2017)

				• ↑Ki67^{+} and LGR5^{+} cells in basal crypts in MSCs (IL-25 and wildtype)	
Rat (DSS)	Syngeneic	BM-MSCs	i.v. injection	• ↓Disease activity ↓histopathology • ↓Pro-inflammatory cytokines and trophic factors in the colon • MSC co-cultured monocytes activated by LPS ↓monocytic TNF-α secretion • MSCs localised to inflamed tissue, predominantly the lamina propria and crypts	(Tanaka et al., 2008)
Rat (DSS)	Syngeneic	BM-MSCs	i.v. injection	• Dose-dependent therapeutic effect on body weight • Reduced epithelial injury • Attenuated loss of mucin secreting cells • Myogenic lineage differentiation of MSCs *in vivo*	(Tanaka et al., 2011)
Rat (DSS)	Xenogeneic	Amnion derived MSCs (human)	i.v. injection	• ↓ Weight loss, colon shortening and DAI • ↓ TNF-α, IL-1β and MIF in colon ↓MCP1 serum • ↓ Histopathology • ↓ Mφ1 ↓Mφ2 N.D. CD3^{+} T lymphocytes • MSC or CM ↓TNF-α ↓ MCP1 in macrophages *in vitro* • MSC-CM ↓NF-kB translocation *in vitro*	(Onishi et al., 2015)
Rat (TNBS)	Allogeneic	AT-MSCs BM-MSCs	i.p. injection i.v. injection	• Intravenously administered MSCs did not migrate to the colon • Intraperitoneally administered MSCs migrated to areas of colonic inflammation (submucosa and muscular layer) • AT-MSCs and BM-MSCs ↓Endoscopic score ↓histopathology ↓Collagen deposition ↓epithelial apoptosis	(Castelo-Branco et al., 2012)
Rat (TNBS)	Allogeneic	AT-MSCs	i.v. injection	• ↓MPO ↓MDA ↓NO *in vivo* • ↑miR-1236 ↓RORγ *in vivo* • miR-1236 mimetic ↓*RORc* expression in HT29 cells *in vitro* and ↓MPO ↓MDA ↓NO induced by TNF-α	(Zhang et al., 2015)
Rat (TNBS)	Allogeneic	AT-MSCs	Local (rectal wall injection)	• Engraftment of MSCs in mucosa and submucosa • ↓Disease activity	(de la Portilla et al., 2018)

Rat (TNBS)	Allogeneic	AT-MSCs	Mesenteric injection	• ↓Disease activity ↓histopathology ↑Colon length ↓Colon weight • ↓MPO • ↑TSG6 ↓TNF-α ↓IL-1β serum ↓IL-17A ↑IL-10 protein and ↓*Il6* ↑*Tgfβ* mRNA	(Fu et al., 2018)
Rat (TNBS)	Allogeneic	BM-MSC extracellular vesicles	i.v. injection	• EV detected in colon after 12h • ↓Histopathology ↓disease activity ↑Colon length • ↓NF-κBp65 (RELA) ↓iNOS ↓TNF-α ↓COX2 ↓IL-1β ↑IL-10 • ↓MPO ↓MDA ↑GSH ↑SOD • ↓c-caspase 3 ↓caspase 8 ↓caspase 9	(Yang et al., 2015)
Rat (TNBS)	Allogeneic	BM-MSCs CXCR4-MSCs	i.v. injection	• MSC over-expressing *Cxcr4* ameliorated colitis	(Liu et al., 2013)
Rat (TNBS)	Allogeneic	BM-MSCs BM-MSCs CXCR4-IL35-MSCs	i.v. injection	• *Cxcr4* and *Il35* overexpressing MSCs • ↓Disease activity ↓histopathology ↑Colon length. • ↑Tregs ↓T_h17 in MLNs and spleen • ↑IL-10 ↓IL-17 ↑FOXP3 ↓RORyt in colon • All effects enhanced by CXCR4-IL35-MSCs	(Nan et al., 2018)
Rat (TNBS)	Allogeneic	BM-MSCs	i.v. injection	• Co-treatment of MSC with granulocyte colony-stimulating factor (MSC/GCSF) via subcutaneous injection • ↓Disease activity only with MSC/GCSF • N.D. for all on histopathology	(Tang et al., 2015b)
Rat (TNBS)	Allogeneic	BM-MSCs	i.v. injection	• ↓Disease activity ↓histopathology • MSCs detected in colon • ↓TNF-α in serum • ↓Nuclear NF-κBp65 in mucosa • ↓*Tnf* ↓*Rela* (NF-kbp65) mRNA	(Zuo et al., 2015)
Rat (TNBS)	Allogeneic	BM-MSCs	Local (Submucosa injection)	• ↓Disease activity ↓histopathology • ↓In lesion size • Intravenously injected MSCs accumulated in lungs • Unexpanded bone marrow cells did not ameliorate colitis	(Hayashi et al., 2008)

				• MSCs differentiate into interstitial cells, fibroblast and myofibroblast *in vivo* • MSCs expressed VEGF and TGF-β1 *in vivo* through immunostaining	
Rat (TNBS)	Syngeneic	AT-MSCs	Local (Submucosa injection)	• ↓ Histopathology of colitis • MSCs secrete trophic factors *in vitro* • ↑Proliferation of colonic epithelium • ↓Neutrophil infiltration in the colon • MSCs selectively localised to inflamed ulcerated areas • Repaired colonic ulcers	(Ando et al., 2008)
Rat (TNBS)	Xenogeneic	Amnion derived MSC Conditioned medium gel (human)	i.v. injection Enema	• ↓Endoscopic damage • ↓Neutrophil ↓Monocyte/ Mφ • ↓T lymphocytes by MSC-CM enema only	(Miyamoto et al., 2017)
Rat (TNBS)	Xenogeneic	AT-MSCs (human)	Local (Endoscopic injection)	• Injection into submucosa confirmed by anti-human IHC • ↑Weight recovery • ↓Endoscopic damage score ↓Stenosis • ↑Colon length N.D. histopathology • ↑*Foxp3,* N.D. *Il10* mRNA	(Martin Arranz et al., 2018)
Rat and mouse (TNBS and DSS)	Syngeneic Xenogeneic	BM-MSC conditioned medium (rat)	Enema	• Treatment with MSC supernatant/conditioned media • Enema, i.p. and i.v. injections • ↓Disease activity ↓histopathology • ↓Epithelial injury • ↓TNF-α, IL6 ↑IL10 in RAW 264.7 macrophages *in vitro* • ↑Mφ2 polarisation *in vitro*	(Watanabe et al., 2013)

APC, antigen presenting cell; ARG, arginase; AT, adipose tissue; BIP, binding immunoglobulin protein; BM, bone marrow; CB, cord blood; CBPL, cord blood-derived platelet lysate; CCL, CC chemokine ligands; CD, Crohn's disease; CGRP, calcitonin gene-related peptide; ChAT, choline acetyltransferase; CM, conditioned medium ; DC, dendritic cell; DSS, dextran sodium sulphate; ER, endoplasmic reticulum; EV, extracellular vesicle ; FOXP3, forkhead box P3; GAL3, Galectin-3; GPx, glutathione peroxidase; GSH, glutathione; HO, haem oxygenase ; i.p., intraperitoneal; i.v., intravenous; IFN, interferon; IL, interleukin; IP-10, interferon-γ-inducible protein 10; iPSC, induced-pluripotent stem cell; KD, knock down; LGR5, leucine-rich repeat-containing G-protein coupled receptor 5 ; LOX,

lipoxygenase; LPMC, lamina propria mononuclear cells; LPS, lipopolysaccharide; LTF, lactoferrin; MCP1, monocyte chemoattractant protein 1; MDA, malondialdehyde; MGP, matrix Gla protein; MHC, major histocompatibility complex; MIF, macrophage migration inhibitory factor; MLN, mesenteric lymph nodes; MMP, matrix metalloproteinase; MPO, myeloperoxidase; Mφ, macrophage; N.D., no difference; NFκB, nuclear factor-κB; NKT, natural killer T lymphocyte; nNOS, neuronal nitric oxide synthase; NOD2, nucleotide-binding oligomerization domain-containing protein 2; PDI, protein disulphide isomerase; PTEN, phosphatase and tensin homolog; RORγt, RAR-related orphan receptor gamma; SAA, serum amyloid A; SCID, severe combined immune deficiency; shRNA, short-hairpin RNA; SOD, superoxide dismutase; STAT, signal transducer and activator of transcription; TGF, transforming growth factor; Th, tyrosine hydroxylase; TLR, toll-like receptors; TNBS, 2,4,6-trinitrobenzenesulfonic acid; TNF, tumour necrosis factor; Treg, regulatory CD4+ T lymphocyte; TSG6, tumour necrosis factor-inducible gene 6 protein; TSP1, thrombospondin 1; UC, umbilical cord; UPR, unfolded protein response; VAChT, vesicular acetylcholine transporter; VCAM, vascular cell adhesion protein; ZO-1, zonula occludens

1.2.3. MSC heterogeneity: tissue sources

Although MSCs are universally capable of trilineage differentiation, adherence to plastic and the expression of specific surface markers, the isolation of MSCs from various tissue sources yields cells with heterogeneous characteristics. In clinical trials for the treatment of IBD, MSCs have been derived from adipose tissue (AT-MSC), bone marrow (BM-MSC) and the umbilical cord (**Figure 1.1C, Table 1.1**). MSCs derived from these sources have also been utilised in experimental colitis, in addition to cells derived from compact-bone, cord blood, amnion, gingiva and the tonsils (**Figure 1.1C, Table 1.2**). In experimental colitis, MSCs have also been derived from induced-pluripotent stem cells (iPSC) (Soontararak et al., 2018). In IBD, the two most studied adult sources of MSCs are bone marrow and adipose tissue. Clinical trials for the treatment of CD-related fistulae predominantly use AT-MSCs; whereas, BM-MSCs take precedence to treat luminal inflammation (**Table 1.2**). Administration of either AT or BM-MSCs produce favourable results in experimental colitis. However, most studies have utilised BM-MSCs which reflects the pattern of clinical studies in the inflammatory luminal pathology of IBD, rather than the fistulising disease, which is not accurately modelled by experimental colitis. Nevertheless, AT-MSCs remain an attractive option for several reasons. Lipoaspirate is a waste product of routine orthopaedic and cosmetic medical procedures and thus, is readily available for allogeneic or xenogeneic administration in humans and experimental models, respectively. Moreover, lipo-aspiration may be perceived as a less invasive procedure by patients. Compared to the bone marrow, MSCs are more easily obtained from lipoaspirate and the yield of AT-MSCs could be up to 500 fold higher than BM-MSCs (Aust et al., 2004, Li et al., 2011, Strioga et al., 2012).

Ideally, MSCs exhibit a high proliferative capacity, colony forming potential and spindle-shaped morphology. Replicative senescence and prolonged culture results in the loss of these traits and maintaining them is a key focus of the field (Neuhuber et al., 2008, Schellenberg et al., 2011, Ayatollahi et al., 2012, Yang et al., 2018).

Several studies have reported that MSCs derived from adipose tissue are optimal over those derived from the bone marrow for these qualities (Kern et al., 2006, Sung et al., 2008, Ikegame et al., 2011, Dmitrieva et al., 2012, Zhu et al., 2012, Stavely et al., 2015a, Stavely et al., 2015b). Additionally, it should be considered that these characteristics are negatively affected by the age of the donor and the period of expansion (Choudhery et al., 2014, Yang et al., 2018). Nevertheless, studies controlling for age and expansion conditions have demonstrated that AT-MSCs have much faster growth kinetics than BM-MSCs in mice and guinea-pigs (Ikegame et al., 2011, Stavely et al., 2015a). Based on their proliferative potential, AT-MSCs appear to be a more suitable source than BM-MSCs; however, this is dependent on the premise that MSCs from various sources are equally efficacious in the treatment of intestinal inflammation.

Heterogeneous gene expression profiles are observed in MSCs derived from bone marrow and adipose tissue (Lee et al., 2004, Wagner et al., 2005). Likewise, the constituents of the MSC secretome and their expression of chemokine receptors is altered depending on the tissue source of derivation (Yoo et al., 2009, Ikegame et al., 2011, Balasubramanian et al., 2012). Variances in *in vitro* characteristics are evident. However, these differences could also affect their therapeutic efficacy *in vivo*. Albeit, studies comparing the value of MSCs from different tissue sources are lacking, especially in clinical trials. In a rat model of 2,4,6-trinitrobenzenesulfonic acid (TNBS)-induced colitis, both allogeneic AT and BM-MSCs administered intraperitoneally reduced endoscopic and histopathologic scores, despite AT-MSCs appearing to have a greater migratory range (Castelo-Branco et al., 2012). Nonetheless, in a similar model of colitis in guinea-pigs, allogeneic BM-MSCs administered intra-luminally appeared to be more effective than AT-MSCs at attenuating weight loss and leukocyte infiltration in the mucosa and near the myenteric neurons embedded between the muscle layers (Stavely et al., 2015a). In other inflammatory models, better outcomes have been reported using allogeneic BM-MSCs for treating experimental lung inflammation in mice (Antunes et al., 2014a, Antunes et al., 2014b). Likewise, xenogeneic human BM-MSCs were more efficacious in attenuating leukocyte recruitment to multiple organs affected by

experimental systemic inflammation (Elman et al., 2014). Conversely, the enhanced migratory potential of AT-MSCs has led to better outcomes in experimental autoimmune encephalomyelitis (Payne et al., 2013a). Together, these studies unequivocally demonstrate that the origin of MSCs can affect their efficacy. Furthermore, these effects may be disease specific and provide an avenue to optimise MSC therapies for various pathologies including IBD.

1.2.4. Efficacy of MSCs in IBD

Clinical trials have evaluated the efficacy and safety of MSC therapies using a variety of dosages and cell sources for UC, as well as the fistulising and inflammatory luminal pathologies of CD (**Table 1.1**). Clinical responses or remission have been achieved in refractory patients, this was predominantly defined as a 100-point reduction in the CD activity index (CDAI) and a CDAI score of lower than 150 points, respectively. Thus far, investigations into the treatment of fistulising CD have progressed more rapidly than other pathologies. In these studies, direct injection of autologous MSCs derived from bone marrow and adipose tissue into rectovaginal, enterocutaneous and complex perianal fistulae has promoted re-epithelialisation and remission in many subjects. MSC treatments have also been effective in conjunction with fibrin glue to seal the fistulae, however the therapeutic effects appeared to be predominantly mediated by MSCs, at least in short-term studies (Garcia-Olmo et al., 2009b, Garcia-Olmo et al., 2010). Furthermore, this affect appears to be characteristic of expanded AT-MSCs as the primary stromal vascular fraction of lipo-aspirate is comparatively ineffective (Garcia-Olmo et al., 2009b). While MSC treatments have demonstrated an ability to heal fistulae, the maintenance of remission in complex fistulae is not observed in all patients; therefore, the long-term effects of MSC treatments are crucial to determine efficacy. The enduring effects of autologous MSC treatments may also be promoted by fibrin glue with co-treated patients maintaining closure after 1 year, albeit in a small cohort (Garcia-Olmo et al., 2015). In a retrospective follow up of

a phase 2 trial, approximately 4 years after the procedure, 1 of the 2 participating patients with closure of CD-related fistula treated with AT-MSC and fibrin glue had relapsed while the other maintained closure (Guadalajara et al., 2012). In studies by another group, sustained closure of fistulae has been achieved in 88-100% of subjects 8-12 months post-therapy with autologous AT-MSCs and fibrin glue (Cho et al., 2013, Lee et al., 2013). In a retrospective analysis, closure of the fistulae was observed in 21/26 subjects; furthermore, approximately 83% of subjects maintained closure of the fistulae from initial healing at 8 weeks post-treatment (Cho et al., 2015). Therapy with BM-MSCs has also been effective for the treatment of CD-related fistulae. In perianal fistulae, complete or incomplete fistula healing was achieved in 7 and 3 out of 10 subjects, respectively, after injection of BM-MSCs into the fistulous tract wall and lumen (Ciccocioppo et al., 2011). Moreover, long-term effects in BM-MSC-treated subjects are also reported with clinical remission achieved in all subjects, 12 months post-treatment, as observed by a decline in CDAI and perianal activity index scores (Ciccocioppo et al., 2011).

Previously, bacterial contamination during expansion has delayed or prevented autologous MSC treatment (García-Olmo et al., 2005, 2010). Furthermore, it is currently unknown whether the MSCs isolated from IBD patients are as functionally competent as those from healthy donors; this remains an important unresolved question given the preference towards autologous therapies by regulatory bodies such as the Food and Drug Administration (FDA) and Therapeutic Goods Administration (TGA). Pre-prepared sources of allogeneic MSCs can be used to avoid unforeseen complication during isolation and *in vitro* expansion. Allogeneic AT-MSCs were demonstrated to heal complex perianal fistula at 24 weeks in 56% of subjects (de la Portilla et al., 2013). Specifically, in CD-related rectovaginal fistulae, closure has been observed in 9/10 patients treated with AT-MSCs at some stage throughout the study, however this was only maintained in 60% after 1 year (Garcia-Arranz et al., 2016). These studies may indicate that allogeneic AT-MSCs are less effective than autologous AT-MSCs; however, fibrin glue was not used which appears to have an additive effect to the efficacy of MSC treatments. Nonetheless, complete closure after allogeneic BM-

MSC injection into the fistulous tract wall has been observed in 80% of subjects treated with $1x10^7$ or $3x10^7$ cells, as opposed to, 33% from the placebo group, which demonstrates the efficacy of allogeneic MSCs (Molendijk et al., 2015). Arguably the greatest evidence for the incorporation of allogeneic MSCs into the clinic for fistulising CD comes from a phase III trial. In this study, expanded allogeneic AT-MSCs (Cx601) yielded a similar efficacy to the corresponding phase I/IIa trial with remission of treatment-refractory complex perianal fistulae achieved in approximately 50% of subjects (Panes et al., 2016). However, this study further demonstrated that the use of allogeneic AT-MSCs was better than placebo and could be used in combination with immunomodulators and anti-TNF-α biologics to improve outcomes. Therefore, local allogeneic MSC administration does not interfere with current treatment regimens and can have a beneficial effect by reducing the need for surgery or systemic immunosuppression. Together, these studies demonstrate that allogeneic MSC treatments are a useful tool to promote fistulae closure and can induce remission in CD patients with a fistulising pathology; nonetheless, considering the generally high incidences of relapse of CD-related fistulae, future studies should investigate the efficacy of repeat treatments. Evidence from various trials have demonstrated differing efficacy which could be dependent on multiple factors that require optimisation.

To improve patient outcomes and the efficacy of MSC treatments, several simple elements of therapy can be addressed. Further studies should determine the optimal tissue source of MSC and compare the effects of autologous and allogeneic administration in a controlled manner. Ideal dosages should also be further investigated. Using autologous AT-MSCs, healing of the fistula appeared to occur in a dose-dependent manner in a range of $3x10^7$ to $40x10^7$ total cells depending on the size of the fistula (Cho et al., 2013). Conversely, in CD-related perianal fistulae, allogeneic BM-MSCs appeared to be significantly more therapeutic at lower doses of $1\text{-}3x10^7$ compared to the highest dose of $9x10^7$ which suggest that injecting too many cells can reduce efficacy (Molendijk et al., 2015). These results could be explained by several variables including the source of MSC and type of fistula treated. Additionally, the use of MSCs as a combination therapy with current

treatments also needs to be elaborated. Remission achieved by allogeneic AT-MSCs was increased in combination with anti-TNF/immunomodulators, TNF alone or neither; but not immunomodulators on their own (Panes et al., 2016). Understanding these caveats is crucial to improving patient outcomes. Furthermore, novel application methods and technologies to improve efficacy should be sought. Recently, a phase 1 trial demonstrated that local administration of autologous AT-MSCs with a bio-absorbable matrix plug could promote the closure of CD-related perianal fistulae in 83% of subjects after 6 months (Dietz et al., 2017). This demonstrates that further progress can be made with advancements in technology in the application of MSCs which remains relatively unexplored in the clinic.

The development of MSC therapies to treat UC and the inflammatory luminal pathology of CD requires an alternate approach to that of fistulising CD. While fistulising CD was predominantly treated by autologous AT-MSCs injected locally; these studies have principally focused on the use of allogeneic BM-MSCs infused systemically. Thus far, the limited number of clinical trials have observed positive results. Patient recruitment is usually limited to those that exhibit substantial progression of the disease and are refractory to current treatment regimens of immunosuppressants and biologics. In studies administering autologous BM-MSCs, unequivocal results have been observed with clinical responses to treatments observed in a third of subjects, while another third underwent surgery due to advancement of the disease (Duijvestein et al., 2010). Albeit, the refractory nature of the disease in these subjects suggest that surgical intervention was a consequence of the inefficacy of MSC treatments, as opposed to MSCs contributing directly to the severity of disease. Moreover, in a study addressing dose-responses of autologous BM-MSCs in small cohorts, a clinical response in CDAI was observed at 2 weeks post-treatment in 50% ($2x10^6$ cells/kg), 25% ($5x10^6$ cells/kg) and 50% ($10x10^6$ cells/kg) of subjects which demonstrated a clear benefit of autologous BM-MSC treatments in some patients; although the effect of dosages on efficacy were unclear (Dhere et al., 2016). No biologics or immunomodulators were permitted in the study. In fistulising CD, MSC treatments appear to have an additive effect to these compounds. However, this may have interfered with the main objective of the

study which was to establish the safety of MSC therapy. Notably, 2 subjects that did not proceed with concomitant therapies in a recent phase 1-2 trial exhibited worsening of the disease; therefore, the concept of utilising MSC treatments as an adjunct treatment should be considered (Gregoire et al., 2018). Less favourable results were observed at 2 weeks in this study with a clinical response reported in 36% of patients (Gregoire et al., 2018). Between these two studies, a similar number of MSCs were injected, albeit these were delivered over different periods. Further considerations to explain these results include the use of allogeneic and cryopreserved MSCs in the latter study. Nevertheless, it should be noted that the majority of trials utilise cryopreserved cells thawed on the day of administration. Moreover, results from a phase 2 study achieved optimistic outcomes in Crohn's colitis and ileocolitis by administering 4 weekly doses of $2x10^6$ cells/kg cryopreserved allogeneic BM-MSCs with clinical responses observed in 80% of subjects (Forbes et al., 2014). Furthermore, half of subjects achieved clinical remission and endoscopic improvement. It should be noted however that the largest decrease in the CDAI was observed 4 weeks after the first treatment, thus it is unclear if these outcomes can be maintained for a long period. In the aforementioned phase 1-2 trial, a decrease in the CDAI activity index was observed in as many as 80% of subjects at week 8; nonetheless, this was reduced to 55.5% by week 12 (Gregoire et al., 2018). This may suggest that the effects of MSC therapy are not enduring and repeated administration is required. Nonetheless, long-term efficacy has been reported in up to 82% of subjects administered with a single slow drop infusion of $1.5\text{-}2x10^8$ allogeneic BM-MSCs at 4-8 month follow up (Lazebnik et al., 2010b). Notably, the first study demonstrating a clinical benefit for the luminal inflammatory pathology of refractory CD was performed over a decade ago (Onken et al., 2006) which utilised commercial allogeneic BM-MSCs (Prochymal®, Osiris Therapeutics). Using these cells, the largest clinical trial to date is expected to be completed in 2020 and will enrol approximately 330 participants with refractory mild-severe CD in a placebo-controlled phase 3 study (NIH identifier: NCT00482092).

Unlike the clinical trials for fistulising CD, AT-MSCs have never been used for the luminal inflammatory pathology of CD. However, allogeneic MSCs derived from the umbilical cord have been utilised in a clinical trial with administration methods similar to that of Forbes et al. (2014), albeit at half the dosage (Zhang et al., 2018). Administration of these cells decreased CDAI, demonstrated endoscopic improvement and reduced corticosteroid dosages after 12 months. Nevertheless, no patient achieved complete remission. Considering that age negatively effects the prototypical characteristics of MSCs, administering cells of early progeny, such as those derived from the umbilical cord, would logically yield better outcomes. However, in experimental models these 'ideal' MSC characteristics do not appear to translate to therapeutic efficacy in intestinal inflammation. In fact, such cells could be less effective (Stavely et al., 2015a). Nonetheless, the first clinical trial administering amnion-derived MSCs is currently underway which will be examined in the treatment of moderate luminal CD (Otagiri et al., 2018).

Fewer clinical trials have been conducted on MSC therapy in UC; however promising outcomes are observed over a long duration which are strengthened by the respectable sample sizes. Similar to studies in the luminal inflammatory pathology of CD, allogeneic MSCs are administered by intravenous infusion. In one study, treatment with a single infusion of BM-MSCs yielded decreases in the morphological indices of UC in 77% of subjects (Lazebnik et al., 2010a). Similarly, long-term remission was achieved in 79% of UC patients during a 4-8 month follow up period (Lazebnik et al., 2010b). When compared to treatments with aminosalycilic acid and glucocorticoids, or, singular infusions of BM-MSCs, 3 weekly MSC infusions resulted in a greater decrease in clinical activity and Mayo endoscopy scores after 12 months (Lazebnik et al., 2012). Moreover, the relative risk of UC after 2 years was lower after 3 weekly MSC infusions compared to the other groups. Likewise, positive outcomes have been achieved via the administration of umbilical cord derived MSCs with 83% of subjects demonstrating a clinical response after 3 months according to Mayo scores. Long-term efficacy was observed with a decline in Mayo scores and histopathology scores after 2 years (Hu et al., 2016). Results from these studies suggest a clear therapeutic benefit is

achieved in UC by the administration of allogeneic MSCs. However, larger multi-centre placebo-controlled clinical trials should be conducted to validate these findings before incorporating MSCs in current treatment regimens.

1.2.5. Safety considerations

The safety concerns and side effects caused by current IBD treatments are major barriers to achieving therapeutic outcomes (**Chapter 1, Section 1.1.1**); therefore, evaluating the tolerance to MSC therapy in IBD patients is critical. In all clinical trials to date, limited serious adverse events have been reported that were attributed to MSC therapies in IBD. Adverse events are reported in these studies (**Table 1.1**); however, this appears to be related to the severity of colitis in the cohort of subjects who are refractory to conventional treatments. This is exemplified in a clinical trial of fistulising CD where the nature of adverse events was similar between subjects treated with MSCs or a placebo (Panes et al., 2016). Moreover, the number of patients with adverse events was less in the MSC-treated cohort (Panes et al., 2016). In fistulising CD, patients have been followed for 1-2 years after the administration of allogeneic or autologous cells with no adverse events associated with MSC treatments (Ciccocioppo et al., 2011, Lee et al., 2013, Cho et al., 2015, Garcia-Arranz et al., 2016). Similarly, no serious events have reported in UC patients intravenously infused with MSCs after a 2-year follow-up. These studies suggest that the risk of adverse events by utilising MSCs may outweigh those produced by the disease itself. Limited data are available on the prospective outcomes of patients intravenously infused with MSCs in the luminal pathology of CD. In one study, it was reported that a subject contracted *C. difficile* infection and another developed appendicitis which could be related to MSC infusions (Dhere et al., 2016). Reactions have also been noted after MSC infusion of autologous cryopreserved cells (Duijvestein et al., 2010). This may have been caused by the dimethyl sulfoxide (DMSO) used to preserve cell viability during the freezing process, which is a known irritant and allergen. In the majority of studies, MSCs were expanded to generate adequate cell numbers, cryopreserved and then thawed on the day of administration. It has been demonstrated that cryopreserved MSCs have reduced

immunomodulatory activity and strongly activate the complement cascade in comparison to MSCs administered directly after expansion (Moll et al., 2014). This correlates with reduced therapeutic efficacy in acute GvHD and haemorrhagic cystitis (Moll et al., 2014). DMSO can be removed from cells immediately prior to administration, however it must also be considered that this results in the loss of stem cell numbers and increases the risk of cell clotting or contamination with pathogens (Perotti et al., 2006).

The long-term effects of MSC treatment (> 2 years) have not yet been fully elucidated therefore, it is still undetermined whether MSC treatments can contribute to the development of colorectal cancer in IBD patients who are already at risk. In one study, dysplastic lesions were discovered in a subject during endoscopy after 42 days post initial MSC treatment and the patient was diagnosed with sigmoidal adenocarcinoma (Forbes et al., 2014). A retrospective biopsy revealed dysplasia upon entry into the study, thus MSCs were not the source of tumorigenesis. However, it is uncertain whether MSCs could contribute to its progression. The cellular phenotype of MSCs post-administration is poorly understood. Differentiation of administered MSCs into aberrant cell types and malignancy *in vivo* has been rarely reported, however, long-term culture *in vitro* can spontaneously transform MSCs which can induce sarcomas when administered into mice (Rubio et al., 2005, Tolar et al., 2007, Donnelly et al., 2014). *In vitro* studies and experimental models such as these, highlight the concern of the development of cancer in IBD patients after MSC therapy. It is recommended that MSCs are only used for therapy at the fourth passage or less to minimise acquired genetic abnormalities in the cells that could lead to uncontrolled proliferation (Ueyama et al., 2012). Typically, MSCs have a limited self-renewal capacity as evidenced by proliferation and clonogenicity (colony forming unit-fibroblast) assays that demonstrate a reduced number of colonies and cells after each passage which is indicative of acquired senescence (Bonab et al., 2006, Schellenberg et al., 2011). This, combined with the available data in experimental models and clinical trials, demonstrates that MSCs have a low probability of tumour formation (Prockop et al., 2010). This also highlights why MSCs derived from primary tissues are

relatively safer than MSCs derived from pluripotent stem cells. The concerns for MSCs to spontaneously induce cancer in IBD patients may be unfounded as MSC therapy can reduce colitis-associated cancer in experimental models (Tang et al., 2015a). Therefore, MSC treatments may reduce the risk of developing colorectal cancer in IBD by supressing inflammation-associated carcinogenesis. Nonetheless, MSCs have been implicated in promoting the progression of previously formed cancerous tissue in experimental models; therefore due diligence is still required (Karnoub et al., 2007, Touboul et al., 2013, Bergfeld et al., 2014).

Several quality control measures should be implemented before MSCs can be considered as a safe and viable option for IBD patients. First, screening patients for cancer must be performed to minimise the chance of MSCs encountering dysplastic tissues; this is particularly pertinent given that MSCs have a propensity to migrate to sites of inflammation and/or hypoxia; environments where cancer cells thrive (Lee and Hong, 2017). Previous cancers and/or recent bouts of chemotherapy experienced by patients should also be added to any potential exclusion criteria. Furthermore, *in vitro* quality control should be considered for MSCs before administration to determine the probability of MSCs becoming tumorigenic themselves. Time restraints may limit the feasibility of performing in-depth tumorigenesis assays before the application of freshly isolated cells. Albeit, abnormalities in proliferation rate and karyotype can be easily detected during the expansion period. Moreover, expansive allogeneic cell lines should be fully characterised due to the increased risk of acquiring genetic abnormalities over subsequent culture (European Medicines Agency, 2008; European Medicines Agency, 2010). Regardless of the above considerations, cells should be assessed for purity, viability, and presence of contaminants such as bacteria, viruses, fungi, mycoplasma and endotoxins. At minimum, MSCs need to be produced according to Good Manufacturing Practice (GMP) guidelines for cellular therapy set by the relevant national regulatory agency.

The efficacy of allogeneic MSC therapy has given rise to the development of allogeneic cell lines that could be used commercially (Onken et al., 2006). Thus far,

therapy with allogeneic MSC cell lines have demonstrated to be well-tolerated and yield a degree of therapeutic efficacy; however, it needs to be determined whether allogeneic MSCs are better than those from autologous sources. This includes assessing the ability of allogeneic MSCs to interact with the host immune system. In one study, no changes were observed in immunoglobulin (Ig)G, IgA or IgM levels at 12 weeks after the intravenous administration of allogeneic MSCs in CD (Gregoire et al., 2018). Conversely, after local administration of allogeneic AT-MSCs for fistulising CD, donor-specific IgG human leukocyte antigen (HLA) class I antibodies were observed in one third of patients and none in placebo (Panes et al., 2016). This did not appear to affect efficacy or the number of adverse events in the study. While MSCs were once considered immune-privileged, it has been accepted that allogeneic MSC can stimulate a cell-mediated or humoral immune response in humans and other species (Berglund et al., 2017, Lohan et al., 2017). Therefore, it is uncertain how repeated treatments can affect patients and the efficacy of MSC treatments. Considering that allogeneic MSCs do not engraft long-term, their immunomodulatory effects may be only transient; therefore, routine treatments are likely to be necessary to treat chronic intestinal inflammation (Ankrum et al., 2014). Moreover, fever and mild allergic reactions were observed directly after infusion of allogeneic MSCs; nevertheless, the DMSO used for the cryopreservation of MSCs is also known to induce a similar response (Duijvestein et al., 2010, Zhang et al., 2018). Nevertheless, the ability of allogeneic MSCs to elicit an immune response, especially after multiple treatments, should not be ignored.

1.2.6. Improving the efficacy of MSC treatments

From the limited evidence in these clinical trials, MSCs did not alter cytokine levels and immune cell populations in every subject (Duijvestein et al., 2010, Gregoire et al., 2018). The pathogenesis of IBD is inconsistent between patients, likewise MSCs are intrinsically variable due to donor differences and cell manufacturing techniques. Therefore, it is probable that current MSC treatments will not be efficacious for all patients. Identifying patients that are likely to respond to MSC

therapy by their disease phenotype could improve these outcomes. Nonetheless, this can only be achieved by experience in the clinical setting and by adding to our fundamental understanding to MSC biology. Alternatively, the functional competency of the MSCs themselves could be responsible for the lack of response in some patients. Previously, the functional competency of autologous MSCs were characterised via a T-lymphocyte proliferation assay and indoleamine IDO expression prior to infusion into CD patients (Dhere et al., 2016). Despite all MSCs passing functional screening, half of the patients did not respond to the treatment. Fortunately, MSCs can act therapeutically through a plethora of mechanisms. Given the multi-faceted nature of IBD, it is unlikely that this mechanism of action will be identical between patients that do respond. Therefore, patterns that predict responses could be identified by broadening assays of functional competency that address many other mechanisms of MSC therapy. The International Society for Cellular Therapy (ISCT) released a paper discussing potential criteria and functional assays to address MSC potency in clinical trials which could be incorporated into those for IBD (Galipeau et al., 2016). It is evident that MSCs are subject to donor heterogeneity, given that factors such as age, disease status, obesity, alcohol and drug use can significantly impact the health of the bone marrow stroma or adipose tissue, the two most common sources of MSCs; thus the health of the donor will translate to variably therapeutic potential of donor MSCs. To circumvent donor variability, pooled sources of allogeneic MSCs have been demonstrated to greatly improve the allo-suppressive effects of MSC therapy in GvHD (Kuci et al., 2016). Similar methods could be used to reduce the variability of MSC therapy in IBD. Furthermore, the functional competency of MSCs can be enhanced. MSCs can be genetically engineered to improve homing and secrete specific factors that may improve their efficacy. In experimental models of colitis the efficacy and homing of MSCs can be improved by over-expressing C-X-C chemokine receptor type 4 (CXCR4), interleukin (IL)-37b and IL-35 or knockdown of miR21 to increase the production of transforming growth factor (TGF)β1 (Liu et al., 2013, Wang et al., 2015, Wu et al., 2015, Chen et al., 2018b, Nan et al., 2018, Yan et al., 2018). Concerns for the safety of patients has led to a reluctance in utilising genetically modified cellular therapies for the time being. Nevertheless,

safer alternatives are available to enhance the efficacy of MSCs therapies. MSCs are responsive to a variety of cytokines and pathogen associated molecular patterns that can be added to *in vitro* cultures before administration to alter their phenotype and the factors they secrete. Experimental models of colitis have demonstrated that the efficacy of MSCs can be enhanced by pre-stimulation with the cytokines interferon (IFN)-γ and IL-25, or activation of the pathogen recognition receptors nucleotide-binding oligomerization domain-containing protein 2 (NOD2) and toll-like receptor (TLR)-3 (Duijvestein et al., 2011, Kim et al., 2013a, Fuenzalida et al., 2016, Qiu et al., 2016, Cheng et al., 2017). In one case study, a patient with refractory CD was treated with MSCs pre-stimulated by IFN-γ which did not induce a therapeutic response (Taddio et al., 2015). Nevertheless, results from experimental colitis suggest pre-stimulation of MSCs is a viable option to optimise treatments.

The efficacy of MSCs can be enhanced by co-treatment *in vivo* with pharmacological agents. Co-administration with granulocyte-colony stimulating factor (GCSF) and a micro-particle that activates NOD2 and TLR-9 signalling have both demonstrated to improve the therapeutic effects of MSCs in experimental colitis (Tang et al., 2015b, Lee et al., 2018). Pharmacological inhibition of MSC-derived proinflammatory factor galectin-3 during *in vitro* culture has also enhanced the immunomodulatory effects of MSCs in experimental colitis (Simovic Markovic et al., 2016). Furthermore, co-administration of umbilical cord blood-derived platelet lysate with AT-MSCs from CD patients potentiated their efficacy in experimental colitis (Forte et al., 2015).

The interaction between MSC therapy and current clinically approved IBD treatments is relatively unestablished. Several clinical trials have administered MSCs in conjunction with routine treatments of biologics, immunomodulators or steroids demonstrating that this does not lead to any adverse effects. Data from MSC administration in fistulising CD suggest that anti-TNFα antibodies and immunomodulators could assist in increasing remission rates; however, these interactions have not been thoroughly explored (Panes et al., 2016). An ongoing

clinical trial in refractory CD will provide preliminary data on the efficacy of MSC treatments alone or in conjunction with current routine treatments (NIH identifier: NCT02532738).

1.2.7. Administration and dosage

Several administration methods to deliver MSCs have been assessed in experimental models of colitis and IBD patients with varying results depending on the location, severity and nature of the pathology. In fistulising CD, MSCs are applied locally to deliver a targeted effect at the site of the fistulae: either intra-luminally or into the wall of the fistulous tract. In the inflammatory luminal pathology of CD and UC, MSCs are currently delivered by intravenous infusions. Compared to fistulising CD, the inflammatory luminal pathology is exhibited broadly throughout the intestinal tract making local delivery impractical. The utilisation of intravenous injections is rationalised by the homing capacity of MSCs to sites of inflammation. Intravenous administration is relatively non-invasive and, therefore, is the preferred option for the delivery of cell-based therapies in clinical settings. Although MSCs have been demonstrated to migrate to the inflamed colon in experimental colitis, many studies have reported that systemically injected, or even intraperitoneally injected, MSCs can accumulate in the spleen, lungs, liver, heart, kidney and mesenteric lymph nodes (MLN) (Hayashi et al., 2008, Liang et al., 2011, Tang et al., 2015a, Song et al., 2017c, Takeyama et al., 2017, Song et al., 2018, Soontararak et al., 2018). If MSC therapies could target the site of inflammation more efficiently, then dosages may be reduced, and patient outcomes improved.

The efficiency of MSC delivery and engraftment in the intestine could be enhanced by optimising homing of the cells or by identifying novel methods of administration. MSCs must be expansively cultured to generate the numbers required for a therapeutic response in IBD patients; however, it should be considered that the size of MSCs increases throughout *in vitro* expansion (Yang et al., 2018). It is unknown whether the physical size or *in vitro* ageing of MSCs can

affect its migratory properties in the treatment of intestinal inflammation. Nonetheless, optimisation of expansion conditions to avert the effects of *in vitro* aging may assist in maintaining homing capacity and efficacy. Alternatively, novel administration methods are being investigated in experimental intestinal inflammation that have permitted MSCs to elicit a therapeutic effect without relying on their homing capabilities (**Figure 1.1D, Table 1.2**). Surgical procedures have been trialled in experimental models to directly deliver MSCs into the inguinal lymph nodes, mesentery and the intestinal wall (Ando et al., 2008, Hayashi et al., 2008, Lopez-Santalla et al., 2017, de la Portilla et al., 2018, Fu et al., 2018). Local endoscopic injection of MSCs is also a viable option which has been shown to ameliorate experimental colitis (Martin Arranz et al., 2018). Nonetheless, these are all invasive procedures and a major goal of IBD therapy is to minimise surgical interventions. Intra-luminal administration of MSCs by enema may be a feasible solution to effectively target the site of inflammation and avoid erroneous biodistribution in other organs. The efficacy of MSCs administered by enema has been demonstrated in mice and guinea-pigs with chemically-induced colitis where they have been demonstrated to engraft into the intestine and reduce inflammation (Robinson et al., 2014, Robinson et al., 2015, Stavely et al., 2015a, Stavely et al., 2015b, Wang et al., 2016, Robinson et al., 2017b). Moreover, the efficacy of enema delivery has been demonstrated using MSCs derived from CD patients in murine dextran sodium sulphate (DSS)-induced colitis (Forte et al., 2015). In the same experimental model, the administration methods of intravenous injection, intraperitoneal injection and enema were directly compared (Wang et al., 2016). Enema and intraperitoneal injections were the most effective for the localisation of MSCs to the colon and produced the highest therapeutic efficacy. Furthermore, MSCs administered by enema did not engraft into other organs like those administered intravenously, or, to a lesser extent, intraperitoneally. Although MSC administration by enema may be safer and efficacious, the distance of pathological manifestations from the rectum in CD could pose limitations; thus, this may only be a suitable application method for colitis.

The engraftment of MSCs into the inflamed intestine has been investigated in experimental colitis. It has been demonstrated that administration of syngeneic MSCs by intravenous injection can engraft and proliferate up to 21 days in murine DSS-induced colitis (Sun et al., 2015). Conversely, xenogeneic MSCs injected intraperitoneally in the same model engraft into the colon at 2h but cannot be detected after 24h despite alleviating colitis (Song et al., 2018). This suggest that MSCs may only be active for a short period of time, however, their therapeutic effects are maintained long after their departure. This can be explained by the ability of MSCs to stimulate other cells remaining in the tissue that can mediate their therapeutic effects. Even so, several studies have demonstrated that MSCs can ameliorate colitis without even homing to the colon, or with very low colonic engraftment, after intravenous and intraperitoneal administration (Song et al., 2017c, Takeyama et al., 2017, Soontararak et al., 2018). In fact, one study reported that less than 1% of MSCs administered intraperitoneally engrafted into the colon and the majority of cells formed aggregates in the peritoneal cavity (Sala et al., 2015). The paracrine activity of these aggregates was described to ameliorate experimental colitis in this study. The therapeutic potential of the paracrine secretion has been supported by the efficacy of administrating the supernatant of cultured MSCs (conditioned media) in guinea-pig and mouse models of chemically-induced colitis (Watanabe et al., 2013, Robinson et al., 2014, Legaki et al., 2016, Hoffman et al., 2018). In these studies, the medium conditioned by xenogeneic MSCs isolated from the bone marrow of healthy donors, or AT-MSCs from CD patients, was demonstrated to ameliorate colitis when applied by enema (Robinson et al., 2014, Hoffman et al., 2018). Nonetheless, allogeneic and xenogeneic conditioned medium has also ameliorated chemically-induced colitis when administered intraperitoneally and intravenously (Watanabe et al., 2013, Legaki et al., 2016).

The development of novel technologies and stem cell-based products may overcome issues of MSC homing or erroneous engraftment. Application of the MSC conditioned medium in the form of a gel to avoid leakage has yielded positive results in TNBS-induced colitis in rats (Miyamoto et al., 2017). Exosomes and

extracellular vesicles isolated from allogeneic and xenogeneic MSCs have also been reported to alleviate chemically-induced colitis in the mouse and rat which presents as another therapeutic option without delivering MSCs themselves (Yang et al., 2015, Mao et al., 2017a). Other innovations that have improved the efficacy or homing of MSCs in experimental colitis include the endoscopic or enema application of MSC-derived spheroids, co-administration with recombinant protein scaffolds and vascular cell adhesion protein-1 (VCAM-1) antibody coating of MSCs (Ko et al., 2010, Molendijk et al., 2016, Barnhoorn et al., 2018, Iwazawa et al., 2018). Recently, *in vitro* grown sheets of allogeneic MSCs were used to ameliorate the ulcerations in the mucosa in experimental colitis when directly transplanted to the affected tissue by endoscopy (Pak et al., 2018). Therefore, specific techniques may continue to be developed that target the different manifestations of IBD, similar to the divergence of the MSC-based treatment methodology for the fistulising and inflammatory luminal pathology of CD. The diversity of these studies demonstrate that several novel MSC-based technologies and application methods can be further developed in pre-clinical models; these are crucial to enhancing the efficacy of MSCs in the clinic. Particularly, the development of stem cell-based products that can be administered without applying the cells themselves may be of interest due to the reservations of erroneous engraftment and the development of cancerous MSCs. The conditioned medium used to derive these therapies is often disposed of as a by-product of MSC expansion. If these methods are efficacious, a reduction in costs of production and characterisation could also be an advantage.

1.2.8. Mechanisms of MSCs action in IBD

Although current human studies in CD and UC are designed to determine the efficacy and safety of MSC therapy, several studies have also attempted to elucidate their mechanisms of action. In fistulising CD, local administration of autologous BM-MSCs increased the number of mucosal and circulating regulatory T-lymphocytes (Tregs) which remained elevated after 12 months post treatment (Ciccocioppo et al., 2011). In IBD, Tregs are thought to be functionally competent,

however they are often reduced in numbers locally and systemically which may contribute to the pathogenesis of the disease (Boden and Snapper, 2008). This supports the immunosuppressive properties of MSC therapy in patients. Likewise, administration with allogeneic AT-MSCs in fistulising CD resulted in a decrease in IL-6 at 52 weeks post treatment in 7/10 patents (Garcia-Arranz et al., 2016). IL-6 is considered a pro-inflammatory cytokine in IBD and has been identified as a therapeutic target (Allocca et al., 2013, Garcia-Arranz et al., 2016). No differences were observed in IL-1β, IL-10, TNF-α and IFN-γ, however this may have been hindered by the detection limit of the assay or sample processing as only low levels of these cytokines were detected as baseline. Altogether, these studies suggest that MSC therapy may function via anti-inflammatory mechanisms in fistulising CD; nevertheless, the closure of fistulae requires tissue regeneration which is also promoted by MSC treatments. It was once considered that the therapeutic benefit of locally injected autologous MSCs could be a result of their differentiation into connective tissue (García-Olmo et al., 2005). Alternatively, transient allogeneic MSCs are also effective at promoting remission of fistulae (Garcia-Arranz et al., 2016); thus, their therapeutic value may be provided by their trophic secretome. In one clinical trial, MSCs were effective in treating both CD-related fistulae and fistulae arising spontaneously in non-CD patients (Garcia-Olmo et al., 2009a). Therefore, specifically in fistulising CD, the value of MSC therapy may be trophic and not solely attributed to immunosuppression by Tregs and reducing IL-6 levels which are involved in the pathogenesis of IBD. While IL-6 was decreased by MSC treatment in fistulising CD, no change in serum levels were induced by intravenous infusion of umbilical cord derived MSCs in the inflammatory luminal pathology of CD after 3 months (Hu et al., 2016). Similarly, no changes were detected in the key pro-inflammatory cytokines TNF-α and IFN-γ. Conversely, levels of these serum cytokines are often altered by MSC treatments in experimental models, however cytokine concentrations have been measured at earlier time-points (**Table 1.3**). Furthermore, cytokine measurements from mucosal biopsies may offer better insight into the levels of inflammation in the intestinal microenvironment, albeit acquisition of samples is a more invasive procedure. In biopsies of the inflamed mucosa, allogeneic BM-MSCs trended to decrease IL-6, however the same

cytokine, along with IL-1β, was significantly elevated in the serum (Duijvestein et al., 2010). The effect of allogeneic BM-MSCs on patterns of TNF-α and IL-10 expression were varied. However, MSCs trended to reduce the proportion of $CD4^+$ T-lymphocytes and increase the proportion of Tregs (5/7 patients) after 6 weeks (Duijvestein et al., 2010). Conversely, no differences have been observed in the populations of blood Treg, naïve T helper (T_h), memory T_h, cytotoxic T-lymphocytes or B-lymphocytes at 12 weeks post-treatment with allogeneic BM-MSCs (Gregoire et al., 2018). However, MSC treatments increased the number of natural killer (NK) cells and NKT-lymphocytes. This immuno-stimulatory activity of allogeneic MSC treatment warrants further exploration considering that IBD patients are often immunocompromised, susceptible to developing colorectal cancer and NK cells appear to play a role in the pathophysiology of IBD (Yadav et al., 2011).

1.2.9. Mechanisms of action in experimental colitis

The success of MSC therapies in refractory patients has given optimism for the future inclusion of MSCs into the treatment regimen for IBD. However, it has been acknowledged that pre-clinical studies are still necessary to elucidate the mechanisms of action and optimise therapies to improve clinical outcomes (Gregoire et al., 2018). Over 80 studies have been conducted in experimental models of colitis with approximately three quarters of them published over the last four years (**Figure 1.1**). Insight into their potential mechanism of action has been provided by these studies which includes promotion of epithelial integrity, immunomodulation, alleviation of oxidative stress and neuroprotection.

1.2.9.1.Epithelial integrity

The intestinal epithelium is a vital barrier between the lamina propria and the luminal microbiome or enterotoxins. Disruption of this barrier facilitates the interaction between foreign luminal contents and the immune system which can lead to inflammation. Therefore, restoration of the epithelial barrier in IBD is a

potential therapeutic target (Okamoto, 2011, Fries et al., 2013). On the macroscopic level, MSCs have been regularly demonstrated to attenuate gross morphological changes in models of experimental colitis (**Table 1.2**). MSCs were able to migrate to damaged tissues, where they reduced ulceration and improved endoscopic scores (Ando et al., 2008, Hayashi et al., 2008, Castelo-Branco et al., 2012, Perez-Merino et al., 2015). MSCs appear to acquire a myofibroblast-like phenotype post-administration in colitis (Hayashi et al., 2008, Tanaka et al., 2011). Considering that myofibroblast are associated with fibrosis, the role of MSCs in contributing to the stricturing pathology could be of concern. Although this appears unwarranted as MSC treatments reduced collagen deposition in experimental colitis suggesting that treatments may actually ameliorate scarring of the tissue (Castelo-Branco et al., 2012, Wang et al., 2016).

Many studies have performed histological examination after MSC treatments which have revealed that MSCs attenuate the loss and discontinuity of the surface columnar epithelial lining and disorganisation of the intestinal crypts (**Table 1.2**). While the intact epithelial layer creates a physical barrier between the tissue and the contents of the lumen, the mucous barrier is also critical in blocking the adherence of pathogenic bacteria (Corazziari, 2009). Mucins that form this barrier can be disrupted or completely lost in IBD (Dorofeyev et al., 2013). Administration of MSCs also ameliorated the loss of mucin secreting goblet cells in experimental colitis (Tanaka et al., 2011, Fawzy et al., 2013). The mechanism of how MSCs restore the epithelial lining could be explained by their trophic secretion (Ando et al., 2008, Watanabe et al., 2013). The protective effect of conditioned medium from MSCs on the epithelial layer highlights the significance of the MSC secretome in this process (Watanabe et al., 2013). Within the secretome, trophic factors were identified including: vascular endothelial growth factor (VEGF), hepatocyte growth factor (HGF) and adiponectin; these were suggested to contribute to the mechanism of MSCs to regenerate the epithelium. Although these factors are secreted by MSCs, levels of VEGF and HGF were found to be reduced after MSC treatments in the inflamed colon; therefore the therapeutic effects of MSCs may be mediated by other factors (Tanaka et al., 2008).

Table 1.3 ***Effects of mesenchymal stem cell treatments on endogenous factors in experimental colitis models***

Factor	Expression level in tissues after MSC treatment	References
15-LOX-1	↓Colon	(Mao et al., 2017b)
	↓Spleen	(Mao et al., 2017b)
Akt	↑Colon	(Hoffman et al., 2018)
ARG1	↑Colon	(Song et al., 2017c, de Aguiar et al., 2018, Song et al., 2018)
	↑Serum	(Ferrer et al., 2016)
ARG2	↑Colon	(Sala et al., 2015)
bFGF	↓Colon	(Tanaka et al., 2008)
BIP	↓Colon	(Banerjee et al., 2015)
Ccl2 (MCP1)	↓Colon	(de Aguiar et al., 2018, Hoffman et al., 2018)
	↓Serum	(Onishi et al., 2015)
CCL22	↑Colon	(Sala et al., 2015)
Ccl23	↑Colon	(Hoffman et al., 2018)
CCL5	↓Colon	(Gonzalez-Rey et al., 2009, González et al., 2009)
CD11b	↓Colon	(Song et al., 2017c)
CXCL10	↓Colon	(Mao et al., 2017b)
	↓Spleen	(Mao et al., 2017b)
Fizz1	↑Colon	(Song et al., 2017c, Song et al., 2018)
FOXP3	↑Colon	(Chen et al., 2013, Sala et al., 2015, Wang et al., 2016, Jo et al., 2018, Martin Arranz et al., 2018, Nan et al., 2018)
	↑Serum	(Sala et al., 2015)

Gata3	↑Colon	(Chen et al., 2013)
GSH	↑Colon	(Ferrer et al., 2016, da Costa Gonçalves et al., 2017)
GSK3B	↑Colon	(Hoffman et al., 2018)
HGF	↓Colon	(Tanaka et al., 2008)
HO-1	↑Colon	(Sala et al., 2015)
IFN-γ	↓Colon	(Gonzalez-Rey et al., 2009, González et al., 2009, Zhang et al., 2009b, Liang et al., 2011, Chen et al., 2013, Wang et al., 2014, Lin et al., 2015, Liu et al., 2015, Song et al., 2017c, de Aguiar et al., 2018)
	N.D. Colon	(Duijvestein et al., 2011)
	↓Serum	(Chen et al., 2013, Forte et al., 2015)
	↓$CD4^+$ T lymphocytes in spleen	(Wang et al., 2015) (Ferrer et al., 2016)
IL-10	↑Colon	(Gonzalez-Rey et al., 2009, González et al., 2009, Zhang et al., 2009b, Chen et al., 2013, Sala et al., 2015, Chao et al., 2016, Lee et al., 2016, Legaki et al., 2016, Wang et al., 2016, Mao et al., 2017b, Song et al., 2017b, Song et al., 2017c, de Aguiar et al., 2018, Fu et al., 2018, Jo et al., 2018, Nan et al., 2018, Song et al., 2018)
	N.D. Colon	(Duijvestein et al., 2011, Martin Arranz et al., 2018)
	↑Serum	(Simovic Markovic et al., 2016, Heidari et al., 2018)(Chen et al., 2013)
	↓Serum	(Forte et al., 2015)
	↑MLN	(Heidari et al., 2018)
	↑Spleen	(Ferrer et al., 2016, Mao et al., 2017b, Heidari et al., 2018)
IL-12 (IL-12p40)	↓Colon	(Gonzalez-Rey et al., 2009, González et al., 2009, Tang et al., 2015a, Chao et al., 2016)
	↓Serum	(Ferrer et al., 2016, Nikolic et al., 2018)
IL-17	↓Colon	(Zhang et al., 2009b, Liang et al., 2011, Chen et al., 2013, Wang et al., 2014, Liu et al., 2015, Song et al., 2017b, Song et al., 2017c, Fu et al., 2018, Nan et al., 2018)
	N.D. Colon	(Duijvestein et al., 2011, Chao et al., 2016)

	↑Colon	(Hoffman et al., 2018)
	↓Serum	(Liang et al., 2011, Chen et al., 2013, Heidari et al., 2018)
	↓MLN	(Heidari et al., 2018)
	↓Spleen	(Ferrer et al., 2016, Heidari et al., 2018)
IL-1α	↓Colon	(Tang et al., 2015a)
	↓Serum	(Ferrer et al., 2016)
IL-1β	↓Colon	(Tanaka et al., 2008, Gonzalez-Rey et al., 2009, González et al., 2009, He et al., 2012, Lin et al., 2015, Onishi et al., 2015, Tang et al., 2015a, Legaki et al., 2016, Mao et al., 2017b, Song et al., 2017a, Song et al., 2017c, Hoffman et al., 2018)
	↓Serum	(González et al., 2009, Chen et al., 2013, Simovic Markovic et al., 2016, Fu et al., 2018, Nikolic et al., 2018)
	↓Spleen	(Ferrer et al., 2016, Mao et al., 2017b)
IL-2	↓Colon	(Chen et al., 2013)
	↓Serum	(Chen et al., 2013, Ferrer et al., 2016)
	↑$CD4^+$ T lymphocytes in spleen	(Wang et al., 2015)
IL-21	↓Colon	(Chao et al., 2016)
IL-23	↓Colon	(Liang et al., 2011, Chao et al., 2016)
IL-4	↑Colon	(Chen et al., 2013)
	↑Serum	(Chen et al., 2013)
IL-5	↓Colon	(Tang et al., 2015a)
	↓Serum	(Ferrer et al., 2016)
IL-6	↓Colon	(Gonzalez-Rey et al., 2009, González et al., 2009, Zhang et al., 2009b, Liang et al., 2011, Chen et al., 2013, Wang et al., 2014, Lin et al., 2015, Liu et al., 2015, Tang et al., 2015a, Chao et al., 2016, Mao et al., 2017b, Song et al., 2017a, de Aguiar et al., 2018, Fu et al., 2018, Hoffman et al., 2018, Song et al., 2018)
	↓Serum	

		(González et al., 2009, Chen et al., 2013, Forte et al., 2015, Ferrer et al., 2016, Nikolic et al., 2018)
	↓Spleen	(Mao et al., 2017b)
IL-8	↓Colon	(Ando et al., 2008)
MIF	↓Colon	(Onishi et al., 2015)
MIP-2	↓Colon	(Gonzalez-Rey et al., 2009, González et al., 2009)
	N.D. Colon	(Onishi et al., 2015)
	↓Serum	(González et al., 2009)
MMP2	↓Colon	(Legaki et al., 2016)
***Mrc1* (CD206)**	↑Colon	(Song et al., 2017c, Song et al., 2018)
***Nos2* (iNOS)**	↓Colon	(Song et al., 2018)
***P65/Rela* (NF-kbp65)**	↑Colon	(Hoffman et al., 2018)
	↓Colon	(Zuo et al., 2015)
PDI	↓Colon	(Banerjee et al., 2015)
pSTAT3	↓Colon	(Jo et al., 2018)
	↓Spleen	(Mao et al., 2017b)
RORyt	↓Colon	(Chen et al., 2013, Nan et al., 2018)
SOD	↑Colon	(Sun et al., 2015)
Tbx21 (T-Bet)	↓Colon	(Chen et al., 2013)
TGFβ (1)	↑Colon	(Liu et al., 2015, Sala et al., 2015, Legaki et al., 2016, Song et al., 2017b, Heidari et al., 2018, Jo et al., 2018) (Chen et al., 2013, Liu et al., 2015, Chao et al., 2016, Fu et al., 2018)
	N.D. Colon	(Lee et al., 2016)
	↑Serum	(Simovic Markovic et al., 2016, Heidari et al., 2018)
	↑MLN	(Heidari et al., 2018)
	↑Spleen	(Ferrer et al., 2016, Heidari et al., 2018)

TNF-α	↓Colon	(Tanaka et al., 2008, Gonzalez-Rey et al., 2009, González et al., 2009, He et al., 2012, Chen et al., 2013, Wang et al., 2014, Lin et al., 2015, Liu et al., 2015, Onishi et al., 2015, Tang et al., 2015a, Zuo et al., 2015, Chao et al., 2016, Legaki et al., 2016, Wang et al., 2016, Mao et al., 2017b, Song et al., 2017c, de Aguiar et al., 2018, Song et al., 2018)
	N.D. Colon	(Duijvestein et al., 2011, Lee et al., 2016)
	↓Serum	(González et al., 2009, Liang et al., 2011, He et al., 2012, Chen et al., 2013, Forte et al., 2015, Zuo et al., 2015, Simovic Markovic et al., 2016, Fu et al., 2018)
	↓Spleen	(Ferrer et al., 2016, Mao et al., 2017b)
TSG6	↑Colon	(Sala et al., 2015, Wang et al., 2016)
	↑Serum	(Sala et al., 2015, Fu et al., 2018)
VEGF	↑Colon	(Hoffman et al., 2018)
	↓Colon	(Tanaka et al., 2008)
Ym1	↑Colon	(Song et al., 2017c, Song et al., 2018)

↑ increase, ↓ decrease, N.D. no difference; 15-LOX-1, 15-lipoxygenase-1; Akt, protein kinase B; ARG1, arginase 1; ARG2, arginase 2; bFGF, basic fibroblast growth factor; BIP, binding immunoglobulin protein; Ccl2 (MCP1), monocyte chemoattractant protein 1; CCL, C-C motif chemokine ligand; CD11b (ITGAM), integrin alpha M ; CXCL, C-X-C motif chemokine ligand; Fizz1, (Retnla), resistin-like alpha; FOXP3, forkhead box P3; Gata3, GATA binding protein 3; GSH, glutathione; GSK3B, glycogen synthase kinase 3 beta; HGF, hepatocyte growth factor; HO-1, haem oxygenase 1; IFN-γ, interferon gamma; IL, interleukin; MIF, macrophage migration inhibitory factor; MIP-2, macrophage inflammatory protein 2; MLN, mesenteric lymph nodes; MMP2, matrix metalloproteinase 2; Mrc1 (CD206), mannose receptor C-type 1; Nos2 (iNOS), inducible nitric oxide synthase; P65 (RELA), nuclear factor NF-kappa-B p65 subunit; PDI, protein disulphide isomerases; pSTAT3, phosphorylated signal transducer and activator of transcription 3; RORyt, RAR-related orphan receptor gamma; SOD, superoxide dismutase; Tbx21 (T-Bet), T-box protein expressed in T lymphocytes; TGFβ, transforming growth factor beta; TNF-α, tumour necrosis factor alpha; TSG6, tumour necrosis factor-inducible gene 6 protein; VEGF, vascular endothelial growth factor; Ym1 (Chil3), chitinase-like 3.

Nevertheless, MSCs could localise to the base of intestinal crypts and express VEGF and TGF-β1; therefore, local concentrations of trophic factors could still be high in this region (Hayashi et al., 2008, Tanaka et al., 2008). Moreover, MSCs may be able to stimulate endogenous mechanisms of repair in the epithelial layer (Sémont et al., 2013). AT-MSCs and iPSC-derived MSCs have been demonstrated to promote the vascularisation of the epithelium (Soontararak et al., 2018). The conditioned medium of MSCs from CD patients can increase the endogenous expression of VEGF-A in epithelial cells and increase their proliferation *in vitro* (Hoffman et al., 2018). Similarly, the conditioned media of MSCs increases the number of epithelial cells expressing the proliferation marker Ki67 *in vivo* (Wang et al., 2016, Hoffman et al., 2018). Furthermore, the epithelial stem cell marker leucine-rich repeat-containing G-protein coupled receptor 5 (LGR5) is increased by MSC treatments (Chen et al., 2013, Soontararak et al., 2018). This may suggest that MSCs promote epithelial regeneration by stimulating the proliferation and differentiation of epithelial progenitors to replace the damaged tissue. It is conflicting whether this process is already activated by inflammation in experimental colitis (Chen et al., 2013, Soontararak et al., 2018). Furthermore, repair of the intestinal epithelial barrier by MSCs has been associated with improved diversity in the microbiota and a reduction in proteobacteria (Soontararak et al., 2018). It is unclear whether the normalisation of the microbiome improved healing or whether regeneration of the epithelium affected the composition of the microbiome; however, evidence of MSCs attenuating loss of mucin secreting goblet cells may support the latter. Additionally, it has been demonstrated that MSC treatments can avert epithelial permeability by enhancing the expression of the tight junction proteins (TJPs) ZO-1, claudin 2, 12 and 15 (Yabana et al., 2009, de Aguiar et al., 2018). MSC treatments were demonstrated to reduce serum levels of D-lactate and diamine oxidase which are indicative of epithelial barrier permeability in conjunction with an increase in E-cadherin expression (Sun et al., 2015). Together these studies indicate that MSCs not only promote the proliferation of epithelial cells to facilitate healing, but they also improve tight junctions to block the penetration of luminal contents, thus, averting antigenic insult to the immune system.

1.2.9.2. Immunomodulation

IBD is an immune disorder and current treatments are focused on supressing or modulating the immune response. MSCs have also demonstrated potent immunosuppressive properties in many studies of experimental colitis. From these studies, a plethora of markers of inflammation have been investigated (**Table 1.3**). The most common observations are an increase in the anti-inflammatory cytokines TGFβ and IL-10, as well as, a decrease in pro-inflammatory cytokines: TNF-α, IL-6, IL-12 (IL-12p40), IL-17, IFN-γ and IL-1β. This demonstrates that MSC treatments can modify the pro-inflammatory signalling milieu of the local microenvironment to alleviate experimental colitis. Changes to these cytokines can also be detected systemically and in other organs harbouring immune cells, such as the spleen and mesenteric lymph nodes (**Table 1.3**). After MSC treatment there is also a reduction in the general number of leukocytes in TNBS and DSS-induced colitis models (Sala et al., 2015, Stavely et al., 2015a). This can be observed throughout the various layers of the colon (Stavely et al., 2015a). However, the combined effects of MSC treatments on specific subpopulations of leukocytes are likely to mediate their therapeutic properties.

The innate immune system provides the initial response to acute inflammation but is also crucial in mediating chronic inflammation in IBD. Of these cells, MSCs have been demonstrated to affect neutrophils, macrophages (Mφ) and dendritic cells (DC) in experimental colitis. Neutrophils are the most abundant of the leukocytes in most mammalian species and their mass infiltration into the intestine is utilised in the diagnosis of IBD. In experimental colitis, MSCs have been demonstrated to avert neutrophil invasion in many studies (**Table 1.2**). This has been demonstrated histologically and by a reduction in their bio-marker myeloperoxidase (MPO), which is an enzyme responsible for their lytic and bactericidal function. A reduction in Mφ and DCs and can also be observed after MSC treatments in experimental colitis which are crucial mediators of chronic inflammation by their contribution to the cytokine signalling milieu and their capabilities for antigen presentation (Onishi

et al., 2015, Simovic Markovic et al., 2016, de Aguiar et al., 2018). These effects may be explained by a reduction in chemokines such as monocyte chemoattractant protein-1 (MCP-1) which is responsible for monocyte recruitment and activation (de Aguiar et al., 2018). This demonstrates that MSCs may limit inflammation by reducing the infiltration of these leukocytes, however, MSCs also appear to alter the properties of Mφs and DCs that reside in the inflamed tissue. These cells are postulated to be responsive to MSC secreted factors; this is highly plausible given that Mφs and DCs are receptive to both pro and anti-inflammatory signals given that they constitutively express cytokine receptors or can be induced to upregulate them in the presence of certain cytokines. This is exemplified by *in vitro* studies which have demonstrated that MSCs decrease the secretion of TNF-α, IL-12, IL-6 and MCP-1 from monocytes or macrophages (Tanaka et al., 2008, González et al., 2009, Onishi et al., 2015, Song et al., 2018). Human and mouse cytokines (and their cognate receptors) share a large degree of homology (Auron et al., 1985, Degrave et al., 1986, Schrader et al., 1986) further validating the therapeutic potential observed in xenogeneic models. Macrophages are dynamic cells with multiple functions including phagocytosis, antigen presentation, T cell activation and key inflammatory cells that are associated with the pathology of many diseases. Macrophages can be polarised towards a pro-inflammatory (Mφ1) or anti-inflammatory phenotype (Mφ2) that assist in regulating the inflammatory response. *In vitro* experiments have demonstrated that xenogeneic MSCs can induce the Mφ2 phenotype in a paracrine manner (Anderson et al., 2013b, Song et al., 2017c, Song et al., 2018). Likewise, MSCs have been demonstrated to alter the cytokine expression profile of DCs in a paracrine manner *in vitro*. MSCs promoted the expression of the anti-inflammatory cytokines IL-10 and TGFβ and reduced the pro-inflammatory cytokines IFN-γ, IL-6 and TNF-α (Jo et al., 2018, Nikolic et al., 2018). Moreover the DC markers that are needed for activation and co-stimulation of T cells (CD86, CD80 and MHCII) were found to be reduced by the paracrine secretion of MSCs (Nikolic et al., 2018). MSC treatments in experimental colitis *in vivo* decreased the levels of Mφs but increase the population of Mφ2 using the surface marker mannose receptor C-type 1 (MRC1; CD206) (Simovic Markovic et al., 2016, Song et al., 2018). This included a decline in Mφs expressing IL-1β or

IL-12 and an increase in Mφs expressing IL-10 (Simovic Markovic et al., 2016). The proteins or genes expressed by Mφ2 were also upregulated in colon tissues by MSC treatments which included MRC1, arginase-1 (*Arg1*), resistin-like beta (*Retnlb*/*Fizz1*) and chitinase-like 3 (*Chil3*/*Ym1*) which further supported that treatments could induce the Mφ2 phenotype (Song et al., 2017c, de Aguiar et al., 2018, Song et al., 2018). Nevertheless, it was reported that xenogeneic application of amnion-derived MSCs also alleviated colitis but reduced both the Mφ1 and Mφ2 phenotypes (Onishi et al., 2015). Therefore, Mφ2 may not be essential to the mechanism of MSC therapy. However, the administration of Mφ2 induced by MSCs *in vitro* successfully attenuates experimental colitis (Anderson et al., 2013b). Thus, Mφ2s appear to be at least partially involved in the mechanisms of action of MSC therapies.

Dendritic cells share most of the same functions as macrophages with a few notable exceptions such as cross-presentation (Villadangos et al., 2007) and the polarisation of T-helper responses. Typically, IL-12 secretion by DCs polarises un-committed T helper cells towards a Th1 phenotype; conversely DCs that secrete IL-4 will polarise T helper cells towards a Th2 phenotype (de Jong et al., 2002); however, there is evidence to suggest that MSCs can influence the phenotype and therefore cytokine secretion by DCs. For example, adoptive transfer of DCs primed by MSCs attenuate experimental colitis which could be mediated by a decrease in signal transducer and activator of transcription 3 (STAT3) signalling and an increase in anti-inflammatory cytokines IL-10 and TGFβ (Jo et al., 2018, Nikolic et al., 2018). Monocyte or DC co-cultures with MSCs reduce T-lymphocyte proliferation and IFN-γ secretion mediated partly by IL-10 (Gonzalez-Rey et al., 2009, Anderson et al., 2013b). Moreover, DCs primed by MSCs increase the expression of the Treg marker, forkhead box P3 (FOXP3), in splenocytes *in vitro*, and administration of both MSCs and MSC-primed DCs increase FOXP3 expression in experimental colitis (Jo et al., 2018). Together this suggests that the MSCs polarise antigen presenting cells which in turn may regulate experimental colitis through polarisation of T helper lymphocyte responses.

In experimental colitis, MSC treatments have been demonstrated to induce anti-inflammatory and immunoregulatory properties in many immune cells. Their ability to directly or indirectly modulate the adaptive immune response is vital in suppressing chronic inflammation. MSCs can alter various subpopulations of T-lymphocytes, however effects to NKT-lymphocytes and B-lymphocytes have also been reported (**Table 1.2**). In DSS-induced colitis, syngeneic MSCs decreased the number of NKT-lymphocytes, conversely, NKT-lymphocytes are increased by allogeneic transplant in CD patients (Simovic Markovic et al., 2016, Gregoire et al., 2018). These results may be explained by host-donor differences, however future studies are required to explore this and the potential implications in therapy. Furthermore, MSCs injected via intravenous routes have been reported to be sequestered in the liver and spleen which are also the largest storage site of NKT-lymphocytes in the body, thus studying the cross-talk between MSC and NKT-lymphocytes is of utmost importance particularly given that NKT-lymphocytes are potent cytokine producers and thus can have a large influence on polarising immune responses (Kronenberg, 2005). Further, NKT-lymphocytes can be primed towards a pro-tumourigenic and anti-tumourigenic phenotype, an important implication if the patient has had a history or cancer (Bedard et al., 2017). A general reduction in the infiltration of $CD4^+$ T-lymphocytes (T helper; T_h) parallels decreased inflammation after MSC treatments in colitis (Zhang et al., 2009b). However, subsets of the T_h population appear to also be altered by MSC therapy. Modifications to the *in vivo* signalling milieu and in markers of T-lymphocytes are observed after MSC treatments which demonstrate that populations of pro-inflammatory T_h1 and T_h17 cells are reduced while Tregs, and possibly T_h2 cells, are increased (**Table 1.3**). These changes are evident in the colon and can often be observed in the MLN, spleen or serum (**Table 1.3**). MSCs co-cultured with lamina propria mononuclear cells decrease IFN-γ and IL-17 in a paracrine manner which are typically pro-inflammatory cytokines produced by Th1 and Th17 cells, respectively (Liang et al., 2011). Co-culture of MSCs with *in vitro* explants of the MLN decrease pro-inflammatory IFN-γ and IL-2, while simultaneously promoting IL-10 secreting T-lymphocytes which demonstrates the induction of an anti-inflammatory phenotype of resident cells (Gonzalez-Rey et al., 2009, González et

al., 2009). In experimental colitis, MSC treatments increase the Treg marker, FOXP3, and the proportions of bona-fide $CD4^+$ Tregs within T-lymphocyte populations (Zhang et al., 2009b, Chen et al., 2013, Heidari et al., 2018). It is uncertain whether MSCs can independently induce the Treg phenotype in colitis, however it has been suggested that this process can occur without altering the levels of $CD103^+$ DCs which are thought to promote their development in the MLN (Takeyama et al., 2017). MSCs mediate the induction of Tregs in the MLN and spleen via paracrine mechanisms as demonstrated by the application of MSC-conditioned medium in experimental colitis (Heidari et al., 2018, Pouya et al., 2018). T-lymphocytes stimulated by MSCs acquire a Treg phenotype, isolation and subsequent administration of these cells attenuates colitis which exemplifies the importance of Tregs in mediating the therapeutic effect of MSCs (Gonzalez-Rey et al., 2009, González et al., 2009). Furthermore, when IL-10 or CD25+ cells were depleted using neutralising antibodies MSCs failed to elicit a therapeutic response which highlights the impact of MSC-Treg cross-talk in the amelioration of inflammation (Gonzalez-Rey et al., 2009). The phenotype of B-lymphocytes can also be altered by MSCs in experimental colitis. Administration of xenogeneic umbilical cord derived MSCs increased the population of Tregs in the MLN and spleen, in addition to $CD5^+$ regulatory B-lymphocytes (Bregs) (Chao et al., 2016). MSCs could directly promote the population of Bregs in splenic lymphocytes *in vitro*. When Bregs were administered in TNBS-induced colitis, inflammation was attenuated and populations of Tregs were increased. Moreover, Bregs could directly inhibit T-lymphocyte differentiation *in vitro* (Chao et al., 2016). The mechanisms of MSC-induction of Bregs, or the therapeutic effects of Bregs themselves, were undefined; however, these cells secrete high levels of IL-10 which is regularly associated with the immunosuppressive effects of MSCs in experimental colitis (**Table 1.3**).

Considering that the conditioned medium of MSCs attenuates experimental colitis; the MSC secretome is key to their therapeutic mechanism. Several studies have collected data on the colonic signalling milieu in experimental colitis after MSC treatment (**Table 1.3**). Depending on the design of the study, these factors could be

endogenous, as observed in xenogeneic studies, or contributed to by both MSCs and endogenous sources, as in syngeneic and allogeneic studies. IL-10 appears to be a key mediator of the immunosuppressive properties of MSCs, however unstimulated MSCs do not appear to secrete IL-10 in culture (Hwang et al., 2009, Melief et al., 2013). Therefore, the elevation in IL-10 is likely to be due to the polarisation of anti-inflammatory leukocytes. Nevertheless, TNF-α, IFN-γ and activation of TLRs can stimulate MSCs to secrete anti-inflammatory factors (English et al., 2007, Waterman et al., 2010). Thus, the potential for the pro-inflammatory cytokines or the microbiome to upregulate anti-inflammatory factors such as IL-10 should not be disregarded.

Elevations in TGFβ are observed concurrently with the therapeutic effects of MSCs in experimental colitis (**Table 1.2**). Likewise, changes in the levels of TGFβ parallel an increase in Tregs in the MLN and spleen (Heidari et al., 2018). Unlike IL-10, MSCs can actively secrete TGF-β1 *in vitro* (Amable et al., 2014). Inhibition of TGF-β1 signalling during MSC therapy inhibits their therapeutic effect in experimental colitis and moreover, recombinant TGF-β1 can replicate the therapeutic effect of MSCs (Wang et al., 2014, Liu et al., 2015). Together this demonstrates the significance of this molecule in the attenuation of inflammation. Nevertheless, some studies have suggested the MSCs actually secrete a relatively small amount of TGFβ and that Mφ2 are the major source of this cytokine in attenuating experimental colitis (Wang et al., 2014, Liu et al., 2015). The ablation of macrophages inhibits MSCs from attenuating colitis which suggest that their immunosuppressive properties are likely mediated by the secretion of anti-inflammatory cytokines from these cells (Liu et al., 2015). However, both immune cells and MSCs are likely to be required and appear to act synergistically. MSCs have been determined to secrete high levels of thrombospondin 1 (TSP1) which assists in the activation of latent TGFβ into its functional form (Takeyama et al., 2017). When TSP1 expression is knocked down, MSCs are unable to attenuate colitis or potentiate the Treg phenotype *in vivo*. Therefore, even if levels of TGFβ are not driven directly by the MSC secretome, it may be required to activate its immunosuppressive properties (Takeyama et al., 2017).

Matrix Gla protein (MGP) has also been recently identified as an important part of the MSC secretome in the attenuation of experimental colitis (Feng et al., 2018). Knockdown of MGP in MSCs revealed that it is partially responsible for decreasing the proliferation and the expression of TNF-α and IFN-γ in cytotoxic and Th lymphocytes *in vitro.* Similarly, MGP was required to reduce the levels of these cytokines and immune cells in experimental colitis (Feng et al., 2018). Notably, MGP expression is heterogeneous in MSC cell lines which could explain some of the variability in MSC treatments (Feng et al., 2018). Some studies have identified that TNF-stimulated gene 6 protein (TSG-6) may also play a role in therapeutic effects of MSC therapy. In these studies, knockdown of TSG-6 blocked xenogeneic and syngeneic MSCs from attenuating experimental colitis (Sala et al., 2015, Song et al., 2017c, Song et al., 2018). Moreover, TSG-6 was demonstrated to be necessary for MSCs to polarise macrophages to Mφ2 *in vitro* and in experimental colitis *in vivo* (Song et al., 2017c, Song et al., 2018). Together these studies demonstrate the complexity of the MSC secretome which contains many therapeutic factors that are likely to work synergistically to modulate inflammation via altering the inflammatory signalling milieu and activating immunosuppressive phenotypes in Mφ, DC and lymphocytes residing within the inflamed tissue.

1.2.9.3. Oxidative stress

Oxidative stress is emerging as a key contributor to the pathophysiology of IBD. A decline in scavenging of free radicals is reported in IBD patients (Lih-Brody et al., 1996, Koutroubakis et al., 2004). Moreover, markers of severe oxidative stress are evident in UC and CD patients (D'Inca et al., 2004, Pereira et al., 2016). In colitis, the activity of several enzymes that participate in the inflammatory response and the endogenous production of reactive oxygen species (ROS) can be increased including NADPH oxidase (NOX), nitric oxide synthase (NOS), lipoxygenase (LOX), cyclooxygenase (COX) and MPO (Piechota-Polanczyk and Fichna, 2014). Furthermore, ROS can directly upregulate several genes involved in the inflammatory response and increase mucosal permeability resulting in enterotoxic

and antigenic insult perpetuating the inflammatory response (Tian et al., 2017). The ability for MSCs to reduce oxidative stress is evidenced by the reduction in lipid peroxidation in experimental colitis (Sun et al., 2015, Zhang et al., 2015). However, the mechanism of MSCs in alleviating oxidative stress may require further exploration. Neutrophils produce a respiratory burst of free radicals including superoxide, hydrogen peroxide (H_2O_2) and hypochlorite generated by NOX and MPO (Zhang et al., 2002, Pattison and Davies, 2006). Many studies have demonstrated the MSCs reduce the levels MPO in experimental colitis (**Table 1.2**). Similarly, it has been reported that MSC treatments can reduce the expression of iNOS and its product nitric oxide (NO) which can react with ROS to form compounds that cause cellular damage via nitrosylation (Zhang et al., 2015, Song et al., 2018). Moreover, levels of the antioxidant glutathione are increased after MSC treatments (da Costa Gonçalves et al., 2017). MSCs increased the level or activity of the superoxide dismutase (SOD) which scavenges the highly reactive superoxide (Sun et al., 2015, da Costa Gonçalves et al., 2017). In intraperitoneal aggregates of MSCs and immune cells, high levels of haem oxygenase-1 was also observed which is important in the catabolism of haem which can contribute to the damage mediated by oxidative stress (Sala et al., 2015). Extracellular vesicles derived from MSCs have similar antioxidative effects and can reduce lipid peroxidation, COX2 and MPO levels and increase GSH and SOD (Yang et al., 2015). In MSCs isolated from CD patients, high levels of lactoferrin was expressed, which has ROS scavenging properties (Hoffman et al., 2018). The conditioned medium had an enhanced therapeutic capacity in experimental colitis compared to MSCs from uninflamed controls with low lactoferrin levels. Moreover, administration of lactoferrin reproduced many of the therapeutic effects of the MSC conditioned medium (Hoffman et al., 2018). Furthermore, MSCs have been demonstrated to reduce endoplasmic stress and the activation of the unfolded protein response in experimental colitis which is likely to contribute to oxidative stress via the generation of ROS in intestinal inflammation (Banerjee et al., 2015, Chong et al., 2017).

1.2.9.4. Neuroprotection

Intestinal inflammation results in neurally-controlled intestinal dysfunctions that manifest concurrently with damage to the nervous system within the gut (Poli et al., 2001, Hansen, 2003, Lomax et al., 2005, De Giorgio et al., 2007, Lakhan and Kirchgessner, 2010). Both the extrinsic and intrinsic enteric nervous system (ENS) can elicit anti-inflammatory phenotypes in populations of leukocytes (Tsuchida et al., 2010, Matteoli et al., 2014, Gabanyi et al., 2016). Therefore, the nervous system has been identified as a therapeutic target to remedy the symptoms and pathophysiology of IBD. Nevertheless, studies investigating the benefit of neuroprotective treatments in colitis are still limited. MSCs have proven to be potent neuroprotective agents in many models of disease in the central and peripheral nervous system (Bouchez et al., 2008, Karussis et al., 2008, Vercelli et al., 2008, Harting et al., 2009, Lanza et al., 2009, Ikegame et al., 2011, Lin et al., 2011a, Matthes et al., 2013, Payne et al., 2013a, Han et al., 2014b). Likewise, MSCs have also demonstrated neuroprotective efficacy for the ENS in TNBS-induced colitis in guinea-pigs. Xenogeneic human BM-MSCs ameliorated the loss of myenteric neurons and restored innervation of gut by enhancing the regrowth of nerve fibres (Robinson et al., 2014). Specifically, an increase in the proportions of cholinergic neurons and decrease in the number of nitrergic neurons were observed after MSC treatment (Robinson et al., 2014, Robinson et al., 2015). These results were associated with restored colonic motility which was initially disturbed by intestinal inflammation (Robinson et al., 2014). The neuroprotective properties of MSCs were dose-dependent (Robinson et al., 2017b). Similar results were observed using the MSC conditioned medium which demonstrated that these effects were mediated by paracrine signalling (Robinson et al., 2014). Likewise, allogeneic MSCs produced similar neuroprotective effects; however, BM-MSCs were more effective than those from AT-MSCs (Stavely et al., 2015a). Notably, this was the first study isolating, characterising and administering MSCs derived from the guinea-pig (Stavely et al., 2015a). Alterations to the ENS were associated with number of leukocytes in proximity to the myenteric ganglia which was attenuated

by MSC treatments (Robinson et al., 2015, Stavely et al., 2015a). This suggest that neuronal damage is likely mediated by the immune system and that MSCs may protect neurons by immunosuppression. Nevertheless, in *in vitro* experiments, guinea-pig MSCs attenuated LPS-induced neuronal loss in a paracrine manner which demonstrated that MSCs could directly protect enteric neurons (Stavely et al., 2015a). This is plausible given that MSCs secrete a variety of neuroprotective and trophic factors (Robinson et al., 2015, Stavely et al., 2015a). TGF-β1 signalling was identified as part of the neuroprotective actions of MSCs in this particular *in vitro* model (Stavely et al., 2015a).

1.2.10. Improving pre-clinical models

Pre-clinical studies have provided valuable insight into the mechanism of action of MSC treatments in intestinal inflammation and have identified avenues for optimisation of the therapy. Nevertheless, many mechanisms that have been outlined in acute animal models of IBD may not be replicated in the human pathology. This is highlighted by studies frequently identifying the promotion of Tregs after MSC treatments in experimental colitis which was not observed in the luminal inflammatory pathology of CD (Gregoire et al., 2018). Experimental studies that investigate the mechanism of MSC therapy are mostly performed in acute models of chemically-induced inflammation (**Figure 1.1E, Table 1.2**). Chronic models that better replicate the pathophysiology of IBD may be required to translate findings to the clinic. Previously the long-term effects of MSC treatments (33 days) have been modelled in DSS-induced colitis, however, MSCs were administered during the first cycle of exposure when the inflammatory profile would still be representative of acute inflammation (Lee et al., 2016). Studies that have determined the concordance of DSS and TNBS-induced colitis to IBD, by comparing their gene expression profiles, suggest that the accuracy of these models is modest. When comparing entire expression profiles from arrays, 16.1% (in 944 genes) concordance was observed in DSS-treated mice (Fang et al., 2010), and 12.5% (in 6142 genes) in TNBS-treated rats (Brenna et al., 2013). In another study, concordance was determined for a selected list of IBD-related genes (32 genes)

which demonstrated reasonable similarity in DSS-treated mice (46.9%) but suggested poor similarity in TNBS-treated mice (6.25%) (te Velde et al., 2007). The most common model of chronic intestinal inflammation is the IL-10 knockout mouse. However, considering that MSCs have been demonstrated to function via the endogenous secretion of IL-10, this model is not feasible to assess the therapeutic mechanisms of MSCs. Even so, only 68.5% concordance (92 genes) was observed with piroxicam-accelerated colitis in interleukin IL-10 knockout mice (Holgersen et al., 2015). *Winnie* mice appear to be a suitable chronic model of colitis that develops spontaneously without experimental intervention or the application of foreign compounds (Heazlewood et al., 2008, Eri et al., 2011). These mice possess a single point missense mutation in the *Muc2* (Mucin 2) gene. The protein is expressed, but is misfolded, triggering endoplasmic reticulum stress and the unfolded protein response in epithelial cells. This disrupts the epithelial barrier and decreases the number of mucin secreting goblet cells which triggers chronic inflammation with an onset at early adulthood similar to IBD (Heazlewood et al., 2008, Stavely et al., 2018a). Likewise, ER stress and altered mucin 2 production are evident in the pathophysiology of IBD and are implicated in its pathogenesis (Boltin et al., 2013, Cao, 2015). *Winnie* mice share many pathophysiological similarities to human UC and an analogous signalling milieu driving the inflammatory phenotype (Heazlewood et al., 2008, Eri et al., 2011, Rahman et al., 2015, Rahman et al., 2016, Robinson et al., 2017a). Considering that *Winnie* mice develop spontaneous chronic colitis without any intervention, this model may be robust and not subject to the variability of some techniques required to induce colitis. Ideally, the concordance of the inflammatory profile in these mice would need to be assessed to validate its accuracy as a model of IBD.

1.2.11. Screening the effects of MSC therapy

Using experimental models, several therapeutic mechanisms for MSC therapy in intestinal inflammation have been proposed. Together, these pre-clinical studies exemplify the multi-faceted function of MSCs. This appears to be one of the major advantages of MSC therapy. Current treatments that target one pathway, such as

biological therapies, are less effective than those targeting several inflammatory pathways, such as corticosteroids. Nevertheless, the complexity of MSC therapy and diverse mechanisms of action has led to some ambiguity in whether these many mechanisms are concurrent, or dependent, on experimental conditions. Furthermore, novel pathways effected by MSCs in colitis may yet be identified. Considering that both the function of MSCs and the pathophysiology of intestinal inflammation are multi-faceted, large-scale screening techniques may be a more efficient method to determine the multiple roles of MSC therapy and unify previously identified mechanisms.

RNA-Sequencing (RNA-Seq) is emerging as a powerful tool to explore changes to the entire transcriptome in disease. Specific pathways could be identified and then studied in detail, which may provide a more meticulous approach to elucidating the mechanisms of MSC therapy. Sequencing of the transcriptome has been performed in cohorts of IBD patients and uploaded to public data repositories with the aim of deciphering its pathogenesis and identifying novel therapeutic targets or biomarkers of the disease (Edgar et al., 2002, Barrett et al., 2012, Peters et al., 2017). Analysis of changes to the transcriptome can be grouped into simplified categories ('terms') by bioinformatics. Public databases are available that allow changes in groups of genes to be classified by their role in biological processes, molecular functions, cellular components, disease pathways and types of protein products (Ashburner et al., 2000, Kanehisa and Goto, 2000, Boutet et al., 2007, Finn et al., 2017). These groups can be analysed for 'enrichment' against all changes to identify terms with a high likelihood of relevance. This may assist in identifying the novel effects of MSC therapy in intestinal inflammation. Terms that contain changes in multiple related genes are detected using this method. Conversely, the transcriptome can be analysed by assessing the largest changes in gene expression. This is a respectable method for identifying disease biomarkers. However, this may be less effective to determine mechanisms of action: slight changes in several genes could have a greater or equal impact on a molecular pathway then a large change in one gene. This technology could be used in the future to take a personalised approach to medicine (Ozsolak and Milos, 2011). Enrichment analysis of functional terms may

be useful to identify analogous pathways in the pathophysiology of IBD, rather than individual genes that may not be affected in all patients. IBD is multi-faceted and the transcriptome is likely to vary between individuals; likewise, MSCs are heterogeneous. Therefore, MSCs may not function via the same pathways in all patients. Analysis of the transcriptome could help identify patients that are likely to respond to MSC treatments. In experimental models, RNA-Seq could be used to comprehensively investigate the changes induced by MSC treatments. In addition, comparing the transcriptome of pre-clinical models to IBD could assist in determining the probability of translating findings from experimental colitis to the human pathology.

1.2.12. Future outlook

Clinical trials have provided some insight to warrant further investigations into MSC therapy for the treatment of intestinal inflammation. At minimum, MSCs appear to be as efficacious as biological therapies in reducing disease activity and promoting remission, with the additional benefit of rarely being associated with severe side effects. Currently, MSCs can reduce the disease activity of IBD in subsets of patient's refractory to all other pharmaceutical options and may be suitable as an adjunct therapy. Data on the long-term safety of MSC treatments in IBD is limited at the present, however, retrospective follow-ups thus far are positive. Cellular therapies are highly dynamic and heterogeneous; this provides avenues for optimisation that can improve outcomes. Nonetheless several outstanding questions remain. It is uncertain how allogeneic MSC treatments will be tolerated after repeated exposure, or whether they offer more therapeutic benefit than autologous MSCs from IBD patients. Optimal dosages are still being explored and there is no consensus on what tissue source of MSC provides more therapeutic value. Furthermore, it is unclear how cryopreservation and expansion methods affect MSC efficacy and immunotolerance. Comparisons between the current literature is impractical due to multiple variables. Groups use different administration regimens, cell production methods and treat different cohorts making any extrapolations between studies equivocal. To optimise therapy

experiments must be performed that specifically address these questions. This may be performed in *in vivo* models of experimental colitis which can make an immediate impact on the clinic by identifying areas of focus for optimisation. Pre-clinal studies have revealed that MSCs can be applied by several novel administration methods that could be favourable due to enhanced efficacy or a lack of erroneous sequestration in healthy organs. Furthermore, many novel stem cell-based products are being developed and tested in experimental models. Many studies have also attempted to advance MSC treatments by using cytokine priming or genetic engineering which can improve outcomes. Further elucidating the mechanisms of action of MSC therapies will be useful to improve treatments. The immunosuppressive activity of MSCs and changes to immune cell populations have been studied extensively. The advancement of high-throughput screening techniques has offered an avenue to explore the multi-faceted therapeutic mechanisms of MSC treatments. Currently, acute models of chemically-induced colitis are utilised to study MSC therapy which largely differs from the pathophysiology of IBD on the molecular level. Future studies should be conducted in chronic models of intestinal inflammation that more accurately reflect the profile of IBD to optimise MSC therapy and decipher its mechanisms. Emerging research has demonstrated that MSCs offer neuroprotective and antioxidative properties that may contribute to the resolution of intestinal inflammation which warrants further investigation.

1.3. The Enteric Nervous System (ENS) in IBD

The ENS has been identified as a therapeutic target to remedy the symptoms and pathophysiology of IBD (Bernardazzi et al., 2016, Margolis and Gershon, 2016). Inflammation of the intestinal tract is associated with diarrhoea and/or constipation, hypersensitivity and pain. Many of these effects are caused via significant changes in neurally-controlled functions, including intestinal motility, secretion and gastrointestinal sensation (Lomax et al., 2005, Hons et al., 2009, Mawe et al., 2009). The ENS spans the length of the intestinal tract and is separated into two distinct plexuses, the submucosal and myenteric (**Figure 1.2**). Within the plexuses, neurons

and glial cells localise into a series of interconnected ganglia that intrinsically regulate intestinal processes including: vasomotor function, secretion, epithelial barrier permeability (submucosal plexus) and the coordination of motility (myenteric plexus) (Furness, 2012). Furthermore, immunomodulatory roles of myenteric neurons and glial cells are emerging (Tsuchida et al., 2010, Matteoli et al., 2014, Pochard et al., 2018). The enteric ganglia contain distinct subpopulations of neurons responsible for the various functions of the gastrointestinal tract. These neurons can be classified according to morphology, neurochemical coding, sites of innervation and electrophysiological properties (Costa and Brookes, 2008). Although the ENS receives sympathetic and parasympathetic input and provides sensory output to the central nervous system (CNS) via primary afferent sensory fibres of dorsal root ganglion (DRG) neurons, many functions can be conducted independently of extrinsic innervation via a nexus of intrinsic microcircuitry. Signalling of the submucosal and myenteric plexuses are not mutually exclusive. Myenteric neurons modulate the efferent functions of submucosal neurons. Moreover, submucosal neurons relay afferent signals to myenteric neurons; thus, bidirectional input is required for homeostatic functioning. The myenteric plexus also contains afferent neurons that project to the mucosa (intrinsic primary afferent neurons) which modulate its functions. However, synchronous muscle contractions are possible without any mucosal input which highlights the importance of myenteric neurons for regulating contractile reflexes in peristalsis. This reflex is mediated by cholinergic, excitatory muscle motor and interneurons, as well as nitrergic, inhibitory muscle motor neurons (Furness, 2000). Albeit, interstitial cells of Cajal which are responsive to excitatory and inhibitory signals from myenteric neurons are also crucial to propagating phasic contractions (Iino et al., 2004, Iino et al., 2008). In experimental colitis, MSCs were shown to attenuate dysmotility which highlights their potential to remedy dysfunctions in neurally-controlled processes induced by intestinal inflammation (Robinson et al., 2014).

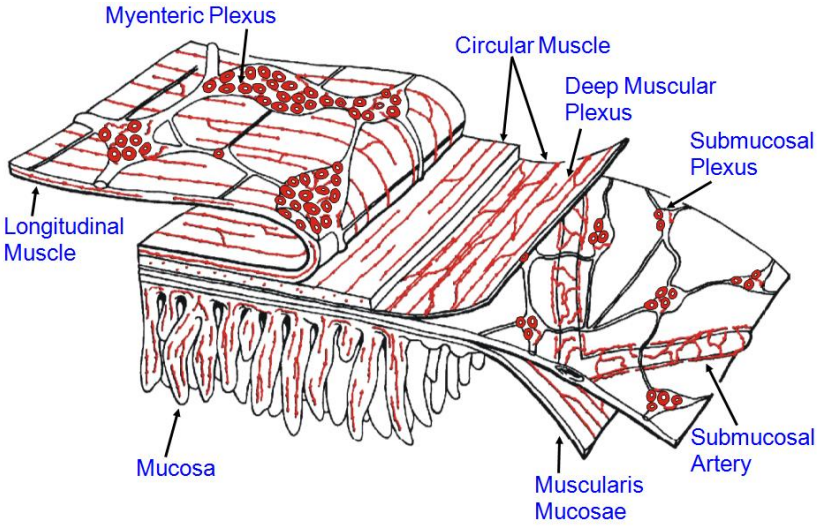

Figure 1.2 ***Arrangement of the enteric plexuses (Furness, 2006)***

Evidence that enteric neurons are closely involved in the pathophysiology of IBD can be deducted from the neurally-controlled gut dysfunctions that manifest concurrently with alterations to the ENS and intestinal inflammation in the human pathology and experimental colitis (Poli et al., 2001, Hansen, 2003, Lomax et al., 2005, De Giorgio et al., 2007, Lakhan and Kirchgessner, 2010). Many alterations to the ENS occur in response to inflammatory stimuli that may explain the abnormal functioning of the neuronal circuitry. Gross structural abnormalities are evident in IBD patients: alterations in nerve fibres and neuronal density are observed in intestinal biopsies (Bishop et al., 1980, Bernardini et al., 2012). This is also prevalent in experimental models of colitis which suggest that these changes are induced by inflammation (Boyer et al., 2005, Lin et al., 2005, Linden et al., 2005a, Sarnelli et al., 2009, Nurgali et al., 2011, Gulbransen et al., 2012). Nevertheless, these changes may be a predisposition to, or perpetuate, inflammation as a prior decrease in neuronal density is directly related to the severity of experimental colitis (Margolis et al., 2011). Intestinal inflammation can also alter the proportions of neurons with varying neurochemical coding in animal models and human IBD, which is not restricted to sites of active inflammation (Schneider et al., 2001, Neunlist et al., 2003a, Lin et al., 2005, Linden et al., 2005a, Boyer et al., 2007, Winston et al., 2013, de Fontgalland et al., 2014). These changes may be explained either by the dynamic nature of neurochemical coding, or the susceptibility for

certain subpopulations to be damaged. These studies demonstrate that conspicuous changes are evident on the level of the ganglia, however, the individual electrochemical properties of neurons are also influenced by intestinal inflammation. Ion channels in enteric neurons are altered following inflammation in humans and in experimental models (Arnold et al., 2003, Linden et al., 2003, Nurgali et al., 2007). Synaptic transmission and the release of neurotransmitters are also affected (Hons et al., 2009, Nurgali et al., 2009). Acute inflammation is a trigger for mechanisms of persistent hyperexcitability in enteric neurons of the ileum and colon (Linden et al., 2003, Nurgali et al., 2007, Nurgali et al., 2011). These electrophysiological changes correlate with disturbed intestinal motility that is persistent after inflammation is completely resolved (Krauter et al., 2007, Lomax et al., 2007a) providing evidence for inefficiency of enteric signalling to return to homeostasis after inflammation. These studies demonstrate a strong connection between the ENS and the immune system. The interaction between these two systems is justified given that in IBD and experimental colitis leukocyte infiltration is observed in close proximity to the enteric ganglia which is termed ‘plexitis’ (Sharkey and Mawe, 2002, Ferrante et al., 2006, Sokol et al., 2009, Bressenot et al., 2013). Enteric neurons are receptive to inflammatory mediators which can cause substantial excitation in humans and animals (Sharkey and Kroese, 2001, Schemann et al., 2005). Therefore, pro-inflammatory paracrine factors released by leukocytes can directly act on enteric neurons and alter their function. Plexitis is predictive of post-operative reoccurrence of IBD which exemplifies that the ENS contributes to the pathophysiology of intestinal inflammation (Ferrante et al., 2006, Sokol et al., 2009, Bressenot et al., 2013).

The prognostic value of plexitis and observations of altered enteric signalling or neurochemical coding in uninflamed areas could suggest that dysfunctions in the ENS precede the immune response; thus, contributing to the progression of the disease (Villanacci et al., 2008). In IBD, antigens or pathogen-associated molecular patterns (PAMPs) interact with leukocytes of the lamina propria which triggers an immune response and therefore inflammation. The ENS appears to have a role in averting the initial immunostimulatory interaction and supressing the subsequent

inflammatory response. Enteric neurons modulate the microbiome and reduce the number of bacteria that contribute to inflammation (Rolig et al., 2017). Mucin secretion by goblet cells is regulated by enteric neurons which provides adhesion sites for non-pathogenic bacteria and creates a barrier for pathogenic bacteria (Thorpe et al., 2013). Cholinergic stimulation of Paneth cells leads to the release of antimicrobial peptides; which provides a mechanism of direct antibiotic defences mediated by the ENS (Busch et al., 2014). These antimicrobial peptides are present in the colon which harbours most of the intestinal microbiome, however, the neurocrine regulation of bactericidal peptides has not yet been elucidated in this region. The physical barrier between luminal contents and the immune system is also strengthened by the ENS. Enteric neurons regulate the differentiation of epithelial stem cells and promote the release of anti-inflammatory factors that may assist in protecting the epithelial barrier (Puzan et al., 2018) Furthermore, submucosal neurons innervating the colonic mucosa maintain epithelial barrier integrity by promoting the expression of tight junction proteins (Neunlist et al., 2003b). Hypermotility is also responsible for the clearance of luminal pathogens and may have a therapeutic role in physiological conditions (Andersen et al., 2006). However, the effects of chronic accelerated transit in IBD on maintaining the physiological microbiome are unexplored. Together, dysregulation in the diverse functions of the ENS are likely to explain the predisposition to inflammation. Moreover, once inflammation is triggered, cholinergic myenteric neurons have been demonstrated to directly induce an anti-inflammatory phenotype in local populations of macrophages (Tsuchida et al., 2010, Matteoli et al., 2014). Thus, enteric neurons may also assist in directly supressing inflammation via neuromodulation. Nevertheless, the ability of enteric neurons, or the subsequently stimulated macrophages to further modulate inflammatory leukocytes in the mucosa or submucosa requires elucidation.

1.3.1. Neuronal loss

Low neuronal density is a predisposition to a higher severity of intestinal inflammation in experimental models; conversely, high neuronal density is

protective (Margolis et al., 2011) Therefore, neuronal loss may predispose or perpetuate intestinal inflammation. In models of acute colitis, neuronal loss is evident in response to inflammation in guinea-pig, mouse and rat models of TNBS or dinitrobenzenesulfonic acid (DNBS)-induced colitis (Sanovic et al., 1999, Boyer et al., 2005, Lin et al., 2005, Linden et al., 2005a, Sarnelli et al., 2009, Stavely et al., 2015a, Stavely et al., 2015b). Likewise, a reduction in the number of neurons is observed in chronic experimental colitis in *Winnie* mice (Rahman et al., 2016). Gross structural degeneration is observed within the enteric ganglia in inflamed regions of UC (Oehmichen and Reifferscheid, 1977, Riemann and Schmidt, 1982). Nonetheless, the quantification of neurons in biopsies from UC patients have been varied with reports observing an increase, decrease or no change (Storsteen, 1953, Neunlist et al., 2003a, Villanacci et al., 2008, Bernardini et al., 2012). This variability could be explained by the different methodology for quantifying neurons in these studies. More recently, Bernardini et al. (2012) observed that the ganglionated area increases by 59% in patients with UC. When neuronal counts were normalised to the size of the ganglia a 61% decrease in neuronal density was observed. This justifies observations from previous studies that have not normalised for size differences between the ganglia and reported no change, or an increase, in neuronal numbers (Storsteen, 1953, Neunlist et al., 2003a, Villanacci et al., 2008). In CD, increased apoptosis is evident in enteric neurons (Bassotti et al., 2009). However, a decrease in apoptosis is observed between patients with UC and controls (Bassotti et al., 2009). Nonetheless, extrapolation from studies using full-thickness biopsies can be equivocal as controls have undergone resection for neoplastic growth and neuronal loss can be caused by neoadjuvant chemotherapy, cancer-related cachexia and the tumours themselves (Janusz, 2010, McQuade et al., 2016, Vicentini et al., 2016). Previously, it was observed in a model of DNBS-induced colitis that cleaved caspase-3 can be present in the cytoplasm of neurons and other cells of the ganglia at 1.5 hours after instillation (Boyer et al., 2005). Furthermore, immunoreactivity for cleaved caspase-3 could not be detected after 4 hours. Only a small proportion of neurons expressed cleaved caspase-3 (1.4%) compared to the total number of neurons lost due to inflammation. Therefore, it is possible that damaged myenteric neurons do not exclusively undergo apoptosis in

the acute stages of inflammation. Furthermore, caspase-3 can also be important in executing physiological processes such as neuroplasticity and synapse formation in the central nervous system CNS, additionally, cellular stress in sensory neurons of the DRG leads to caspase-3 activation despite their perseverance (Cheng and Zochodne, 2003, D'Amelio et al., 2010). Therefore, it should be considered that neurons can be robust against traditional pathways of apoptosis and may express caspase-3 as part of their physiology. In other pathologies, apoptosis is not the only mediator of enteric neuronal loss (Bassotti et al., 2007). It is becoming increasingly recognised that neuronal death can occur via many pathways including caspase-independent apoptosis, various forms of necrosis and programmed necrosis, or necroptosis (Yakovlev and Faden, 2004). Many traditional cell death pathways are not always exclusive of one another and several novel pathways exist. Thus, investigations into cell death pathways other than apoptosis may explain the low numbers of apoptotic neurons despite significant neuronal loss in experimental colitis. Moreover, the mechanisms of neuropathy in chronic experimental inflammation are unestablished.

1.3.2. Plexitis and inflammation in the ENS

The induction of intestinal inflammation in animal models perturbs the ENS which is likely mediated by proinflammatory leukocytes. This is plausible given the occurrence of plexitis in chemically-induced colitis which accompanies neuronal damage, altered peristaltic reflexes and dysmotility (Sanovic et al., 1999, Boyer et al., 2005, Kinoshita et al., 2007). Plexitis is defined by abnormally high numbers of leukocytes that reside inside, or surround, the enteric ganglia (Lemmens et al., 2017, Milassin et al., 2017). This can include any of the leukocyte subpopulations if they are present in abnormally high quantities (Lemmens et al., 2017, Milassin et al., 2017). In IBD, several studies have indicated that submucosal and myenteric plexitis is an indicator of future inflammatory relapse when observed in non-inflamed segments of resected bowel (Ferrante et al., 2006, Sokol et al., 2009, Bressenot et al., 2013, Misteli et al., 2015, Lemmens et al., 2017, Milassin et al., 2017). This may suggest that enteric plexitis contributes to the progression of

intestinal inflammation. Both CD and UC associate with higher levels of mast cells near the submucosal ganglia as well as lymphocytes inside and surrounding the myenteric ganglia compared to control tissues from caecal adenocarcinoma patients (Lemmens et al., 2017). Lymphocytes and plasmocytes were detected in the submucosal and myenteric plexuses of CD patients (Milassin et al., 2017). Eosinophils and neutrophils were rarely detected (Milassin et al., 2017). Conversely, in experimental models of intestinal inflammation granulocytes are observed in proximity to enteric neurons which may mediate perturbations in the ENS (Sanovic et al., 1999, Sayani et al., 2004, Boyer et al., 2005, Filippone et al., 2018a). Eosinophils and neutrophils have both been associated with neuronal loss in models of DNBS-induced colitis (Sanovic et al., 1999, Boyer et al., 2005). Sanovic et al. (1999) demonstrated that eosinophils infiltrate to the myenteric plexus 6 hours after the initiation of colitis when neuronal loss begins to occur. Peak levels of neutrophil infiltration to the myenteric plexus occurred at 48 hours after DNBS administration; however, the greatest decline in neuronal numbers occurred 24 hours before. This suggests that eosinophils may play a larger role than neutrophils in inflammation-induced enteric neuropathy. This is supported by a recent study that also determined that eosinophilic plexitis was associated with neuropathy in guinea-pigs exposed to TNBS (Filippone et al., 2018a). Moreover, when the eotaxin-1/C-C chemokine receptor type 3 (CCR3) axis was inhibited, eosinophils failed to migrate, and neuronal loss was averted (Filippone et al., 2018a). The corticosteroid budesonide was shown to attenuate the activity of myeloperoxidase (MPO) which is predominantly expressed by neutrophils; this paralleled the aversion of neuronal loss (Sanovic et al., 1999). This is further illustrated by the application of antibodies specifically targeting neutrophils which also attenuated neuronal loss (Boyer et al., 2005).

Muscularis macrophages are typically the only resident leukocytes found in close proximity to the myenteric ganglia in physiological conditions (De Schepper et al., 2018). These cells exhibit a stellate morphology, similar to that of microglia in the CNS, and can regulate the physiological functions of myenteric neurons (Muller et al., 2014, De Schepper et al., 2018). Muscularis macrophages seed the intestine

prenatally, however, it has not been elucidated whether this pool takes residence throughout the lifespan, or whether they are repopulated by circulating monocytes (De Schepper et al., 2018). The role of macrophages in the physiological maintenance of the ENS is beginning to be elucidated; dysregulation in this system could potentially contribute to neuronal loss. It has been suggested that macrophages phagocytose myenteric neurons as a continual physiological mechanism of ganglionic remodelling (Kulkarni et al., 2017). The ganglia are reportedly repopulated by a local pool of adult progenitors capable of neuronal differentiation. Thus, loss of neuronal density could be reflective of an imbalance in neuronal phagocytosis and regeneration. It has been postulated that macrophages can migrate to the myenteric plexus in inflammatory conditions, and therefore, could contribute to the inflammatory signalling milieu involved in neuronal damage (Kinoshita et al., 2007). Nevertheless, the contribution of myenteric remodelling and neurogenesis in intestinal inflammation is equivocal as previous studies in chemically-induced colitis demonstrate that neuronal numbers do not increase despite the resolution of inflammation at timepoints up to 56 days after exposure (Sanovic et al., 1999, Lin et al., 2005, Linden et al., 2005a). However, other studies support the presence of neurogenesis in DSS-induced colitis which demonstrated that inflammation could cause an increase in the number of enteric neurons via a 5-Hydroxytryptamine (5-HT) receptor 4 (5-HT_4R)-dependent mechanism (Belkind-Gerson et al., 2015). Conversely, in the same model, decreases in neuronal density due to increased neuronal death were reported (Gulbransen et al., 2012). The controversial results of these studies highlight the complexity of the regulation of neuronal density in intestinal inflammation. This could be dependent on multiple factors including, but not limited to, the degree of inflammation, species, models of inflammation and methods of quantification. The microbiota and mucosal 5-HT levels can also affect neuronal density; both can be altered in inflammation and could contribute to some of the variability in these results (Bertrand et al., 2010, Robinson et al., 2016, De Vadder et al., 2018, Stavely et al., 2018b). Even so, neuronal numbers appear to be dynamic as they are subjected to cell death and remodelling depending on environmental cues that are obviously imbalanced in intestinal inflammation.

1.3.3. Immunomodulation

Early studies established that enteric neurons are responsive to cytokines which can modulate excitation and neurotransmitter release (Inoue et al., 1999, Xia et al., 1999, Kelles et al., 2000). Moreover, enteric neurons can express immuno-stimulatory cytokines and chemokines including TNF-α, IL-8 and C-C chemokine ligand 4 (Tixier et al., 2006, Coquenlorge et al., 2014). Likewise, it is becoming increasingly evident that neurotransmitters and neuropeptides can directly act on leukocytes to supress the immune system (Pacheco et al., 2010, de Jonge, 2013). However, the neurotransmitters acetylcholine (ACh), substance P and vasoactive intestinal peptide can also be produced by leukocytes associated with the innate and adaptive immune response (Delgado, 2003, Wessler and Kirkpatrick, 2008, Mashaghi et al., 2016, Fujii et al., 2017). This highlights the close interaction between the nervous and immune systems. Bilateral communication between these systems may be critical to mitigating an exuberant inflammatory response in the intestine. In the myenteric plexus, muscularis macrophages are the most probable leukocyte population to be regulated by enteric neurons by virtue of their proximity and receptivity to neurotransmitters. While these macrophages typically possess an Mφ2 phenotype, their dysregulation is becoming evident in the pathophysiology of various intestinal disorders including colitis (Kinoshita et al., 2007, De Schepper et al., 2018). The sympathetic nervous system can enhance the anti-inflammatory phenotype of muscularis macrophages which is mediated by the β2 adrenergic receptor (Gabanyi et al., 2016). Cholinergic myenteric neurons can also directly enhance the anti-inflammatory properties of muscularis macrophages (Tsuchida et al., 2010, Matteoli et al., 2014). This was achieved by the excitatory stimulation of cholinergic myenteric neurons via vagal afferent nerves or by activation of 5-HT_4R (Tsuchida et al., 2010, Matteoli et al., 2014). These studies demonstrate that myenteric neurons stimulated artificially can modulate the local immune response; however it is predicted that intrinsic reflexes may have a similar role (Chavan et al., 2017). It has been established in models of chemically-induced colitis that pro-inflammatory mediators can supress cholinergic neurotransmission in the ENS (Xia

et al., 1999, Kelles et al., 2000). Dysregulation in cholinergic signalling is prominent in acute and chronic models of intestinal inflammation which contributes to dysmotility (Poli et al., 2001, Robinson et al., 2017a). Furthermore, tobacco smoking can independently promote remission or reduce the incidence and severity of disease in UC, which is likely mediated by nicotine (McGrath et al., 2004, Thomas et al., 2005). Therefore, it is plausible that dysregulation in nicotinic neurotransmission may contribute to the pathophysiology of the disease. Previously, it was identified by our group and others that choline acetyltransferase (ChAT; ACh synthesis) immunoreactive neurons or vesicular acetylcholine transporter (VAChT; ACh vesicular packaging) expression are reduced in acute and chronic experimental models of colitis, as well as in UC patients; this was often associated with enteric neuropathy (Neunlist et al., 2003a, Lin et al., 2005, Robinson et al., 2014, Rahman et al., 2015, Robinson et al., 2015, Stavely et al., 2015a, Stavely et al., 2015b, Rahman et al., 2016, Robinson et al., 2017b). If cholinergic myenteric neurons are responsible for maintaining the anti-inflammatory phenotype of resident leukocytes, then this may provide one mechanism of how decreased neuronal density increases the severity of intestinal inflammation. Conversely, intestinal neurotransmitters or neuropeptides may have a role in promoting intestinal inflammation (de Jonge, 2013). Neuropeptide Y (NPY) has been implicated in DSS-induced colitis where it is upregulated and has a pro-inflammatory role which may be mediated by the NPY Y1 receptor (Hassani et al., 2005, Chandrasekharan et al., 2008). Substance P and CGRP release from sensory nerve fibres have also been associated with establishing inflammation in chemically-induced colitis (Engel et al., 2011, Engel et al., 2012). Leukocytes are directly receptive to both neuropeptides (Stanisz, 2001, Assas et al., 2014). High levels of substance P have been reported in the inflamed regions of UC, which includes expression in the myenteric ganglia (Goldin et al., 1989, Neunlist et al., 2003a). While substance P induces the secretion of pro-inflammatory mediators, CGRP may confer an anti-inflammatory effect in experimental acute colitis which appears to be inefficient in UC (Stanisz, 2001, Engel et al., 2012, Li et al., 2013a). Enteric glial cells may also contribute to chronic intestinal inflammation (Pochard et al., 2018). The glial cell specific protein S100 calcium-binding protein B (S100B)

is upregulated in UC patients, and when released, may stimulate the secretion of inflammatory mediators (Cirillo et al., 2009, Cirillo et al., 2011, Capoccia et al., 2015). Together these studies highlight that the nervous system can modulate the immune response and is not merely a bystander to intestinal inflammation. Several of these mechanisms appear to be dysregulated in IBD which exemplifies the role of the nervous system in the pathophysiology of the disease.

1.3.4. Oxidative stress in the ENS

Oxidative stress and the immune response are heavily interlinked in inflammatory disorders. Reactive oxygen species (ROS) up-regulate the production of pro-inflammatory cytokines; likewise, pro-inflammatory cytokines can promote mitochondrial superoxide production and the expression of nitric oxide synthase (NOS) (Bhat et al., 1999, Naik and Dixit, 2011, Cao et al., 2013). Oxidative stress is prominent in experimental models of chemically-induced colitis and IBD (Lih-Brody et al., 1996, Sundaram et al., 2003, Lakhan and Kirchgessner, 2010, Roberts et al., 2013, Piechota-Polanczyk and Fichna, 2014). The observation that oxidative stress can precede the onset of the immune response is suggestive of its contribution to the pathophysiology of chronic intestinal inflammation (Rezaie et al., 2007). Although pro-inflammatory mediators can alter the ENS, oxidative stress could also contribute to its damage and dysregulation. In general, neurons are particularly susceptible to oxidative insult from free radicals which is a result of their higher energy demand and O_2 consumption, excess mitochondria-derived superoxide, autooxidation of neurotransmitters, excitotoxicity, poor antioxidant defences and limited replicative potential (Friedman, 2011). Neurons of the ENS also appear to exhibit a sensitivity to oxidative stress which has been implicated in neuronal damage in models of chemotherapy, diabetes and physiological aging (Thrasivoulou et al., 2006, Chandrasekharan et al., 2011, McQuade et al., 2016, McQuade et al., 2018). In a diabetic model, resident macrophages were also shown to be affected by oxidative stress which can result in the loss of their anti-inflammatory phenotype (Choi et al., 2008). Therefore, the ENS is not exempt from the interplay between oxidative stress and the immune system. Similarly, oxidative

stress is predicted to be a key contributor to ENS dysfunction in the pathophysiology of IBD (Lakhan and Kirchgessner, 2010). This is illustrated in chemically-induced colitis which causes oxidative stress in the ENS, and consequentially, dysfunction in neurally-controlled intestinal functions (Roberts et al., 2013). In a model of parasitic ileitis, the largest changes in lipid peroxidation were observed in the muscle layers compared to mucosa and plasma (Sundaram et al., 2003). Therefore, the muscle layers of the intestine may be susceptible to oxidative injury. Likewise, myenteric neurons contained within the muscle layers are not resistant to oxidative stress induced by intestinal inflammation (Brown et al., 2016). Oxidative stress alters the electrophysiological properties of enteric neurons, damages neuronal membranes and can cause neuronal death (Gaginella et al., 1992, Wada-Takahashi and Tamura, 2000, Roberts et al., 2013, Brown et al., 2016). In intestinal inflammation, the neuropathic role of oxidative stress in mediating neuronal cell death is exemplified by the administration of the antioxidant N-acetyl cysteine (NAC) which attenuates neuronal loss *in vivo* (Brown et al., 2016). Additionally, NAC did not appear to directly ameliorate the inflammatory response which suggests that oxidative insult in colitis contributes more to neuropathy than pro-inflammatory cytokines. In the same study high levels of oxidised glutathione (GSSG)/reduced glutathione (GSH) were observed indicating that myenteric neurons were under an oxidative reduction-oxidation (redox) environment. Furthermore, high levels of the free radical, superoxide ($O_2^{\cdot -}$), were observed in the myenteric plexus. An increase in $O_2^{\cdot -}$ derived specifically from the mitochondria can be observed concomitantly with enteric neuropathy after chemotherapy (McQuade et al., 2016, McQuade et al., 2018). Therefore, mitochondrial-derived $O_2^{\cdot -}$ could also be responsible for neuronal loss in intestinal inflammation which requires elucidation. Hydrogen peroxide (H_2O_2) is another free radical which is prevalent in the muscle layers of the colon in TNBS and DSS models of colitis (Shi et al., 2010). Oxidative stress in enteric neurons is commonly modelled by applying this compound to enteric neuronal cell lines and primary cultures which highlights its potential neurotoxicity (Lourenssen et al., 2009, Pouokam et al., 2009, Abdo et al., 2010, Korsak et al., 2012, Bianco et al., 2016, Bubenheimer et al., 2016). Nevertheless, $O_2^{\cdot -}$ and H_2O_2 are not mutually exclusive;

increased mitochondria-derived $O_2^{\cdot -}$ levels parallel cytosolic H_2O_2 concentrations and exogenous H_2O_2 can increase $O_2^{\cdot -}$ production (Aon et al., 2010).

Myenteric neurons appear to exhibit the highest density of mitochondria in the muscular region which may rationalise their susceptibility to increases in $O_2^{\cdot -}$ production in pathological conditions (Berghe et al., 2002). The local oxygen gradients could also affect ROS generation by the mitochondria and the redox balance. Excessive ROS is produced at a lower-energy oxidative environment or at a higher-energy reductive environment (Aon et al., 2010). A reductive environment is usually attributed to hypoxic conditions and tissue hypoxia has been studied in depth in the brain as a cause of neuronal loss (Choi, 1995). However, in intestinal inflammation, the redox environment of myenteric neurons is oxidative, and thus, may not be hypoxic (Brown et al., 2016). Under physiological conditions, the kinetics of $O_2^{\cdot -}$ production by the mitochondria are directly proportional to the levels of O_2; this has been demonstrated in neurons (Kwak et al., 2006, D'Agostino et al., 2007, Murphy, 2009, Matott et al., 2014). Therefore, there is also potential for an hyperoxic environment to cause neuronal damage (Chang et al., 2007). The mitochondria are also critical to maintaining the electrophysiological properties of myenteric neurons. Inhibiting complexes of the electron transport chain (ETC) causes mitochondrial dysfunction and increases cytosolic Ca^{2+} which results in sustained hyperpolarisation (Berghe et al., 2002). Neurons are dependent on the mitochondria, Ca^{2+} signalling and ion transport for homeostatic signalling; oxidative stress can cause dysfunction in all of these processes, thus, providing a potential explanation for their perturbed function under oxidative conditions (Kourie, 1998, Görlach et al., 2015). Likewise, a high Ca^{2+} load is associated with increased mitochondria-derived ROS and can contribute to cell death through the voltage and Ca^{2+}-dependent mitochondrial permeability transition pore. The co-dependency of ROS and Ca^{2+} transport in enteric neurons may explain their propensity for oxidative stress-induced neuropathy. The nitrosative product, nitric oxide (NO), is also considered to contribute to oxidative stress. $O_2^{\cdot -}$ and NO can react to form the compound peroxynitrite which damages proteins, lipids and DNA (Dijkstra et al., 1998, Pacher et al., 2007). It has been demonstrated *in vivo* that

oxidative stress is associated with a selective loss of neuronal NOS (nNOS) immunoreactive enteric neurons which may be explained by a nitrosylating mechanism of damage (Rivera et al., 2011a, Rivera et al., 2011b). Similar observations are made when oxidative stress is induced artificially in enteric neurons *in vitro* using menadione sodium bisulphite (Voukali et al., 2011). However, in intestinal inflammation neuronal loss appears to be indiscriminate of neurochemical coding and nNOS expressing neurons are not specifically decreased (Linden et al., 2005a, Winston et al., 2013, Stavely et al., 2015a, Stavely et al., 2015b, Bubenheimer et al., 2016).

1.4. MSCs in Oxidative Stress

MSCs have been used as tools to treat a plethora of diseases associated with inflammation both in animal models and clinical trials. Extensive research has established the anti-inflammatory and trophic value of MSCs treatments; however, many gaps in knowledge remain. The effect of MSC treatments on oxidative injury is one aspect that has been widely overlooked. Recently, the role of MSCs in ameliorating oxidative stress has received considerable attention in several studies.

1.4.1. MSCs are resistant to oxidative stress

MSCs themselves are highly resistant to oxidative insult. The effects of ionising radiation are limited on MSCs which has been attributed to their ability to scavenge free radicals (Chen et al., 2006). Valle-Prieto and Conget (2010) demonstrated that MSCs were resistant directly to oxidative and nitrosative stimulus *in vitro* and associated this with constitutively expressed antioxidant enzymes SOD1, SOD2, catalase (CAT) and glutathione peroxidase (GPx), in addition to high levels of total glutathione. Depletion of the latter resulted in a loss of tolerance to oxidative stress. Notably, MSCs appear to possess a unique ability to share their constitutively expressed antioxidant factors with other cells and the microenvironment; such as SOD1, which is not usually secreted by cells (Klein et al., 2017). In addition to wielding constitutive antioxidants, MSCs are also capable of significant adaptions

in response to redox stress. MSCs exposed to LPS produce oxidative and nitrosative free radicals (Gorbunov et al., 2013). In parallel, several adaptive processes are observed including the upregulation and/or nuclear translocation of redox-sensitive factors (nuclear factor kappa-light-chain-enhancer of activated B lymphocytes, NFκB; thioredoxin, TRX1; apurinic/apyrimidinic endodeoxyribonuclease 1, APEX1/REF1; nuclear factor erythroid 2–related factor 2, NRF2; forkhead box O3, FOXO3 and haem oxygenase 1, HO-1), as well as mitochondrial remodelling and autophagy. MSCs were also observed to constitutively express heat-shock protein 70 (HSP70) and NAD-dependent deacetylase sirtuin-3, mitochondrial (SIRT3) (Gorbunov et al., 2013), which may also play a role in the resistance of MSCs to oxidative/nitrosative injury. The advantageous ability of MSCs to tolerate and respond to the oxidative environment may be critical to their engraftment and therapeutic efficacy in sites of tissue injury.

1.4.2. MSC treatments reduce oxidative stress

A hallmark of high oxidative/nitrosative stress is damage to DNA, lipids and proteins. In the rat kidney, DNA oxidation was reduced by administration of allogeneic BM-MSCs after ischemia-reperfusion injury (Liu et al., 2012). In the same tissue, DNA oxidation was reduced after cisplatin-induced injury using exosomes derived from human UC-MSCs; these results were confirmed *in vitro* with renal proximal tubular cells (Zhou et al., 2013). The same authors also observed a reduction in lipid peroxidation both *in vivo* and *in vitro* (Zhou et al., 2013). A similar reduction in lipid peroxidation has also been observed in allogeneic models of spontaneous stroke, LPS-induced lung injury and testicular torsion injury in rats (Pulavendran et al., 2010, Calió et al., 2014, Hsiao et al., 2015). Additional studies in mice investigating allogeneic BM-MSC application in hepatotoxic injury and *E. coli*-induced lung injury, also observed decreased lipid peroxidation (Pulavendran et al., 2010, Shalaby et al., 2014). In these studies, Pulavendran et al. (2010) demonstrated that MSCs were more efficacious than haematopoietic stem cells at reducing lipid peroxidation in the liver. Therefore, antioxidative properties appear to be specific to MSCs. The timing of treatments

may also affect their ability to attenuate lipid peroxidation. Shalaby et al. (2014) demonstrated that MSC administration during inflammation was less effective than MSC pre-treatment to avert lipid peroxidation in the lungs. In a model of canine spinal cord injury, allogeneic AT-MSCs also demonstrated antioxidant activity with a reduction in lipid peroxidation and protein oxidation, however no significant effects were observed for nitrosylation (Kim et al., 2015). Many studies have observed a reduction in inflammation-induced iNOS and nNOS expression after MSC treatment (Shalaby et al., 2014, Robinson et al., 2015, Stavely et al., 2015a, Stavely et al., 2015b, Song et al., 2018). However, NO can be produced by non-human MSCs which is critical to their immunomodulatory function and may explain their inefficacy in attenuating nitrosylation in some models (Ren et al., 2009, Kim et al., 2015). While the effects of MSCs on nitrosative stress are unclear, these studies are in agreement that MSCs can reduce markers of oxidative stress.

1.4.3. Antioxidative mechanisms of MSCs

The potential for MSCs to attenuate oxidative injury is unequivocally demonstrated by the reduction in lipid peroxidation, DNA and protein oxidation in several models of disease. Nonetheless, the mechanism of MSC action remains ambiguous and is likely disease dependent (Iyer et al., 2010, Pulavendran et al., 2010, DeSantiago et al., 2013, Shalaby et al., 2014). Current literature indicates that the protective effects of MSC therapy in oxidative injury can be explained by their ability to modulate the inflammatory response, enhance antioxidant defences, avert perturbations of mitochondrial function, augment oxidative phosphorylation, manipulate mitochondria-associated cell death signalling, or a combination of these mechanisms (Iyer et al., 2010, Pulavendran et al., 2010, DeSantiago et al., 2013, Shalaby et al., 2014).

1.4.3.1. Inflammation and free radicals

Immune function is regulated by free radicals and the redox system; leukocytes and pro-inflammatory mediators enhance the formation of free radicals and perturb the

redox environment creating a positive feedback cycle (Kim et al., 2013b). The immunomodulatory action of MSCs is a well-documented phenomenon, however their role in the interactions between the immune system and oxidative stress is poorly understood. It was previously demonstrated that allogeneic BM-MSC treatment can reduce markers of inflammation in the serum including pro-inflammatory cytokines and perturbed thiol/disulphide redox pairings responsible for free radical scavenging (Iyer et al., 2010). Decreased levels of IL-1β and TNF-α superseded restoration of redox homeostasis. This suggests that the aversion of oxidative injury is secondary to the immunomodulation of pro-inflammatory signalling, at least in acute inflammation. Neutrophils appear to be key mediators of oxidative stress in inflammation. These cells harbour an abundance of MPO, a major catalyst for hypochlorite and NO-derived oxidants (Zhang et al., 2002, Pattison and Davies, 2006). MSCs have been demonstrated to attenuate the infiltration of neutrophils and reduce MPO levels in several disease models (Gonzalez-Rey et al., 2009, Pulavendran et al., 2010, El-Attar et al., 2012). Furthermore, MSCs can dampen the respiratory burst of neutrophils and ameliorate their deleterious effects by the upregulation of SOD3 (Raffaghello et al., 2008, Jiang et al., 2016). Conversely, several *in vitro* studies demonstrate that MSCs directly reduce oxidative injury in many cell types; thus, the antioxidative properties of MSC therapy may not solely be explained by the immunomodulation of leukocytes (Kim et al., 2008, Liu et al., 2010, Ohkouchi et al., 2012, DeSantiago et al., 2013, Zhou et al., 2013, Cui et al., 2017). This is highlighted in *in vivo* and organotypic *in vitro* models of myocardial ischemia-reperfusion injury where MSC-derived exosomes ameliorated infarction injury without altering leukocyte recruitment (Arslan et al., 2013). In *in vivo* experiments, protein oxidation was reduced by MSC-derived exosomes after one hour; neutrophils were yet to infiltrate into the tissue. After 24 hours, MSCs reduced peripheral blood leukocyte numbers and neutrophil infiltration into the myocardium; thus, the antioxidative activity of MSCs preceded the infiltration of leukocytes (Arslan et al., 2013). This suggests that MSCs can attenuate oxidative stress-induced tissue injury which can limit the recruitment of immune cells and subsequent inflammation.

1.4.3.2. Antioxidant defence and scavenging

The antioxidant effects of MSCs may be explained by their ability to improve levels of several antioxidant defences as demonstrated in *in vivo* and in cell culture experiments. In endotoxin-induced sepsis, MSC treatments improved levels of reduced cysteine and glutathione indicating normalisation of the redox system (Iyer et al., 2010). Exosomes derived from human umbilical cord MSCs were also observed to increase GSH in cisplatin-induced renal injury both *in vivo* and *in vitro* (Zhou et al., 2013). Likewise, an increase in GSH is observed after MSC treatment in the injured lungs of *E.coli*-exposed mice (Shalaby et al., 2014). The authors reported an increase in GPx and glutathione reductase which catalyses the reduction of GSSG to GSH which may explain these observations. In addition, MSCs increased the expression of CAT and SOD which was also previously reported in a model of hepatotoxic injury (Pulavendran et al., 2010, Shalaby et al., 2014). Enhanced expression of the redox regulated antioxidant enzyme HO-1 has also been reported in a model of BM-MSC-treated renal ischemia-reperfusion injury (Liu et al., 2012). Considering that MSCs can express most of these antioxidant enzymes, it is equivocal whether the tissues stimulated by MSCs, or the engrafted MSCs themselves contributed to the increased expression of antioxidant defences (Gorbunov et al., 2013, Klein et al., 2017).

Studies using MSC-conditioned medium are suggestive that paracrine secretion of antioxidants and scavengers by MSCs may attenuate oxidative stress. Media that is conditioned by MSCs has an enhanced antioxidant capacity which is reflective of the factors secreted by MSCs (Kim et al., 2008). MSC-conditioned medium is a more effective antioxidant for hydroxyl radicals than medium conditioned by lung fibroblasts which illustrate the unique antioxidant properties of MSCs (Waszak et al., 2012). Extracellularly secreted SOD3 is thought to be a major contributor to the antioxidant properties of MSCs which is synergistically promoted by TNF-α and IFN-γ and correlates with their ability to rescue neurons from NO-induced cell death *in vitro* (Kemp et al., 2010). Neuroprotection was suggested to be achieved by averting peroxynitrite formation.

These studies support the concept that MSCs can directly scavenge free radicals in a paracrine manner; however, MSC could also alter endogenous antioxidant defences and ROS production in the host. In *in vitro* studies, ROS generated by H_2O_2-stimulated alveolar basal epithelial adenocarcinoma cells was decreased in transwell co-culture with BM-MSCs as indicated by the cellular probe 6-carboxy-2',7'-dichlorodihydrofluorescein diacetate (Ohkouchi et al., 2012). A similar result was observed with the conditioned medium from human placental MSCs in tert-Butyl hydroperoxide treated umbilical endothelial cells (Liu, 2010). In this study, MSC-CM increased SOD2 protein expression in umbilical endothelial cells on the transcriptional level which was regulated by glycoprotein 130 (gp130)-signal transducer and activator of transcription (STAT3) signalling. Knockdown of either SOD2 or STAT3 in endothelial cells decreased the anti-apoptotic effects of the MSC-conditioned medium. Using the same oxidative stimulus, the conditioned medium from AT-MSCs can promote the activity or levels of SOD and GPx in human dermal fibroblast (Kim et al., 2008). *In vivo*, allogeneic BM-MSC treatments were shown to reduce $O_2^{\cdot -}$ production in a rat model of spontaneous stroke which highlights the therapeutic potential of SODs secreted by MSCs and/or upregulated in cells targeted by MSCs (Calió et al., 2014).

1.4.3.3. Mitochondria, oxidative phosphorylation and bioenergetics

Dysfunction in mitochondria can cause cellular injury which is mediated through the generation of $O_2^{\cdot -}$ and proteins that initiate cellular apoptosis. Depolarisation of the mitochondrial membrane potential (Ψ_{mito}) is a hallmark of mitochondrial dysfunction and pending cell death. The potential for MSCs to directly attenuate Ψ_{mito} dysfunction has been demonstrated in an *in vitro* model of ischemia-reperfusion injury in mouse ventricular myocytes (DeSantiago et al., 2013). Within five minutes of reperfusion, cells exhibited an exaggerated mitochondrial membrane hyperpolarisation which was reduced by conditioning the reperfusion solution with MSCs. The exaggerated hyperpolarisation was followed by a continuous depolarisation in controls after 15 minutes which was also attenuated

by the paracrine secretion of MSCs. Decay of the Ψ_{mito} was likely a result of the mitochondrial permeability transition pore opening. The exaggerated hyperpolarisation of the Ψ_{mito} was also averted by a mitochondrial ROS scavenger which simultaneously decreased mitochondrial $O_2^{\cdot -}$ generation demonstrating the close relationship between these events. Similarly, MSC secretion decreased mitochondrial $O_2^{\cdot -}$ which led to the suggestion that MSCs may also attenuate Ψ_{mito} dysfunction via scavenging of $O_2^{\cdot -}$. Depolarisation of the Ψ_{mito} in cisplatin-treated renal proximal tubular cells has also been reportedly attenuated using exosomes derived from umbilical cord MSCs (Zhou et al., 2013). *In vitro*, BM-MSC were demonstrated to upregulate uncoupling protein 2 (UCP2) transcription in H_2O_2-treated alveolar basal epithelial adenocarcinoma cells which reduces the formation of mitochondria-derived $O_2^{\cdot -}$ by lowering the proton-motive force across the mitochondrial membrane and provides another potential mechanism for the alleviation of mitochondrial dysfunction (Ohkouchi et al., 2012). This was regulated by the paracrine secretion of stanniocalcin-1 by MSCs which enhanced UCP2, correlating with cell survival and decreased ROS generation. MSCs secreted stanniocalcin-1 may also attenuate inflammation as it decreases mitochondrial ROS and subsequent activation of the nucleotide-binding oligomerization domain (NOD)-like receptor protein 3 (NLRP3) inflammasome (Oh et al., 2014). BM-MSCs inhibited the activity of the NLRP3 inflammasome in primed macrophages, which are overactive in IBD, and is responsible for recognising damage-associated molecular patterns (DAMPs) and initiating the inflammatory cascade through activation and secretion of IL-1β (Lazaridis et al., 2017, Liu et al., 2017). Collectively, these studies demonstrate that MSCs can ameliorate mitochondrial dysfunction in a paracrine manner with diverse therapeutic outcomes.

Recently, a concept has emerged that MSCs may be able to alter oxidative phosphorylation and bioenergetics in cells through donation of mitochondria themselves. Phinney et al. (2015) observed that oxidative stress caused by *in vitro* culture of MSCs in hyperoxic (21% O_2: normoxic atmosphere) conditions promoted the generation of mitochondrial $O_2^{\cdot -}$, Ψ_{mito} depolarisation and subsequent mitophagy with mitochondria loaded into phagosomes and shuttled to the plasma

membrane. These effects were reduced by culturing MSCs closer to a normoxic oxygen concentration (5% O_2: hypoxic atmosphere). Macrophages engulfed the blebs containing the partially depolarised mitochondria which fused with mitochondria endogenous to the macrophages. MSCs and exosome-treated macrophages exhibited altered bioenergetics which attenuated both their decreased oxygen consumption rate and increased mitochondrial $O_2^{\cdot -}$ production induced by silica *in vitro*; however, these effects could not be elicited when human fibroblasts were substituted for MSCs. In a mouse model of silica-induced lung injury, GAPDH transcripts for human BM-MSC derived-exosomes and fibroblasts disappeared after 14 days (Phinney et al., 2015). However, mitochondrial human cyclooxygenase-1 transcripts were observed at day 28 in only human BM-MSC and exosome treated animals suggesting that MSCs can transfer mitochondria *in vivo* across the xenogeneic barrier. Similarly, Islam et al. (2012) observed mitochondrial transfer from human BM-MSCs to alveolar epithelium in a mouse model of LPS-induced lung injury. This phenomenon only occurred in the LPS-treated lung and was not observed in phosphate buffered saline-treated animals. BM-MSC administration attenuated decreased intracellular ATP in the alveoli caused by lung injury; notably ATP (visualised by a molecular probe) was predominantly restored at the site of mitochondrial transfer and immediately surrounding alveoli. MSCs with a mutation in connexin 43, a protein involved in the formation of gap junctions, were unable transfer mitochondria despite being functionally competent and subsequently did not restore ATP, surfactant secretion or reduce leukocyte infiltration. The therapeutic use of MSCs to deliver functional mitochondria to damaged tissue is an intriguing concept and warrants further study; however, another recent advancement reported by Panfoli et al. (2016) suggests that the exosomes of MSCs are capable of oxidative phosphorylation independent of the mitochondria. Subsets of MSC-derived exosomes isolated from the umbilical cord of term newborns were discovered to contain complexes of the electron transport chain (ETC) embedded in the membrane. These exosomes possessed an electrochemical membrane potential, consumed O_2 and produced ATP. The therapeutic application of these exosomes is yet to be investigated, nonetheless, this

may present a viable tool to restore dysfunctional oxidative phosphorylation and ATP synthesis in damaged cells.

1.4.4. Cell death signalling axis

It has been well-established that an oxidative environment initiates cell death signalling (Ryter et al., 2007). Many studies have investigated mitochondrial pathways of apoptosis to explain the protective effects of MSC therapy in tissue injury and cell death (Li et al., 2008, Xiang et al., 2009, Lin et al., 2011a, Qi and Wu, 2013, Aziz et al., 2014, Hsiao et al., 2015, Li et al., 2015, Qin et al., 2015, Gu et al., 2016). The B-cell lymphoma 2 (BCL-2) family of apoptotic regulators contain proteins responsible for mediating the permeabilisation of the outer mitochondrial membrane (Bcl-2-associated X, BAX; Bcl-2 interacting killer, BIK; BH3 interacting-domain death agonist, BID) via their insertion and formation of homomeric and heteromeric pores; contrarily, this protein family also contains inhibitors that intercept their proapoptotic counterparts (BCL-2, BCL-xL) (Shamas-Din et al., 2013). Upon outer mitochondrial membrane permeabilisation, soluble apoptogenic factors are released into the cytoplasm and initiate apoptosis via caspase dependent mechanisms. Thus, the effect of MSCs on the balance between members of the BCL-2 family have been investigated in several studies to elucidate their cytoprotective properties.

Human MSCs decrease levels of BAX in models of testicular torsion injury and the quinolinic acid model of Huntington's disease (Lin et al., 2011a, Hsiao et al., 2015). Rat BM-MSCs can also reduce BAX levels in oxygen and glucose deprived adrenal pheochromocytoma (PC12) cells *in vitro* (Gu et al., 2015). These studies suggest that MSCs reduce proapoptotic signalling; additionally, allogeneic BM-MSCs treatments can also increase levels of anti-apoptotic BCL-2 in spontaneous stroke. Allogeneic rat BM-MSCs have been observed to both downregulate BAX and upregulate BCL-2 in models of streptozotocin-induced diabetic nephropathy, D-galactosamine and LPS-induced acute liver injury and cisplatin-induced acute kidney injury (Qi and Wu, 2013, Aziz et al., 2014, Cai et al., 2015). Similarly, AT-

MSCs increase Bcl-xL and concomitantly decrease BAX in radiation-induced thrombocytopenia; fibroblasts have no effect, which illustrates that this is a unique property of MSC treatments (Zhang et al., 2016). Likewise, MSCs can alter levels of these apoptotic proteins in cisplatin-treated renal proximal tubular cells *in vitro*, which suggests that this effect is directly mediated by MSCs (Qi and Wu, 2013). This is supported by similar results using transwell cultures and the conditioned medium of MSCs which have demonstrated that BCL-2 and BAX are altered in a paracrine manner in oxygen and glucose deprived primary hippocampal neurons and cortical astrocytes or 2,5-hexanedione-treated adrenal pheochromocytoma (PC12) cells (Li et al., 2015, Gu et al., 2016). These studies suggest that MSCs can regulate both pro and anti-apoptotic members of the BCL-2 family to protect cells from apoptosis in various pathologies. In parallel to the changes in the expression of BCL-2 family proteins, MSCs can avert translocation of apoptogenic cytochrome *c* and apoptosis-inducible factor from the mitochondria into the cytoplasm to activate caspases (Xiang et al., 2009, Lin et al., 2011a). Furthermore, these studies demonstrated reductions in inactive and activated caspase-3 expression *in vivo*, as well as activated caspase-3 and caspase-9 expression *in vitro* (Xiang et al., 2009, Lin et al., 2011a, Qi and Wu, 2013, Hsiao et al., 2015, Li et al., 2015, Qin et al., 2015). Thus, the ability of MSCs to manipulate mitochondria-associated cell death signalling appears to be critical in avoiding cellular death in a wide variety of *in vitro* and *in vivo* models of disease.

Conversely, MSCs have been demonstrated to attenuate cellular degeneration and necrosis in ischemia-reperfusion injury *in vivo* without altering members of the BCL-2 family; this may suggest that the interaction of MSCs with this particular pathway of cell death is disease dependent (Liu et al., 2012). The effects of MSCs on many pathways of cell death are yet to be explored. In cortical neurons, MSCs were determined to downregulate receptor interacting protein kinase1 (RIP1) and 3 (RIP3) which instigate intracellular signalling for necroptosis (Kong et al., 2017). This suggests that MSCs can regulate pathways of cell death other than apoptosis which should be considered in future studies. This could be achieved by investigating DAMPs accompanying oxidative stress-induced injury that are

associated with alternate pathways of cellular death (Janko et al., 2014, Andersson et al., 2018).

1.5. High-Mobility Group Box 1 in Intestinal Inflammation and Neurons

1.5.1. Role of HMGB1 in cellular functions

High-mobility group box 1 (HMGB1) is a highly-conserved and constitutively expressed nuclear protein that stabilises the nucleosome and regulates transcription by its DNA binding properties in normal physiology (Park et al., 2004, Lotze and Tracey, 2005). However, HMGB1 is emerging as an alarmin to cellular stress and key mediator of the pathophysiology of several diseases (Andersson et al., 2018). Upon synthesis, HMGB1 enters the nucleus via binding at its two nuclear localisation sites. Under conditions of cellular stress, these sites can be hyperacetylated. Subsequently, HMGB1 accumulates in the cellular cytoplasm and is released actively by leukocytes, or passively by cells undergoing necrosis (premature, non-programmed cell death) or necroptosis (programmed cell death without cellular fragmentation) (Yiting et al., 2016). Once HMGB1 is released, it functions as a DAMP. Its specific DAMP activity depends on posttranslational modifications that are controlled by the local redox environment and result in mutually exclusive functions. In the nucleus HMGB1 is primarily in its fully reduced form (all-thiol HMGB1). However, HMGB1 can be reversibly partially-oxidised (disulfide HMGB1) or irreversibly fully-oxidised (sulfonyl HMGB1). All-thiol HMGB1 acts as a direct chemoattractant for leukocytes by binding C-X-C chemokine ligand 12 (CXCL12) and subsequently activating C-X-C chemokine receptor type 4 (CXCR4). Disulfide HMGB1 signals via toll-like receptor (TLR)-2 and TLR-4 which promotes the secretion of pro-inflammatory cytokines and chemokines from leukocytes (Park et al., 2004). A direct immunomodulatory function for sulfonyl HMGB1 is yet to be identified, but it has been theorised that it may represent an inactivated form of HMGB1 in a process that could help avert chronicity in HMGB1-mediated inflammation.

1.5.2. HMGB1 in intestinal inflammation

HMGB1 has been established to contribute to the pathophysiology of inflammatory and autoimmune diseases (Andersson and Tracey, 2011, Magna and Pisetsky, 2014). Likewise, HMGB1 expression is elevated in IBD patients and in animal models of colitis which may be suggestive of a causative role to intestinal inflammation (Davé et al., 2009, Yamasaki et al., 2009, Vitali et al., 2011, Vitali et al., 2013, Palone et al., 2014). In IBD, HMGB1 is secreted at high levels, and can be detected in faeces, which has shown potential as a non-invasive marker for paediatric and adult cases (Vitali et al., 2011, Palone et al., 2014). It was demonstrated in both TNBS-induced colitis and IL-$10^{-/-}$ mice that HMGB1 levels parallel the onset and alleviation of inflammation (Davé et al., 2009). Therefore, HMGB1 appears to have a role in the intestinal immune response. The pre-established role of HMGB1 in inflammatory diseases, combined with its high expression in IBD patients, rationalises the approach of blocking HMGB1 signalling as a potential therapeutic treatment for IBD (Andersson and Tracey, 2011). Improvements in intestinal inflammation were observed by pharmacological and antibody-mediated inhibition of HMGB1 in DSS-induced colitis as a preventative treatment (Yamasaki et al., 2009, Vitali et al., 2013). Nonetheless, the efficacy of HMGB1 inhibition in spontaneous chronic intestinal inflammation has not yet been studied.

HMGB1 is ubiquitously expressed by virtually all cell types, however its role in mediating damage to the CNS is particularly of interest. HMGB1 has been identified to participate in mediating damage and inflammation in ischemia, reperfusion, haemorrhage and physical trauma (Gong et al., 2011, Ohnishi et al., 2011, Kim et al., 2012, Okuma et al., 2014). In these pathologies, the inflammatory process is unique and HMGB1 appears to facilitate a mechanism of ‘sterile’ inflammation which can be defined as inflammation in the absence of exogenous pathogens or antigens. Similarly, HMGB1 has recently been characterised in the myenteric plexus and was implicated in the neurotoxic effects of chemotherapeutic agents (Nurgali et al., 2018, Stojanovska et al., 2018). Therefore, HMGB1 may be

vital in mediating local inflammation in the myenteric ganglia, which like the CNS, may be relatively 'sterile' by virtue of its distance from the intestinal lumen. In *in vitro* and *in vivo* models of experimental sub-arachnoid haemorrhage, HMGB1 translocation was predominantly observed in neurons and rarely in glial cells (Sun et al., 2014). Likewise, HMGB1 translocation was only observed in MAP-2 positive neurons and not astrocytes or microglia in traumatic brain injury (Okuma et al., 2014). Inhibition of HMGB1 signalling in the CNS can attenuate inflammation, oxidative stress and excitotoxicity which demonstrate its multiple roles in mediating neuronal damage (Gong et al., 2011, Kim et al., 2012). Together this suggests that, in the CNS, HMGB1 is released almost exclusively from neurons, and thus, may be a specific neuronal signalling mechanism that activates the inflammatory response and promotes local tissue damage. The expression and role of HMGB1 in the ENS under inflammatory conditions is yet to be elucidated.

1.5.3. HMGB1 in oxidative stress

HMGB1 has been implicated in many pathologies involving oxidative injury (Gong et al., 2011, Kim et al., 2012, Lau et al., 2014). Oxidative stress and changes in the redox status are critical to the alarmin and DAMP activity of HMGB1; however, ROS and oxidative insult can also promote cytoplasmic HMGB1 translocation and release (Tang et al., 2007, Tsung et al., 2007, Tang et al., 2011). The relationship between oxidative stress and HMGB1 appears to be bilateral as it has been demonstrated that HMGB1 can also promote the generation of ROS (Kim et al., 2012). In DSS-induced colitis, HMGB1 levels are reduced by the application of the anti-inflammatory and ROS scavenging agent ethyl pyruvate (Davé et al., 2009). Furthermore, upregulation of the antioxidant enzyme HO-1 coincided with a reduction in HMGB1 (Davé et al., 2009). This may support that HMGB1 release is driven by oxidative stress in intestinal inflammation. The free radicals, H_2O_2 and $O_2^{\cdot -}$, can induce HMGB1 translocation and release (Gauley and Pisetsky, 2009, Tang et al., 2011). SOD mimetics reduce HMGB1 secretion and are being considered for treatment of pathologies associated with HMGB1-induced damage (Janko et al., 2014). Furthermore, SOD1 and SOD2 can attenuate HMGB1 release

and cell death in conditions of metabolic stress (Lee et al., 2010). These studies suggest that $O_2^{\cdot -}$ is a major contributor to cellular HMGB1 release. Myenteric neurons have previously been demonstrated to contain elevated levels of $O_2^{\cdot -}$ in chemically-induced colitis; therefore, it is plausible that HMGB1 expression may be affected in these cells during intestinal inflammation.

1.5.4. Role of HMGB1 in cell death

High levels of ROS are observed during apoptosis and necrosis. Changes in the position of HMGB1 are also associated with cell death. During apoptosis HMGB1 irreversibly binds to nuclear DNA; contrariwise, HMGB1 translocation into the cytoplasm is a feature of necrotic and necroptotic cell death pathways (Janko et al., 2014, Andersson et al., 2018). Therefore, the compartmentalisation of HMGB1 can be indicative of alternate cell death pathways. During apoptosis, HMGB1 release is limited, and is predominantly heavily oxidised or bound to DNA. During necrosis, HMGB1 is suggested to be passively released in large quantities (Lee et al., 2010, Andersson et al., 2018). HMGB1 released from necrotic cells can be fully-reduced and partially-oxidised, resulting in a potentially pro-inflammatory effect (Venereau et al., 2012). It has also been suggested that passive release of HMGB1 from necrotic cells is predominantly in a reversibly oxidised form which consists of 90% of the total pool of HMGB1 (Urbonaviciute et al., 2009). High levels of ROS are evident in necrosis which may account for the oxidation of HMGB1 (Janko et al., 2014, Negroni et al., 2015). This supports the hypothesis that HMGB1 derived from necrotic cells is pro-inflammatory, whereas HMGB1 released during apoptosis may not elicit an inflammatory response due the lower concentration and affinity for DNA. Post-translational modifications to HMGB1 have only been studied in these two traditional pathways of cell death (Tang et al., 2016). Further studies are required to determine the state of HMGB1 on other cell death pathways. Additionally, it has not been elucidated whether these modifications during cell death can be disease or tissue specific. While HMGB1 is released during cell death, it has also been demonstrated to contribute to cytotoxicity in a broad range of cell types, including renal cells, hepatocytes and neurons of the CNS (Ohnishi et al.,

2011, Gwak et al., 2012, Kim et al., 2012, Lau et al., 2014). The mechanism of HMGB1 in promoting cell death is unclear; however, it has been postulated that extracellularly released HMGB1 can induce translocation and further release of HMGB1 in other cells (Okuma et al., 2014). This is likely mediated by the activation of receptors with an affinity for HMGB1. TLR-4 is receptive to semi-oxidised HMGB1 and can induce further HMGB1 translocation; this may indicate that HMGB1 can function via a self-driven signalling cascade between cells in the local tissue environment (Gauley and Pisetsky, 2009). Myenteric neurons express the major receptors for HMGB1 including the receptor for advanced glycation end-products (RAGE), TLR-2 and TLR-4 (Venereau et al., 2012, Chen et al., 2015, Burgueño et al., 2016). Therefore, it is probable that these cells are receptive to HMGB1 signalling. Previously, it was demonstrated that the TLR-4 agonist, LPS, is neurotoxic in myenteric neurons (Stavely et al., 2015a). LPS is an exogenous ligand that would typically not be present in the myenteric plexus, however, HMGB1 offers the prospect of an endogenous ligand that can cause neuronal damage via a similar mechanism. Nevertheless, it must be considered that HMGB1 can bind to this receptor in its semi-oxidised form. Considering that increased ROS is common in enteric neuronal pathologies this is plausible. Moreover, muscularis macrophages also express TLR-4, and therefore, may be receptive to HMGB1 (Hori et al., 2008). Thus, HMGB1 signalling may explain the link between plexitis, neuronal damage and oxidative stress in the ENS of the inflamed intestine which needs to be elucidated.

1.6. The ENS as a target for MSC therapy in IBD

While the ENS is ingrained in the pathophysiology of IBD; investigations into neuroprotective treatments are limited. The application of MSCs to attenuate damage to the ENS is rationalised by their therapeutic value observed in a number of experimental models of neuropathies. These include favourable outcomes in experimental autoimmune encephalomyelitis, ischemic or traumatic brain injury, spinal cord or peripheral nerve injury, amyotrophic lateral sclerosis, diabetic neuropathies and models of neurodegenerative diseases such as Huntington’s and

Parkinson's (Lu et al., 2005, Bouchez et al., 2008, Karussis et al., 2008, Shibata et al., 2008, Vercelli et al., 2008, Harting et al., 2009, Lanza et al., 2009, Ikegame et al., 2011, Lin et al., 2011a, Uccelli et al., 2011, Matthes et al., 2013, Payne et al., 2013a, Wang et al., 2013b, Han et al., 2014b). Together these data provided a solid foundation for using MSCs to improve neurological function and attenuate neuronal damage. Subsequently, it was demonstrated that MSCs also exhibited neuroprotective effects in the ENS of guinea-pigs with TNBS-induced colitis through a series of papers exploring the effects of various doses, species and tissue sources as well as time-points of MSC treatments (Robinson et al., 2014, Robinson et al., 2015, Stavely et al., 2015a, Stavely et al., 2015b, Robinson et al., 2017b). These studies have offered insight into the potential therapeutic application of MSCs to remedy neuronal or nerve fibre loss and changes to neurochemical coding. After treatment, neurons also appear to be functionally competent as observed by the restoration of colonic motility patterns (Robinson et al., 2014). Nevertheless, these studies are limited by the use of chemically-induced models of colitis which does not adequately reflect the pathogenesis or molecular mechanisms of inflammation in IBD. As mentioned in Section 1.2.10, the *Winnie* mouse model of spontaneous chronic colitis has been demonstrated to replicate the inflammatory and neurological pathophysiology of UC (Heazlewood et al., 2008, Eri et al., 2011, Rahman et al., 2015, Rahman et al., 2016, Robinson et al., 2017a). Therefore, these mice may offer a more suitable model to study the effect of MSC therapy on alterations to the ENS in chronic intestinal inflammation. Moreover, this model could be useful to elucidate the underlying mechanisms of enteric neuronal damage in chronic inflammation, and likewise, MSC-mediated neuroprotection.

In chemically-induced colitis, the ability of MSCs to avert plexitis coincides with the attenuation of neuronal loss and dysfunction in the ENS (Robinson et al., 2015, Stavely et al., 2015a, Stavely et al., 2015b). The immunomodulatory capabilities of MSCs are well-established and it has been shown in several models of inflammation that MSCs reduce leukocyte recruitment (Antunes et al., 2014a, Antunes et al., 2014b, Elman et al., 2014, Stavely et al., 2015a, Wang et al., 2016). In TNBS-induced colitis, MSCs have been demonstrated to reduce leukocyte infiltration as

indicated by myeloperoxidase activity and leukocyte counts in the mucosa and submucosa (Ando et al., 2008, Liang et al., 2011, Stavely et al., 2015a). Therefore, the attenuation of leukocyte recruitment may participate in the neuroprotective value of MSCs. Maintenance of the epithelial barrier is also critical to perpetuating or reinitiating inflammation driven by the immune reaction to luminal antigens and PAMPs. In experimental colitis, epithelial cells can regenerate rapidly after the initial inflammatory insult, however this is limited in mucin secreting cells (Tanaka et al., 2011). Considering that mucus provides a barrier for luminal pathogens, this may provide one mechanism for chronic intestinal inflammation (Thorpe et al., 2013). MSC treatments increase mucin secreting goblet cells in experimental colitis (Tanaka et al., 2011, Fawzy et al., 2013). Enteric neurons regulate the differentiation of epithelial stem cells and mucin secretion itself (Phillips et al., 1984, Puzan et al., 2018). Therefore, the absence of mucin secreting cells or changes in the epithelial barrier post-colitis could underlie changes in enteric neuronal signalling, which likewise, is dysregulated after inflammation. Moreover, the therapeutic value of MSCs for the ENS and epithelial barrier may therefore limit the immuno-stimulatory insult and further inflammation-induced damage to the ENS.

The immunosuppressive properties of MSCs may contribute to the aversion of neuronal damage; however, MSCs can also directly act on enteric neurons via their paracrine secretion (Stavely et al., 2015a). MSCs secrete various trophic factors that have been linked to their neuroprotective effects in the CNS (Teixeira et al., 2013). Many of these factors have roles in the ENS and might be involved in enteric neuroprotection (Robinson et al., 2015). Administration of glial cell-derived neurotrophic factor (GDNF), which is secreted by MSCs, has previously been shown to rescue enteric neuropathy (Anitha et al., 2006, Whone et al., 2012). Brain-derived neurotrophic factor (BDNF) is also secreted by MSCs and is involved in neuronal growth, differentiation and synaptic plasticity and is present in the ENS where it amplifies enteric signalling (Boesmans et al., 2008, Cohen-Cory et al., 2010). In *in vitro* experiments, BDNF has been demonstrated to avert NO-induced neuronal death (Wilkins et al., 2009). Trophic factors promoting angiogenesis have

also been implicated in MSC-mediated neuroprotection, however these may be more relevant to ischemia- associated neuropathies (Ikegame et al., 2011). In addition to immunomodulation, cytokines may directly provide neuroprotection. IL-6 secreted by MSCs is suggested to be partially responsible for their ability to recover neurons from oxygen-glucose deprivation *in vitro* (Huang et al., 2014). Furthermore, TGF-β is secreted by MSCs and is regarded to have neuroprotective roles in the CNS and ENS (Dobolyi et al., 2012, Stavely et al., 2015a). The contribution of MSC-secreted factors to enteric neuroprotection is plausible given that MSCs can rescue LPS-stimulated myenteric neurons in a paracrine fashion *in vitro* (Stavely et al., 2015a). However, MSCs may also secrete antioxidants, such as superoxide dismutase (SOD) 3, which was demonstrated to be at least partially responsible for the protection of CNS neurons from NO-induced damage *in vitro* (Kemp et al., 2010). MSCs have been demonstrated to alleviate oxidative stress in experimental models of neurological pathologies of the CNS and in *in vitro* neuronal cultures (Lanza et al., 2009, Calió et al., 2014, Kim et al., 2015, de Godoy et al., 2018). Considering that the ENS appears to be susceptible to oxidative stress in intestinal inflammation, the antioxidative properties of MSCs may offer one explanation for their neuroprotective effects on myenteric neurons. This may be plausible taking into account that MSCs were recently demonstrated to ameliorate oxidative stress in chemically-induced colitis by normalising the redox state and increasing SOD activity (Sun et al., 2015, da Costa Gonçalves et al., 2017).

1.7. Summary

Due to the limited efficacy and high toxicity of current treatments, the development of novel therapies is crucial for improving outcomes for patients with IBD. MSC therapies have promoted positive outcomes in patients that are refractory to conventional treatment options, and thus, have shown promise as a prospective clinical option. The limited side effects produced by MSCs in clinical trials have demonstrated an advantage over current pharmacological and biological therapies. Nevertheless, a clinical response is not observed in every patient, further highlighting the complexity of the underlying pathophysiology of IBD. Fortunately, cellular therapies are easily manipulated by culture conditions, pre-stimulation,

adjuvant treatments and genetic modification, which could assist in improving patient outcomes. To develop and optimise MSC therapies, their mechanism of action must be fully elucidated. To date, most studies have been conducted in models of acute chemically-induced colitis and have predominantly explored the role of MSCs in immunomodulation. Discrepancies in these mechanisms are beginning to emerge between these models and clinical data; therefore, alternative models may be required for clinical relevance. MSC treatments have not been investigated in chronic models of experimental colitis which could provide more accurate inferences to the human pathology. The reported mechanisms and effects of MSC treatments in experimental colitis are multi-faceted and diverse. It is uncertain which of these processes may occur in spontaneous chronic colitis or IBD. High-throughput transcriptomics is a valid option to objectively assess these processes and their potential clinical relevance. Furthermore, this may facilitate more directed exploration into novel mechanisms of MSC therapies. In addition to immunomodulation, there are two key mechanisms that have emerged to explain the efficacy of MSC treatments: 1) reduction of oxidative stress and 2) attenuation of damage to the nervous system. These effects appear to be mediated by MSC paracrine secretion and may be independent of their immunomodulatory properties to an extent. The ENS is sensitive to oxidative stress-induced dysfunction in multiple pathologies, including colitis. Therefore, the previously described effects of MSCs on oxidative stress and neuroprotection may be linked. Nevertheless, understanding the effects of MSCs on oxidative stress and neuronal damage can be problematic, as the initial extent of these changes has not been clarified in experimental chronic colitis and IBD. Screening tools may be useful to improve our understanding of the relationship between intestinal inflammation, oxidative stress and the ENS. Particularly, the mechanisms of neuronal loss in intestinal inflammation require exploration. MSCs have previously been identified to avert both apoptotic and necroptotic death in neurons of the CNS. Apoptosis alone does not appear to explain the loss of neurons in acute colitis. Studying novel molecules associated with neuronal death may assist in identifying the mechanisms of neuronal loss and MSC-mediated neuroprotection. Translocation of the HMGB1 protein has previously been identified concomitantly with the death of CNS

neurons. Moreover, HMGB1 is a novel biomarker of IBD; thus, its function in intestinal inflammation and enteric neuropathy requires examination.

CHAPTER TWO

Human Adult Stem Cells Derived from Adipose Tissue and Bone Marrow Attenuate Enteric Neuropathy in the Guinea-pig Model of Acute Colitis

STAVELY, R., ROBINSON, A. M., MILLER, S., BOYD, R., SAKKAL, S. & NURGALI, K. 2015. Human adult stem cells derived from adipose tissue and bone marrow attenuate enteric neuropathy in the guinea-pig model of acute colitis. *Stem Cell Research & Therapy*, 6**,** 244.

2.1. Summary

Introduction: Mesenchymal stem cells (MSCs) have been identified as a viable treatment for inflammatory bowel disease (IBD). Experimental models have been predominated by MSCs derived from bone marrow (BM-MSCs) whereas the majority of clinical trials have used MSCs derived from adipose tissue (AT-MSCs), thus there is little consensus on the optimal tissue source. The therapeutic efficacies of these MSCs are yet to be compared in context of the underlying dysfunction of the enteric nervous system innervating the gastrointestinal tract concomitant with IBD. This study aims to characterise the *in vitro* properties of MSCs and compare their *in vivo* therapeutic potential for the treatment of enteric neuropathy associated with intestinal inflammation. **Methods:** BM-MSCs and AT-MSCs were validated and characterised *in vitro*. In *in vivo* experiments, guinea-pigs received either 2,4,6-trinitrobenzene-sulfonate acid (TNBS) for the induction of colitis or sham treatment by enema. MSCs were administered at a dose of $1x10^6$ cells via enema 3 hours after the induction of colitis. Colon tissues were collected 24 and 72 hours after TNBS administration to assess the level of inflammation and damage to the ENS. MSC migration to the myenteric plexus *in vivo* was elucidated by immunohistochemistry and *in vitro* using a modified Boyden chamber assay. **Results:** Cells exhibited multipotency and a typical surface immunophenotype for validation as bona fide MSCs. *In vitro* characterisation revealed increased growth kinetics, clonogenicity and spindle-shaped morphology in AT-MSCs compared to BM-MSCs. *In vivo*, BM-MSCs were comparatively more effective than AT- MSCs in attenuating leukocyte infiltration and neuronal loss in the myenteric plexus. MSCs from both sources equally ameliorated body weight loss, gross morphological damage to the colon, changes in the neurochemical coding of neuronal subpopulations, the reduction in density of extrinsic and intrinsic nerve fibres innervating the colon and the generation of mitochondria-derived superoxide. MSCs from both sources migrated to the myenteric plexus in *in vivo* colitis and in an *in vitro* assay. **Conclusion:** Results of *in vitro* experiments suggest that AT-MSCs are ideal for cellular expansion. However, *in vivo* studies demonstrate that for clinical application BM-MSCs were more therapeutic in the treatment of enteric neuropathy

and plexitis. These characteristics should be considered when deciding on the MSC tissue source.

2.2. Abbreviations

AT-MSCs	mesenchymal stem cells derived from adipose tissue
BM-MSCs	mesenchymal stem cells derived from bone marrow
CFU-f	colony forming unit-fibroblast
CGRP	calcitonin gene-related peptide
ChAT	choline acetyltransferase
DMSO	dimethyl sulfoxide
ENS	enteric nervous system
FBS	foetal bovine serum
IBD	inflammatory bowel disease
LMMP	longitudinal muscle and myenteric plexus
LPS	lipopolysaccharide
MSCs	mesenchymal stem cells
NDS	normal donkey serum
nNOS	neuronal nitric oxide synthase
PDL	population doubling level
PGP 9.5	protein gene product 9.5
TH	tyrosine hydroxylase
TNBS	2,4,6-trinitrobenzene-sulfonate acid
VAChT	vesicular acetylcholine transporter

2.3. Introduction

Mesenchymal stem cells (MSCs) otherwise known as multipotent stromal cells have been proposed as a potential treatment option for chronic inflammation and neurological damage (Wei et al., 2013). These cells are identified by their multipotency as implied by name (Dominici et al., 2006), however it is the numerous other characteristics that attract investigations into their therapeutic potential. MSCs are readily isolated from adult bone marrow or adipose tissue (Zuk et al., 2002, Chamberlain et al., 2007, Mosna et al., 2010). *In vitro*, MSCs are easily purified due to their adherence to plastic and proliferation, generating high yields of cells for treatments (Caplan, 1991). The immune evasive nature of MSCs may also be exploited for allogeneic and, if required, xenogeneic transplantation (Li et al., 2012, Ankrum et al., 2014). Once administered, MSCs migrate towards sites of inflammation by chemotaxis (Karp and Leng Teo, 2009). Engrafted MSCs can then exert immunomodulatory activities and promote endogenous repair mechanisms through secretion of cytokines in addition to angiogenic and trophic factors (Wu et al., 2007, Chen et al., 2008, Ma et al., 2013, Sémont et al., 2013). These traits make MSCs ideal candidates to target both the inflammatory pathology and structural damage to the intestines of inflammatory bowel disease (IBD) patients.

Current treatments for IBD often fail to maintain periods of remission effectively throughout the prolonged course of illness due to their inefficacy or toxicity (Pithadia and Jain, 2011), thus necessitating the development of novel therapies. Clinical trials of MSC application in IBD have recognised their therapeutic efficacy, feasibility and safety. Specifically, MSCs have shown promise in the treatment of the fistulising and inflammatory luminal pathologies of Crohn's disease (Duijvestein et al., 2010, Ciccocioppo et al., 2011). Clinical remission and endoscopic improvement has been observed in over half of patients with Crohn's colitis and ileocolitis refractory to conventional treatments after MSC therapy (Forbes et al., 2014). However, further studies are crucial to optimise MSC therapy for better treatment outcomes.

Investigating the facets of MSCs derived from different tissue sources may provide an opportunity to improve therapy. In experimental models and clinical trials, MSCs from either bone marrow or adipose tissue have been used. Experimental models have been predominated by MSCs derived from bone marrow (BM-MSCs) whereas the majority of clinical trials have used MSCs derived from adipose tissue (AT-MSCs) (Stavely et al., 2014), thus there is little consensus on the optimal tissue source of MSCs. The favoured use of AT-MSCs in the clinic is presumably owing to the availability and less invasiveness of obtaining adipose tissue (Strioga et al., 2012). Furthermore, the cell yield of AT-MSCs is predicted to be 500 fold of BM-MSCs (Fraser et al., 2006). Nonetheless, differences in the functional efficacy of these MSCs could influence the preference of tissue source.

Studies directly comparing BM-MSCs and AT-MSCs are limited. However, MSC application in different *in vivo* models of various inflammatory conditions indicate that BM-MSCs exhibit functionally better immunomodulatory properties (Roemeling-van Rhijn et al., 2013, Antunes et al., 2014a, Antunes et al., 2014b, Elman et al., 2014). Conversely, AT-MSCs have been reported to be functionally better than BM-MSCs in ameliorating the clinical and pathological severity of autoimmune demyelination due to their enhanced ability to migrate to the central nervous system (Payne et al., 2013a). In intestinal inflammation, studies have largely investigated MSC protection of the mucosal integrity and polarisation of the pro-inflammatory signalling milieu (González et al., 2009, Tanaka et al., 2011, Castelo-Branco et al., 2012, He et al., 2012, Anderson et al., 2013b, Fawzy et al., 2013). Recently, we have demonstrated that human BM-MSCs can attenuate neuropathy in the enteric nervous system (ENS) of guinea-pigs with colitis (Robinson et al., 2014). Comparisons between BM-MSCs and AT-MSCs are yet to be elucidated in the context of inflammation-induced neurological damage concomitant with intestinal inflammation.

The colon is innervated extrinsically by parasympathetic vagus nerve fibres, sympathetic and sensory afferent fibres of the dorsal root ganglion (Phillips and Powley, 2007). Intrinsic innervation is governed by the ENS which can function

independently of extrinsic input and justifies its label as ‘the little brain’ (Epstein et al., 1996). The ENS consists of a network of neurons and glial cells spanning the length of the gastrointestinal tract which form the ganglia. The ganglia, containing individual neuronal subpopulations, are localised within the submucosal plexus regulating secretion and vasodilation, and the myenteric plexus coordinating muscular contraction (Furness, 2012). Persistent intestinal inflammation associates with disruption to the ENS causing symptomatic gut dysfunctions (Hansen, 2003, Lomax et al., 2005, De Giorgio et al., 2007, Lakhan and Kirchgessner, 2010). Neuropathy and axonal damage are likely to be consequential of inflammation in the bowel (Boyer et al., 2005, Linden et al., 2005a, Sarnelli et al., 2009, Nurgali et al., 2011). However, in non-inflamed regions, the invasion of leukocytes to the level of the enteric plexuses, termed plexitis, may be an indicator of inflammatory relapse (Ferrante et al., 2006, Sokol et al., 2009, Bressenot et al., 2013). Furthermore, the neurochemical coding that defines neuronal subpopulations is altered in animal models of intestinal inflammation and IBD patients (Schneider et al., 2001, Neunlist et al., 2003a, Linden et al., 2005a, Boyer et al., 2007, de Fontgalland et al., 2014). These changes are not only responsible for the symptoms of IBD but can perpetuate further intestinal inflammation. Thus, the ENS presents as a therapeutic target for IBD**.** In this study we performed a comparison in the *in vitro* characteristics and *in vivo* therapeutic efficacy of BM-MSCs and AT-MSCs for the treatment of inflammation-induced neurological changes in the colon.

2.4. Methods

2.4.1. Animals

Male and female Hartley guinea-pigs weighing 140-280g were received from the South Australian Health and Medical Research Institute (SAHMRI). All guinea-pigs were housed in a temperature-controlled environment with 12-hour day/night cycles and had *ad libitum* access to food and water. The average weight of guinea-pigs that underwent experimental procedures was 248±5g. All procedures were performed under approval of the Victoria University Animal Experimentation

Ethics Committee (ethics number AEETH 12-012) and conducted according to the Australian National Health and Medical Research Council (NHMRC) Code of Practice for the Care and Use of Animals for Scientific Purposes.

2.4.2. Cell culture and passaging

Pre-established cell lines of human MSCs (Tulane University, USA) were derived from the bone marrow and adipose tissue of four donors. MSCs were cultured to the fourth passage for all subsequent experiments and exhibited a viability of minimum 95% at the time of injection. Cells were plated at an initial density of 60 cells/cm^2 and incubated in expansion medium (α-MEM supplemented with 100 U/mL penicillin/streptomycin, 1% glutaMAX (Gibco®, Life Technologies, Melbourne, Australia) and 16.5% foetal bovine serum (FBS; mesenchymal stem cell-qualified, Gibco®)) which was replenished every 48-72h for 10-14 days until the cells were 70-85% confluent (maximum). MSCs were trypsinised and either reseeded for expansion or collected for *in vitro* experiments and *in vivo* treatment of guinea-pigs. All MSC cultures were incubated at 37ºC in 5% CO_2 throughout the study.

2.4.3. Surface marker expression

MSCs were immunolabelled as previously described (Payne et al., 2013b) with CD29-Alexa Fluor 488 (clone TS2/16), CD34-phycoerythrin (PE) (clone 581), CD45-PerCPCy5.5 (clone H130), CD44-Brilliant Violet 421 (clone IM7), CD73-Brilliant Violet 421 (clone AD2), and CD90-Alexa Fluor 647 (clone 5E10) (1:100) (BioLegend, San Diego, USA). Data were acquired on a BD FACSCanto II flow cytometer with FACSDiva v6.1 software (BD Biosciences, Melbourne, Australia). Unlabelled cells were incubated with 7-Aminoactinomycin D (7-AAD) (1:20) (Life Technologies) for 1min before acquisition to determine the viability of the cell suspensions.

2.4.4. Differentiation assay

The differentiation potential of MSCs was assessed using the StemPro® Adipogenesis Differentiation Kit and StemPro® Osteogenesis Differentiation Kit according to manufacturer's instructions (Life Technologies). To detect adipogenesis, MSCs were fixed in 10% neutral buffered formalin after 2 weeks in culture and lipid vacuoles were stained with Oil red O (Sigma-Aldrich, Sydney, Australia) in 60% (v/v) isopropanol. Cells were then counterstained with haematoxylin. To detect osteogenesis, MSCs were fixed in 10% neutral buffered formalin after 3 weeks in culture and calcium deposits were stained with 2% (w/v) Alizarin red S (Sigma-Aldrich) in distilled water.

2.4.5. Colony forming unit-fibroblast (CFU-f) assay

MSCs were seeded in 90mm size petri dishes at low density (100 cells/dish). Expansion medium was changed every 3-4 days. After 2 weeks in culture, MSCs were fixed and stained with 0.5% (w/v) crystal violet (Sigma-Aldrich) in methanol for 30min before colonies containing >50 cells (CFU-f) (Bourin et al., 2013) were counted under a dissection microscope.

2.4.6. MSC growth kinetics and cell morphology

To assess cell proliferation, MSCs were cultured in triplicates and seeded at 60 cells/cm^2 in 25cm^2 cell culture flasks containing 5mL of expansion medium which was replaced every 48-72h. Cells were trypsinised and counted with a haemocytometer at days 3, 7 and 14. The population doubling level (PDL) was calculated using the formula PDL= ($\log^2$ [final no. of cells]) - ($\log^2$ [initial cells seeded]) (Cristofalo et al., 1998). For morphological studies, MSCs were seeded at 100 cells/cm^2 in 6 well plates and analysed after 48h. MSCs were morphologically characterised into one of two categories defined by the presence of elongated cell bodies with long thin processes (spindle) or flat bodies with irregular processes (flat).

2.4.7. Induction of colitis and MSC administration

To induce colitis, 2,4,6-trinitrobenzene-sulfonate acid (TNBS) (Sigma-Aldrich) was dissolved in 30% ethanol to a concentration of 30mg/kg and administered intrarectally 7cm proximal to the anus (total volume of 300µL) by a lubricated silicone catheter (Nurgali et al., 2011). Guinea-pigs were anesthetised with isoflurane (1-4% in O_2) during the procedure and held at an inverted angle to prevent leakage. Sham-treated guinea-pigs underwent the same procedure without administration of TNBS. Guinea-pigs were treated with MSCs 3h after TNBS administration at the peak of tissue damage (Pontell et al., 2009). Each animal was treated with MSCs derived from a separate donor. MSCs were administered by enema at a dose of $1x10^6$ cells in 300µL of sterile PBS. Guinea-pigs were weighed and monitored daily following treatment. At 24 or 72h after TNBS administration, animals were culled via stunning and exsanguination (Nurgali et al., 2009). Segments of the distal colon were collected for histological and immunohistochemical studies.

2.4.8. Tissue preparation

Colon tissues were cut along the mesenteric border, stretched and pinned flat with the mucosal side up for wholemount preparations. Tissue samples were fixed overnight at 4°C in Zamboni's fixative (2% formaldehyde and 0.2% picric acid) and subsequently washed in dimethyl sulfoxide (DMSO) (Sigma-Aldrich) (3x10min) and PBS (3x10min) to remove fixative. Samples for histology were fixed in 10% buffered formalin solution and stored in 70% ethanol until embedding.

2.4.9. Immunohistochemistry

Immunohistochemistry was performed on wholemount preparations of the longitudinal muscle and myenteric plexus (LMMP). The preparations were dissected by removing the mucosa, submucosa and circular muscle layers to expose

the myenteric plexus. LMMPs were incubated in 10% normal donkey serum (NDS; Merck Millipore, Melbourne, Australia) at room temperature for 1h before immunolabelling. For neuronal counting, LMMPs were incubated overnight at 4ºC with primary antibodies: anti-Hu (mouse, clone 15A7.1, 1:500; Merck Millipore), anti-neuronal nitric oxide synthase (nNOS) (goat, 1:500; Novus Biologicals, Littleton, USA), anti-choline acetyltransferase (ChAT) (goat, 1:500; Merck Millipore), anti-CD45 (mouse, clone IH-1, 1:200; Abcam, Melbourne Australia) and anti-protein gene product 9.5 (PGP9.5) (rabbit, 1:500; Abcam). For analysis of immunoreactive (IR) area density, LMMP tissues were incubated with primary antibodies: anti-calcitonin gene-related peptide (CGRP) (rabbit, 1:3000; Sigma-Aldrich), anti-tyrosine hydroxylase (TH) (sheep, 1:1000; Merck Millipore) and anti-vesicular acetylcholine transporter (VAChT) (goat, 1:500; Merck Millipore). Tissues were washed (3x10min PBS) and incubated for 2 hours at room temperature with secondary antibodies: donkey anti-mouse Alexa Fluor 594 (1:200), donkey anti-goat FITC 488 (1:200), donkey anti-mouse FITC 488 (1:200) and donkey anti-rabbit Alexa Fluor 594 (1:200), donkey anti-sheep FITC 488 (1:200) and donkey anti-goat Alexa Fluor 647 (1:200) (all from Jackson Immunoresearch, West Grove, USA). After washing, tissues were mounted on glass slides with fluorescent mounting medium (DAKO). For cross sections, tissues were frozen in optimal cutting temperature compound (Tissue-Tek) and sections were cut at a thickness of 20µm. Cross sections were labelled with rabbit anti-α-actin (1:1000; Abcam) followed by donkey anti-rabbit Alexa Fluor 594 (1:200) and FITC conjugated anti-human human leukocyte antigen (HLA)-A, B, C (1:50; BioLegend).

2.4.10. Histology

Tissues were embedded in paraffin and cut into 5µm sections which were then deparaffinised, cleared, and rehydrated in graded ethanol. Cross sections of the colon were stained with haematoxylin and eosin and mounted on glass slides with distrene plasticizer xylene (DPX) mountant. Gross morphological damage in cross sections of the distal colon was assessed by histological grading of four parameters: mucosal flattening (0 = normal, 3 = severe flattening), occurrence of haemorrhagic

sites (0 = none, 3 = frequent sites), loss of goblet cells (0 = normal, 3 = severe loss of cells) and variation of the circular muscle (0 = normal, 3 = considerable thickening of muscular layer) (Nurgali et al., 2007, Robinson et al., 2014).

2.4.11. MitoSOX Red staining

To assess mitochondria-derived superoxide production in the myenteric plexus, colon segments were placed in carbogenated physiological saline (NaCl 118 mM, KCl 4.8 mM, $NaHCO_3$ 25 mM, NaH_2PO_4 1.0 mM, $MgSO_4$ 1.2 mM, glucose 11.1 mM and $CaCl_2$ 2.5mM, pH 7.4) with 3μM nicardipine (Sigma-Aldrich) to inhibit muscle contraction. Tissues were pinned in physiological saline and immediately, the mucosa, submucosa and circular smooth muscles were removed to expose the myenteric plexus. Tissues were incubated in physiological saline with MitoSOX Red (1:1000) (Molecular Probes®, Thermofisher, Melbourne, Australia), a mitochondria-specific, fluorogenic superoxide indicator, for 40min at 37°C and were then washed 3×10min in physiological saline prior to being fixed in 4% paraformaldehyde overnight at 4°C. After 3×10min washes in PBS, the tissue was mounted onto glass slides with DAKO fluorescence mounting medium and visualized by confocal microscopy.

2.4.12. Imaging

Confocal microscopy was performed using Eclipse Ti confocal laser scanning system (Nikon, Tokyo, Japan). Z-series images were acquired at a thickness of 0.5μm (512x512 pixels) and converted into maximum intensity projections using NIS-Elements Software (Nikon). The number of myenteric neurons Hu-IR, nNOS-IR, and ChAT-IR, as well as CD45-IR cells were counted within eight randomly captured images (total area size $2mm^2$) per preparation. CGRP-IR, TH-IR and VAChT-IR were assessed by measuring the density of immunoreactivity per area (total area size 1 mm^2). Image J software (National Institute of Health, Bethesda, MD, USA) was employed to convert images from RGB to greyscale 8 bit then to binary; particles were then analysed to obtain the percentage area of

immunoreactivity (Rahman et al., 2015). MitoSOX fluorescence was observed in stained LMMP tissues. Eight randomly captured images were acquired per preparation in a 0.4mm^2 (400,000μm^2) field of view. The arbitrary fluorescence in these images was analysed using the mean grey value (mean fluorescence intensity) within traces of the ganglia by Image J software (NIH, USA). The average mean fluorescence intensity from these eight images per was calculated. Gross morphological damage in haematoxylin and eosin-stained colon sections was visualised using an Olympus BX53 microscope (Olympus Imaging, Sydney, Australia) and images were captured with CellSenseTM software. Cellular imaging *in vitro* was performed on an Olympus IX81 inverted microscope (Olympus) using the same software.

2.4.13. MSC migration assay

The distal colon was collected and myenteric plexuses were isolated as of Grundmann et al. (2015). Tissues were trypsinised for 10min before cells were seeded into 24-well plates pre-coated with poly-L-lysine and laminin containing media. Myenteric plexuses were cultured for 7 days with the media changed every second day. Medium containing lipopolysaccharide (LPS) (20ng/mL; Sigma-Aldrich) was added to cultures for 8h to stimulate inflammatory conditions prior to the migration assay. The media conditioned by cells of the myenteric plexus were collected, pooled together and filtered through 0.2μm pore filter to serve as a chemoattractant in the bottom well of the Boyden chamber. Controls contained unconditioned media without FBS, with equivalent FBS, or FBS with added LPS (20ng/mL). Top wells of the Boyden chamber (pore size 8μm, Corning) were loaded with 2x10^5 BM-MSCs or AT-MSCs. After 72h in culture chambers were washed in PBS and cells in the bottom wells were collected by trypsinisation and counted by haemocytometry.

2.4.14. Statistical analysis

Data analysis was performed using GraphPad Prism v6 (GraphPad Software Inc., San Diego, USA). Data were analysed using Student's *t*-test (two-tailed) and one-way or two-way ANOVA for multiple group comparisons followed by Tukey's and Sidak's post hoc test. For all analysis $P<0.05$ was considered significant. All data were presented as mean ± standard error of the mean (SEM).

2.5. Results

2.5.1. *In vitro* validation and characterisation of BM-MSCs and AT-MSCs

All experiments were conducted using MSCs cultured until the fourth passage. Flow cytometry was used to validate the immunophenotype of MSCs. Cell surface expression of positive MSC markers CD29, CD44, CD73 and CD90 was observed in BM-MSCs (98.5%, 98.8%, 98.0% and 98.9%, respectively) and AT-MSCs (99.9%, 99.8%, 99.9% and 99.6% respectively) (**Figure 2.1A**). BM-MSCs demonstrated negligible expression of non-MSC markers CD34 (2.5%) and CD45 (3.6%). In AT-MSCs, the expression of CD34 was low (10.3%) while CD45 was negligible (1.6%). Thus, the immunophenotype of BM-MSCs and AT-MSCs were in compliance with MSC definition (Dominici et al., 2006).

MSCs adhered to plastic and proliferated to form monolayer cultures (**Figure 2.1B-B′**). In addition, BM-MSCs appeared more sparsely distributed than AT-MSCs. The multipotent potential of MSCs was assessed by exposing cells to adipogenic and osteogenic differentiation media. MSCs stained positive with Oil Red O indicative of successful induction to adipocytes with lipid filled vacuoles (**Figure 2.1C-D′**). Confirmation of differentiation to osteogenic lineage was revealed by Alizarin red S staining of calcium deposition (**Figure 2.1E-F′**). Both BM-MSCs and AT-MSCs exhibited multipotency and therefore were considered bona fide MSCs. A CFU-f assay was performed to compare the clonogenicity between BM-MSCs and AT-MSCs. The percentage of MSCs capable of developing into colonies was greater in AT-MSC cultures (39.0±0.6%) compared to those of BM-MSCs (14.3±3.0%, $P<0.01$) after 2 weeks (**Figure 2.2A-A′, B,** n=3 independent

cultures/group). Subpopulations of MSCs were quantified by the morphological properties of their cell bodies *in vitro* (**Figure 2.2C-D′**).

Figure 2.1 ***Phenotypic and functional validation of BM-MSCs and AT-MSCs***

(A) BM-MSCs and AT-MSCs analysed for cell surface antigen expression of known positive (CD29, CD44, CD73 and CD90) and negative (CD34 and CD45) MSC markers. Red closed histograms represent MSCs labelled with antibodies against the surface antigen indicated on the right-hand side of each row. Blue open histograms show isotype controls. BM-MSCs **(B)** and AT-MSCs (**B′)** adhered to plastic with a perceptible appearance typical of MSCs in culture. Scale bar=200μm. BM-MSCs and AT-MSCs cultured without **(C-D)** and with **(C′-D′)** adipogenesis differentiation medium for 14 days and stained with Oil red O. Scale bar=50μm. BM-MSCs and AT-MSCs cultured without **(E-F)** and with **(E′-F′)** osteogenesis differentiation medium for 21 days and stained with Alizarin red S. Scale bar=200μm.

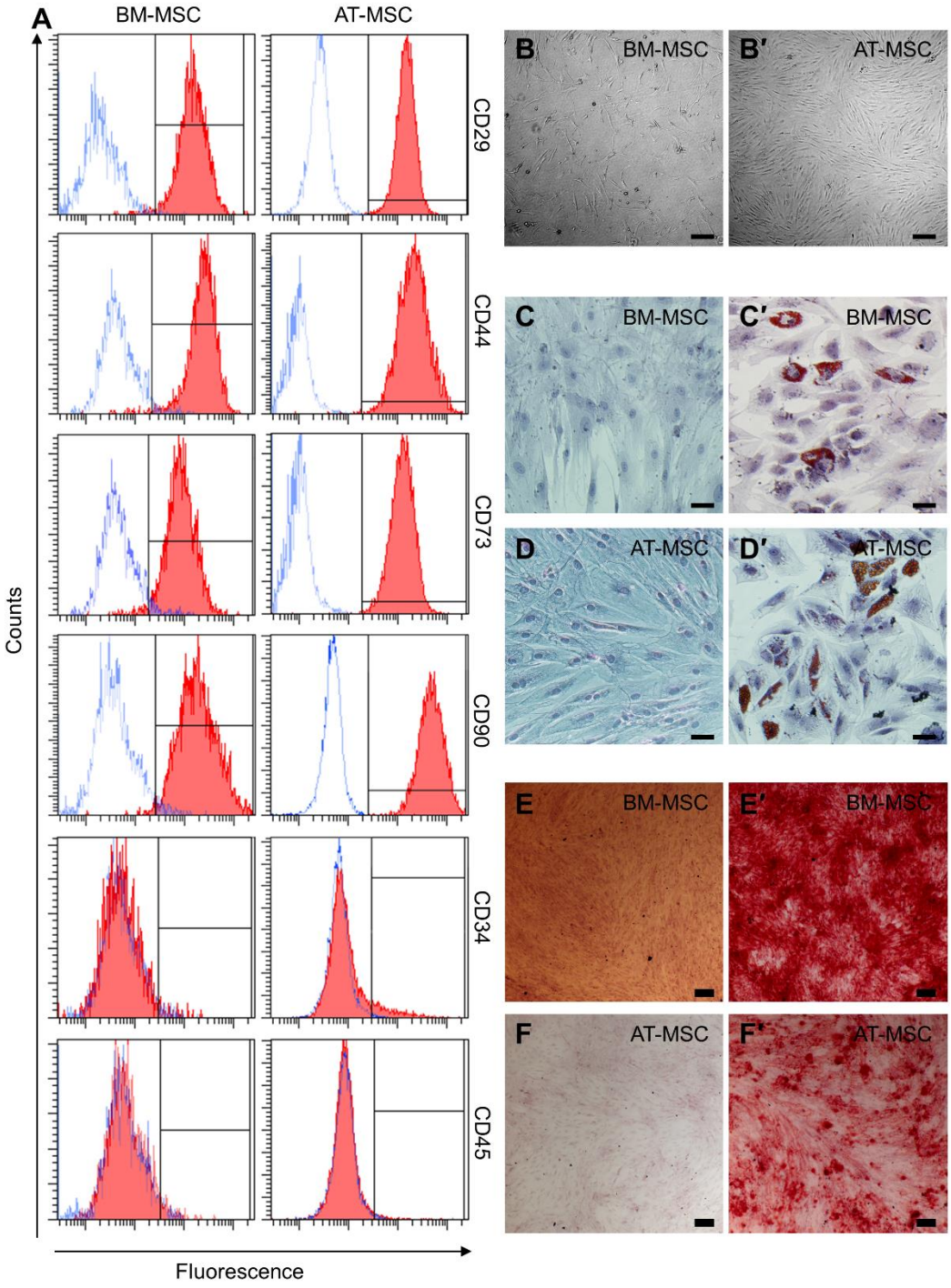
A
BM-MSC
AT-MSC
CD29
CD44
CD73
CD90
CD34
CD45
Counts
Fluorescence
B
BM-MSC
B′
AT-MSC
C
BM-MSC
C′
BM-MSC
D
AT-MSC
D′
AT-MSC
E
BM-MSC
E′
BM-MSC
F
AT-MSC
F′
AT-MSC

Figure 2.2 ***In vitro clonogenicity, morphology, and growth kinetics of MSCs***

Clonogenicity of BM-MSCs **(A)** and AT-MSCs **(A′)** determined by a colony forming unit-fibroblast (CFU-f) assay (n=3 independent cultures/group). **(B)** CFU-f counts quantified as a percentage of the total viable cells seeded. **(C-D′)** Morphological subpopulations exhibited by BM-MSCs **(C-C′)** and AT-MSCs **(D-D′)** in culture. MSC morphology defined according to the presence of long thin spindles ('spindle': **C-D**) or flat cells with atypical processes ('flat': **C′-D′**) (scale bar=50μm). **(E)** Quantitative analysis of MSC morphological types. Data expressed as a percentage of the total cell number in each population (n=6 independent cultures/group). **(F)** The population doubling level (PDL) of proliferating MSCs recorded at 3, 7 and 14 days after seeding (n=3 independent cultures/group/time point). ***P*<0.01, ****P*<0.001, *****P*<0.0001.

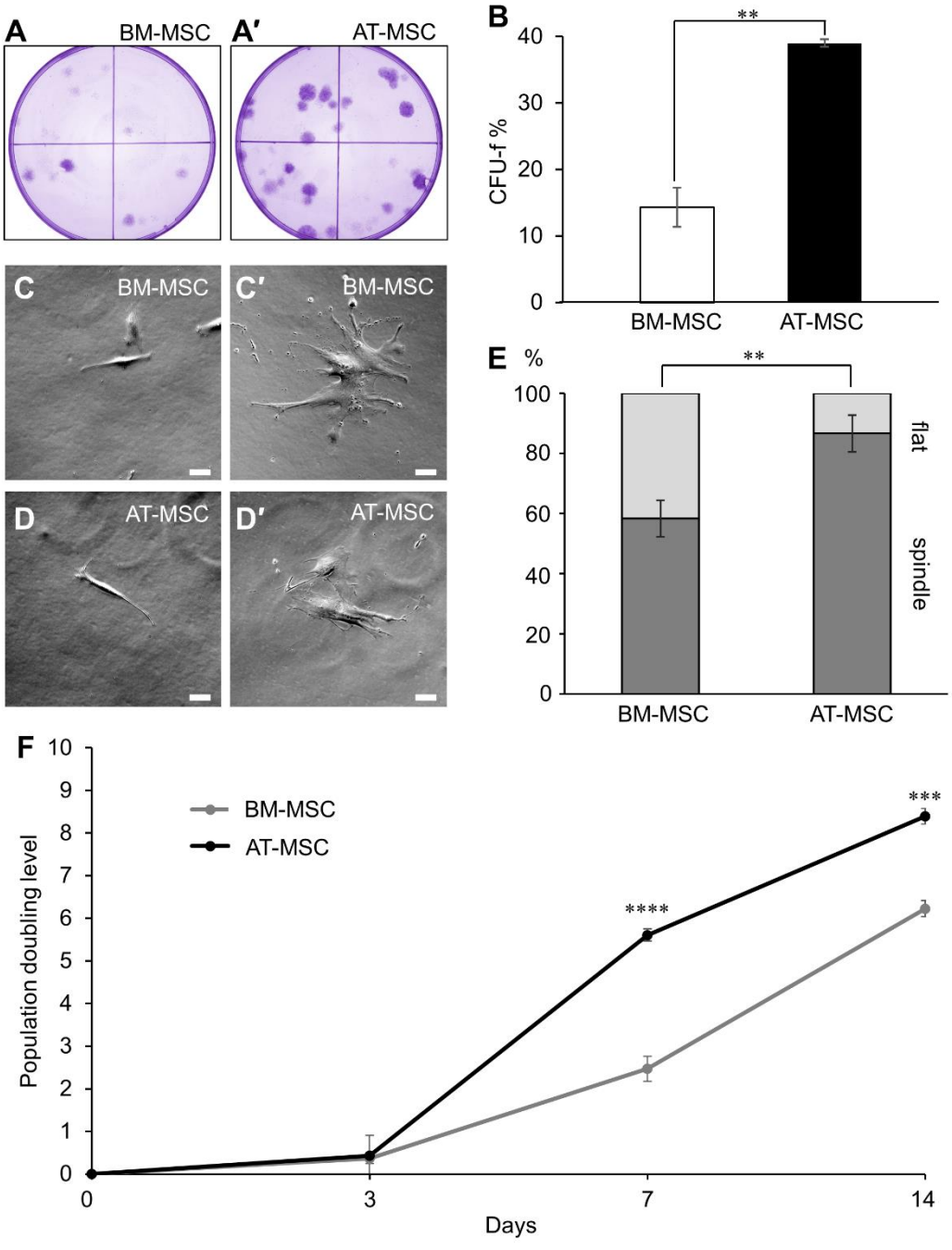
A
BM-MSC
A′
AT-MSC
C
BM-MSC
C′
BM-MSC
D
AT-MSC
D′
AT-MSC
B
CFU-f %
40
30
20
10
0
**
BM-MSC
AT-MSC
E
%
100
80
60
40
20
0
**
flat
spindle
BM-MSC
AT-MSC
F
Population doubling level
10
9
8
7
6
5
4
3
2
1
0
BM-MSC
AT-MSC
****
***
0
3
7
14
Days

Two prominent morphological types were exhibited in MSC cultures consisting of cells with long thin 'spindle' shapes (**Figure 2.2C, D**) and 'flat' cells with irregular processes (**Figure 2.2C′, D′**). Cell populations with a 'spindle' morphology were more readily exhibited by AT-MSCs (86.7±6.1%) than BM-MSCs (58.3±6.0%, $P<0.01$, n=6 independent cultures/group, **Figure 2.2E**). In contrary, a higher population of cells with a 'flat' morphology was observed in BM-MSCs (41.7±6.0%) in comparison to AT-MSCs (13.3±6.1%, $P<0.01$). The growth kinetics of MSCs were quantified over 14 days in culture and an assessment was made on the population doubling rate (**Figure 2.2F**). No difference in the PDL was observed between BM-MSCs (0.4±0.1) and AT-MSCs (0.4±0.5) after 3 days (n=3 independent cultures/group/time point). Higher PDL was observed in AT-MSC compared to BM-MSC cultures at day 7 (5.6±0.1 vs 2.5±0.3, $P<0.0001$) continuing to day 14 (8.4±0.2 vs 6.2±0.2, $P<0.001$). Thus the *in vitro* AT-MSC phenotype exhibited characteristics associated with superior cellular expansion.

2.5.2. BM-MSCs and AT-MSCs comparably ameliorate histological damage and weight loss associated with TNBS-induced colitis

Gross morphological damage was assessed in haematoxylin and eosin-stained cross sections of the colon. No damage was observed in sham-treated guinea-pigs (histological score = 0, **Figure 2.3A-A′**). At 24 and 72h following the induction of TNBS-induced colitis, changes to the colonic architecture were observed including flattening of the mucosa, haemorrhagic sites, loss of goblet cells and altered presentation of the circular muscle layer (histological score = 2.3) (**Figure 2.3B-B′**). These changes were attenuated in both BM-MSC and AT-MSC-treated animals at 24h and 72h (histological score = 0-1, **Figure 2.3C-C′, D-D′**). The body weight of guinea-pigs was recorded before and after treatment at 24, 48 and 72h (**Figure 2.3E, Table 2.1**, n=4 animals/group/time point). No differences in weight were observed between treatment groups after 24h. By 48 and 72h, the body weight of TNBS group was lower compared to sham (both $P<0.001$).

Figure 2.3 ***Effects of MSC treatment on histological changes and body weight in colitis***

Colonic structure assessed via haematoxylin and eosin staining of cross sections from tissues collected at 24h **(A-D)** and 72h **(A′-D′)** post TNBS administration. Scale bar=50μm. **(E)** Body weight recorded at 24, 48 and 72h after TNBS administration and expressed as the change from baseline measurements. **P*<0.05, ***P*<0.01, ****P*<0.001, n=4 animals/group/time point.

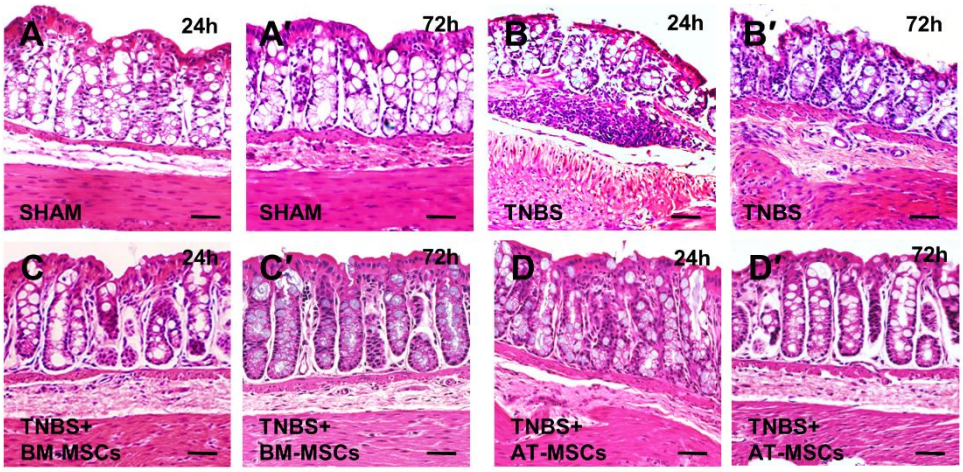
A
24h
SHAM
A'
72h
SHAM
B
24h
TNBS
B'
72h
TNBS
C
24h
TNBS+
BM-MSCs
C'
72h
TNBS+
BM-MSCs
D
24h
TNBS+
AT-MSCs
D'
72h
TNBS+
AT-MSCs

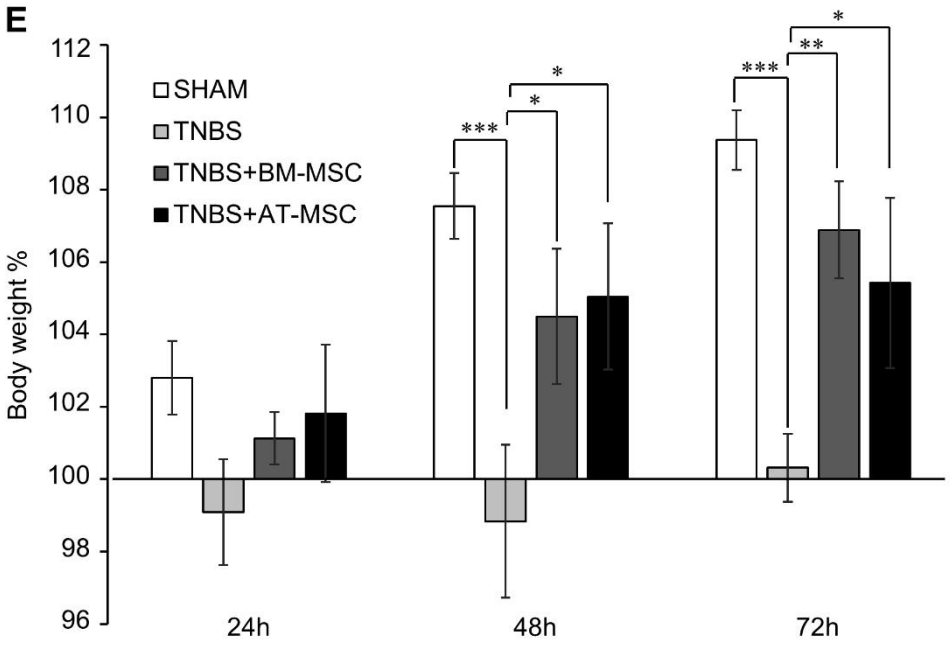
E
Body weight %
112
110
108
106
104
102
100
98
96
SHAM
TNBS
TNBS+BM-MSC
TNBS+AT-MSC
***
*
*
***
**
*
24h
48h
72h

Table 2.1 ***Effects of mesenchymal stem cells derived from bone marrow and adipose tissue on body weight (%) in TNBS-induced colitis***

Time after treatment	Treatment Groups			
	Sham	TNBS	TNBS+BM-MSC	TNBS+AT-MSC
24h	102.8±1.0	99.1±1.5	101.1±0.7	101.8±1.9
48h	107.5±0.9	98.8±2.1 †††	104.5±1.9 *	105.0±2.0 *
72h	109.4±0.8	100.3±0.9 †††	106.9±1.3 **	105.4±2.4 *

TNBS – 2,4,6-trinitrobenzene sulfonic acid, BM-MSC – bone marrow derived MSC, AT-MSC – adipose tissue derived MSC, *P<0.05, **P<0.01, significantly different to TNBS; †††P<0.001, significantly different to sham.

The reduction in body weight was ameliorated by both BM-MSC (48h, $P<0.05$ and 72h, $P<0.01$) and AT-MSC treatments (48h and 72h $P<0.05$). Therefore BM-MSCs and AT-MSCs were equally effective in attenuating colitis-induced weight loss.

2.5.3. BM-MSCs are more efficient than AT-MSCs in attenuating leukocyte infiltration to the level of the myenteric ganglia

The number of leukocytes in proximity to the myenteric plexus were quantified in LMMP preparations of the guinea-pig colon (**Figure 2.4A-D′**, n=4 animals/group/time point). Elevated leukocyte counts (cells/area) were observed in TNBS groups at 24h (104.8±5.0) and 72h (71.8±3.2) compared to shams (24h: 19.8±1.0 and 72h: 19.8±1.6, both $P<0.001$; **Figure 2.4E**). At 24h, elevated leukocyte levels were attenuated by BM-MSC (40.0±3.3, $P<0.01$) and AT-MSC (50.5±9.9, $P<0.05$) treatments. However, the number of leukocytes was still elevated in AT-MSC-treated animals in comparison to sham ($P<0.05$). By 72h, TNBS-induced leukocyte infiltration was mitigated by BM-MSC (24.0±1.7, $P<0.01$) and AT-MSC (25.0±3.2, $P<0.01$) treatments to levels comparable to shams. These results demonstrate that both MSC types can attenuate plexitis, however BM-MSCs appear to act faster.

2.5.4. BM-MSCs and AT-MSCs have comparable efficacy for attenuating inflammation-induced enteric neuropathy

The pan-neuronal marker HuC/D was used to assess the neuroprotective efficacy of MSCs in wholemount LMMP preparations (**Figure 2.5A-D′**, n=4 animals/group/time point). In comparison to sham, the administration of TNBS resulted in neuronal loss at 24h ($P<0.0001$) which persisted at 72h ($P<0.001$, **Figure 2.5E, Table 2.2**). The loss of neurons was ameliorated at both time points by BM-MSC (24h: $P<0.0001$ and 72h: $P<0.01$) and AT-MSC treatments (24h: $P<0.001$ and 72h: $P<0.01$). However, AT-MSC treatment was less effective and differences to the sham groups were observed at 24 and 72h (both $P<0.05$, **Figure 2.5E**).

Figure 2.4 ***Effects of MSCs on leukocyte infiltration to the myenteric plexus***

(A-D′) CD45-IR leukocytes (green) visualised on the level of myenteric neurons labelled with anti-PGP9.5 (red) by confocal microscopy in LMMP wholemounts prepared from colon collected at 24 **(A-D)** and 72h **(A′-D′)** post treatment. Scale bar=50µm. **(E)** CD45-IR leukocytes quantified in a 2mm^2 area of the myenteric plexus in the colon. *P<0.05, **P<0.01, ***P<0.001, n=4 animals/group/time point.

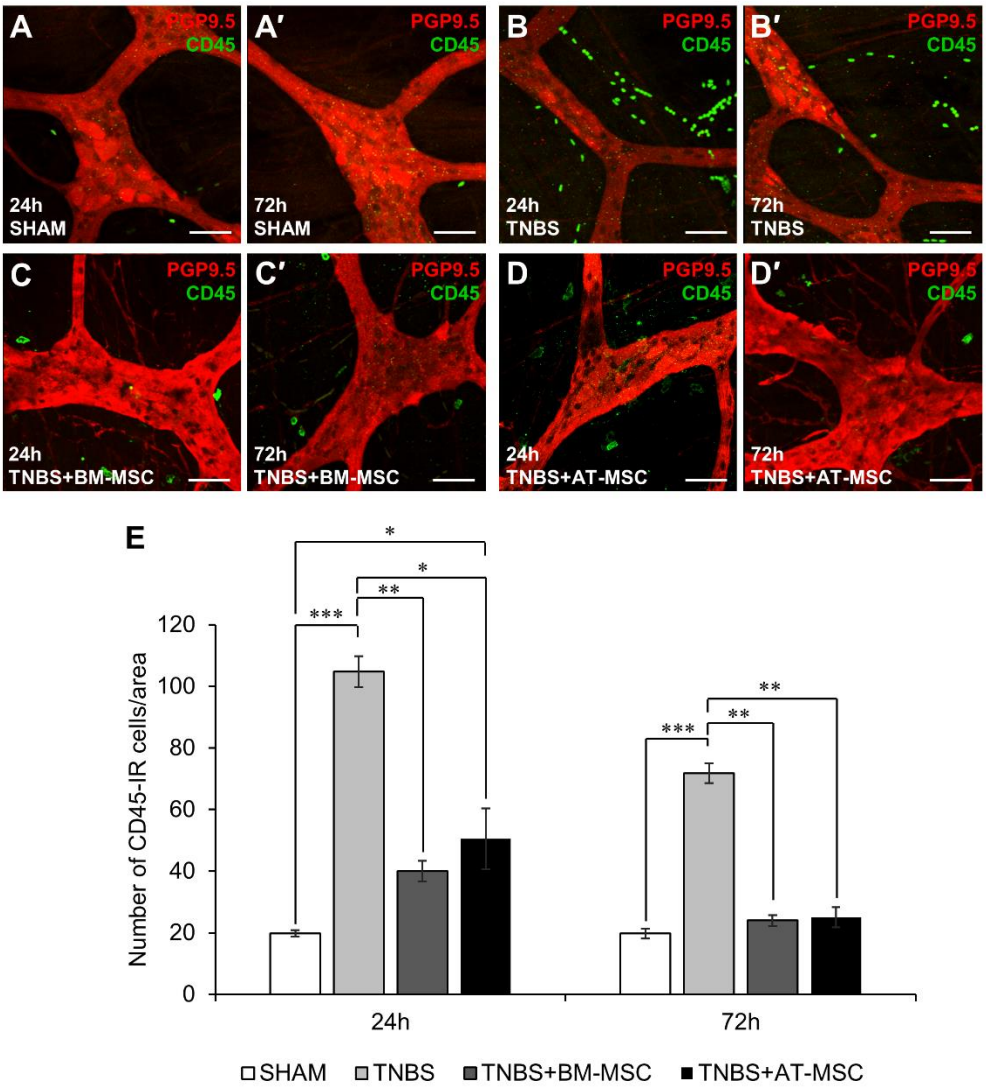
A
PGP9.5
CD45
24h
SHAM
A′
PGP9.5
CD45
72h
SHAM
B
PGP9.5
CD45
24h
TNBS
B′
PGP9.5
CD45
72h
TNBS
C
PGP9.5
CD45
24h
TNBS+BM-MSC
C′
PGP9.5
CD45
72h
TNBS+BM-MSC
D
PGP9.5
CD45
24h
TNBS+AT-MSC
D′
PGP9.5
CD45
72h
TNBS+AT-MSC
E
Number of CD45-IR cells/area
120
100
80
60
40
20
0
*
*
**
***
**
**
***
24h
72h
SHAM
TNBS
TNBS+BM-MSC
TNBS+AT-MSC

Figure 2.5 ***Effects of BM-MSCs and AT-MSCs on the total number of myenteric neurons***

(A-D′) Neuronal cell bodies in the myenteric plexus were labelled with the pan-neuronal marker anti-HuC/D antibody at 24 **(A-D)** and 72h **(A′-D′)** post treatment. Scale bar=50µm. **(E)** The total number of neuronal bodies were quantified within a $2mm^2$ area of the myenteric plexus. **P*<0.05, ***P*<0.01, ****P*<0.001, *****P*<0.0001, n=4 animals/group/time point.

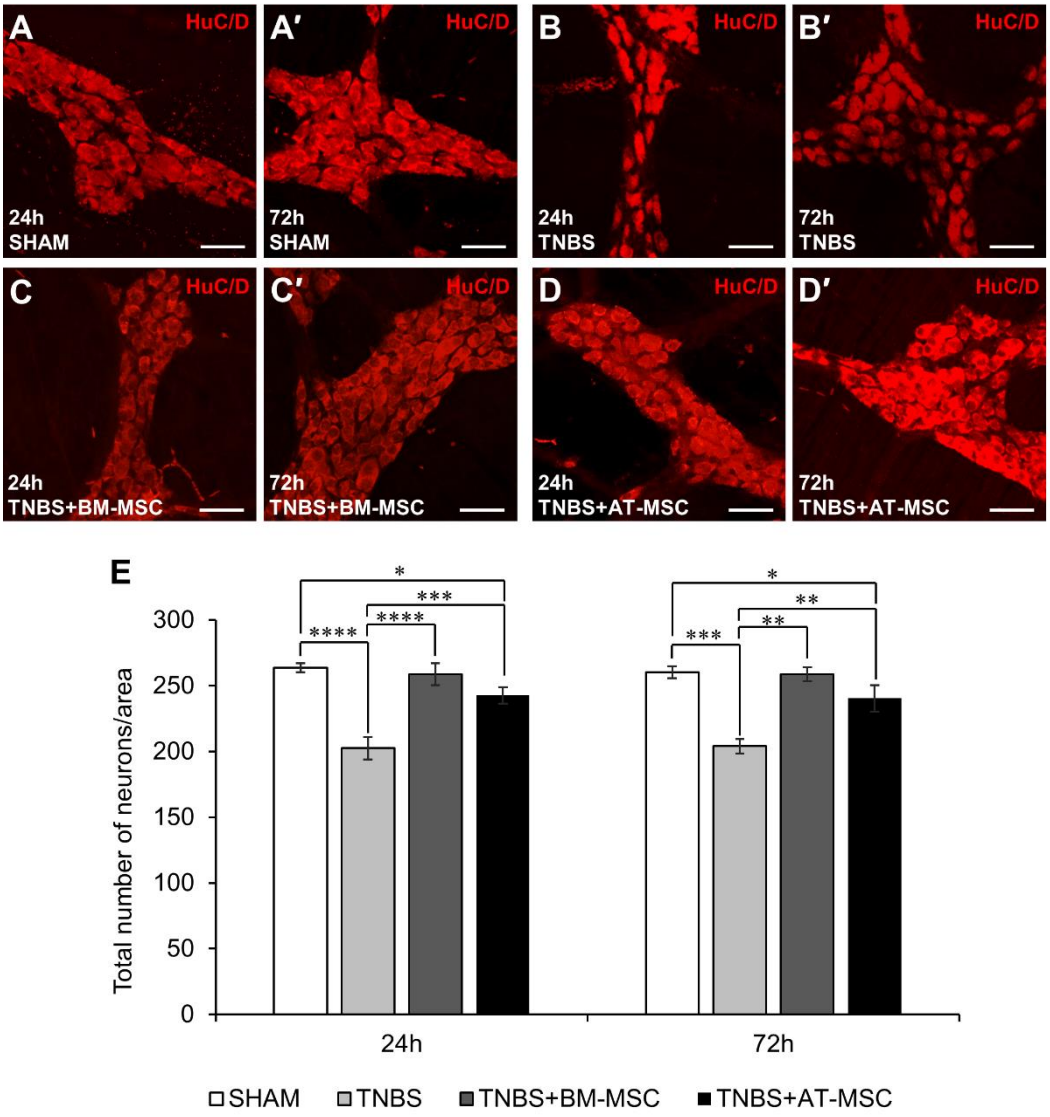
A
HuC/D
24h
SHAM
A′
HuC/D
72h
SHAM
B
HuC/D
24h
TNBS
B′
HuC/D
72h
TNBS
C
HuC/D
24h
TNBS+BM-MSC
C′
HuC/D
72h
TNBS+BM-MSC
D
HuC/D
24h
TNBS+AT-MSC
D′
HuC/D
72h
TNBS+AT-MSC
E
Total number of neurons/area
300
250
200
150
100
50
0
*
***
****
****
*
**
***
**
24h
72h
SHAM
TNBS
TNBS+BM-MSC
TNBS+AT-MSC

Table 2.2 ***Effects of mesenchymal stem cells derived from bone marrow and adipose tissue on myenteric neurons in TNBS-induced colitis***

Time after treatment	Treatment groups			
	Sham	TNBS	TNBS+BM-MSC	TNBS+AT-MSC
		Total number of myenteric neurons/2mm²		
24h	263.8±3.5	202.5±8.4 ††††	258.8±2.9 ****	242.8±6.2 *** †
72h	262.0±5.1	204.0±5.4 †††	258.8±7.6 **	240.5±10.0 ** †
		Total number of nNOS-IR neurons/2mm²		
24h	52.3±1.8	70.0±4.9 †††	55.0±3.2 **	53.5±2.6 **
72h	52.5±1.0	70.5±3.2 †††	55.3±2.7 **	57.3±1.7 *
		Proportion of nNOS-IR neurons/2mm² (%)		
24h	19.9±0.9	34.8±2.8 ††††	21.3±1.2 ****	22.1±1.1 ****
72h	20.2±0.3	34.6±1.8 ††††	21.4±1.3 ****	23.9±0.7 ***
		Total number of ChAT-IR neurons/2mm²		
24h	163.5±2.1	111.3±5.7 ††††	148.3±4.6 ****	144.5±4.9 *** †
72h	157.8±6.3	112.3±1.7 ††††	147.5±7.3 ****	145.3±3.4 ***
		Proportion of ChAT-IR neurons/2mm² (%)		
24h	62.0±1.4	55.1±2.9	57.3±1.6	59.5±0.9
72h	59.1±0.9	55.2±2.3	57.1±3.0	60.7±2.5

TNBS – 2,4,6-trinitrobenzene sulfonic acid, BM-MSC – bone marrow derived MSC, AT-MSC – adipose tissue derived MSC, nNOS – neuronal nitric oxide synthase, ChAT – choline acetyltransferase, IR – immunoreactive, *P<0.05, **P<0.01, ***P<0.001, ****P<0.0001, significantly different to TNBS; †P<0.05, †††P<0.001, ††††P<0.0001, significantly different to sham.

Inhibitory and excitatory neurons, defined by nNOS-IR and ChAT-IR respectively, were quantified within the myenteric ganglia (**Figures 2.6A-D′ & 2.7A-D′, Table 2.2**, n=4 animals/group/time point). Increased numbers (both $P<0.001$) and proportions (both $P<0.0001$) of nNOS-IR neurons were observed in myenteric ganglia from TNBS groups at 24 and 72h compared to sham (**Figure 2.6E-F, Table 2.2**). BM-MSC and AT-MSC treatments attenuated these changes in the total number (BM-MSC: 24h and 72h, $P<0.01$ and AT-MSC: 24h, $P<0.01$ and 72h, $P<0.05$) and proportion of nNOS-IR neurons at both time points (BM-MSC: 24h and 72h, $P<0.0001$; AT-MSCs: 24h, $P<0.0001$ and 72h, $P<0.001$). The total numbers of ChAT-IR neurons were decreased at both 24 and 72h after TNBS administration compared to sham ($P<0.0001$ for both time points) (**Figure 2.6E, Table 2.2**). The loss of ChAT-IR neurons was attenuated at 24 and 72h by treatments with BM-MSCs ($P<0.0001$) and AT-MSCs ($P<0.001$ for both time points). However, the number of ChAT-IR neurons were still less than sham after AT-MSC treatment at 24h ($P<0.05$). Quantification of the proportion of ChAT-IR neurons revealed no differences between groups (**Figure 2.6F, Table 2.2**). Thus, although both BM-MSCs and AT-MSCs were effective in attenuating neuronal loss and changes in nNOS and ChAT immunoreactivity, AT-MSCs were less efficacious compared to BM-MSCs in treating neuropathy.

2.5.5. BM-MSCs and AT-MSCs mitigate the loss of nerve fibres in the inflamed colon

Immunoreactivity for CGRP (sensory), TH (sympathetic) and VAChT (cholinergic) was assessed within the myenteric plexus in LMMP preparations (**Figures 2.8A-D′, 2.9A-D′ & 2.10A-D′, Table 2.3**). At 24 and 72h, TNBS administered groups exhibited decreased density of CGRP immunoreactivity (**Figure 2.8E**, $P<0.0001$ for both time points) compared to shams. At these time points, BM-MSC and AT-MSC treatments attenuated the loss of CGRP immunoreactivity (BM-MSC: $P<0.001$ for both time points; AT-MSC: 24h, $P<0.05$ and 72h $P<0.001$). However, the loss of CGRP-IR was not prevented to the levels of sham groups by BM-MSCs ($P<0.01$ for both time points) and AT-MSCs (24h, $P<0.001$ and 72h, $P<0.01$) treatments.

Figure 2.6 ***Effects of BM-MSCs and AT-MSCs on nitrergic myenteric neurons***

(A-D′) Nitrergic (nNOS-IR) neurons were visualised in the myenteric plexus at 24 **(A-D)** and 72h **(A′-D′)**. Scale bar=50µm. The total number of nNOS-IR neurons **(E)** and the proportion of nNOS-IR neurons to the total number of HuC/D-IR neurons **(F)** were quantified within a 2mm^2 area of the myenteric plexus in the guinea-pig colon. **P*<0.05, ***P*<0.01, ****P*<0.001, *****P*<0.0001, n=4 animals/group/time point.

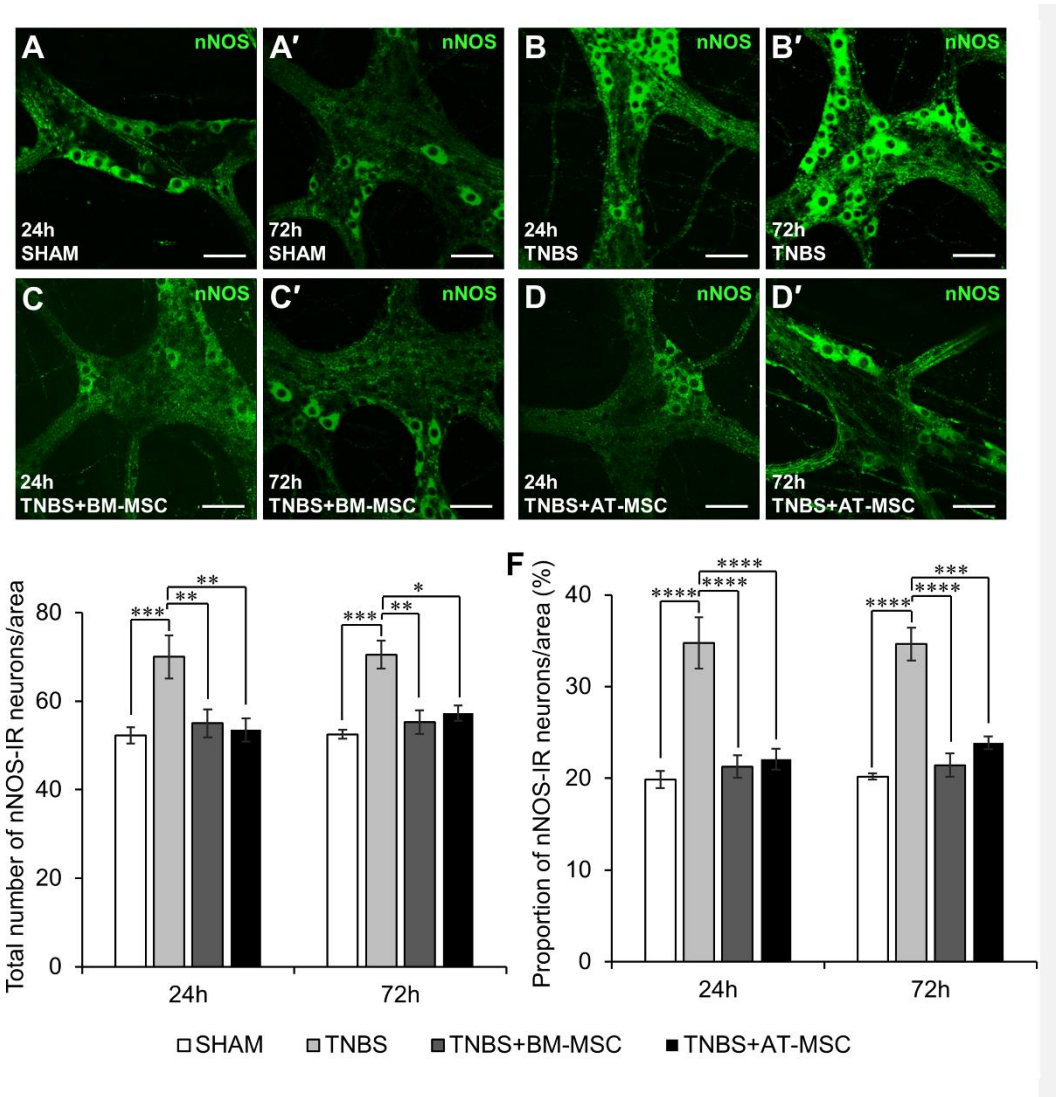
A
nNOS
24h
SHAM
A′
nNOS
72h
SHAM
B
nNOS
24h
TNBS
B′
nNOS
72h
TNBS
C
nNOS
24h
TNBS+BM-MSC
C′
nNOS
72h
TNBS+BM-MSC
D
nNOS
24h
TNBS+AT-MSC
D′
nNOS
72h
TNBS+AT-MSC
F
Total number of nNOS-IR neurons/area
Proportion of nNOS-IR neurons/area (%)
24h
72h
SHAM
TNBS
TNBS+BM-MSC
TNBS+AT-MSC

Figure 2.7 ***Effects of BM-MSCs and AT-MSCs on cholinergic myenteric neurons***

(A-D′) Cholinergic (ChAT-IR) neurons in the myenteric plexus at 24 **(A-D)** and 72h **(A′-D′)**. Scale bar=50µm. The total number of ChAT-IR neurons **(E)** and the proportion of ChAT-IR neurons to the total number of HuC/D-IR neurons **(F)** were quantified within a 2mm^2 area of the myenteric plexus in the guinea-pig colon. **P*<0.05, ****P*<0.001, *****P*<0.0001, n=4 animals/group/time point.

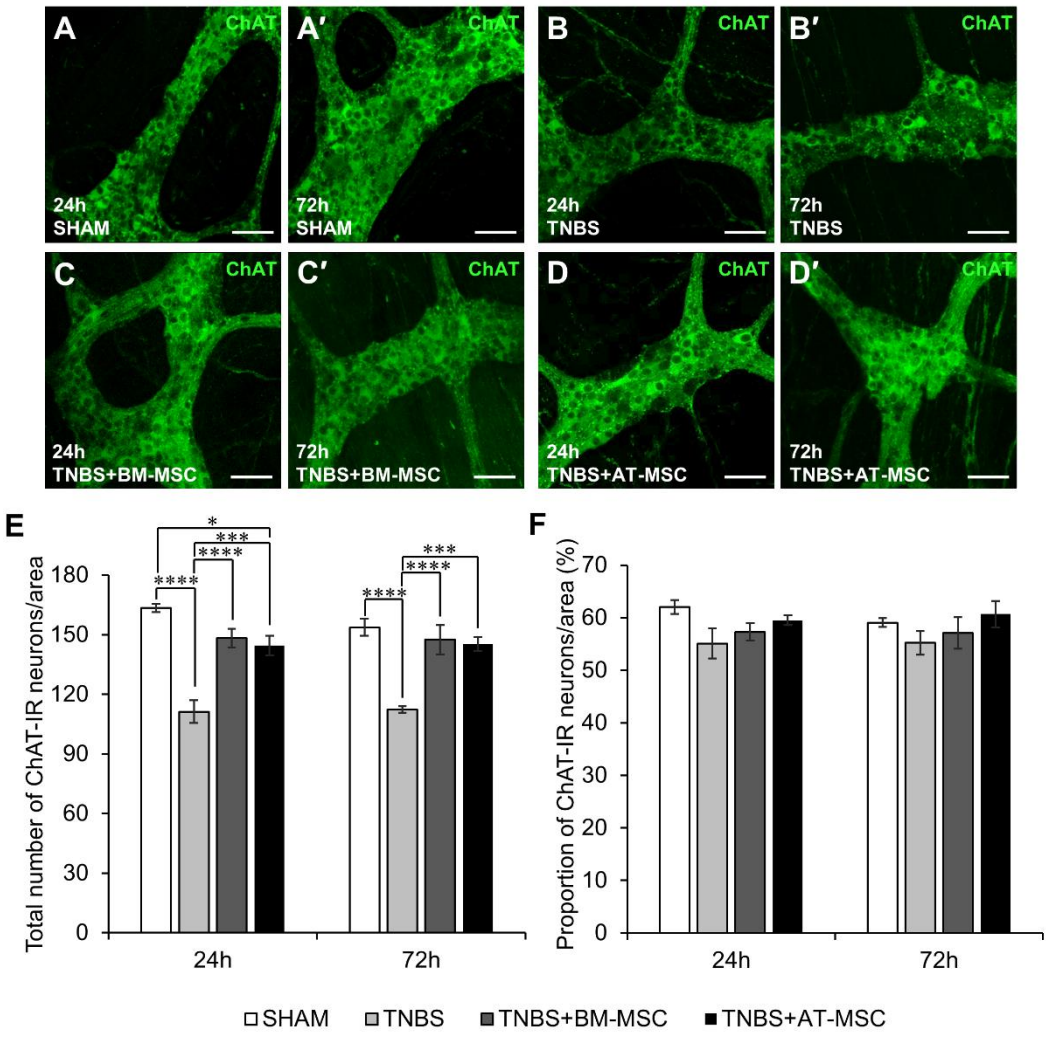
A
ChAT
24h
SHAM
A′
ChAT
72h
SHAM
B
ChAT
24h
TNBS
B′
ChAT
72h
TNBS
C
ChAT
24h
TNBS+BM-MSC
C′
ChAT
72h
TNBS+BM-MSC
D
ChAT
24h
TNBS+AT-MSC
D′
ChAT
72h
TNBS+AT-MSC
E
Total number of ChAT-IR neurons/area
0
30
60
90
120
150
180
*
***
****
****
****
***
****
24h
72h
F
Proportion of ChAT-IR neurons/area (%)
0
10
20
30
40
50
60
70
24h
72h
SHAM
TNBS
TNBS+BM-MSC
TNBS+AT-MSC

Figure 2.8 ***Effects of BM-MSCs and AT-MSCs on CGRP-IR nerve fibres in the myenteric plexus***

(A-D′) CGRP-IR in the myenteric plexus at 24h **(A-D)** and 72h **(A′-D′)**. Scale bar=100µm. **(E)** Area percentage quantification of CGRP-IR within a 1mm^2 area of the myenteric plexus in the guinea-pig colon. *P<0.05, **P<0.01, ***P<0.001, ****P<0.0001, n=3 animals/group/time point.

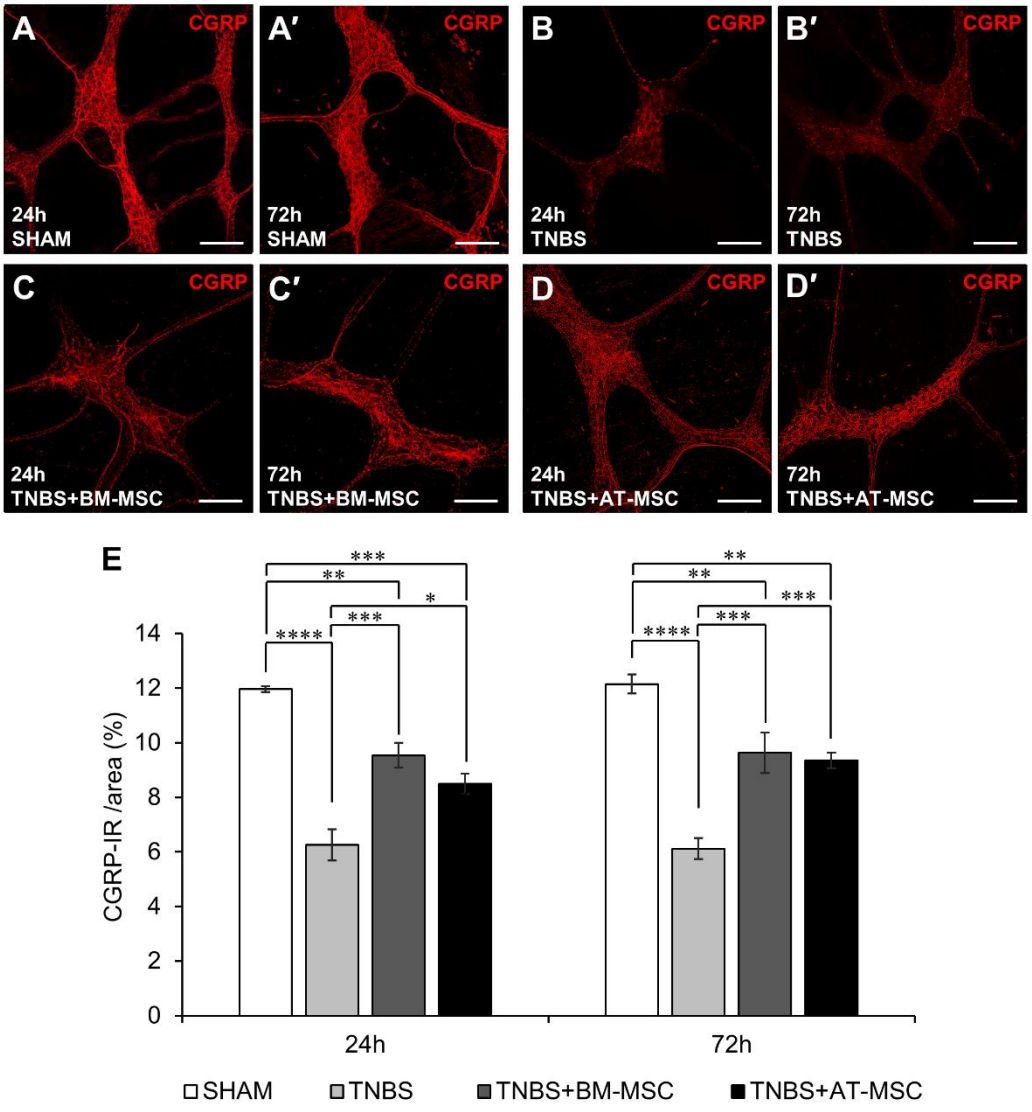
A
CGRP
24h
SHAM
A′
CGRP
72h
SHAM
B
CGRP
24h
TNBS
B′
CGRP
72h
TNBS
C
CGRP
24h
TNBS+BM-MSC
C′
CGRP
72h
TNBS+BM-MSC
D
CGRP
24h
TNBS+AT-MSC
D′
CGRP
72h
TNBS+AT-MSC
E
CGRP-IR /area (%)
0
2
4
6
8
10
12
14
24h
72h
SHAM
TNBS
TNBS+BM-MSC
TNBS+AT-MSC

Figure 2.9 ***Effects of BM-MSCs and AT-MSCs on TH-IR nerve fibres in the myenteric plexus***

(A-D′) TH-IR nerve fibres in the myenteric plexus at 24h **(A-D)** and 72h **(A′-D′)**. Scale bar=100µm. **(E)** Area percentage quantification of TH-IR nerve fibres within a 1mm^2 area of the myenteric plexus in the guinea-pig colon. *P<0.05, **P<0.01, n=3 animals/group/time point.

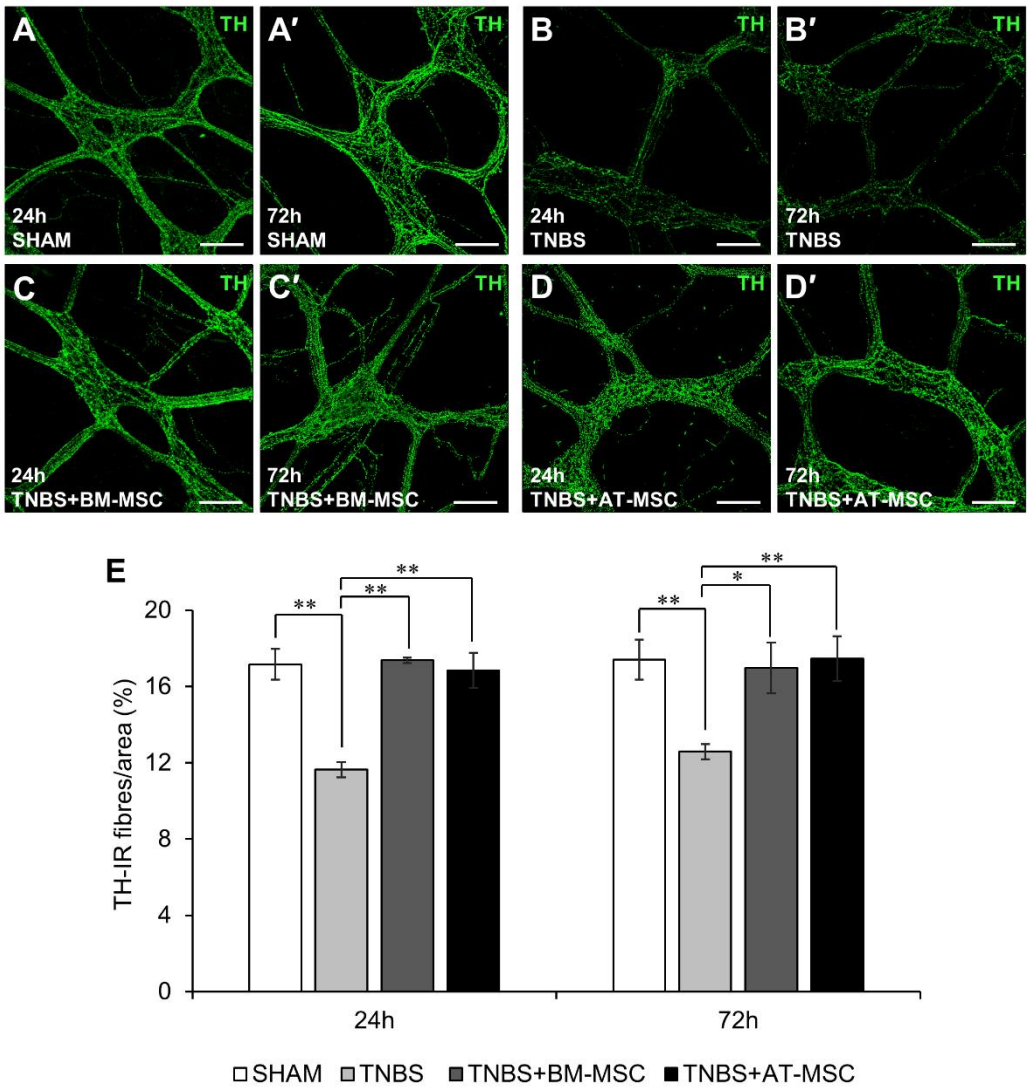
A
TH
24h
SHAM
A′
TH
72h
SHAM
B
TH
24h
TNBS
B′
TH
72h
TNBS
C
TH
24h
TNBS+BM-MSC
C′
TH
72h
TNBS+BM-MSC
D
TH
24h
TNBS+AT-MSC
D′
TH
72h
TNBS+AT-MSC
E
TH-IR fibres/area (%)
0
4
8
12
16
20
**
**
**
**
**
*
24h
72h
SHAM
TNBS
TNBS+BM-MSC
TNBS+AT-MSC

Figure 2.10 ***Effects of BM-MSCs and AT-MSCs on VAChT-IR nerve fibres in the myenteric plexus***

(A-D′) VAChT-IR nerve fibres in the myenteric plexus at 24h **(A-D)** and 72h **(A′-D′)**. Scale bar=100µm. **(E)** Area percentage quantification of VAChT-IR nerve fibres within a $1mm^2$ area of the myenteric plexus in the guinea-pig colon. ****$P<0.0001$, n=3 animals/group/time point.

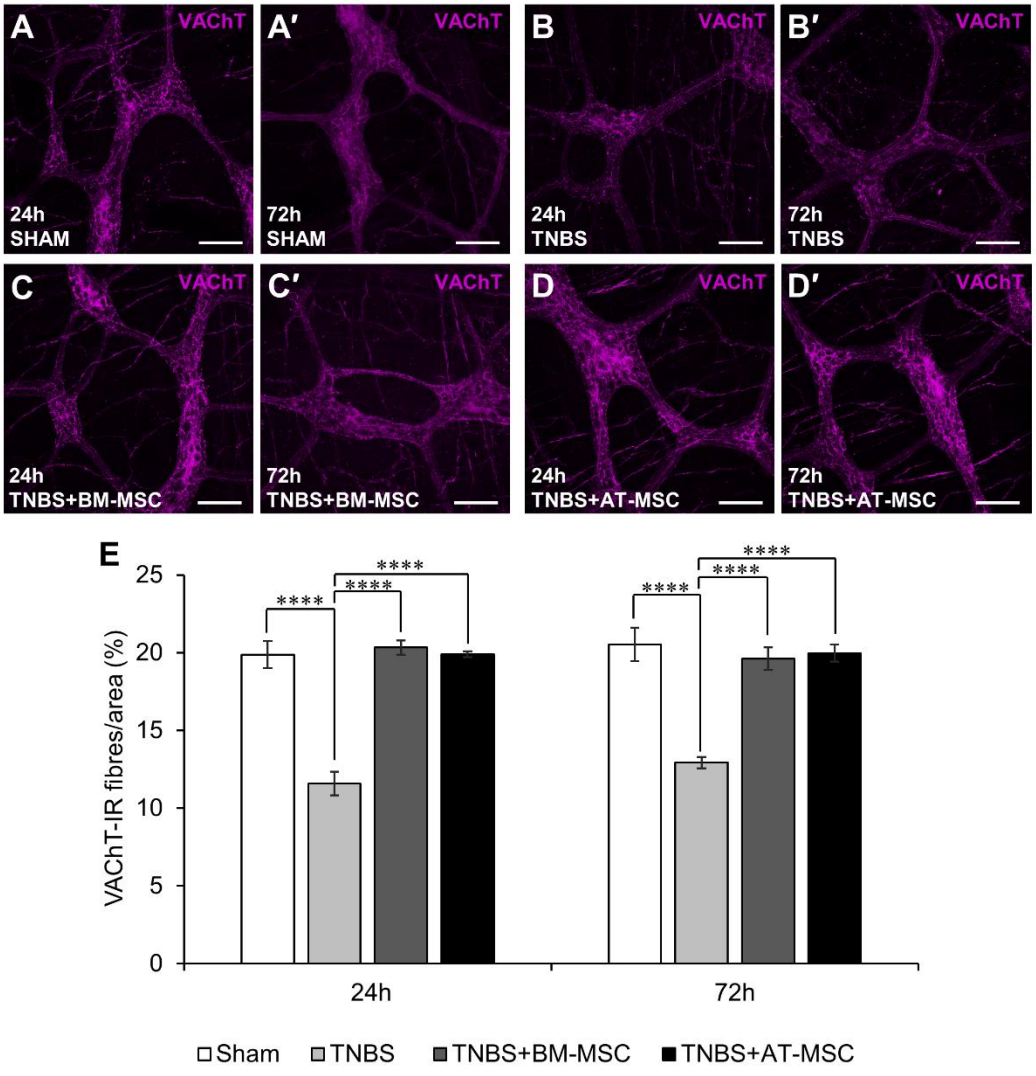
A
VAChT
24h
SHAM
A′
VAChT
72h
SHAM
B
VAChT
24h
TNBS
B′
VAChT
72h
TNBS
C
VAChT
24h
TNBS+BM-MSC
C′
VAChT
72h
TNBS+BM-MSC
D
VAChT
24h
TNBS+AT-MSC
D′
VAChT
72h
TNBS+AT-MSC
E
VAChT-IR fibres/area (%)
25
20
15
10
5
0
****
****
****
****
****
****
24h
72h
Sham
TNBS
TNBS+BM-MSC
TNBS+AT-MSC

Table 2.3 ***Effects of mesenchymal stem cells derived from bone marrow and adipose tissue on nerve fibre density in TNBS-induced colitis***

Time after treatment	Treatment groups			
	Sham	TNBS	TNBS+BM-MSC	TNBS+AT-MSC
		Level of CGRP immunoreactivity /1mm² (%)		
24h	12.0±0.1	6.3±0.6 ††††	9.5±0.5 *** ††	8.5±0.4 * †††
72h	12.2±0.4	6.1±0.4 ††††	9.6±0.7 *** ††	9.4±0.3 *** ††
		Density of TH-IR nerve fibres/1mm² (%)		
24h	17.2±0.8	11.6±0.4 ††	17.4±0.1 **	16.8±0.9 **
72h	17.4±1.1	12.6±0.4 ††	17.0±1.3 *	17.5±1.2 **
		Density of VAChT-IR nerve fibres/1mm² (%)		
24h	19.9±0.9	11.6±0.8 ††††	20.3±0.5 ****	19.9±0.2 ****
72h	20.5±1.1	12.9±0.4 ††††	19.6±0.7 ****	20.0±0.6 ****

TNBS – 2,4,6-trinitrobenzene sulfonic acid, BM-MSC – bone marrow derived MSC, AT-MSC – adipose tissue derived MSC, CGRP – calcitonin gene-related peptide, TH – tyrosine hydroxylase, VAChT – vesicular acetylcholine transporter, IR – immunoreactive, **P*<0.05, ***P*<0.01, ****P*<0.001, *****P*<0.0001, significantly different to TNBS; ††*P*<0.01, †††*P*<0.001, ††††*P*<0.0001, significantly different to sham.

Similar loss in density was observed after TNBS administration in TH-IR (**Figure 2.9E**, both $P<0.01$) and VAChT-IR nerve fibres (**Figure 2.10E**, both $P<0.0001$) compared to shams. BM-MSC and AT-MSC treatments ameliorated the loss of TH-IR (BM-MSC: 24h, $P<0.01$ and 72h, $P<0.05$; AT-MSC: $P<0.01$ for both time points) and VAChT-IR (all $P<0.0001$) nerve fibres. BM-MSCs and AT-MSCs were equally efficacious in attenuating the loss of nerve fibre immunoreactivity.

2.5.6. BM-MSCs and AT-MSCs reduce levels of superoxide produced by mitochondria in the myenteric plexus under inflammatory conditions

Mitochondria-derived superoxide levels in the myenteric ganglia were visualised in LMMPs probed with MitoSOX, a dye that targets mitochondria in live cells and fluoresces upon selective oxidation by superoxide (**Figure 2.11A-D′**). High levels of MitoSOX fluorescence were observed in the myenteric ganglia compared to other regions of the LMMP. Superoxide levels in the myenteric ganglia were quantified by measuring the fluorescence of MitoSOX in confocal images (mean fluorescence intensity). Exposure to TNBS resulted in elevated MitoSOX fluorescence (mean fluorescence intensity) within the myenteric ganglia at 24h (52.0±3.5 arb. units) and 72h (55.2±7.8 arb. units) compared to sham-treated animals (24h: 9.8±0.5 arb. units, 72h: 10.0±0.8 arb. units; $P<0.0001$ for both time points). At 24h, treatment of TNBS exposed animals with either BM-MSCs (23.8±1.0 arb. units) or AT-MSCs (21.1±2.8 arb. units) lowered MitoSOX fluorescence (BM-MSC: $P<0.001$, AT-MSC: $P<0.0001$) to levels similar to controls. Likewise, at 72h, BM-MSCs (22.7±1.2 arb. units) and AT-MSCs (34.2±6.8 arb. units) lowered MitoSOX fluorescence (BM-MSC: $P<0.0001$, AT-MSC: $P<0.01$) compared to TNBS-exposed animals; nonetheless levels were still elevated after AT-MSC treatment compared to uninflamed controls ($P<0.01$).

2.5.7. BM-MSCs and AT-MSCs migrate to the myenteric plexus

BM-MSCs and AT-MSCs were detected in cross sections of the colon at 24h and 72h as defined by HLA-IR (**Figure 2.12A-D″**).

Figure 2.11 ***Effects of BM-MSCs and AT-MSCs on mitochondria-derived superoxide levels in the myenteric plexus***

(A-D′) Mitochondria-derived superoxide visualised by the fluorescent probe MitoSOX in the myenteric plexus at 24h **(A-D)** and 72h **(A′-D′)**. Scale bar=100µm. **(E)** Mean fluorescence intensity (arbitrary units) of the myenteric ganglia in images of LMMPs from the guinea-pig colon labelled with MitoSOX. ***P*<0.01, ****P*<0.001, *****P*<0.0001, n=4 animals/group/time point.

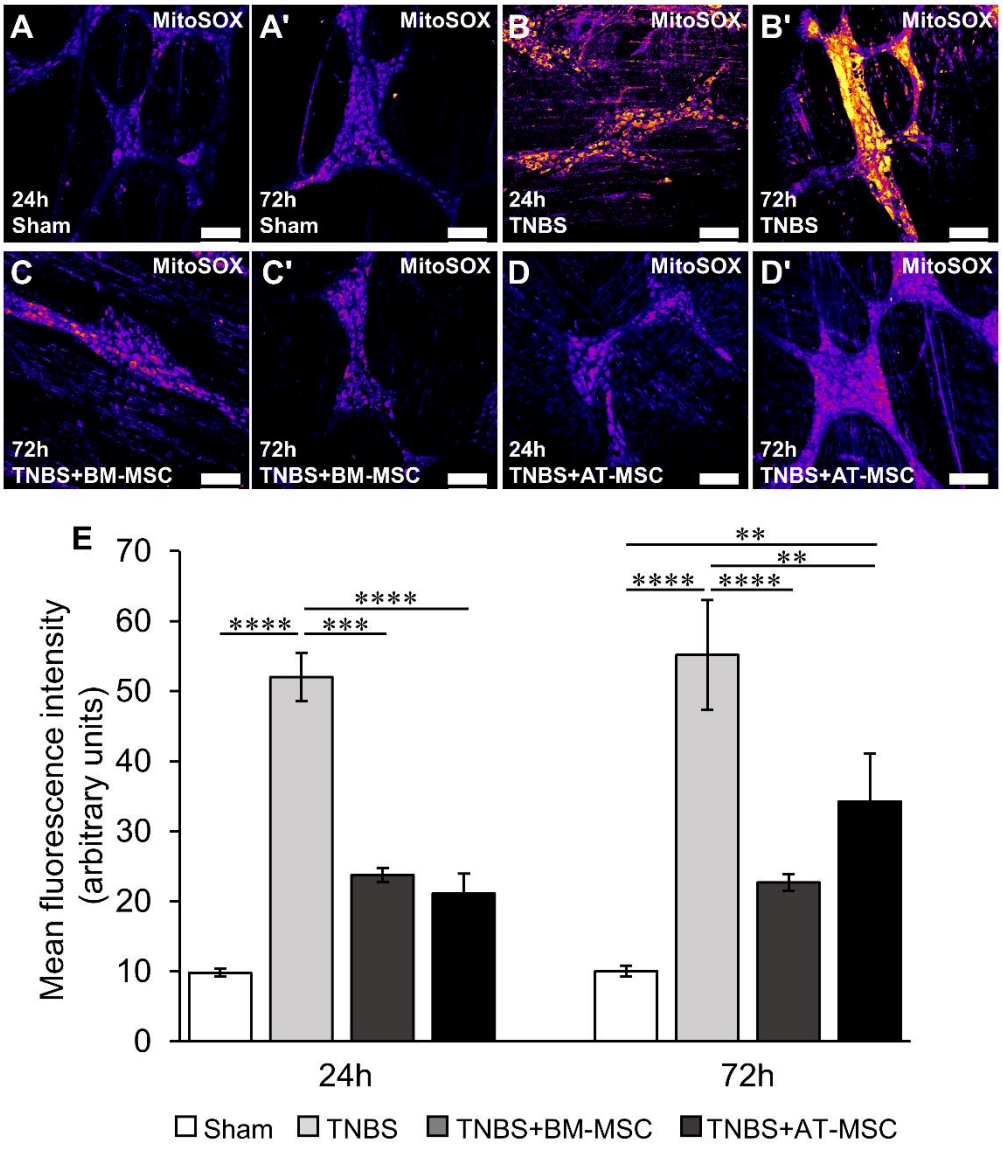
A
MitoSOX
24h
Sham
A'
MitoSOX
72h
Sham
B
MitoSOX
24h
TNBS
B'
MitoSOX
72h
TNBS
C
MitoSOX
72h
TNBS+BM-MSC
C'
MitoSOX
72h
TNBS+BM-MSC
D
MitoSOX
24h
TNBS+AT-MSC
D'
MitoSOX
72h
TNBS+AT-MSC
E
Mean fluorescence intensity (arbitrary units)
0
10
20
30
40
50
60
70
****
***
****
**
****
**
24h
72h
Sham
TNBS
TNBS+BM-MSC
TNBS+AT-MSC

Figure 2.12 ***In vivo migration of BM-MSCs and AT-MSCs***

(A-D″) Cross sections of the guinea-pig colon after treatment with BM-MSCs **(A-B)** and AT-MSCs **(C-D)** labelled with anti-HLA **(A-D)** to detect human MSCs and anti-α-actin to visualise smooth muscle **(A′-D′)**. Scale bar=50μm. **(E′-F′)** High magnification confocal images (x100) of myenteric ganglia from BM-MSC **(E-E′)** and AT-MSC-treated guinea-pigs **(F-F′)**. Scale bar=10μm.

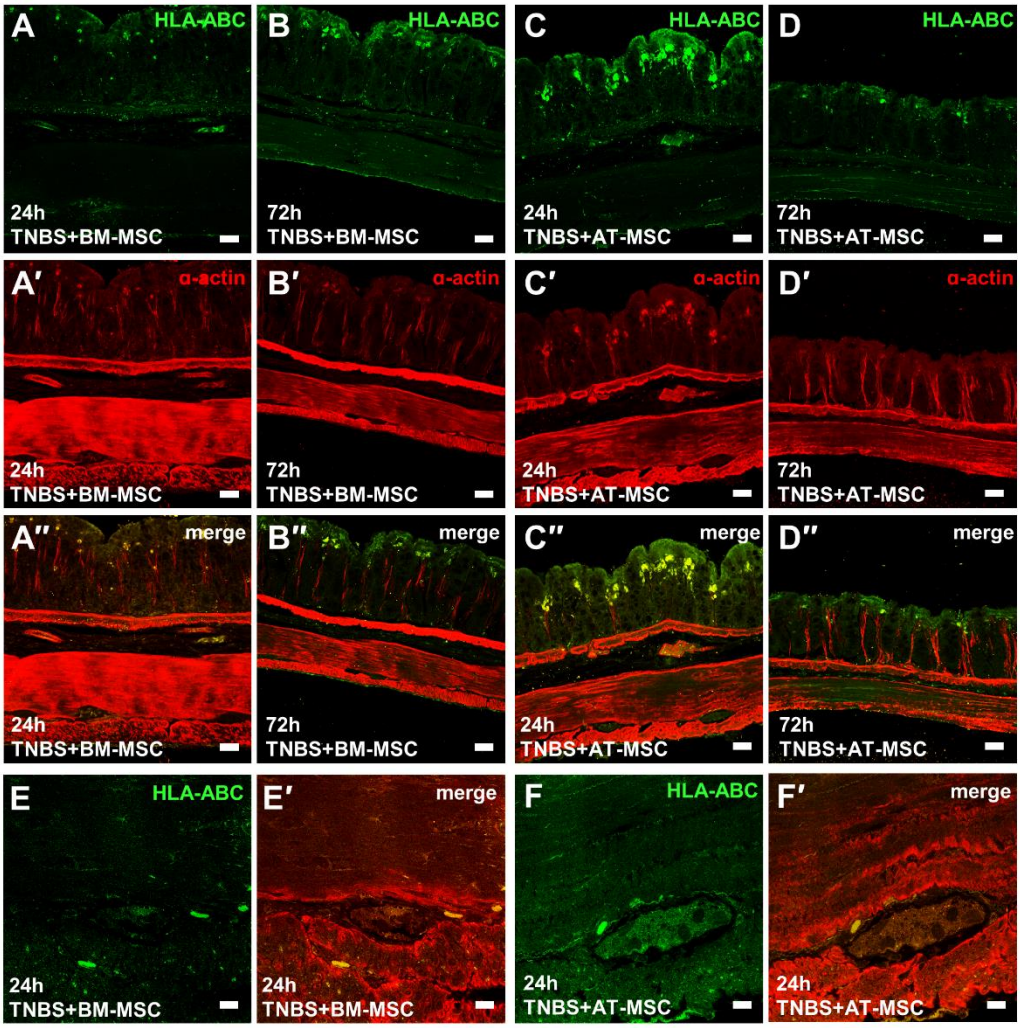
A
HLA-ABC
24h
TNBS+BM-MSC
B
HLA-ABC
72h
TNBS+BM-MSC
C
HLA-ABC
24h
TNBS+AT-MSC
D
HLA-ABC
72h
TNBS+AT-MSC
A′
α-actin
24h
TNBS+BM-MSC
B′
α-actin
72h
TNBS+BM-MSC
C′
α-actin
24h
TNBS+AT-MSC
D′
α-actin
72h
TNBS+AT-MSC
A″
merge
24h
TNBS+BM-MSC
B″
merge
72h
TNBS+BM-MSC
C″
merge
24h
TNBS+AT-MSC
D″
merge
72h
TNBS+AT-MSC
E
HLA-ABC
24h
TNBS+BM-MSC
E′
merge
24h
TNBS+BM-MSC
F
HLA-ABC
24h
TNBS+AT-MSC
F′
merge
24h
TNBS+AT-MSC

Predominantly, MSCs were observed within the mucosa and to a lesser extent in the submucosa. Relatively low number of HLA-IR cells was observed in the muscle layers. High magnification confocal images (x100) confirmed the presence of HLA-IR cells at the level of the myenteric ganglia in both BM-MSC (**Figure 2.12E-E′**) and AT-MSC (**Figure 2.12F-F′**) treated groups.

To assess the migration of MSCs to the inflamed myenteric plexus, an *in vitro* migration assay was performed using LPS stimulated neurons as a chemoattractant (**Figure 2.13**). BM-MSCs and AT-MSCs had a higher affinity to migrate to the conditioned medium of LPS-stimulated myenteric neurons (BM-MSC: $5.6\pm0.4\times10^3$; AT-MSC: $4.5\pm0.2\times10^3$) compared to control media without FBS (BM-MSC: $3.3\pm0.5\times10^3$; AT-MSC: $2.2\pm0.2\times10^3$, $P<0.01$ for both) or supplemented with FBS (BM-MSC: $2.9\pm0.3\times10^3$, $P<0.001$; AT-MSC: $2.6\pm0.5\times10^3$, $P<0.05$) and medium containing the same amount of LPS (20 ng/mL) as the conditioned medium of LPS-stimulated myenteric neurons (BM-MSC: $2.0\pm0.2\times10^3$, $P<0.0001$; AT-MSC: $2.3\pm0.3\times10^3$, $P<0.01$). No differences in migration were observed between BM-MSCs and AT-MSCs.

2.6. Discussion

This is the first study comparing the neuroprotective efficacy of AT-MSCs and BM-MSCs in a model of colitis. *In vitro,* AT-MSCs possessed a superior phenotype for cellular expansion. Both AT-MSCs and BM-MSCs demonstrated therapeutic efficacy in the amelioration of weight loss, histopathology, leukocyte infiltration to the myenteric plexus, neuronal loss, altered neurochemical expression and damage to nerve fibres. However, AT-MSCs appeared less effective in the attenuation of plexitis, neuropathy and reduction in ChAT immunoreactivity.

MSCs used in this study were validated according to the guidelines of the International Society for Cellular Therapy (Dominici et al., 2006). BM-MSCs and AT-MSCs displayed a typical surface marker phenotype including positive expression of CD29, CD44, CD73, and CD90 in addition to negligible expression of CD45.

Figure 2.13 ***In vitro migration of BM-MSCs and AT-MSCs***

Quantification of MSC migration towards the conditioned media of cultured myenteric plexus (MP) cells pre-stimulated with LPS in a modified Boyden chamber assay. $^{**}P<0.01$, $^{***}P<0.001$, $^{****}P<0.0001$, n=4 independent cultures/group.

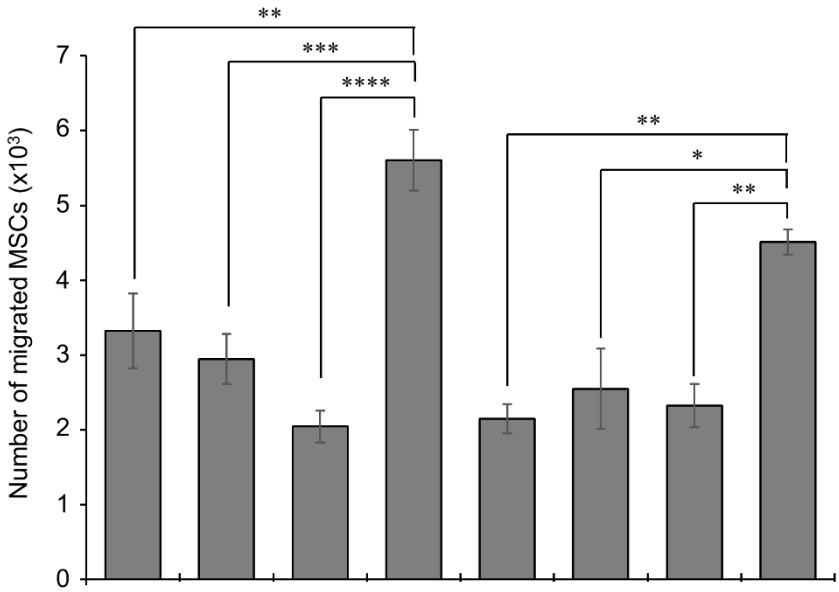

BM-MSC	+	+	+	+	-	-	-	-
AT-MSC	-	-	-	-	+	+	+	+
MP culture	-	-	-	+	-	-	-	+
LPS	-	-	+	+	-	-	+	+
FBS	-	+	+	+	-	+	+	+

AT-MSCs exhibited low positive expression of CD34, however it is now accepted that $CD34^{+}$ MSCs are a common subpopulation residing in the adipose tissue (Lin et al., 2012b). MSCs from both sources demonstrated multipotency by differentiation into adipocytes and osteocytes when cultured in media supplemented with appropriate differentiation factors. Both cell types were plastic adherent and proliferated to form colonies, a definitive characteristic of MSCs.

In vitro expansion of MSC cultures is fundamental to obtain appropriate numbers for therapeutic application. Our results show that after an initial ~3day lag period, AT-MSCs proliferate at a higher rate than BM-MSCs yielding greater quantities of cells. Other studies have shown similar differences in proliferation exhibited by BM-MSCs and AT-MSCs (Ikegame et al., 2011, Dmitrieva et al., 2012, Zhu et al., 2012). The ability of MSCs to form colonies is reflective of their expansive capacity (Schellenberg et al., 2012). The CFU-f assay is regarded as the gold standard for identifying clonogenic MSCs (Friedenstein et al., 1970). Both MSC types were capable of developing colony forming units. However, AT-MSCs produced more than twice the number of colony forming units compared to BM-MSCs. Similar results have been reported in multiple human MSC lines (Schellenberg et al., 2012). The heterogeneous *in vitro* characteristics of BM-MSCs and AT-MSCs were further elucidated by defining morphological subpopulations. AT-MSC cultures were dominated by cells with 'spindle' morphology. Inversely, the proportion of 'flat' MSCs was greater in BM-MSC cultures. In agreement with these results, rat AT-MSCs have also been observed to contain higher populations of 'spindle' shaped cells with higher proliferative capacity (Taghi et al., 2012). Evidence of a direct relationship between MSC morphology and expansive characteristics arise from the parallels of decreasing proliferation and clonogenicity (Bonab et al., 2006, Schellenberg et al., 2011) and increasing populations of 'flat' MSCs (Neuhuber et al., 2008) over subsequent passaging. Nonetheless, differences in proliferation and clonogenicity between BM-MSCs and AT-MSCs are observed consistently at equivalent passages (Ikegame et al., 2011, Dmitrieva et al., 2012, Schellenberg et al., 2012, Zhu et al., 2012). In our study, colony forming units were predominantly populated by 'spindle' MSCs suggesting a link between morphology and

clonogenicity. It should be noted that 'flat' MSCs were also observed to be clonogenic; however, these colonies were rarely detected by the CFU-f assay due to their inferior proliferative nature. Nonetheless, these data collectively suggest that morphological subpopulations may be indicative of expansion potential, which could be useful information when propagating MSC therapies in the clinic. Due to the great number of MSCs required for human therapy, the *in vitro* phenotype is a crucial consideration to determine the favourable source of MSC treatment in the clinic. AT-MSCs were shown to exhibit superior *in vitro* properties. However, the *in vivo* therapeutic efficacy of MSCs from different sources also requires attention. In our study, the efficacy of BM-MSCs and AT-MSCs was assessed in an *in vivo* model of intestinal inflammation induced by administering TNBS which initiated an immune response to hapten modified autologous proteins (Wirtz et al., 2007). Lack of weight gain is commonly observed in this model and reflective of the inflammatory state (Linden et al., 2003, Lomax et al., 2007a). This effect was comparably attenuated in guinea-pigs treated with BM-MSCs and AT-MSCs. The histopathological severity of experimental colitis has been evaluated to determine the effectiveness of MSC treatments (Ando et al., 2008, González et al., 2009, Fawzy et al., 2013, Wang et al., 2014). In our study, both MSC treatments similarly prevented disruption to the epithelial lining, inflammatory infiltrate and changes to the colonic architecture. Previous comparisons of allogeneic rat MSCs from these tissue sources in experimental colitis are in agreement with these observations (Castelo-Branco et al., 2012). While MSCs from both sources were seemingly equally beneficial in attenuating the manifestations of TNBS-induced colitis, we further investigated their therapeutic efficacy for the treatment of enteric neuropathy associated with intestinal inflammation.

The increased number of leukocytes in proximity to myenteric ganglia upon administration of TNBS, indicative of plexitis, was prevented by both MSC treatments. However, leukocyte numbers were still elevated after AT-MSC treatment compared to shams at early stages of inflammation which suggests that AT-MSCs exert their immunomodulatory effects slower than BM-MSCs. Previous studies in various pathologies appear to be in agreement that BM-MSCs are

superior to AT-MSCs in preventing leukocyte infiltration and inflammation (Roemeling-van Rhijn et al., 2013, Antunes et al., 2014a, Antunes et al., 2014b, Elman et al., 2014). The infiltration of leukocytes to the myenteric plexus in the resected bowel of Crohn's disease patients is predictive of inflammatory relapse requiring repeated surgery (Ferrante et al., 2006, Sokol et al., 2009). Enteric neurons express receptors for inflammatory mediators, activation of which causes substantial excitation in enteric neurons (Xia et al., 1999). Inflammation-induced neuronal death and axonal damage leads to changes in neurally-controlled intestinal functions (Törnblom et al., 2002, Lindberg et al., 2009).

Neuronal loss was observed in animals administered with TNBS in our study consistent with previous reports (Boyer et al., 2005, Linden et al., 2005a, Nurgali et al., 2011). Both BM-MSCs and AT-MSCs attenuated neuronal loss in animals with colitis, however BM-MSCs were more effective compared to AT-MSCs. In the myenteric plexus, the two major subpopulations of excitatory and inhibitory muscle motor and interneurons, ChAT-IR (cholinergic) and nNOS-IR (nitrergic), were further investigated (Furness, 2000). Changes in the neurochemical coding of these neurons are associated with altered coordination of muscular contractions and dysmotility in humans and animals (Wattchow et al., 2008, Suply et al., 2012, Winston et al., 2013). Intestinal dysmotility is a symptom of IBD, however it may also contribute to disease progression through dysfunctional propulsive clearance of enterotoxins that promote additional inflammatory bouts (Wood, 2007). Administration of TNBS resulted in decreased numbers of cholinergic neurons. Cholinergic neuronal loss was attenuated by both BM-MSCs and AT-MSCs. Similar to total neuronal counts, AT-MSCs were less effective at attenuating cholinergic neuronal loss at 24h. The unchanged proportion of cholinergic neurons may be attributed to the parallel loss of total myenteric neurons (Linden et al., 2005a). Intestinal inflammation induced by TNBS increased the total numbers and proportions of nNOS-IR nitrergic neurons. Similar changes to the neurochemical coding of enteric neurons have been observed after acute pancreatitis (Lin et al., 2011b) and in experimental models of colitis (Winston et al., 2013) and Crohn's disease patients (Belai et al., 1997, Boyer et al., 2007). Furthermore, neurons in the

central nervous system reportedly increase in nNOS expression in response to inflammatory stimuli (Wu et al., 1998, Di Girolamo et al., 2003). MSCs from both sources similarly attenuated neurochemical alterations in nitrergic neurons. Excessive nitric oxide has been linked to neuropathy in enteric neurons upon intestinal inflammation (Hogaboam et al., 1995) and likewise with peripheral motor neurons (Wu and Li, 1993, Higashimori et al., 2008). Thus, attenuating increases in nNOS could be partially responsible for the therapeutic action of MSCs in neuropathy.

The loss of nerve fibres in the myenteric plexus was prominent after TNBS administration in our study. TH-IR nerve fibres represent extrinsic noradrenergic sympathetic fibres in the myenteric plexus projecting to the ganglia, mucosa and blood vessels which regulate motility and vasomotor function (Furness, 2000, Stebbing et al., 2001, Lomax et al., 2007b). Sympathetic neurotransmitters can have pro and anti-inflammatory effects depending on concentration (Straub et al., 2006). Damage to sympathetic nerve fibres have been reported in Crohn's disease patients (Straub et al., 2008). In acute experimental colitis, sympathectomy improves outcomes but conversely has adverse effects in chronic models (Straub et al., 2008). This suggests that sympathetic innervation may possess beneficial ant-inflammatory properties in chronic stages of intestinal inflammation. Immunoreactivity for VAChT identifies cholinergic fibres from a broad range of neurons including extrinsic vagal, intrinsic excitatory muscle motor neurons, ascending and descending interneurons, primary afferent neurons and intestinofugal afferent neurons (Lomax and Furness, 2000). The loss of innervation from these fibres may have repercussions in immunomodulation. Acetylcholine has been identified as a potent immunomodulator. The inflammatory reflex mediated through the efferent and afferent arms of cholinergic vagal fibres innervating the mucosa is suggested to prevent the release of pro-inflammatory mediators from macrophages via the α7 nicotinic cholinergic receptor (Tracey, 2002, Cailotto et al., 2012). In our study, the loss of cholinergic fibres coincided with the loss of cholinergic neurons in the myenteric plexus, suggesting that most damaged fibres

were of intrinsic origin. Both BM-MSC and AT-MSC treatments attenuated the loss of cholinergic and sympathetic nerve fibres to levels comparable with controls.

In the myenteric plexus, sensory extrinsic afferent fibres as well as intrinsic afferent neurons and fibres are immunoreactive for CGRP. Reduced CGRP immunoreactivity was observed in the myenteric plexus from inflamed animals. In ulcerative colitis, lack of CGRP expression correlates with disease activity scores and may be a useful marker of disease progression (Li et al., 2013a). Furthermore, abrogation of CGRP signalling via neutralising antibodies or associated receptor antagonist promotes inflammation in experimental colitis (Reinshagen et al., 1998). Together this suggests that sensory nerve fibres may play an anti-inflammatory role. In our study, BM-MSCs and AT-MSCs attenuated the loss of CGRP immunoreactivity, although levels remained lower compared to shams. This may be reflective of chemorepulsive mechanisms inhibiting sensory fibre projections (Tang et al., 2004), which might be an endogenous mechanism to prevent pain or hypersensitivity, however this needs to be elucidated.

Oxidative stress in the ENS is predicted to play a major role in the disease progression of inflammatory bowel disease (Lakhan and Kirchgessner, 2010). High levels of reactive oxygen species are present in models of gastrointestinal inflammation and in human IBD; observations of oxidative stress can even precede the onset of inflammation (Rezaie et al., 2007). Furthermore, oxidative stress and neuronal loss are also evident in the ENS of patients with gastrointestinal dysfunction consequential of diabetes (Chandrasekharan et al., 2011). Our results indicate that MSC therapy can avert increased superoxide production in the myenteric plexus resulting from TNBS-induced inflammation. While it may be likely that pro-inflammatory immune cells are responsible for enteric neuronal damage in TNBS-induced colitis our results demonstrated that immune cell infiltration decreases from 24h to 72h in contrast to the increases in superoxide production which was maintained throughout the experiment. Previous studies suggest that alterations to enteric signalling persist after the resolution of inflammation; data from this study may support oxidative stress as an underlying

cause of these prolonged perturbations (Linden et al., 2003, Nurgali et al., 2007, Nurgali et al., 2011). Nevertheless, damage to the enteric nervous system may be a result of bilateral communication between oxidative stress and the pro-inflammatory response considering that reactive oxygen species up-regulate the production of pro-inflammatory cytokines (Naik and Dixit, 2011); and likewise, pro-inflammatory cytokines promote the formation of ROS including mitochondrial-derived superoxide production (Cao et al., 2013).

In our study, BM-MSCs were more efficacious at ameliorating neuropathy and plexitis. This correlation may suggest immunomodulatory effects are responsible for the neuroprotective properties exerted by MSCs. However, this does not explain the equality of BM-MSCs and AT-MSCs in attenuating inflammation-induced damage to nerve fibres and changes to neurochemical coding observed in our study. Both BM-MSCs and AT-MSCs release neurotrophic factors including nerve growth factor, brain derived neurotrophic factor, neurotrophin-3 and glial derived neurotrophic factor (Taghi et al., 2012). These factors have all been linked to neuroprotective effects (Wilkins et al., 2009, Zhang et al., 2012, Morcuende et al., 2013). Thus, the neuroprotective action of MSCs may occur via immunomodulation, directly by paracrine secretion of neurotrophic factors or synergistically through both. Furthermore, the neuroprotective efficacy of MSCs could be associated with their ability to migrate and engraft in proximity to enteric neurons.

In our study, MSCs administered by enema migrated transmurally from the mucosa to the myenteric ganglia, although most MSCs were observed in the mucosa. The low number of MSCs migrating to the muscle layers, relative to the mucosa, might be due to the short length of experiments in this study as greater numbers of MSCs migrating to the muscle layers have been observed at late stages of experimental colitis (Robinson et al., 2014). To assess the chemotactic properties of MSCs, an *in vitro* assay was designed to determine MSC migration toward secreted factors released by cultured cells of the myenteric plexus under simulated inflammatory conditions. Both AT-MSCs and BM-MSCs migrated towards the milieu of LPS-

damaged neurons within a 72h period. In agreement with our *in vivo* data, the proportion of MSCs with chemotactic affinity was low and differences were not observed between tissue sources. In other neuroinflammatory models, such as experimental autoimmune encephalomyelitis, AT-MSCs were more therapeutic than BM-MSCs due to their enhanced migratory capabilities (Payne et al., 2013a). In the rat model of intestinal inflammation, it has been reported that intraperitoneally injected AT-MSCs migrated from the peritoneum through to the epithelial layer, whereas BM-MSCs only localised to the peritoneum surface, muscular layers and submucosa by 72h (Castelo-Branco et al., 2012). The direction of migration suggests a high chemotactic affinity to the mucosal, or possibly submucosal layers, where tissue damage is most prominent. The dissimilarities between BM-MSC and AT-MSC migration in these studies could be explained by their differential expression of chemokine receptors (Balasubramanian et al., 2012). In addition, the morphological analysis performed in our study may suggest that BM-MSCs, containing greater proportions of large 'flat' cells, may be limited in migration due to their physical size. Nonetheless, MSC migration did not appear to greatly influence the therapeutic outcomes of this study or that conducted by Castelo-Branco et al. (2012). The low affinity of MSC migration to the myenteric plexus in our study suggest that either low numbers of MSCs are required to exert therapeutic effects on myenteric neurons, or, the proximity of MSCs is irrelevant to their neuroprotective mechanism. Investigations into paracrine secretion may explain the differences observed in this study between BM-MSCs and AT-MSCs.

2.7. Conclusion

Optimisation of MSC therapies is of critical importance for their clinical application. Identifying the ideal tissue source of MSCs for the treatment of intestinal inflammation may lead to improved therapeutic outcomes. *In vitro*, AT-MSCs were determined to have greater proliferation, clonogenicity and 'spindle' morphology suggesting that AT-MSCs are ideal for cellular expansion. *In vivo,* both BM-MSCs and AT-MSCs ameliorated weight loss, histopathological changes, plexitis, neuropathy, changes to neuronal neurochemical coding, loss of nerve fibres

and the generation of mitochondria-derived superoxide in the myenteric ganglia, however, BM-MSCs appeared to be more effective in the treatment of neuropathy and plexitis. These differences could not be explained by migration capacity to the myenteric plexus both *in vivo* and *in vitro.* Future studies should determine the role of paracrine secretion in the neuroprotective efficacy of MSCs in addition to their direct and indirect interactions with myenteric neurons. The benefits between the expansiveness of AT-MSCs and the increased efficacy of BM-MSCs to target neurological manifestation should be considered when selecting MSCs to treat intestinal inflammation.

CHAPTER THREE

Mesenchymal Stem Cell Therapy Ameliorates Inflammation in Spontaneous Chronic Colitis

3.1. Summary

Current treatments for inflammatory bowel disease (IBD) are ineffective in many patients to halt the disease progression or can only be used for short durations due to their toxicity. Mesenchymal stem cells (MSCs) have been proposed as an alternative treatment for IBD and their therapeutic value has been observed in patients who are refractory to conventional treatments. Experimental models are required to understand the mechanisms and to improve the efficacy of MSC therapy in the clinic. Murine models of chemically-induced colitis by 2,4,6-trinitrobenzenesulfonic acid (TNBS) or dextran sodium sulphate (DSS) are the only models currently being used to explore MSC treatments. Recent clinical data have not supported immunomodulatory mechanisms of MSC therapy, such as the induction of regulatory T lymphocytes (Treg), which is observed in experimental models. This may be due to acute nature of inflammation in chemically-induced colitis which does not mimic the chronic inflammatory signalling milieu of IBD. To date, no studies have explored MSC treatments in a chronic model of colitis. The *Winnie* mouse model of spontaneous chronic colitis demonstrates resemblance to human UC and may offer a better representation of the inflammatory environment. In this study, *Winnie* mice underwent a treatment regimen of four bone marrow-derived MSC (BM-MSC) injections over two weeks delivered by enema. Mice were culled 24h after the final treatment. Disease activity was evaluated, and distal colons were collected for RNA isolation, immunohistochemistry and histological examination. The total number of leukocytes (CD45) and Treg cells expressing the transcription factor, forkhead box P3 (FOXP3), were evaluated in the distal colon. High-throughput RNA sequencing and bioinformatics were performed to assess the changes in the transcriptome in the distal colon of *Winnie* mice treated by BM-MSCs. Data describing the effects of MSC therapies on the expression of inflammation-associated factors in chemically-induced colitis were collated from the literature. The gene expression of these factors was evaluated in BM-MSC-treated *Winnie* mice. This was performed to explore the concordance between the effects of MSC therapy on the inflammatory signalling milieu in acute and chronic colitis. The profile of inflammatory genes in

Winnie mice were compared to the transcriptome of IBD patients retrieved from the Gene Expression Omnibus data repository. The results of this study revealed that BM-MSC treatments decreased the disease activity of colitis in *Winnie* mice. Stool consistency and colon weight was improved by BM-MSCs in *Winnie* mice. The increased number of leukocytes in the colon was reduced after BM-MSC treatments. Levels of FOXP3 expressing cells were not decreased by BM-MSC therapy similar to results reported in IBD. However, the proportion of FOXP3 expressing leukocytes increased due to a decline in the total population of leukocytes. BM-MSC treatments changed the expression of 1171 genes in *Winnie* mice. Analysis of the transcriptome revealed that BM-MSCs downregulated many genes associated with the pro-inflammatory response in *Winnie* mice. BM-MSC treatments in *Winnie* mice induced similar changes in the expression of half of the assessed genes previously reported to be affected by MSC treatment in chemically-induced colitis. However, half of these genes were oppositely regulated by MSCs in *Winnie* mice. This may suggest that BM-MSCs act via novel mechanisms of action in the resolution of chronic inflammation. Comparison of inflammatory genes in the transcriptome of *Winnie* mice and IBD patients revealed that this model replicated UC with a high degree of accuracy not observed previously in models of chemically-induced colitis. These data offer valuable direction to explore the therapeutic effects BM-MSCs in chronic colitis, to identify novel molecular targets for IBD treatment and develop a successful approach to MSC therapy in the clinic.

3.2. Abbreviations

BM-MSC	bone marrow-derived MSC
CD	Crohn's disease
DAI	disease activity index
DAVID	database for annotation, visualization and integrated discovery
DEG	differentially expressed gene
DMSO	dimethyl sulfoxide
DSS	dextran sodium sulphate
FBS	foetal bovine serum
FOXP3	forkhead box P3
GEO	Gene Expression Omnibus
GO	gene ontologies
IBD	inflammatory bowel disease
IL	interleukin
KEGG	Kyoto Encyclopedia of Genes and Genomes
KLK	kallikreins
MSC	mesenchymal stem cells
MUC2	mucin 2
NDS	normal donkey serum
NSAIDs	nonsteroidal anti-inflammatory drugs
OCT	optimal cutting temperature
PMN	polymorphonucleated neutrophils
Reg3	regenerating islet-derived protein 3
RIN	RNA integrity number
RNA-Seq	RNA-Sequencing
SPINK	serine protease inhibitor Kazal-type
TNBS	2,4,6-trinitrobenzenesulfonic acid
TNF	tumour necrosis factor
Tregs	regulatory T lymphocytes
UC	ulcerative colitis

3.3. Gene Symbols

1100001g20rik (Wfdc21)	WAP four-disulphide core domain 21
2210407c18rik	RIKEN cDNA 2210407C18 gene
Adam8	a disintegrin and metallopeptidase domain 8
Adamtsl4	ADAMTS-like 4
Adcy8	adenylate cyclase 8
Adm	adrenomedullin
Alox12	arachidonate 12-lipoxygenase
Alox15	arachidonate 15-lipoxygenase
Anxa1	annexin A1
Anxa2	annexin A2
Apod	apolipoprotein D
Areg	amphiregulin
Arg1	arginase, liver
Arg2	arginase type II
Batf2	basic leucine zipper transcription factor, ATF-like 2
Bglap3	bone gamma-carboxyglutamate protein 3
Bmp8b	bone morphogenetic protein 8b
Bmper	BMP-binding endothelial regulator
Bnip3	BCL2/adenovirus E1B interacting protein 3
C1qtnf3	C1q and tumour necrosis factor related protein 3
C2	complement component 2 (within H-2S)
Capg	capping protein (actin filament), gelsolin-like
Ccdc88b	coiled-coil domain containing 88B
Ccl3	chemokine (C-C motif) ligand 3
Ccl4	chemokine (C-C motif) ligand 4
Ccl5	chemokine (C-C motif) ligand 5
Ccl7	chemokine (C-C motif) ligand 7
Ccl8	chemokine (C-C motif) ligand 8
Ccl28	chemokine (C-C motif) ligand 28

Ccrl2	chemokine (C-C motif) receptor-like 2
Cd274	CD274 antigen
Cd300lf	CD300 molecule like family member F
Cd33	CD33 antigen
Cd47	CD47 antigen
Cd55	CD55 molecule, decay accelerating factor for complement
Cd6	CD6 antigen
Cdh3	cadherin 3
Cdsn	corneodesmosin
Ceacam10	carcinoembryonic antigen-related cell adhesion molecule 10
Cebpb	CCAAT/enhancer binding protein (C/EBP), beta
Ces2f	carboxylesterase 2F
Ces2g	carboxylesterase 2G
Cfh	complement component factor h
Chi3l1	chitinase-3-like protein 1
Chi3l3	chitinase-3-like protein 3
Chit1	chitinase 1 (chitotriosidase)
Chrd	chordin
Cldn1	claudin 1
Cldn4	claudin 4
Clec4d	C-type lectin domain family 4, member d
Clec4e	C-type lectin domain family 4, member e
Clec5a	C-type lectin domain family 5, member a
Col12a1	collagen, type XII, alpha 1
Col17a1	collagen, type XVII, alpha 1
Cpxm1	carboxypeptidase X 1 (M14 family)
Csf2rb	colony stimulating factor 2 receptor, beta, low-affinity (granulocyte-macrophage)
Csf3r	colony stimulating factor 3 receptor (granulocyte)
Csta	cystatin-A
Ctgf	connective tissue growth factor
Ctsk	cathepsin K

Cxcl2	chemokine (C-X-C motif) ligand 2
Cxcl3	chemokine (C-X-C motif) ligand 3
Cxcl5	chemokine (C-X-C motif) ligand 5
Cxcl9	chemokine (C-X-C motif) ligand 9
Cxcl14	chemokine (C-X-C motif) ligand 14
Cxcl16	chemokine (C-X-C motif) ligand 16
Cxcr2	chemokine (C-X-C motif) receptor 2
Defb6	defensin beta 6
Dmbt1	deleted in malignant brain tumours 1
Dmkn	dermokine
Dsc3	desmocollin 3
Dtx3l	deltex 3-like, E3 ubiquitin ligase
Emilin2	elastin microfibril interfacer 2
F10	coagulation factor X
F13a1	coagulation factor XIII, A1 subunit
F3	coagulation factor III
Fabp5	fatty acid binding protein 5, epidermal
Fas	fas (TNF receptor superfamily member 6)
Fcer1g	Fc receptor, IgE, high affinity I, gamma polypeptide
Fcgr4	Fc receptor, IgG, low affinity IV
Foxp3	forkhead box P3
Fpr1	formyl peptide receptor 1
Fpr2	formyl peptide receptor 2
Fst	follistatin
Gata3	GATA binding protein 3
Gbp2	guanylate binding protein 2
Gbp3	guanylate binding protein 3
Gbp5	guanylate binding protein 5
Gbp6	guanylate binding protein 6
Gbp7	guanylate binding protein 7
Gch1	GTP cyclohydrolase 1
Glb1l2	galactosidase, beta 1-like 2

Gp1bb	glycoprotein Ib, beta polypeptide
Grem1	gremlin 1, DAN family BMP antagonist
Gsdma	gasdermin A
Gzma	granzyme A
H2q7	histocompatibility 2, Q region locus 7
H2-q7	histocompatibility 2, Q region locus 7
Hbb	hemoglobin beta chain complex
Hilpda	hypoxia inducible lipid droplet associated
Hk2	hexokinase 2
Hk3	hexokinase 3
Hmox1	heme oxygenase 1
Hp	haptoglobin
I830012o16rik (Ifit3b)	interferon-induced protein with tetratricopeptide repeats 3B
Icam1	intercellular adhesion molecule 1
Ido1	indoleamine 2,3-dioxygenase 1
Ier3	immediate early response 3
Ifi47	interferon gamma inducible protein 47
Ifi204	interferon activated gene 204
Ifit1	interferon-induced protein with tetratricopeptide repeats 1
Ifit2	interferon-induced protein with tetratricopeptide repeats 2
Ifit3	interferon-induced protein with tetratricopeptide repeats 3
Ifitm1	interferon induced transmembrane protein 1
Ifitm6	interferon induced transmembrane protein 6
Ifng	interferon gamma
Igf1	insulin-like growth factor 1
Igfbp2	insulin-like growth factor binding protein 2
Igfbp3	insulin-like growth factor binding protein 3
Iigp1	interferon inducible GTPase 1
Il1a	interleukin 1 alpha
Il1b	interleukin 1 beta
Il1f9	interleukin 1 family, member 9

Il1r2	interleukin 1 receptor, type II
Il21	interleukin 21
Il2ra	interleukin 2 receptor, alpha chain
Il33	interleukin 33
Il4ra	interleukin 4 receptor, alpha
Il6	interleukin 6
Il18bp	interleukin 18 binding protein
Il18rap	interleukin 18 receptor accessory protein
Inhba	inhibin beta-A
Irg1 (Acod1)	aconitate Decarboxylase 1
Irgm1	immunity-related GTPase family M member 1
Isg20	interferon-stimulated protein
Itga2	integrin alpha 2
Itgam	integrin alpha M
Itgav	integrin alpha V
Itgax	integrin alpha X
Itgb6	integrin beta 6
Klk8	kallikrein related-peptidase 8
Klk13	kallikrein related-peptidase 13
Krt1	keratin 1
Krt4	keratin 4
Krt6a	keratin 6A
Krt10	keratin 10
Krt16	keratin 16
Krtdap	keratinocyte differentiation associated protein
Lama3	laminin, alpha 3
Lamc2	laminin, gamma 2
Lbp	lipopolysaccharide binding protein
Lcn2	lipocalin 2
Lgals7	lectin, galactose binding, soluble 7
Lgi2	leucine-rich repeat LGI family, member 2
Lif	leukemia inhibitory factor

Lipk	lipase, family member K
Lipm	lipase, family member M
Lox	lysyl oxidase
Lrg1	leucine-rich alpha-2-glycoprotein 1
Ltb4r1	leukotriene B4 receptor 1
Ltbp2	latent transforming growth factor beta binding protein 2
Ltf	lactotransferrin
Ly6a	lymphocyte antigen 6 complex, locus A
Mfap4	microfibrillar-associated protein 4
Mmp3	matrix metallopeptidase 3
Mmp7	matrix metallopeptidase 7
Mmp8	matrix metallopeptidase 8
Mmp9	matrix metallopeptidase 9
Mmp10	matrix metallopeptidase 10
Mmp12	matrix metallopeptidase 12
Mmp13	matrix metallopeptidase 13
Mrc1	mannose receptor, C type 1
Msln	mesothelin
Nfil3	nuclear factor, interleukin 3, regulated
Nlrp3	NLR family, pyrin domain containing 3
Nod2	nucleotide-binding oligomerization domain containing 2
Nos2	nitric oxide synthase 2, inducible
Nucb2	nucleobindin 2
Oas2	2'-5' oligoadenylate synthetase 2
Oas3	2'-5' oligoadenylate synthetase 3
Olfm4	olfactomedin 4
Olr1	oxidised low density lipoprotein (lectin-like) receptor 1
Osm	oncostatin M
Osmr	oncostatin M receptor
Padi4	peptidyl arginine deiminase, type IV
Parp9	poly (ADP-ribose) polymerase family, member 9
Pfkfb3	6-phosphofructo-2-kinase/fructose-2,6-biphosphatase 3

Pglyrp1	peptidoglycan recognition protein 1
Pi15	peptidase inhibitor 15
Pim1	proviral integration site 1
Pirb	paired Ig-like receptor B
Pla1a	phospholipase A1 member A
Pla2g2e	phospholipase A2, group IIE
Plat	plasminogen activator, tissue
Plaur	plasminogen activator, urokinase receptor
Ppbp	pro-platelet basic protein
Prkcd	protein kinase C, delta
Prss12	protease, serine 12 neurotrypsin (motopsin)
Prss27	protease, serine 27
Psapl1	prosaposin-like 1
Ptafr	platelet-activating factor receptor
Rac3	RAS-related C3 botulinum substrate 3
Reg3b	regenerating islet-derived 3 beta
Reg3g	regenerating islet-derived 3 gamma
Rel	reticuloendotheliosis oncogene
Retnlb	resistin like beta
Retnlg	resistin like gamma
Ripk3	receptor-interacting serine-threonine kinase 3
Rorc	RAR-related orphan receptor gamma
Rptn	repetin
S100a8	S100 calcium binding protein A8 (calgranulin A)
S100a9	S100 calcium binding protein A9 (calgranulin B)
S100a14	S100 calcium binding protein A14
Saa3	serum amyloid A 3
Samhd1	SAM domain and HD domain, 1
Sbsn	suprabasin
Selp	selectin, platelet
Sema7a	sema domain, immunoglobulin domain

Serpina3j	serine (or cysteine) peptidase inhibitor, clade A (alpha-1 antiproteinase, antitrypsin), member 3J
Serpina10	(alpha-1 antiproteinase, antitrypsin), member 10serine (or cysteine) peptidase inhibitor, clade A
Serpinb3a	serine (or cysteine) peptidase inhibitor, clade B (ovalbumin), member 3A
Serpinb8	serine (or cysteine) peptidase inhibitor, clade B, member 8
Serpinb11	serine (or cysteine) peptidase inhibitor, clade B (ovalbumin), member 11
Serpine1	serine (or cysteine) peptidase inhibitor, clade E, member 1
Serpine2	serine (or cysteine) peptidase inhibitor, clade E, member 2
Sfrp1	secreted frizzled-related protein 1
Sfrp4	secreted frizzled-related protein 4
Slfn2	schlafen 2
Slfn4	schlafen 4
Socs1	suppressor of cytokine signalling 1
Socs3	suppressor of cytokine signalling 3
Sphk1	sphingosine kinase 1
Spink5	serine peptidase inhibitor, Kazal type 5
Spns2	spinster homolog 2
Spp1	secreted phosphoprotein 1
Sprr3	small proline-rich protein 3
Stx11	syntaxin 11
Sulf1	sulfatase 1
Tac1	tachykinin 1
Tacstd2	tumour-associated calcium signal transducer 2
Tap1	transporter 1, ATP-binding cassette, sub-family B (MDR/TAP)
Tarm1	T cell-interacting, activating receptor on myeloid cells 1
Tbx21	T-box 21
Tgm1	transglutaminase 1, K polypeptide
Tgtp1	T cell specific GTPase 1

Thpo	thrombopoietin
Timp1	tissue inhibitor of metalloproteinase 1
Tinagl1	tubulointerstitial nephritis antigen-like 1
Tlr2	toll-like receptor 2
Tmem173	transmembrane protein 173
Tmprss11a	transmembrane protease, serine 11a
Tmprss11bnl (Tmprss11b)	transmembrane protease, serine 11b
Tmprss11d	transmembrane protease, serine 11d
Tmprss11g	transmembrane protease, serine 11g
Tnf	tumour necrosis factor
Tnfrsf1b	tumour necrosis factor receptor superfamily, member 1b
Tnfrsf9	tumour necrosis factor receptor superfamily, member 9
Tnfrsf11b	tumour necrosis factor receptor superfamily, member 11b (osteoprotegerin)
Tnfrsf12a	tumour necrosis factor receptor superfamily, member 12a
Trem1	triggering receptor expressed on myeloid cells 1
Trim10	tripartite motif-containing 10
Trim15	tripartite motif-containing 15
Trim29	tripartite motif-containing 29
Trim30a	tripartite motif-containing 30A
Trp63	transformation related protein 63
Usp18	ubiquitin specific peptidase 18
Wfdc18	WAP four-disulfide core domain 18
Zap70	zeta-chain (TCR) associated protein kinase
Zbp1	Z-DNA binding protein 1

3.4. Introduction

Inflammatory bowel disease (IBD) consists of a set of idiopathic disorders, predominantly ulcerative colitis (UC) and Crohn's disease (CD), which are characterised by remitting and relapsing periods of severe inflammation in the intestinal tract. In UC, inflammation is localised in the mucosa/submucosa of the colon and continuously ascends from the rectum. In contrast, inflammation in CD can be observed as transmural skip lesions throughout the gastrointestinal tract. Progressive inflammation in the intestinal tract can lead to several debilitating sequelae including: diarrhoea and/or constipation, severe abdominal pain, ulceration, strictures and fistulae. Treatments for IBD aim to supress inflammation and include nonsteroidal anti-inflammatory drugs (NSAIDs), corticosteroids, aminosalicylates, methotrexate and biological therapies. For many patients, these treatments are ineffective to halt the disease progression or can only be used for a short duration due to their toxicity. Up to 90% of CD patients require surgical resection of the bowel (Lewis and Maron, 2010); this demonstrates the difficulty of managing the disease by current pharmacological and biological interventions.

Mesenchymal stem cells (MSCs) have been proposed as an alternative treatment for IBD with therapeutic value observed for fistulising and luminal pathologies of the disease (**Chapter 1, Table 1.1**). These cells can be readily isolated from a variety of adult tissue sources and expanded for autologous and allogeneic transplant (**Chapter 1, Section 1.2.2 & 1.2.3**). While these cells are capable of multipotent differentiation, they possess various qualities that appear to be of benefit in intestinal inflammation (**Chapter 1, Table 1.2**). There is a large body of evidence on the trophic support offered by MSCs, nonetheless, they are also able to migrate to sites of inflammation, where they engraft and modulate the immune response (Wu et al., 2007, Chen et al., 2008, Ma et al., 2013, Sémont et al., 2013). These properties make MSC therapy an intriguing proposition to treat the structural and inflammatory perturbations associated with IBD. Early clinical trials have demonstrated that remission can be achieved using MSC therapy in patients that are unresponsive to conventional treatments (Forbes et al., 2014). In addition, an

abundance of literature has reported positive outcomes in murine models of chemically-induced colitis which is predominately attributed to the anti-inflammatory effects and immunomodulatory properties of MSCs (**Chapter 1, Table 1.2**). Experimental models offer valuable insight into the optimisation of MSC therapy for clinical applications and have assisted in uncovering its immunomodulatory mechanisms in colitis. Studies have attributed the immunomodulatory properties of MSCs to the polarisation of regulatory T lymphocytes (Tregs) in chemically-induced colitis (**Chapter 1, Table 1.2**). In DSS-induced colitis, an increase in the number of cells expressing the Treg transcription factor, forkhead box P3 (FOXP3), has been observed in the colon after administration of MSCs by intravenous, intraperitoneal and intra-luminal injections (Sala et al., 2015, Wang et al., 2016, Soontararak et al., 2018). However, in a recent clinical trial of MSC therapy in refractory IBD patients, an increase in (Tregs) was not observed (Gregoire et al., 2018). Therefore, the mechanisms of MSC treatments in the human pathology may vary to chemically-induced models. These models are often acute and reversible by removal of the chemical stimulus, thus, may not reflect the alterations caused by chronic inflammation in the human pathology. To accurately determine the mechanisms of action of MSC therapy and optimise treatments, a model that better replicates the pathology of IBD is required.

The *Winnie* mouse is a promising model of spontaneous chronic colitis to evaluate the efficacy of pre-clinical therapies for IBD. These mice possess a single point missense mutation in the *Muc2* (Mucin 2) gene. Mucin 2 has been implicated in the pathogenesis of IBD and is the major component of the mucous barrier separating the luminal microbiome and the host (Boltin et al., 2013). This protein is misfolded, triggering endoplasmic reticulum stress and the unfolded protein response in epithelial cells which disrupts the epithelial barrier and triggers chronic inflammation with an onset at early adolescence (Heazlewood et al., 2008, Stavely et al., 2018a). Likewise, these mechanisms are evident in the pathophysiology of IBD (Cao, 2015). *Winnie* mice share many pathophysiological similarities to human UC and an analogous signalling milieu driving the inflammatory phenotype (Heazlewood et al., 2008, Eri et al., 2011, Rahman et al., 2015, Rahman et al., 2016,

Robinson et al., 2017a). The mechanisms of MSC therapy in a model of spontaneous chronic colitis are yet to be elucidated. In this study, the therapeutic effects of MSC treatments will be evaluated in *Winnie* mice spontaneous chronic inflammation. The potential mechanisms of MSC treatments in chronic inflammation will be assessed by analysis of the mRNA transcriptome and compared to markers previously identified in chemically-induced models of colitis (**Chapter 1, Table 1.3**). Furthermore, markers of inflammation will be compared between *Winnie* mice and IBD patients to establish the relevance of this model to human IBD.

3.5. Methods

3.5.1. Animals

Male *Winnie* mice aged 14 weeks (total n=14) were obtained from Victoria University (Melbourne, Victoria, Australia). *Winnie* mice were compared to age matched male C57BL/6 mice (total n=10) obtained from the Animal Resource Centre (Perth, Western Australia, Australia). All mice had *ad libitum* access to food and water and were housed in a temperature-controlled environment with a 12-h day/night cycle. Mice were acclimatised for at least one week at the Western Centre for Health, Research and Education (Melbourne, Victoria, Australia). All mice were culled by cervical dislocation and the distal portion of the colon was collected for subsequent experiments. All animal experiments in this study complied with the guidelines of the Australian Code of Practice for the Care and Use of Animals for Scientific Purposes and were approved by the Victoria University Animal Experimentation Ethics Committee.

3.5.2. Cell culture and passaging

MSCs used in this study were derived from human bone marrow (BM-MSC) and obtained from Tulane University, USA. BM-MSCs used in this study were previously extensively characterised for cell surface markers, differentiation

potential, proliferation, colony formation, morphology and adherence to plastic (Stavely et al., 2015b) (**Chapter 2, Figures 2.1 & 2.2**) and conform to the guidelines set by the International Society for Cell Therapy (Dominici et al., 2006). Cells were plated at a seeding density of 60 cells/cm^2 and cultured at 37ºC in 5% CO_2 and ambient air using expansion medium (α-MEM supplemented with 100 U/mL penicillin/streptomycin, 1% glutaMAX [Gibco®, Life Technologies, Melbourne, Australia, for all]) and 16.5% foetal bovine serum (FBS; mesenchymal stem cell-qualified, Gibco®, Life Technologies) which was replenished every 48-72h for 10-14 days until the cells were 70-85% confluent. BM-MSCs used for animal treatments had a viability of over 95% after trypsinisation and were used only at the fourth passage and not later to minimise genetic abnormalities in the cells (Ueyama et al., 2012).

3.5.3. MSC administration

BM-MSCs were administered into *Winnie* mice with chronic colitis by enema. A lubricated silicone catheter was inserted 3cm proximal to the anus of mice anesthetised with 2% isoflurane. *Winnie* mice were treated with two doses of $4x10^6$ BM-MSCs in 100µL of sterile PBS and subsequently received two replenishment doses of $2x10^6$ BM-MSCs in the same volume of sterile PBS. All treatments were administered 4 days apart. Sham-treated *Winnie* mice underwent the same procedure on the same days with an injection of sterile PBS at the same volume (*Winnie*-sham). Mice were culled 24h after the final treatment.

3.5.4. Evaluation of colitis

Clinical signs of colonic inflammation in *Winnie* mice are characterised by changes to colon weight and body weight, diarrhoea, rectal prolapses and rectal bleeding (Heazlewood et al., 2008, Eri et al., 2011). Faecal pellets were collected from mice in isolated collection cages for up to an hour. Pellets were weighed for wet weight immediately after collection to prevent evaporation. Faecal pellets were dried in a fan forced oven at 60ºC for 24h to remove all moisture. Faecal water content was

calculated as the difference expressed as a percentage between wet and dry pellets. Animals were closely monitored for clinical symptoms throughout the experimental procedures. Daily body weights were recorded to calculate weight loss, which was expressed as a percentage of the weight recorded on the day of culling to the maximum observed weight. Directly after culling, the entire colon including the caecum was excised and weighed. Colons were immediately placed into Krebs physiological saline (composition in mmol L−1: NaCl, 117; NaH2PO4, 1.2; MgSO4, 1.2; CaCl2, 2.5; KCl, 4.7; NaHCO3, 25; and glucose, 11) to be photographed and measured to calculate the colon weight:length ratio. Colitis was confirmed by a disease activity index (DAI) which included symptoms of chronic diarrhoea (faecal water content: 60-64%=1, 65-69%=2, 70-74%=3, 75-79%=4, ≥80%=5), rectal manifestations (bleeding=1, prolapse=2), weight loss (from highest recorded weight: 1-4%=1, 5-9%=2, ≥10%=3), and ratios of colon weight:length from the caecum to the anus (0.0110-0.0140=1, 0.0141-0.0160=2, 0.0161-0.0180=3, 0.0181-0.0200=4, ≥0.0200=5) (Stavely et al., 2018a).

3.5.5. Histology

Segments of the colon were opened and pinned in sylgard (Dow Corning, Midland, USA) elastomer-lined dishes where they were fixed overnight in 10% neutral buffered formalin. Tissues were then subjected to 3×10min washes in PBS and were prepared for paraffin embedding by immersing tissues in subsequent solutions of 70, 80, 95 and 100% ethanol, xylene and paraffin wax at 56° (2×1h each). After tissues were embedded into paraffin blocks (Paraffin embedding system TBS88, Medite, Germany), 20µm cross sections were cut with a microtome and mounted onto glass microscope slides. The sections were deparaffinised in a 37°C oven, cleared with xylene (3×5min) and rehydrated in graded ethanol concentrations (100, 90, 75 and 50%, 1×3min each) prior to staining haematoxylin (1×5min) (Sigma-Aldrich, Sydney, Australia) (1×30min). Slides were then rinsed in distilled water and counterstained with eosin (1×5min) before dehydration in 100% ethanol (2×3min) and clearing in xylene (2×10min). Distrene plasticizer xylene (DPX) mounting medium (VWR International, Brisbane, Australia) and coverslips were

applied to slides before imaging using an Olympus BX53 microscope (Olympus Imaging, Sydney, Australia). Large intestine inflammation and damage scores of histological sections were evaluated for several parameters as previously described in the *Winnie* mouse model (Heazlewood et al., 2008). This included crypt architecture (0 = normal architecture, 1 = irregular architecture, 2 = moderate crypt loss at 10-50%, 3 = severe crypt loss at 50-90%, 4 = small-medium size ulcers of 10 crypt widths, 5 = large ulcers more than 10 crypt widths), crypt length of the distal colon (0 = < 150µm, 1 = 150-200µm, 2 = 200-250µm, 3 = 250-300µm, 4 = >300µm), crypt abscesses (0 = no crypt abscesses, 1 = 1-5, 2 = 6-10, 3 = >10), tissue damage (0 = no damage, 1 = discrete lesion, 2 = mucosal erosion, 3 = extensive mucosal damage), goblet cell loss (0 = <10%, 1 = 10-25%, 2 =25-50%, 3 = >50%), inflammatory cell infiltration (0 = normal lamina propria infiltration, 1 = increasing leukocytes in lamina propria, 2 = confluence of leukocytes extending to sub-mucosa, 3 = transmural extension of inflammatory infiltrate), number of lamina propria polymorphonucleated neutrophils (PMN) within 0.015mm^2 images taken at 100X magnification (0 = 0-5 PMNs, 1 = 6-10 PMNs, 2 =11-20 PMNs, 3 = > 20 PMNs).

3.5.6. Immunohistochemistry

For immunohistochemical studies, distal colon segments were viewed under a dissection microscope, cut along the mesenteric border and pinned into a sylgard elastomer-coated petri dish. Tissues were pinned without stretching to protect the structure of the mucosa. All tissues were fixed overnight at 4°C in Zamboni's fixative solution (2% formaldehyde and 0.2% picric acid) with subsequent washes in dimethyl sulfoxide (DMSO) (Sigma-Aldrich) (3x10min) to permeabilise the tissues and 0.1 M PBS (3x10min) to remove DMSO and the fixative. To prepare cross sections, tissues were embedded in optimal cutting temperature (OCT) compound (Tissue Tek-Sakura, Tokyo, Japan). Using a cryostat (Leica Biosystems, Wetzlar, Germany), 20µm sections were cut from the OCT embedded colon and were mounted onto glass slides. Tissue sections were thawed prior to incubation with 10% NDS (Merck Millipore, Melbourne, Australia) and 0.5% Triton X-100

diluted in 0.1 M PBS at room temperature to minimise non-specific binding that could arise from subsequent immunolabeling. Sections were washed (3x10min of 0.1 M PBS for all proceeding wash steps) and were incubated with the primary antibodies rat anti-CD45 (1:200) (BioLegend, San Diego, USA) and rabbit anti-FOXP3 (1:500) (Abcam, Melbourne Australia) with 2% NDS, overnight at 4°C. Sections were washed as previous, and then incubated with the secondary antibodies Alexa Fluor 488 donkey anti-rat and Alexa Fluor 594 donkey anti-rabbit (both, 1:500; Jackson Immunoresearch, West Grove, USA) with 2% NDS for 1h at room temperature. Sections were subjected to an additional wash step and were mounted on to glass slides for imaging using DAKO fluorescence mounting medium (Agilent Technologies, Melbourne, Australia) to preserve the tissue and fluorescent signal.

3.5.7. Imaging and analysis

The levels of CD-45 and FOXP3 immunofluorescence were visualised using an Eclipse Ti confocal laser scanning system (Nikon, Tokyo, Japan). For each sample, eight Z-series images were randomly acquired using the 20X objective at a thickness of 2µm. Identical image acquisition settings were retained for all samples. All images were collected as .ND2 files which contained all metadata including fluorescence signals at all Z levels. Images were visualised using Image J v1.50b open source software (National Institute of Health, Bethesda, USA) (Schneider et al., 2012, Rueden et al., 2017) with the Image J ND2 Reader plugin and were converted into maximum intensity projections in 16-bit .TIFF format. Each image contained a field of view of $0.4mm^2$ ($400{,}000\mu m^2$) Using the same software, regions of interest were set to include the mucosa/submucosa and eliminate the lumen and muscle layers. This was necessary to address the differences in the size of the mucosa between C57BL/6 and *Winnie* mice. 16-bit images were analysed by binary thresholding for immunoreactivity. Identical threshold levels were set for every image. The binary particles were then analysed to obtain the total area (mm^2) of CD45 immunoreactivity per image (Rahman et al., 2015). This area was then made into a region of interest and applied to binary threshold images of FOXP3

immunoreactivity. The total area of co-localised CD45 and FOXP3 was measured in these images (mm^2). Values were expressed as the average area of immunoreactivity for CD45 or CD45 and FOXP3 within these $0.4mm^2$ images from eight images analysed per mouse.

3.5.8. Statistical analysis

Data analysis for the clinical parameters of colitis, histology and immunohistochemistry was performed using GraphPad Prism v7 (GraphPad Software Inc., San Diego, USA). One-way ANOVA was performed with a post hoc Holm-Sidak test for multiple comparisons. For these analyses $P \leq 0.05$ was considered significant and data were presented as mean ± standard error of the mean (SEM).

3.5.9. RNA extraction

The distal colon was collected from mice and snap frozen in liquid nitrogen immediately after culling and stored at -80°C until RNA was extracted. Tissues were placed in separate tubes containing 1000µL of TRIzol® reagent at 4°C (Thermo Fisher Scientific, Melbourne, Australia) and two metallic beads each. Tubes were then placed in a homogenising bead beater (TissueLyser LT, Qiagen, Melbourne, Australia) and were pulsed at 50 oscillations per second for 2x5 minutes to dissociate the tissues with a 1min break in between. To perform phase separation of RNA, the TRIzol tissue homogenate solution was removed from homogenisation tubes and 200µL of chloroform was added. Solutions were mixed by shaking for 15s, incubated for 3min at room temperature and centrifuged at 12000G for 15min at 4°C. From this solution the aqueous phase containing RNA was removed and incubated with 500µL of absolute isopropanol at room temperature for 10min before centrifugation at 12000G for 10min at 4ºC to obtain RNA pellets. The RNA pellets were washed in 500µL of 75% ethanol and spun at 5000G for 5min to remove contaminating phenols and recollect the pellet. Pellets were dissolved in 100µL of pure nucleotide free H_2O for processing using the RNeasy Mini Kit

(Qiagen). Briefly, a mixture of 350µL proprietary RLT buffer containing 1% 2-mercaptoethanol and 250µL of absolute ethanol was added to the resuspended RNA. The solution was then transferred to silica-membrane RNeasy spin columns and spun at 8000G for 15s to bind RNA. Samples were washed by spinning with 350µL of proprietary RW1 buffer at 8000G for 15s before and after an on-column DNA denaturing step with DNase (Qiagen) incubated for 15min at room temperature. Samples were then washed by two spins with 500µL proprietary RPE buffer for 15s at 8000G and spun dry at 8000G for 1min. Purified RNA was collected in 36µL of nuclease-free water spun at 8000G for 1min and frozen at -80°C for use in experiments.

3.5.10. RNA concentrations and quality control

The concentration of RNA in each sample was quantified by a Qubit 1.0 fluorometer (Invitrogen, Thermofisher, Melbourne, Australia) using the Qubit® RNA Broad Range Assay Kit (Life Technologies) according to the manufacturer's protocol. Briefly, 10µL of supplied standards and 10µL of sample RNA (diluted 1:2 in nuclease-free water) was added to clear PCR tubes with 190µL of Qubit® RNA working solution containing an RNA-specific fluorometric. Tubes were incubated for 2min at room temperature before readings were taken for fluorometric quantitation specific to RNA in the samples. Contaminates (such as phenol) were evaluated in RNA samples using a DeNovix DS-11 spectrophotometer (Gene Target Solutions, Sydney, Australia). Absorbance (A) scores for all samples were between 1.8 – 2.0 for A260/A280 ratios and 2.0-2.2 for A260/A230 ratios, suggesting that nucleotide purity was high. The quality of RNA was assessed using an 2100 Bioanalyzer (Agilent Technologies) microfluidics platform with the RNA 6000 Nano Kit (Agilent Technologies) according to the manufacturer's protocol. All samples were free from contamination of genomic DNA and 16S ribosomal RNA from bacteria. Samples were of very high quality and had minimal degradation with RNA integrity number (RIN) values between 9.9-10/10.

3.5.11. High-throughput RNA-Sequencing of mRNA

An experimental design similar to Seaman et al. (2015) was employed for RNA-Sequencing (RNA-Seq) experiments. Samples of RNA (n=7/group) from C57BL/6 and *Winnie* mice, treated with either vehicle or BM-MSCs, were pooled into groups containing equal concentrations of RNA totalling at least 3µg of RNA at 100ng/µL in nuclease-free water. Samples were submitted to the Australian Genome Research Facility (AGRF, Melbourne, Australia) for polyA purification of mRNA from total RNA samples, RNA-Seq library perpetration and high-throughput sequencing using a 100bp single-end read protocol on the Illumina HiSeq 2500 System. A data yield of approximately 2.5-3.2 Gb were acquired per sample. Base calling was performed using HiSeq Control Software (HCS) v2.2.68 and Real Time Analysis (RTA) v1.18.66.3. Sequencing data were generated using the Illumina bcl2fastq 2.20 pipeline. The quality of raw reads was assessed by FASTQC at a kmer size of 7 (Andrews, 2010). In addition, 1000 raw reads were randomly selected for alignment to the NCBI nonredundant nucleotide database using Blast+ v2.7.1 (Camacho et al., 2009). To map raw reads, the STAR v2.6.0c program was used to align reads to the mouse reference genome (GRCm38) (Dobin et al., 2013). Optical duplicates were removed, and the alignment file was sorted by coordinates using Sequence Alignment/Map(SAM) tools v1.8.0 (Li et al., 2009). Read summarisation of the raw counts per gene was determined using featureCounts v1.6.2 program of the software package subread (Liao et al., 2014). Differentially expressed genes (DEG) from raw mapped reads were evaluated by the R package DEGseq v 1.34.0 (Wang et al., 2009). Data followed a normal distribution when presented as volcano plots with LogFC on the X axis and -Log10 of the *P* value and the Y axis (**Appendix A, Figures S1-2**). DEGs were identified with a *P* value of <0.001 using the Benjamini-Hochberg correction (Benjamini and Hochberg, 1995). Resulting datasets were additionally cleaned by cut-offs for lowly expressed genes with <10 counts in a group and low changes in expression between ±0.5LogFC. The expression of several genes was validated by RT-PCR; LogFC values between PCR and RNA-Seq data shared a high degree of similarity (R^2 = 0.9611, F = 148.3, *P*<0.0001) (**Appendix A, Figure S3**). Up and downregulated DEGs were analysed

for enriched gene ontology (GO) terms (Ashburner et al., 2000) associated with biological processes, molecular function and cellular components using a rank-based method with a $P<0.001$ threshold by the web-based tool GOrilla (Eden et al., 2009). Selected, enriched gene ontologies (GO) identified using GOrilla were visualised as interaction maps by the R package clusterProfiler v3.8.1 (Yu et al., 2012). Analysis of enrichment of Kyoto Encyclopedia of Genes and Genomes (KEGG) pathways (Kanehisa and Goto, 2000) was performed in up and downregulated DEGs separately (Hong et al., 2014) using the web-based tool DAVID (database for annotation, visualization and integrated discovery) with a $P<0.05$ threshold and the Benjamini-Hochberg correction (Dennis et al., 2003, Huang et al., 2008b, Huang et al., 2008a). The fold regulation of genes identified in enriched KEGG pathways were visualised as heat maps using the gplots R package (Warnes et al., 2009).

Gene expression data on the transcriptome of human IBD patients were obtained from the National Centre for Biotechnology Information (NCBI) Gene Expression Omnibus (GEO) public data repository (Edgar et al., 2002, Barrett et al., 2012). Data obtained in the GEO is de-identifiable before submission. The expression profile of the inflamed intestine from IBD patients and of the healthy colon regions from uninflamed controls undergoing resection of non-obstructive colorectal adenocarcinoma was produced by high-throughput sequencing using Illumina HiSeq 2500 platform and uploaded by Peters et al. (2017) as reads per kilobase of transcript, per million mapped reads (RPKM). Similar to our methods, poly-A purified mRNA was used in this study from RNA isolated using TRIzol obtained from samples of snap frozen 50mm fragments of excised tissue. These data are accessible through GEO series accession number GSE83687 at https://www.ncbi.nlm.nih.gov/geo/. Gene expression of colon samples were used from this dataset including: male (n=14) and female (n=20) controls, male (n=19) and female (n=11) patients with UC and male (n=7) and female (n=4) patients with CD (total n=75).

3.6. Results

3.6.1. BM-MSCs ameliorate the severity of spontaneous chronic colitis

To determine the therapeutic value of MSCs in spontaneous chronic colitis, *Winnie* mice were treated with BM-MSCs via enema, an application method which has been demonstrated previously to be effective in acute models of colitis (Robinson et al., 2014, Forte et al., 2015, Robinson et al., 2015, Stavely et al., 2015a, Stavely et al., 2015b, Cury et al., 2016, Wang et al., 2016, Robinson et al., 2017b). Colons collected from *Winnie* mice treated with a vehicle (PBS) via enema were morphologically distinct from C57BL/6 mice with an observable thickening in colon diameter, soft content and dark colour which was less pronounced in *Winnie* mice treated with BM-MSCs (**Figure 3.1A**).

Disease activity scores for colitis, consisting of prolapse and bleeding, changes in colon morphology, stool consistency and weight loss, were evaluated in C57BL/6 and *Winnie* mice treated with either PBS as a sham or BM-MSCs (**Figure 3.1B**). The disease activity index was significantly increased in *Winnie*-sham mice (9.2±0.4) compared to C57BL/6 mice (0.2±0.2, $P<0.0001$) (n=5 animals/group). Treatment with BM-MSCs attenuated the disease activity of colitis in *Winnie* mice (5.7±0.7, $P<0.001$, n=7 animals), albeit to levels remaining higher then C57BL/6 mice ($P<0.0001$). No differences in weight loss were observed between *Winnie* mice treated with PBS or BM-MSCs.

Changes to the length and weight of the colon are often used as an indication of colitis in animal models. No differences between the colon length of C57BL/6 mice (99.1±3.5mm, n=5 animals), sham treated (94.5±4.2mm, n=5 animals) and BM-MSC treated *Winnie* mice (93.9±1.8mm, n=7 animals) were observed (**Figure 3.2A**).

Figure 3.1 ***Effects of BM-MSC treatments on colon morphology and the disease activity scores in the Winnie mouse model of spontaneous chronic colitis***

A) Photographical representation of colons obtained from C57BL/6 mice, *Winnie* mice treated with PBS (sham) and *Winnie* mice treated with BM-MSCs. **B)** Disease activity Index (DAI) of colitis consisting of rectal bleeding/prolapse, colon weight:length ratio, presence of diarrhoea and weight loss in C57BL/6 mice, *Winnie*-sham and *Winnie* mice treated with BM-MSCs. ***$P<0.001$ between *Winnie*-sham and *Winnie*+MSC, ††††$P<0.0001$ between C57BL/6 and both *Winnie*-sham and *Winnie*+MSC. C57BL/6 and *Winnie*-sham: n=5 animals/group, *Winnie*+MSC: n=7 animals.

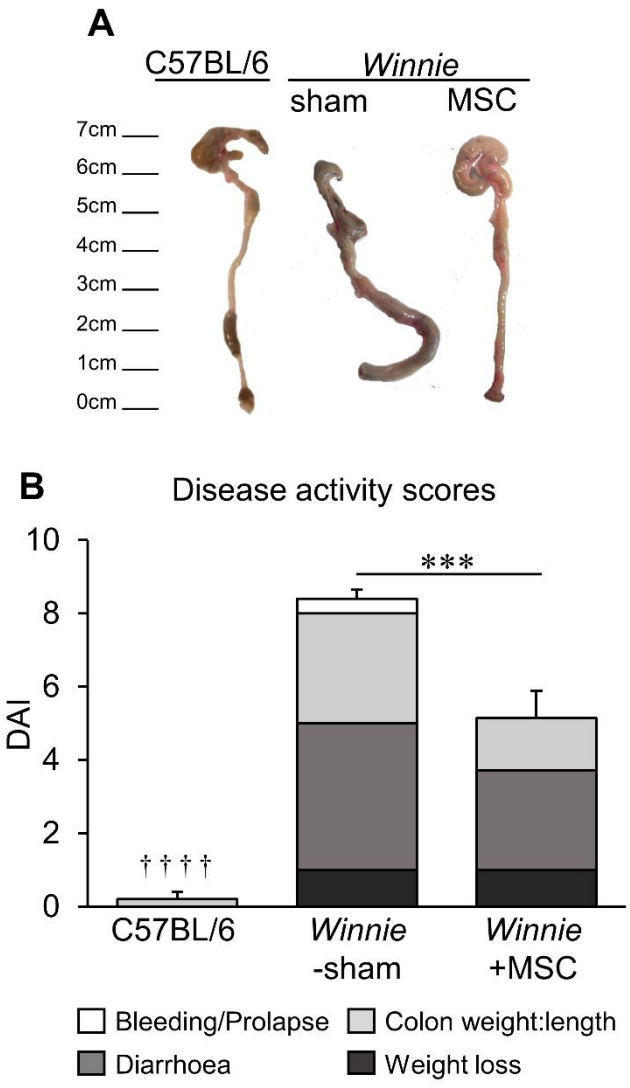
A
C57BL/6
Winnie
sham
MSC
7cm
6cm
5cm
4cm
3cm
2cm
1cm
0cm
B
Disease activity scores
DAI
10
8
6
4
2
0
***
††††
C57BL/6
Winnie
-sham
Winnie
+MSC
Bleeding/Prolapse
Colon weight:length
Diarrhoea
Weight loss

Figure 3.2 ***Effects of BM-MSC treatments on the size of the colon in Winnie mice***

Alterations in colon morphology measured by the length (mm) of the colon from caecum to rectum **(A)**, colon weight (g) **(B)** and the colon weight:length ratio **(C)** in C57BL/6 mice, *Winnie* mice treated with PBS (sham) and *Winnie* mice treated with BM-MSCs. **P*<0.05 between *Winnie*-sham and *Winnie*+MSC, ††††*P*<0.0001 between C57BL/6 and *Winnie*-sham, ‡‡*P*<0.01, ‡‡‡*P*<0.001 between C57BL/6 and *Winnie*+MSC. C57BL/6 and *Winnie*-sham: n=5 animals/group, *Winnie*+MSC: n=7 animals.

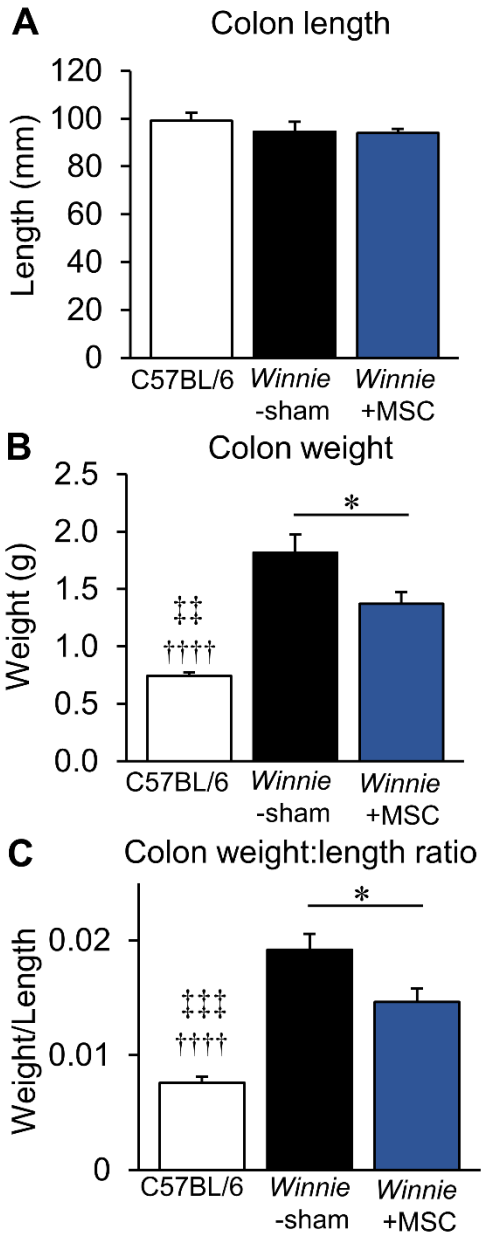
A
Colon length
Length (mm)
120
100
80
60
40
20
0
C57BL/6
Winnie -sham
Winnie +MSC
B
Colon weight
Weight (g)
2.5
2.0
1.5
1.0
0.5
0.0
*
‡‡
††††
C57BL/6
Winnie -sham
Winnie +MSC
C
Colon weight:length ratio
Weight/Length
0.02
0.01
0
*
‡‡‡
††††
C57BL/6
Winnie -sham
Winnie +MSC

Conversely, colon weight was significantly increased in *Winnie*-sham (1.81±0.16g, n=5 animals) compared to C57BL/6 mice (0.74±0.03g, $P<0.0001$, n=5 animals) (**Figure 3.2B**). Treatment of *Winnie* mice with BM-MSCs decreased the weight of the colon (1.37±0.10g, $P<0.05$, n=7 animals), however colons were heavier than those of C57BL/6 mice ($P<0.01$) (**Figure 3.2B**). Similar results were observed when colon weight was normalised to colon length with higher colon weight:length ratios in *Winnie*-sham mice (0.0192±0.0014, n=5 animals) compared to C57BL/6 mice (0.0076±0.0005, $P<0.0001$, n=5 animals) and BM-MSC-treated *Winnie* mice (0.0146±0.0011, $P<0.05$, n=7 animals). Nonetheless, colon weight:length ratios in BM-MSC-treated *Winnie* mice also remained elevated compared C57BL/6 mice ($P<0.001$) (**Figure 3.2C**).

Stool consistency was measured by the faecal water content of pellets collected from mice in isolated cages prior to culling (**Figure 3.3A**). The percentage of faecal water content was the lowest in C57BL/6 mice (57.6±0.8%, n=5 animals) compared to both *Winnie*-sham (79.2±1.4%, $P<0.0001$, n=5 animals) and *Winnie* mice treated with BM-MSCs (72.7±2.2%, $P<0.0001$, n=7 animals) Nevertheless, *Winnie* mice demonstrated improvements in stool consistency with BM-MSC treatments ($P<0.05$) (**Figure 3.3A**). Weight loss is regularly used as a clinical parameter of murine colitis (Wirtz et al., 2007, Chassaing et al., 2014); therefore, the percentage of weight lost was evaluated (**Figure 3.3B**). C57BL/6 continuously gained weight throughout the study (n=5 animals), however, both sham-treated (-1.58±0.23%, n=5 animals) and BM-MSC-treated (-1.64±0.51%, n=7 animals) *Winnie* mice exhibited modest, but significant ($P<0.01$ for both), weight loss (**Figure 3.3B**).

3.6.2. BM-MSC treatments reduce gross morphological damage and leukocyte recruitment in chronic colitis

Haematoxylin and eosin staining was performed in cross sections of the distal colon to evaluate gross morphological damage to the colon including changes to crypt architecture, crypt length and presence of abscesses, tissue damage, loss of goblet cells and leukocyte infiltration (Heazlewood et al., 2008) (**Figure 3.4A-A″**).

Figure 3.3 ***Effects of BM-MSC treatments on stool consistency and weight loss in Winnie mice***

A) Faecal water content expressed as the percentage of water weight in faecal pellets. **B)** Weight loss was expressed as the percentage of weight lost recorded on the day of culling compared to the highest recorded weight during acclimation and treatment periods. C57BL/6 mice, *Winnie* mice treated with PBS (sham) and *Winnie* mice treated with BM-MSCs. **P*<0.05 between *Winnie*-sham and *Winnie*+MSC, ††*P*<0.01, ††††*P*<0.0001 between C57BL/6 and *Winnie*-sham, ‡‡*P*<0.01, ‡‡‡‡*P*<0.0001 between C57BL/6 and *Winnie*+MSC. C57BL/6 and *Winnie*-sham: n=5 animals/group, *Winnie*+MSC: n=7 animals.

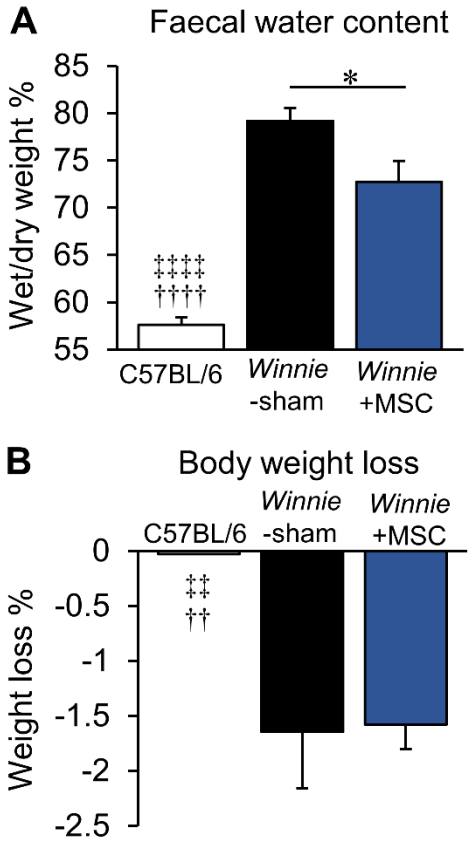
A
Faecal water content
Wet/dry weight %
85
80
75
70
65
60
55
*
‡‡‡‡
††††
C57BL/6
Winnie
-sham
Winnie
+MSC
B
Body weight loss
Weight loss %
0
-0.5
-1
-1.5
-2
-2.5
C57BL/6
Winnie
-sham
Winnie
+MSC
‡‡
††

Figure 3.4 ***Gross morphology of the distal colon from Winnie mice after BM-MSC treatment***

A-A′′) Gross morphology of the distal colon was visualised by H&E staining in cross sections from C57BL/6 mice **(A)**, *Winnie* mice treated with PBS (sham) **(A′)** and *Winnie* mice treated with BM-MSCs **(A′′)** (scale bar = 50µm). **B)** Quantification of histological scoring in colonic cross sections. ***$P<0.001$, ****$P<0.0001$; n=7 animals/group.

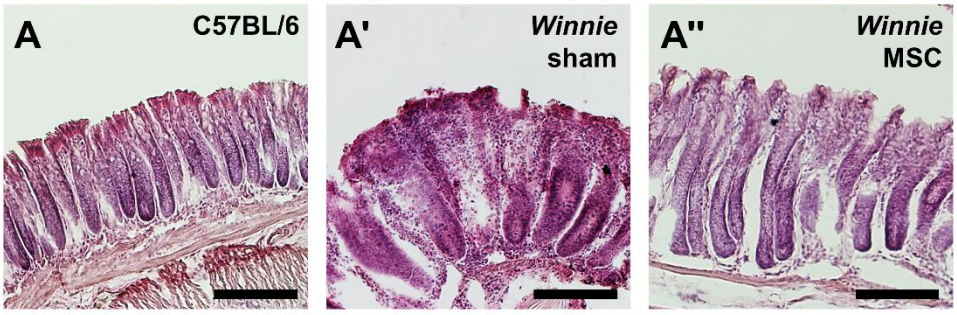
A
C57BL/6
A'
Winnie
sham
A''
Winnie
MSC

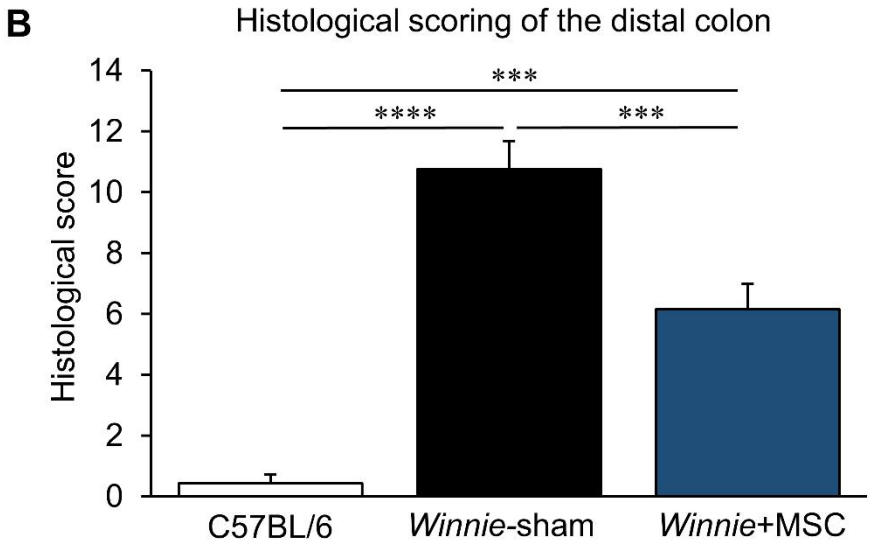
B
Histological scoring of the distal colon
Histological score
14
12
10
8
6
4
2
0
***
****
***
C57BL/6
Winnie-sham
Winnie+MSC

Histological scores were elevated in sham-treated (10.8±0.9, $P<0.0001$, n=7 animals) and BM-MSC-treated *Winnie* mice (6.1±0.9, $P<0.001$, n=7 animals) compared to C57BL/6 mice (0.4±0.3, n=7 animals) However, BM-MSC treatment reduced histological scores in *Winnie* mice ($P<0.001$) (**Figure 3.4B**).

Immune cell infiltration was assessed in cross sections of the distal colon by immunohistochemistry using the pan-leukocyte marker CD45 (**Figure 3.5A-C**). The average area of leukocytes within 0.4mm^2 images was greatly higher in *Winnie*-sham mice (0.105±0.020mm^2, n=7 animals) compared to C57BL/6 controls (0.046±0.009mm^2, $P<0.05$, n=4 animals). Treatment with BM-MSCs (0.047±0.008mm^2, n=6 animals) reduced the level of leukocytes in *Winnie* mice ($P<0.05$) to levels similar to C57BL/6 mice (**Figure 3.5D**). No differences were observed between the total level of CD45$^+$FOXP3$^+$ leukocytes in the distal colon of C57BL/6 (0.011±0.002mm^2, n=4 animals) and sham-treated *Winnie* mice (0.011±0.003mm^2, n=7 animals) or BM-MSC-treated *Winnie* mice (0.010±0.003mm^2, n=6 animals) (**Figure 3.5D**). Nonetheless, the ratio of CD45$^+$FOXP3$^+$ to CD45$^+$ leukocytes was decreased in *Winnie*-sham mice (0.09±0.01) compared to C57BL/6 controls (0.27±0.01, $P<0.001$). A lower ratio was also observed in BM-MSC-treated *Winnie* mice (0.15±0.03) to C57BL/6 mice ($P<0.01$); however, the ratio of FOXP3$^+$ leukocytes was elevated compared to *Winnie*-sham mice ($P<0.05$) (**Figure 3.5E**).

3.6.3. Anti-inflammatory signatures of BM-MSC treatments in chronic colitis

To evaluate the effects of BM-MSC treatments on the inflammatory profile of colitis, the transcriptome was assessed by high-throughput RNA-Seq. Deferentially expressed genes (DEG) were calculated and cut-offs were applied to these datasets revealing 5619 DEGs between sham-treated *Winnie* and control C57BL/6 mice, and 1171 DEGs between BM-MSC-treated and sham-treated *Winnie* mice.

Figure 3.5 ***Effects of BM-MSC treatment on leukocyte and FOXP3 immunoreactivity in the distal colon***

A-C) $CD45^+$ leukocytes, **A′-C′)** $FOXP3^+$ cells and **A′′-C′′)** $CD45^+FOXP3^+$ leukocytes in the distal colon were visualised by immunofluorescence in cross sections from C57BL/6 mice **(A-A′′)**, *Winnie*-sham **(B-B′′)** and *Winnie* mice treated with BM-MSCs **(C-C′′)** (scale bar = 50µm). **D)** Quantification of the area of CD45 fluorescence, and the area of FOXP3 immunoreactivity (IR) colocalised with CD45, in colonic cross sections. **E)** Ratio of $CD45^+FOXP3^+$ to $CD45^+$ immunofluorescence in the distal colon. **P*<0.05, ***P*<0.01, ****P*<0.001; C57BL/6: n=4 animals, *Winnie*-sham: n=7 animals, *Winnie*+MSC: n=6 animals.

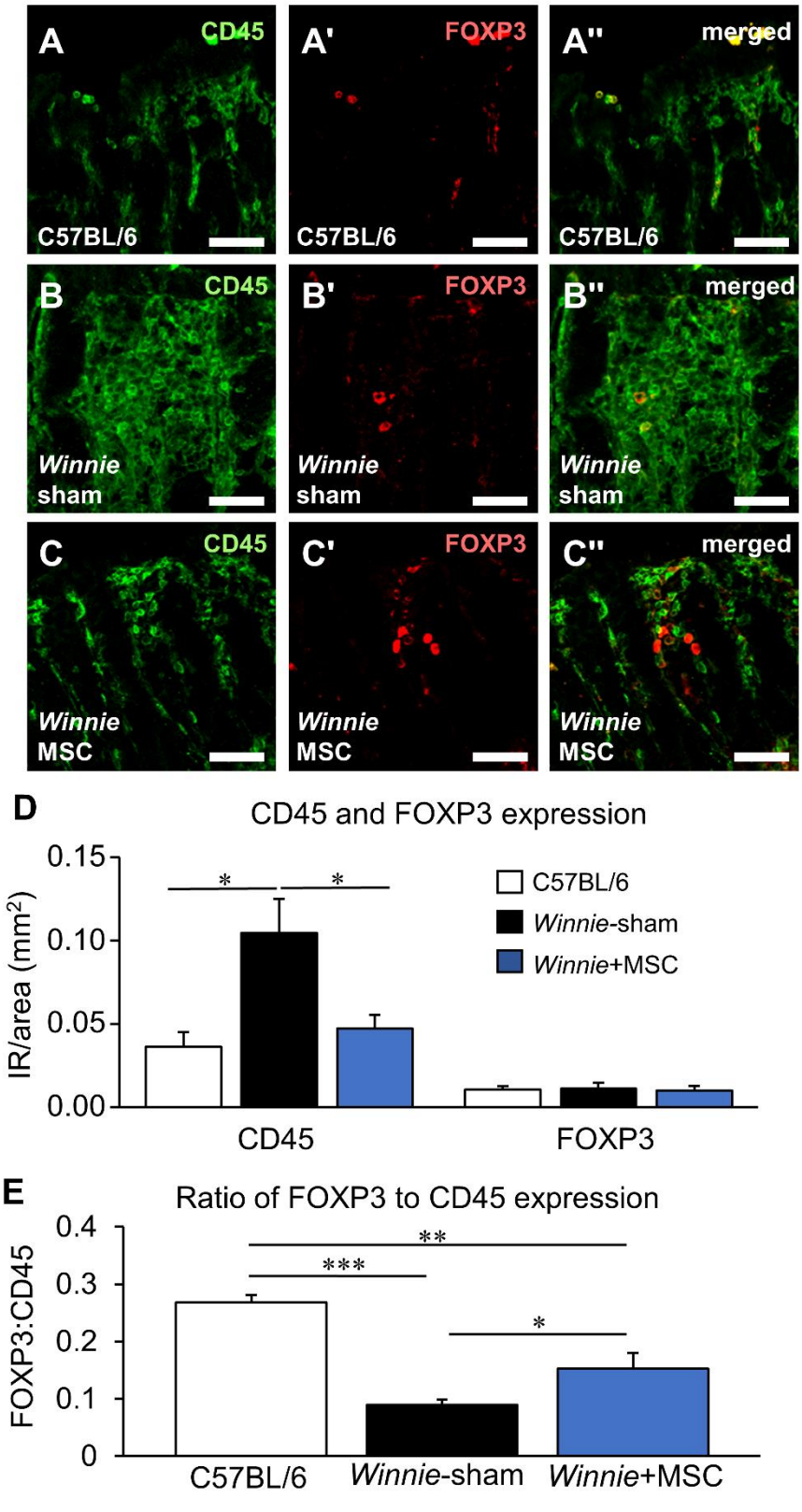
A
CD45
C57BL/6
A'
FOXP3
C57BL/6
A''
merged
C57BL/6
B
CD45
Winnie
sham
B'
FOXP3
Winnie
sham
B''
merged
Winnie
sham
C
CD45
Winnie
MSC
C'
FOXP3
Winnie
MSC
C''
merged
Winnie
MSC
D
CD45 and FOXP3 expression
IR/area (mm2)
0.15
0.10
0.05
0.00
*
*
C57BL/6
Winnie-sham
Winnie+MSC
CD45
FOXP3
E
Ratio of FOXP3 to CD45 expression
FOXP3:CD45
0.4
0.3
0.2
0.1
0
**
***
*
C57BL/6
Winnie-sham
Winnie+MSC

The effects of BM-MSC therapy on downregulated DEGs compared to *Winnie*-sham mice were summarised and annotated by analysing the enrichment of terms from the GO database. This was performed using the tool GOrilla which determines GO term enrichment in ranked (LogFC) DEGs. Analysis of the enrichment of GO terms associated with biological processes in top-ranked DEGs downregulated by BM-MSC treatments in *Winnie* mice revealed an abundance of processes related to the inflammatory and defence response (**Figures 3.6-3.8, Table 3.1**). Many of these terms were enriched in top-ranked DEGs upregulated in *Winnie* mice compared to uninflamed controls which suggest that BM-MSCs reduced multiple inflammatory processes in chronic colitis (**Appendix A, Tables S1-2**). Due to the large number of GO terms associated with inflammation, top hierarchical GO terms that encompassed multiple inflammation-associated biological processes were reported to avoid redundancy (**Appendix A, Tables S1-2**). The biological processes, *response to external biotic stimulus, immune response, leukocyte migration, inflammatory response, regulation of (endo)peptidase activity* and *H_2O_2-induced neuron death* were enriched in top-ranked DEGs upregulated in *Winnie* mice compared to C57BL/6 controls (**Figure 3.6A**). These terms, in addition to *epithelial cell differentiation,* were also enriched in top-ranked DEGs downregulated by BM-MSC treatments in *Winnie* mice. Several DEGs downregulated by BM-MSC treatments in *Winnie* mice were expressed across multiple terms with the most frequent being *Reg3b, Tnf, S100a9, Il1b, Nlrp3, Spink5, Gata3, S100a8, Tlr2, Lbp, Ptafr, Ccl5, Ifng, Cxcl5, Cxcl2, Ltf, Cxcl3, Ppbp, Reg3g, Adam8, Il1a, Ccl3* and *Trp63* (**Figure 3.6B-C**). Many of the homologs for these genes are upregulated in IBD patients (Taman et al., 2018) and *Tnf,* a key therapeutic target of IBD, was associated with the most biological processes. A network map representing gene-term interactions was generated to demonstrate how inflammation and multiple biological processes are linked via genes downregulated by BM-MSC treatments in *Winnie* mice. This included *neuronal apoptosis* through *Reg3b, Tnf, Il1b, Gata3, Adam8* and *Ccl3*, as well as, *epithelial cell differentiation* through *Tnf, Spink5, Gata3, Il1a, Reg3g, Krt16, Krt6a* and *Ifng* (**Figure 3.6C**).

GO terms associated with molecular function were analysed which revealed an enrichment in inflammation-associated terms *chemokine receptor binding*, *cytokine receptor binding* and *cytokine activity* in top-ranked DEGs upregulated in *Winnie* mice compared to uninflamed controls and in downregulated DEGs between BM-MSC and sham-treated *Winnie* mice (**Figure 3.7A, Table 3.1**). In *Winnie* mice after BM-MSC treatment, several downregulated DEGs were expressed across these terms with the most frequent being cytokines: *Il1f9, Tnf, Ifng, Inhba, Il1b, Lif, Osm, Il1a,* chemokines: *Ppbp, Ccl5, Cxcl5, Cxcl2, Ccl3, Ccl4, Cxcl14, Cxcl3, Ccrl2* and *Defb6* with dual chemoattractant and antimicrobial activity (**Figure 3.7B**). The genes interacting between these molecular functions were visualised (**Figure 3.7C**). Cytokines and chemokines were identified that were associated with the biological processes, *neuronal apoptosis*, through *Tnf, Il1b, Gata3, Adam8* and *Ccl3*, as well as, *epithelial differentiation,* through *Tnf, Gata3, Il1a* and *Ifng,* which suggest that inflammatory paracrine mechanisms interacting with the epithelium and nervous system were downregulated by BM-MSCs.

Analysis of GO terms associated with cellular components revealed an enrichment in terms associated with cellular secretion including *extracellular region* and *extracellular space* in top-ranked DEGs upregulated in *Winnie*-sham mice compared to uninflamed controls and in downregulated DEGs in BM-MSC-treated *Winnie* mice compared to *Winnie*-sham (**Figure 3.8A, Table 3.1**). The GO term *secretory granule* was also enriched by BM-MSC treatments in *Winnie* mice. All downregulated DEGs associated with the *secretory granule* are expressed by epithelial cells including *Krtdap, Klk13, Reg3b, Olfm4, Reg3b, Spink5* and *Klk10,* with all genes, except *Klk10,* being represented in the *extracellular region* and *extracellular space* (**Figure 3.8B-C**). Together this may highlight the importance of the epithelial secretion in the therapeutic effects of BM-MSC treatment. Likewise, UC is associated with upregulation in epithelial genes including *REG* family genes analogous to those downregulated by BM-MSCs; furthermore dysregulated expression of these genes persist during remission (Planell et al., 2013).

Figure 3.6 ***Effects of BM-MSCs on biological processes in the distal colon of Winnie mice***

A) Gene counts of top-ranked genes for selected GO terms describing biological processes associated with colonic inflammation. Enriched GO terms were identified in upregulated differentially expressed genes using RNA-Seq between *Winnie* mice vs C57BL/6 mice (black bars) and in downregulated differentially expressed genes between *Winnie* mice treated with BM-MSCs vs sham-treated *Winnie* mice (blue bars) by *GOrilla*. Genes were ranked by LogFC with a ±0.5 cut off and a *P* value of <0.001 for analysis. **B)** Binary matrix of differentially expressed genes (green) associated with greatest number of GO terms identified in genes downregulated by BM-MSC treatment in *Winnie* mice. **C)** An interaction network of differentially expressed genes and selected enriched GO terms from downregulated genes after BM-MSC treatment in *Winnie* mice. Matrices were generated and plotted using *clusterProfiler*. Red text depicts genes associated with the regulation of neuron apoptotic process and H_2O_2-induced neuron death. Red borders depict key biomarkers of colonic inflammation.

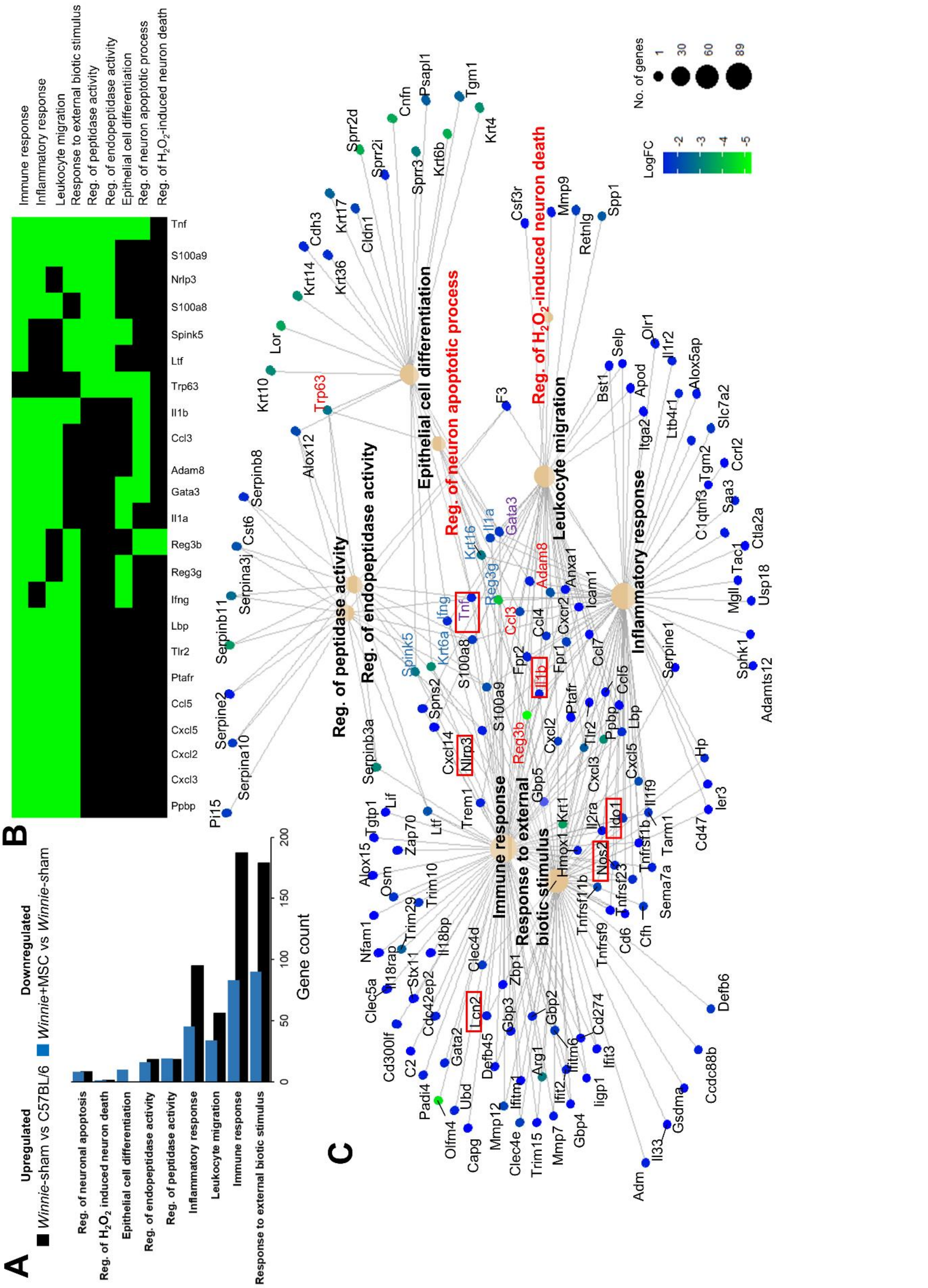

A
Upregulated
Downregulated
Winnie-sham vs C57BL/6
Winnie+MSC vs Winnie-sham
Reg. of neuronal apoptosis
Reg. of H_2O_2 induced neuron death
Epithelial cell differentiation
Reg. of endopeptidase activity
Reg. of peptidase activity
Inflammatory response
Leukocyte migration
Immune response
Response to external biotic stimulus
Gene count
B
Immune response
Inflammatory response
Leukocyte migration
Response to external biotic stimulus
Reg. of peptidase activity
Reg. of endopeptidase activity
Epithelial cell differentiation
Reg. of neuron apoptotic process
Reg. of H_2O_2-induced neuron death
Tnf
S100a9
Nrlp3
S100a8
Spink5
Ltf
Trp63
Il1b
Ccl3
Adam8
Gata3
Il1a
Reg3b
Reg3g
Ifng
Lbp
Tlr2
Ptafr
Ccl5
Cxcl5
Cxcl2
Cxcl3
Ppbp
C
Reg. of peptidase activity
Reg. of endopeptidase activity
Epithelial cell differentiation
Reg. of neuron apoptotic process
Reg. of H_2O_2-induced neuron death
Leukocyte migration
Inflammatory response
Immune response
Response to external biotic stimulus
No. of genes
LogFC

Figure 3.7 ***Effects of BM-MSCs on molecular function in the distal colon of Winnie mice***

A) Gene counts of top-ranked genes for selected GO terms describing molecular function associated with colonic inflammation. Enriched GO terms were identified in upregulated differentially expressed genes using RNA-Seq between *Winnie* mice vs C57BL/6 mice (black bars) and in downregulated differentially expressed genes between *Winnie* mice treated with BM-MSCs vs sham-treated *Winnie* mice (blue bars) by *GOrilla*. Genes were ranked by LogFC with a ±0.5 cut off and a *P* value of <0.001 for analysis. **B)** Binary matrix of differentially expressed genes (green) associated with greatest number of GO terms identified in genes downregulated by BM-MSC treatment in *Winnie* mice. **C)** An interaction network of differentially expressed genes and selected enriched GO terms from downregulated genes after BM-MSC treatment in *Winnie* mice. Matrices were generated and plotted using *clusterProfiler*. Red text depicts genes associated with the regulation of neuron apoptotic process, blue text depicts genes associated with epithelial differentiation and purple text depicts both. Red borders depict key biomarkers of colonic inflammation.

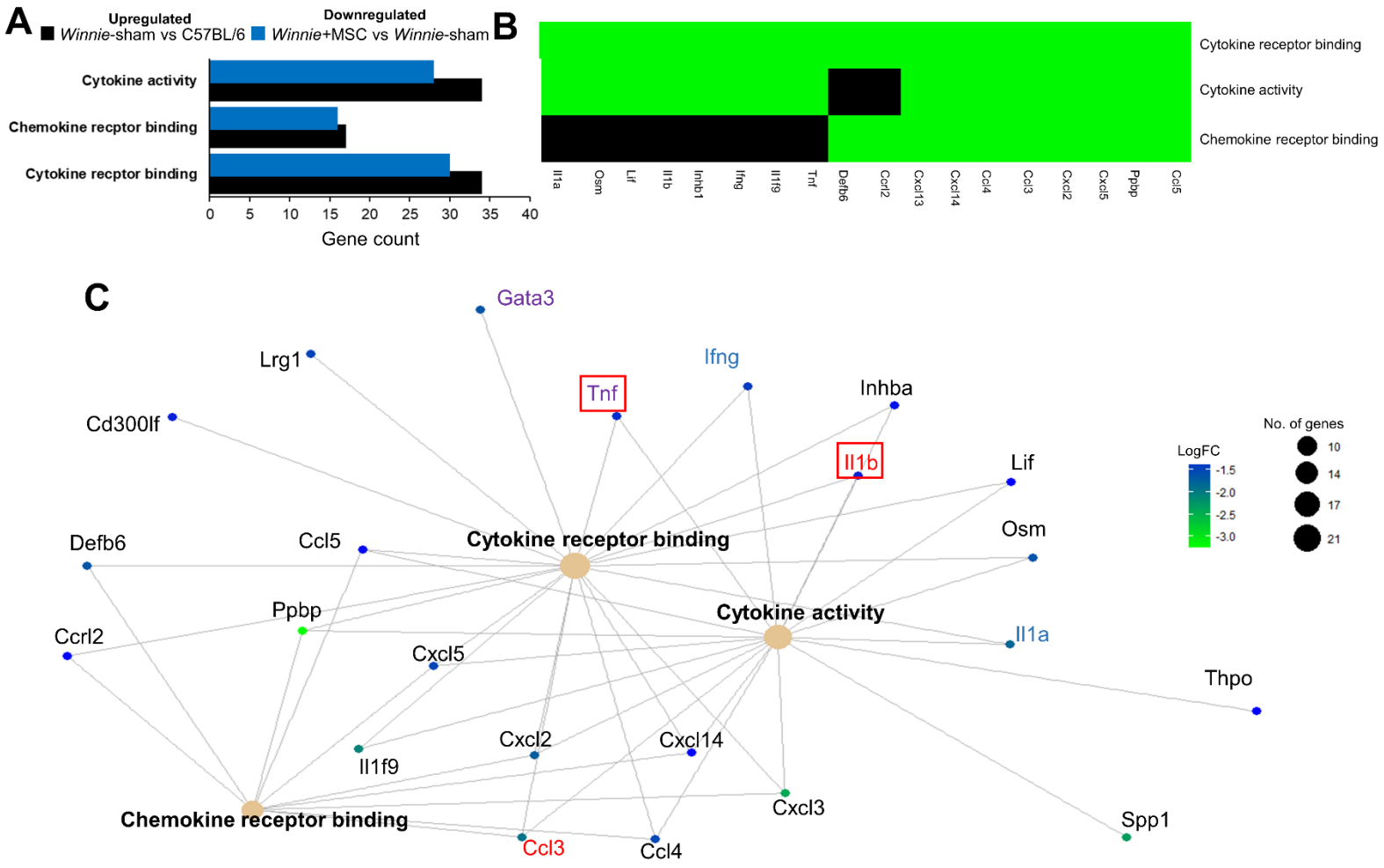
A
Upregulated
Winnie-sham vs C57BL/6
Downregulated
Winnie+MSC vs Winnie-sham
Cytokine activity
Chemokine recptor binding
Cytokine recptor binding
0 5 10 15 20 25 30 35 40
Gene count
B
Cytokine receptor binding
Cytokine activity
Chemokine receptor binding
Il1a Osm Lif Il1b Inhb1 Ifng Il1f9 Tnf Defb6 Ccrl2 Cxcl13 Cxcl14 Ccl4 Ccl3 Cxcl2 Cxcl5 Ppbp Ccl5
C
Gata3
Lrg1
Ifng
Tnf
Inhba
Cd300lf
Il1b
Lif
Osm
Defb6
Ccl5
Cytokine receptor binding
Ppbp
Cytokine activity
Ccrl2
Il1a
Cxcl5
Thpo
Cxcl2
Cxcl14
Il1f9
Cxcl3
Chemokine receptor binding
Spp1
Ccl3
Ccl4
LogFC
-1.5
-2.0
-2.5
-3.0
No. of genes
10
14
17
21

Figure 3.8 ***Effects of BM-MSCs on cellular components in the distal colon of Winnie mice***

A) Gene counts of top-ranked genes for selected GO terms describing cellular components associated with colonic inflammation. Enriched GO terms were identified in upregulated differentially expressed genes using RNA-Seq between *Winnie* mice vs C57BL/6 mice (black bars) and in downregulated differentially expressed genes between *Winnie* mice treated with BM-MSCs vs sham-treated *Winnie* mice (blue bars) by *GOrilla*. Genes were ranked by LogFC with a ±0.5 cut off and a *P* value of <0.001 for analysis. **B)** Binary matrix of differentially expressed genes (green) associated the GO term 'secretory granule' (all identified genes were associated with the epithelial layer) and key biomarkers of colonic inflammation in genes downregulated by BM-MSC treatment in *Winnie* mice. **C)** An interaction network of differentially expressed genes and selected enriched GO terms from downregulated genes after BM-MSC treatment in *Winnie* mice. Matrices were generated and plotted using *clusterProfiler*. Red text depicts genes associated with the regulation of neuron apoptotic process and H_2O_2-induced neuron death, blue text depicts genes associated with epithelial differentiation and purple text depicts both. Red borders depict key biomarkers of colonic inflammation and green borders depict neuroinflammatory markers.

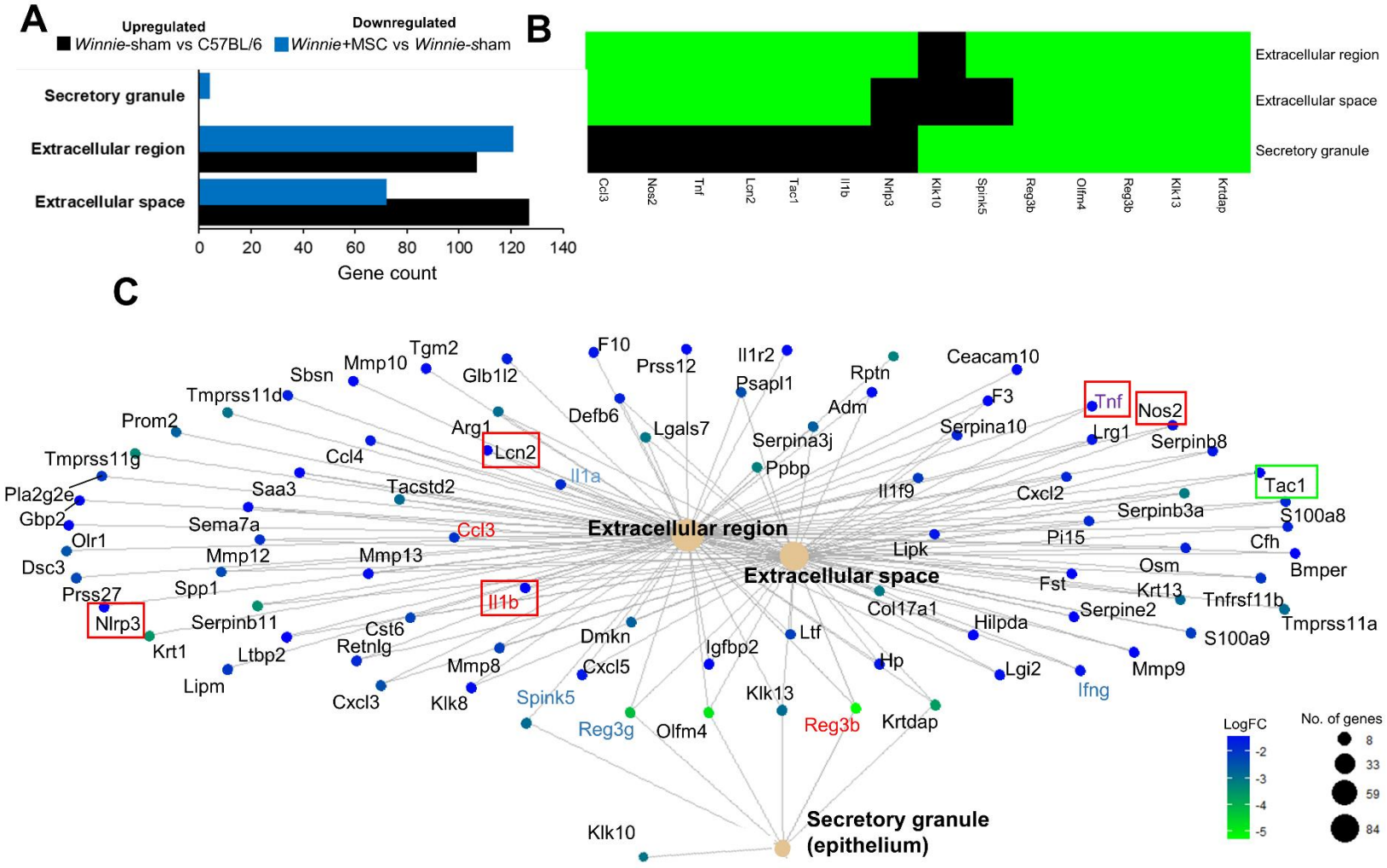
A
Upregulated
Winnie-sham vs C57BL/6
Downregulated
Winnie+MSC vs Winnie-sham
Secretory granule
Extracellular region
Extracellular space
0
20
40
60
80
100
120
140
Gene count
B
Extracellular region
Extracellular space
Secretory granule
Ccl3
Nos2
Tnf
Lcn2
Tac1
Il1b
Nrlp3
Klk10
Spink5
Reg3b
Olfm4
Reg3b
Klk13
Krtdap
C
Extracellular region
Extracellular space
Secretory granule
(epithelium)
Tgm2
Mmp10
Sbsn
Glb1l2
Tmprss11d
Prom2
Arg1
Lcn2
Ccl4
Tmprss11g
Pla2g2e
Saa3
Tacstd2
Gbp2
Sema7a
Olr1
Mmp12
Mmp13
Dsc3
Spp1
Prss27
Nlrp3
Serpinb11
Krt1
Ltbp2
Cst6
Retnlg
Lipm
Cxcl3
Klk8
Mmp8
Spink5
Reg3g
Olfm4
Cxcl5
Dmkn
Igfbp2
Ltf
Klk13
Reg3b
Krtdap
Hp
Klk10
F10
Prss12
Il1r2
PsapI1
Rptn
Defb6
Lgals7
Adm
Serpina3j
Ppbp
Il1a
Il1b
Il1f9
Ceacam10
F3
Serpina10
Tnf
Nos2
Lrg1
Serpinb8
Cxcl2
Tac1
Serpinb3a
S100a8
Pi15
Cfh
Lipk
Osm
Bmper
Fst
Krt13
Tnfrsf11b
Col17a1
Serpine2
Tmprss11a
Hilpda
S100a9
Lgi2
Mmp9
Ifng
LogFC
-2
-3
-4
-5
No. of genes
8
33
59
84

Table 3.1 ***Selected enriched gene ontologies identified in differentially expressed genes downregulated in Winnie mice treated with BM-MSCs compared to sham-treated Winnie mice***

GO Term	Description	*P* value	FDR q-value	Genes
		Biological Process		
GO:0006955	Immune response	1.37E-12	3.17E-09	*Fas, Cxcl3, Samhd1, Stx11, Pirb ,Arg1 ,H2Q7, Il1b, Il1a, Cxcl9, Il18rap, Osm, Oas3, Trim29, Oas2, Lif, Cd55, Fcer1g, Prkcd, Tinagl1, Cxcl14, Cd6, Clec4e, Tnfrsf1b, Il18bp, Gata3, Pglyrp1, Padi4, Nod2, Tap1, Anxa1, Clec4d, Rel, Nlrp3, Reg3g, Ccrl2, Tnf, Zap70, Lbp, Tmem173, Icam1, Tarm1, Trim30a, Ifitm1, Cd274, Cxcl2, Ifit1, Cxcl5, Irgm1, Cfh, Il1f9, Ccl3, Ltf, Iigp1, Ccl4, Irg1, Isg20, Ccl7, Ccl8, Ccl5, Dtx3l, Krt1, Trim15, Zbp1, Ifng, C2, Krt16, Reg3b, Ifit3, Ifit2, S100a8, S100a9, Clec5a, Trim10, Parp9, Nfil3, Il2ra, Krt6a, Tlr2, Cxcr2, Il4ra, Lcn2, Ppbp*
GO:0043207	Response to external biotic stimulus	3.42E-11	4.74E-08	*Gbp7, Gbp6, Cxcl3, Samhd1, Gbp5, 1100001G20Rik, Arg1, Il1b, Cxcl9, Gsdma, Oas3, Ly6a, Oas2, Ptafr, Prkcd, Fcer1g, Mmp12, Retnlb, Cxcl16, Gch1, Saa3, Cd6, I830012O16Rik, Itgax, Itgav, Clec4e, Tnfrsf1b, Pglyrp1, 2210407C18Rik, Gbp2, Mmp7, Lrg1, Nod2, Ccdc88b, Clec4d, Cd47, Reg3g, Nlrp3, Tnf, Mrc1, Lbp, Tmem173, Gbp3, Trim30a, Ifitm1, Bnip3, Cd274, Nos2, Cxcl2, Cxcl5, Ifit1, Ifi204, Irgm1, Il33, Ier3, Il1f9, Iigp1, Ltf, Cebpb, Ido1, Irg1, Ifitm6, Isg20, Adm, Ccl5, Dtx3l, Zbp1, Slfn2, Usp18, Hp, Ifng, Slfn4, Defb6, Reg3b, Batf2, Ifit3, Ifit2, S100a9, Gzma, Parp9, Serpine1, Dmbt1, Tlr2, Fcgr4, Krt6a, Il4ra, Tgtp1, Lcn2, Ppbp*
GO:0006954	Inflammatory response	6.38E-10	4.42E-07	*Cxcl3, Sphk1, Icam1, Lbp, Gbp5, Il1b, Il1a, Nos2, Fpr1, Adam8, Fpr2, Cxcl2, Cxcl5, Ltb4r1, Ptafr, Ccl3, Il1f9, Ccl4, Irg1, Ido1, Saa3, Ccl7, Ccl5, Cd6, Tac1, Olr1, Hp, Tnfrsf1b, Krt16, Reg3b, Sema7a, S100a8, S100a9, Anxa1, Il2ra, Reg3g, Nlrp3, Selp, Tlr2, Chi3l1, Ccrl2, Cxcr2, Tnf, Chi3l3, Ppbp*
GO:0050900	Leukocyte migration	1.05E-08	4.54E-06	*Cxcl3, Spns2, Retnlg, Lbp, Icam1, Il1b, Cxcl9, Adam8, Fpr1, Fpr2, Cxcl2, Cxcl5, Csf3r, Fcer1g, Il1f9, Ccl3, Ccl4, Cxcl16, Ccl7, Ccl8, Ccl5, Itgam, Ifng, Trem1, Gata3, S100a8, S100a9, Mmp9, Anxa1, Spp1, Selp, Cxcr2, Tnf, Ppbp*
GO:0030855	Epithelial cell differentiation	3.49E-04	2.75E-02	*Tgm1, Krt10, Sprr3, Spink5, Krt4, Psapl1*
GO:0052548	Regulation of endopeptidase activity	5.50E-04	3.97E-02	*Alox12, Serpinb3a, Spink5, Serpina10, S100a8, Mmp9, S100a9, Serpine2, Serpinb11, Trp63, Nlrp3, Ltf, F3, Serpina3j, Tnf, Serpinb8*
GO:0052547	Regulation of peptidase activity	7.36E-04	5.05E-02	*Alox12, Serpinb3a, Spink5, Serpina10, Wfdc18, S100a8, Mmp9, S100a9, Serpine2, Pi15, Serpinb11, Trp63, Csta, Nlrp3, Ltf, F3, Serpina3j, Tnf, Serpinb8*
GO:0043523*	Regulation of neuron apoptotic process	1.68E-02	5.53E-01	*Il1b, Tnf, Adam8, Gata3, Ccl3, Trp63, Reg3g, Reg3b*

Molecular Function				
GO:0005126	Cytokine receptor binding	7.01E-06	5.78E-03	*Cxcl3, Il1b, Il1a, Cxcl9, Osm, Cxcl2, Cxcl5, Lif, Bmp8b, Grem1, Cd300lf, Ccl3, Il1f9, Ccl4, Cxcl16, Cxcl14, Ccl7, Ccl8, Ccl5, Ifng, Defb6, Ccl28, S100a14, Gata3, Lrg1, Inhba, Ccrl2, Nucb2, Tnf, Ppbp*
GO:0005125	Cytokine activity	9.08E-05	4.99E-02	*Cxcl3, Areg, Il1b, Il1a, Cxcl9, Osm, Cxcl2, Lif, Cxcl5, Bmp8b, Timp1, Il33, Grem1, Il1f9, Ccl3, Ccl4, Cxcl16, Cxcl14, Ccl7, Ccl8, Ccl5, Ifng, Thpo, Pglyrp1, Inhba, Spp1, Tnf, Ppbp*
GO:0042379	Chemokine receptor binding	3.18E-04	5.83E-02	*Cxcl3, Defb6, S100a14, Ccl28, Cxcl9, Cxcl2, Cxcl5, Ccl3, Ccl4, Cxcl16, Cxcl14, Ccrl2, Ccl7, Ccl8, Ccl5, Ppbp*
Cellular Component				
GO:0005615	Extracellular space	1.79E-06	3.28E-04	*Emilin2, Fas, Ces2g, Areg, 1100001G20Rik, Arg1, Capg, Hbb, Apod, Retnlb, Cxcl14, Cxcl16, F10, Chrd, Fabp5, Dmkn, F3, Chi3l1, Anxa2, Col12a1, Klk8, Col17a1, Icam1, Nos2, Il33, Ltbp2, Grem1, Csta, Ltf, Serpina3j, Adm, Ctsk, Ifng, Mfap4, C1qtnf3, Reg3b, S100a8, S100a9, Igfbp3, Inhba, Serpine1, Plat, Igfbp2, Spp1, Igf1, Lgi2, Ppbp, Msln, Sulf1, Cxcl3, Serpinb3a, Serpina10, Pla1a, Il1b, Il1a, Cxcl9, Osm, Serpine2, Lif, Pi15, Serpinb11, Timp1, Mmp13, Cdsn, Krtdap, Tinagl1, Fst, Mmp12, Saa3, Serpinb8, Bmper, Tac1, Itgam, Il18bp, Tnfrsf9, Bglap3, Pglyrp1, Mmp3, Mmp7, Lrg1, Mmp8, Mmp9, Anxa1, Psapl1, Lox, Reg3g, Tnf, Tnfrsf11b, Retnlg, Lbp, Lamc2, Olfm4, Cpxm1, Cxcl2, Cxcl5, Adamtsl4, Bmp8b, Cfh, Ces2f, Ccl3, Il1f9, Ccl4, Chit1, Ctgf, Ccl7, Ccl8, Klk13, Ccl5, Hp, Defb6, Sfrp1, Lgals7, C2, Thpo, Tacstd2, Sfrp4, Sema7a, Hilpda, Selp, Nucb2, Lcn2*
GO:0005576	Extracellular region	5.29E-06	7.72E-04	*Dsc3, Cxcl3, Tmprss11a, Serpina10, 1100001G20Rik, Il1b, Sbsn, Il1a, Osm, Serpine2, Tmprss11g, Pi15, Ceacam10, Mmp13, Lipk, Krtdap, Mmp10, Mmp12, Fst, Saa3, Bmper, Tac1, Spink5, F10, Prss27, Lipm, Wfdc18, Bglap3, Glb1l2, Pla2g2e, Mmp7, Mmp8, Mmp9, Psapl1, Dmkn, Reg3g, Nlrp3, Chi3l1, Tnf, Chi3l3, Tnfrsf11b, Retnlg, Klk8, Col17a1, Rptn, Olfm4, Cxcl2, Cxcl5, Prss12, Tmprss11bnl, Ltbp2, Cfh, Il1f9, Ccl3, Ltf, Ccl4, Adm, Tmprss11d, Olr1, Hp, Ifng, Defb6, Lgals7, Reg3b, S100a8, S100a9, Il1r2, Hilpda, Spp1, Igfbp2, Lgi2, Lcn2*
GO:0030141	Secretory granule	3.38E-04	2.24E-02	*Krtdap, Reg3g, Reg3b, Olfm4*

GO – gene ontology. *Enriched in clusterProfiler R package

Downregulation in markers of IBD including *Nlrp3, Nos2, Lcn2, Tnf and Il1b,* as well as the neuroinflammatory marker *Tac1,* were also observed under the GO terms *extracellular region* and *extracellular space* suggesting that pro-inflammatory paracrine secretion was inhibited by BM-MSC treatments (**Figure 3.8C**).

3.6.4. Anti-inflammatory pathways and gene expression after BM-MSC treatments in chronic colitis

Enrichment analysis of KEGG pathways was performed on DEGs to identify the potential mechanisms of action of BM-MSCs in colonic inflammation (**Appendix A, Tables S3-6**). Enriched pathways were associated with inflammation in downregulated DEGs between BM-MSC and sham-treated *Winnie* mice and included: *cytokine-cytokine receptor interaction, tumour necrosis factor (TNF) signalling pathway, hematopoietic cell lineage, complement and coagulation cascades, inflammatory bowel disease, toll-like receptor signalling pathway, Jak-STAT signalling pathway, chemokine signalling pathway and natural killer cell mediated cytotoxicity* (**Figure 3.9A, Table 3.2**). In contrast, all identified inflammation-associated pathways were also enriched in upregulated DEGs between *Winnie*-sham and C57BL/6 mice (**Figure 3.9A**). All DEGs downregulated by BM-MSC treatments in *Winnie* mice belonging to the *inflammatory bowel disease* pathway, including *Tnf, Il1b, Il4ra, Il1a, Ifng, Lif, Nod2, Il18rap* and *Tlr2*, were linked to other enriched inflammatory pathways (**Figure 3.9B**). The most frequently identified genes in inflammatory pathways were *Tnf, Il1b, Il4ra, Ccl5, Il1a, Ifng, Lif, Il2ra, Csf3r, Thpo, Ccl3, Cxcl9* and *Ccl4* which were associated with three or more of these pathways (**Figure 3.9B**). These data support the potent immunomodulatory properties of BM-MSCs through regulation of multiple pathways associated with inflammation. The fold regulation for all DEGs after BM-MSC treatment in these inflammation-associated KEGG pathways were compiled and compared to their fold regulation in *Winnie* mice and IBD patients to their respective uninflamed controls (**Figure 3.10, Table 3.3**). Treatment with BM-MSCs downregulated the expression of 72 genes in *Winnie* mice that were associated with these KEGG pathways.

Figure 3.9 ***Effects of BM-MSCs on Kyoto Encyclopedia of Genes and Genome (KEGG) pathways associated with colonic inflammation***

A) Enrichment scores for KEGG pathways associated with colonic inflammation determined by *DAVID* functional analysis of upregulated differentially expressed genes identified using RNA-Seq between *Winnie* mice vs C57BL/6 mice (black bars) and in downregulated differentially expressed genes between *Winnie* mice treated with BM-MSCs vs sham-treated *Winnie* mice (blue bars). Differentially expressed genes used for the KEGG enrichment analysis had a cut off between ±0.5 LogFC and enriched KEGG terms had a *P* value of <0.05. **B)** Binary matrix of differentially expressed genes (green) associated with greatest number of KEGG pathways identified in genes downregulated by BM-MSC treatment in *Winnie* mice.

A

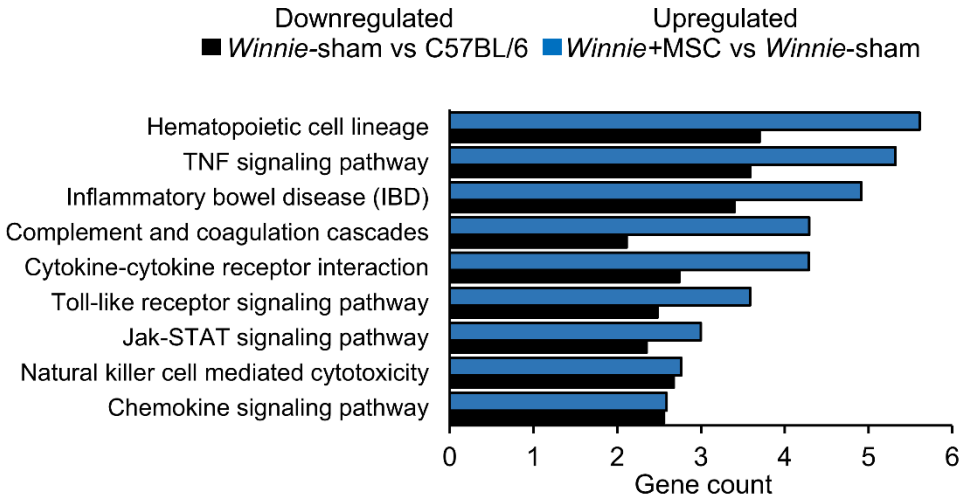
Downregulated
Upregulated
Winnie-sham vs C57BL/6
Winnie+MSC vs Winnie-sham
Hematopoietic cell lineage
TNF signaling pathway
Inflammatory bowel disease (IBD)
Complement and coagulation cascades
Cytokine-cytokine receptor interaction
Toll-like receptor signaling pathway
Jak-STAT signaling pathway
Natural killer cell mediated cytotoxicity
Chemokine signaling pathway
0
1
2
3
4
5
6
Gene count

B

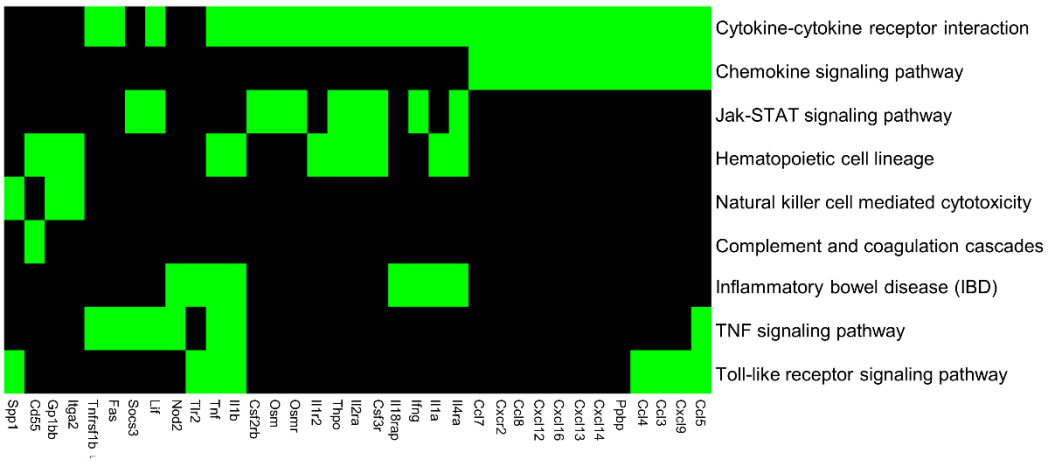
Cytokine-cytokine receptor interaction
Chemokine signaling pathway
Jak-STAT signaling pathway
Hematopoietic cell lineage
Natural killer cell mediated cytotoxicity
Complement and coagulation cascades
Inflammatory bowel disease (IBD)
TNF signaling pathway
Toll-like receptor signaling pathway
Spp1
Cd55
Gp1bb
Itga2
Tnfrsf1b
Fas
Socs3
Lif
Nod2
Tlr2
Tnf
Il1b
Csf2rb
Osm
Osmr
Il1r2
Thpo
Il2ra
Csf3r
Il18rap
Ifng
Il1a
Il4ra
Ccl7
Cxcr2
Ccl8
Cxcl12
Cxcl16
Cxcl13
Cxcl14
Ppbp
Ccl4
Ccl3
Cxcl9
Ccl5

Table 3.2 ***Selected enriched KEGG pathways identified in differentially expressed genes downregulated in Winnie mice treated with BM-MSCs compared to sham-treated Winnie mice***

KEGG Term	Description	Fold Enrichment	Count	*P* Value	Benjamini FDR	Genes
mmu04060	Cytokine-cytokine receptor interaction	4.29	29	9.68E-11	2.10E-08	*Il1r2, Ccl3, Tnf, Osmr, Tnfrsf12a, Il4ra, Cxcl9, Ccl8, Cxcr2, Ccl5, Ccl4, Ccl7, Lif, Tnfrsf1b, Tnfrsf11b, Ifng, Il1b, Csf3r, Csf2rb, Fas, Il1a, Thpo, Il18rap, Il2ra, Osm, Tnfrsf9, Ppbp, Cxcl14, Cxcl16*
mmu04668	TNF signalling pathway	5.32	16	2.41E-07	2.61E-05	*Icam1, Tnf, Cebpb, Socs3, Mmp9, Cxcl3, Cxcl2, Ifi47, Ccl5, Mmp3, Lif, Nod2, Tnfrsf1b, Ripk3, Il1b, Fas*
mmu04640	Hematopoietic cell lineage	5.61	13	2.67E-06	1.93E-04	*Il1r2, Tnf, Il2ra, Il4ra, Itga2, Itgam, Cd55, Gp1bb, Cd33, Il1b, Csf3r, Il1a, Thpo*
mmu04610	Complement and coagulation cascades	4.29	9	1.07E-03	2.31E-02	*Plat, Cd55, F10, F13a1, F3, Serpine1, Cfh, C2, Plaur*
mmu05321	Inflammatory bowel disease (IBD)	4.91	8	1.08E-03	2.11E-02	*Nod2, Tnf, Il18rap, Ifng, Il4ra, Tlr2, Il1b, Il1a*
mmu04620	Toll-like receptor signalling pathway	3.59	10	1.76E-03	2.69E-02	*Ctsk, Ccl3, Tnf, Cxcl9, Tlr2, Il1b, Lbp, Ccl5, Ccl4, Spp1*
mmu04630	Jak-STAT signalling pathway	3.00	12	2.09E-03	2.79E-02	*Osm, Lif, Il2ra, Osmr, Socs3, Socs1, Ifng, Il4ra, Pim1, Csf2rb, Csf3r, Thpo*
mmu04062	Chemokine signalling pathway	2.59	14	2.86E-03	3.39E-02	*Ccl3, Cxcl14, Cxcl5, Ppbp, Adcy8, Cxcl3, Cxcl16, Cxcl2, Cxcl9, Ccl8, Cxcr2, Ccl5, Ccl4, Ccl7*
mmu04512	ECM-receptor interaction	3.29	8	1.03E-02	9.33E-02	*Cd47, Lama3, Gp1bb, Itgav, Itgb6, Itga2, Lamc2, Spp1*
mmu04066	HIF-1 signalling pathway	2.79	8	2.40E-02	1.66E-01	*Pfkfb3, Hk3, Serpine1, Ifng, Hk2, Igf1, Nos2, Timp1*
mmu04650	Natural killer cell mediated cytotoxicity	2.76	8	2.51E-02	1.68E-01	*Icam1, Tnf, Rac3, Ifng, Zap70, Fcgr4, Fcer1g, Fas*

mmu04514	Cell adhesion molecules (CAMs)	2.24	10	3.41E-02	2.04E-01	*Icam1, Selp, Cldn4, Itgav, Cd274, Cldn1, Cdh3, Cd6, H2-Q7, Itgam*

Figure 3.10 ***Changes in the expression of inflammation-associated genes in the colon***

Heat map representation of the fold regulation of genes determined by RNA-Seq in enriched KEGG pathways associated with colonic inflammation identified by *DAVID* functional analysis of downregulated differentially expressed genes between *Winnie* mice treated with BM-MSCs vs sham-treated *Winnie* mice. Fold regulation was determined between *Winnie* and C57BL/6 mice, *Winnie* mice treated with BM-MSCs and sham-treated *Winnie* mice, males and female patients with ulcerative colitis, as well as, male and female patients with Crohn's disease compared to the colon of uninflamed sex-matched controls (left to right columns). Upregulated genes and downregulated genes were visualised as red and green gradients up to >10 fold and <-5 fold, respectively. Genes failing the initial cut off between ±0.5logFC are represented as black (no change).

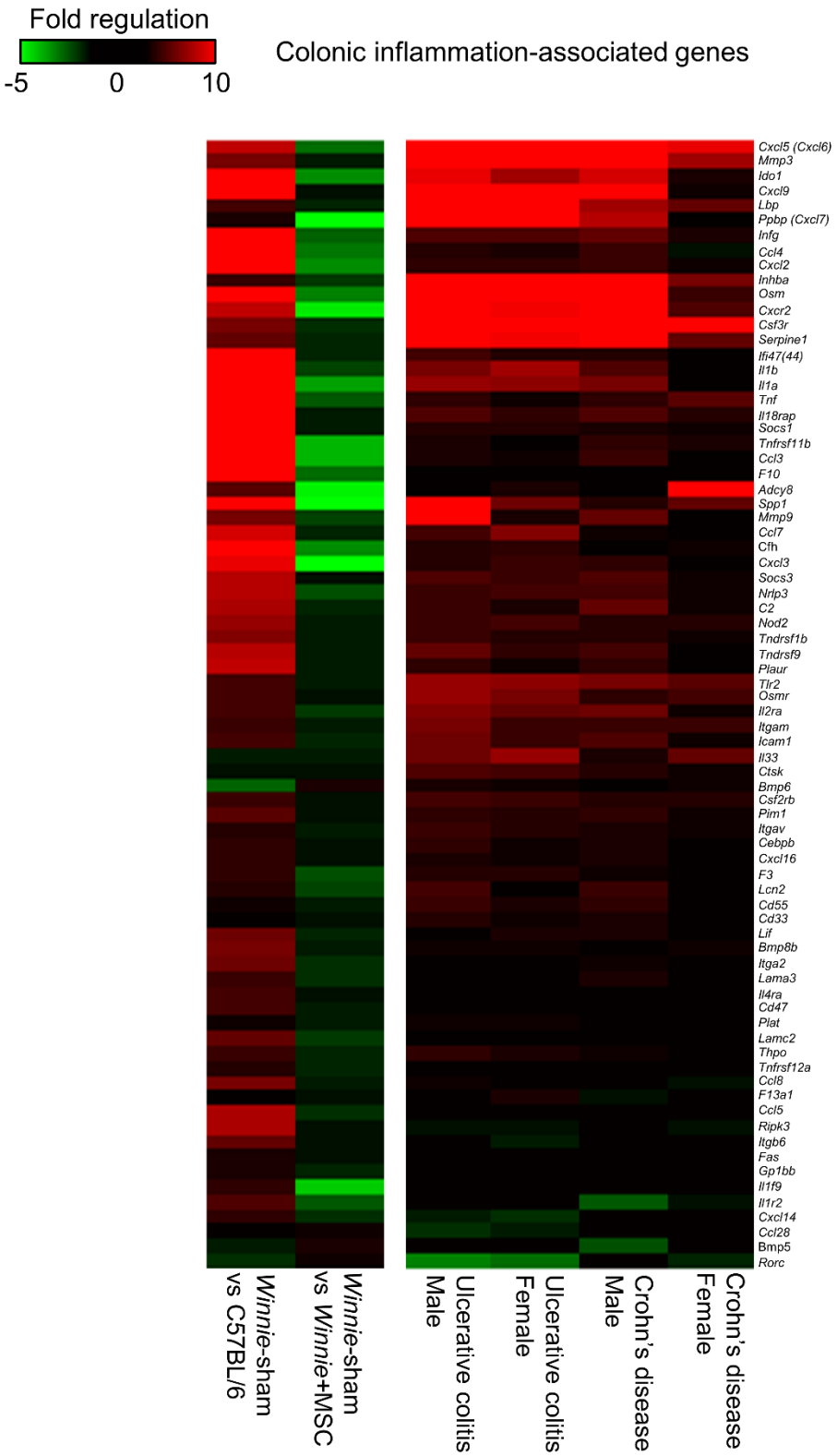
Fold regulation
-5
0
10
Colonic inflammation-associated genes
Cxcl5 (Cxcl6)
Mmp3
Ido1
Cxcl9
Lbp
Ppbp (Cxcl7)
Infg
Ccl4
Cxcl2
Inhba
Osm
Cxcr2
Csf3r
Serpine1
Ifi47(44)
Il1b
Il1a
Tnf
Il18rap
Socs1
Tnfrsf11b
Ccl3
F10
Adcy8
Spp1
Mmp9
Ccl7
Cfh
Cxcl3
Socs3
Nrlp3
C2
Nod2
Tndrsf1b
Tndrsf9
Plaur
Tlr2
Osmr
Il2ra
Itgam
Icam1
Il33
Ctsk
Bmp6
Csf2rb
Pim1
Itgav
Cebpb
Cxcl16
F3
Lcn2
Cd55
Cd33
Lif
Bmp8b
Itga2
Lama3
Il4ra
Cd47
Plat
Lamc2
Thpo
Tnfrsf12a
Ccl8
F13a1
Ccl5
Ripk3
Itgb6
Fas
Gp1bb
Il1f9
Il1r2
Cxcl14
Ccl28
Bmp5
Rorc
Winnie-sham vs C57BL/6
Winnie-sham vs Winnie+MSC
Ulcerative colitis Male
Ulcerative colitis Female
Crohn's disease Male
Crohn's disease Female

Table 3.3 ***Fold regulation of genes associated with MSC-mediated immunomodulation identified in KEGG pathways***

Gene	*Winnie* MSC vs *Winnie*-sham	*Winnie*-sham vs C57BL/6	UC male vs control male	UC female vs control female	CD male vs control male	CD female vs control female
Ppbp (Cxcl7)	-9.3	2.0	70.5	28.3	7.5	1.4
Cxcl3	-5.4	9.1	2.4	2.9	2.6	1.4
Spp1	-5.0	10.5	13.3	4.7	2.3	4.5
Adcy8	-4.8	4.3	0.0	1.8	0.0	20.7
Cxcr2	-4.7	7.8	30.3	9.3	10.1	3.9
Il1f9	-4.2	2.6	0.0	0.0	0.0	0.0
Tnfrsf11b	-3.9	12.1	1.8	1.1	2.5	1.8
Ccl3	-3.9	13.8	1.9	1.5	2.9	-1.3
Il1a	-3.5	15.9	6.4	5.8	5.2	1.3
Cxcl2	-3.4	54.8	2.7	2.8	3.2	1.4
Ido1	-3.3	267.4	9.1	6.4	8.4	2.0
Cfh	-3.2	10.1	2.3	2.7	1.2	1.7
Osm	-3.1	17.1	23.3	11.1	12.7	3.1
Ccl4	-2.9	87.0	2.3	2.1	2.9	-1.5
Cxcl5 (Cxcl6)	-2.9	7.8	245.4	59.0	50.3	9.1
F10	-2.8	14.4	-1.2	-1.2	-1.4	-1.4
Ifng	-2.7	107.0	3.6	3.9	4.3	1.9
Il1r2	-2.5	3.7	-1.1	-1.1	-2.5	-1.5
Tnf	-2.5	19.5	2.7	1.6	2.7	4.2
Nlrp3	-2.3	7.1	2.9	3.3	3.5	1.6
F3	-2.3	2.8	2.2	2.2	1.7	1.2
Lcn2	-2.3	2.5	3.5	1.2	3.2	1.2
Il1b	-2.3	21.4	5.0	6.5	3.8	1.3
Mmp9	-2.2	5.2	16.0	2.0	4.6	1.4
Inhba	-2.1	3.1	44.3	13.0	39.5	5.3
Il2ra	-2.1	3.5	5.5	4.6	4.8	1.8
Lamc2	-2.0	4.5	1.0	1.2	1.4	-1.2
Ccl5	-2.0	6.9	-1.1	1.1	1.1	-1.4
Itga2	-1.9	4.9	1.1	1.1	1.5	1.4
Csf3r	-1.9	5.3	24.9	10.1	11.8	10.6
Cxcl14	-1.9	2.8	-1.6	-1.9	-1.2	-1.3
Lama3	-1.9	2.9	1.3	1.2	1.8	1.2
Lbp	-1.8	3.5	109.2	60.4	6.8	4.6
Thpo	-1.8	2.9	2.7	1.8	1.6	-1.2
Lif	-1.8	4.6	1.1	2.0	1.8	1.2
Tnfrsf12a	-1.8	2.4	1.3	1.2	1.1	-1.0
Ccl7	-1.8	8.3	3.3	5.5	1.6	1.0
Gp1bb	-1.8	1.9	0.0	0.0	0.0	0.0
Ifi47/44	-1.8	31.5	3.3	2.3	2.3	1.2
C2	-1.7	6.9	3.0	2.1	4.3	1.6
Icam1	-1.7	3.2	4.9	3.2	3.8	1.6
Serpine1	-1.7	4.5	22.7	9.4	10.0	4.3
Tnfrsf9	-1.7	7.4	4.3	2.8	3.4	-1.2
Tnfrsf1b	-1.7	5.7	2.9	2.3	2.4	1.5
Plat	-1.7	1.7	1.5	1.5	1.2	1.2
Il18rap	-1.7	12.6	3.8	2.8	3.6	2.4
Cd47	-1.7	3.3	1.0	1.1	1.0	1.0
Tlr2	-1.7	3.6	6.3	5.9	5.1	4.1
Il33	-1.7	-1.7	4.7	6.3	2.1	4.3
Plaur	-1.7	7.8	2.6	1.5	2.8	-1.3
Bmp8b	-1.6	5.1	1.6	1.5	1.0	1.4
Mmp3	-1.6	5.0	270.6	34.9	49.4	6.7
Itgam	-1.6	2.9	5.1	3.0	3.0	2.9
Nod2	-1.6	6.1	3.1	3.4	2.2	2.2
Cd55	-1.6	1.5	3.2	1.8	2.6	1.4
Socs1	-1.6	15.7	2.3	2.4	2.1	1.5
Ccl8	-1.6	5.3	1.7	1.2	-1.4	-1.5
Itgav	-1.6	2.3	2.9	2.2	1.8	1.6
F13a1	-1.6	0.7	1.3	2.1	-1.4	-1.0
Cebpb	-1.5	2.8	2.6	1.7	1.9	1.0
Osmr	-1.5	3.5	6.1	5.1	2.8	3.3
Fas	-1.5	2.0	-1.2	1.3	1.1	0.8
Cd33	-1.5	1.2	2.3	1.6	2.0	1.1

Pim1	-1.5	4.2	2.7	2.4	2.5	1.7
Ctsk	-1.5	-1.5	3.7	3.4	2.4	1.6
Ripk3	-1.5	7.1	-1.5	-1.5	-1.2	-1.5
Cxcl9	-1.5	169.8	15.0	11.8	16.4	1.5
Cxcl16	-1.5	2.8	1.9	1.5	1.9	1.1
Itgb6	-1.5	4.4	-1.4	-1.7	1.4	1.1
Csf2rb	-1.5	3.0	3.3	3.0	2.1	2.3
Il4ra	-1.5	3.4	1.4	1.1	1.3	1.1
Socs3	-1.4	7.3	3.8	3.0	3.6	1.7
Ccl28	1.4	-1.1	-1.9	-1.7	-1.2	-1.3
Rorc	1.6	-1.9	-3.2	-2.8	-1.4	-1.8
Bmp5	1.9	-1.6	-1.4	-1.3	-2.3	-1.1
Bmp6	2.0	-2.8	1.9	1.7	1.2	1.4

UC - Ulcerative colitis, CD – Crohn’s disease.

BM-MSC treatments also upregulated the expression of 4 genes associated with these pathways, including *Bmp5* and *Bmp6,* which have been negatively associated with inflammation (Bramlage et al., 2006, Varas et al., 2015), as well as, *Ccl28* and *Rorc,* which were downregulated in UC. The top 20 genes downregulated by BM-MSCs contained key markers of IBD including *Il1a, Ido1, Ifng, Tnf,* and *Nlrp3,* in addition to genes involved in chemotaxis and extravasation, including *Ppbp (Cxcl7), Cxcl3, Spp1, Adcy8, Cxcr2, Ccl3, Cxcl2, Osm, Ccl4* and *Cxcl5(Cxcl6)*; all of which were upregulated in both *Winnie* mice and IBD patients.

Genes previously associated with the anti-inflammatory activity of MSCs in animal models of chemically-induced colitis were identified by analysis of 81 studies in the literature (**Chapter 1, Table 1.3**). Changes in these genes were assessed in *Winnie* mice treated with BM-MSCs and baseline changes were determined in *Winnie* mice and IBD patients compared to their uninflamed controls (**Figure 3.11, Table 3.4**). Similar to the reported effects of MSCs in chemically-induced colitis, BM-MSC treatments in *Winnie* mice downregulated the expression of *Il6, Ifng, Il1b, Il1a, Tnf, Cxcl2, Tbx21* and *Itgam*, which were upregulated in *Winnie* mice and IBD patients. Furthermore, BM-MSC treatments downregulated *Nos2, Arg1, Gata3, Mrc1* and *Hmox1* which were again upregulated in *Winnie* mice and IBD patients; in contrast these genes were upregulated by MSCs in chemical models of colitis. The genes *Foxp3* and *Il21* were upregulated in IBD patients and *Winnie* mice; however, these genes were further upregulated by BM-MSC treatment in *Winnie* mice. In chemically-induced colitis MSCs also increased *Foxp3*, however, *Il21* was decreased. Contrarily, BM-MSC treatments in *Winnie* mice increased *Rorc* which was decreased in chemically-induced colitis. Nonetheless, *Rorc* was downregulated in both *Winnie* mice and IBD patients which may suggest that BM-MSCs corrected its expression in chronic colitis. In addition, *Winnie* mice administered with BM-MSCs exhibited a decrease in *Alox15* and *Ccl5,* as well as, *Retnlb, Chi3l3,* and *Arg2* which are reportedly upregulated by MSCs in models of chemically-induced colitis; however, these genes had dissimilar regulation between *Winnie* mice and IBD patients compared to their inflamed controls and therefore highlights some of the divergence between murine colitis and colitis in human IBD.

Figure 3.11 ***Changes in the expression of genes associated with MSC activity in colitis***

Genes associated with MSC functions in models of colitis were determined by analysis of 81 studies in the literature. Heat map representation of the fold regulation of genes associated with BM-MSC function determined by RNA-Seq. Fold regulation was determined between *Winnie* and C57BL/6 mice, *Winnie* mice treated with BM-MSCs and sham-treated *Winnie* mice, males and female patients with ulcerative colitis, as well as, male and female patients with Crohn's disease compared to the colon of uninflamed sex-matched controls (left to right columns). Upregulated genes and downregulated genes were visualised as red and green gradients up to >10 fold and <-5 fold, respectively. Genes failing the initial cut off between ±0.5logFC are represented as black (no change).

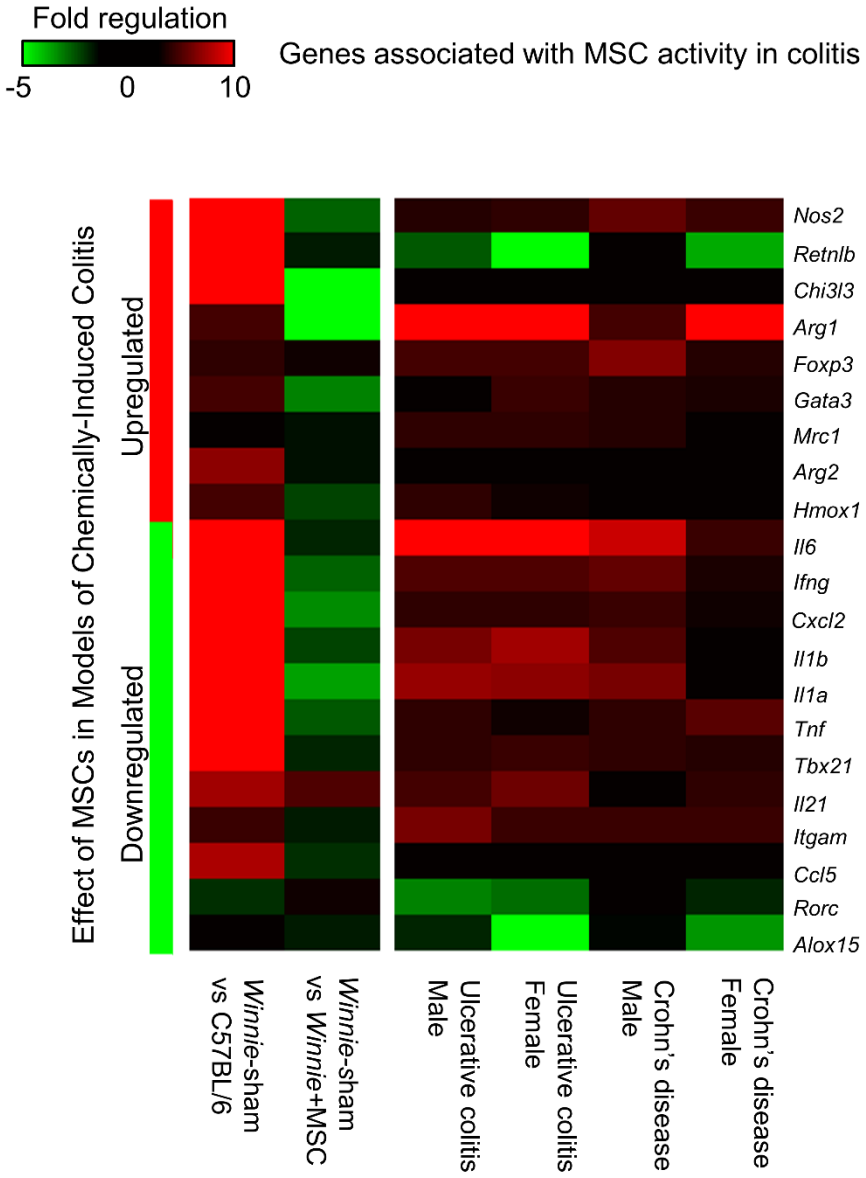
Fold regulation
-5
0
10
Genes associated with MSC activity in colitis
Effect of MSCs in Models of Chemically-Induced Colitis
Upregulated
Downregulated
Nos2
Retnlb
Chi3l3
Arg1
Foxp3
Gata3
Mrc1
Arg2
Hmox1
Il6
Ifng
Cxcl2
Il1b
Il1a
Tnf
Tbx21
Il21
Itgam
Ccl5
Rorc
Alox15
Winnie-sham vs C57BL/6
Winnie-sham vs Winnie+MSC
Ulcerative colitis Male
Ulcerative colitis Female
Crohn's disease Male
Crohn's disease Female

Table 3.4 ***Fold regulation of genes associated with BM-MSC-mediated immunomodulation of chemically-induced colitis***

Factor	Effect of MSCs In chemical colitis	*Winnie* MSC vs *Winnie*-sham	*Winnie*-sham vs C57BL/6	UC male vs control male	UC female vs control female	CD male vs control male	CD female vs control female
Il21	-	3.73	6.69	3.47	4.75	1.38	2.75
Rorc	-	1.58	-1.90	-3.17	-2.78	-1.36	-1.82
Itgam	-	**-1.62**	2.87	5.06	3.04	2.99	2.89
Alox15	-	**-1.70**	-1.05	-1.82	-5.62	-1.41	-3.49
Tbx21	-	**-1.74**	18.39	2.54	3.09	2.59	2.14
Il6	-	**-1.79**	102.56	14.93	18.69	7.92	3.18
Ccl5	-	**-1.95**	6.91	-1.10	1.14	1.08	-1.38
Il1b	-	**-2.29**	21.38	5.04	6.48	3.79	1.28
Tnf	-	**-2.46**	19.47	2.73	1.61	2.73	4.15
Ifng	-	**-2.68**	107.02	3.60	3.86	4.31	1.90
Il1a	-	**-3.54**	15.85	6.38	5.82	5.19	1.33
Foxp3	+	**1.48**	2.53	3.49	3.35	5.48	2.27
Arg2	+	-1.48	5.89	1.37	1.27	1.04	-1.05
Retnlb	+	-1.69	62.86	-2.50	-7.24	-1.03	-3.67
Hmox1	+	-2.27	3.22	2.64	1.58	-1.11	-1.02
Nos2	+	-2.66	103.90	2.18	2.82	4.58	3.08
Gata3	+	-3.17	3.34	1.36	3.11	2.25	2.00
Cxcl2	+	-3.35	54.82	2.67	2.83	3.17	1.42
Chi3l3	+	-7.16	32.70	0.00	0.00	0.00	0.00
Arg1	+	-7.59	3.46	11.65	9.67	3.39	10.06

UC - Ulcerative colitis, CD – Crohn's disease, (-) – downregulated by MSC treatments in chemically-induced colitis, (+) – upregulated by MSC treatments in chemically-induced colitis. Fold regulation values for genes sharing expression patterns in BM-MSC-treated *Winnie* mice and MSC-treated chemical colitis in bold.

The concordance of gene expression in *Winnie* mice and human IBD for genes that were altered by BM-MSC treatments in *Winnie* mice was evaluated. Genes associated with the anti-inflammatory activity of BM-MSCs in colitis were determined by enriched KEGG pathways in this study, and genes identified as modulating the anti-inflammatory activity of MSCs from the literature. In total, the expression patterns of 85 genes were changed between BM-MSC and sham-treated *Winnie* mice which was associated with their anti-inflammatory activity. The expression pattern of these genes was evaluated between *Winnie* mice and IBD patients compared to their respective uninflamed controls (**Figure 3.12**). Compared to *Winnie* mice, 76.5% of genes had similar expression in IBD patients with 65 genes showing similarity in males or females with either UC and CD. Of these genes, males and females with UC (90.7%, for both) and males with CD (87.7%) shared similar concordance in expression patterns with *Winnie* mice, as opposed to females with CD (63.1%) which were the least similar to *Winnie* mice.

3.7. Discussion

In this study, it was demonstrated that BM-MSCs can attenuate chronic colonic inflammation and the expression of various novel inflammatory genes in the *Winnie* mouse model of spontaneous chronic colitis. Treatment with BM-MSCs reduced disease activity demonstrated by improved stool consistency, decreased colon weight, reduced histopathology of colitis and improved gross morphological architecture of the colon. BM-MSC treatments reduced the infiltration of leukocytes into the distal colon observed through histological and immunohistochemical analysis. The number of $FOXP3^{+}$ leukocytes was unchanged by BM-MSC treatments; however, their proportion was increased due to a reduction in the total number of leukocytes. Analysis of the transcriptome revealed that BM-MSCs downregulated genes associated with inflammatory processes and pathways that were previously unrecognised to be associated with the immunomodulatory activity of MSCs in chemically-induced colitis. Many genes that were associated with MSC treatments in chemically-induced colitis were also altered by BM-MSC treatments in *Winnie* mice.

Figure 3.12 ***Homology of genes in Winnie mice and IBD patients in colonic inflammation-associated genes altered by BM-MSC treatments***

Heat map representation of upregulated (red) and downregulated (green) genes associated with colonic inflammation determined by RNA-Seq. Target genes of BM-MSC therapy in the *Winnie* mouse model of spontaneous colitis were identified. The homology in expression of these genes was determined in *Winnie* mice and IBD patients compared to their respective uninflamed controls. Genes failing the initial cut off between ±0.5logFC are represented as black (no change).


Regulation
Down
Up
Concordance of expression with Winnie mice
91%
91%
88%
63%
Rorc
Cxcl9
Ido1
Ifng
Cxcl2
Tnf
Osm
Socs1
Il18rap
Spp1
Cxcr2
Cxcl5(Cxcl6)
Socs3
Nlrp3
C2
Nod2
Tnfrsf1b
Csf3r
Mmp3
Serpine1
Pim1
Tlr2
Il2ra
Osmr
Lbp
Icam1
Inhba
Csf2rb
Itgam
Itgav
Foxp3
Tbx21
Il6
Nos2
Arg1
Ifi47/44
Ccl4
Il1b
Il1a
Ccl3
Cxcl3
Ccl7
Plaur
Tnfrsf9
Mmp9
Thpo
F3
Cebpb
Cxcl16
Ppbp(Cxcl7)
Cd55
Gata3
Lif
Tnfrsf11b
Lcn2
Bmp5
Lama3
Itga2
Bmp8b
Cfh
Il21
Adcy8
Hmox1
Plat
Ccl8
Ulcerative colitis Male
Ulcerative colitis Female
Crohn's disease Male
Crohn's disease Female

However, several differences were observed suggesting that BM-MSCs act through alternative mechanisms in chronic inflammation. The expression of inflammation-associated genes shared high concordance in *Winnie* mice and IBD patients, particularly those with UC. This demonstrates that *Winnie* mice offer a reliable model of IBD appropriate for testing MSC therapy. Furthermore, the efficacy of BM-MSC treatments and mechanisms of action identified in the *Winnie* model may be translated to human patients more accurately than those in other models.

MSCs can be sourced from a range of different tissues and their application into animal models is either xenogeneic (human to animal), allogeneic (same species) or syngeneic (minor genetic variation). In our study, xenogeneic human MSCs derived from the bone marrow were used for the treatment of murine chronic colitis. Previously, we observed similar results in the guinea-pig model of TNBS-induced colitis using xenogeneic human MSCs and allogeneic guinea-pig MSCs (Stavely et al., 2015a, Stavely et al., 2015b). Furthermore, BM-MSCs has stronger therapeutic potential compared to those derived from adipose tissue as demonstrated in a model of TNBS-induced colitis (Stavely et al., 2015a, Stavely et al., 2015b). Studies in other models appear to be in consensus with these finding by demonstrating enhanced efficacy of BM-MSCs against leukocyte activation, recruitment and inflammation (Zhu et al., 2012, Antunes et al., 2014a, Antunes et al., 2014b, Elman et al., 2014). In addition, MSCs are typically applied intravenously or by intraperitoneal injection in studies of experimental colitis. Subsequently, MSCs become sequestered in various organs throughout the body including the lung, liver and spleen; the long-term effects of erroneous MSC homing are not yet fully understood (Scarfe et al., 2018). In our study, MSC administration was performed by enema. Previously, our lab has demonstrated an efficacy of MSCs administered by enema for treating experimental colitis in the guinea-pig model of TNBS-induced colitis (Robinson et al., 2014, Stavely et al., 2015a, Stavely et al., 2015b, Robinson et al., 2017b). Other labs have achieved similar results in rats or mice by administering MSCs or their conditioned medium by enema in TNBS-induced colitis (Watanabe et al., 2013, Cury et al., 2016, Wang et al., 2016, Miyamoto et al., 2017). Furthermore, Wang et al. (2016) demonstrated in a mouse model of DSS-

induced colitis that MSCs delivered by enema are not erroneously entrapped in tissues other than the colon compared to those administered intraperitoneally and intravenously. Additionally, MSCs administered by enema are more effective than those administered through the other routes in the *Winnie* model (Robinson, Stavely & Nurgali, unpublished), thus MSCs injected intra-luminally may provide a more targeted therapeutic approach for the treatment of colitis.

The therapeutic application of MSCs in experimental chemically-induced colitis has been extensively investigated; similar to our study, predominantly positive outcomes have been achieved in reducing the severity of colitis. In these studies, MSCs attenuated rectal bleeding, inflammation-induced loss of body weight, improved stool consistency and reduced histopathological severity of colitis after DSS or TNBS exposure in rats and mice (Tanaka et al., 2008, Gonzalez-Rey et al., 2009, Zuo et al., 2013, Xie et al., 2017) (**Chapter 1, Table 1.2**). In the *Winnie* model of spontaneous chronic colitis, BM-MSCs alleviated these manifestations of colitis apart from a slight loss of body weight observed in both treated and untreated *Winnie* mice. In addition, BM-MSCs reduced the weight of the colon which was initially increased in *Winnie* mice, however no differences in colon length were observed between *Winnie* mice and controls. This is consistent with studies in TNBS-induced colitis as opposed to DSS-induced colitis where colon shortening is prominent (Motavallian-Naeini et al., 2012, Chassaing et al., 2014).

The immunomodulatory capabilities of MSCs are well established and it has been shown in models of inflammation that MSCs can attenuate leukocyte infiltrate into inflamed tissues (Roemeling-van Rhijn et al., 2013, Thin Luu et al., 2013, Antunes et al., 2014b, Kay et al., 2017). In models of chemically-induced colitis, MSCs have been demonstrated to supress leukocyte infiltration as indicated by decreased leukocyte counts in the mucosa and submucosa and reduced myeloperoxidase activity (Ando et al., 2008, Zhang et al., 2009b, Liang et al., 2011, Stavely et al., 2015a). In our study the number of leukocytes recruited to the distal colon was reduced to near control levels by BM-MSC treatment. Analysis of the transcriptome validated that the reduction in leukocyte numbers translated to a decrease in

inflammatory biomarkers associated with IBD including *Nlrp3, Ido1, Nos2, Lcn2, Il1b, Tnf* and a reduction in a plethora of pro-inflammatory cytokines and chemokines. Many GO terms associated with inflammation were enriched in genes downregulated by BM-MSC treatments. This included genes associated with cytokine/chemokine signalling and the extracellular space confirming that the paracrine signalling milieu that drives inflammation in colitis was downregulated by BM-MSC treatments. In addition, there was considerable overlap between genes associated with the immune/inflammatory response and leukocyte migration, which on the molecular level supports our observations of reduced colitis disease activity and leukocyte numbers after MSC treatment. Furthermore, many of these genes were associated with a response to external biotic stimulus which is the most widely accepted aetiology of the chronic inflammatory pathology of IBD (Matsuoka and Kanai, 2015). It was previously demonstrated that *Winnie* mice exhibit alterations to the microbiome that parallel those observed in human IBD patients (Robinson et al., 2016), this indicates that the inflammation associated with biotic stimuli may reflect the human pathology and highlights the value of using *Winnie* mice as pre-clinical model to study therapeutic interventions including MSC therapy.

In addition to GO terms associated with inflammation, terms related to epithelial cell differentiation and neuronal death have been identified. Furthermore, an overlap between inflammatory processes and these terms was observed in many genes downregulated by MSC treatments. This highlights the interplay between these cell types and immune cells as both the epithelium and nervous system play important non-canonical roles in the immune response, particularly in the intestinal tract. Alterations to the intrinsic enteric nervous system are reported in IBD and animal models of colitis and may contribute to the progression and severity of the disease (Lomax et al., 2005, Lomax et al., 2007a, Nurgali et al., 2007, Nurgali, 2009, Nurgali et al., 2009, Lakhan and Kirchgessner, 2010, Nurgali et al., 2011, Bernardini et al., 2012). Furthermore, the extrinsic innervation of the intestinal tract can modulate the immune response through the cholinergic anti-inflammatory reflex (Tracey, 2002). In the presented study, BM-MSCs also downregulated *Tac1* which encodes the neuropeptides neurokinin A and substance P; the latter is

involved in neuroimmune interactions with high levels paralleling disease severity in UC and constitutively high levels present in CD (Tavano et al., 2012).

The GO term *secretory granule* of the cellular compartment was also identified in genes downregulated by BM-MSC treatments in *Winnie* mice. These genes included: *Spink5,* Regenerating islet-derived protein 3 (Reg3) family members *Reg3g* and *Reg3b,* tissue kallikreins *Klk10* and *Klk13*, *Olfm4* and *Krtdap.* All are expressed by epithelial cells and have roles in intestinal inflammation and IBD. The serine protease inhibitor Kazal-type (SPINK) family is associated with susceptibility loci to coeliac disease and *SPINK5* is downregulated in the intestinal mucosa of coeliac disease patients (Wapenaar et al., 2007). Intestinal tissue kallikreins (KLK) are predicted to have various functions in the pathophysiology of IBD as facilitators of inflammation and secretory diarrhoea through kinins and bradykinin receptors (Stadnicki, 2011). *OLFM4*, which regulates innate immunity against bacteria, is highly upregulated and secreted in the mucus of CD and UC patients (Gersemann et al., 2012). Gene variants in *KRTDAP* were recently identified in a paediatric IBD cohort (Shaw et al., 2018). Furthermore, murine Reg3 family members, *Reg3g* and *Reg3b,* have antimicrobial activity and are upregulated in colitis. They are thought to assist in the resolution of inflammation and promote epithelial proliferation via STAT3 in chemically-induced colitis (Ratsimandresey et al., 2016); the human gene *REG3A* is also highly upregulated in IBD (van Beelen Granlund et al., 2013). While models of chemically-induced colitis suggest that these genes may be involved in the mechanisms of the epithelial response associated with the resolution of colitis, their contribution to resolving chronic colitis in *Winnie* mice and IBD is questionable. In previous studies, MSC-mediated resolution of chemically-induced colitis was associated with increased epithelial proliferation and stem cell numbers in the crypts which was indicative of mucosal repair (Chen et al., 2013, Soontararak et al., 2018). Considering that hypertrophy of the mucosa is common in *Winnie* mice in our study and IBD (Beck and Podolsky, 1999, MacDonald et al., 2000), mechanisms to repair the mucosa appear to be already chronically active and are ineffective in resolving inflammation. Therefore, our observations of reduced hypertrophy of the mucosa in *Winnie* mice by BM-

MSC treatments may reflect their positive effects in chronic colitis, as opposed to MSCs increasing epithelial cell proliferation as reported in chemically-induced colitis. These data may indicate that BM-MSCs dampen the inflammatory response in the epithelium which may be due to their immunomodulatory activity. Furthermore, this may also explain why intra-luminal injection of BM-MSCs by enema is highly effective as many MSCs will interact with the epithelial cells of the mucosa through either direct contact or paracrine signalling (Wang et al., 2016). Albeit, it has been demonstrated that MSCs injected intra-luminally can engraft and migrate into the submucosa and muscle layers of the colon (Stavely et al., 2015b, Robinson et al., 2017b).

Analysis of KEGG pathways revealed the genes downregulated by BM-MSC treatments in *Winnie* mice were associated with *cytokine-cytokine receptor interaction, hematopoietic cell lineage, complement and coagulation cascades, toll-like receptor signalling pathway, Jak-STAT signalling pathway, chemokine signalling pathway* and *natural killer cell mediated cytotoxicity*. These pathways were all associated with genes upregulated in *Winnie* mice in the presented study, and, previously, in patients with UC (Cardinale et al., 2014). Notably, genes downregulated by BM-MSCs were also associated with the *TNF signalling pathway*, which is a major target for biologic therapy currently in the clinic for the treatment of IBD.

Concordance in gene expression between *Winnie* mice and human IBD were assessed in genes altered by BM-MSC treatment to determine the accuracy of the *Winnie* model of colitis to represent IBD-like inflammation. Furthermore, this may provide an indication of how reproducible findings from BM-MSC-treated *Winnie* mice may be in the human pathology. Similar patterns of expression were observed in 76.5% of inflammation-associated genes. *Winnie* mice accurately represented UC with 90.7% similarity in the expression of these genes, as well as, 87.7%. similarity to males with CD. Studies determining concordance of DSS and TNBS models to IBD have yielded modest results. When comparing entire expression profiles from arrays, 16.1% (of 944 genes) concordance in DSS-treated mice (Fang

et al., 2010), and 12.5% (of 6142 genes) in TNBS-treated rats (Brenna et al., 2013) was observed. In another study, concordance was determined for a selected list of IBD-related genes (32 genes) which demonstrated reasonable similarity in DSS-treated mice (46.9%), but only 6.25% similarity in TNBS-treated mice (te Velde et al., 2007). In comparison, transfer of $CD4^{+}CD45RB^{high}$ T lymphocytes into immunodeficient mice resulted in 93.75% concordance (te Velde et al., 2007). Other models including piroxicam-accelerated colitis in interleukin (IL)-10 knockout mice and adoptive transfer of CD4+CD25- leukocytes in immunodeficient mice, demonstrated a concordance of 68.5% and 57.6%, respectively, compared to IBD-associated genes (92 genes) (Holgersen et al., 2015). Considering that *Winnie* mice develop spontaneous chronic colitis without any intervention, and their immune profile highly resembles that of UC, the *Winnie* model is an accurate model of colitis that is not subject to the variability of experimental techniques used to induce colitis. This positions the *Winnie* mice as a robust model to study BM-MSC therapy, and indeed other pre-clinical treatments for IBD.

Many factors were previously reported to be decreased on the protein or gene expression level in the colon by MSC treatments in chemically-induced colitis. Several of these were also downregulated by BM-MSCs in *Winnie* mice. This included genes for key pro-inflammatory cytokines *Il6, Ifng, Il1b,* and *Tnf,* which were identified in numerous studies. Additional similarities were observed after MSC treatment in the downregulation of several factors: *Il1a,* pro-inflammatory cytokine*; Cxcl2 (MIP-2),* polymorphonuclear leukocyte chemoattractant; *Tbx21* (T-bet), Th1 lymphocyte commitment; and *Itgam* (CD11b), often used as a macrophage marker but can be expressed in multiple innate leukocytes. All these genes were upregulated in *Winnie* mice and IBD. Moreover, changes in these genes after MSC treatment represent some of the common effects of MSC therapy in acute and chronic colitis models. Previously it was also reported that amelioration of chemically-induced colitis by MSCs associated with upregulation of *Arg1* and *Mrc1,* which are associated with type 2 macrophage polarisation (Song et al., 2017c, de Aguiar et al., 2018, Song et al., 2018); *Gata3,* which is suggested to be a

marker for Th2 lymphocytes (Chen et al., 2013); *Hmox1*, which may regulate chemokine signalling in intestinal epithelial cells (Onyiah et al., 2018); and *Nos2* (iNOS), which is involved in the anti-pathogenic response but excessive NO production associates with severe colitis (Dhillon et al., 2014). These genes were already upregulated in *Winnie* mice and IBD patients. BM-MSCs downregulated these genes which corrected their expression in *Winnie* mice. Therefore, MSC treatments in *Winnie* mice and chemical-induced colitis produced different effects on the level of gene expression. Similarly, downregulation of *Rorc* (RORγt), which is often considered a marker of Th17 commitment, by MSCs was observed in chemically-induced colitis (Chen et al., 2013). However, this was downregulated in *Winnie* mice and IBD patients compared to inflamed controls and upregulated by BM-MSC treatments in *Winnie* mice. Several studies have also reported an increase in FOXP3 after MSC treatments in chemically-induced colitis (**Chapter 1, Table 1.2**). FOXP3 is a key transcription factor in the commitment to the Treg phenotype. The immunomodulatory effects of MSC treatment associate with the number of Tregs in murine colitis (Gonzalez-Rey et al., 2009, González et al., 2009, Zhang et al., 2009b, Takeyama et al., 2017). Even though *Foxp3* was upregulated in *Winnie* mice with similar expression observed in IBD patients, *Foxp3* was further upregulated after BM-MSC treatments in *Winnie* mice on the gene level. However, no differences were observed between the number of FOXP3+ leukocytes in the distal colon between C57BL/6 and *Winnie* mice treated with sham or BM-MSCs. Nevertheless, the proportion of FOXP3+ leukocytes was increased by BM-MSC treatment. Previous studies suggest that MSCs promote the polarisation of regulatory T lymphocytes (Gonzalez-Rey et al., 2009, González et al., 2009). Our data in BM-MSC-treated *Winnie* mice indicates that the increased proportion of FOXP3+ leukocytes could also be explained by an overall decrease in leukocyte infiltration while the number of FOXP3+ leukocytes remain unchanged.

While we observed changes in the expression of many factors previously associated with the resolution of chemically-induced colitis after MSC treatment, high-throughput screening of the mRNA transcriptome allowed us to identify a plethora of genes that were associated with the immunomodulatory capabilities of BM-

MSCs. Within the top ten genes downregulated by BM-MSCs in inflammation-associated KEGG pathways, many factors were implicated in IBD. This included: *Ppbp* (Cxcl7), which is highly upregulated in epithelial cells of UC patients (Kruidenier et al., 2006); *Cxcl3* and *Cxcr2*, which were recently determined to be upregulated in UC (Taman et al., 2018); *Spp1* (osteopontin), upregulated in UC (Masuda et al., 2003); *Il1f9* (IL-36γ), upregulated in UC (Nishida et al., 2016), decreased Treg and increased Th9 lymphocytes which are responsible for inflammation in experimental colitis (Harusato et al., 2017); *Adcy8*, involved in macrophages initiating the innate anti-viral host defence (Dhillon et al., 2014); *Tnfrsf11b* (osteoprotegerin), a non-invasive biomarker of IBD (De Voogd et al., 2016); *Ccl3* (MIP-1α), broadly upregulated in epithelium, stroma and leukocytes in tissues from IBD patients (Banks et al., 2003); *Ido1*, highly upregulated in UC (Ciorba, 2013); and *Cfh* (Complement factor H), which has not been studied in colitis to the best of our knowledge, nonetheless changes in the complement system in IBD have been reported many years ago (Ross et al., 1979). Notably, many genes of recent interest were also downregulated by BM-MSCs including: *Nlrp3* which is overactive in peripheral blood mononuclear cells from IBD patients (Lazaridis et al., 2017); *Lbp* and *Tlr2*, which are involved in pathogen recognition (Kordjazy et al., 2018); as well as *Lcn-2* and *Mmp9*, which have recently shown promise as non-invasive faecal biomarkers of IBD (Buisson et al., 2018).

3.8. Conclusion

Considerable progression has been made in studies exploring MSCs as a tool to ameliorate the inflammatory pathology of IBD. While human trials and animal models have shown promise for MSC therapy, mechanisms of action must be fully understood to optimise clinical translation. Sequencing of the transcriptome has uncovered substantial evidence in the pathophysiology of many diseases including IBD. Utilising this technology to study the effects of MSC therapy may offer direction for many researchers in the field. In *Winnie* mice, BM-MSC treatments induced changes in gene expression that were similar to those reported in acute models of chemically-induced colitis. However, multiple differences were observed

and many gene targets that may play novel roles in the resolution of inflammation were identified. Comparison of inflammatory genes in the transcriptome of *Winnie* mice and IBD patients revealed that this model replicated UC with a high degree of accuracy not observed in models of chemically-induced colitis. Models of chronic colitis, such as *Winnie* mice, are necessary to study the mechanisms of MSCs in IBD and develop a successful approach to MSC therapy in the clinic.

CHAPTER FOUR

Mesenchymal Stem Cell Therapy Ameliorates Chronic Inflammation-induced Alterations to the Enteric Nervous System

4.1. Summary

The enteric nervous system (ENS) has been identified as a therapeutic target for inflammatory bowel disease (IBD). Despite this, a thorough screen for alterations in the nervous system has not been performed in IBD patients or pre-clinical models. Furthermore, investigations into neuroprotective treatments for intestinal inflammation are limited. Recently, we determined that mesenchymal stem cells (MSCs) possess potent neuroprotective properties in an acute model of intestinal inflammation. However, a neuroprotective benefit of MSC therapy in chronic colitis is currently uncharacterised. The *Winnie* mouse model of spontaneous chronic colitis closely resembles human ulcerative colitis (UC) and is a robust pre-clinical model to examine prospective treatments. In this study, we evaluated inflammation-induced alterations to the ENS in the *Winnie* model of colitis. Furthermore, the potential neuroprotective properties of MSC therapy in chronic experimental colitis were investigated. *Winnie* mice underwent bone marrow-derived MSC (BM-MSC) or sham treatments over two weeks delivered by enema. Mice were culled 24h after the final treatment and distal colons were collected for RNA isolation and immunohistochemistry. High-throughput RNA sequencing and bioinformatics were performed to analyse nervous system-associated genes in the mRNA transcriptome. Results were compared to the transcriptome of colon samples from IBD patients retrieved from the Gene Expression Omnibus data repository. The number of neurons (microtubule-associated protein 2) and leukocytes (CD45) were evaluated in the myenteric plexus. Similar alterations to the expression of genes associated with cholinergic, purinergic, glutaminergic and NPY-ergic signalling were observed in *Winnie* mice and IBD patients. Changes on the gene level that were associated with neurotransmission, structural changes and neurogenic inflammation were found in both *Winnie* mice and IBD patients. Subsequent treatment with BM-MSCs normalised the expression for many of these genes in *Winnie* mice. Structural changes of the myenteric ganglia and immune cell infiltration were confirmed in *Winnie* mice by immunohistochemistry: plexitis, ganglionic hypertrophy and decreased neuronal density were identified. The degree of plexitis correlated positively with the disease activity of colitis, and negatively,

with neuronal density. BM-MSC treatments alleviated myenteric plexitis and increased neuronal density to near control levels. Based on the results of this study, we have concluded that the expression of genes related to changes in colon innervation in *Winnie* mice are similar to those observed in IBD patients. Using transcriptome sequencing, multiple affected pathways have been identified. Thus, *Winnie* mice share similar molecular signatures and structural changes with IBD patients, and, therefore, represent a reliable pre-clinical model of IBD to test neuroprotective treatments. The results of this study are suggestive that BM-MSCs could be efficacious for attenuating alterations to the enteric nervous system in a clinical setting.

4.2. Abbreviations

5-HT4R	5-hydroxytryptamine receptor 4
ACh	acetylcholine
BM-MSC	bone marrow derived MSC
CCR3	C-C chemokine receptor type 3
ChAT	choline acetyltransferase
CNS	central nervous system
DAPI	4',6-diamidino-2-phenylindole
DMSO	dimethyl sulfoxide
DSS	dextran sodium sulphate
ENS	enteric nervous system
FBS	foetal bovine serum
GABA	γ-aminobutyric acid
GDNF	glial cell line-derived neurotrophic factor
GO	gene ontology
IBD	inflammatory bowel disease
KEGG	Kyoto Encyclopedia of Genes and Genomes
LMMP	longitudinal muscle and myenteric plexus
MAP-2	microtubule associated protein 2
MPO	myeloperoxidase
MSC	mesenchymal stem cell
Mφ2	type 2 macrophage
NDS	normal donkey serum
NPY	neuropeptide Y
RIN	RNA integrity number
RNA-Seq	RNA-Sequencing
S100B	S100 calcium-binding protein B
TNBS	2,4,6-trinitrobenzenesulfonic acid
UC	ulcerative colitis
VAChT	vesicular acetylcholine transporter
β-CGRP	β-calcitonin gene-related peptide

4.3. Gene Symbols

Adra1a	adrenergic receptor, alpha 1a
Adra1b	adrenergic receptor, alpha 1b
Adra2b	adrenergic receptor, alpha 2b
Adrb2	adrenergic receptor, beta 2
Adrb3	adrenergic receptor, beta 3
Ano1	anoctamin 1, calcium activated chloride channel
Calb2	calbindin 2
Calcb	calcitonin-related polypeptide, beta
Chat	choline acetyltransferase
Chrna1	cholinergic receptor, nicotinic, alpha polypeptide 1 (muscle)
Chrna3	cholinergic receptor, nicotinic, alpha polypeptide 3
Chrna9	cholinergic receptor, nicotinic, alpha polypeptide 9
Chrnb4	cholinergic receptor, nicotinic, beta polypeptide 4
Elavl2	ELAV (embryonic lethal, abnormal vision, Drosophila)-like 2 (Hu antigen B)
Elavl3	ELAV (embryonic lethal, abnormal vision, Drosophila)-like 3 (Hu antigen C)
Elavl4	ELAV (embryonic lethal, abnormal vision, Drosophila)-like 4 (Hu antigen D)
Gabra1	gamma-aminobutyric acid (GABA) A receptor, subunit alpha 1
Gabrd	gamma-aminobutyric acid (GABA) A receptor, subunit delta
Gabre	gamma-aminobutyric acid (GABA) A receptor, subunit epsilon
Gabrg2	gamma-aminobutyric acid (GABA) A receptor, subunit gamma 2
Gabrp	gamma-aminobutyric acid (GABA) A receptor, pi
Gabrr2	gamma-aminobutyric acid (GABA) C receptor, subunit rho 2
Gfra1	glial cell line derived neurotrophic factor family receptor alpha 1
Gria2	glutamate receptor, ionotropic, AMPA2 (alpha 2)
Gria4	glutamate receptor, ionotropic, AMPA4 (alpha 4)
Grin1	glutamate receptor, ionotropic, NMDA1 (zeta 1)

Grin2b	glutamate receptor, ionotropic, NMDA2B (epsilon 2)
Grin2d	glutamate receptor, ionotropic, NMDA2D (epsilon 4)
Grin3a	glutamate receptor ionotropic, NMDA3A
Grina	glutamate receptor, ionotropic, N-methyl D-aspartate-associated protein 1 (glutamate binding)
Htr2a	5-hydroxytryptamine (serotonin) receptor 2A
Htr3a	5-hydroxytryptamine (serotonin) receptor 3A
Htr4	5-hydroxytryptamine (serotonin) receptor 4
Mtap2/Map2	microtubule associated protein 2
Ndn	necdin
Neu3	neuraminidase 3
Npy	neuropeptide Y
Npy1r	neuropeptide Y receptor Y1
Npy2r	neuropeptide Y receptor Y2
Npy6r	neuropeptide Y receptor Y6
Nrg1	neuregulin 1
Ntf3	neurotrophin 3
Ntng1	netrin G1
P2rx1	purinergic receptor P2X, ligand-gated ion channel, 1
P2rx3	purinergic receptor P2X, ligand-gated ion channel, 3
P2rx5	purinergic receptor P2X, ligand-gated ion channel, 5
P2rx6	purinergic receptor P2X, ligand-gated ion channel, 6
P2ry4	pyrimidinergic receptor P2Y, G-protein coupled, 4
Ramp2	receptor (calcitonin) activity modifying protein 2
Ramp3	receptor (calcitonin) activity modifying protein 3
Ret	ret proto-oncogene
S100b	S100 protein, beta polypeptide, neural
Slc6a4	solute carrier family 6 (neurotransmitter transporter, serotonin), member 4
Slc6a12	solute carrier family 6 (neurotransmitter transporter, betaine/GABA), member 12

Slc6a15	solute carrier family 6 (neurotransmitter transporter), member 15
Slc18a3	solute carrier family 18 (vesicular monoamine), member 3
Slc22a3	solute carrier family 22 (organic cation transporter), member 3
Stx11	syntaxin 11
Stx1a	syntaxin 1A (brain)
Syn2	synapsin II
Syt1	synaptotagmin I
Syt2	synaptotagmin II
Syt8	synaptotagmin VIII
Syt12	synaptotagmin XII
Syt13	synaptotagmin XIII
Syt16	synaptotagmin XVI
Syt17	synaptotagmin XVII
Tac1	tachykinin 1
Th	tyrosine hydroxylase
Uchl1	ubiquitin carboxy-terminal hydrolase L1 (PGP 9.5)

4.4. Introduction

The enteric nervous system (ENS) has been identified as a therapeutic target to remedy the symptoms and pathophysiology of inflammatory bowel disease (IBD) (Bernardazzi et al., 2016, Margolis and Gershon, 2016). Despite recent advancements in gene sequencing technology, alterations in the intestinal innervation have not been thoroughly explored on the level of gene expression in IBD patients. Furthermore, only a limited number of pre-clinical studies have investigated the benefit of neuroprotective treatments for intestinal inflammation. The ENS spans the length of the intestinal tract and is separated into two distinct plexuses, the submucosal and myenteric. Within the plexuses, neurons and glial cells form interconnected ganglia that intrinsically regulate intestinal processes including: vasomotor function, secretion, epithelial barrier permeability and the coordination of motility. In the presence of intestinal inflammation, gut dysfunctions manifest concurrently with disturbances to the ENS (Poli et al., 2001, Hansen, 2003, Lomax et al., 2005, De Giorgio et al., 2007, Lakhan and Kirchgessner, 2010). Structural abnormalities including axonal damage and neuropathy are prominent in animal models of chemically-induced colitis (Boyer et al., 2005, Lin et al., 2005, Linden et al., 2005a, Sarnelli et al., 2009, Nurgali et al., 2011, Gulbransen et al., 2012). Similarly, alterations in nerve fibres and neuronal density are observed in biopsies from IBD patients (Bishop et al., 1980, Bernardini et al., 2012). Intestinal inflammation can alter the proportion of enteric neuronal subpopulations defined by their neurochemical coding in animal models and IBD. (Schneider et al., 2001, Neunlist et al., 2003a, Lin et al., 2005, Winston et al., 2013). Dysfunction is also evident in the electrophysiological properties of individual neurons in models of chemically-induced colitis (Linden et al., 2003, Krauter et al., 2007, Nurgali et al., 2007, Nurgali et al., 2009, Nurgali et al., 2011, Linden, 2013). These changes persist long after the resolution of inflammation which indicates that it is difficult for enteric neurons to fully recuperate from the inflammatory insult (Krauter et al., 2007, Lomax et al., 2007a). This may be mediated by pro-inflammatory cytokines acting directly on enteric neurons which can have excitatory effects and supress cholinergic neurotransmission (Xia et al., 1999,

Kelles et al., 2000). Together, these studies demonstrate a strong connection between the ENS and the pathophysiology of intestinal inflammation. This is exemplified by the high levels of leukocyte infiltration within proximity of the enteric plexus (plexitis) in IBD and animal models of colitis (Sanovic et al., 1999, Sayani et al., 2004, Boyer et al., 2005, Ferrante et al., 2006, Kinoshita et al., 2007, Sokol et al., 2009, Bressenot et al., 2013). This accompanies neuronal damage in animal models of chemically-induced colitis which is linked to altered peristaltic reflexes and motility (Sanovic et al., 1999, Boyer et al., 2005, Kinoshita et al., 2007). Moreover, plexitis is prognostic of future inflammatory relapse, and thus, may contribute to the pathophysiology of IBD (Ferrante et al., 2006, Sokol et al., 2009, Bressenot et al., 2013). Due to the parallels between intestinal inflammation and damage to the ENS, neuroprotection is emerging as a therapeutic strategy for alleviating IBD.

Recently, we have published a series of papers that have demonstrated the potential of mesenchymal stem cell (MSC) therapy to protect the ENS from inflammation-induced alterations in the guinea-pig model of 2,4,6-trinitrobenzenesulfonic acid (TNBS)-induced colitis (Robinson et al., 2014, Robinson et al., 2015, Stavely et al., 2015a, Stavely et al., 2015b, Robinson et al., 2017b). These studies provide evidence for the potential therapeutic application of MSC therapy for IBD; nonetheless, these findings would be better explored in a model that progresses in a similar manner to IBD. The *Winnie* mouse model of spontaneous chronic colitis has recently been demonstrated to replicate the pathophysiology of human ulcerative colitis (UC) (Heazlewood et al., 2008, Eri et al., 2011) and similar perturbations to the ENS have been observed (Rahman et al., 2015, Rahman et al., 2016, Robinson et al., 2017a). Therefore, this model is ideal to establish the neuroprotective benefits of MSC therapy in chronic intestinal inflammation. The objectives of this study are to screen for inflammation-induced alterations to the ENS using high-throughput RNA sequencing in the *Winnie* mouse model of spontaneous chronic colitis and investigate the potential neuroprotective effects of MSC therapy.

4.5. Methods

4.5.1. Animals

Male *Winnie* mice aged 14 weeks (total n=14) were obtained from Victoria University (Melbourne, Victoria, Australia). *Winnie* mice were compared to age matched male C57BL/6 mice (total n=10) obtained from the Animal Resource Centre (Perth, Western Australia, Australia). All mice had *ad libitum* access to food and water and were housed in a temperature-controlled environment with a 12-h day/night cycle. Mice were acclimatised for one week at the Western Centre for Health, Research and Education (Melbourne, Victoria, Australia). All mice were culled by cervical dislocation and the distal portion of the colon was collected for subsequent experiments. All animal experiments in this study complied with the guidelines of the Australian Code of Practice for the Care and Use of Animals for Scientific Purposes and were approved by the Victoria University Animal Experimentation Ethics Committee.

4.5.2. Cell culture and passaging

The MSCs used in this study were derived from human bone marrow (BM-MSC) and were obtained from Tulane University, USA. These BM-MSCs were extensively characterised for cell surface markers, differentiation potential, proliferation, colony formation, morphology and adherence to plastic (Stavely et al., 2015b) (**Chapter 2, Figures 2.1 & 2.2**) and conform to the guidelines set by the International Society for Cell Therapy (Dominici et al., 2006). BM-MSCs were cultured to generate the required numbers for animal treatments as previously described (**Chapter 3, Section 3.5.2**). Cells prepared for administration had a viability of over 95% after trypsinisation and were used only at the fourth passage to minimise the chance of acquiring genetic abnormalities (Ueyama et al., 2012).

4.5.3. MSC administration

BM-MSCs were administered into *Winnie* mice with chronic colitis by enema. A lubricated silicone catheter was inserted 3cm proximal to the anus of mice anesthetised with 2% isoflurane. *Winnie* mice were treated with two doses of $4x10^6$ BM-MSCs in 100µL of sterile PBS and subsequently received two replenishment doses of $2x10^6$ BM-MSCs in the same volume of sterile PBS. All treatments were administered 4 days apart. Sham-treated *Winnie* mice underwent the same procedure on the same days with an injection of sterile PBS at the same volume (*Winnie*-sham). Mice were culled 24h after the final treatment.

4.5.4. Immunohistochemistry

Immunohistochemistry was performed on wholemount preparations of the longitudinal muscle and myenteric plexus (LMMP) and cross sections of the distal colon. Segments of the distal colon were viewed under a dissection microscope, cut along the mesenteric border and pinned mucosal side up in a silicon-lined Petri dish. For wholemount preparations, tissues were stretched and pinned taught before fixation. Conversely, tissues for cross sectional immunohistochemistry were loosely pinned to protect the structure of the mucosa. All tissues were fixed overnight at 4°C in Zamboni's fixative (2% formaldehyde and 0.2% picric acid) with subsequent washes in dimethyl sulfoxide (DMSO) (Sigma-Aldrich, Sydney, Australia) (3x10min) to permeabilise the tissues and 0.1 M PBS (3x10min) to remove DMSO and the fixative. Fixed and washed wholemount preparations were micro-dissected to remove the mucosa, submucosa and circular muscle layers to expose the LMMP. Wholemount LMMP preparations were incubated in PBS containing 10% normal donkey serum (NDS) (Merck Millipore, Sydney, Australia) and 0.5% Triton X-100 at room temperature for 1h before immunolabelling. Tissues were washed (3x10min of 0.1 M PBS for all proceeding wash steps) and incubated overnight at 4ºC with the primary antibodies chicken anti-microtubule associated protein 2 (MAP-2) (1:5000) (Abcam, Melbourne, Australia) and rat anti-CD45 (1:200) (BioLegend, San Diego, USA). After additional washing, tissues were incubated for 2 hours at room temperature with the secondary antibodies Alexa Fluor 594 donkey anti-chicken (1:500) and Alexa Fluor 488 donkey anti-rat (1:500)

(Jackson ImmunoResearch, West Grove, USA). Wholemounts were washed again before being stained with 4',6-diamidino-2-phenylindole (DAPI) and mounted on glass slides with fluorescent mounting medium (DAKO) (Agilent Technologies, Melbourne, Australia). Immunohistochemistry in tissue cross sections was performed using the methodology previously described (**Chapter 3, Section 3.5.6**). Sections were labelled with the primary antibody chicken anti-microtubule associated protein (MAP)-2 (1:5000) and secondary antibody Alexa Fluor 594 donkey anti-chicken (1:500; Jackson Immunoresearch). Sections were stained with the nuclei marker, DAPI, for 2min prior to being washed and mounted for imaging.

4.5.5. Imaging and analysis

Immunoreactivity for MAP-2, CD-45 and DAPI staining was visualised using an Eclipse Ti confocal laser scanning system (Nikon, Tokyo, Japan). For wholemount preparations, Z-series images were randomly acquired using the 40X objective at a thickness of 1µm. In cross sections, Z-series images were randomly acquired using the 60X objective at a thickness of 2µm. All images were collected as .ND2 files which contained all metadata including fluorescence signals at all Z levels. Images were visualised using Image J v1.50b open source software (National Institute of Health, Bethesda, USA) (Schneider et al., 2012, Rueden et al., 2017) with the Image J ND2 Reader plugin and were converted into maximum intensity projections in 16-bit .TIFF format. In wholemount preparations, the average neuronal density was calculated in images within a $0.1mm^2$ (316.23µm x 316.23µm = $100,000µm^2$) field of view using Image J software as previously described (Gulbransen et al., 2012). Analysis was performed in eight randomly captured images per preparation. The size of each myenteric ganglion was quantified ($µm^2$). The number of MAP-2 immunoreactive neurons within this area was enumerated using the cell counter plugin of ImageJ software. Values were expressed as the number of neurons per $0.01mm^2$ (100µm x 100µm = $10,000µm^2$) area of ganglia. For analysis of MAP-2 immunoreactive neurons in cross sections, the number of neurons were quantified in eight nonadjacent sections in a field of view of $0.04mm^2$ (200µm x 200µm = $40,000µm^2$) per image using the cell counter plugin of ImageJ software. Leukocytes

immunoreactive for CD-45 were quantified in images of wholemount preparations within a 0.1mm^2 (316.23µm x 316.23µm = 100,000µm^2) field of view using the cell counter plugin of ImageJ software. Leukocytes were further classified by their location in relation to the myenteric ganglia (intra-ganglionic, periphery of ganglia, extra-ganglionic) and by their morphology (rounded or stellate). For all analyses average mean values were calculated from eight images per mouse.

4.5.6. Statistical analysis

Data analysis was performed using GraphPad Prism v7 (GraphPad Software Inc., San Diego, USA). A one-way ANOVA was performed with a post hoc Holm-Sidak test for multiple comparisons. X, Y correlations were determined using a linear regression analysis with *P* values for significant slope relationships recorded. For all analyses $P \leq 0.05$ was considered significant. All data were presented as mean ± standard error of the mean (SEM).

4.5.7. RNA extraction and quality control

Total RNA was extracted from segments of the distal colon as previously described (**Chapter 3, Section 3.5.9**). Briefly, snap frozen colon was dissociated with a homogenising bead beater (TissueLyser LT, Qiagen, Melbourne, Australia) and RNA was extracted from the tissue homogenate using TRIzol® reagent (Thermo Fisher Scientific, Melbourne, Australia) and spin columns from the RNeasy Mini Kit (Qiagen, Melbourne, Australia). The concentration of RNA in each sample was quantified by a Qubit 1.0 fluorometer (Invitrogen, Thermo Fisher Scientific) using the Qubit® RNA Broad Range Assay Kit (Life Technologies) according to manufacturer's protocol. Contaminates (such as phenol) were evaluated in RNA samples using a DeNovix DS-11 spectrophotometer (Gene Target Solutions, Sydney, Australia). Absorbance (A) scores for all samples were between 1.8 – 2.0 for A260/A280 ratios and 2.0-2.2 for A260/A230 ratios, suggesting that nucleotide purity was high. The quality of RNA was assessed using an 2100 Bioanalyzer (Agilent Technologies) microfluidics platform with the RNA 6000 Nano Kit

(Agilent Technologies) according to the manufacturer's protocol. All samples were free from contamination of genomic DNA and 16S ribosomal RNA from bacteria. All samples were of very high quality and had minimal degradation with RNA integrity number (RIN) values between 9.9-10/10.

4.5.8. High-throughput RNA-Sequencing and bioinformatics

High-throughput sequencing of Poly-A tail purified mRNA was performed as described previously (**Chapter 3, Section 3.5.11**) with an experimental design similar to Seaman et al. (2015). Samples of RNA (n=7/group) from C57BL/6 and *Winnie* mice treated with either sham or BM-MSC enemas were submitted to the Australian Genome Research Facility (AGRF, Melbourne, Australia) and met all quality control criteria. High-throughput sequencing was performed using a 100bp single-end read protocol on the Illumina HiSeq 2500 System. Raw data were processed, and gene reads were mapped as previously described (**Chapter 3, Section 3.5.11**). Genes expression from raw mapped reads were calculated by the R package DEGseq v 1.34.0 and genes with a LogFC value between ±0.5 were omitted from further analysis (Wang et al., 2009). Gene expression data on the transcriptome of human IBD patients were obtained from the National Centre for Biotechnology Information (NCBI) Gene Expression Omnibus (GEO) public data repository as previously described (**Chapter 3, Section 3.5.11**) (Edgar et al., 2002, Barrett et al., 2012). Data were uploaded by Peters et al. (2017); similar to our methods, RNA was extracted by TRIzol, purified for mRNA and the same sequencing platform was used. These data are accessible through GEO series accession number GSE83687 at https://www.ncbi.nlm.nih.gov/geo/. Gene expression of colon samples used from this dataset included: male (n=14) and female (n=20) controls, male (n=19) and female (n=11) patients with UC and male (n=7) and female (n=4) patients with CD (total n=75). Gene sets that were representative of the ENS and common neurotransmitter receptors were collated from gene expression data. The fold regulation of genes were visualised as heat maps using the gplots R package (Warnes et al., 2009). These genes were analysed for enriched terms using the web-based tool DAVID (database for annotation,

visualization and integrated discovery) with a $P<0.001$ threshold and the Benjamini-Hochberg correction (Dennis et al., 2003, Huang et al., 2008b, Huang et al., 2008a). To categorise alterations to the ENS by function and related gene products, data were analysed for enrichment using public databases including: InterPro protein families (Finn et al., 2017), Kyoto Encyclopedia of Genes and Genomes (KEGG) pathways (Kanehisa and Goto, 2000), Swiss-Prot keywords (Boutet et al., 2007) and gene ontologies (GO) associated with biological processes, molecular function and cellular components (Ashburner et al., 2000). Furthermore, functional clustering of ENS genes and neurotransmitter receptors were performed by DAVID using the above databases to identify groups of genes in individual signalling pathways of neurotransmission (*i.e.* cholinergic, nitrergic). Terms and genes associated with individual signalling pathways in functional gene clusters were presented as node-edge network maps using Gephi v0.9.2 open-source network analysis and visualisation software (Bastian et al., 2009) with aesthetic alterations to vector graphics files performed on Inkscape v0.92.3 (Bah, 2009).

4.6. Results

4.6.1. BM-MSCs ameliorate alterations to enteric nervous system- associated gene expression in spontaneous chronic colitis

Previously, we determined that BM-MSC treatment via enema reduced the disease activity of spontaneous chronic colitis and reduced multiple inflammatory processes in *Winnie* mice (**Chapter 3, Section 3.6**). Alterations to the nervous system were screened in *Winnie* mice with chronic inflammation and in those with the inflammation attenuated by BM-MSC treatments. Genes that are expressed in the nervous system were investigated in datasets of the transcriptome produced by RNA-Sequencing (RNA-Seq). To date, criteria for genes defining ENS specific terms have not been contributed to gene annotation databases of gene groups, functions or associated pathways (*i.e.* GO or KEGG pathways). Therefore, a panel of genes that represent the ENS was developed. This was accomplished by identifying proteins or genes that are highly expressed by the ENS, or those that are absent in mice modelling Hirschsprung's disease (lacking an ENS) in previously published studies (Krammer et al., 1994, Costa et al., 2000, Anlauf et al., 2003, Furness, 2006, Heanue and Pachnis, 2006, Geramizadeh et al., 2013). Differences in gene expression of various ENS-related genes were detected in *Winnie* mice with chronic colitis and in human IBD patients compared to uninflamed controls (**Figure 4.1, Table 4.1**). Furthermore, changes in ENS-associated genes were detected after treatment of *Winnie* mice with BM-MSCs. Within the top ten genes upregulated by BM-MSC treatments in *Winnie* mice, all these genes were also downregulated in *Winnie*-sham compared to C57BL/6 mice. This included genes associated with neurotransmitter production (*Chat:* acetylcholine, ACh and *Npy*: neuropeptide Y, NPY) and transport (*Slc18a3*: ACh; *Slc22a3*: 5-HT, histamine, norepinephrine and dopamine; *Slc6a15*: neuronal amino acids). The genes *Elavl2* and *Elavl3* coding for the Hu proteins (pan-neuronal cell body marker) were upregulated by BM-MSC treatments. Genes coding membrane bound proteins *Ntng1* (axonal guidance) and *Gfra1* (glial cell line-derived neurotrophic factor (GDNF) receptor) were also upregulated. Within the top ten genes downregulated by BM-MSC treatments in

Winnie mice, genes that produce ligands associated with neurogenic inflammation including: *Calcb* (β-calcitonin gene-related peptide, β-CGRP), *Tac1* (Neurokinin A and substance P) and *S100b* (glial cell subpopulation) were observed. Several genes involved in vesicle trafficking were downregulated by BM-MSC treatments (*Syt16, Syt8, Syt1, Stx1a* and *Stx11*). As was the expression of *Th* (tyrosine hydroxylase, TH; dopamine and norepinephrine synthesis)

Changes in the expression of genes from the major neurotransmitter receptor families present in the colon were determined between *Winnie*-sham mice and human IBD patients compared to uninflamed controls, as well as BM-MSC and sham-treated *Winnie* mice (**Figure 4.2, Table 4.2**). The majority neurotransmitter receptors that were downregulated in *Winnie*-sham mice compared to C57BL/6 mice. Numerous alterations to gene expression were induced by BM-MSC treatments in *Winnie* mice with the top ten genes upregulated including: the γ-aminobutyric acid (GABA)-ergic receptor *Gaber*; purinergic receptors *P2ry4* and *P2rx1*; adrenergic receptors *Adra2b, Adra1b* and *Adra1a*; nicotinic receptors *Chrna3* and *Chrna9;* and glutaminergic receptors *Gria4* and *Grin2d*. The top ten downregulated genes included: GABA-ergic receptors *Gabrp, Gabrd, Gabra1, Gabrr2* and *Gabrg2*; glutaminergic receptors *Grin2b* and *Grin3a*; (NPY)-ergic receptors *Npy6r* and *Npy2r;* and the serotonergic receptor *Htr2a*.

The nervous system is highly divergent in mammals; some genes may not be homologous or commonly expressed between humans and other mammalian species (Sousa et al., 2017). Therefore, investigating overall changes to signalling systems may offer more value than comparing the expression of individual genes. All ENS-associated genes and neurotransmitter receptors were analysed for functional clusters and groups of genes associated with specific neurotransmitter families (**Figures 4.3 and 4.4, Table 4.3**) (**Appendix A, Tables S7-13**).

Figure 4.1 ***Changes in the expression of genes associated with cells in the ENS within the colon***

Heat map of the fold regulation of genes identified by RNA-Seq between control C57BL/6, *Winnie*-sham, *Winnie* BM-MSC-treated mice and IBD patients that selectively represent cells of the enteric nervous system and the neurochemical coding of enteric neurons. Upregulated and downregulated genes were visualised as red and green gradients up to >5 or <-5 folds, respectively. Genes failing the initial cut off between ±0.5logFC are represented as black (no change).

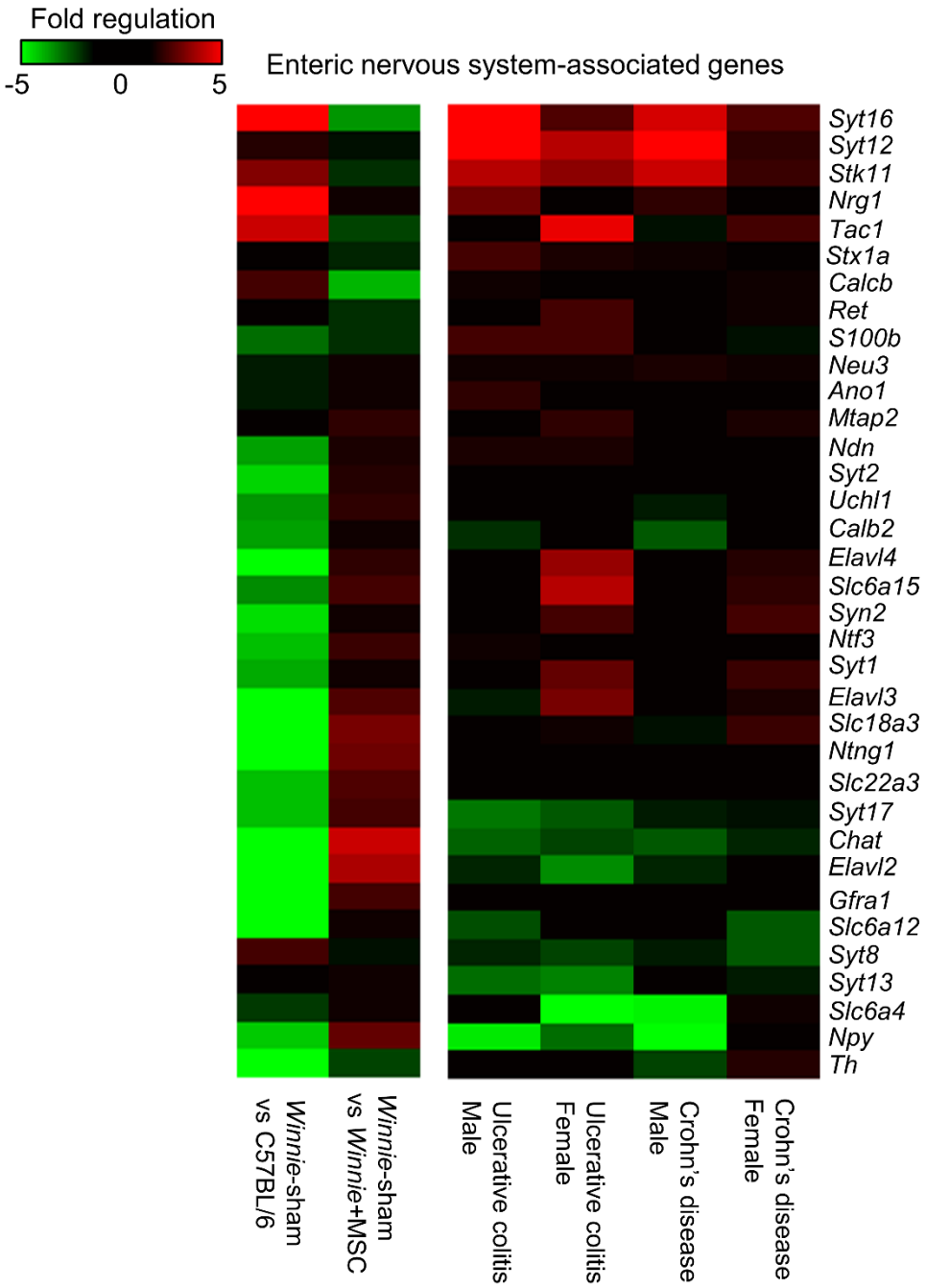
Fold regulation
-5
0
5
Enteric nervous system-associated genes
Syt16
Syt12
Stk11
Nrg1
Tac1
Stx1a
Calcb
Ret
S100b
Neu3
Ano1
Mtap2
Ndn
Syt2
Uchl1
Calb2
Elavl4
Slc6a15
Syn2
Ntf3
Syt1
Elavl3
Slc18a3
Ntng1
Slc22a3
Syt17
Chat
Elavl2
Gfra1
Slc6a12
Syt8
Syt13
Slc6a4
Npy
Th
Winnie-sham vs C57BL/6
Winnie-sham vs Winnie+MSC
Ulcerative colitis Male
Ulcerative colitis Female
Crohn's disease Male
Crohn's disease Female

Table 4.1 ***Fold regulation of ENS-associated genes***

Gene	*Winnie MSC vs Winnie*-sham	*Winnie*-sham *vs* C57BL/6	*UC male vs control male*	*UC female vs control female*	*CD male vs control male*	*CD female vs control female*
Chat	4.2	-5.4	-2.6	-2.3	-2.5	-1.9
Elavl2	3.7	-7.2	-1.8	-3.3	-1.9	-5.8
Slc18a3	2.9	-6.6	1.1	1.5	-1.5	2.1
Ntng1	2.8	-8.1	1.2	1.4	-1.2	1.4
Npy	2.7	-4.1	-4.6	-2.8	-6.3	1.2
Slc22a3	2.4	-4.0	-1.2	-1.3	-1.3	-1.1
Elavl3	2.3	-5.3	-1.7	2.9	-1.4	1.6
Slc6a15	2.2	-3.2	1.1	3.8	-1.3	1.9
Syt17	2.2	-4.0	-2.9	-2.5	-1.7	-1.5
Gfra1	2.2	-7.9	-1.3	1.2	1.0	-1.0
Ntf3	2.1	-4.1	1.4	1.2	-1.2	1.1
Mtap2	2.0	-1.1	1.4	2.4	-1.1	1.6
Elavl4	2.0	-5.9	1.1	3.4	1.0	1.7
Uchl1	1.9	-3.4	-1.1	1.4	-1.6	-1.1
Syt2	1.7	-4.4	-1.4	-1.0	1.1	-1.3
Ndn	1.6	-3.5	1.6	1.7	-1.1	-1.1
Ano1	1.6	-1.7	1.9	1.3	1.2	1.0
Syn2	1.6	-4.5	1.4	2.2	-1.2	2.2
Neu3	1.5	-1.7	1.5	1.6	1.6	1.5
Syt1	1.5	-3.7	-1.4	2.6	-1.3	2.0
Slc6a12	1.5	-8.2	-2.4	-1.2	-1.4	-2.6
Syt13	1.5	-1.1	-2.8	-3.2	-1.2	-1.6
Nrg1	1.4	5.9	2.8	1.3	1.9	-1.1
Slc6a4	1.4	-2.1	-1.2	-8.1	-4.8	1.4
Calb2	1.4	-3.5	-1.9	1.3	-2.5	-1.3
Syt12	-1.5	1.7	18.7	3.9	7.4	1.9
Syt8	-1.5	2.2	-1.7	-2.2	-1.6	-2.5
Stx1a	-1.9	-1.0	2.2	1.6	1.5	1.3
S100b	-1.9	-2.8	2.2	2.2	-1.0	-1.5
Ret	-1.9	1.1	1.2	2.2	-1.0	1.5
Stx11	-1.9	3.1	3.9	3.3	4.1	2.1
Th	-2.2	-23.3	-1.1	-1.3	-2.3	1.7
Tac1	-2.2	4.2	1.4	4.6	-1.4	2.2
Syt16	-3.4	7.1	38.9	2.4	4.4	2.5
Calcb	-3.9	2.2	1.4	1.1	1.1	1.4

UC - Ulcerative colitis, CD – Crohn's disease.

Figure 4.2 ***Changes in the expression of neurotransmitter receptor genes in the colon***

Heat map of the fold regulation of genes identified by RNA-Seq between control C57BL/6, *Winnie*-sham, *Winnie* BM-MSC-treated mice and IBD patients that selectively represent neurotransmitter receptors in the distal colon. Upregulated genes and downregulated genes were visualised as red and green gradients up to >5 or <-5 folds, respectively. Genes failing the initial cut off between ±0.5logFC are represented as black (no change). Note: NPY6R is a pseudogene encoding a protein currently considered to be non-functional in humans.

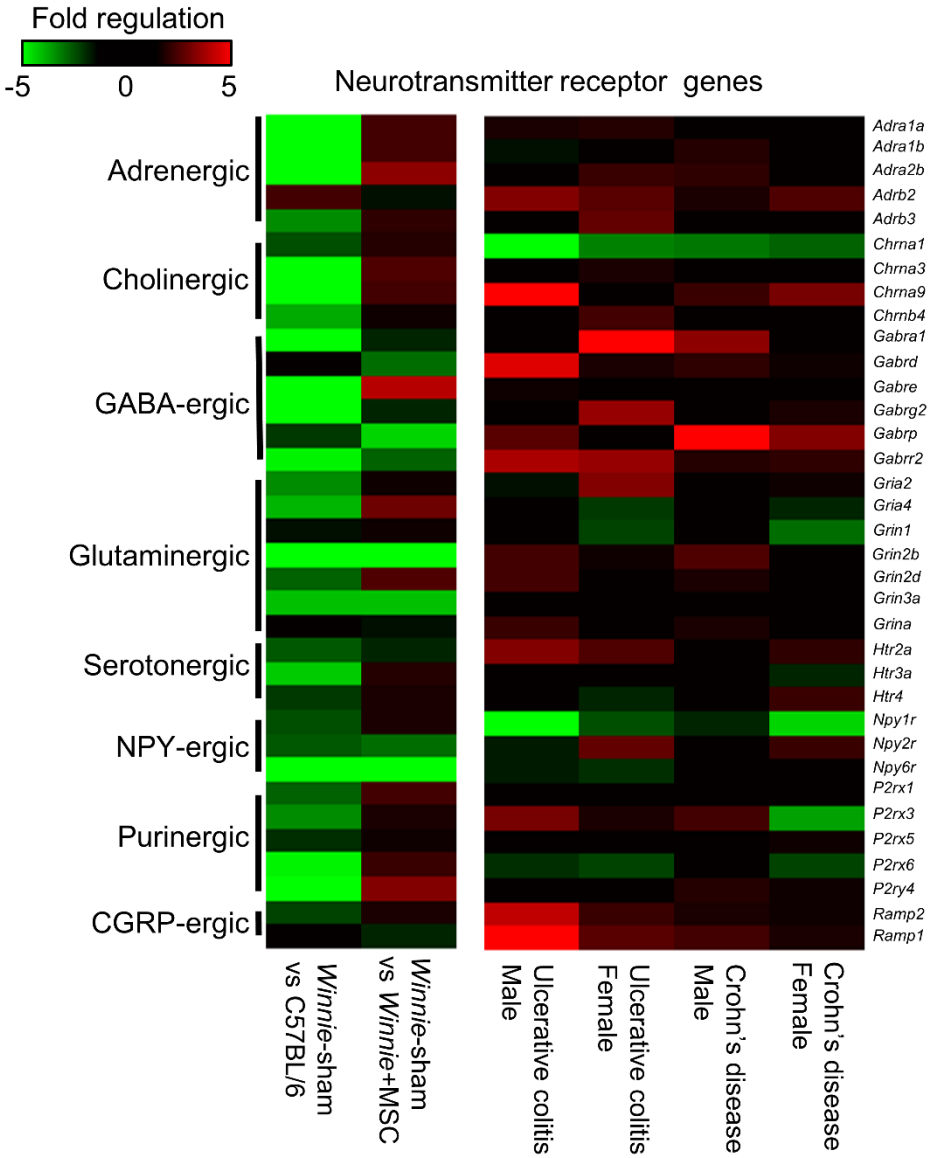
Fold regulation
-5
0
5
Neurotransmitter receptor genes
Adrenergic
Cholinergic
GABA-ergic
Glutaminergic
Serotonergic
NPY-ergic
Purinergic
CGRP-ergic
Adra1a
Adra1b
Adra2b
Adrb2
Adrb3
Chrna1
Chrna3
Chrna9
Chrnb4
Gabra1
Gabrd
Gabre
Gabrg2
Gabrp
Gabrr2
Gria2
Gria4
Grin1
Grin2b
Grin2d
Grin3a
Grina
Htr2a
Htr3a
Htr4
Npy1r
Npy2r
Npy6r
P2rx1
P2rx3
P2rx5
P2rx6
P2ry4
Ramp2
Ramp1
Winnie-sham vs C57BL/6
Winnie-sham vs Winnie+MSC
Ulcerative colitis Male
Ulcerative colitis Female
Crohn's disease Male
Crohn's disease Female

Table 4.2 ***Fold regulation of neurotransmitter receptor genes***

Gene	*Winnie* MSC vs *Winnie*-sham	*Winnie* - sham vs C57BL/6	UC male vs control male	UC female vs control female	CD male vs control male	CD female vs control female
Gabre	3.9	-9.0	1.4	1.1	1.1	1.1
Adra2b	3.4	-8.1	1.2	2.1	1.9	1.3
P2ry4	3.1	-5.4	1.1	-1.4	1.7	1.5
Gria4	2.9	-3.8	-1.1	-2.1	-1.2	-1.7
Grin2d	2.4	-2.7	2.3	-1.4	1.7	-1.2
Chrna3	2.4	-5.6	-1.2	1.6	-1.3	1.1
Adra1b	2.2	-9.9	-1.5	-1.3	1.7	1.3
Chrna9	2.2	-11.7	8.1	1.2	2.1	3.0
Adra1a	2.2	-19.7	1.7	1.8	1.3	1.1
P2rx1	2.2	-2.7	1.2	-1.1	-1.3	1.0
P2rx6	2.1	-4.8	-2.0	-2.2	-1.2	-2.3
Adrb3	1.9	-3.2	1.2	2.7	1.3	1.1
Chrna1	1.8	-2.4	-5.0	-3.2	-3.1	-2.6
Htr3a	1.7	-4.1	1.1	-1.2	-1.0	-1.8
Htr4	1.7	-2.1	-1.4	-1.8	1.3	2.0
P2rx3	1.7	-3.3	2.9	1.7	2.3	-3.6
Ramp2	1.6	-2.2	4.0	2.1	1.6	1.5
Npy1r	1.6	-2.3	-5.3	-2.4	-1.8	-4.3
Grin1	1.6	-1.6	-1.3	-2.2	1.0	-2.8
Chrnb4	1.5	-3.7	-1.2	2.3	-1.1	1.1
Gria2	1.5	-3.3	-1.5	3.1	-1.0	1.6
P2rx5	1.5	-2.0	1.3	-1.0	1.2	1.5
Grina	-1.4	1.0	2.0	1.3	1.7	-1.1
Adrb2	-1.5	2.3	3.1	2.5	1.6	2.3
Ramp3	-1.8	-1.2	5.1	2.5	2.3	1.6
Htr2a	-1.8	-2.5	3.1	2.4	1.0	1.9
Gabrg2	-1.8	-8.1	-1.3	3.4	-1.2	1.7
Gabra1	-1.8	-16.6	1.1	6.1	3.3	0.0
Gabrr2	-2.7	-4.8	3.7	3.4	1.8	2.0
Gabrd	-2.9	-1.1	4.5	1.6	2.0	1.5
Npy2r	-2.9	-2.5	-1.6	2.6	-1.4	2.1
Grin3a	-4.0	-4.0	0.9	1.2	1.2	1.2
Gabrp	-4.4	-2.1	2.5	1.3	6.1	3.1
Npy6r	-6.3	-6.2	-1.6	-1.9	-1.0	1.3
Grin2b	-16.1	-16.1	2.2	1.5	2.4	-1.1

UC - Ulcerative colitis, CD – Crohn's disease. Note: NPY6R is a pseudogene encoding a protein currently considered to be non-functional in humans.

Similar results were observed in functional clusters identified in *Winnie*-sham mice and UC patients for cholinergic, ionotropic purinergic, glutaminergic and NPY-ergic signalling. Nonetheless, adrenergic and GABA-ergic signalling were associated with clusters of upregulated genes in UC patients, while regulation of serotonergic signalling associated genes was varied with possible sexual dimorphisms. Compared to control C57BL/6 mice, all genes associated with these signalling pathways were downregulated in *Winnie*-sham mice. Between BM-MSCs and sham-treated *Winnie* mice, functional clusters were identified that contained upregulated genes associated with nicotinic (**Figure 4.3**), purinergic (**Figure 4.4**), adrenergic and glutaminergic signalling, as well as, downregulated genes associated with GABA-ergic signalling. Upregulation of individual genes associated with serotonergic signalling were also identified. Regulation of genes associated with NPY-ergic signalling were varied.

To simplify and group changes to the nervous system, ENS-associated genes with expression levels altered by BM-MSC treatments were analysed for enriched terms in a variety of databases. This included: InterPro protein families (**Figure 4.5A**), KEGG pathways (**Figure 4.5B**), Swiss-Prot keywords (**Figure 4.5C**) and gene ontologies (**Figure 4.6A-C**) (**Table 4.4**). Analysis of protein families confirmed some results from the functional cluster analysis with an enrichment in the terms *P2X purinoreceptor, adrenergic receptor, nicotinic acetylcholine receptor* and *glutamate receptor* observed in genes upregulated between BM-MSC and sham-treated *Winnie* mice and downregulated between *Winnie*-sham mice compared to C57BL/6 mice. After BM-MSC treatment in *Winnie* mice, the KEGG pathways *cAMP signalling pathway, calcium signalling pathway* and *neuroactive ligand-receptor interaction* were enriched in upregulated genes which coincided with the upregulation of various neurotransmitter-receptor families. These KEGG pathways were also enriched in genes downregulated between *Winnie*-sham and C57BL/6 mice. Enriched terms of Swiss-Prot keywords in genes upregulated by BM-MSC-treated *Winnie* mice were predominantly associated with the cell membrane including terms: *postsynaptic cell membrane, synapse, cell junction, ion transport, ligand-gated ion channel* and *receptor*.

Figure 4.3 ***Alterations in gene expression associated with cholinergic signalling in Winnie mice after BM-MSCs treatments and in ulcerative colitis patients***

Node-edge network map of terms and genes associated with the cholinergic signalling pathway in functional gene clusters [C#] identified by DAVID using the InterPro (IPR), KEGG and GO databases. Upregulated genes or terms identified in clusters of upregulated genes in male (UC-M) and female (UC-F) patients with ulcerative colitis compared to non-inflamed controls denoted as red nodes and edges. Downregulated genes or terms identified in clusters of upregulated genes in UC and *Winnie* mice compared to non-inflamed controls denoted as green nodes and edges. Upregulated genes or terms identified in clusters of upregulated genes in BM-MSC-treated *Winnie* mice compared to sham-treated counterparts denoted as blue nodes and edges.

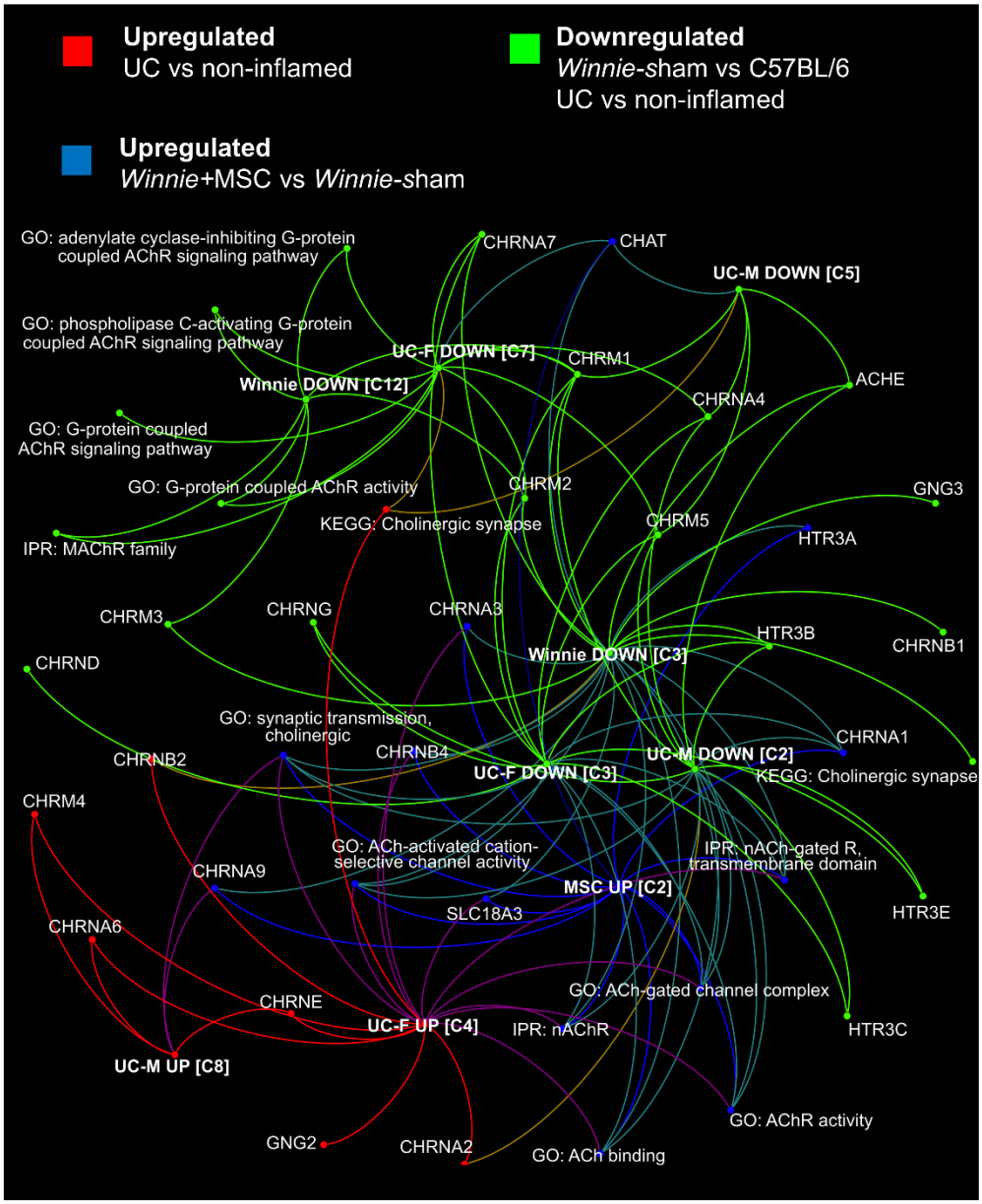
Upregulated
UC vs non-inflamed
Downregulated
Winnie-sham vs C57BL/6
UC vs non-inflamed
Upregulated
Winnie+MSC vs Winnie-sham
GO: adenylate cyclase-inhibiting G-protein coupled AChR signaling pathway
CHRNA7
CHAT
UC-M DOWN [C5]
GO: phospholipase C-activating G-protein coupled AChR signaling pathway
UC-F DOWN [C7]
CHRM1
ACHE
Winnie DOWN [C12]
CHRNA4
GO: G-protein coupled AChR signaling pathway
GO: G-protein coupled AChR activity
CHRM2
GNG3
KEGG: Cholinergic synapse
CHRM5
HTR3A
IPR: MAChR family
CHRM3
CHRNG
CHRNA3
HTR3B
CHRNB1
Winnie DOWN [C3]
CHRND
GO: synaptic transmission, cholinergic
CHRNA1
CHRNB4
UC-M DOWN [C2]
CHRNB2
UC-F DOWN [C3]
KEGG: Cholinergic synapse
CHRM4
GO: ACh-activated cation-selective channel activity
IPR: nACh-gated R, transmembrane domain
CHRNA9
MSC UP [C2]
HTR3E
SLC18A3
CHRNA6
GO: ACh-gated channel complex
CHRNE
UC-F UP [C4]
IPR: nAChR
HTR3C
UC-M UP [C8]
GO: AChR activity
GNG2
CHRNA2
GO: ACh binding

Figure 4.4 ***Alterations in gene expression associated with purinergic signalling in Winnie mice after BM-MSCs treatments and in ulcerative colitis patients***

Node-edge network map of terms and genes associated with the purinergic signalling pathway in functional gene clusters [C#] identified by DAVID using the InterPro (IPR), KEGG and GO databases. Upregulated genes or terms identified in clusters of upregulated genes in male (UC-M) and female (UC-F) patients with ulcerative colitis compared to non-inflamed controls denoted as red nodes and edges. Downregulated genes or terms identified in clusters of upregulated genes in UC and *Winnie* mice compared to non-inflamed controls denoted as green nodes and edges. Upregulated genes or terms identified in clusters of upregulated genes in BM-MSC-treated *Winnie* mice compared to sham-treated counterparts denoted as blue nodes and edges.

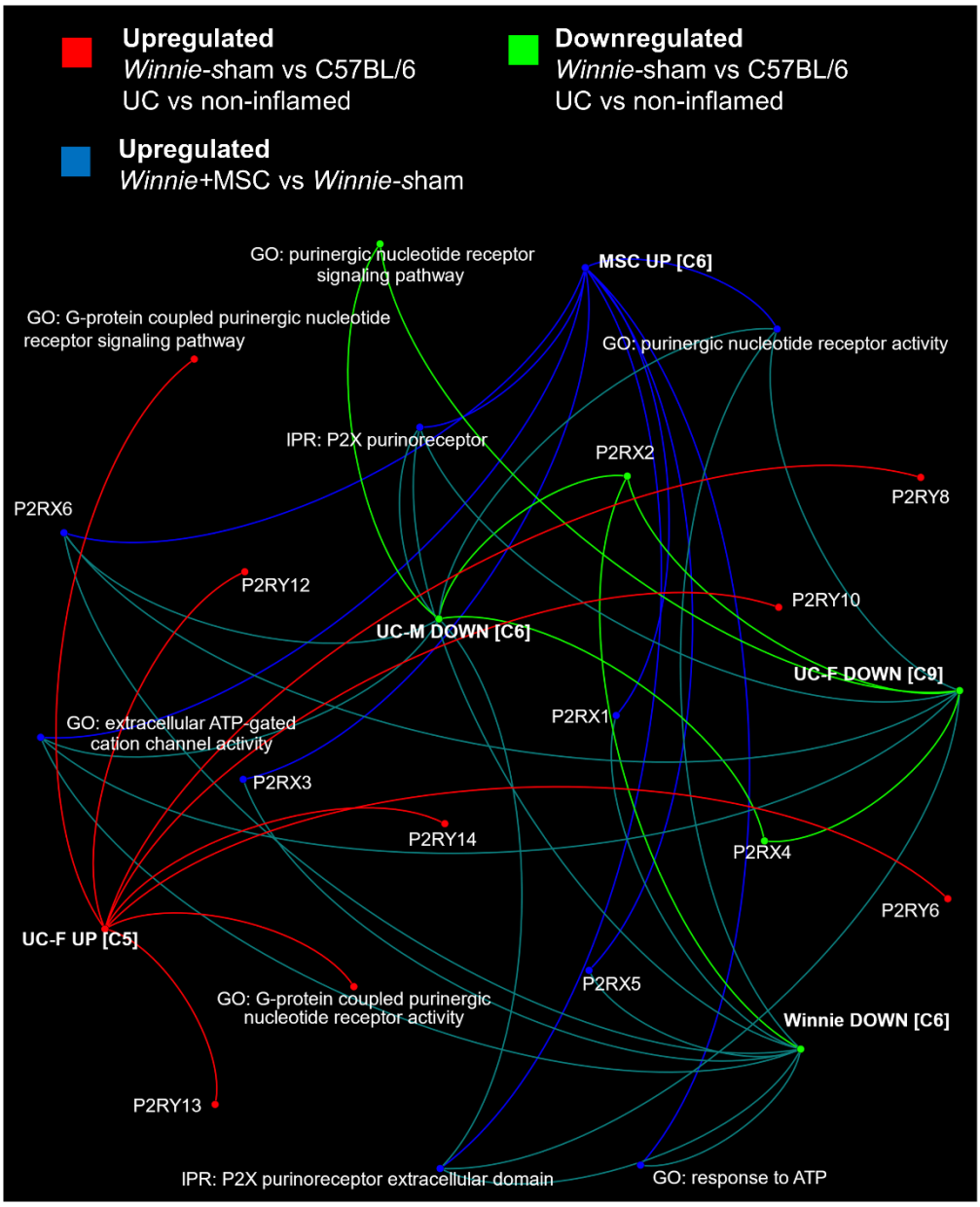
Upregulated
Winnie-sham vs C57BL/6
UC vs non-inflamed
Downregulated
Winnie-sham vs C57BL/6
UC vs non-inflamed
Upregulated
Winnie+MSC vs Winnie-sham
GO: purinergic nucleotide receptor signaling pathway
MSC UP [C6]
GO: G-protein coupled purinergic nucleotide receptor signaling pathway
GO: purinergic nucleotide receptor activity
IPR: P2X purinoreceptor
P2RX2
P2RY8
P2RX6
P2RY12
P2RY10
UC-M DOWN [C6]
UC-F DOWN [C9]
GO: extracellular ATP-gated cation channel activity
P2RX1
P2RX3
P2RY14
P2RX4
P2RY6
UC-F UP [C5]
P2RX5
GO: G-protein coupled purinergic nucleotide receptor activity
Winnie DOWN [C6]
P2RY13
IPR: P2X purinoreceptor extracellular domain
GO: response to ATP

Table 4.3 ***Summary of neurotransmission pathways identified in functional cluster analysis***

Pathway	*Winnie*+MSC vs *Winnie*-sham		*Winnie*-sham vs C57BL/6		UC Male vs control		UC Female vs control	
Cholinergic	↑ (6) Nic	C2	↓ (16) Nic ↓ (3) Mus	C3 C12	↓ (11) Nic ↓ (5) Mix ↑ (4) Mix	C2 C5 C8	↓ (11) Nic ↓ (7) Mus ↑ (9) Nic	C3 C3 C4
Purinergic	↑ (4) P2RX	C6	↓ (5) P2RX	C6	↓ (3) P2RX	C6	↓ (3) P2RX ↑ (6) P2RY	C9 C5
Adrenergic	↑ (4)	C9	↓ (6)	C9	↑ (4)	C5	↑ (5)	C7
Glutaminergic	↑ (4)	C4	↓ (9)	C4	↓ (3)	C7	↓ (4)	C5
GABA-ergic	↓ (5)	C1	↓ (10)	C2	↑ (9)	C2	↑ (13)	C2
Serotonergic	↑ (3)	G	↓ (9)	C8	↑ (6)	C4	↓ (7) ↑ (7)	C6 C6
NPY-ergic	↑ (2) ↓ (2)	G G	↓ (4)	C15	↓ (4)	C4	↓ (3)	G

↑ - upregulated, ↓ - downregulated, C – cluster, G – gene list, GABA - γ-aminobutyric acid, Mus – muscarinic family, Mix – mixture of nicotinic and muscarinic family, NPY - neuropeptide Y, Nic - nicotinic family, P2RY - G-protein coupled purinergic receptors, P2RX - ligand-gated purinergic receptors, UC - Ulcerative colitis. Number of genes in clusters or gene list in brackets. Full dataset in **Appendix A**, **Tables S7-13**.

Figure 4.5 ***Categorical terms summarising the effects of BM-MSCs on the ENS in Winnie mice***

Bar charts representing the gene counts within up to ten terms from InterPro **(A)**, KEGG **(B)** and Swiss-Prot **(C)** databases. Enriched terms were identified in nervous system and neurotransmitter-associated gene sets. Number of downregulated genes in *Winnie*-sham mice compared to C57BL/6 controls represented as black bars. Number of downregulated genes in BM-MSC-treated *Winnie* mice compared to *Winnie*-sham represented as yellow bars. Number of upregulated genes in BM-MSC-treated *Winnie* mice compared to *Winnie*-sham represented as blue bars. No enrichment of these terms was detected in genes upregulated in *Winnie*-sham mice compared to C57BL/6 controls. Analysis performed using DAVID. Top ten terms ranked by *P* values with a cut off of $P<0.001$.

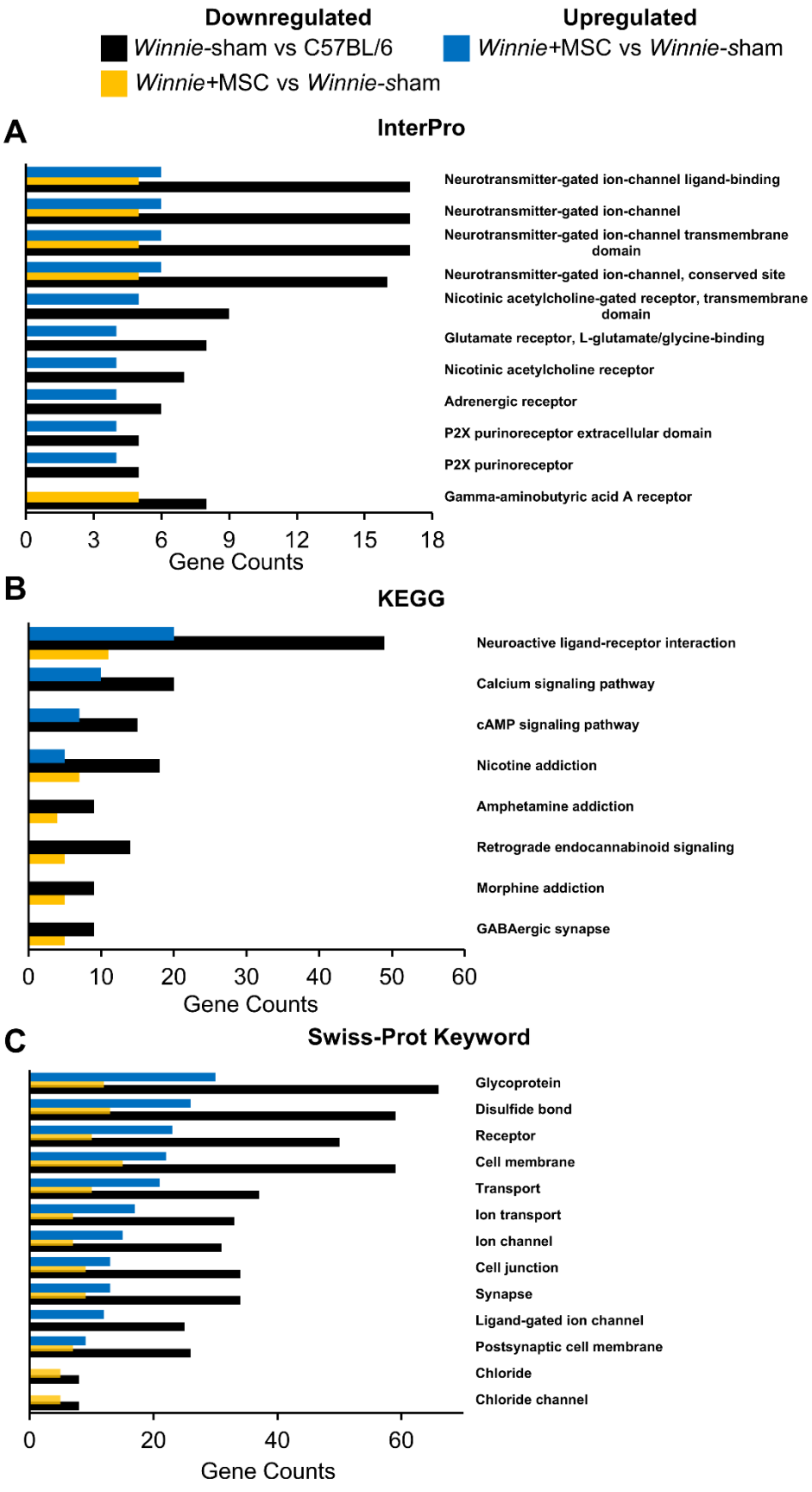
Downregulated
Winnie-sham vs C57BL/6
Winnie+MSC vs Winnie-sham
Upregulated
Winnie+MSC vs Winnie-sham
A
InterPro
Neurotransmitter-gated ion-channel ligand-binding
Neurotransmitter-gated ion-channel
Neurotransmitter-gated ion-channel transmembrane domain
Neurotransmitter-gated ion-channel, conserved site
Nicotinic acetylcholine-gated receptor, transmembrane domain
Glutamate receptor, L-glutamate/glycine-binding
Nicotinic acetylcholine receptor
Adrenergic receptor
P2X purinoreceptor extracellular domain
P2X purinoreceptor
Gamma-aminobutyric acid A receptor
0 3 6 9 12 15 18
Gene Counts
B
KEGG
Neuroactive ligand-receptor interaction
Calcium signaling pathway
cAMP signaling pathway
Nicotine addiction
Amphetamine addiction
Retrograde endocannabinoid signaling
Morphine addiction
GABAergic synapse
0 10 20 30 40 50 60
Gene Counts
C
Swiss-Prot Keyword
Glycoprotein
Disulfide bond
Receptor
Cell membrane
Transport
Ion transport
Ion channel
Cell junction
Synapse
Ligand-gated ion channel
Postsynaptic cell membrane
Chloride
Chloride channel
0 20 40 60
Gene Counts

Figure 4.6 ***Gene ontologies summarising the effects of BM-MSCs on the ENS in Winnie mice***

Bar charts representing the gene counts within up to ten terms from the GO databases for molecular function **(A)**, biological process **(B)** and cellular component **(C)**. Number of downregulated genes in *Winnie*-sham mice compared to C57BL/6 controls represented as black bars. Number of downregulated genes in BM-MSC-treated *Winnie* mice compared to *Winnie*-sham represented as yellow bars. Number of upregulated genes in *Winnie*-sham mice compared to C57BL/6 controls represented as grey bars. Number of upregulated genes in BM-MSC-treated *Winnie* mice compared to *Winnie*-sham represented as blue bars. Analysis performed using DAVID. Top ten terms ranked by *P* values with a cut off of $P<0.001$.

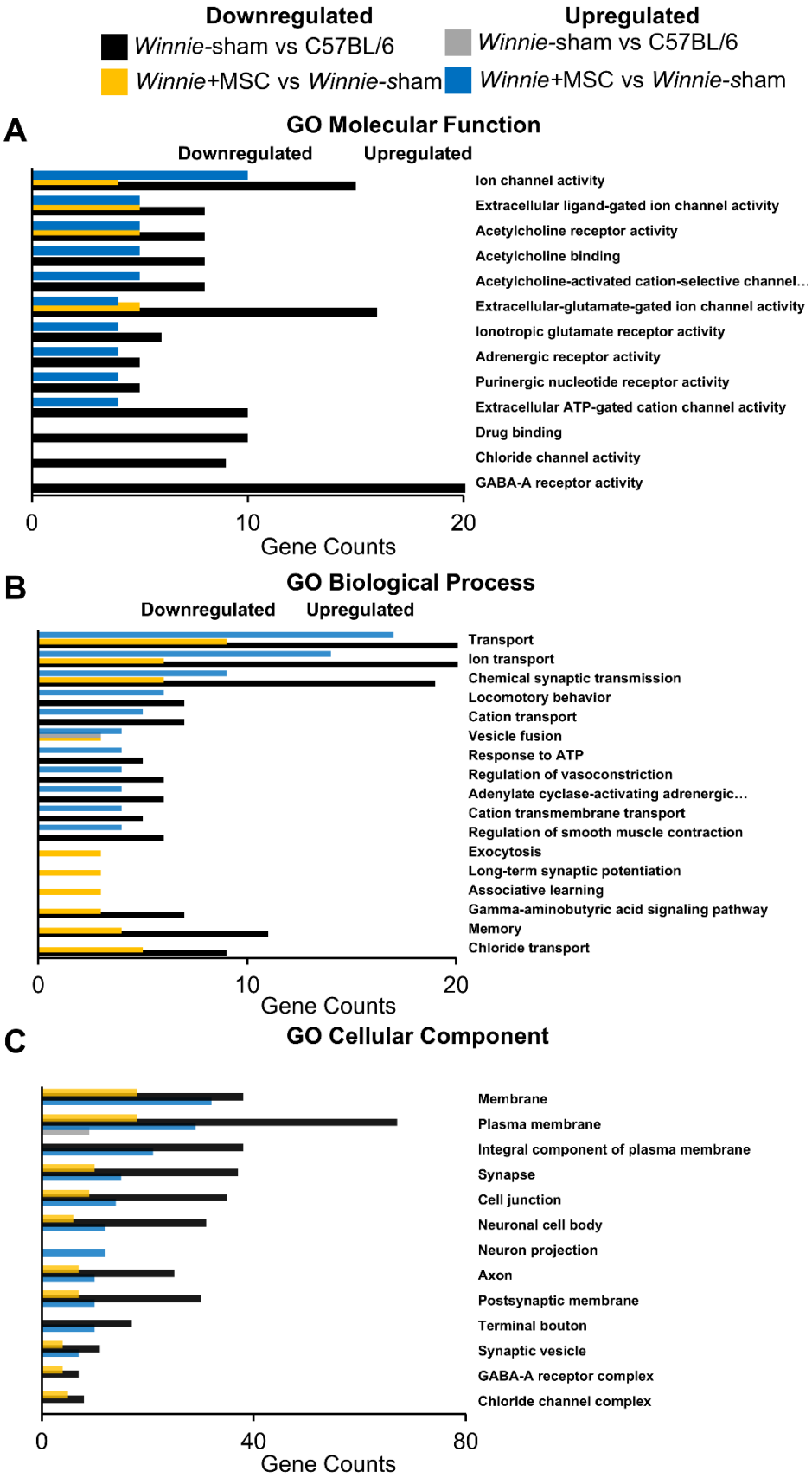
Downregulated
Winnie-sham vs C57BL/6
Winnie+MSC vs Winnie-sham
Upregulated
Winnie-sham vs C57BL/6
Winnie+MSC vs Winnie-sham
A
GO Molecular Function
Downregulated
Upregulated
Ion channel activity
Extracellular ligand-gated ion channel activity
Acetylcholine receptor activity
Acetylcholine binding
Acetylcholine-activated cation-selective channel...
Extracellular-glutamate-gated ion channel activity
Ionotropic glutamate receptor activity
Adrenergic receptor activity
Purinergic nucleotide receptor activity
Extracellular ATP-gated cation channel activity
Drug binding
Chloride channel activity
GABA-A receptor activity
0
10
20
Gene Counts
B
GO Biological Process
Downregulated
Upregulated
Transport
Ion transport
Chemical synaptic transmission
Locomotory behavior
Cation transport
Vesicle fusion
Response to ATP
Regulation of vasoconstriction
Adenylate cyclase-activating adrenergic...
Cation transmembrane transport
Regulation of smooth muscle contraction
Exocytosis
Long-term synaptic potentiation
Associative learning
Gamma-aminobutyric acid signaling pathway
Memory
Chloride transport
0
10
20
Gene Counts
C
GO Cellular Component
Membrane
Plasma membrane
Integral component of plasma membrane
Synapse
Cell junction
Neuronal cell body
Neuron projection
Axon
Postsynaptic membrane
Terminal bouton
Synaptic vesicle
GABA-A receptor complex
Chloride channel complex
0
40
80
Gene Counts

Table 4.4 ***Enriched terms from GO, KEGG, InterPro and Swiss-Prot keywords databases in ENS and neurotransmitter receptor associated genes altered by BM-MSCs in Winnie mice***

Upregulated GO biological process

Ref	Term	Fold Enrich.	Count	*P* Value	BH	Genes
GO:0006811	Ion transport	9.42	14	1.03E-09	3.96E-07	*Ano1, Grin1, Slc6a15, Gria4, P2rx6, P2rx1, Gria2, Grin2d, P2rx3, Chrnb4, Slc22a3, Htr3a, Chrna1, Chrna3*
GO:0007268	Chemical synaptic transmission	20.57	9	9.09E-09	1.75E-06	*Gria2, Slc6a12, P2rx3, Slc6a4, Grin1, Htr4, Slc18a3, Gria4, Chat*
GO:0006810	Transport	3.67	17	3.98E-06	5.10E-04	*Ramp2, Slc6a12, Ano1, Grin1, Slc6a4, Slc6a15, Gria4, P2rx6, Gria2, P2rx1, Grin2d, P2rx3, Chrnb4, Slc22a3, Htr3a, Chrna1, Chrna3*
GO:0006940	Regulation of smooth muscle contraction	120.95	4	4.05E-06	3.90E-04	*P2rx1, Chrnb4, Adra2b, Chrna3*
GO:0098655	Cation transmembrane transport	120.95	4	4.05E-06	3.90E-04	*P2rx6, P2rx1, P2rx3, Chrnb4*
GO:0007626	Locomotory behaviour	21.84	6	7.00E-06	5.38E-04	*Adra1b, Chrnb4, Npy1r, Nrg1, Elavl4, Chrna3*
GO:0071880	Adenylate cyclase-activating adrenergic receptor signalling pathway	82.76	4	1.36E-05	8.71E-04	*Adrb3, Adra1b, Adra1a, Adra2b*
GO:0019229	Regulation of vasoconstriction	78.62	4	1.59E-05	8.76E-04	*P2rx1, Adra1b, Adra1a, Adra2b*
GO:0033198	Response to ATP	78.62	4	1.59E-05	8.76E-04	*P2rx5, P2rx6, P2rx1, P2rx3*
GO:0006812	Cation transport	26.92	5	3.21E-05	0.001545	*Chrna9, P2rx3, Grin1, Ano1, Chrna1*
GO:0007274	Neuromuscular synaptic transmission	58.24	4	4.04E-05	0.001727	*Ntf3, P2rx3, Chrna1, Chat*
GO:0007271	Synaptic transmission, cholinergic	52.41	4	5.58E-05	0.002146	*Chrna9, Chrnb4, Chrna1, Chrna3*
GO:0051291	Protein heterodimerization	21.60	5	7.64E-05	0.00267	*Syt1, P2rx6, P2rx1, Chrnb4, Chrna3*
GO:0019228	Neuronal action potential	46.25	4	8.17E-05	0.002617	*P2rx5, P2rx1, P2rx3, Chrna1*
GO:0042391	Regulation of membrane potential	20.26	5	9.79E-05	0.002897	*Grin1, Ano1, Chrnb4, Chrna1, Chrna3*
GO:0007267	Cell-cell signalling	19.08	5	1.24E-04	0.003394	*Adrb3, Npy, Adra1b, Adra1a, Adra2b*
GO:0051260	Protein homo-oligomerization	11.97	6	1.25E-04	0.003206	*P2rx5, Syt1, P2rx6, P2rx1, P2rx3, Slc6a4*
GO:0032098	Regulation of appetite	147.41	3	1.68E-04	0.004034	*Npy, Htr4, Slc22a3*
GO:0006836	Neurotransmitter transport	34.94	4	1.90E-04	0.004293	*Slc6a12, Slc6a4, Slc6a15, Slc18a3*
GO:0006906	Vesicle fusion	32.09	4	2.45E-04	0.005226	*Syt1, Syt2, Syt13, Syt17*

GO:0008217	Regulation of blood pressure	25.36	4	4.92E-04	0.009914	*Ramp2, Npy, P2rx1, Npy1r*
GO:0019233	Sensory perception of pain	20.42	4	9.26E-04	0.017683	*Ndn, Uchl1, Grin1, Npy1r*

Downregulated GO biological process

Ref	Term	Fold Enrich.	Count	*P* Value	BH	Genes
GO:0007268	Chemical synaptic transmission	27.42	6	1.70E-06	5.21E-04	*Gabrd, Gabrg2, Grin2b, Npy2r, Tac1, Htr2a*
GO:0006821	Chloride transport	49.14	5	2.45E-06	3.75E-04	*Gabrr2, Gabrd, Gabrg2, Gabra1, Gabrp*
GO:0007613	Memory	37.89	4	1.35E-04	0.013706	*S100b, Grin2b, Th, Htr2a*
GO:0007214	Gamma-aminobutyric acid signalling pathway	94.34	3	4.17E-04	0.03149	*Gabrr2, Gabrg2, Gabra1*
GO:0006811	Ion transport	8.08	6	5.76E-04	0.034774	*Gabrr2, Gabrd, Gabrg2, Gabra1, Grin2b, Gabrp*
GO:0006810	Transport	3.88	9	9.16E-04	0.045812	*Gabrr2, Gabrd, Ramp3, Gabrg2, Stx1a, Gabra1, Grin2b, Stx11, Gabrp*
GO:0008306	Associative learning	63.74	3	9.17E-04	0.039443	*Adrb2, Grin2b, Tac1*

Upregulated GO molecular function

Ref	Term	Fold Enrich.	Count	P Value	BH	Genes
GO:0005216	Ion channel activity	21.83	10	5.18E-10	7.87E-08	*P2rx6, Gria2, P2rx1, P2rx3, Grin2d, Grin1, Chrnb4, Gria4, Chrna1, Chrna3*
GO:0004889	Acetylcholine-activated cation-selective channel activity	103.11	5	1.26E-07	9.57E-06	*Chrna9, Chrnb4, Htr3a, Chrna1, Chrna3*
GO:0042166	Acetylcholine binding	97.68	5	1.59E-07	8.07E-06	*Chrna9, Chrnb4, Slc18a3, Chrna1, Chrna3*
GO:0015464	Acetylcholine receptor activity	92.80	5	1.99E-07	7.55E-06	*Chrna9, Chrnb4, Htr3a, Chrna1, Chrna3*
GO:0004931	Extracellular ATP-gated cation channel activity	212.11	4	5.96E-07	1.81E-05	*P2rx5, P2rx6, P2rx1, P2rx3*
GO:0001614	Purinergic nucleotide receptor activity	185.60	4	9.52E-07	2.41E-05	*P2rx5, P2rx6, P2rx1, P2rx3*
GO:0004935	Adrenergic receptor activity	148.48	4	2.03E-06	4.41E-05	*Adrb3, Adra1b, Adra1a, Adra2b*
GO:0005230	Extracellular ligand-gated ion channel activity	45.27	5	3.99E-06	7.58E-05	*Gabre, Chrnb4, Htr3a, Chrna1, Chrna3*
GO:0004970	Ionotropic glutamate receptor activity	82.49	4	1.36E-05	2.30E-04	*Gria2, Grin2d, Grin1, Gria4*
GO:0005234	Extracellular-glutamate-gated ion channel activity	82.49	4	1.36E-05	2.30E-04	*Gria2, Grin2d, Grin1, Gria4*
GO:0030276	Clathrin binding	32.28	4	2.41E-04	0.00365	*Syt1, Syt2, Syt13, Syt17*

Downregulated GO molecular function

Ref	Term	Fold Enrich.	Count	*P* Value	BH	Genes
GO:0004890	GABA-A receptor activity	208.68	5	5.94E-09	5.41E-07	*Gabrr2, Gabrd, Gabrg2, Gabra1, Gabrp*
GO:0005230	Extracellular ligand-gated ion channel activity	96.71	5	1.53E-07	6.94E-06	*Gabrr2, Gabrd, Gabrg2, Gabra1, Gabrp*
GO:0005254	Chloride channel activity	62.94	5	8.82E-07	2.68E-05	*Gabrr2, Gabrd, Gabrg2, Gabra1, Gabrp*
GO:0008144	Drug binding	28.32	4	3.15E-04	0.007139	*Adrb2, Gabra1, Grin2b, Htr2a*

Upregulated GO cellular component

Ref	Term	Fold Enrich.	Count	*P* Value	BH	Genes
GO:0005887	Integral component of plasma membrane	8.15	21	5.76E-14	6.11E-12	*Gabre, Slc6a12, Slc6a4, Grin1, Htr4, Slc6a15, Npy1r, P2rx5, Adrb3, P2rx6, Gria2, P2rx1, Chrna9, P2rx3, Adra1b, Syt13, Slc18a3, Slc22a3, Adra1a, Adra2b, Nrg1*
GO:0045202	Synapse	12.98	15	2.58E-12	1.37E-10	*Syt1, Gabre, Syt2, Grin1, Gria4, Calb2, Gria2, Grin2d, Syn2, Chrnb4, Syt13, Htr3a, Nrg1, Chrna1, Chrna3*
GO:0043195	Terminal bouton	38.67	10	2.96E-12	1.05E-10	*Syt1, Gria2, Npy, Syt2, P2rx3, Syn2, Grin1, Slc18a3, Gria4, Calb2*
GO:0045211	Postsynaptic membrane	19.68	10	1.28E-09	3.38E-08	*Gria2, Chrna9, P2rx1, Grin2d, Grin1, Chrnb4, Gria4, Htr3a, Chrna1, Chrna3*
GO:0043005	Neuron projection	12.48	12	1.51E-09	3.20E-08	*Syt1, Gria2, Npy, P2rx1, Slc6a12, P2rx3, Slc6a4, Map2, Chrnb4, Slc18a3, Calb2, Chat*
GO:0030054	Cell junction	8.52	14	3.36E-09	5.94E-08	*Syt1, Gabre, Syt2, Grin1, Gria4, P2rx6, Chrna9, Gria2, Grin2d, Syn2, Chrnb4, Htr3a, Chrna1, Chrna3*
GO:0043025	Neuronal cell body	9.82	12	1.82E-08	2.76E-07	*P2rx6, Gria2, P2rx3, Uchl1, Map2, Grin1, Gfra1, Gria4, Htr3a, Elavl4, Chrna3, Chat*
GO:0005886	Plasma membrane	2.60	29	5.60E-08	7.42E-07	*Syt1, Syt2, Ano1, Uchl1, Slc6a4, Adrb3, P2ry4, Grin2d, Syn2, Adra2b, Htr3a, Chrna1, Nrg1, Chrna3, Ramp2, Grin1, Htr4, Ntng1, Gria4, Npy1r, P2rx5, Gria2, P2rx1, Adra1b, Chrnb4, Adra1a, Gfra1, Neu3, Syt17*
GO:0030424	Axon	11.81	10	1.06E-07	1.25E-06	*Syt1, Syt2, P2rx3, Uchl1, Slc18a3, Gfra1, Npy1r, Htr3a, Nrg1, Chat*
GO:0008021	Synaptic vesicle	24.27	7	3.55E-07	3.77E-06	*Syt1, Gria2, Syt2, Syn2, Grin1, Slc18a3, Npy1r*
GO:0016020	Membrane	2.00	32	2.63E-06	2.53E-05	*Syt1, Syt2, Slc6a4, Ano1, Uchl1, Adrb3, P2ry4, Grin2d, Slc22a3, Htr3a, Chrna1, Chrna3, Ramp2, Slc6a12, Grin1, Htr4, Ntng1, Slc6a15, Gria4, Npy1r, Elavl4, P2rx6, Gria2, P2rx1, P2rx3, Adra1b, Chrnb4, Syt13, Adra1a, Gfra1, Neu3, Syt17*
GO:0005639	Integral component of nuclear inner membrane	116.52	4	4.67E-06	4.12E-05	*P2rx5, P2rx6, P2rx1, P2rx3*
GO:0005892	Acetylcholine -gated channel complex	102.81	4	6.96E-06	5.67E-05	*Chrna9, Chrnb4, Chrna1, Chrna3*
GO:0016021	Integral component of membrane	1.97	31	7.32E-06	5.55E-05	*Syt1, Syt2, Ano1, Slc6a4, Adrb3, P2ry4, Grin2d, Slc22a3, Adra2b, Htr3a, Chrna1, Nrg1, Chrna3, Ramp2, Ntf3, Slc6a12, Grin1, Htr4, Slc6a15, Gria4, Npy1r, P2rx6, Gria2,*

						P2rx1, P2rx3, Adra1b, Chrnb4, Syt13, Adra1a, Gfra1, Slc18a3
GO:0030672	Synaptic vesicle membrane	35.81	5	1.04E-05	7.33E-05	*Syt1, Gria2, Syt2, Syn2, Slc18a3*
GO:0014069	Postsynaptic density	12.80	7	1.45E-05	9.63E-05	*P2rx6, Gria2, Syn2, Map2, Grin1, Gria4, Chrna3*
GO:0030425	Dendrite	6.24	7	7.34E-04	0.0045 7	*Gria2, Map2, Grin1, Gria4, Nrg1, Elavl4, Chrna3*

Downregulated GO cellular component

Ref	Term	Fold Enrich.	Count	*P* Value	BH	Genes
GO:0045202	Synapse	16.93	10	1.67E-09	1.22E-07	*Gabrr2, Gabrd, Gabrg2, Stx1a, Gabra1, Grin2b, Syt12, Syt8, Grin3a, Gabrp*
GO:0045211	Postsynaptic membrane	26.96	7	1.24E-07	4.53E-06	*Gabrr2, Gabrd, Gabrg2, Gabra1, Grin2b, Grin3a, Gabrp*
GO:0034707	Chloride channel complex	92.92	5	1.86E-07	4.52E-06	*Gabrr2, Gabrd, Gabrg2, Gabra1, Gabrp*
GO:0005886	Plasma membrane	3.16	18	3.45E-07	6.29E-06	*Gabrd, Ramp3, Gabrg2, Stx1a, Ret, Gabra1, Npy2r, Syt12, Syt8, Tac1, Npy6r, Gabrr2, Adrb2, Grin2b, Syt16, Stx11, Gabrp, Htr2a*
GO:0030054	Cell junction	10.72	9	6.17E-07	9.01E-06	*Gabrr2, Gabrd, Gabrg2, Stx1a, Gabra1, Grin2b, Syt12, Grin3a, Gabrp*
GO:1902711	GABA-A receptor complex	189.97	4	9.81E-07	1.19E-05	*Gabrr2, Gabrd, Gabrg2, Gabra1*
GO:0030424	Axon	16.17	7	2.47E-06	2.57E-05	*Gabrr2, Gabrg2, Ret, Adrb2, Th, Tac1, Htr2a*
GO:0016021	Integral component of membrane	2.24	18	6.23E-05	5.68E-04	*Gabrd, Ramp3, Gabrg2, Stx1a, Ret, Gabra1, Npy2r, Syt12, Syt8, Npy6r, Gabrr2, Adrb2, Grin2b, Grina, Syt16, Stx11, Gabrp, Htr2a*
GO:0016020	Membrane	2.20	18	8.01E-05	6.49E-04	*Gabrd, Ramp3, Gabrg2, Stx1a, Ret, Gabra1, Npy2r, Syt12, Syt8, Npy6r, Grin3a, Gabrr2, Adrb2, Grin2b, Grina, Stx11, Gabrp, Htr2a*
GO:0043025	Neuronal cell body	9.61	6	2.60E-04	0.0018 99	*Ret, S100b, Th, Tac1, Grin3a, Htr2a*
GO:0008021	Synaptic vesicle	27.14	4	3.62E-04	0.0024	*Stx1a, Grin2b, Th, Stx11*

Upregulated KEGG pathways

Ref	Term	Fold Enrich.	Count	*P* Value	BH	Genes
mmu04080	Neuroactive ligand-receptor interaction	16.42	20	7.29E-20	3.13E-18	*Gabre, Grin1, Htr4, Gria4, Npy1r, P2rx5, Adrb3, P2rx6, Gria2, P2ry4, P2rx1, Chrna9, P2rx3, Grin2d, Adra1b, Chrnb4, Adra1a, Adra2b, Chrna1, Chrna3*
mmu04020	Calcium signalling pathway	13.00	10	2.95E-08	6.34E-07	*P2rx5, Adrb3, P2rx6, P2rx1, P2rx3, Grin2d, Grin1, Htr4, Adra1b, Adra1a*
mmu05033	Nicotine addiction	29.24	5	2.00E-05	2.87E-04	*Gabre, Gria2, Grin2d, Grin1, Gria4*
mmu04024	cAMP signalling pathway	8.31	7	1.33E-04	0.0014 31	*Gria2, Npy, Grin2d, Grin1, Htr4, Gria4, Npy1r*

Downregulated KEGG pathways

Ref	Term	Fold Enrich.	Count	*P* Value	BH	Genes
mmu04080	Neuroactive ligand-	18.62	11	1.03E-11	4.11E-10	*Gabrr2, Gabrd, Gabrg2, Adrb2, Gabra1, Grin2b, Npy2r, Npy6r, Grin3a, Gabrp, Htr2a*

	receptor interaction					
mmu05033	Nicotine addiction	84.44	7	6.33E-11	1.27E-09	*Gabrr2, Gabrd, Gabrg2, Gabra1, Grin2b, Grin3a, Gabrp*
mmu04727	GABAergic synapse	27.73	5	1.87E-05	2.49E-04	*Gabrr2, Gabrd, Gabrg2, Gabra1, Gabrp*
mmu05032	Morphine addiction	25.94	5	2.43E-05	2.43E-04	*Gabrr2, Gabrd, Gabrg2, Gabra1, Gabrp*
mmu04723	Retrograde endocannabinoid signalling	23.42	5	3.64E-05	2.91E-04	*Gabrr2, Gabrd, Gabrg2, Gabra1, Gabrp*
mmu05031	Amphetamine addiction	28.81	4	2.64E-04	0.001758	*Stx1a, Grin2b, Th, Grin3a*

Upregulated InterPro

Ref	Term	Fold Enrich.	Count	*P* Value	BH	Genes
IPR018000	Neurotransmitter-gated ion-channel, conserved site	64.12	6	3.14E-08	2.98E-06	*Gabre, Chrna9, Chrnb4, Htr3a, Chrna1, Chrna3*
IPR006029	Neurotransmitter-gated ion-channel transmembrane domain	62.60	6	3.55E-08	1.69E-06	*Gabre, Chrna9, Chrnb4, Htr3a, Chrna1, Chrna3*
IPR006201	Neurotransmitter-gated ion-channel	62.60	6	3.55E-08	1.69E-06	*Gabre, Chrna9, Chrnb4, Htr3a, Chrna1, Chrna3*
IPR006202	Neurotransmitter-gated ion-channel ligand-binding	62.60	6	3.55E-08	1.69E-06	*Gabre, Chrna9, Chrnb4, Htr3a, Chrna1, Chrna3*
IPR027361	Nicotinic acetylcholine-gated receptor, transmembrane domain	121.71	5	6.51E-08	2.06E-06	*Chrna9, Chrnb4, Htr3a, Chrna1, Chrna3*
IPR001429	P2X purinoreceptor	250.38	4	3.63E-07	8.62E-06	*P2rx5, P2rx6, P2rx1, P2rx3*
IPR027309	P2X purinoreceptor extracellular domain	250.38	4	3.63E-07	8.62E-06	*P2rx5, P2rx6, P2rx1, P2rx3*
IPR002233	Adrenergic receptor	194.74	4	8.68E-07	1.65E-05	*Adrb3, Adra1b, Adra1a, Adra2b*
IPR002394	Nicotinic acetylcholine receptor	109.54	4	5.72E-06	9.06E-05	*Chrna9, Chrnb4, Chrna1, Chrna3*
IPR019594	Glutamate receptor, L-glutamate/glycine-binding	97.37	4	8.31E-06	1.13E-04	*Gria2, Grin2d, Grin1, Gria4*
IPR001508	NMDA receptor	97.37	4	8.31E-06	1.13E-04	*Gria2, Grin2d, Grin1, Gria4*
IPR001320	Ionotropic glutamate receptor	97.37	4	8.31E-06	1.13E-04	*Gria2, Grin2d, Grin1, Gria4*
IPR006548	Splicing factor ELAV/HuD	328.63	3	2.92E-05	3.47E-04	*Elavl2, Elavl3, Elavl4*
IPR002343	Paraneoplastic encephalomyelitis antigen	164.31	3	1.36E-04	0.001429	*Elavl2, Elavl3, Elavl4*
IPR001565	Synaptotagmin	73.03	3	7.30E-04	0.006913	*Syt1, Syt2, Syt17*
IPR000175	Sodium	65.73	3	9.04E-04	0.00778	*Slc6a12, Slc6a4, Slc6a15*

Downregulated InterPro

Ref	Term	Fold Enrich.	Count	*P* Value	BH	Genes
IPR006028	Gamma-aminobutyric acid A receptor	194.65	5	8.53E-09	5.37E-07	*Gabrr2, Gabrd, Gabrg2, Gabra1, Gabrp*
IPR018000	Neurotransmitter-gated ion-channel, conserved site	109.19	5	9.63E-08	3.03E-06	*Gabrr2, Gabrd, Gabrg2, Gabra1, Gabrp*
IPR006201	Neurotransmitter-gated ion-channel	106.59	5	1.06E-07	2.23E-06	*Gabrr2, Gabrd, Gabrg2, Gabra1, Gabrp*
IPR006029	Neurotransmitter-gated ion-channel transmembrane domain	106.59	5	1.06E-07	2.23E-06	*Gabrr2, Gabrd, Gabrg2, Gabra1, Gabrp*
IPR006202	Neurotransmitter-gated ion-channel ligand-binding	106.59	5	1.06E-07	2.23E-06	*Gabrr2, Gabrd, Gabrg2, Gabra1, Gabrp*

Upregulated Keywords

Ref	Term	Fold Enrich.	Count	*P* Value	BH	Genes
KEYWORD	Ligand-gated ion channel	79.32	12	2.11E-18	1.52E-16	*P2rx6, Gria2, Chrna9, P2rx1, P2rx3, Grin2d, Grin1, Chrnb4, Gria4, Htr3a, Chrna1, Chrna3*
KEYWORD	Ion channel	21.54	15	2.95E-15	1.08E-13	*Gabre, Ano1, Grin1, Gria4, P2rx5, P2rx6, Gria2, P2rx1, Chrna9, Grin2d, P2rx3, Chrnb4, Htr3a, Chrna1, Chrna3*
KEYWORD	Ion transport	13.25	17	3.64E-14	8.74E-13	*Gabre, Ano1, Grin1, Slc6a15, Gria4, P2rx5, P2rx6, Gria2, P2rx1, Chrna9, P2rx3, Grin2d, Chrnb4, Slc22a3, Htr3a, Chrna1, Chrna3*
KEYWORD	Glycoprotein	3.79	30	2.85E-12	5.13E-11	*Syt1, Syt2, Ano1, Uchl1, Slc6a4, Adrb3, P2ry4, Grin2d, Slc22a3, Htr3a, Chrna1, Chrna3, Ramp2, Ntf3, Slc6a12, Grin1, Htr4, Ntng1, Slc6a15, Gria4, Npy1r, P2rx6, Gria2, P2rx1, P2rx3, Adra1b, Chrnb4, Adra1a, Gfra1, Slc18a3*
KEYWORD	Synapse	17.57	13	4.63E-12	6.67E-11	*Gabre, Syt1, Gria2, Chrna9, Grin2d, Syt2, Syn2, Grin1, Chrnb4, Gria4, Htr3a, Chrna1, Chrna3*
KEYWORD	Disulphide bond	4.02	26	9.97E-11	1.20E-09	*Slc6a4, Adrb3, P2ry4, Chrna9, Grin2d, Adra2b, Htr3a, Chrna1, Chrna3, Ramp2, Gabre, Ntf3, Slc6a12, Grin1, Ntng1, Htr4, Gria4, Npy1r, P2rx6, P2rx1, Gria2, P2rx3, Chrnb4, Adra1b, Adra1a, Gfra1*
KEYWORD	Transport	5.33	21	1.77E-10	1.82E-09	*Ramp2, Gabre, Slc6a12, Slc6a4, Ano1, Grin1, Slc6a15, Gria4, P2rx5, P2rx6, Gria2, P2rx1, Chrna9, P2rx3, Grin2d, Chrnb4, Slc18a3, Slc22a3, Htr3a, Chrna1, Chrna3*
KEYWORD	Receptor	4.25	23	1.03E-09	9.24E-09	*Ramp2, Gabre, Grin1, Htr4, Gria4, Npy1r, P2rx5, Adrb3, P2rx6, Gria2, Chrna9, P2ry4, P2rx1, P2rx3, Grin2d, Adra1b, Chrnb4, Adra1a, Gfra1, Adra2b, Htr3a, Chrna1, Chrna3*
KEYWORD	Postsynaptic cell membrane	24.68	9	2.27E-09	1.82E-08	*Gria2, Chrna9, Grin2d, Grin1, Chrnb4, Gria4, Htr3a, Chrna1, Chrna3*
KEYWORD	Cell junction	9.49	13	5.34E-09	3.85E-08	*Gabre, Syt1, Gria2, Chrna9, Grin2d, Syt2, Syn2, Grin1, Chrnb4, Gria4, Htr3a, Chrna1, Chrna3*
KEYWORD	Membrane	2.11	38	6.03E-09	3.94E-08	*Syt1, Syt2, Slc6a4, Ano1, Uchl1, Adrb3, Chrna9, P2ry4, Grin2d,*

						Slc22a3, Adra2b, Htr3a, Chrna1, Nrg1, Chrna3, Gabre, Ramp2, Ntf3, Slc6a12, Grin1, Htr4, Ntng1, Slc6a15, Gria4, Npy1r, P2rx5, P2rx6, Gria2, P2rx1, P2rx3, Adra1b, Chrnb4, Syt13, Slc18a3, Adra1a, Gfra1, Neu3, Syt17
KEYWORD	Transmembrane helix	2.36	34	1.08E-08	6.48E-08	*Syt1, Syt2, Slc6a4, Ano1, Adrb3, Chrna9, P2ry4, Grin2d, Slc22a3, Adra2b, Htr3a, Chrna1, Nrg1, Chrna3, Ramp2, Gabre, Ntf3, Slc6a12, Grin1, Htr4, Slc6a15, Gria4, Npy1r, P2rx5, P2rx6, Gria2, P2rx1, P2rx3, Adra1b, Chrnb4, Syt13, Slc18a3, Adra1a, Gfra1*
KEYWORD	Transmembrane	2.36	34	1.15E-08	6.40E-08	*Syt1, Syt2, Slc6a4, Ano1, Adrb3, Chrna9, P2ry4, Grin2d, Slc22a3, Adra2b, Htr3a, Chrna1, Nrg1, Chrna3, Ramp2, Gabre, Ntf3, Slc6a12, Grin1, Htr4, Slc6a15, Gria4, Npy1r, P2rx5, P2rx6, Gria2, P2rx1, P2rx3, Adra1b, Chrnb4, Syt13, Slc18a3, Adra1a, Gfra1*
KEYWORD	Palmitate	14.29	9	1.59E-07	8.19E-07	*Adrb3, Syt1, Gria2, Htr4, Adra1b, Adra1a, Gria4, Adra2b, Npy1r*
KEYWORD	Lipoprotein	7.42	12	3.30E-07	1.58E-06	*Adrb3, Syt1, Gria2, Uchl1, Htr4, Ntng1, Adra1b, Gfra1, Adra1a, Gria4, Adra2b, Npy1r*
KEYWORD	Cell membrane	2.82	22	3.79E-06	1.71E-05	*Gabre, Slc6a4, Grin1, Ano1, Htr4, Ntng1, Gria4, Npy1r, Adrb3, Gria2, P2ry4, Chrna9, Grin2d, Adra1b, Chrnb4, Gfra1, Adra1a, Adra2b, Htr3a, Chrna1, Neu3, Chrna3*
KEYWORD	Neurotransmitter transport	52.17	4	5.78E-05	2.45E-04	*Slc6a12, Slc6a4, Slc6a15, Slc18a3*

Downregulated Keywords

Ref	Term	Fold Enrich.	Count	*P* Value	BH	Genes
KEYWORD	Synapse	24.86	9	9.20E-10	5.70E-08	*Gabrr2, Gabrd, Gabrg2, Stx1a, Gabra1, Grin2b, Syt12, Grin3a, Gabrp*
KEYWORD	Postsynaptic cell membrane	39.22	7	1.35E-08	4.18E-07	*Gabrr2, Gabrd, Gabrg2, Gabra1, Grin2b, Grin3a, Gabrp*
KEYWORD	Chloride channel	107.18	5	1.05E-07	2.18E-06	*Gabrr2, Gabrd, Gabrg2, Gabra1, Gabrp*
KEYWORD	Cell junction	13.43	9	1.11E-07	1.72E-06	*Gabrr2, Gabrd, Gabrg2, Stx1a, Gabra1, Grin2b, Syt12, Grin3a, Gabrp*
KEYWORD	Chloride	73.59	5	4.89E-07	6.06E-06	*Gabrr2, Gabrd, Gabrg2, Gabra1, Gabrp*
KEYWORD	Ion channel	20.54	7	6.18E-07	6.38E-06	*Gabrr2, Gabrd, Gabrg2, Gabra1, Grin2b, Grin3a, Gabrp*
KEYWORD	Cell membrane	3.93	15	9.73E-07	8.61E-06	*Ramp3, Gabrd, Gabrg2, Stx1a, Ret, Gabra1, Npy2r, Syt8, Npy6r, Grin3a, Gabrr2, Adrb2, Grin2b, Gabrp, Htr2a*
KEYWORD	Disulphide bond	4.10	13	7.68E-06	5.95E-05	*Gabrr2, Gabrd, Ramp3, Gabrg2, Calcb, Ret, Adrb2, Gabra1, Grin2b, Npy2r, Npy6r, Htr2a, Gabrp*
KEYWORD	Ion transport	11.15	7	2.07E-05	1.43E-04	*Gabrr2, Gabrd, Gabrg2, Gabra1, Grin2b, Grin3a, Gabrp*
KEYWORD	Transport	5.19	10	3.64E-05	2.25E-04	*Gabrr2, Gabrd, Ramp3, Gabrg2, Stx1a, Gabra1, Grin2b, Grin3a, Stx11, Gabrp*
KEYWORD	Transmembrane helix	2.42	17	5.72E-05	3.23E-04	*Gabrd, Ramp3, Gabrg2, Stx1a, Ret, Gabra1, Npy2r, Syt12, Syt8, Npy6r, Grin3a, Gabrr2, Adrb2, Grin2b, Grina, Gabrp, Htr2a*
KEYWORD	Transmembrane	2.41	17	5.92E-05	3.06E-04	*Gabrd, Ramp3, Gabrg2, Stx1a, Ret, Gabra1, Npy2r, Syt12, Syt8, Npy6r, Grin3a, Gabrr2, Adrb2, Grin2b, Grina, Gabrp, Htr2a*
KEYWORD	Membrane	2.04	18	2.29E-04	0.00109	*Gabrd, Ramp3, Gabrg2, Stx1a, Ret, Gabra1, Npy2r, Syt12, Syt8, Npy6r,*

						Grin3a, Gabrr2, Adrb2, Grin2b, Grina, Stx11, Gabrp, Htr2a
KEYWORD	Glycoprotein	3.10	12	3.43E-04	0.001519	*Gabrr2, Gabrd, Ramp3, Gabrg2, Ret, Adrb2, Gabra1, Grin2b, Npy2r, Npy6r, Gabrp, Htr2a*
KEYWORD	Receptor	3.77	10	4.30E-04	0.001776	*Gabrd, Ramp3, Ret, Adrb2, Gabra1, Grin2b, Npy2r, Npy6r, Grin3a, Htr2a*

Databases used: GO, gene ontology; KEGG, Kyoto Encyclopedia of Genes and Genomes; InterPro, protein families and Swiss-Prot, keywords; Ref, database identifier; Fold enrich., enrichment scores; BH, Benjamini-Hochberg value.

Similar results were observed between InterPro protein families and GO molecular functions for enriched terms in genes downregulated between *Winnie*-sham and C57BL/6 mice, as well as those upregulated between BM-MSC and sham-treated *Winnie* mice, this included: *purinergic nucleotide receptor activity, adrenergic receptor activity, ionotropic glutamate receptor activity* and *acetylcholine binding* (**Figure 4.6A**). Likewise, in genes downregulated in *Winnie*-sham compared to C57BL/6 mice and those upregulated by BM-MSCs in *Winnie* mice, the GO biological processes *chemical synaptic transmission* and *response to ATP* were enriched, as well as important neurally-controlled processes in colitis (*regulation of smooth muscle contraction* and *regulation of vasoconstriction*) (**Figure 4.6B**). Analysis of the GO cellular component also demonstrated that the machinery of chemical signalling such as the *synaptic vesicle*, *terminal bouton, postsynaptic membrane, cell junction* and *synapse* was downregulated in *Winnie*-sham compared to C57BL/6 mice and upregulated by BM-MSCs in *Winnie* mice (**Figure 4.6C**). Genes downregulated in *Winnie*-sham compared to C57BL/6 mice were also associated with the structure of the nervous system, which conversely were enriched in genes upregulated by BM-MSC treatments in *Winnie* mice. This included the cellular components of *axon, neuron projection and neuronal cell body*.

4.6.2. BM-MSCs restore myenteric neuronal density

Transcriptome analysis revealed that the neuronal markers *Elavl2*, *Elavl3*, *Elavl4* and *Uchl1* were downregulated in *Winnie* mice compared to C57BL/6 controls except for *Mapt2* (MAP-2) which was unchanged between sham-treated Winnie mice and C57BL/6 mice. Therefore, we investigated MAP-2 expression on the protein level in wholemount LMMP preparations of the distal colon. All neuronal markers were upregulated in *Winnie* mice after MSC treatment compared to sham-treated *Winnie* mice. The size of the myenteric ganglia was assessed to determine if gross structure to the ganglia could explain the alterations in the expression of ENS-associated genes.

Figure 4.7 ***Size of myenteric ganglia in C57BL/6, BM-MSC and sham-treated Winnie mice***

A-C) Myenteric ganglia were observed by immunofluorescence using the neuronal marker MAP-2 in LMMP wholemount preparations from the distal colon of C57BL/6 mice **(A)**, sham-treated *Winnie* mice **(B)** and *Winnie* mice treated with BM-MSCs **(C)** (scale bar = 50µm). **D)** Quantitative analysis of ganglia size. **P*<0.05; C57BL/6: n=7 animals, *Winnie*-sham: n=8 animals, *Winnie*+MSC: n=5 animals.

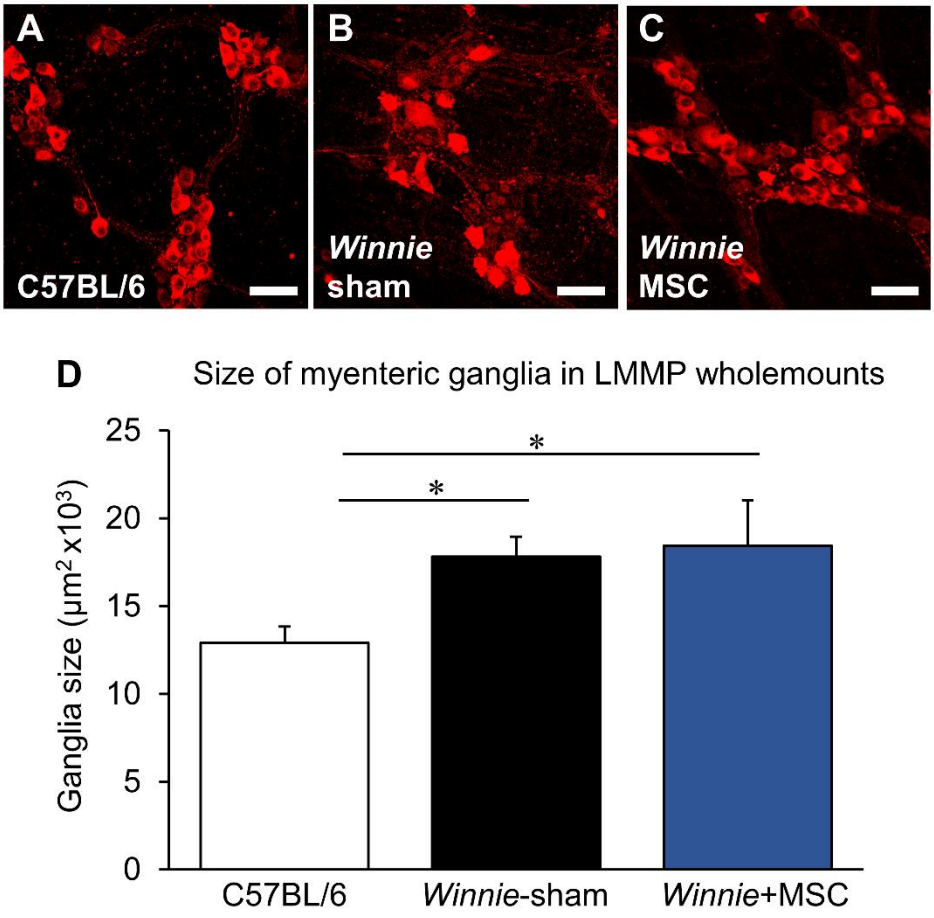
A
C57BL/6
B
Winnie
sham
C
Winnie
MSC
D
Size of myenteric ganglia in LMMP wholemounts
Ganglia size (µm² x10³)
25
20
15
10
5
0
*
*
C57BL/6
Winnie-sham
Winnie+MSC

Despite gene expression data indicating that the majority of ENS-associated genes were downregulated between *Winnie*-sham and C57BL/6 mice, the size of myenteric ganglia was larger in *Winnie*-sham mice (17804.0±1138.0μm^2, n=8 animals) compared to those in C57BL/6 controls (12911.9±923.6μm^2, $P<0.05$, n=7 animals) (**Figure 4.7A-D**). Likewise, the myenteric ganglia in C57BL/6 controls were smaller than BM-MSC-treated *Winnie* mice (18442.6±2566.9μm^2, $P<0.05$, n=5 animals). Furthermore, there was no difference in the size of the ganglia between sham and BM-MSC-treated *Winnie* mice. Enumeration of the neuronal density within the ganglia revealed neuronal loss in *Winnie*-sham mice (16.9±0.7 neurons/area, n=8 animals) compared to C57BL/6 mice (22.5±0.7 neurons/area, $P<0.01$, n=6 animals) (**Figure 4.8A-D**). Treatment with BM-MSCs corrected the decline in neuronal density (23.7±1.5 neurons/area, $P<0.01$, n=5 animals) in *Winnie* mice to similar levels observed in C57BL/6 mice (**Figure 4.8A-D**). Likewise, in cross sections of the distal colon, a significant reduction in myenteric neurons was observed in *Winnie*-sham mice (13.8±0.8 neurons/area) compared to C57BL/6 mice (23.0±2.0 neurons/area) which was restored in *Winnie* mice treated with BM-MSCs to control levels (23.4±2.4 neurons/area, $P<0.01$ for both) (**Figure 4.9A-D**; n=5 animals/group). Together, these data suggest that changes to neuronal density, and not the size of myenteric ganglia, may account for the increase in the expression of ENS-specific genes after BM-MSC treatment.

4.6.3. BM-MSCs reduce plexitis in the myenteric ganglia

Plexitis has been associated with the severity of IBD. Using the marker CD45, leukocytes were visualised in LMMP wholemount preparations (**Figure 4.10A-C**). Leukocytes could be observed in proximity to the myenteric ganglia using the pan-neuronal marker MAP-2. The majority of leukocytes lined the edges of the myenteric ganglia (ganglia periphery) in C57BL/6 and *Winnie* mice.

Figure 4.8 ***Effects of BM-MSC treatments on myenteric neuronal counts in wholemount LMMP preparations from the distal colon of Winnie mice***

A-C) Neurons within the myenteric ganglia were observed by immunofluorescence using the neuronal marker MAP-2 in fresh fixed LMMP wholemount preparations from the distal colon of C57BL/6 mice **(A)**, sham-treated *Winnie* mice **(B)** and *Winnie* mice treated with BM-MSCs **(C)** (scale bar = 50µm). **D)** Quantitative analysis of myenteric neuronal density within the ganglia expressed per ganglionated area. $^{**}P<0.01$; C57BL/6: n=6 animals, *Winnie*-sham: n=8 animals, *Winnie*+MSC: n=5 animals.

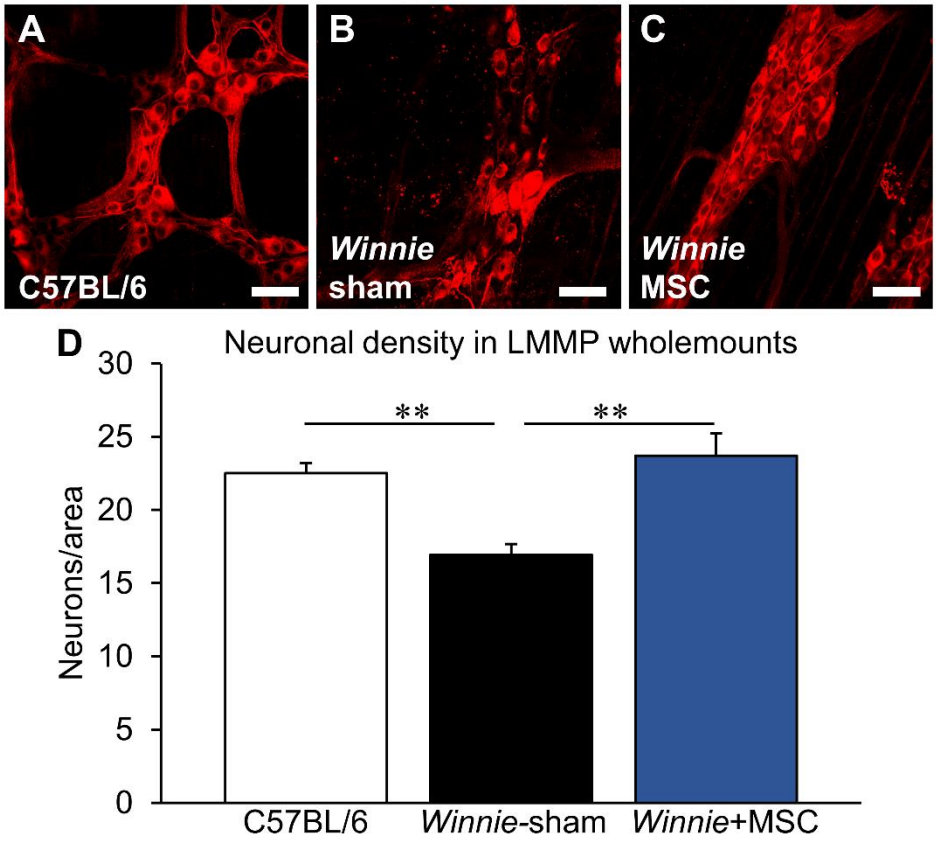
A
C57BL/6
B
Winnie
sham
C
Winnie
MSC
D
Neuronal density in LMMP wholemounts
Neurons/area
30
25
20
15
10
5
0
**
**
C57BL/6
Winnie-sham
Winnie+MSC

Figure 4.9 ***Effects of BM-MSC treatments on myenteric neurons in cross sections of distal colon from Winnie mice***

A-C′′) Neurons within the myenteric ganglia were observed by immunofluorescence using the neuronal marker MAP-2 **(A-C)** and the nuclear marker DAPI **(A′-C′)** in cross sections from the distal colon of C57BL/6 mice **(A-A′′)**, sham-treated *Winnie* mice **(B-B′′)** and *Winnie* mice treated with BM-MSCs **(C-C′′)** (scale bar = 50µm). **D)** Quantification of myenteric neurons per area in colonic cross sections. ***P*<0.01; n=5 animals/group.

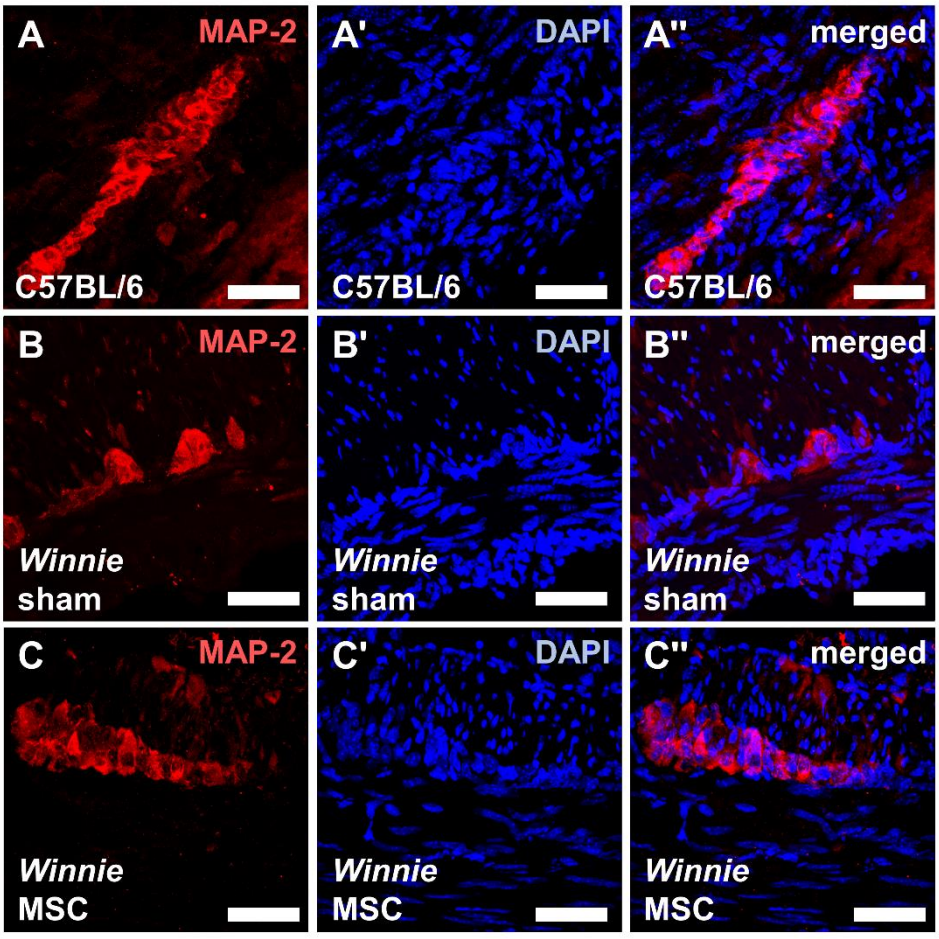
A
MAP-2
C57BL/6
A'
DAPI
C57BL/6
A''
merged
C57BL/6
B
MAP-2
Winnie
sham
B'
DAPI
Winnie
sham
B''
merged
Winnie
sham
C
MAP-2
Winnie
MSC
C'
DAPI
Winnie
MSC
C''
merged
Winnie
MSC

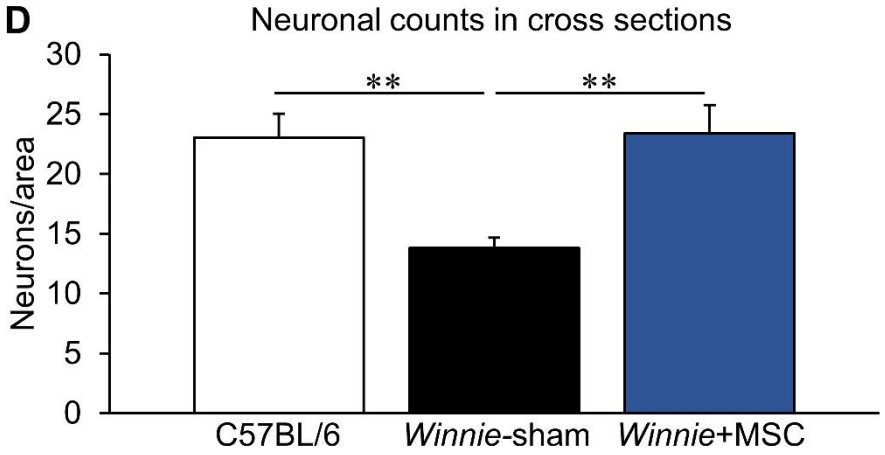
D
Neuronal counts in cross sections
Neurons/area
30
25
20
15
10
5
0
**
**
C57BL/6
Winnie-sham
Winnie+MSC

Many leukocytes were localised outside the myenteric ganglia (extra-ganglionic), however, a smaller number was also observed to infiltrate into the ganglia (intra-ganglionic) in direct contact with myenteric neurons. The total number of leukocytes quantified in LMMPs were significantly elevated in *Winnie*-sham mice compared to C57BL/6 mice ($P<0.0001$) (**Figure 4.11A, Table 4.5**, n=5 animals/group). When leukocytes were quantified according to location, increased cell numbers were observed in all regions, including intra-ganglionic ($P<0.01$), ganglia periphery ($P<0.0001$) and extra-ganglionic ($P<0.01$). When *Winnie* mice were treated with BM-MSCs, total leukocyte numbers remained elevated compared to C57BL/6 mice ($P<0.001$) as well as on the periphery of the ganglia ($P<0.0001$) and extra-ganglionic region ($P<0.05$) (**Figure 4.11B, Table 4.5**, n=5 animals/group). Nevertheless, compared to *Winnie*-sham mice, BM-MSC treatments reduced the total number of leukocytes ($P<0.01$), intra-ganglionic leukocytes ($P<0.05$) and leukocytes on the ganglia periphery ($P<0.01$), but not in the extra-ganglionic region. Within the leukocytes at the level of the myenteric plexus, distinct morphological populations could be observed that resembled either a rounded or stellate structure. The total number of rounded leukocytes were increased in *Winnie* mice compared to C57BL/6 controls ($P<0.01$), and furthermore, were decreased in *Winnie mice* when treated with BM-MSCs ($P<0.05$) (**Figure 4.11B, Table 4.5**, n=5 animals/group). Specifically, increased numbers of rounded leukocytes were observed in the intra-ganglionic area in *Winnie*-sham mice compared to BM-MSC-treated *Winnie* mice ($P<0.05$) and C57BL/6 mice ($P<0.01$) which contained similar levels. Furthermore, rounded leukocytes were increased on the periphery of the ganglia in sham-treated *Winnie* mice ($P<0.0001$) compared to controls which were reduced by treatments with BM-MSCs in *Winnie* mice ($P<0.05$); albeit to levels remaining higher than controls ($P<0.05$). High levels of rounded leukocytes were also observed in the extra-ganglionic region of *Winnie* mice ($P<0.05$), however this was not affected by BM-MSC treatments. Compared to C57BL/6 controls, the total number of stellate-shaped leukocytes were increased in both sham ($P<0.0001$) and BM-MSC-treated ($P<0.001$) *Winnie* mice (**Figure 4.11C, Table 4.5**, n=5 animals/group).

Figure 4.10 ***Leukocyte numbers in proximity to myenteric neurons in the distal colon of Winnie mice***

A-C) Leukocytes in proximity to the myenteric ganglia were observed by immunofluorescence using the pan-leukocyte marker CD-45 (green) and the neuronal marker MAP-2 (red) in LMMP wholemount preparations from the distal colon of C57BL/6 mice **(A)**, sham-treated *Winnie* mice **(B-B′)** and *Winnie* mice treated with BM-MSCs **(C)** (scale bar = 20µm).

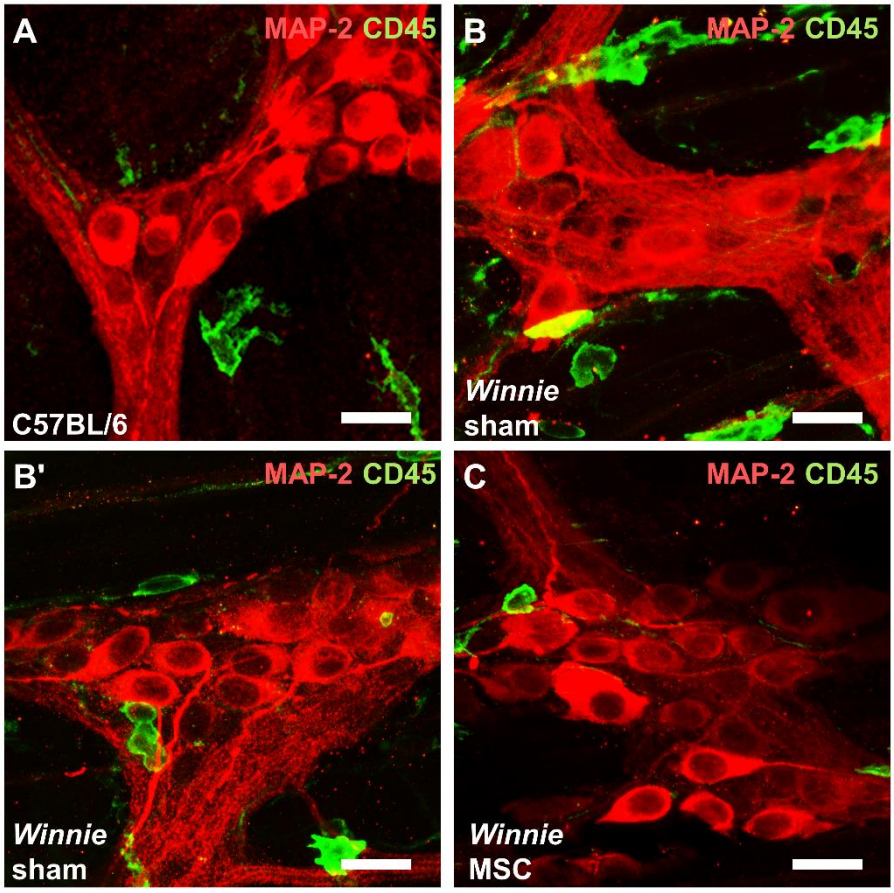
A
MAP-2 CD45
C57BL/6
B
MAP-2 CD45
Winnie
sham
B'
MAP-2 CD45
Winnie
sham
C
MAP-2 CD45
Winnie
MSC

Figure 4.11 ***Effects of BM-MSC treatments on leukocytes in the distal colon of Winnie mice***

A) CD-45 immunoreactive (IR) cells (leukocytes) in the myenteric plexus quantified per area and categorised by location in proximity to the myenteric ganglia including intra-ganglionic, periphery of the ganglia and extra-ganglionic. Leukocytes were further subdivided into distinct rounded **(B)** and stellate-shaped **(C)** morphological groups. Linear correlations were observed between **D)** the total number of CD-45 IR cells/area and disease activity index scores, as well as, **E)** the number of rounded CD-45 IR cells/area on the periphery of the ganglia and neuronal density. **P*<0.05, ***P*<0.01, ****P*<0.001, *****P*<0.0001; n=5 animals/group.

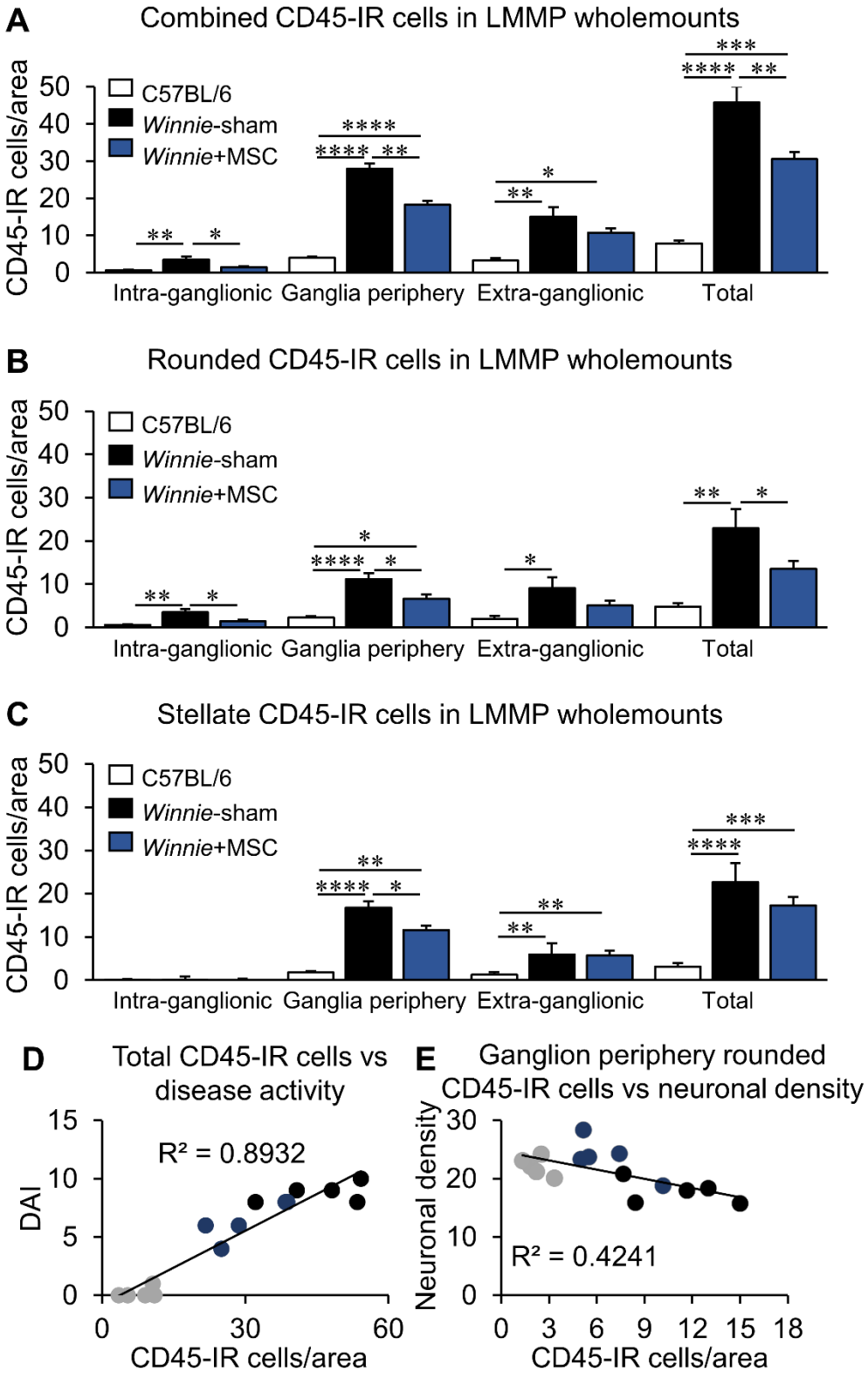
A
Combined CD45-IR cells in LMMP wholemounts
CD45-IR cells/area
C57BL/6
Winnie-sham
Winnie+MSC
Intra-ganglionic
Ganglia periphery
Extra-ganglionic
Total
B
Rounded CD45-IR cells in LMMP wholemounts
C
Stellate CD45-IR cells in LMMP wholemounts
D
Total CD45-IR cells vs disease activity
R² = 0.8932
DAI
CD45-IR cells/area
E
Ganglion periphery rounded CD45-IR cells vs neuronal density
R² = 0.4241
Neuronal density

Table 4.5 ***Effects of BM-MSC treatment on the number of leukocytes in proximity to the myenteric ganglia***

	C57BL/6	*Winnie*-sham	*Winnie*+MSC
Location		**Rounded CD45-IR cells/area**	
Intra-ganglionic	0.59±0.13	3.47±0.82 **	1.44±0.36 †
Ganglia periphery	2.24±0.34	11.15±1.38 ****	6.65±0.98 * †
Extra-ganglionic	1.99±0.64	9.10±2.49 *	5.03±1.16
Total	4.81±0.78	22.90±4.42 **	13.50±1.91 †
		Stellate CD45-IR cells/area	
Intra-ganglionic	0.07±0.07	0.03±0.03	0.00±0.00
Ganglia periphery	1.76±0.48	16.79±2.64 ****	11.61±0.82 ** †
Extra-ganglionic	1.27±0.48	5.98±0.65 **	5.72±0.98 **
Total	3.13±0.97	22.66±3.14 ****	17.30±1.58 ***
		Total CD45-IR cells/area	
Intra-ganglionic	0.65±0.19	3.50±0.81 **	1.44±0.36 †
Ganglia periphery	4.00±0.75	27.94±2.34 ****	18.27±1.49 **** ††
Extra-ganglionic	3.26±0.89	15.08±2.43 **	10.75±2.03 *
Total	7.91±1.48	45.76±4.16 ****	30.51±3.48 *** ††

IR – immunoreactive. *P<0.05, **P<0.01, ***P<0.001, ****P<0.0001 significantly different to C57BL/6. †P<0.05, ††P<0.01 significantly different to *Winnie*-sham; n=5 animals/group.

Region specific differences were observed with BM-MSC treatments inducing a decrease in stellate leukocyte numbers in *Winnie* mice on the periphery of the ganglia ($P<0.05$) which also contained the highest portion of these cells. Stellate leukocyte numbers remained elevated compared to controls in *Winnie*-sham and BM-MSC-treated *Winnie* mice on the periphery of the ganglia ($P<0.0001$ and $P<0.01$, respectively) or in the extra-ganglionic area ($P<0.01$ for both). These cells were rarely observed within the ganglia. To determine the relationship between plexitis and the disease severity in our model, a linear regression analysis was performed. A significant regression was found for the total number of leukocytes in proximity to the myenteric ganglia and disease activity scores for colitis ($F(1,13) = 108.7$, $P<0.0001$) with an R^2 of 0.8932 (**Figure 4.11D, Table 4.6**; n=15 pooled, n=5 animals/group). Predicted disease activity scores were - 0.78+(0.21×no. of leukocytes in all regions). This relationship appeared to be independent of leukocyte morphology or proximity to the ganglia with significant correlations observed in all permutations except for stellate-shaped cells inside the ganglia (**Table 4.6**). In addition, linear regression was used to determine the relationship between plexitis and neuropathy (**Table 4.7**). The highest correlation was identified in a regression equation for the number of rounded leukocytes located on the periphery of the ganglia ($F(1,13) = 9.573$, $P<0.01$) with an R^2 of 0.4241 (**Figure 4.11E, Table 4.7**; n=15 pooled, n=5 animals/group). Predicted neuronal density was 24.732-(0.5263×no. of peripheral, rounded leukocytes). Similarly, neuronal density was also negatively correlated with the number of rounded leukocytes in all regions or those that were intra-ganglionic (**Table 4.7**). Similar relationships to plexitis and disease activity or neuropathy were observed independently in sham-treated and BM-MSC treated *Winnie* mice.

4.7. Discussion

This is the first study investigating the effects of BM-MSC therapy on the ENS in the *Winnie* mouse model of spontaneous chronic colitis. Notably, this study also provides the first data on expression patterns of ENS-specific genes in an animal model of intestinal inflammation and human IBD using high-throughput sequencing technology.

Table 4.6 ***Linear regression correlations between leukocyte counts in proximity to the myenteric plexus and disease activity index scores***

	Morphology	R square	F	*P* value
Intra-ganglionic	Round	0.4688	11.47	**0.0049**
	Stellate	0.06874	0.9596	0.3452
	Total	0.4538	10.8	**0.0059**
Ganglia periphery	Round	0.7958	50.66	**<0.0001**
	Stellate	0.7313	35.37	**<0.0001**
	Total	0.8745	90.58	**<0.0001**
Extra-ganglionic	Round	0.4804	12.02	**0.0042**
	Stellate	0.7898	48.84	**<0.0001**
	Total	0.7475	38.49	**<0.0001**
All	Round	0.6699	26.38	**0.0002**
	Stellate	0.7965	50.87	**<0.0001**
	Total	0.8932	108.7	**<0.0001**

Significant correlations in bold.

Table 4.7 ***Linear regression correlations between leukocyte counts in proximity to the myenteric plexus and myenteric neuronal counts***

	Morphology	R square	F	*P* value
Intra-ganglionic	Round	0.3923	8.393	**0.0125**
	Stellate	0.01053	0.138	0.7159
	Total	0.4036	8.796	**0.0109**
Ganglia periphery	Round	0.4241	9.573	**0.0085**
	Stellate	0.0767	1.08	0.3177
	Total	0.2004	3.258	0.0943
Extra-ganglionic	Round	0.2361	4.019	0.0663
	Stellate	0.08137	1.152	0.3027
	Total	0.2147	3.555	0.0819
All	Round	0.3406	6.716	**0.0224**
	Stellate	0.08187	1.159	0.3012
	Total	0.2372	4.042	0.0656

Significant correlations in bold.

On the level of gene expression, similarities were observed between murine chronic colitis and human IBD in alterations to expression patterns of genes associated with cholinergic, purinergic, glutaminergic and NPY-ergic signalling. Spontaneous chronic colitis induced changes in gene expression that were associated with neurotransmission, structural alterations in the ENS and neurogenic inflammation. Subsequent treatment with BM-MSCs normalised the expression for many of these genes. The size of the myenteric ganglia was larger in *Winnie* mice with chronic inflammation compared to non-inflamed controls. Whilst the majority of ENS-specific genes were downregulated in these mice, this may be explained by structural changes within the ganglia with a reduction in neuronal density observed in *Winnie* mice. BM-MSC therapy reduced leukocyte numbers on the level of the myenteric ganglia which correlated well with reduced disease severity. Furthermore, BM-MSCs reduced infiltration of leukocytes that had a rounded morphology; this correlated with reduced neuronal density which suggests an immunological component accounting for the reduction of neurons and remodelling of the ganglia in chronic colitis. The neuroprotective activity of BM-MSCs may explain the normalisation in the regulation of many ENS-specific genes.

Our analysis revealed an over-representation of genes associated with structural damage to the nervous system, therefore we decided to verify this using immunohistochemistry. Prominent neuronal loss was observed in the myenteric ganglia of *Winnie* mice which is consistent with previous reports (Rahman et al., 2016). We observed a loss in neuronal density (approximately 25%) in wholemount preparations from *Winnie* mice; these results are within the ranges of neuronal loss reported previously in guinea-pig, mouse and rat models of TNBS or DNBS-induced colitis (Sanovic et al., 1999, Boyer et al., 2005, Lin et al., 2005, Linden et al., 2005a, Sarnelli et al., 2009, Stavely et al., 2015a, Stavely et al., 2015b). Gross structural degeneration is observed within the enteric ganglia in inflamed regions of UC (Oehmichen and Reifferscheid, 1977, Riemann and Schmidt, 1982). Even so, results in studies quantifying neuronal numbers in resected tissue from UC patients have been varied with reports observing an increase, decrease or no change (Storsteen, 1953, Neunlist et al., 2003a, Villanacci et al., 2008, Bernardini et al.,

2012). In full-thickness biopsies, control tissue is usually sourced from patients undergoing resection for colorectal cancer. This can confound results as neuronal loss can be caused by neoadjuvant chemotherapy, cancer-related cachexia and the tumours themselves (Janusz, 2010, McQuade et al., 2016, Vicentini et al., 2016). This variability may be attributed to the methods of quantifying neuronal loss. In the most recent study, Bernardini et al. (2012) observed that the ganglionated area increases by 59% in patients with UC; when neuronal counts were normalised a 61% decrease in neuronal density was observed. This justifies observations from previous studies that have not normalised for size differences between the ganglion and reported no change or an increase in neuronal numbers (Storsteen, 1953, Neunlist et al., 2003a, Villanacci et al., 2008). Similar to UC patients, the size of the myenteric ganglia was larger in *Winnie* mice compared to uninflamed controls despite a reduction in neuronal density. Furthermore, no differences were observed between the size of the ganglia in BM-MSC-treated and untreated *Winnie* mice.

Neuroprotective effects of BM-MSC treatments in the *Winnie* mouse model of spontaneous chronic colitis were observed by increased myenteric neuronal counts in cross sections and wholemount preparations from the distal colon. Previously, our group has demonstrated the neuroprotective potential of MSCs in the ENS of guinea-pigs with TNBS-induced colitis through a series of papers exploring the effects of doses, time-points, MSC tissue sources and species of MSC treatments (Robinson et al., 2014, Robinson et al., 2015, Stavely et al., 2015a, Stavely et al., 2015b, Robinson et al., 2017b). The results of the presented study strengthen the body of evidence supporting the use of BM-MSCs as a treatment of myenteric neuropathy induced by intestinal inflammation by using a model that better reflects human IBD. Considering the resemblance of structural changes to the myenteric plexus in *Winnie* mice and UC, the mechanisms of MSC-mediated neuroprotection in murine colitis may translate more accurately to chronic human IBD than previous studies.

Enteric plexitis has been demonstrated to have a close association with inflammatory relapse after resection in IBD patients; thus, linking neuro-

immunological changes to the disease pathology (Ferrante et al., 2006, Sokol et al., 2009, Bressenot et al., 2013). Our results demonstrate that plexitis correlates with disease severity in *Winnie* mice; and furthermore, these were both reduced by BM-MSC treatments (**Chapter 3, Figure 3.1**). The immunomodulatory capabilities of MSCs are well-established and it has been shown in several models of inflammation that MSCs reduce leukocyte recruitment (Antunes et al., 2014a, Antunes et al., 2014b, Elman et al., 2014, Stavely et al., 2015a, Wang et al., 2016). In TNBS-induced colitis, MSCs have been demonstrated to reduce leukocyte infiltration as indicated by myeloperoxidase activity and leukocyte counts in the mucosa and submucosa (Ando et al., 2008, Liang et al., 2011, Stavely et al., 2015a). In addition, the presented results are aligned with previous studies by our group investigating the effect of MSC treatments on plexitis in guinea-pigs with TNBS-induced colitis (Robinson et al., 2015, Stavely et al., 2015a, Stavely et al., 2015b). In *Winnie* mice, the majority of leukocytes were concentrated around the periphery of the ganglia; albeit higher numbers of leukocytes were observed in all regions. BM-MSC treatment reduced the number of leukocytes on the edges of the ganglia and those inside the ganglia to levels of C57BL/6 mice. The relationship between plexitis and disease activity appeared to be indiscriminate to the proximity of leukocytes to the ganglia and their morphology. In contrast, neuropathy appeared to be more dependent on the number leukocytes with a rounded morphology located inside and on the edges of the myenteric ganglia. Previously, eosinophils and neutrophils have been implicated in plexitis-induced neuropathy in models of dinitrobenzene sulfonic acid (DNBS)-induced colitis (Sanovic et al., 1999, Boyer et al., 2005). Sanovic et al. (1999) demonstrated that eosinophilic myenteric plexitis occurs 6h post DNBS administration; neuronal loss began at the same time-point. Peak neutrophilic infiltration to the level of the myenteric plexus occurred 48h after DNBS administration despite the greatest decline in neuronal numbers occurring after 24h; therefore, it was predicted that eosinophils may play a larger role in neuropathy. Recently, it was also demonstrated that attenuation of eosinophilic myenteric plexitis via inhibiting the eotaxin 1- C-C chemokine receptor type 3 (CCR3) axis confers neuroprotection in guinea-pigs exposed to TNBS (Filippone et al., 2018a). Nonetheless, application of the corticosteroid budesonide can

ameliorate neuronal loss in a dose-dependent manner that parallels a reduction in the neutrophil marker, myeloperoxidase (MPO) (Sanovic et al., 1999). Furthermore, Boyer et al. (2005) demonstrated that pre-treatment of mice exposed to DNBS with antibodies targeting neutrophils reduced neuronal loss. Together these data suggest that neutrophils and eosinophils have a role in neuropathy, or at least in chemically-induced colitis. However, it is unclear whether acute plexitis in these studies are secondary to the innate inflammatory response mediated by neutrophils in the mucosa. In the presented study, infiltration of leukocytes with a similar rounded morphology to neutrophils and eosinophils were observed in *Winnie* mice. An ongoing project within our group is currently defining these leukocyte populations in chronic inflammation (Filippone et al., 2018b).

Resident muscularis macrophages also reside near the myenteric plexus which mediate the physiological function of myenteric neurons; these cells exhibit a stellate profile (similar to microglia in the central nervous system, CNS) which were morphologically equivalent to the stellate-shaped leukocytes lining the ganglia in our study (Muller et al., 2014, De Schepper et al., 2018). While these macrophages typically have an anti-inflammatory phenotype (Mφ2), their dysregulation is also becoming evident in the pathophysiology of various intestinal disorders including damage to the ENS and dysmotility in colitis (Kinoshita et al., 2007, De Schepper et al., 2018). Furthermore, it has been demonstrated that these resident macrophages can lose their anti-inflammatory phenotype in response to oxidative stress as evidenced in the stomach of a diabetic animal model (Choi et al., 2008). Conversely, the anti-inflammatory properties of muscularis macrophages can be enhanced in intestinal inflammation by cholinergic signalling from myenteric neurons stimulated by vagal afferent nerve fibres (Matteoli et al., 2014). Similarly, 5-Hydroxytryptamine receptor 4 (5-HT_4R) agonist can also exert anti-inflammatory effects mediated through myenteric cholinergic neurons acting on resident muscularis macrophages (Tsuchida et al., 2010). Interestingly, genes associated with cholinergic neurotransmission, ACh synthesis (*ChAT*) and the 5-HT_4R were downregulated in *Winnie* mice and human UC patients compared to non-inflamed controls and upregulated by BM-MSC treatments in *Winnie* mice. Furthermore, the

sympathetic nervous system can also enhance the anti-inflammatory phenotype of muscularis macrophages mediated by the beta-2 adrenergic receptor as demonstrated in a model of luminal bacterial infection (Gabanyi et al., 2016). While interactions between luminal pathogens and the immune system are implicated in the development of chronic colitis in MUC2-deficient mice (Morampudi et al., 2016, Robinson et al., 2016), and possibly the therapeutic effect of BM-MSCs (**Chapter 3, Section 3.6.3**), *Adrb2* was upregulated in *Winnie* mice and IBD patients but downregulated by BM-MSCs. Furthermore, BM-MSC treatments did not enhance *Th* expression (Tyrosine hydroxylase, norepinephrine synthesis) despite yielding therapeutic effects. Therefore, in chronic colitis, dysfunction in this sympathetic anti-inflammatory pathway may not be associated with the pathophysiology of the disease.

Neurons are sensitive to pro-inflammatory mediators which can cause dysfunction and cell death (Downen et al., 1999, Xia et al., 1999, Kelles et al., 2000). Therefore, it could be hypothesised that BM-MSCs increased the myenteric neuronal density in *Winnie* mice by reducing the levels of harmful paracrine factors derived from infiltrating leukocytes. However, emerging research is beginning to reveal the complexity of immune interactions with the maintenance of the ENS. A recent study by Kulkarni et al. (2017) suggest that macrophages phagocytose myenteric neurons in a continuous physiological mechanism of ganglionic remodelling. These neurons are reportedly replaced by a pool of resident precursor cells. Therefore, it is also possible that neuronal loss in intestinal inflammation is an imbalance in neuronal phagocytosis and regeneration. The role of myenteric remodelling and neurogenesis in intestinal inflammation remains contentious as studies have demonstrated that enteric neurons do not regenerate after chemically-induced colitis at time points up to 56 days after exposure, despite the absence of inflammation (Sanovic et al., 1999, Lin et al., 2005, Linden et al., 2005a). Nonetheless, the neurogenesis paradigm supports a recent study by Belkind-Gerson et al. (2015) which suggests that neuronal numbers increase in dextran sodium sulphate (DSS)-induced colitis. Considering that studies in similar models have reported decreases in neuronal density due to neuronal cell death (Gulbransen et al., 2012), the number

of myenteric neurons may depend on many factors including the degree of inflammation, species, models of inflammation and methods of quantification. Even so, this demonstrates that neuronal numbers are likely to be dynamic and subjected to death and remodelling depending on environmental cues that are obviously imbalanced in intestinal inflammation. In the context of MSC-therapy, our results suggest that the increase in neuronal density correlated with a reduction in leukocyte numbers in the myenteric ganglia. This suggests that BM-MSCs may have promoted neuronal survival by reducing infiltrating (i.e. non-resident) leukocyte numbers, which subsequently reduced chemotactic signalling, leukocyte recruitment and attenuated the release of inflammatory paracrine factors that are associated with neuropathy. Alternatively, BM-MSCs have been demonstrated to release many neuroprotective and trophic factors (Robinson et al., 2015, Stavely et al., 2015a); therefore it cannot be ruled out that BM-MSCs directly reduced neuronal damage via trophic support which assisted with the survival and repair of damaged enteric neurons.

The ability of MSCs to reduce leukocyte recruitment to the mucosa and submucosal layers has been reported extensively in chemically-induced colitis (Ando et al., 2008, Zhang et al., 2009b, Liang et al., 2011, Stavely et al., 2015a). While it is known that muscularis macrophages seed the intestine prenatally, it is uncertain whether this pool is replenished by circulating monocytes over time, or whether these cells constitute the original population throughout the lifespan (De Schepper et al., 2018). Nonetheless, macrophages and neutrophils can infiltrate to the myenteric plexus in inflammatory conditions (Sayani et al., 2004, Kinoshita et al., 2007). It is unconfirmed in our study whether the decrease in the number of leukocytes in *Winnie* mice treated with BM-MSCs represents a reduction in the infiltration of circulating monocytes/macrophages or neutrophils, or the division of resident leukocytes.

Analysis of gene expression data revealed that BM-MSCs downregulated secreted factors associated with neurogenic inflammation in colitis such as *Tac1*, *S100b* and *Calcb* which encode for the proteins substance P, S100 calcium-binding protein B

(S100B) and β-CGRP (the dominant enteric CGRP isoform (Muddhrry et al., 1988)), respectively. Conversely the gene encoding NPY, which is also associated with neurogenic inflammation, was upregulated by BM-MSC treatments in *Winnie* mice. Substance P and CGRP are released by extrinsic sensory neurons (although both are found in intrinsic myenteric neurons) which drives the progression of inflammation in chemically-induced colitis (Engel et al., 2011, Engel et al., 2012). Substance P can directly activate immune cells to secrete pro-inflammatory cytokines and chemokines (Stanisz, 2001). Leukocytes also express CGRP receptors and are subject to immunomodulation by CGRP (Assas et al., 2014). Nonetheless, CGRP appears to confer an anti-inflammatory effect as CGRP receptor antagonism can promote susceptibility to oxazolone-induced colitis (Engel et al., 2012) and UC disease severity negatively correlates with CGRP levels (Li et al., 2013a). In contrast, our study suggests that β-CGRP is upregulated in IBD and *Winnie* mice compared to non-inflamed controls. Similarly, we observed that the substance P gene *Tac1* was upregulated in *Winnie* mice and UC; high levels have previously been reported in the inflamed regions of UC, including an increase of substance P immunoreactive myenteric neurons (Goldin et al., 1989, Neunlist et al., 2003a). Although S100B is constitutively expressed in the intestine, its expression is upregulated in UC patients where it is released by enteric glia which appears to stimulate the release of inflammatory mediators (Cirillo et al., 2009, Cirillo et al., 2011, Capoccia et al., 2015). Likewise, we observed an upregulation of *S100B* in UC, however, this was downregulated in *Winnie* mice, albeit BM-MSC treatments reduced levels even further. The neuropeptide NPY has also been implicated in DSS-induced colitis where it is upregulated and has a pro-inflammatory role (Chandrasekharan et al., 2008). Conversely, NPY levels were reduced in chronic inflammation in our study with lower levels in *Winnie* mice and UC patients compared to non-inflamed controls. These levels were increased by BM-MSC treatments. Considering that NPY is expressed in sympathetic fibres and intrinsically throughout the ENS it might play a role in the neuroprotective action of BM-MSCs to the ENS (de Jonge, 2013).

While BM-MSCs have demonstrated an ability to restore structural changes to the ENS; specific neuronal subpopulations may be more important than others in the development of symptoms and sequelae of intestinal inflammation. Previously, we have identified a loss in choline acetyltransferase (ChAT; ACh synthesis) immunoreactive neurons or vesicular acetylcholine transporter (VAChT; ACh vesicular packaging) expression in TNBS-induced colitis in the guinea-pig and spontaneous chronic colitis in *Winnie* mice (Robinson et al., 2014, Rahman et al., 2015, Robinson et al., 2015, Stavely et al., 2015b, Stavely et al., 2015a, Rahman et al., 2016, Robinson et al., 2017b). In the present study, these observations are reinforced on the gene expression level with reduced *ChAT* and *Slc18a3* (VAChT) expression in *Winnie* mice. Moreover, these were both upregulated by BM-MSCs treatments which is similar to previous results in TNBS-induced colitis in guinea-pigs on the protein level (**Chapter 2, Section 2.5.4 & 2.5.5**). Similar results have been observed in TNBS-induced colitis in rats and UC patients with a downregulation of ChAT immunoreactive neurons in the myenteric plexus which parallels our gene expression results in IBD patients (Neunlist et al., 2003a, Lin et al., 2005). Furthermore, *Winnie* mice exhibited downregulation of *Chrna3* and *Chrnb4* which are transcripts for the α3β4 subunits of the pentameric α3β4 nicotinic receptor, or, ganglionic nicotinic ACh receptor, which is the major nicotinic receptor in the enteric ganglia. Both of these genes were upregulated by BM-MSCs. Thus, there are several disturbances to the cholinergic system that appear to be ameliorated by BM-MSCs in chronic inflammation including ACh synthesis and vesicular loading, as well, as alterations in the expression of target receptors. It has been established in models of chemically-induced colitis that pro-inflammatory mediators can supress cholinergic neurotransmission in the ENS (Xia et al., 1999, Kelles et al., 2000). Therefore, cholinergic dysfunction appears to be consistent in animal models and human IBD. Nicotinic signalling in particular may be dysfunctional in UC as tobacco smoking reduces the incidence and severity of the disease and nicotine can promote remission independently (McGrath et al., 2004, Thomas et al., 2005). The potential anti-inflammatory mechanisms of cholinergic myenteric neurons have been discussed, however these neurons are also the major excitatory muscle motor neurons involved in smooth muscle contraction. In our

study, the GO biological process *regulation of smooth muscle contraction* was enriched in genes downregulated in *Winnie* mice and upregulated by BM-MSCs. The effect of altered cholinergic signalling on dysmotility in colitis is highlighted by a reduction in choline uptake, acetylcholine release and contractile response to stimulation of enteric nerves in DNBS-treated rats (Poli et al., 2001). In addition, inflammation can also disrupt purinergic signalling and cause dysmotility in TNBS-exposed guinea-pigs and DSS-exposed mice which is thought to be mediated by oxidative stress and disturbed purine synthesis (Roberts et al., 2013). Interestingly, BM-MSC treatments attenuated the downregulation of purinergic receptors, particularly the P2X receptor family which were downregulated in *Winnie* mice and UC patients. Excess extracellular ATP and purinergic signalling has been reported as a mechanism of neuronal cell death in intestinal inflammation in different models of colitis (Gulbransen et al., 2012). Neuropathy can cause dysfunctions in multiple neurally-controlled processes including motility (Boyer et al., 2005). Along with neuronal loss, *Winnie* mice also exhibit dysmotility due to dysfunction in cholinergic and purinergic signalling to smooth muscle cells which results in diarrhoea that does not appear to be of secretory origin (Robinson et al., 2017a). BM-MSC treatments increased neuronal density and altered gene expression associated with cholinergic and purinergic signalling in *Winnie* mice which might contribute to the reduced faecal water content of stools after BM-MSC treatment (**Chapter 3, Figure 3.3**).

4.8. Conclusion

The expression of many ENS-associated genes was influenced by BM-MSC treatments in *Winnie* mice. These genes were associated with multiple nervous system-controlled gastrointestinal functions which demonstrated that BM-MSCs could have a broad effect on neural innervation in chronic inflammation. Genes associated with neurotransmission pathways were downregulated by chronic inflammation in *Winnie* mice. These were ameliorated by BM-MSC treatments including cholinergic and purinergic signalling genes which control physiological

functions of the ENS, as well as, immunomodulation and neuronal damage. BM-MSCs treatments ameliorated neuronal loss, which may explain their effects on upregulating many neuronal and synapse associated genes. Plexitis may be a cause of neuronal loss in chronic inflammation which was linked with the infiltration of leukocytes with a rounded morphology as opposed to stellate-shaped cells that could resemble the resident muscularis macrophages. Gene expression associated with the nervous system is disturbed by chronic inflammation in *Winnie* mice and IBD. We have shown for the first time that there are strong correlations between both the *Winnie* model of colitis and clinical IBD in ENS-associated gene expression within the colon. Treatments in *Winnie* mice may be clinically relevant since they share similar molecular signatures. These insights demonstrated that BM-MSCs are capable of at least partially restoring homeostasis in the ENS in *Winnie* mice. Taken together, these data are suggestive that BM-MSCs could be efficacious for attenuating alterations to the ENS in a clinical setting.

CHAPTER FIVE

Mesenchymal Stem Cells Attenuate Inflammation-Induced Oxidative Stress in Myenteric Neurons

5.1. Summary

DNA adducts caused by high levels of oxidation are a biomarker for inflammatory bowel disease (IBD) and are indicative of oxidative stress. It has become widely accepted that oxidative stress is not only a marker of IBD but also contributes to the chronicity of intestinal inflammation. Neurons are susceptible to oxidative insult and models of acute intestinal inflammation have identified that oxidative stress is prominent in the enteric nervous system (ENS) which may contribute to the pathophysiology of IBD. Mesenchymal stem cell (MSC) treatments possess multiple properties that may attenuate the oxidative pathology of intestinal inflammation including: immunomodulatory activity that averts the generation of reactive oxygen species (ROS), direct scavenging or detoxification of free radicals and the ability to promote antioxidant defences in host tissues. The antioxidative properties of MSCs have been demonstrated in experimental models of neurological pathologies in the central nervous system and in neuronal cultures *in vitro*. Therefore, MSCs are a potential candidate therapy to alleviate oxidative stress in the ENS. *Winnie* mice with spontaneous chronic colitis underwent a treatment regimen of four bone marrow-derived MSC (BM-MSC) injections over two weeks delivered by enema. Mice were culled 24h after the final treatment and distal colons were collected for RNA isolation and immunohistochemistry. High-throughput RNA sequencing and bioinformatics were performed to screen the genes upregulated by BM-MSC treatments and to identify changes in genes specifically associated with oxidative stress. Results were compared to the transcriptome of IBD patients retrieved from the Gene Expression Omnibus data repository to explore clinical relevance. The neuroprotective properties of BM-MSC treatments were examined in myenteric neurons exposed to oxidative stress inducing stimuli *in vitro.* BM-MSCs increased the expression of genes involved in endogenous antioxidant defences. Furthermore, several genes that were redox sensitive or involved in the production of free radicals were downregulated by BM-MSC treatments which illustrated that an antioxidative mechanism was involved in their therapeutic effect. BM-MSCs corrected the patterns of expression for several oxidative-stress associated genes that were dysregulated in both *Winnie* mice and IBD patients. The antioxidative properties of BM-MSCs were confirmed by a

reduction in DNA/RNA oxidation in the inflamed colon. Intestinal inflammation resulted in high levels of DNA/RNA oxidation and mitochondria-derived superoxide specifically in the myenteric ganglia which was alleviated by BM-MSC treatments. Oxidative stress inducing stimuli was identified to cause myenteric neuronal loss *in vitro* which could be attenuated by the secretion of BM-MSCs-derived factors. Inhibition of SOD1 blocked BM-MSCs from protecting myenteric neurons from oxidative-induced injury, and therefore, may mediate their therapeutic effects.

5.2. Abbreviations

•OH	hydroxyl radical
8-OHdG	8-hydroxy-2'-deoxyguanosine
BM-MSCs	bone marrow-MSCs
CD	Crohn’s disease
COX	cyclooxygenase
DAPI	4',6-diamidino-2-phenylindole
DEG	differentially expressed genes
DMSO	dimethyl sulfoxide
DNBS	dinitrobenzene sulfonic acid
DNBS	dinitrobenzene sulfonic acid
DSS	dextran sodium sulphate
DUOX	dual oxidases
ENS	enteric nervous system
ETC	electron transport chain
FBS	foetal bovine serum
FC	fold change
FMO	flavin-containing monooxygenase
GO	gene ontology
GPx	glutathione peroxidase
GSH	reduced glutathione
GSSG	oxidised glutathione
GST	glutathione S-transferases
H_2O_2	hydrogen peroxide
HIF-1	hypoxia-inducible factor-1
HO-1	haem oxygenase 1
IBD	inflammatory bowel disease
IL	interleukin
iNOS	inducible NOS
KEGG	Kyoto Encyclopedia of Genes and Genomes
LMMP	longitudinal muscle myenteric plexus

LOX	lipoxygenase
MAP-2	microtubule associated protein 2
Mmp9	matrix metallopeptidase 9
MPO	myeloperoxidase
mPTP	mitochondrial permeability transition pore
MSC	mesenchymal stem cells
NAC	N-acetyl cysteine
NDS	normal donkey serum
NLRP3	NOD-like receptor protein 3
nNOS	neuronal NOS
NO	nitric oxide
NOD	nucleotide-binding oligomerization domain
NOS	nitric oxide synthase
NOX	nicotinamide adenine dinucleotide phosphate, reduced NADPH)-oxidase
NQO	ribosyldihydronicotinamide dehydrogenase, quinone
$O_2^{\cdot -}$	superoxide anion
OCT	optimal cutting temperature
PBS	phosphate buffered saline
redox	reduction-oxidation
RIN	RNA integrity number
ROS	reactive oxygen species
SEM	standard error of the mean
SOD	superoxide dismutase
SOD1	SOD-Cu-Zn
TNBS	2,4,6-trinitrobenzenesulfonic acid
TNF	tumour necrosis factor
UC	ulcerative colitis

5.3. Gene Symbols

5330417C22Rik	RIKEN cDNA 5330417C22 gene
Abat	4-aminobutyrate aminotransferase
Abca8a	ATP-binding cassette, sub-family A (ABC1), member 8a
Abca9	ATP-binding cassette, sub-family A (ABC1), member 9
Abcb1a	ATP-binding cassette, sub-family B (MDR/TAP), member 1A
Abcc3	ATP-binding cassette, sub-family C (CFTR/MRP), member 3
Abcg2	ATP-binding cassette, sub-family G (WHITE), member 2
Abcg3	ATP-binding cassette, sub-family G (WHITE), member 3
Abcg5	ATP-binding cassette, sub-family G (WHITE), member 5
Abcg8	ATP-binding cassette, sub-family G (WHITE), member 8
Abo	ABO blood group (transferase A, alpha 1-3-N-acetylgalactosaminyltransferase, transferase B, alpha 1-3-galactosyltransferase)
Acer1	alkaline ceramidase 1
Acox2	acyl-Coenzyme A oxidase 2, branched chain
Acsl3	acyl-CoA synthetase long-chain family member 3
Acsm3	acyl-CoA synthetase medium-chain family member 3
Acss1	acyl-CoA synthetase short-chain family member 1
Acss2	acyl-CoA synthetase short-chain family member 2
Acta1	actin, alpha 1, skeletal muscle
Adam23	a disintegrin and metallopeptidase domain 23
Adipoq	adiponectin, C1Q and collagen domain containing
Agt	angiotensinogen (serpin peptidase inhibitor, clade A, member 8)
Ahcyl2	S-adenosylhomocysteine hydrolase-like 2
Ak4	adenylate kinase 4
Akr1c14	aldo-keto reductase family 1, member C14
Akr1c19	aldo-keto reductase family 1, member C19
Aldh1a1	aldehyde dehydrogenase family 1, subfamily A1
Aldh1a7	aldehyde dehydrogenase family 1, subfamily A7
Aldh1b1	aldehyde dehydrogenase 1 family, member B1

Aldh2	aldehyde dehydrogenase 2, mitochondrial
Aldh6a1	aldehyde dehydrogenase family 6, subfamily A1
Aldob	aldolase B, fructose-bisphosphate
Alox5ap	arachidonate 5-lipoxygenase activating protein
Alpi	alkaline phosphatase, intestinal
Amt	aminomethyltransferase
Amy1	amylase 1, salivary
Angptl4	angiopoietin-like 4
Ank3	ankyrin 3, epithelial
Ano7	anoctamin 7
Anxa1	annexin A1
Apod	apolipoprotein D
Aqp11	aquaporin 11
Aqp8	aquaporin 8
Aspa	aspartoacylase
Atp1a2	ATPase, Na+/K+ transporting, alpha 2 polypeptide
B3galt2	UDP-Gal:betaGlcNAc beta 1,3-galactosyltransferase, polypeptide 2
Bag2	BCL2-associated athanogene 2
BC021891	cDNA sequence BC021891
Bnip3	BCL2/adenovirus E1B interacting protein 3
Cacna1e	calcium channel, voltage-dependent, R type, alpha 1E subunit
Cacna2d2	calcium channel, voltage-dependent, alpha 2/delta subunit 2
Car3	carbonic anhydrase 3
Car4	carbonic anhydrase 4
Cbr3	carbonyl reductase 3
Cbs	cystathionine beta-synthase
Ccdc141	coiled-coil domain containing 141
Ccl5	chemokine (C-C motif) ligand 5
Cd36	CD36 antigen
Cdx2	caudal type homeobox 2
Ces1d	carboxylesterase 1D

Cftr	cystic fibrosis transmembrane conductance regulator
Chd6	chromodomain helicase DNA binding protein 6
Chpt1	choline phosphotransferase 1
Chrna3	cholinergic receptor, nicotinic, alpha polypeptide 3
Cit	citron
Clcn2	chloride channel, voltage-sensitive 2
Cntnap1	contactin associated protein-like 1
Col4a5	collagen, type IV, alpha 5
Col4a6	collagen, type IV, alpha 6
Col6a1	collagen, type VI, alpha 1
Col6a2	collagen, type VI, alpha 2
Col6a3	collagen, type VI, alpha 3
Col27a1	collagen, type XXVII, alpha 1
Cox8b	cytochrome c oxidase subunit VIIIb
Cps1	carbamoyl-phosphate synthetase 1
Creb3l1	cAMP responsive element binding protein 3-like 1
Csad	cysteine sulfinic acid decarboxylase
Cth	cystathionase (cystathionine gamma-lyase)
Cybrd1	cytochrome b reductase 1
Cyp2c55	cytochrome P450, family 2, subfamily c, polypeptide 55
Cyp2c68	cytochrome P450, family 2, subfamily c, polypeptide 68
Cyp2d12	cytochrome P450, family 2, subfamily d, polypeptide 12
Cyp2d22	cytochrome P450, family 2, subfamily d, polypeptide 22
Cyp2d9	cytochrome P450, family 2, subfamily d, polypeptide 9
Cyp2e1	cytochrome P450, family 2, subfamily e, polypeptide 1
Cyp2s1	cytochrome P450, family 2, subfamily s, polypeptide 1
Cyp39a1	cytochrome P450, family 39, subfamily a, polypeptide 1
Cyp4f14	cytochrome P450, family 4, subfamily f, polypeptide 14
Dclk1	doublecortin-like kinase 1
Ddc	dopa decarboxylase
Ddx3y	DEAD (Asp-Glu-Ala-Asp) box polypeptide 3, Y-linked
Dgkg	diacylglycerol kinase, gamma

Dgkh	diacylglycerol kinase, eta
Dhrs11	dehydrogenase/reductase (SDR family) member 11
Dnah8	dynein, axonemal, heavy chain 8
Dnm1	dynamin 1
Dpp4	dipeptidylpeptidase 4
Dpyd	dihydropyrimidine dehydrogenase
Duox1	dual oxidase 1
Duoxa1	dual oxidase maturation factor 1
Edil3	EGF-like repeats and discoidin I-like domains 3
Edn1	endothelin 1
Efemp1	epidermal growth factor-containing fibulin-like extracellular matrix protein 1
Eif2s3y	eukaryotic translation initiation factor 2, subunit 3, structural gene Y-linked
Eno3	enolase 3, beta muscle
Ephx2	epoxide hydrolase 2, cytoplasmic
Ern2	endoplasmic reticulum (ER) to nucleus signalling 2
Etv4	ets variant 4
Fabp2	fatty acid binding protein 2, intestinal
Fabp4	fatty acid binding protein 4, adipocyte
Fasn	fatty acid synthase
Fat4	FAT atypical cadherin 4
Fbn2	fibrillin 2
Fgfr3	fibroblast growth factor receptor 3
Flt3	FMS-like tyrosine kinase 3
Fmo1	flavin containing monooxygenase 1
Fmo2	flavin containing monooxygenase 2
Fmo4	flavin containing monooxygenase 4
Fmo5	flavin containing monooxygenase 5
Foxo3	forkhead box O3
Fut9	fucosyltransferase 9

Galnt5	UDP-N-acetyl-alpha-D-galactosamine:polypeptide N-acetylgalactosaminyltransferase 5
Gcg	glucagon
Gch1	GTP cyclohydrolase 1
Glul	glutamate-ammonia ligase (glutamine synthetase)
Gm1123	predicted gene 1123
Gnao1	guanine nucleotide binding protein, alpha O
Gpd1	glycerol-3-phosphate dehydrogenase 1 (soluble)
Gpt	glutamic pyruvic transaminase, soluble
Greb1l	growth regulation by estrogen in breast cancer-like
Gria4	glutamate receptor, ionotropic, AMPA4 (alpha 4)
Grin2d	glutamate receptor, ionotropic, NMDA2D (epsilon 4)
Gsta3	glutathione S-transferase, alpha 3
Gsta4	glutathione S-transferase, alpha 4
Gstm1	glutathione S-transferase, mu 1
Gstm3	glutathione S-transferase, mu 3
Gstm6	glutathione S-transferase, mu 6
Gstm7	glutathione S-transferase, mu 7
Hao2	hydroxyacid oxidase 2
Hba-a2	hemoglobin alpha, adult chain 2
Hbb-b1	hemoglobin, beta adult major chain
Hepacam2	HEPACAM family member 2
Hhip	Hedgehog-interacting protein
Hk2	hexokinase 2
Hk3	hexokinase 3
Hmga2	high mobility group AT-hook 2
Hmgcs2	3-hydroxy-3-methylglutaryl-Coenzyme A synthase 2
Hmmr	hyaluronan mediated motility receptor (RHAMM)
Hmox1	heme oxygenase 1
Hp	haptoglobin
Hpd	4-hydroxyphenylpyruvic acid dioxygenase
Hpgd	hydroxyprostaglandin dehydrogenase 15 (NAD)

Hpgds	hematopoietic prostaglandin D synthase
Hsd3b2	hydroxy-delta-5-steroid dehydrogenase, 3 beta- and steroid delta-isomerase 2
Hunk	hormonally upregulated Neu-associated kinase
Igdcc4	immunoglobulin superfamily, DCC subclass, member 4
Igfbp6	insulin-like growth factor binding protein 6
Igsf10	immunoglobulin superfamily, member 10
Igsf9	immunoglobulin superfamily, member 9
Il1b	interleukin 1 beta
Inpp5j	inositol polyphosphate 5-phosphatase J
Irgm1	immunity-related GTPase family M member 1
Irs2	insulin receptor substrate 2
Itgav	integrin alpha V
Ivd	isovaleryl coenzyme A dehydrogenase
Iyd	iodotyrosine deiodinase
Jph4	junctophilin 4
Kcna2	potassium voltage-gated channel, shaker-related subfamily, member 2
Kcnf1	potassium voltage-gated channel, subfamily F, member 1
Kcnj10	potassium inwardly-rectifying channel, subfamily J, member 10
Kcnk3	potassium channel, subfamily K, member 3
Kdr	kinase insert domain protein receptor
Kif12	kinesin family member 12
Kit	kit oncogene
Krt1	keratin 1
Lama2	laminin, alpha 2
Lamb1	laminin B1
Lcn2	lipocalin 2
Lipe	lipase, hormone sensitive
Lipg	lipase, endothelial
Lpcat1	lysophosphatidylcholine acyltransferase 1

Lpl	lipoprotein lipase
Lrig1	leucine-rich repeats and immunoglobulin-like domains 1
Lrig3	leucine-rich repeats and immunoglobulin-like domains 3
Lrp1	low density lipoprotein receptor-related protein 1
Ltbp4	latent transforming growth factor beta binding protein 4
Ltc4s	leukotriene C4 synthase
Mamdc2	MAM domain containing 2
Man2a2	mannosidase 2, alpha 2
Map2k6	mitogen-activated protein kinase kinase 6
Map3k13	mitogen-activated protein kinase kinase kinase 13
Mb	myoglobin
Mep1a	meprin 1 alpha
Mep1b	meprin 1 beta
Mertk	c-mer proto-oncogene tyrosine kinase
Mks1	Meckel syndrome, type 1
Mlxipl	MLX interacting protein-like
Mmp3	matrix metallopeptidase 3
Mmp9	matrix metallopeptidase 9
Mybpc2	myosin binding protein C, fast-type
Myh4	myosin, heavy polypeptide 4, skeletal muscle
N4bp2	NEDD4 binding protein 2
Nid2	nidogen 2
Nod2	nucleotide-binding oligomerization domain containing 2
Nos2	nitric oxide synthase 2, inducible
Nov	nephroblastoma overexpressed gene
Nox1	NADPH oxidase 1
Nqo1	NAD (P)H dehydrogenase, quinone 1
Nr3c2	nuclear receptor subfamily 3, group C, member 2
Nrg1	neuregulin 1
Oas2	2'-5' oligoadenylate synthetase 2
Oas3	2'-5' oligoadenylate synthetase 3
Oplah	5-oxoprolinase (ATP-hydrolysing)

P2rx1	purinergic receptor P2X, ligand-gated ion channel, 1
P2ry4	pyrimidinergic receptor P2Y, G-protein coupled, 4
Pak6	p21 protein (Cdc42/Rac)-activated kinase 6
Palld	palladin, cytoskeletal associated protein
Papln	papilin, proteoglycan-like sulfated glycoprotein
Pcca	propionyl-Coenzyme A carboxylase, alpha polypeptide
Pck1	phosphoenolpyruvate carboxykinase 1, cytosolic
Pde2a	phosphodiesterase 2A, cGMP-stimulated
Pdgfra	platelet derived growth factor receptor, alpha polypeptide
Pdk2	pyruvate dehydrogenase kinase, isoenzyme 2
Pdk4	pyruvate dehydrogenase kinase, isoenzyme 4
Pik3cg	phosphoinositide-3-kinase, catalytic, gamma polypeptide
Pik3r3	phosphatidylinositol 3 kinase, regulatory subunit, polypeptide 3 (p55)
Pim1	proviral integration site 1
Pipox	pipecolic acid oxidase
Pla2g3	phospholipase A2, group III
Plcb2	phospholipase C, beta 2
Pld2	phospholipase D2
Plin1	perilipin 1
Pltp	phospholipid transfer protein
Pm20d1	peptidase M20 domain containing 1
Pnpla3	patatin-like phospholipase domain containing 3
Ppargc1b	peroxisome proliferative activated receptor, gamma, coactivator 1 beta
Prkcd	protein kinase C, delta
Prss30	protease, serine 30
Ptch1	patched 1
Ptprm	protein tyrosine phosphatase, receptor type, M
Ptpru	protein tyrosine phosphatase, receptor type, U
Rab3b	RAB3B, member RAS oncogene family
Rab3c	RAB3C, member RAS oncogene family

Rab4a	RAB4A, member RAS oncogene family
Rac3	RAS-related C3 botulinum substrate 3
Ramp2	receptor (calcitonin) activity modifying protein 2
Rapgef3	Rap guanine nucleotide exchange factor (GEF) 3
Rasd2	RASD family, member 2
Rasef	RAS and EF hand domain containing
Rcan2	regulator of calcineurin 2
Reg3b	regenerating islet-derived 3 beta
Ret	ret proto-oncogene
Ripk3	receptor-interacting serine-threonine kinase 3
Rorc	RAR-related orphan receptor gamma
Runx2	runt related transcription factor 2
S100a8	S100 calcium binding protein A8 (calgranulin A)
S100a9	S100 calcium binding protein A9 (calgranulin B)
S100g	S100 calcium binding protein G
Sall1	sal-like 1 (Drosophila)
Scn2b	sodium channel, voltage-gated, type II, beta
Sema5a	sema domain, seven thrombospondin repeats (type 1 and type 1-like), transmembrane domain (TM) and short cytoplasmic domain, (semaphorin) 5A
Sgk1	serum/glucocorticoid regulated kinase 1
Shank2	SH3/ankyrin domain gene 2
Slc2a10	solute carrier family 2 (facilitated glucose transporter), member 10
Slc2a4	solute carrier family 2 (facilitated glucose transporter), member 4
Slc7a11	solute carrier family 7 (cationic amino acid transporter, y+ system), member 11
Slc9a2	solute carrier family 9 (sodium/hydrogen exchanger), member 2
Slc9a3	solute carrier family 9 (sodium/hydrogen exchanger), member 3

Slc10a5	solute carrier family 10 (sodium/bile acid cotransporter family), member 5
Slc12a8	solute carrier family 12 (potassium/chloride transporters), member 8
Slc13a2	solute carrier family 13 sodium-dependent dicarboxylate transporter), member 2
Slc15a1	solute carrier family 15 (oligopeptide transporter), member 1
Slc16a5	solute carrier family 16 (monocarboxylic acid transporters), member 5
Slc20a1	solute carrier family 20, member 1
Slc26a2	solute carrier family 26 (sulfate transporter), member 2
Slc26a3	solute carrier family 26, member 3
Slc27a1	solute carrier family 27 (fatty acid transporter), member 1
Slc34a2	solute carrier family 34 (sodium phosphate), member 2
Slc36a2	solute carrier family 36 (proton/amino acid symporter), member 2
Slc43a1	solute carrier family 43, member 1
Slfn5	schlafen 5
Sned1	sushi, nidogen and EGF-like domains 1
Sord	sorbitol dehydrogenase
Sphk1	sphingosine kinase 1
St6gal1	beta galactoside alpha 2,6 sialyltransferase 1
Stk10	serine/threonine kinase 10
Sult1a1	sulfotransferase family 1A, phenol-preferring, member 1
Sult2b1	sulfotransferase family, cytosolic, 2B, member 1
Svep1	sushi, von Willebrand factor type A, EGF and pentraxin domain containing 1
Syn2	synapsin II
Tap1	transporter 1, ATP-binding cassette, sub-family B (MDR/TAP)
Tcf21	transcription factor 21
Tek	endothelial-specific receptor tyrosine kinase
Tmem173	transmembrane protein 173

Tnf	tumor necrosis factor
Trpm6	transient receptor potential cation channel, subfamily M, member 6
Trpv3	transient receptor potential cation channel, subfamily V, member 3
Ttll10	tubulin tyrosine ligase-like family, member 10
Tusc5	tumor suppressor candidate 5
Ube2l6	ubiquitin-conjugating enzyme E2L 6
Ugdh	UDP-glucose dehydrogenase
Ugt1a7c	UDP glucuronosyltransferase 1 family, polypeptide A7C
Ugt2b34	UDP glucuronosyltransferase 2 family, polypeptide B34
Ugt2b35	UDP glucuronosyltransferase 2 family, polypeptide B35
Upk3b	uroplakin 3B
Usp2	ubiquitin specific peptidase 2
Vdr	vitamin D receptor
Wars	tryptophanyl-tRNA synthetase
Wnk4	WNK lysine deficient protein kinase 4
Zan	zonadhesin
Zap70	zeta-chain (TCR) associated protein kinase

5.4. Introduction

The reduction-oxidation (redox) environment regulates many physiological and pathophysiological mechanisms in cellular biology. Oxidative stress refers to a deviation from the physiological redox state and an increase in pro-oxidants, or free radicals, that structurally change lipids, proteins and DNA in a way that causes pathology or damage to a cell (Sies, 2015). The most widely studied free radicals are reactive oxygen species (ROS) which can also include reactive molecules that have a stable charge. The three major endogenous ROS include the superoxide anion ($O_2^{\cdot -}$), hydroxyl radical (•OH), and hydrogen peroxide (H_2O_2) (Birben et al., 2012, Schieber and Chandel, 2014). $O_2^{\cdot -}$ is predominantly generated by nicotinamide adenine dinucleotide phosphate, reduced (NADPH)-oxidase (NOX) family enzymes or, by the mitochondria, as a by-product of oxidative phosphorylation (Dan Dunn et al., 2015). The level of mitochondria-derived $O_2^{\cdot -}$ depends on metabolic substrates, cytosolic Ca^{2+} levels, pH and oxygen tension (Aon et al., 2010). $O_2^{\cdot -}$ generated from complexes of the electron transport chain (ETC) are highly reactive and can damage the mitochondrion (Chen et al., 2009). The detoxification of $O_2^{\cdot -}$ into H_2O_2 is mediated by superoxide dismutase (SOD) (Dan Dunn et al., 2015). However, H_2O_2 can also be generated in various metabolic processes and by dual oxidases (DUOX) (De Deken et al., 2014). While H_2O_2 is more stable than $O_2^{\cdot -}$, its detoxification is crucial as it possesses a weak peroxide bond that makes it susceptible to reacting with metals, such as Fe^{2+}, to generate reactive •OH through the Fenton reaction (Winterbourn, 1995). Both, H_2O_2 and $O_2^{\cdot -}$, are diffusible across cell membranes and can affect many cellular processes (Bienert et al., 2006, Fisher, 2009).

Oxidative stress has been associated with many pathologies, however, neurons are particularly susceptible to oxidative insult due to their high metabolic demands and reliance on oxidative phosphorylation (Friedman, 2011). Likewise, oxidative stress has been demonstrated to damage the enteric nervous system (ENS) in models of chemotherapy, diabetes and physiological aging (Thrasivoulou et al., 2006, Chandrasekharan et al., 2011, McQuade et al., 2016, McQuade et al., 2018). Oxidative stress is also prominent in experimental intestinal inflammation and

inflammatory bowel disease (IBD) which has been predicted to contribute to dysfunction in the ENS and the disease pathophysiology (Lih-Brody et al., 1996, Sundaram et al., 2003, Lakhan and Kirchgessner, 2010, Roberts et al., 2013, Piechota-Polanczyk and Fichna, 2014). Oxidative stress is augmented by a number of enzymes that participate in the intestinal inflammatory response, including: NOX, nitric oxide synthase (NOS), lipoxygenase (LOX), cyclooxygenase (COX) and myeloperoxidase (MPO) (Piechota-Polanczyk and Fichna, 2014). Furthermore, ROS upregulate several genes involved in the inflammatory response and increased mucosal permeability resulting in enterotoxic and antigenic insult, thus, perpetuating the inflammatory response (Tian et al., 2017). This may also be mediated by mitochondrial dysfunction which can cause metabolic and oxidative stress in IBD and contributes to the pathogenesis of chronic intestinal inflammation (Schoultz et al., 2011, Novak and Mollen, 2015). H_2O_2 is present at high concentrations in intestinal inflammation and is a potent enteric neurotoxin (Lourenssen et al., 2009, Shi et al., 2010). During experimental colitis, high levels of $O_2^{\cdot -}$ are also observed in the myenteric ganglia (Brown et al., 2016). Free radicals can alter the electrophysiological properties of enteric neurons, damage neuronal membranes and cause neurotoxicity (Gaginella et al., 1992, Wada-Takahashi and Tamura, 2000, Roberts et al., 2013, Brown et al., 2016). Therefore, alleviating oxidative stress may reduce damage to ENS in intestinal inflammation.

Mesenchymal stem cells (MSCs) exhibit multiple properties that can ameliorate oxidative stress. MSCs can supress ROS generation associated with the immune response, promote the expression of endogenous antioxidant defences and directly scavenge or detoxify free radicals via a complement of constitutively expressed antioxidant enzymes (**Chapter 1, Section 1.4**). Previously, MSCs have been demonstrated to alleviate intestinal inflammation by modulating the immune response (**Chapter 1, Section 1.2.9.2 & Chapter 3**) (Gonzalez-Rey et al., 2009, González et al., 2009, Anderson et al., 2013b). Recently, MSCs were also demonstrated to ameliorate concomitant oxidative stress in acute dextran sodium sulphate (DSS)-induced colitis by normalising the redox state and increasing SOD activity (Sun et al., 2015, da Costa Gonçalves et al., 2017). However, the

antioxidant properties of MSCs have not been investigated in a spontaneous chronic model of colitis. Previously, we demonstrated that bone marrow-MSCs (BM-MSCs) can attenuate myenteric neuropathy (**Chapter 2, Figure 2.5 & Chapter 4, Figure 4.8**). MSCs have also been demonstrated to be therapeutic in experimental models of neurological pathologies of the central nervous system and in neuronal cultures *in vitro* by reducing oxidative stress (Lanza et al., 2009, Calió et al., 2014, Kim et al., 2015, de Godoy et al., 2018). Therefore, MSC treatments may reduce damage to the ENS by alleviating oxidative stress associated with intestinal inflammation. In this study, the effects of BM-MSCs on oxidative stress were investigated in the *Winnie* mouse model of spontaneous chronic inflammation to elucidate their mechanisms of neuroprotection.

5.5. Methods

5.5.1. Animals

For organotypic *in vitro* studies, male C57BL/6 mice aged 14 weeks (total n=22) were obtained from the Animal Resource Centre (Perth, Western Australia, Australia). For *in vivo* experiments, male *Winnie* mice aged 14 weeks (total n=14) were obtained from Victoria University (Melbourne, Victoria, Australia). *Winnie* mice were compared to age matched male C57BL/6 mice (n=10) obtained from the Animal Resource Centre (Perth, Western Australia, Australia). All mice had *ad libitum* access to food and water and were housed in a temperature-controlled environment with a 12-h day/night cycle. Mice were acclimatised for one week at the Western Centre for Health, Research and Education (Melbourne, Victoria, Australia). All mice were culled by cervical dislocation and the distal portion of the colon was collected for subsequent experiments. All animal experiments in this study complied with the guidelines of the Australian Code of Practice for the Care and Use of Animals for Scientific Purposes and were approved by the Victoria University Animal Experimentation Ethics Committee.

5.5.2. Cell culture and passaging

The MSCs used in this study were derived from human bone marrow (BM-MSC) and were obtained from Tulane University, USA. These BM-MSCs were extensively characterised for cell surface markers, differentiation potential, proliferation, colony formation, morphology and adherence to plastic (Stavely et al., 2015b) (**Chapter 2, Figures 2.1 & 2.2**) and conform to the guidelines set by the International Society for Cell Therapy (Dominici et al., 2006). BM-MSCs were cultured as previously described to generate the required numbers for animal treatments and cell culture experiments (**Chapter 3, Section 3.5.2**). Cells prepared for *in vivo* and *in vitro* experiments had a viability of over 95% after trypsinisation and were used only at the fourth passage to minimise the chance of acquiring genetic abnormalities (Ueyama et al., 2012).

5.5.3. Organotypic culture of myenteric ganglia

Tissues collected from the distal portion of the colon were viewed under a dissection microscope, cut along the mesenteric border and pinned mucosal side up in a silicon-lined Petri dish containing Hank's balanced salt solution (Sigma-Aldrich, Sydney, Australia). The preparations were immediately dissected to remove the mucosa and submucosa layers before being cut into 1.5cm^2 sheets. The organotypic sheet preparations were loosely pinned into 24-well cell culture plates that were modified to contain a silicon elastomer (Sylgard; Dow Corning, USA) that covered the bottom of the wells with a depth of ~5mm. Preparations were incubated (37°C, 5% CO_2) for 24h in α-MEM supplemented with 100 U/mL penicillin/streptomycin, 1% glutaMAX and 5% (v/v) foetal bovine serum (FBS) (Gibco®, Life Technologies, Melbourne, Australia, for all), unless stated otherwise. Hyperoxic oxygen tension, and the chemical H_2O_2, were utilised as oxidative stimuli in organotypic preparations. A hyperoxic environment was formed using a self-contained modular incubator (Billups-Rothenberg, Inc., San Diego, CA, USA). Tissue culture plates were placed into the modular incubator before it was purged

with a gas mixture of 95% O_2 and 5% CO_2 for 5min (D'Agostino et al., 2007, Matott et al., 2014). The modular incubator was then sealed air-tight and placed into the same incubator as the control preparations. H_2O_2 has been utilised as an *in vitro* or *in vitro* oxidative stimulus for enteric neurons in several studies (Lourenssen et al., 2009, Pouokam et al., 2009, Abdo et al., 2010, Korsak et al., 2012, Bianco et al., 2016, Bubenheimer et al., 2016). Organotypic cultures were exposed to H_2O_2 diluted in α-MEM at a final concentration of 100µM. An equal volume of the α-MEM vehicle was applied to control cultures. Organotypic preparations were co-cultured with BM-MSCs at a concentration of 1×10^5 cells per well. BM-MSCs were either directly cultured in the wells of organotypic tissues, or, for paracrine experiments, were placed in a transwell semipermeable insert (0.4µm pore size; Sigma-Aldrich) that contained the same media as organotypic cultures. To assess the role of SOD1, the antagonist LCS-1 (Sigma-Aldrich), was applied to organotypic cultures at a final concentration of 10µM. For these experiments, the dimethyl sulfoxide (DMSO) vehicle for LCS-1 was present in all cultures at a concentration of 0.05% (v/v). The effects of DMSO was assessed in control, H_2O_2 and H_2O_2+BM-MSC treated organotypic cultures. In all experiments, organotypic preparations were cultured for 24h before being fixed overnight at 4°C in Zamboni's fixative (2% formaldehyde and 0.2% picric acid). Preparations were subsequently washed in DMSO (Sigma-Aldrich) (3x10min), to permeabilise the tissue, and phosphate buffered saline (PBS) (3x10min), to remove DMSO and the fixative for immunohistochemical experiments.

5.5.4. MSC administration

BM-MSCs were administered into *Winnie* mice with chronic colitis by enema. A lubricated silicone catheter was inserted 3cm proximal to the anus of mice anesthetised with 2% isoflurane. *Winnie* mice were treated with two doses of $4x10^6$ BM-MSCs in 100µL of sterile PBS and subsequently received two replenishment doses of $2x10^6$ BM-MSCs in the same volume of sterile PBS. All treatments were administered 4 days apart. Sham-treated *Winnie* mice underwent the same

procedure on the same days with an injection of sterile PBS at the same volume (*Winnie*-sham). Mice were culled 24h after the final treatment.

5.5.5. Immunohistochemistry

Antibody labelling of fixed organotypic preparations was performed using the methodology previously described for the immunolabeling of wholemount preparations (**Chapter 4, Section 4.5.4**). Organotypic preparations were labelled with the primary antibody chicken anti-microtubule associated protein (MAP)-2 (1:5000; Abcam) and secondary antibody Alexa Fluor 594 donkey anti-chicken (1:500; Jackson Immunoresearch, West Grove, USA) prior to being washed with PBS (3x10min) and mounted for imaging.

Cross sections of the distal colon from *in vivo* experiments were prepared using the methodology previously described (**Chapter 3, Section 3.5.6**). Immunohistochemical procedures followed previously detailed methodology (**Chapter 3, Section 3.5.6**) with the exception of an additional procedure to block endogenous mouse immunoglobin (Ig). Briefly, sections were incubated in 10% normal donkey serum (NDS) (Merck Millipore, Sydney, Australia) and Triton X-100 at room temperature for 1h before immunolabelling. Sections were then incubated for an additional 1h at room temperature with the goat unconjugated affinity purified F(ab) fragment anti-mouse IgG (H+L) antibody (1:100; Abcam, Melbourne, Australia). This additional blocking step was performed to improve labelling with monoclonal mouse primary antibodies and reduce background labelling (Lu and Partridge, 1998). Sections were washed with PBS (3x10min) and incubated overnight at 4°C with the primary antibodies chicken anti-MAP-2 (1:5000) and mouse anti-8-hydroxy-2'-deoxyguanosine (8-OHdG) (1:200; Abcam). Sections were washed as described above and incubated with Alexa Fluor 594 donkey anti-chicken (1:500) and Alexa Fluor 488 donkey anti-mouse (1:500; Jackson Immunoresearch) for 1h at room temperature before being mounted for imaging.

5.5.6. MitoSOX Red fluorescent staining

The production of $O_2^{\cdot -}$ in the myenteric plexus was assessed in freshly excised colon segments. Tissues were collected in physiological saline (composition in mmol L^{-1}: NaCl, 117; NaH2PO4, 1.2; MgSO4, 1.2; CaCl2, 2.5; KCl, 4.7; NaHCO3, 25; and glucose, 11) containing 3μM nicardipine (Sigma-Aldrich) to inhibit muscle contraction. The solution of physiological saline was gently bubbled with carbogen throughout the entire procedure. Tissues were viewed under a dissection microscope, cut along the mesenteric border and pinned in a silicon-lined Petri dish containing physiological saline. The mucosa, submucosa and circular smooth muscle was immediately removed to expose the myenteric plexus and longitudinal muscle (LMMP). Tissues were incubated for 40min at 37°C in physiological saline containing MitoSOX Red (1:1000) (Molecular Probes®, Thermofisher, Melbourne, Australia), a fluorogenic indicator of $O_2^{\cdot -}$ derived from the mitochondria. Tissues were then washed in physiological saline (3×10min) prior to being fixed in 4% paraformaldehyde overnight at 4°C. Paraformaldehyde was removed by washing the tissues with PBS (3×10min) before they were mounted onto glass slides with DAKO fluorescence mounting medium (Agilent Technologies, Melbourne, Australia) and visualised by confocal microscopy.

5.5.7. Imaging and analysis

An Eclipse Ti confocal laser scanning system (Nikon, Tokyo, Japan) was used to visualise MAP-2 and 8-OHdG immunofluorescence or the MitoSOX red fluorogenic probe. Identical acquisition settings were used between samples in all experiments. Images were collected as .ND2 files which contained all metadata including fluorescence signals at all Z levels. Images were visualised using Image J v1.50b open source software (National Institute of Health, Bethesda, USA) (Schneider et al., 2012, Rueden et al., 2017) with the Image J ND2 Reader plugin and were converted into maximum intensity projections in 16-bit .TIFF format. All subsequent analysis was performed using Image J. For all analyses, average mean values were calculated from eight individual images per sample.

For organotypic preparations, Z-series images were randomly acquired using the 40X objective at a thickness of 1µm. The average neuronal density was calculated within a 0.1mm^2 (316.23µm x 316.23µm = 100,000µm^2) field of view per image as previously described (Gulbransen et al., 2012) (**Chapter 4, Section 4.5.5**). Analysis was performed in eight randomly captured images per preparation. Values were expressed as the average number of neurons per 0.01mm^2 (100µm x 100µm = 10,000µm^2) area of ganglia.

Immunoreactivity for 8-OHdG in the mucosa/submucosa and muscle layers was visualised in cross sections of the distal colon. Z-series images were randomly acquired using the 20X objective at a thickness of 10µm. Eight randomly captured 16-bit images were analysed with a field of view of 0.4mm^2 (632.5µm x 632.5µm = 400,000µm^2) per image. Regions of interest were manually applied to the mucosa/submucosa and muscle layers. The fluorescence intensity of 8-OHdG immunoreactivity was measured as the mean grey value (mean fluorescence intensity) of the pixels within the regions of interest (Ray-Gallet et al., 2011, Kunda et al., 2012).

To measure 8-OHdG adducts in MAP-2 immunoreactive myenteric neurons, Z-series images were randomly acquired using the 60X objective at a thickness of 1µm. Eight randomly captured 16-bit images were analysed with a field of view of 0.04mm^2 (200µm x 200µm = 40,000µm^2) per individual image. Regions of interest were set over MAP-2 immunoreactive neurons. Images of 8-OHdG immunofluorescence were converted to binary images by thresholding for high intensity labelling (Rahman et al., 2015). Regions of interests defining the location of MAP-2 immunoreactive neurons were overlayed onto binary 8-OHdG images. Binary particles were then analysed to obtain the percentage area of 8-OHdG immunoreactivity within the area of myenteric neurons.

Mitochondria-derived superoxide ($O_2^{\cdot -}$) was visualised using the MitoSOX fluorogenic probe in wholemount LMMP preparations as previously described

(**Chapter 2, Section 2.4.12**). Eight Z-series images were randomly acquired per preparation using the 40X objective at a thickness of 1µm. Analysed images contained a field of view of 0.1mm^2 (316.23µm x 316.23µm = 100,000µm^2) per individual image. Regions of interest were set to determine MitoSOX fluorescence within the myenteric ganglia. The fluorescence intensity of $O_2^{\cdot -}$ in the ganglia was measured as the mean grey value (mean fluorescence intensity) of the pixels within the regions of interest.

5.5.8. Statistical analysis

Data analysis was performed using GraphPad Prism v7 (GraphPad Software Inc., San Diego, CA, USA). For direct comparisons, data were analysed using Student's *t*-test (two-tailed). For multiple groups, a one-way ANOVA was performed with a post hoc Holm-Sidak test for multiple comparisons. For all analyses $P \leq 0.05$ was considered significant. All data were presented as mean ± standard error of the mean (SEM).

5.5.9. RNA extraction and quality control

Total RNA was extracted from segments of the distal colon as previously described (**Chapter 3, Section 3.5.9**). Briefly, snap frozen colon was dissociated with a homogenising bead beater (TissueLyser LT, Qiagen, Melbourne, Australia) and RNA was extracted from the tissue homogenate using TRIzol® reagent (Thermo Fisher Scientific, Melbourne, Australia) and spin columns from the RNeasy Mini Kit (Qiagen, Melbourne, Australia). The concentration of RNA in each sample was quantified by a Qubit 1.0 fluorometer (Invitrogen, Thermo Fisher Scientific) using the Qubit® RNA Broad Range Assay Kit (Life Technologies) according to manufacturer's protocol. Contaminates (such as phenol) were evaluated in RNA samples using a DeNovix DS-11 spectrophotometer (Gene Target Solutions, Sydney, Australia). Absorbance (A) scores for all samples were between 1.8 – 2.0 for A260/A280 ratios and 2.0-2.2 for A260/A230 ratios, suggesting that nucleotide purity was high. The quality of RNA was assessed using an 2100 Bioanalyzer

(Agilent Technologies) microfluidics platform with the RNA 6000 Nano Kit (Agilent Technologies) according to the manufacturer's protocol. All samples were free from contamination of genomic DNA and 16S ribosomal RNA from bacteria. All samples were of very high quality and had minimal degradation with RNA integrity number (RIN) values between 9.9-10/10.

5.5.10. High-throughput RNA-Sequencing and bioinformatics

High-throughput sequencing of Poly-A tail purified mRNA was performed as described previously (**Chapter 3, Section 3.5.11**) with an experimental design similar to Seaman et al. (2015). Samples of RNA (n=7/group) from C57BL/6 and *Winnie* mice treated with either sham or BM-MSC enemas were submitted to the Australian Genome Research Facility (AGRF, Melbourne, Australia) and met all quality control criteria. High-throughput sequencing was performed using a 100bp single-end read protocol on the Illumina HiSeq 2500 System. Raw data were processed, and gene reads were mapped as previously described (**Chapter 3, Section 3.5.11**). Gene expression from raw mapped reads were calculated by the R package DEGseq v 1.34.0 (Wang et al., 2009). Differentially expressed genes (DEGs) were identified using the same package with a *P* value cut-off of <0.001 using the Benjamini-Hochberg correction (Benjamini and Hochberg, 1995). Resulting datasets were additionally cleaned by cut-offs for lowly expressed genes with <10 counts in a group and low changes in expression between ±0.5LogFC. Upregulated DEGs were analysed for enriched gene ontology (GO) terms (Ashburner et al., 2000) associated with biological processes, molecular function and cellular components using a rank-based method with a $P<0.001$ threshold by the web-based tool GOrilla (Eden et al., 2009). Selected, enriched gene ontologies identified using GOrilla were visualised as interaction maps by the R package clusterProfiler v3.8.1 (Yu et al., 2012). Upregulated DEGs were analysed for enrichment in the databases InterPro protein families (Finn et al., 2017) and Kyoto Encyclopedia of Genes and Genomes (KEGG) pathways (Kanehisa and Goto, 2000) using the web-based tool DAVID with a $P<0.05$ threshold and the Benjamini-Hochberg correction (Dennis et al., 2003, Huang et al., 2008b, Huang et

al., 2008a). Gene expression data on the transcriptome of human IBD patients were obtained from the National Centre for Biotechnology Information (NCBI) Gene Expression Omnibus (GEO) public data repository as previously described (**Chapter 3, Section 3.5.11**) (Edgar et al., 2002, Barrett et al., 2012). Data were uploaded by Peters et al. (2017); similar to our methods RNA was extracted by TRIzol, purified for mRNA and used the same sequencing platform. These data are accessible through GEO series accession number GSE83687 at https://www.ncbi.nlm.nih.gov/geo/. Gene expression of colon samples were used from this dataset including: male (n=14) and female (n=20) controls, male (n=19) and female (n=11) patients with ulcerative colitis (UC) and male (n=7) and female (n=4) patients with Crohn's disease (CD) (total n=75). Gene sets that were representative oxidative stress were collated from the gene ontology database for the terms *response to oxidative stress* (GO:0006979) and *antioxidant activity* (GO:0016209). The fold regulation of these genes were visualised as heat maps using the gplots R package (Warnes et al., 2009).

5.6. Results

5.6.1. BM-MSC treatments in chronic colitis upregulate genes associated with metabolism, detoxification and ion transport

Treatments with BM-MSCs were previously demonstrated to ameliorate leukocyte infiltration and inflammation in chronic colitis which paralleled a reduction in the expression of pro-inflammatory cytokines and chemokines (**Chapter 3, Section 3.6.3 & 3.6.4**). However, prior studies have also demonstrated that MSCs can upregulate endogenous processes in host tissue that can contribute to their therapeutic effect (Liu et al., 2010, Pulavendran et al., 2010, Liu et al., 2012, Shalaby et al., 2014). Therefore, the transcriptome was examined after BM-MSC treatments in chronic colitis to identify the processes that were upregulated by the therapy. This was assessed by high-throughput RNA-Seq performed on mRNA extracted from the distal colon of control C57BL/6 mice, *Winnie* treated with sham enema and *Winnie* mice treated with BM-MSCs. Analysis revealed 5619 DEGs

between *Winnie*-sham and control C57BL/6 mice and 1171 DEGs between BM-MSC and sham-treated *Winnie* mice. Many enriched InterPro protein families were observed in DEGs upregulated by BM-MSCs in *Winnie* mice (**Figure 5.1A, Table 5.1**). Within the top 15 enriched protein families, *Epidermal growth factor-like domain, EGF-like conserved site, Immunoglobulin I-set, Immunoglobulin subtype 2* and *Insulin-like growth factor binding protein N-terminal* were also enriched in DEGs downregulated in *Winnie*-sham compared to C57BL/6 mice. These families, along with *Tyrosine-protein kinase, receptor class III conserved site,* contained upregulated genes of growth factor receptors and extracellular matrix proteins that are involved in wound healing, angiogenesis, cell growth and cell survival. Families of metabolic enzymes were also enriched in DEGs upregulated in BM-MSC and sham-treated *Winnie* mice and DEGs downregulated in *Winnie* mice compared to C57BL/6 mice. These included *Cytochrome P450 E-class group I* and *Aldehyde dehydrogenase conserved site* which are associated with detoxification or the prevention of oxidative stress (Nebert and Russell, 2002, Ohsawa et al., 2003, Singh et al., 2013). Similarly, several other protein families that participate in detoxification and protection from oxidative stress were detected including *Glutathione S-transferase Mu class, Glutathione S-transferase C-terminal, Glutathione S-transferase N-terminal, Flavin monooxygenase FMO, Flavin monooxygenase-like* and *Dimethylaniline monooxygenase N-oxide-forming (Sharma et al., 2004, Cashman and Zhang, 2006)*; however these were only observed in DEGs upregulated by BM-MSC treatments in *Winnie* mice and were unaffected in *Winnie*-sham and C57BL/6 mice. Many genes within these groups are associated with antioxidative properties. An antioxidant effect of BM-MSC treatments is supported by previous analysis of KEGG pathways revealing that BM-MSCs downregulated genes associated with redox sensitive hypoxia-inducible factor-1 (HIF-1) signalling in *Winnie* mice (**Chapter 3, Table 3.2**).

Figure 5.1 ***Categorical terms grouping genes upregulated and downregulated by BM-MSCs in Winnie mice***

Bar charts representing the gene counts within the top fifteen terms enriched in deferentially expressed genes from InterPro **(A)** and KEGG **(B)** databases. Number of downregulated genes in *Winnie*-sham mice compared to C57BL/6 controls represented as black bars. Number of downregulated genes in BM-MSC-treated *Winnie* mice compared to *Winnie*-sham represented as yellow bars. Number of upregulated genes in *Winnie*-sham mice compared to C57BL/6 controls represented as grey bars. Number of upregulated genes in BM-MSC-treated *Winnie* mice compared to *Winnie*-sham represented as blue bars. Analysis performed using DAVID. Top fifteen terms ranked by *P* values with a cut off of $P<0.001$.

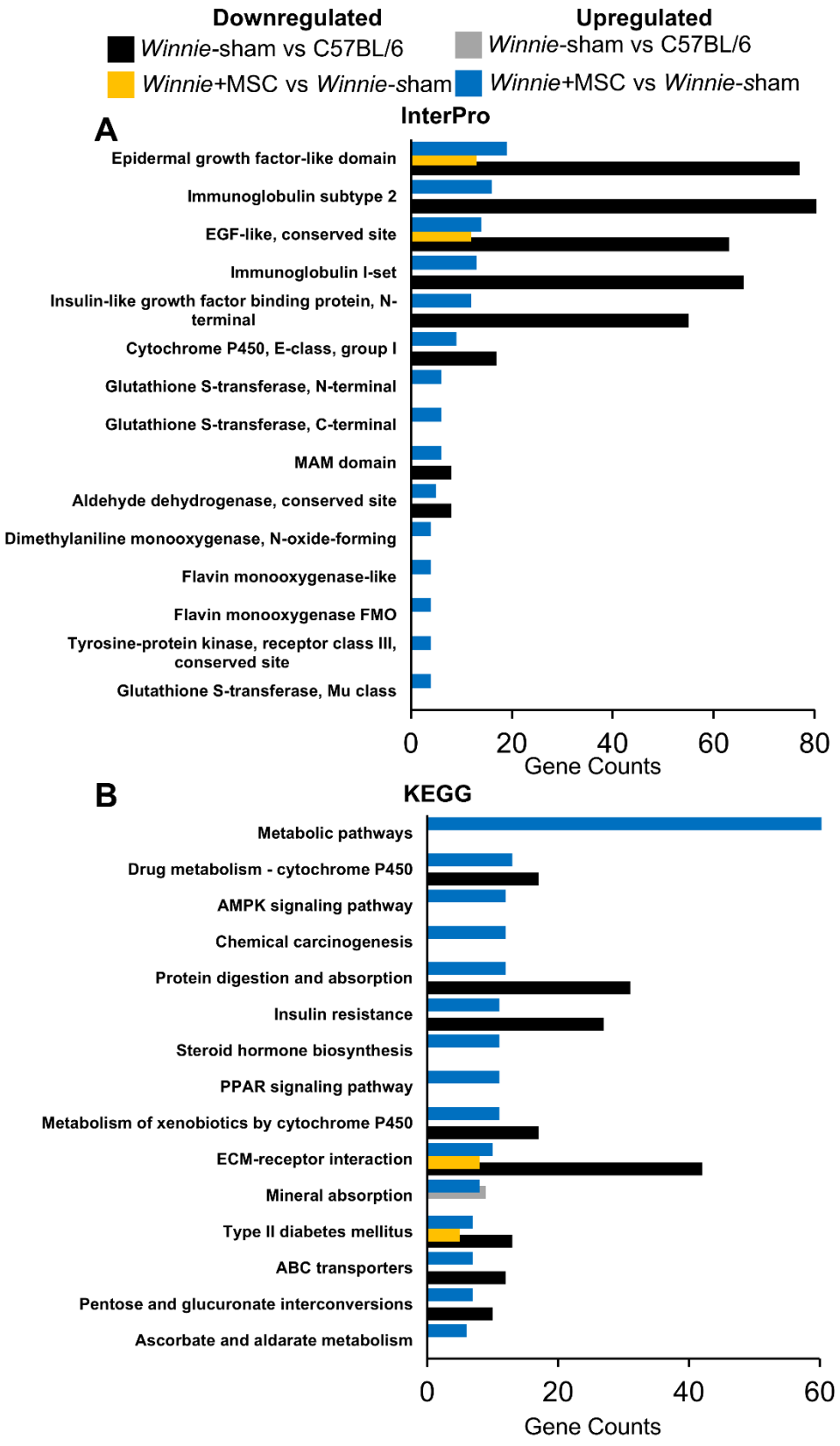
Downregulated
Winnie-sham vs C57BL/6
Winnie+MSC vs Winnie-sham
Upregulated
Winnie-sham vs C57BL/6
Winnie+MSC vs Winnie-sham
A
InterPro
Epidermal growth factor-like domain
Immunoglobulin subtype 2
EGF-like, conserved site
Immunoglobulin I-set
Insulin-like growth factor binding protein, N-terminal
Cytochrome P450, E-class, group I
Glutathione S-transferase, N-terminal
Glutathione S-transferase, C-terminal
MAM domain
Aldehyde dehydrogenase, conserved site
Dimethylaniline monooxygenase, N-oxide-forming
Flavin monooxygenase-like
Flavin monooxygenase FMO
Tyrosine-protein kinase, receptor class III, conserved site
Glutathione S-transferase, Mu class
0
20
40
60
80
Gene Counts
B
KEGG
Metabolic pathways
Drug metabolism - cytochrome P450
AMPK signaling pathway
Chemical carcinogenesis
Protein digestion and absorption
Insulin resistance
Steroid hormone biosynthesis
PPAR signaling pathway
Metabolism of xenobiotics by cytochrome P450
ECM-receptor interaction
Mineral absorption
Type II diabetes mellitus
ABC transporters
Pentose and glucuronate interconversions
Ascorbate and aldarate metabolism
0
20
40
60
Gene Counts

Table 5.1 ***Enrichment analysis of genes upregulated by BM-MSCs in Winnie mice using the InterPro database***

InterPro Term	Description	Fold Enrich.	Count	*P* Value	BH	Genes
IPR000742	Epidermal growth factor-like domain	3.28	19	2.29E-05	2.19E-02	*Svep1, Adam23, Ltbp4, Zan, Efemp1, Nid2, Edil3, Lama2, Lrp1, Sned1, Fat4, Tek, Mep1a, Mep1b, Cntnap1, Hhip, Fbn2, Nrg1, Lamb1*
IPR000998	MAM domain	13.62	6	5.61E-05	2.68E-02	*Ptprm, Mamdc2, Zan, Mep1a, Mep1b, Ptpru*
IPR013098	Immunoglobulin I-set	3.61	13	2.69E-04	8.31E-02	*Igdcc4, Fgfr3, Mybpc2, Lrig1, Papln, Lrig3, Palld, Kdr, Igsf10, Ccdc141, Pdgfra, Nrg1, Igsf9*
IPR009030	Insulin-like growth factor binding protein, N-terminal	3.77	12	3.52E-04	8.17E-02	*Lama2, Nov, Lrp1, Svep1, Sned1, 5330417c22rik, Fat4, Ltbp4, Igfbp6, Efemp1, Nid2, Fbn2*
IPR003081	Glutathione S-transferase, Mu class	23.35	4	4.71E-04	8.72E-02	*Gstm1, Gstm3, Gstm6, Gstm7*
IPR001824	Tyrosine-protein kinase, receptor class III, conserved site	20.43	4	7.40E-04	1.13E-01	*Flt3, Pdgfra, Kit, Kdr*
IPR016160	Aldehyde dehydrogenase, conserved site	11.35	5	8.19E-04	1.07E-01	*Aldh1a1, Aldh6a1, Aldh1b1, Aldh2, Aldh1a7*
IPR004046	Glutathione S-transferase, C-terminal	7.91	6	8.56E-04	9.85E-02	*Gstm1, Gsta3, Gstm3, Gstm6, Hpgds, Gstm7*
IPR003598	Immunoglobulin subtype 2	2.70	16	9.45E-04	9.67E-02	*Igdcc4, Fgfr3, Gm1123, Mybpc2, Lrig1, Papln, Lrig3, Kit, Hepacam2, Palld, Kdr, Ccdc141, Igsf10, Pdgfra, Nrg1, Igsf9*
IPR002401	Cytochrome P450, E-class, group I	4.43	9	9.50E-04	8.79E-02	*Cyp2d9, Cyp2c55, Cyp39a1, Cyp2d22, Cyp2s1, Cyp2c68, Cyp2d12, Cyp4f14, Cyp2e1*
IPR000960	Flavin monooxygenase FMO	18.16	4	1.09E-03	9.15E-02	*Fmo4, Fmo5, Fmo1, Fmo2*
IPR020946	Flavin monooxygenase-like	18.16	4	1.09E-03	9.15E-02	*Fmo4, Fmo5, Fmo1, Fmo2*
IPR012143	Dimethylaniline monooxygenase, N-oxide-forming	18.16	4	1.09E-03	9.15E-02	*Fmo4, Fmo5, Fmo1, Fmo2*
IPR004045	Glutathione S-transferase, N-terminal	7.43	6	1.15E-03	8.86E-02	*Gstm1, Gsta3, Gstm3, Gstm6, Hpgds, Gstm7*
IPR013032	EGF-like, conserved site	2.90	14	1.15E-03	8.24E-02	*Svep1, Adam23, Ltbp4, Efemp1, Zan, Edil3, Nid2, Lrp1, Sned1, Fat4, Tek, Hhip, Fbn2, Nrg1*

Fold enrich., enrichment scores; BH, Benjamini-Hochberg value

KEGG pathways enriched in DEGs upregulated by BM-MSCs in *Winnie* mice were predominantly associated with metabolism, with 65 DEGs associated with *Metabolic pathways* (**Figure 5.1B, Table 5.2**). A broad range of enriched pathways were related to cytochrome P450 detoxification and the metabolism, transport or signalling of proteins, simple carbohydrates, cholesterols, fatty acids and minerals which all together may reflect the restoration of physiological metabolism and functioning of the intestine after BM-MSC treatment.

Enrichment analysis of GO biological process terms also revealed that BM-MSCs upregulated DEGs associated with detoxification and ion homeostasis. This included: *xenobiotic metabolic process,* as well as, the processes *transmembrane transport, monovalent inorganic cation transport, monovalent inorganic cation homeostasis, cation transport* and *regulation of pH* (**Figure 5.2, Table 5.3**). The term *branching morphogenesis of an epithelial tube* was also enriched in DEGs upregulated by BM-MSCs in *Winnie* mice and may be reflective of restoration of the epithelial barrier. This is supported by the upregulation of the transcripts *Slc9a3, Slc9a2* and *Slc26a3* by BM-MSCs which are expressed on the apical membrane of epithelial cells and are involved in the regulation of ionic transport including pH and cation homeostasis (Lohi et al., 2002, Guan et al., 2006). Furthermore, dysfunction in these genes are associated with congenital diarrhoea and could contribute to the pathophysiology of intestinal inflammation (Mäkelä et al., 2002, Xu et al., 2011). Similarly, several GO terms related to molecular function detected in DEGs upregulated by BM-MSCs in *Winnie* mice were associated with maintaining ion gradients including *excitatory extracellular ligand-gated ion channel activity, substrate-specific channel activity, inorganic molecular entity transmembrane transporter activity, inorganic cation transmembrane transporter activity, ion channel activity* and *transmembrane transporter activity* (**Figure 5.3, Table 5.3**). Furthermore, *monooxygenase activity* was enriched which contained the flavin-containing monooxygenase (FMO) family genes. The terms *nucleotide binding* and *ATP binding* were also enriched in BM-MSC-treated *Winnie* mice.

Table 5.2 ***Enrichment analysis of genes upregulated by BM-MSCs in Winnie mice using the Kyoto Encyclopedia of Genes and Genomes (KEGG) database***

KEGG Term	Description	Fold Enrich.	Count	*P* Value	BH	Genes
mmu00982	Drug metabolism - cytochrome P450	2.43	13	6.01E-07	1.39E-04	*Gsta3, Cyp2e1, Gstm6, Gstm7, Gstm1, Fmo4, Fmo5, Gstm3, Ugt2b35, Ugt1a7c, Ugt2b34, Fmo1, Fmo2*
mmu00980	Metabolism of xenobiotics by cytochrome P450	2.06	11	2.17E-05	2.50E-03	*Gstm1, Gsta3, Gstm3, Ugt2b35, Ugt2b34, Ugt1a7c, Cyp2s1, Cyp2e1, Cbr3, Gstm6, Gstm7*
mmu01100	Metabolic pathways	12.17	65	2.53E-05	1.94E-03	*Amt, Cyp2c68, Cyp2s1, Acss2, Acss1, Aspa, Ugt1a7c, Ces1d, Plcb2, Hpd, Aldh6a1, Amy1, Ddc, Cyp2c55, Cyp2e1, Cbr3, Chpt1, Pnpla3, Man2a2, Glul, Cth, Aldh1b1, Hao2, Abat, Pla2g3, Pcca, Hsd3b2, Fut9, Alpi, Sord, Galnt5, Aldob, Ugdh, Pipox, Aldh1a1, Lpcat1, Inpp5j, Csad, Ivd, Dgkg, Fasn, Eno3, Aldh1a7, Acsl3, Hpgds, St6gal1, B3galt2, Cox8b, Acer1, Ephx2, Cyp4f14, Dgkh, Cps1, Pck1, Acsm3, Ugt2b35, Ugt2b34, Hmgcs2, Lipg, Aldh2, Gpt, Ahcyl2, Dpyd, Abo, Cbs*
mmu04974	Protein digestion and absorption	2.25	12	7.19E-05	4.14E-03	*Slc15a1, Col27a1, Slc9a3, Col6a3, Mep1a, Col6a2, Col6a1, Mep1b, Atp1a2, Col4a6, Dpp4, Col4a5*
mmu05204	Chemical carcinogenesis	2.25	12	1.08E-04	5.00E-03	*Gstm1, Gsta3, Cyp2c55, Gstm3, Ugt2b35, Ugt2b34, Ugt1a7c, Cyp2c68, Sult1a1, Cyp2e1, Gstm6, Gstm7*
mmu03320	PPAR signalling pathway	2.06	11	1.53E-04	5.89E-03	*Lpl, Slc27a1, Cd36, Plin1, Fabp4, Fabp2, Adipoq, Acsl3, Pltp, Angptl4, Pck1*
mmu04978	Mineral absorption	1.5	8	2.17E-04	7.13E-03	*Slc26a3, Vdr, Trpm6, Clcn2, Slc9a3, Cybrd1, S100g, Atp1a2*
mmu00140	Steroid hormone biosynthesis	2.06	11	3.09E-04	8.88E-03	*Cyp2d9, Hsd3b2, Cyp2c55, Ugt2b35, Cyp2d22, Ugt2b34, Ugt1a7c, Cyp2c68, Cyp2d12, Sult2b1, Cyp2e1*
mmu00040	Pentose and glucuronate interconversions	1.31	7	7.06E-04	1.80E-02	*Sord, Ugt2b35, Ugt2b34, Ugt1a7c, Aldh1b1, Ugdh, Aldh2*
mmu00053	Ascorbate and aldarate metabolism	1.12	6	1.21E-03	2.77E-02	*Ugt2b35, Ugt2b34, Ugt1a7c, Aldh1b1, Ugdh, Aldh2*
mmu04512	ECM-receptor interaction	1.87	10	1.44E-03	2.98E-02	*Lama2, Cd36, Col27a1, Col6a3, Col6a2, Col6a1, Lamb1, Col4a6, Hmmr, Col4a5*
mmu04152	AMPK signalling pathway	2.25	12	1.75E-03	3.31E-02	*Pik3cg, Irs2, Cd36, Slc2a4, Fasn, Creb3l1, Cftr, Foxo3, Pik3r3, Adipoq, Lipe, Pck1*
mmu04931	Insulin resistance	2.06	11	1.96E-03	3.42E-02	*Pik3cg, Slc27a1, Irs2, Cd36, Slc2a4, Mlxipl, Creb3l1, Pik3r3, Prkcd, Ppargc1b, Pck1*
mmu02010	ABC transporters	1.31	7	2.63E-03	4.25E-02	*Abca9, Abcb1a, Abca8a, Abcc3, Cftr, Abcg3, Abcg2*

Fold enrich., enrichment scores; BH, Benjamini-Hochberg value.

Figure 5.2 ***Effects of BM-MSCs on biological processes in the distal colon of Winnie mice***

A) Gene counts of top-ranked genes for selected representative terms describing biological processes from the gene ontology (GO) database. Enriched GO terms were identified in downregulated differentially expressed genes using RNA-Seq between *Winnie* mice vs C57BL/6 mice (black bars) and in upregulated differentially expressed genes between *Winnie* mice treated with BM-MSCs vs sham-treated *Winnie* mice (blue bars) by *GOrilla*. Genes were ranked by LogFC with a ±0.5 cut off and a *P* value of <0.001 for analysis. **B)** Binary matrix of differentially expressed genes (green) associated with greatest number of GO terms identified in genes upregulated by BM-MSC treatment in *Winnie* mice. **C)** An interaction network of differentially expressed genes and selected enriched GO terms from upregulated genes after BM-MSC treatment in *Winnie* mice.

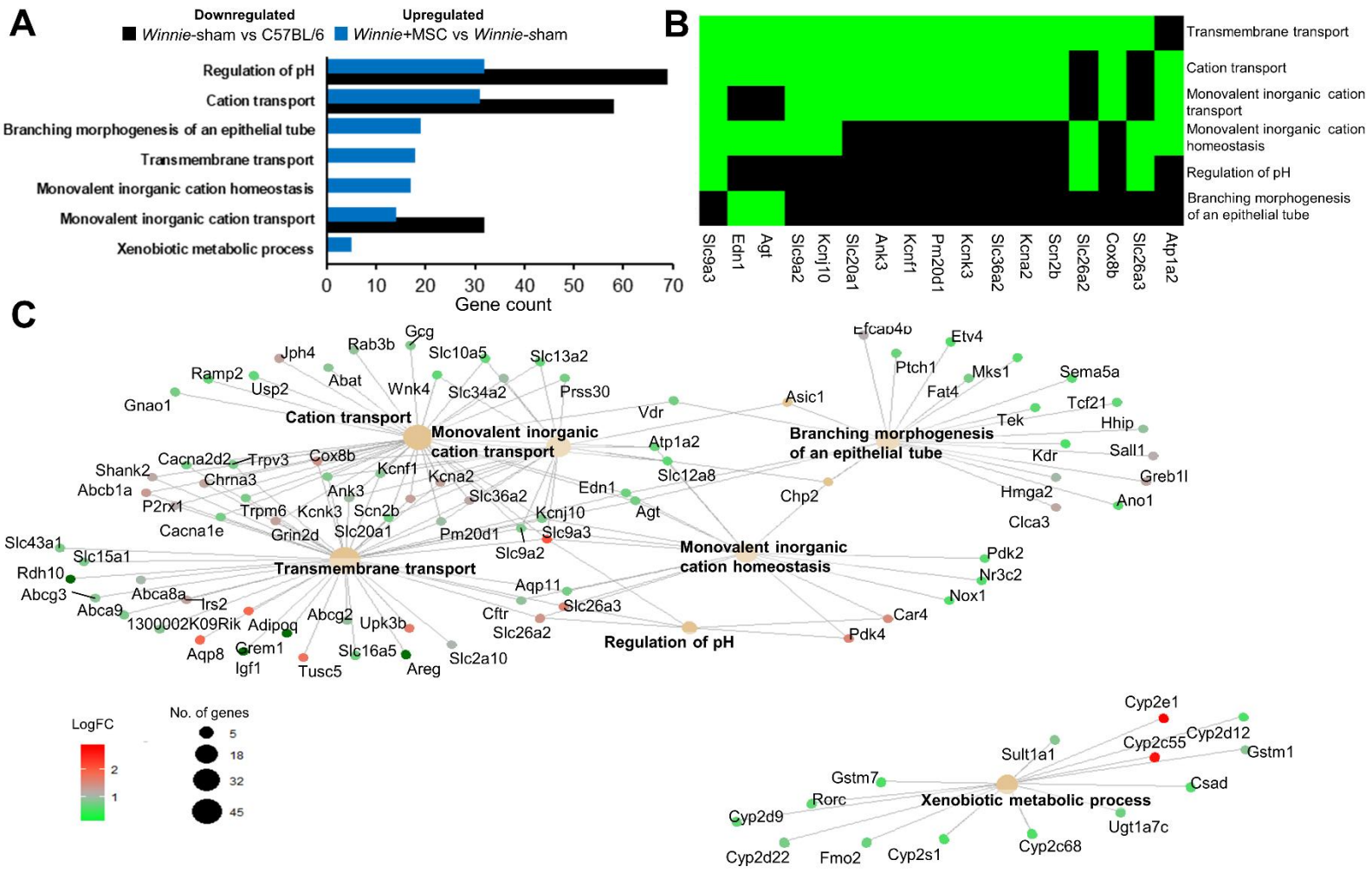
A
Downregulated
Upregulated
Winnie-sham vs C57BL/6
Winnie+MSC vs Winnie-sham
Regulation of pH
Cation transport
Branching morphogenesis of an epithelial tube
Transmembrane transport
Monovalent inorganic cation homeostasis
Monovalent inorganic cation transport
Xenobiotic metabolic process
0 10 20 30 40 50 60 70
Gene count
B
Transmembrane transport
Cation transport
Monovalent inorganic cation transport
Monovalent inorganic cation homeostasis
Regulation of pH
Branching morphogenesis of an epithelial tube
Slc9a3 Edn1 Agt Slc9a2 Kcnj10 Slc20a1 Ank3 Kcnf1 Pm20d1 Kcnk3 Slc36a2 Kcna2 Scn2b Slc26a2 Cox8b Slc26a3 Atp1a2
C
Cation transport
Monovalent inorganic cation transport
Transmembrane transport
Monovalent inorganic cation homeostasis
Regulation of pH
Branching morphogenesis of an epithelial tube
Xenobiotic metabolic process
LogFC
No. of genes
5
18
32
45
2
1

Figure 5.3. ***Effects of BM-MSCs on molecular functions in the distal colon of Winnie mice***

A) Gene counts of top-ranked genes for selected representative terms describing molecular functions from the gene ontology (GO) database. Enriched GO terms were identified in downregulated differentially expressed genes using RNA-Seq between *Winnie* mice vs C57BL/6 mice (black bars) and in upregulated differentially expressed genes between *Winnie* mice (blue bars) treated with BM-MSCs vs sham-treated *Winnie* mice by *GOrilla*. Genes were ranked by LogFC with a ±0.5 cut off and a *P* value of <0.001 for analysis. **B)** Binary matrix of differentially expressed genes (green) associated with greatest number of GO terms identified in genes upregulated by BM-MSC treatment in *Winnie* mice. **C)** An interaction network of differentially expressed genes and selected enriched GO terms from upregulated genes after BM-MSC treatment in *Winnie* mice.

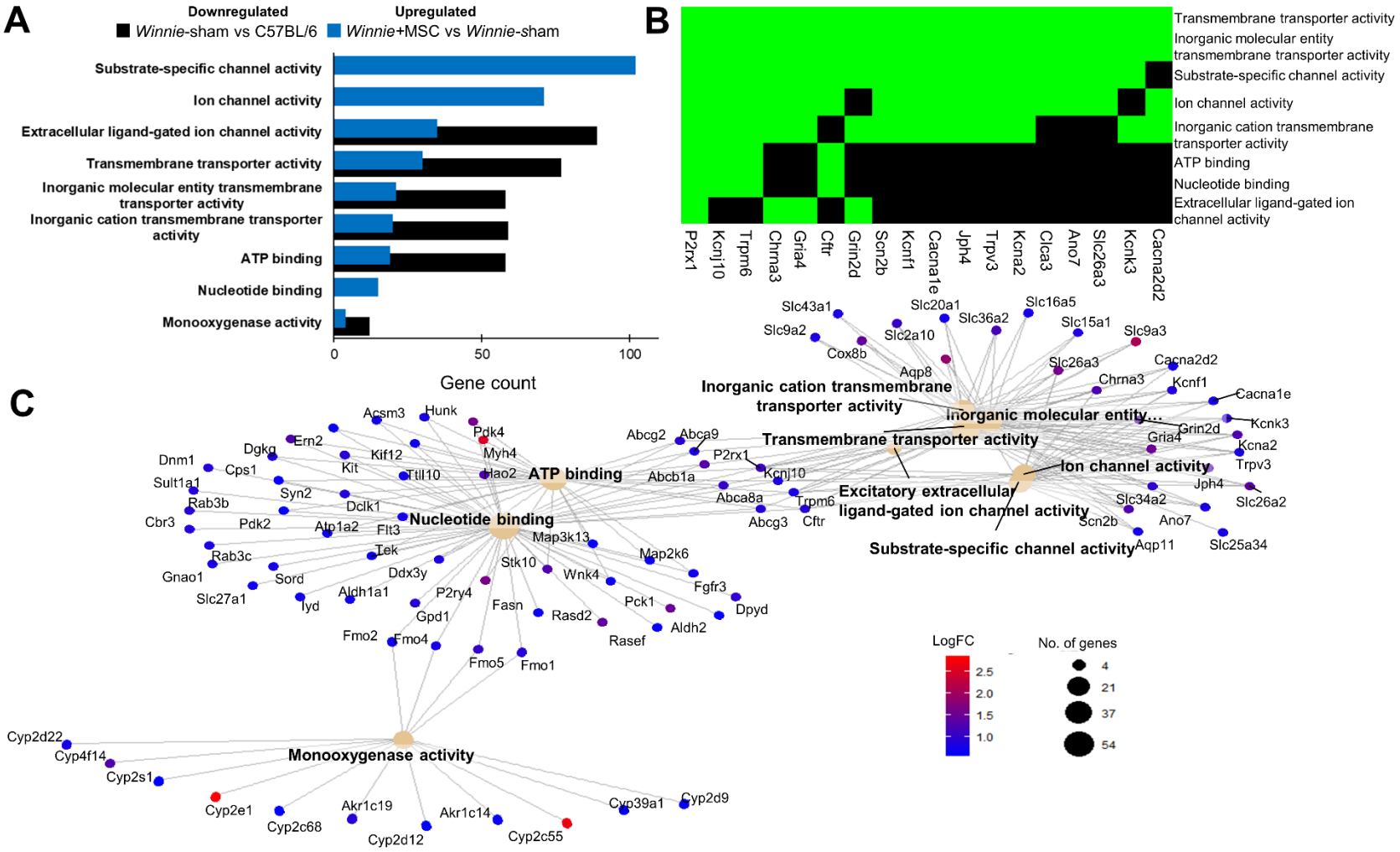
A
Downregulated
Upregulated
Winnie-sham vs C57BL/6
Winnie+MSC vs Winnie-sham
Substrate-specific channel activity
Ion channel activity
Extracellular ligand-gated ion channel activity
Transmembrane transporter activity
Inorganic molecular entity transmembrane transporter activity
Inorganic cation transmembrane transporter activity
ATP binding
Nucleotide binding
Monooxygenase activity
0
50
100
Gene count
B
Transmembrane transporter activity
Inorganic molecular entity transmembrane transporter activity
Substrate-specific channel activity
Ion channel activity
Inorganic cation transmembrane transporter activity
ATP binding
Nucleotide binding
Extracellular ligand-gated ion channel activity
P2rx1
Kcnj10
Trpm6
Chrna3
Gria4
Cftr
Grin2d
Scn2b
Kcnf1
Cacna1e
Jph4
Trpv3
Kcna2
Clca3
Ano7
Slc26a3
Kcnk3
Cacna2d2
C
Inorganic cation transmembrane transporter activity
Inorganic molecular entity...
Transmembrane transporter activity
Ion channel activity
Excitatory extracellular ligand-gated ion channel activity
Substrate-specific channel activity
ATP binding
Nucleotide binding
Monooxygenase activity
LogFC
No. of genes

Table 5.3 ***Enrichment analysis of genes upregulated by BM-MSCs in Winnie mice using the gene ontology (GO) database***

GO Term	Description	*P* Value	FDR q-value	Genes
Biological Process				
GO:0006805	Xenobiotic metabolic process	1.91E-04	1.65E-01	*Cyp2e1, Cyp2c55, Gstm1, Sult1a1, Cyp2d22, Ugt1a7c, Fmo2, Cyp2d9, Rorc, Csad, Cyp2c68, Gstm7, Cyp2s1, Cyp2d12*
GO:0015672	Monovalent inorganic cation transport	2.02E-04	1.55E-01	*Slc9a3, Cox8b, Scn2b, Kcna2, Slc36a2, Kcnk3, Slc34a2, Pm20d1, Kcnf1, Ank3, Kcnj10, Slc9a2, Prss30, Slc20a1, Atp1a2, Slc13a2, Slc10a5, Wnk4, Slc12a8*
GO:0055067	Monovalent inorganic cation homeostasis	3.88E-04	2.45E-01	*Slc9a3, Pdk4, Slc26a3, Car4, Slc26a2, Cftr, Kcnj10, Slc9a2, Aqp11, Agt, Edn1, Atp1a2, Slc12a8, Pdk2, Nr3c2, Nox1*
GO:0055085	Transmembrane transport	4.48E-04	2.39E-01	*Slc9a3, Aqp8, Adipoq, Tusc5, Upk3b, Slc26a3, Cox8b, Slc26a2, Abcb1a, Scn2b, Grin2d, Kcna2, Chrna3, Irs2, Shank2, Slc36a2, P2rx1, Slc2a10, Abca8a, Kcnk3, Pm20d1, Abcg2, Cftr, Kcnf1, Abcg3, Ank3, Kcnj10, Slc9a2, Abca9, Slc15a1, Trpm6, Slc43a1, Trpv3, Aqp11, Cacna1e, Agt, Slc16a5, Slc20a1, Cacna2d2, Edn1*
GO:0048754	Branching morphogenesis of an epithelial tube	5.02E-04	2.32E-01	*Greb1l, Sall1, Hmga2, Hhip, Fat4, Agt, Vdr, Edn1, Ptch1, Tcf21, Tek, Sema5a, Mks1, Etv4*
GO:0006812	Cation transport	7.39E-04	3.01E-01	*Slc9a3, Cox8b, Abcb1a, Scn2b, Grin2d, Kcna2, Chrna3, Jph4, Shank2, Slc36a2, P2rx1, Kcnk3, Slc34a2, Pm20d1, Rab3b, Abat, Kcnf1, Gcg, Ank3, Kcnj10, Slc9a2, Trpm6, Trpv3, Gnao1, Cacna1e, Agt, Vdr, Prss30, Slc20a1, Cacna2d2, Edn1, Atp1a2, Usp2, Ramp2, Slc13a2, Slc10a5, Wnk4*
GO:0006885	Regulation of pH	7.55E-04	2.75E-01	*Slc9a3, Pdk4, Slc26a3, Car4, Slc26a2*
Molecular Function				
GO:0005231	Excitatory extracellular ligand-gated ion channel activity	4.48E-05	2.46E-02	*Gria4, Chrna3, Grin2d, P2rx1*
GO:0022838	Substrate-specific channel activity	1.19E-04	3.28E-02	*Jph4, Ano7, Trpm6, Cacna1e, Kcnf1, Kcnj10, Slc26a3, Clca3, Scn2b, Gria4, Kcna2, Chrna3, Kcnk3, Cftr, Grin2d, Aqp8, Aqp11, Trpv3, P2rx1*
GO:0015318	Inorganic molecular entity transmembrane transporter activity	3.37E-04	3.09E-02	*Slc36a2, Trpm6, Slc20a1, Slc26a3, Kcna2, Slc15a1, Slc34a2, Slc9a2, Trpv3, Aqp8, Aqp11, P2rx1, Slc16a5, Slc2a10, Jph4, Ano7, Cacna1e, Kcnf1, Kcnj10, Cacna2d2, Slc43a1, Clca3, Scn2b, Gria4, Chrna3, Kcnk3, Cftr, Grin2d, Slc9a3, Slc26a2*
GO:0022890	Inorganic cation transmembrane transporter activity	3.66E-04	3.18E-02	*Jph4, Slc36a2, Trpm6, Cacna1e, Kcnf1, Kcnj10, Slc20a1, Cacna2d2, Scn2b, Gria4, Kcna2, Chrna3, Kcnk3, Slc15a1, Grin2d, Slc9a3, Slc34a2, Slc9a2, Trpv3, P2rx1, Slc2a10*
GO:0000166	Nucleotide binding	4.49E-04	3.52E-02	*Fasn, Gpd1, Oas3, Cbr3, Hk3, Oas2, Pik3cg, Prkcd, Cit, Ugdh, Wnk4, Ivd, Gch1, Abcb1a, Sult1a1, Adck3, Rac3, Dclk1, Pdgfra, Kit, Tek, Acsl3, Stk10, Abcg3, Nod2, Pdk2, Cftr, Pim1, Abo, Map2k6, Rab3b, Dnah8, Pck1, Tmem173, Dhrs11, Abcc3, Oplah, Cps1, Slc27a1, Acss2, Irgm1, Dpyd, N4bp2, Sgk1, Map3k13, Ripk3, Dgkg, Fmo2, Pnpla3, Iyd, P2ry4, Hunk, Pcca, Runx2, Dnm1, Ddx3y, Ern2, Bag2, Fmo4, Eif2s3y, Ttll10, Rasd2, Acsm3, Hk2, BC021891, P2rx1, Rab3c, Hao2, Aldh2, Aldh1a1, Chd6, Tap1, Wars, Rab4a, Flt3, Fmo1, Gnao1, Fmo5, Acss1, Cdx2, Fgfr3, Trpm6, Kdr, Glul, Kif12, Sord, Abca9, Abca8a, Myh4, Pde2a, Mertk, Hpgd, Pdk4, Atp1a2, Ube2l6, Kcnj10, Abcg2, Syn2, Rasef, Rapgef3*
GO:0004497	Monooxygenase activity	4.54E-04	3.40E-02	*Cyp39a1, Cyp2d12, Cyp4f14, Cyp2d9, Cyp2e1, Fmo4, Fmo2, Cyp2c55, Cyp2c68, Cyp2s1, Cyp2d22, Akr1c14, Fmo1, Akr1c19, Fmo5*
GO:0005216	Ion channel activity	4.76E-04	3.41E-02	*Jph4, Ano7, Trpm6, Cacna1e, Kcnf1, Kcnj10, Cacna2d2, Slc26a3, Clca3, Gria4, Kcna2, Scn2b, Chrna3, Cftr, Slc26a2, Trpv3, P2rx1*
GO:0005524	ATP binding	8.95E-04	5.47E-02	*Sphk1, Abcg8, Ddx3y, Ern2, Oas3, Hk3, Oas2, Pik3cg, Ttll10, Prkcd, Cit, Acsm3, Hk2, Wnk4, Ak4, BC021891, P2rx1, Abcb1a, Adck3, Dclk1, Pdgfra, Abcg5, Acta1, Kit, Acsl3, Tek, Stk10, Chd6, Abcg3, Nod2, Pdk2, Tap1,*

GO:0022857	Transmembrane transporter activity	9.00E-04	5.30E-02	*Wars, Cftr, Flt3, Pim1, Slfn5, Acss1, Map2k6, Dnah8, Fgfr3, Zap70, Trpm6, Kdr, Glul, Abcc3, Cps1, Oplah, Kif12, Ret, Acss2, Abca9, Abca8a, Myh4, N4bp2, Sgk1, Map3k13, Ripk3, Mertk, Pdk4, Ube2l6, Atp1a2, Kcnj10, Dgkg, Abcg2, P2ry4, Hunk, Syn2, Runx2, Pcca, Pak6 Slc36a2, Trpm6, Slc20a1, Slc26a3, Kcna2, Abca9, Abca8a, Slc15a1, Slc34a2, Slc9a2, Trpv3, Aqp8, Aqp11, Slc16a5, P2rx1, Abcb1a, Slc2a10, Jph4, Ano7, Cacna1e, Kcnf1, Kcnj10, Abcg2, Cacna2d2, Abcg3, Slc43a1, Clca3, Scn2b, Gria4, Chrna3, Kcnk3, Cftr, Grin2d, Slc9a3, Slc26a2*

FDR, false discovery rate.

Several genes within these terms were ATP dependent transporters or ion channels, including *Cftr* which is also present on the apical border of epithelial cells and is critical in many physiological intestinal functions (De Lisle and Borowitz, 2013). Together, analysis of protein families, pathways and gene ontologies indicated that BM-MSCs upregulated many genes that are associated with the maintenance of physiological processes of the colon. This included genes associated with metabolism and antioxidant defences. Metabolic and oxidative stress are evident in IBD which is associated with mitochondrial dysfunction and contributes to the pathogenesis of chronic intestinal inflammation (Schoultz et al., 2011, Novak and Mollen, 2015).

5.6.2. BM-MSC treatments alter the expression of oxidative stress-related genes

To assess changes in the transcriptome related to oxidative stress, a gene list was compiled and changes in gene expression were determined for DEGs within the terms *response to oxidative stress* (GO:0006979) and *antioxidant activity* (GO:0016209) (**Figure 5.4, Table 5.4**). Compared to uninflamed controls, both IBD patients and *Winnie* mice exhibited upregulation of the oxidative stress-associated genes *Itgav, Mmp3, Mmp9, Il1b, Hmox1, Anxa1, Alox5ap, Slc7a11, Bnip3* and *Hk3, as well as* downregulation of *Aldh6a1***,** *Aldh2***,** *Pdk2* and *Ppargc1b*. These patterns of expression were reversed by BM-MSC treatments in *Winnie* mice. The top genes upregulated by BM-MSCs in *Winnie* mice included: *Car3* and *Adipoq* which protect cells from oxidative stress-induced cell death (Ren et al., 2017, Silagi et al., 2018), *Cd36,* reduces inflammation in murine colitis (Oz et al., 2009), *Rcan2,* maintenance of neurological function (Sanna et al., 2006), alcohol dehydrogenase genes and glutathione-S-transferases. Several genes associated with oxidative stress were downregulated by BM-MSC treatments in *Winnie* mice. Many of these genes are associated with oxidative insult including: the pro-inflammatory genes, *Lcn2, Nos2, Tnf, S100a8* and *S100a9,* which are redox sensitive or contribute to ROS production; H_2O_2 generating, *Acox2, Duox1* and *Duoxa1* and haemoglobin genes *Hbb-b1, Hba-a2* and *Hp.*

Figure 5.4 ***Changes in the expression of genes associated with oxidative stress***

Heat map of the fold regulation of genes identified by RNA-Seq that selectively represent responses to oxidative stress or antioxidant activity. Fold regulation was determined between *Winnie* and C57BL/6 mice, *Winnie* mice treated with BM-MSCs and sham-treated *Winnie* mice, males and female patients with ulcerative colitis, as well as, male and female patients with Crohn's disease compared to the colon of uninflamed sex-matched controls (left to right columns). Upregulated and downregulated genes were visualised as red and green gradients between >5 and <-5 folds, respectively. Genes failing the initial cut off between ±0.5logFC are represented as black (no change).

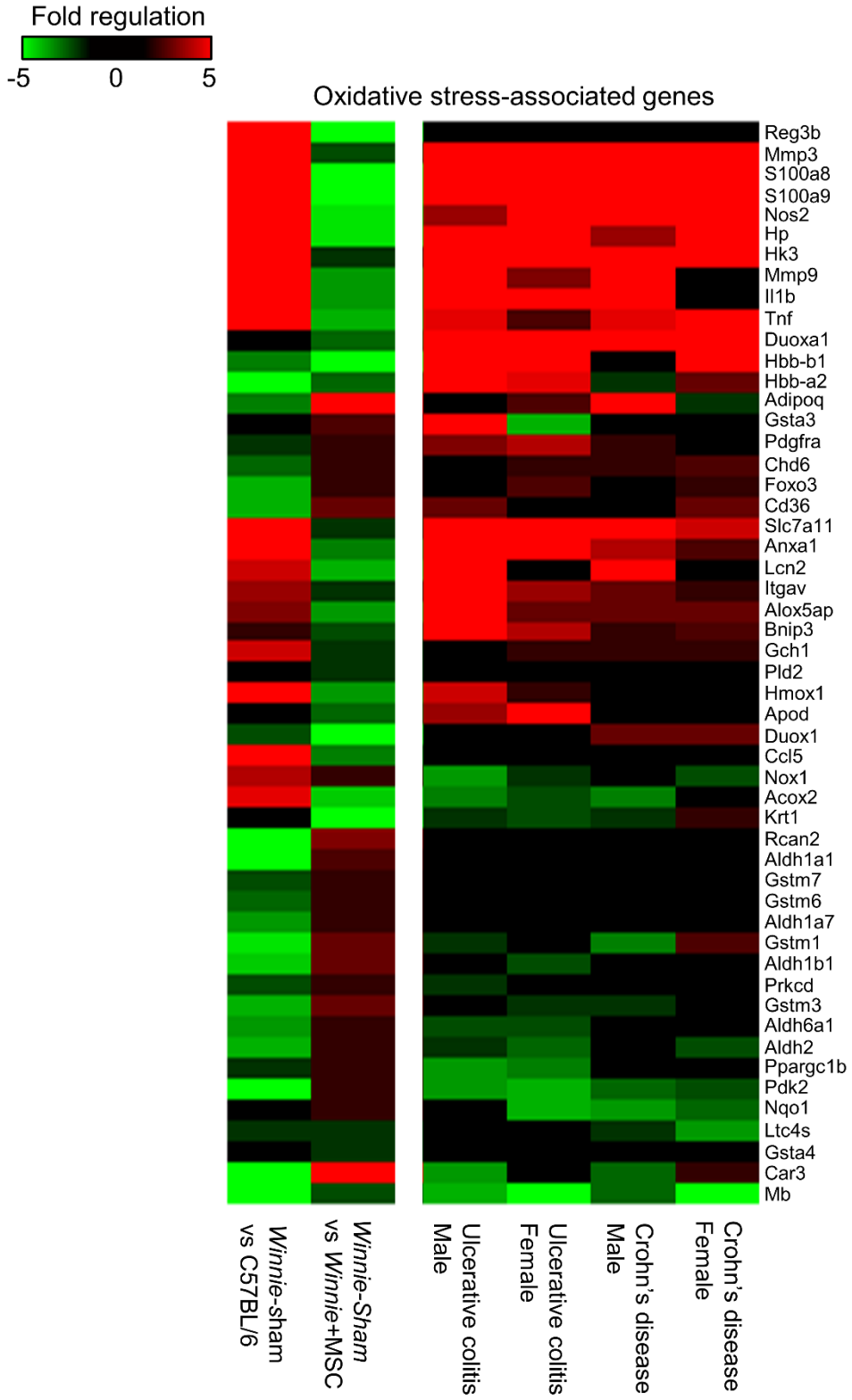
Fold regulation
-5
0
5
Oxidative stress-associated genes
Reg3b
Mmp3
S100a8
S100a9
Nos2
Hp
Hk3
Mmp9
Il1b
Tnf
Duoxa1
Hbb-b1
Hbb-a2
Adipoq
Gsta3
Pdgfra
Chd6
Foxo3
Cd36
Slc7a11
Anxa1
Lcn2
Itgav
Alox5ap
Bnip3
Gch1
Pld2
Hmox1
Apod
Duox1
Ccl5
Nox1
Acox2
Krt1
Rcan2
Aldh1a1
Gstm7
Gstm6
Aldh1a7
Gstm1
Aldh1b1
Prkcd
Gstm3
Aldh6a1
Aldh2
Ppargc1b
Pdk2
Nqo1
Ltc4s
Gsta4
Car3
Mb
Winnie-sham vs C57BL/6
Winnie-Sham vs Winnie+MSC
Ulcerative colitis Male
Ulcerative colitis Female
Crohn's disease Male
Crohn's disease Female

Table 5.4. ***Fold regulation of oxidative stress-associated genes***

Gene	*Winnie* MSC vs *Winnie*-sham	*Winnie*-sham vs C57BL/6	UC male vs control male	UC female vs control female	CD male vs control male	CD female vs control female
Car3	4.3	-9.0	-2.2	-1.1	-1.9	1.5
Adipoq	3.7	-2.1	1.3	1.7	9.9	-1.5
Rcan2	2.1	-6.1	1.2	1.3	-1.2	-1.2
Gstm3	1.9	-2.3	-1.2	-1.5	-1.6	-1.4
Cd36	1.9	-2.4	1.9	1.3	-1.2	1.9
Gstm1	1.8	-2.8	-1.6	-1.2	-2.0	1.7
Aldh1b1	1.8	-2.5	-1.3	-1.8	1.0	-1.4
Gsta3	1.7	1.1	4.8	-2.4	0.0	0.0
Aldh1a1	1.7	-4.2	1.1	-1.4	-1.3	-1.0
Aldh1a7	1.6	-2.1	0.0	0.0	0.0	0.0
Pdk2	1.6	-4.1	-2.2	-2.4	-1.8	-1.6
Ppargc1b	1.6	-1.4	-2.3	-2.0	-1.0	-1.0
Aldh2	1.6	-2.3	-1.6	-1.9	-1.3	-1.7
Nox1	1.5	2.4	-2.1	-1.5	1.1	-1.7
Gstm6	1.5	-1.8	0.0	0.0	0.0	0.0
Aldh6a1	1.5	-2.3	-1.6	-1.6	-1.1	-1.2
Gstm7	1.5	-1.6	0.0	0.0	0.0	0.0
Nqo1	1.5	-1.0	1.3	-2.4	-2.2	-1.9
Foxo3	1.5	-2.4	1.3	1.6	1.2	1.5
Pdgfra	1.4	-1.6	2.0	2.3	1.5	1.4
Chd6	1.4	-1.9	1.2	1.4	1.5	1.7
Prkcd	1.4	-1.7	-1.4	-1.3	-1.2	-1.1
Gch1	-1.4	2.6	-1.0	1.5	1.5	1.5
Gsta4	-1.5	-1.2	-1.1	-1.0	-1.2	-1.1
Pld2	-1.5	1.1	1.3	1.2	1.2	1.0
Hk3	-1.5	4.7	10.8	5.1	5.3	3.7
Ltc4s	-1.5	-1.4	1.3	-1.4	-1.6	-2.2
Slc7a11	-1.6	6.5	3.6	3.5	3.1	2.5
Itgav	-1.6	2.3	2.9	2.2	1.8	1.6
Mmp3	-1.6	5.0	270.6	34.9	49.4	6.7
Bnip3	-1.7	1.4	3.0	2.3	1.4	1.7
Mb	-1.8	-16.0	-2.4	-5.8	-1.8	-3.1
Apod	-1.8	-1.3	2.2	3.1	-1.1	1.1
Hba-a2	-1.9	-3.8	6.6	2.7	-1.6	1.9
Duoxa1	-1.9	-1.4	6.3	3.4	4.6	3.4
Ccl5	-1.9	6.9	-1.1	1.1	1.1	-1.4
Anxa1	-2.0	3.1	3.8	3.2	2.4	1.7
Alox5ap	-2.2	2.1	3.0	1.8	1.8	1.8
Mmp9	-2.2	5.2	16.0	2.0	4.6	1.4
Hmox1	-2.3	3.2	2.6	1.6	-1.1	-1.0
Il1b	-2.3	21.4	5.0	6.5	3.8	1.3
Lcn2	-2.3	2.5	3.5	1.2	3.2	1.2
Tnf	-2.5	19.5	2.7	1.6	2.7	4.2
Acox2	-2.6	2.8	-2.1	-1.7	-2.0	-1.3
Nos2	-2.7	103.9	2.2	2.8	4.6	3.1
Hp	-2.8	12.1	26.4	9.2	2.3	5.3
Hbb-b1	-3.3	-2.1	9.3	3.6	-1.2	4.0
S100a8	-3.4	29.8	120.2	23.7	18.3	19.5
S100a9	-4.3	17.3	74.0	12.6	10.8	9.7
Duox1	-5.3	-1.8	1.1	1.4	1.8	1.8
Krt1	-11.7	1.0	-1.5	-1.7	-1.5	1.4
Reg3b	-37.7	2245.1	0.0	0.0	0.0	0.0

UC - Ulcerative colitis, CD – Crohn's disease.

5.6.3. BM-MSCs ameliorate oxidative stress in chronic colitis

Levels of 8-OHdG in chronic inflammation were assessed by immunohistochemistry in cross sections of the distal colon by labelling 8-OHdG (**Figure 5.5A-A′′**). This molecule is produced by oxidation of DNA/RNA and forms adducts which are a biomarker of endogenous oxidative stress-induced DNA damage. In *Winnie*-sham mice, high levels of 8-OHdG immunofluorescence (mean fluorescence intensity) was observed in the mucosal (629.2±23.8 arb. units) and muscle layers (651.6±80.2 arb. units) of the colon compared to the mucosa (354.6±52.9 arb. units, $P<0.001$) and muscle (298.0±18.8 arb. units, $P<0.0001$) of control C57BL/6 mice (**Figure 5.5B**; n=6 animals/group). 8-OHdG immunofluorescence was observed throughout the colon. Negative controls with affinity purified F(ab) fragment anti-mouse IgG and secondary antibody illustrated that this pattern of expression was accurate (**Figure 5.5A′′′**). Treatment with BM-MSCs reduced 8-OHdG levels in the mucosal (381.8±39.7 arb. units, $P<0.01$) and muscle (483.3±43.9 arb. units, $P<0.05$) layers of *Winnie* mice; however, levels were still more elevated in the muscle than control C57BL/6 mice ($P<0.05$) (**Figure 5.5B**; n=6 animals/group). Localisation of 8-OHdG to myenteric neurons was determined by measuring the area of 8-OHdG immunoreactive adducts in myenteric neurons labelled by MAP-2 (**Figure 5.6A-C′′′**). In myenteric neurons, 8-OHdG was greatly elevated in *Winnie*-sham mice (30.6±5.5%, n=7 animals) compared to C57BL/6 mice (12.7±3.8%, $P<0.05$, n=6 animals) (**Figure 5.6D**). 8-OHdG levels returned to near control values in *Winnie* mice treated with BM-MSCs (12.7±3.6%, $P<0.05$, n=7 animals) (**Figure 5.6D**).

5.6.4. BM-MSCs directly attenuate oxidative stress-induced myenteric neuropathy

The neuroprotective value of BM-MSCs against oxidative stressed-induced myenteric neuropathy was investigated in organotypic cultures. The effects of organotypic culture on neuronal loss was determined in LMMPs from the distal colon of C57BL/6 (**Figure 5.7A-B**).

Figure 5.5 ***Effects of BM-MSC on DNA/RNA damage in the distal colon***

A-B) DNA/RNA oxidative damage, a biomarker of oxidative stress in intestinal inflammation, was observed in the distal colon by immunofluorescence of 8-OHdG in cross sections from C57BL/6 mice **(A′)**, sham-treated *Winnie* mice **(A″)** and *Winnie* mice treated with BM-MSCs **(A″)** (scale bar = 100µm). The efficacy of the endogenous mouse Ig blocking procedure was assessed in negative controls with affinity purified F(ab) fragment anti-mouse IgG and a secondary antibody **(A‴)**. Under standardised image acquisition settings, no fluorescence was observed (top) **(A‴)**. **D)** Quantification of the mean fluorescence intensity of 8-OHdG fluorescence in the mucosa and muscle of colonic cross sections. **P*<0.05, ***P*<0.01, ****P*<0.001, *****P*<0.0001; n=6 animals/group.

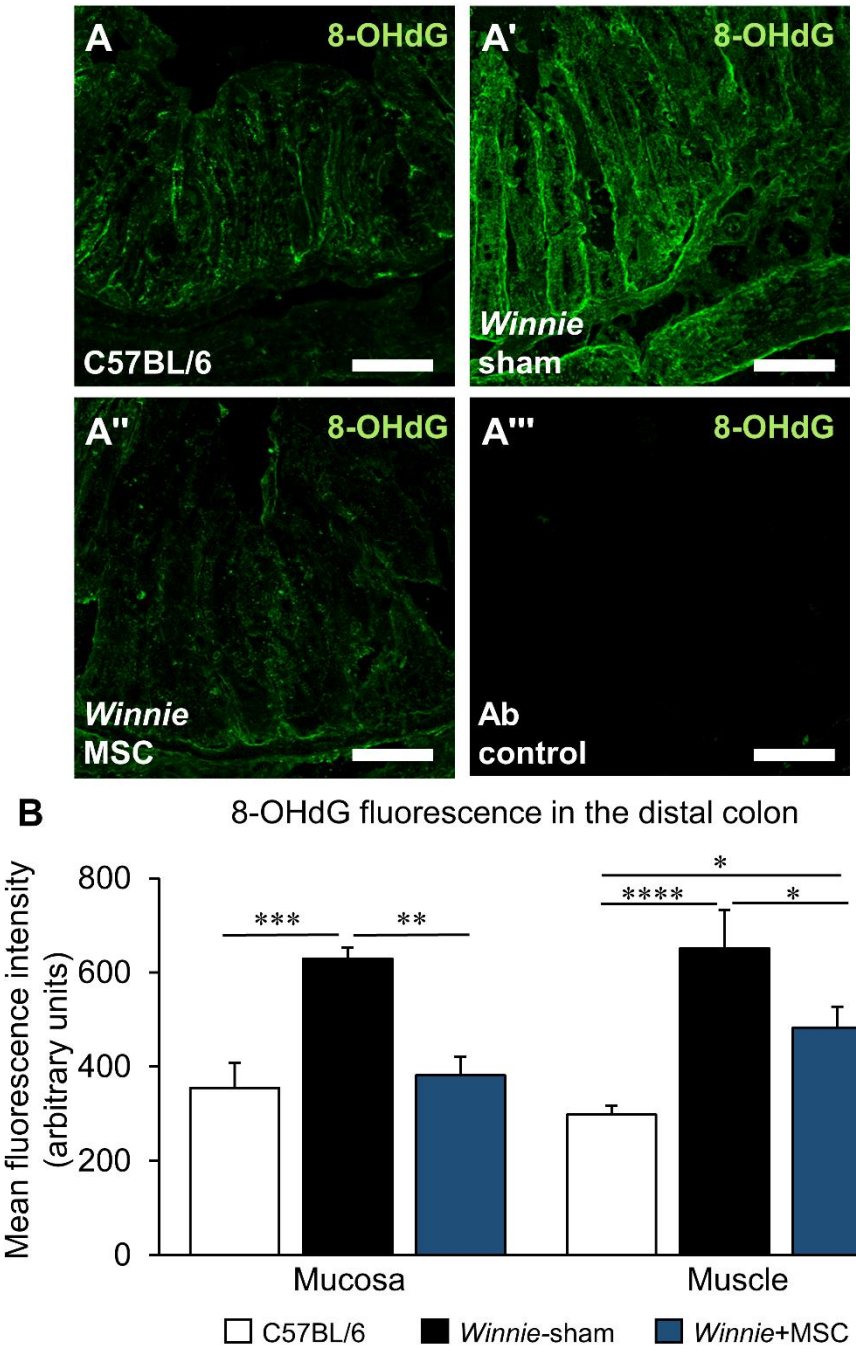
A
8-OHdG
C57BL/6
A'
8-OHdG
Winnie
sham
A''
8-OHdG
Winnie
MSC
A'''
8-OHdG
Ab
control
B
8-OHdG fluorescence in the distal colon
Mean fluorescence intensity
(arbitrary units)
800
600
400
200
0
***
**
*
****
*
Mucosa
Muscle
C57BL/6
Winnie-sham
Winnie+MSC

Figure 5.6 ***Effects of BM-MSC treatments on DNA/RNA damage in the myenteric ganglia of Winnie mice***

A-C′′′) DNA/RNA oxidative damage in neurons within the myenteric ganglia was visualised by immunofluorescence using the neuronal marker MAP-2 **(A-C)** and the DNA/RNA damage marker 8-OHdG **(A′-C′)**. Adducts of 8-OHdG were observed in binary images of 8-OHdG immunofluorescence **(A′′-C′′)**. Co-localisation of 8-OHdG adducts with MAP-2 was viewed in merged images in cross sections from the distal colon of C57BL/6 mice **(A-A′′′)**, sham-treated *Winnie* mice **(B-B′′′)** and *Winnie* mice treated with BM-MSCs **(C-C′′′)** (scale bar = 20µm). **D)** Quantification of 8-OHdG adducts as a percent of the area in the myenteric neurons in colonic cross sections. **P*<0.05; C57BL/6: n=6 animals, *Winnie*-sham and *Winnie*+MSC: n=7 animals.

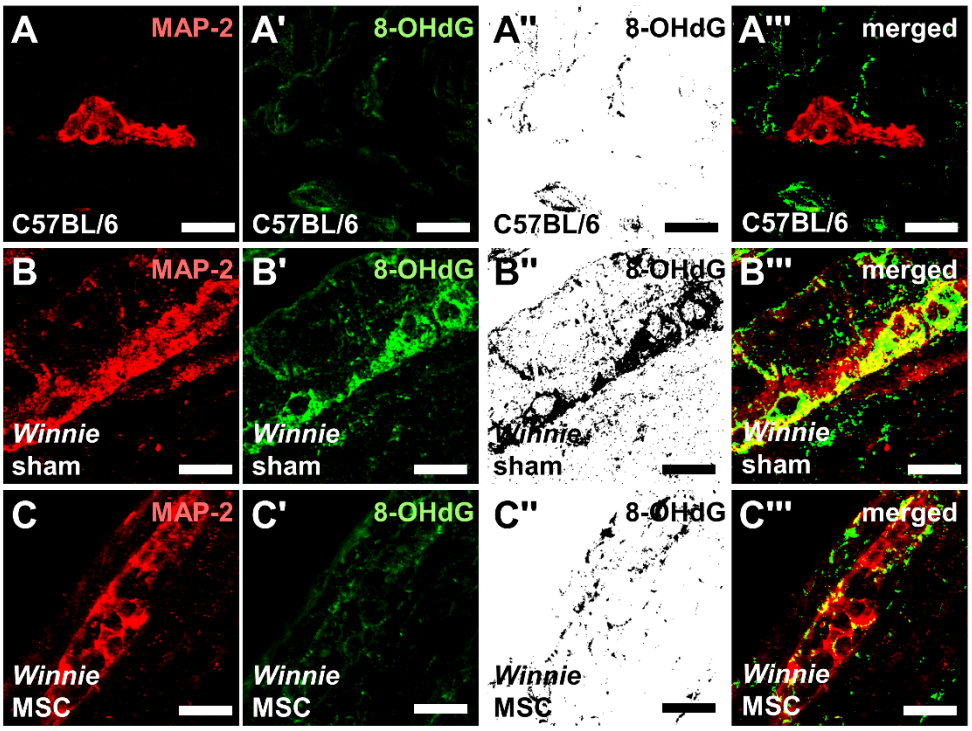
A
MAP-2
C57BL/6
A'
8-OHdG
C57BL/6
A''
8-OHdG
C57BL/6
A'''
merged
C57BL/6
B
MAP-2
Winnie
sham
B'
8-OHdG
Winnie
sham
B''
8-OHdG
Winnie
sham
B'''
merged
Winnie
sham
C
MAP-2
Winnie
MSC
C'
8-OHdG
Winnie
MSC
C''
8-OHdG
Winnie
MSC
C'''
merged
Winnie
MSC

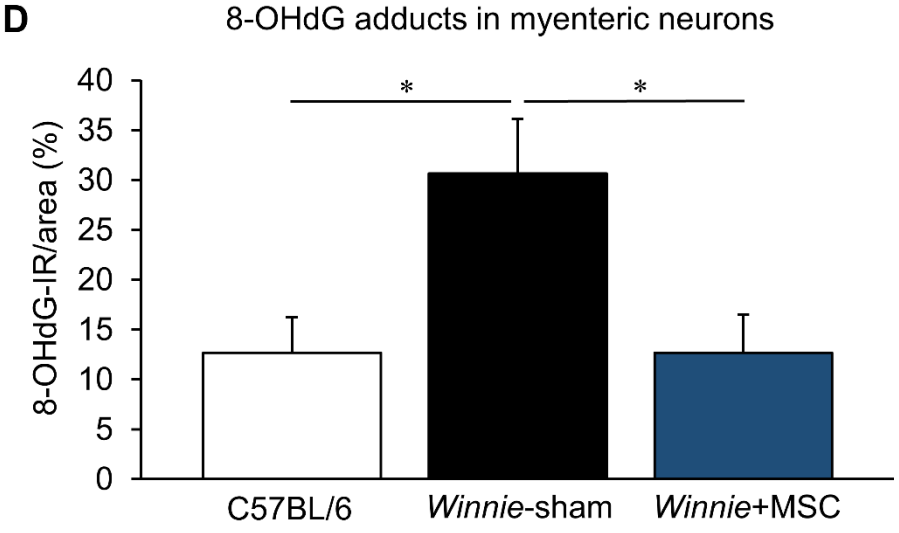
D
8-OHdG adducts in myenteric neurons
8-OHdG-IR/area (%)
40
35
30
25
20
15
10
5
0
*
*
C57BL/6
Winnie-sham
Winnie+MSC

No differences were observed in the neuronal density of myenteric neurons between fresh fixed wholemount tissues (22.5±0.7 neurons/area) and tissues that had been freshly peeled, subjected to organotypic culture for 24h and then fixed (22.5±1.2 neurons/area) (**Figure 5.7C**; n=6 independent samples/group). Organotypic cultures were exposed to hyperoxic conditions to model oxidative stress in myenteric neurons (**Figure 5.8A-C**). A significant reduction in myenteric neuronal density was observed in tissues cultured in hyperoxia (5% CO_2, 95% O_2) (16.8±0.8 neurons/area, n=7 independent samples) compared to those cultured under atmospheric normoxia (5% CO_2 and ambient O_2 [~21%]) (22.9±0.9 neurons/area, $P<0.01$, n=8 independent samples) (**Figure 5.8D**). BM-MSCs applied directlty to organotypic cultures reduced the loss of myenteric neurons caused by hyperoxia (22.1±2.5 neurons/area, $P<0.05$, n=5 independent samples) (**Figure 5.8D**).

In addition, the neuroprotective effects of BM-MSCs in organotypic cultures were evaluated in chemically-induced oxidative stress using H_2O_2, an extensively studied neurotoxic agent (**Figure 5.9A-D**). Application of H_2O_2 at a final concentration of 100µM significantly reduced neuronal density (16.2±0.7 neurons/area, n=5 independent samples) in organotypic cultures compared to tissues cultured for 24h in standard culture medium (22.5±1.2, neurons/area, $P<0.01$, n=6 independent samples) (**Figure 5.9E**). Neuronal loss induced by H_2O_2 was ameliorated by incubating organotypic cultures directly with BM-MSCs (21.9±1.2 neurons/area, $P<0.01$, n=5 independent samples). Similar results were observed when organotypic cultures and BM-MSCs were separated by a semi-permeable (4µm pore-size) transwell insert (22.3±0.5 neurons/area, $P<0.01$, n=4 independent samples) suggesting that MSCs reduce neuropathy in a paracrine fashion (**Figure 5.9E**).

5.6.5. BM-MSCs confer neuroprotection by reducing superoxide production

Mitochondrial-derived $O_2^{\cdot -}$ was measured in the myenteric ganglia using the fluorescent dye MitoSOX.

Figure 5.7 ***Evaluation of myenteric neuronal density in organotypic culture***

A-B) Neurons within the myenteric ganglia were observed by immunofluorescence using the neuronal marker MAP-2 in wholemount LMMP preparations of the distal colon from C57BL/6 mice. Wholemounts that were fixed straight after the animal was culled **(A)** were compared to those subjected to organotypic culture for 24h **(B)** (scale bar = 50µm). **C)** Quantification of myenteric neuron density expressed as the number of neurons per ganglionated area; n=5 independent samples/group.

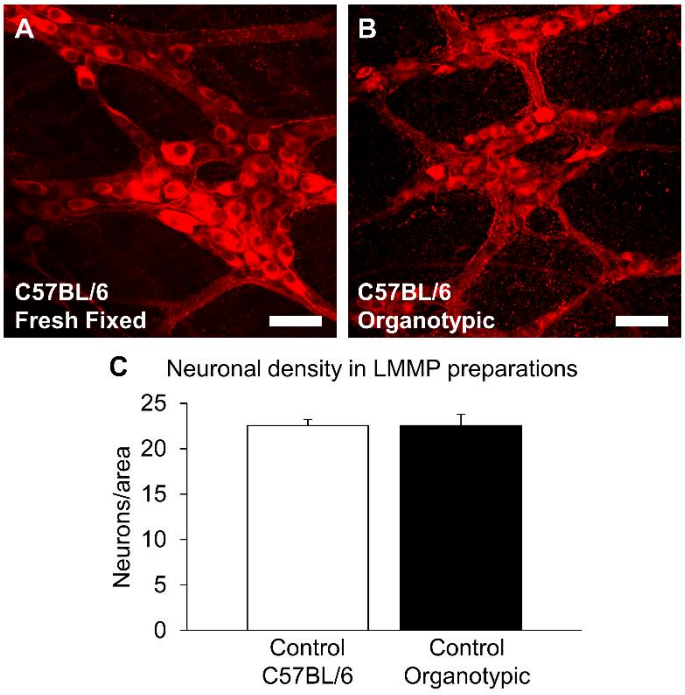
A
C57BL/6
Fresh Fixed
B
C57BL/6
Organotypic
C
Neuronal density in LMMP preparations
Neurons/area
25
20
15
10
5
0
Control
C57BL/6
Control
Organotypic

Figure 5.8 ***Effects of BM-MSCs on hyperoxia-induced myenteric neuropathy in organotypic culture***

A-C) Neurons within the myenteric ganglia observed by immunofluorescence using the neuronal marker MAP-2 in distal colon organotypic cultures. Tissues were cultured for 24h in control **(A)**, hyperoxic ($\uparrow O_2$) condition **(B)** and hyperoxia with $1x10^5$ BM-MSCs **(C)** (scale bar = 50µm). **D)** Quantification of myenteric neuron density expressed as the number of neurons per ganglionated area. $*P<0.05$, $**P<0.01$; control: n=8 independent samples, $\uparrow O_2$: n=7 independent samples, $\uparrow O_2$ + MSC: n=5 independent samples.

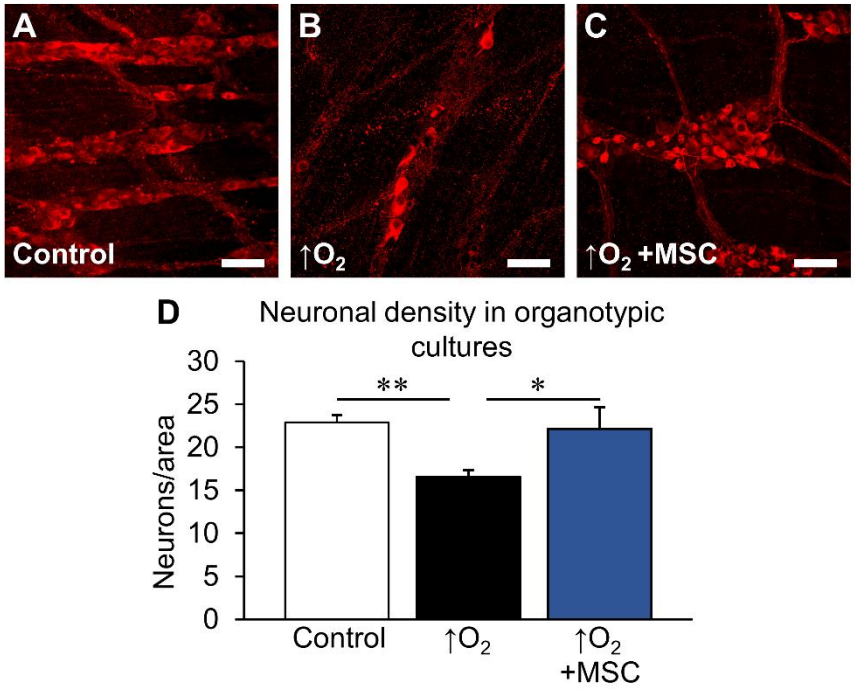
A
Control
B
↑O2
C
↑O2 +MSC
D
Neuronal density in organotypic cultures
Neurons/area
30
25
20
15
10
5
0
**
*
Control
↑O2
↑O2 +MSC

Figure 5.9 ***Effects of BM-MSCs on hydrogen peroxide (H_2O_2)-induced myenteric neuropathy in organotypic culture***

A-D) Neurons within the myenteric ganglia observed by immunofluorescence using the neuronal marker MAP-2 in distal colon organotypic cultures. Tissues were cultured for 24h in standard culture medium **(A)** and exposed to either 100µM H_2O_2 **(B)**, 100µM H_2O_2 with $1x10^5$ BM-MSCs in 4µm pore size transwell inserts **(C)** or 100µM H_2O_2 with $1x10^5$ BM-MSCs applied directly to organotypic cultures **(D)** (scale bar = 50µm). **E)** Quantification of myenteric neuron density expressed as the number of neurons per ganglionated area. $^{**}P<0.01$; control: n=6 independent samples, H_2O_2: n=5 independent samples, H_2O_2 + MSC Transwell: n=4 independent samples, H_2O_2 + MSC direct: n=5 independent samples.

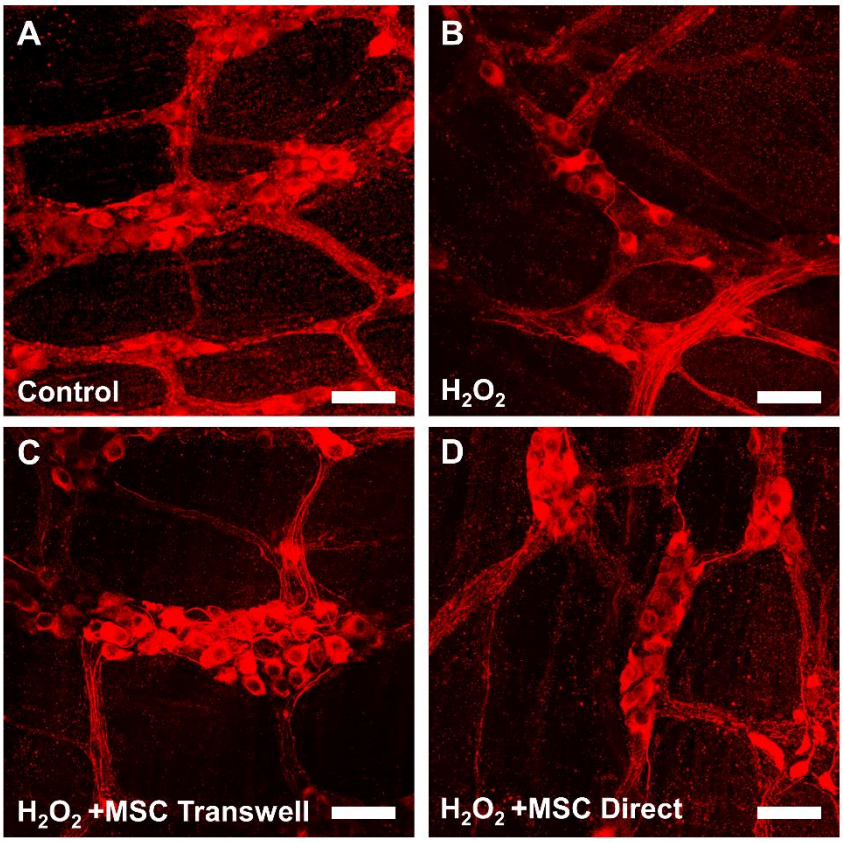
A
Control
B
H_2O_2
C
H_2O_2 +MSC Transwell
D
H_2O_2 +MSC Direct

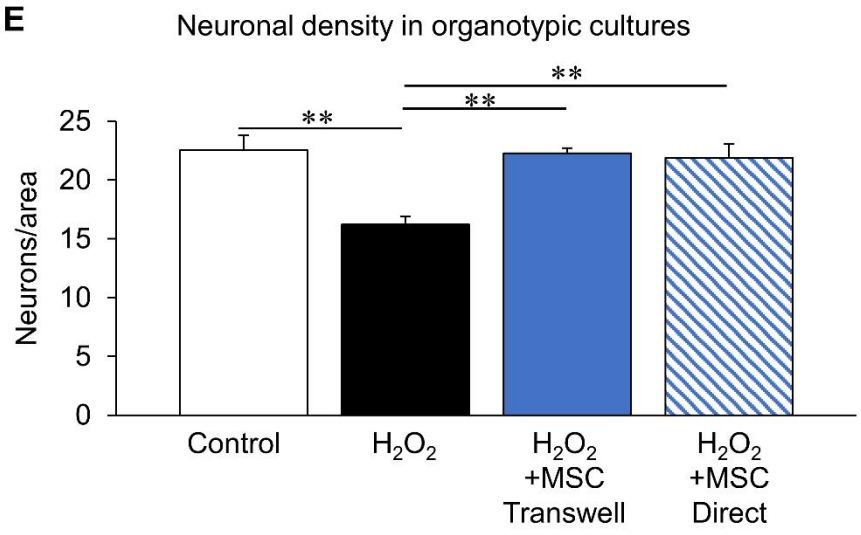
E
Neuronal density in organotypic cultures
Neurons/area
25
20
15
10
5
0
**
**
**
Control
H_2O_2
H_2O_2 +MSC Transwell
H_2O_2 +MSC Direct

High levels of $O_2^{\cdot -}$, as indicated by the intensity of fluorescence, were observed in the myenteric ganglia in comparison to the muscle layer suggesting that the myenteric plexus is the major source of mitochondrial-derived $O_2^{\cdot -}$ in LMMPs (**Figure 5.10A-C**). In *Winnie*-sham mice, $O_2^{\cdot -}$ levels (mean fluorescence intensity) in the myenteric ganglia (127.5±22.5 arb. units, n=6 animals) were more than twice the levels of that observed in control C57BL/6 mice (50.4±3.2 arb. units, $P<0.05$, n=5 animals). Treatment with BM-MSCs reduced $O_2^{\cdot -}$ levels in *Winnie* mice (69.8±10.0 arb. units, $P<0.05$, n=5 animals) to levels comparable to controls (**Figure 5.10D**).

BM-MSCs were recently determined to secrete SOD-Cu-Zn (SOD1) which has a primary role in the detoxification of mitochondrial-derived $O_2^{\cdot -}$ (Klein et al., 2017). To examine the potential role of SOD1 in BM-MSC-mediated myenteric neuroprotection, the SOD1 inhibitor, LCS-1, was applied to organotypic cultures (**Figure 5.11A-F**). Neuronal density was similar in organotypic preparations cultured in standard medium (22.9±0.9 neurons/area, n=8 independent samples) and those treated with LCS-1 at a final concentration of 10µM (22.7±1.7 neurons/area, n=4 independent samples) (**Figure 5.11G**). Application of H_2O_2 with LCS-1 (15.6±0.7 neurons/area, n=4 independent samples) or without LCS-1 (16.7±1.0 neurons/area, n=9 independent samples) similarly reduced neuronal density compared to controls in standard culture medium ($P<0.01$ for both) and those with LCS-1 only ($P<0.05$ for both) (**Figure 5.11G**). In cultures treated with H_2O_2, the application of BM-MSCs maintained neuronal density (22.5±1.2 neurons/area, n=9 independent samples) to levels observed in controls; however, when LCS-1 was added to these cultures, the neuroprotective effect of BM-MSCs was inhibited (16.5±0.9 neurons/area, $P<0.01$, n=6 independent samples) (**Figure 5.11G**). Furthermore, neuronal density in these cultures were similar to that observed after the application of H_2O_2 alone and H_2O_2 with LCS-1, and lower than control ($P<0.01$) or LCS-1 only ($P<0.05$) treated tissues. All groups in these experiments contained 0.05% (v/v) DMSO either as a vehicle for LCS-1 or as a sham vehicle. DMSO can be cytotoxic, with a particular sensitivity observed in neurons (Galvao et al., 2014).

Figure 5.10 ***Effects of BM-MSC treatments on mitochondrial superoxide levels in myenteric neurons in the distal colon of Winnie mice***

A-C) Mitochondrial-derived superoxide ($O_2^{\cdot -}$) in the myenteric ganglia was visualised by the fluorescent probe MitoSOX in LMMP wholemount preparations of the distal colon from C57BL/6 mice **(A)**, sham-treated *Winnie* mice **(B)** and *Winnie* mice treated with BM-MSCs **(C)** (scale bar = 50µm). Presented images are pseudo-coloured (LUT: 'heat', ImageJ) for greater visual distinction. **D)** The mean fluorescence intensity of the myenteric ganglia in single channel 16-bit images were quantified to determine the intensity of MitoSOX fluorescence. All images were captured using the same acquisition settings. **P*<0.05; C57BL/6: n=5 animals, *Winnie*-sham: n=6 animals, *Winnie*+MSC: n=5 animals.

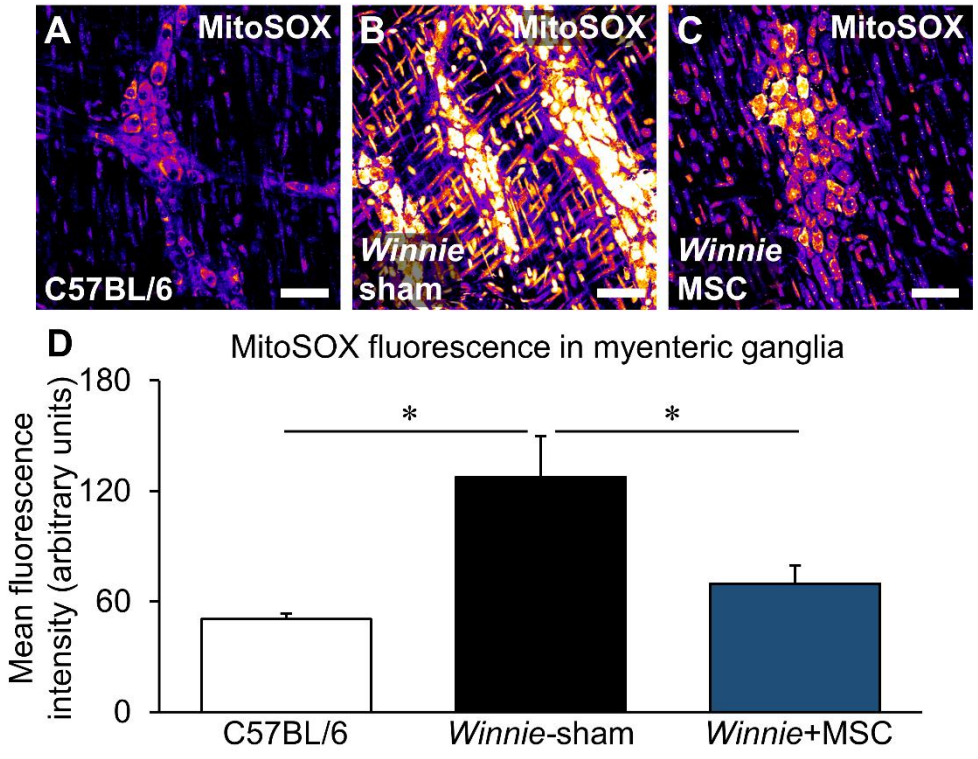
A
MitoSOX
C57BL/6
B
MitoSOX
Winnie
sham
C
MitoSOX
Winnie
MSC
D
MitoSOX fluorescence in myenteric ganglia
Mean fluorescence intensity (arbitrary units)
180
120
60
0
*
*
C57BL/6
Winnie-sham
Winnie+MSC

Figure 5.11 ***Role of superoxide dismutase [Cu-Zn] (SOD1) in BM-MSC-mediated neuroprotection of organotypically-cultured myenteric neurons***

A-F) Neurons within the myenteric ganglia observed by immunofluorescence using the neuronal marker MAP-2 in distal colon organotypic cultures. Tissues were cultured for 24h in standard culture medium **(A)** and exposed to either 100µM H_2O_2 **(B)**, 100µM H_2O_2 with $1x10^5$ BM-MSCs **(C)**, 10µM LCS-1 (SOD1 inhibitor) **(D)**, 100µM H_2O_2 with 10µM LCS-1 **(E)** or 100µM H_2O_2 with 10µM LCS-1 and $1x10^5$ BM-MSCs **(F)** (scale bar = 50µm). DMSO was used as a solvent for LCS-1. Each group contained a total concentration of 0.05% (v/v) DMSO. **G-H)** Quantification of myenteric neuron density expressed as the number of neurons per ganglionated area. Myenteric neurons were quantified to test the effects of the superoxide dismutase [Cu-Zn] (SOD1) inhibitor LCS-1 **(G)** and the solvent DMSO **(H)** on MSC mediated neuroprotection. **G)** $*P<0.01$, $**P<0.01$; control: n=8 independent samples, H_2O_2: n=9 independent samples, H_2O_2 + MSC n=9 independent samples, LCS-1: n=4 independent samples, H_2O_2 + LCS-1: n=4 independent samples, H_2O_2 + MSC + LCS-1: n=6 independent samples. **H)** n=6 independent samples/group.

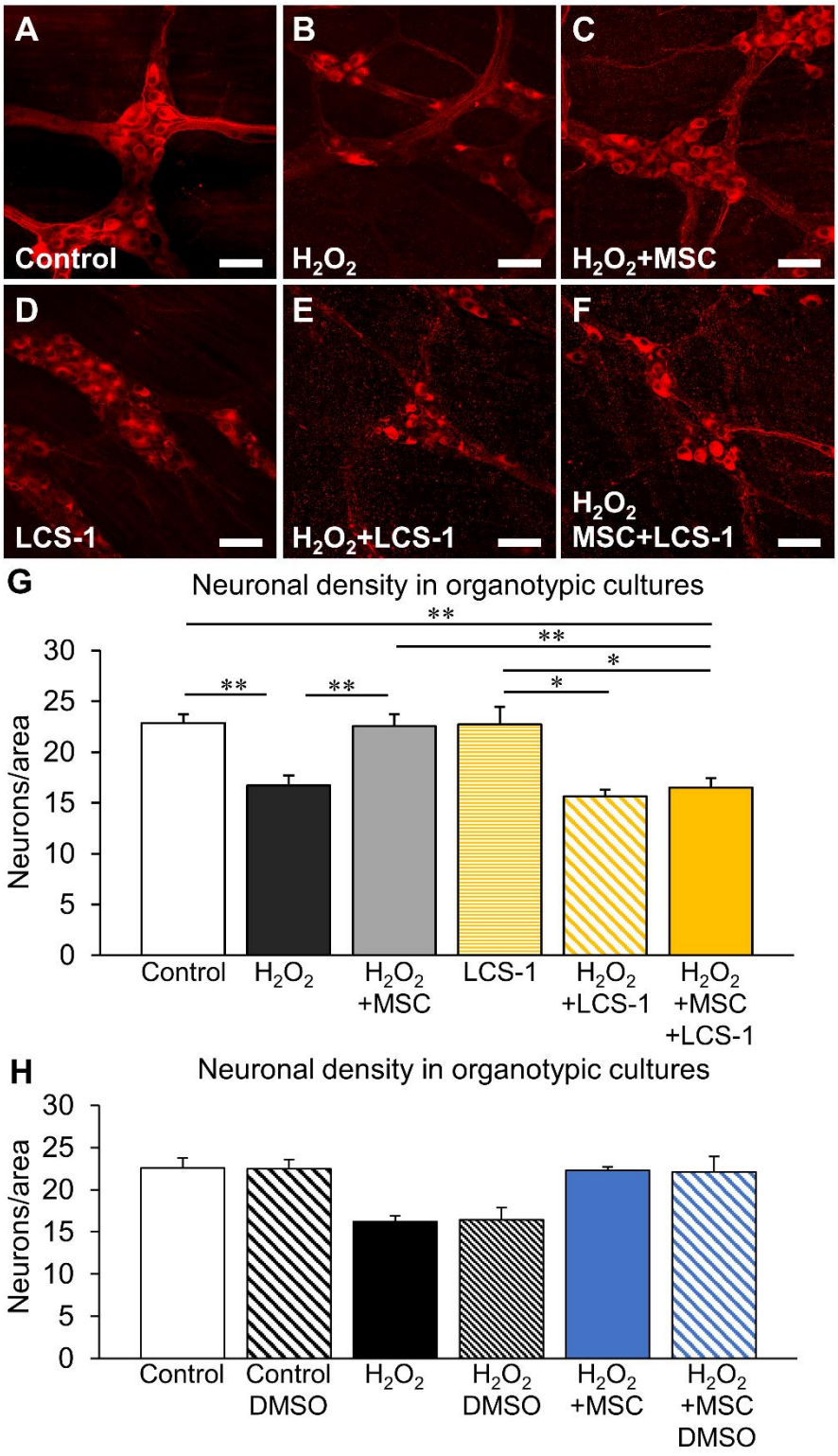
A
Control
B
H2O2
C
H2O2+MSC
D
LCS-1
E
H2O2+LCS-1
F
H2O2
MSC+LCS-1
G
Neuronal density in organotypic cultures
Neurons/area
0
5
10
15
20
25
30
**
**
**
*
*
Control
H2O2
H2O2 +MSC
LCS-1
H2O2 +LCS-1
H2O2 +MSC +LCS-1
H
Neuronal density in organotypic cultures
Neurons/area
0
5
10
15
20
25
30
Control
Control DMSO
H2O2
H2O2 DMSO
H2O2 +MSC
H2O2 +MSC DMSO

The impact of the DMSO vehicle for LCS-1 on the neuronal density of H_2O_2 and BM-MSC treated organotypic cultures was determined (**Figure 5.11H**). No differences in neuronal density were observed after the application of DMSO at a final concentration of 0.05% (v/v) in controls (control: 22.5±1.2 neurons/area vs control + DMSO: 22.5±1.1 neurons/area), tissues treated with H_2O_2 (H_2O_2: 16.2±0.7 neurons/area vs H_2O_2 + DMSO: 16.5±1.4 neurons/area), or those treated with H_2O_2 and BM-MSC (H_2O_2 + MSC: 22.3±0.4 neurons/area vs H_2O_2 + MSC+ DMSO: 22.1±1.8 neurons/area) (**Figure 5.11H**; n=6 independent samples/group).

5.7. Discussion

In this study we observed that the application of BM-MSCs in the *Winnie* mouse model of spontaneous chronic colitis upregulated many genes associated with metabolism, detoxification, ion homeostasis and ATP signalling. BM-MSCs increased the expression of genes involved in endogenous antioxidant defences and downregulated several genes that were redox sensitive, or involved in the production of free radicals, which suggested that an antioxidative mechanism may be involved in their therapeutic effect. Furthermore, BM-MSCs corrected the patterns of expression for several oxidative stress-associated genes in *Winnie* mice. Many of these genes were dysregulated in both *Winnie* mice and IBD patients compared to their uninflamed controls. The antioxidative properties of BM-MSCs were confirmed by a reduction in oxidative stress biomarker, 8-OHdG, which is indicative of DNA/RNA oxidation in the inflamed colon. BM-MSCs directly attenuated oxidative stress-induced myenteric neuropathy in organotypic models. Furthermore, these effects were observed in a paracrine manner which suggests that BM-MSC-derived secreted factors were responsible. High levels of DNA/RNA oxidation and mitochondria-derived $O_2^{\cdot -}$ were observed in the myenteric ganglia of *Winnie* mice suggesting that myenteric neurons are susceptible to oxidative injury; these levels were returned to near control levels after BM-MSC treatment. In *in vitro* experiments, SOD1 inhibition blocked the paracrine neuroprotective properties of BM-MSCs in oxidative-induced injury of myenteric neurons. Thus, the antioxidant effects of BM-MSCs in myenteric neurons may be mediated by SOD1.

In IBD, oxidative stress has a bidirectional relationship with inflammation and is entrenched in the pathology of the disease (Lih-Brody et al., 1996, Piechota-Polanczyk and Fichna, 2014). Our study revealed that BM-MSCs can reduce oxidative stress in chronic colitis as demonstrated by their ability to decrease oxidation products of DNA/RNA and the expression of transcripts that are upregulated in response to oxidative stress. The ability of MSCs to reduce DNA oxidation has previously been demonstrated with allogeneic BM-MSCs and human umbilical cord-MSCs in rat models of ischemia-reperfusion and cisplatin-induced renal injury, respectively (Liu et al., 2012, Zhou et al., 2013). MSCs have also previously been demonstrated to attenuate oxidative stress concomitant with (DSS)-induced colitis (Sun et al., 2015, da Costa Gonçalves et al., 2017). Similar to our results in the *Winnie* mice, the products of DNA oxidation are evident in UC and CD patients (D'Inca et al., 2004, Pereira et al., 2016). The antioxidant properties of MSC therapy may have been mediated by several concurrent mechanisms.

Treatment of *Winnie* mice with BM-MSCs altered the expression of genes associated with oxidative stress. Many of these genes had similar patterns of expression in *Winnie* mice and IBD patients and have roles in the pro-inflammatory response. *Lcn2* is upregulated in response to oxidative stress (Roudkenar et al., 2007), likewise, induction of *Nos2* is redox sensitive, and its product nitric oxide (NO), is a nitrosative species (Piechota-Polanczyk and Fichna, 2014). *Alox5ap*, which regulates 5-LOX (5-lipoxygenase) activity, is also associated with lipoxygenase generated ROS and is a rate limiting step in inflammatory leukotriene synthesis (Liu et al., 2018). Notably, the inducible NOS (iNOS) and 5-LOX systems are thought to be key components in the development of experimental colitis through oxidative stress (Mittal et al., 2007). The pro-inflammatory cytokine *Tnf* can increase ROS production and mitochondrial damage (Suematsu et al., 2003). Similarly, *S100a8* and *S100a9* increase the nucleotide-binding oligomerization domain (NOD)-like receptor protein 3 (NLRP3) inflammasome activity by increasing ROS (Simard et al., 2013). Redox inducible genes that are associated with antioxidant properties or the resolution of inflammation were also upregulated

in *Winnie* mice and IBD patients. This included: *Anxa1*, involved in epithelial repair and resolution of chemically induced-colitis (Rhee et al., 2000, Sheikh and Solito, 2018); *Hk3*, a regulator of mitochondrial biogenesis (Wyatt et al., 2010); *Hmox1*, ameliorates chemically induced-colitis and has antioxidant properties via catabolism of free radical generating haem (Sebastián et al., 2018); as well as *Hp*, which binds haemoglobin to avert its pro-oxidant effects (Folsted et al., 2017). Nonetheless, upregulation of these genes in *Winnie* mice and IBD was undoubtedly insufficient to avert colitis. Increased expression of *Slc7a11* was observed in *Winnie* mice and IBD patients which is upregulated by redox stress to import cysteine in exchange for glutamate for the synthesis of the potent antioxidant glutathione; however, this is also associated with neuronal death (Conrad and Sato, 2012). The oxidative stress-sensor *Bnip3* was also upregulated in chronic inflammation which instigates necroptotic cell death and has been implicated in oxidative stress-induced neuronal loss (Zhang et al., 2007, Kubli et al., 2008). *Winnie* mice and IBD patients also exhibited downregulation in several aldehyde dehydrogenases, which can reduce oxidative and electrophilic stress (Singh et al., 2013). Similarities were also observed between *Winnie* mice and IBD in downregulated mitochondrial genes including: *Aldh2*, protective against oxidative stress (Ohsawa et al., 2003); *Pdk2*, redirects mitochondrial pyruvate from oxidative phosphorylation that generates mitochondrial $O_2^{\cdot -}$ (Gray et al., 2014); and *Ppargc1b*, increases mitochondrial biogenesis and reduces ROS generation (Galmes-Pascual et al., 2017). Together, these data demonstrate that *Winnie* mice share similar alterations to IBD patients in redox sensitive gene expression and the machinery involved in ROS production. Considering that BM-MSCs corrected the dysregulation of these genes in *Winnie* mice, some of these changes may be clinically relevant to the mechanisms of MSC therapy in human IBD.

The antioxidative properties of MSCs have been observed in several animal models of disease which have been attributed to either their immunosuppressive properties, promotion of antioxidant defences, or their ability to scavenge free radicals (**Chapter 1, Section 1.4**). Inflammation and free radical generation are interdependent processes in intestinal inflammation (Piechota-Polanczyk and

Fichna, 2014). Neutrophils which are abundant in colitis produce a respiratory burst of free radicals including $O_2^{\cdot -}$, H_2O_2 and hypochlorite generated by NOX and MPO critical to their lytic microbicidal function (Zhang et al., 2002, Pattison and Davies, 2006). Additionally, pro-inflammatory factors may stimulate ROS production; tumour necrosis factor (TNF)α can increase NOX activity in colon epithelial cells and iNOS is induced in UC patients by NFκB which is activated in epithelial cells by TNF-α or pathogen associated molecular patterns (Andresen et al., 2005, Kuwano et al., 2008, Wullaert et al., 2010). In our study, *Tnf* and *Nos2* gene expression were reduced by BM-MSCs. It has been proposed that the free radicals generated in intestinal inflammation disrupt epithelial integrity by damaging cytoskeletal and tight junction proteins, thus, allowing luminal contents to interact with the immune system (Tian et al., 2017). This includes pathogen molecular patterns and antigens activating the innate and adaptive immune response, respectively. Considering the contribution of inflammation to ROS generation, this may create a perpetual cycle of chronic inflammation (Tian et al., 2017). Alternatively, ROS signalling can directly promote inflammation. The NLRP3 inflammasome responds to damage patterns and extracellular ATP by activating interleukin (IL)-1β in a process that is triggered by ROS (Abais et al., 2015). This process is overactive in IBD and animal models of colitis (Lazaridis et al., 2017, Liu et al., 2017). Notably, scavenging of ROS, including that derived from mitochondrial $O_2^{\cdot -}$, has been demonstrated to inhibit NLRP3 activity in macrophages and reduce matrix metallopeptidase 9 (MMP9) expression in the amelioration of DSS-induced colitis (Dashdorj et al., 2013, Chen et al., 2018a). In *Winnie* mice, BM-MSCs reduced *Mmp9, Nlrp3* and *Il1b* expression and upregulated many genes associated with ATP-binding. Similarly, MSCs have been demonstrated to reduce NLRP3 inflammasome activation in mouse and human macrophages *in vitro* by reducing ROS (Oh et al., 2014). Furthermore, MSCs have been established to reduce MPO levels in colitis, which in addition, has been demonstrated to parallel their antioxidant activity in *E. coli*-induced acute lung injury (Shalaby et al., 2014, Lin et al., 2015, Chao et al., 2016, Wang et al., 2016). Considering the interplay between ROS and the immune response it is difficult to determine if one process take precedence in the therapeutic mechanism of MSC

treatments in inflammation. Nonetheless, it has been observed in murine endotoxin-induced inflammation that the restoration of redox homeostasis by MSCs supersedes a reduction in the pro-inflammatory cytokines IL-1β and TNF-α (Iyer et al., 2010). Even so, the role of antioxidant defences in the development of chronic colitis should not be disregarded as mutations in the antioxidant enzymes ribosyldihydronicotinamide dehydrogenase, quinone (NQO) and SOD2, as well as a deficiency in glutathione S-transferases (GST)s predict an undesirable disease progression and response to therapies in UC (Mittal et al., 2007, Kosaka et al., 2009).

In *Winnie* mice, BM-MSC treatments upregulated endogenous antioxidant defence genes including *Nqo* and several *Gst* family genes. BM-MSCs also upregulated many genes in *Winnie* mice associated with metabolism, including aldehyde dehydrogenases which were downregulated in IBD patients compared to controls. Previous studies have established that MSCs can increase the levels of antioxidant compounds and enzymes to reduce oxidative stress in other animal models of disease (**Chapter 1, Section 1.4.3.2**). In these studies, MSCs were shown to increase glutathione peroxidase (GPx), glutathione reductase, catalase and SOD in models of *E. coli*-induced lung injury and hepatotoxic injury (Pulavendran et al., 2010, Shalaby et al., 2014). Expression of the antioxidant enzyme haem oxygenase 1 (HO-1) was also promoted by BM-MSCs in renal ischemia-reperfusion injury (Liu et al., 2012), which conversely, was downregulated by BM-MSCs in *Winnie* mice on the level of gene expression in our study. However, this gene is redox sensitive, and we observed that similar redox sensitive genes were downregulated by BM-MSC treatments which reflected a reduction in oxidative stress. In *in vivo* studies, it can be unclear whether the source of these antioxidants is from host tissues or the MSCs themselves. Although MSCs express antioxidant enzymes and can scavenge free radicals, *in vitro* studies have demonstrated that MSCs can promote endogenous mechanisms to alleviate oxidative stress in targeted cells (Kim et al., 2008, Liu et al., 2010). In these studies, the conditioned medium of MSCs increased SOD and GPx in tert-Butyl hydroperoxide exposed endothelial cells and dermal fibroblast while decreasing oxidative stress and promoting cell survival

(Kim et al., 2008, Liu et al., 2010). The antioxidant genes observed by RNA-Seq in our study were transcripts of murine origin. Considering that the BM-MSCs used in our study were xenogeneic, these results unequivocally demonstrate that BM-MSCs can promote endogenous defence mechanisms against oxidative stress in the host tissue *in vivo*.

The nervous system is highly sensitive to injury by excessive free radical production due to multiple reasons including, but not limited to, high energy demand and O_2 consumption, excess mitochondria-derived $O_2^{\cdot -}$, autooxidation of neurotransmitters, excitotoxicity, poor antioxidant defences and limited replicative potential (Friedman, 2011). The ENS is also considered to be susceptible to oxidative injury with enteric neuropathy linked to excessive ROS production and oxidative stress in animal models of chemotherapy, diabetes and physiological aging (Thrasivoulou et al., 2006, Chandrasekharan et al., 2011, McQuade et al., 2016, McQuade et al., 2018). Likewise, oxidative stress in the ENS has been predicted to contribute to the pathophysiology of intestinal inflammation (Lakhan and Kirchgessner, 2010). In addition to causing neuronal death, oxidative stress and free radicals can alter the electrophysiological properties of enteric neurons and injure neural membranes leading to dysfunctional signalling in neurally-controlled processes such as dysmotility in colitis (Gaginella et al., 1992, Wada-Takahashi and Tamura, 2000, Roberts et al., 2013). In a model of ileitis in the rabbit induced by the parasite *Eimeria magna*, increased lipid peroxidation was observed with the biggest changes occurring in the muscle layer compared to mucosa and plasma (Sundaram et al., 2003). Similarly, levels of DNA/RNA oxidation appeared to be increased more in the muscle layers of *Winnie* mice. Based on immunofluorescence, myenteric neurons appeared to be the most affected cell type in this region. Specifically in colitis, Brown et al. (2016) observed oxidative stress in the myenteric ganglia of dinitrobenzene sulfonic acid (DNBS)-treated mice, which exhibited higher levels of oxidised (GSSG)/reduced glutathione (GSH) and $O_2^{\cdot -}$ during inflammation than controls. Importantly, oxidative stress was demonstrated to be the key contributing factor to neuropathy with the antioxidant N-acetyl cysteine (NAC) attenuating inflammation-induced neuronal loss *in vivo*.

Furthermore, this antioxidant did not attenuate acute inflammation which indicated that neuronal damage is directly dependent on ROS, rather than pro-inflammatory mediators, in acute colitis. The same group repeated findings of inflammation-induced oxidative stress while also observing that neuronal loss appears to be indiscriminate of neurochemical coding in colitis (Linden et al., 2005b, Bubenheimer et al., 2016). In multiple enteric neuropathies, there is a propensity for deficits in neuronal NOS (nNOS) immunoreactive neurons which has been attributed largely to the free radical and nitrosylating properties of NO (Rivera et al., 2011a). Furthermore, in myenteric organotypic models, menadione sodium bisulphite used to induce oxidative stress decreases the number of nNOS immunoreactive neurons (Voukali et al., 2011). Nevertheless, several studies have demonstrated that nNOS neurons are not specifically decreased in colitis (Winston et al., 2013, Stavely et al., 2015b, Stavely et al., 2015a) and we found no changes in nNOS expression (Rahman et al., 2015); therefore, the free radicals involved in neuronal damage appear to be oxidative, rather than nitrosative, species.

Multiple free radicals could be responsible for oxidative stress-induced neuronal damage *in vivo*. H_2O_2 is a potent enteric neurotoxin and is prevalent in the muscle layers of experimental colitis (Lourenssen et al., 2009, Shi et al., 2010). H_2O_2 is produced as a metabolic by-product of *Acox2* and as the main function of *Duox1* which were downregulated by BM-MSCs in *Winnie* mice (Fransen et al., 2012). The expression of *Duoxa1,* which assists the maturation and transport of DUOX1 was also downregulated by BM-MSCs and the membrane transporter *Aqp8* which regulates cellular levels of H_2O_2 and mitochondrial ROS was upregulated (Tamma et al., 2018). Increased mitochondria-derived $O_2^{\cdot -}$ levels parallel cytosolic H_2O_2 concentrations; likewise, exogenously applied H_2O_2 increases $O_2^{\cdot -}$ (Aon et al., 2010). High levels of $O_2^{\cdot -}$ derived specifically from the mitochondria were observed in LMMP preparations from *Winnie* mice; the highest levels were observed in myenteric neurons. Similar observations have been made in mice with chemotherapy-induced neuropathy (McQuade et al., 2016, McQuade et al., 2018). In LMMP preparations, myenteric neurons exhibit the highest density of mitochondria which may explain their susceptibility to large increases in $O_2^{\cdot -}$

(Berghe et al., 2002). The level of mitochondria-derived $O_2^{\cdot -}$ depends on metabolic substrates, cytosolic Ca^{2+} levels, pH and oxygen tension (Aon et al., 2010). Notably, BM-MSC treatments in *Winnie* mice improved the expression of many genes associated with metabolism and detoxification, ion transport and the regulation of pH. Mitochondria play a vital role in maintaining proper electrophysiological signalling in myenteric neurons. Inhibition of various parts of the electron transport chain and mitochondrial dysfunction result in hyperpolarisation of myenteric neurons which has been attributed to an increase in cytosolic Ca^{2+} (Berghe et al., 2002). ROS is established to have a close coregulatory relationship with Ca^{2+} and ion transport (Görlach et al., 2015). Neurons are dependent on Ca^{2+} signalling, ion transport and mitochondria for homeostatic signalling; therefore, there is a high risk of altered neuronal functioning in conditions of oxidative stress (Kourie, 1998, Görlach et al., 2015). Furthermore, increased Ca^{2+} load is associated increased mitochondrial ROS and cell death through the voltage and Ca^{2+}-dependent mitochondrial permeability transition pore (mPTP). In *Winnie* mice and IBD patients an upregulation of *Bnip3* was observed. *Bnip3* induces caspase-independent cell death through opening of the mPTP and calcium dependent signalling (Gustafsson, 2011, Graham et al., 2015). The propensity for ROS to alter Ca^{2+} transport in enteric neurons may explain why the ENS is vulnerable to oxidative-stress induced neuropathy.

In the present study, BM-MSC treatments reduced mitochondria-derived $O_2^{\cdot -}$ levels in the myenteric neurons of *Winnie* mice. Similarly, MSCs have also been demonstrated to reduce $O_2^{\cdot -}$ and mitochondrial dysfunction in pathologies involving oxidative stress in the brain, lungs and in ventricular myocytes (DeSantiago et al., 2013, Calió et al., 2014, Li et al., 2018). In the mitochondria, excessive $O_2^{\cdot -}$ and H_2O_2 is produced in a lower-energy oxidative environment due to decreased scavenging ability, or, at a higher-energy reductive environment (such as hypoxia) which increases the direct production of $O_2^{\cdot -}$ by the respiratory chain (Aon et al., 2010). This is somewhat paradoxical considering that $O_2^{\cdot -}$ production is directly proportional to O_2 concentrations in normal kinetics of oxidative phosphorylation (Murphy, 2009). The proposition that intestinal inflammation is

associated with hypoxia is a corollary of experiments observing an upregulation in HIF-1a in animal models and IBD (Karhausen et al., 2004, Xue et al., 2013, Shah, 2016). Nevertheless, a decrease in GSH or GSH/GSSG levels is observed in UC and CD patients, indicating a more oxidative environment, as opposed to a reductive one, which contradicts this hypothesis (Tsunada et al., 2003, S. Pinto et al., 2013, Rana et al., 2014). Myenteric neurons also exhibit a similar oxidative redox environment in experimental colitis (Brown et al., 2016). Furthermore, a decline in the scavenging of free radicals is reported in IBD patients which also supports the presence of an oxidative redox environment (Lih-Brody et al., 1996, Koutroubakis et al., 2004). It has been well established that HIF-1a is degraded in oxygenated cells and stabilised in conditions of hypoxia (Huang et al., 1998). Paradoxically, a hyperoxic environment has also been demonstrated to upregulate HIF-1a in tumours and the brain of mice exposed to increased oxygen tension (Benderro et al., 2012, Terraneo et al., 2014). In the intestinal epithelium intervention with hyperoxia causes ROS generation and severe injury (Zhao et al., 2018); however whether tissues could be made hyperoxic in colitis is debatable. In UC, blood flow is decreased in the mucosa and submucosa when the disease is 'inactive' and, conversely, is increased in the 'active' state (Hultén et al., 1977). This suggests that tissue oxygenation is increased during active inflammation which is a relatively hyperoxic environment. Our results demonstrate that haemoglobin genes *Hbb-b1* and *Hba-a2* are increased in IBD patients and, furthermore, downregulated in the absence of inflammation in BM-MSC-treated *Winnie* mice. Therefore, it could be speculated that increased oxygen delivery has a role in mediating colitis. Alternatively, haemoglobin can also contribute to oxidative stress by generating free radicals via Fe^{+2} through the Fenton reaction (Winterbourn, 1995). Nevertheless, concomitant erythema and decreased oxygen tension on the mucosal surface has been observed in rabbits with experimental colitis (Hauser et al., 1988). If the inflamed colon is hypoxic, this could be the consequence of increased oxygen consumption by neutrophils which promote HIF-1α expression in mice with TNBS-induced colitis and reduce oxygen levels *in vitro* via respiratory burst (Campbell et al., 2014). On the other hand, it is accepted that ROS, including H_2O_2, and pro-inflammatory cytokines, such as TNF-α and IL-1β, can upregulate

stable HIF-1α expression without hypoxia (Movafagh et al., 2015). Considering these cytokines and ROS are prevalent in intestinal inflammation it could be speculated that they also regulate HIF-1α expression. Collectively, there are many contradictions regarding the redox status of colitis and the cause of oxidative stress that require further investigation.

Our results demonstrate that BM-MSCs attenuated ROS production in myenteric neurons, however, it is uncertain whether MSCs directly protect neurons from oxidative stress. To determine the direct effects of oxidative stress and BM-MSCs on myenteric neurons, organotypic cultures were exposed to hyperoxia and H_2O_2. These stimuli were chosen to mimic the oxidative redox environment of myenteric neurons in colitis (Aon et al., 2010, Brown et al., 2016). Hyperoxia is a novel method to induce oxidative stress in enteric neurons, however, ROS generation has been demonstrated to be dose-dependent with oxygen tension in neurons (Kwak et al., 2006, D'Agostino et al., 2007, Matott et al., 2014). Furthermore, hyperoxia has been demonstrated to cause cell death in cortical neurons via lipid peroxidation and ATP dependent Ca^{2+} transport (Chang et al., 2007). Conversely, H_2O_2 is commonly used to model oxidative stress-induced damage to enteric neurons using various cell lines and methods of primary culture (Lourenssen et al., 2009, Pouokam et al., 2009, Abdo et al., 2010, Korsak et al., 2012, Bianco et al., 2016). Furthermore, H_2O_2 has been validated to cause oxidative stress in LMMPs from C57BL/6 mice, as used in our study (Bubenheimer et al., 2016). Both hyperoxia and H_2O_2 resulted in neuronal loss which demonstrates that oxidative stress can have a direct effect on myenteric neurons. Treatment with BM-MSCs reduced neuronal loss from both oxidative stimuli which demonstrates that BM-MSCs can attenuate oxidative stress and its effects directly. Similar results have been demonstrated in other models of oxidative stress-induced neuropathy, including H_2O_2-induced neuropathy in immortalised retinal ganglion cells (Cui et al., 2017, de Godoy et al., 2018). Furthermore, BM-MSCs functioned in a paracrine manner which suggests that secreted factors of BM-MSCs are able to mitigate the effects of oxidative stress.

BM-MSCs constitutively express and can secrete SOD1 (Valle-Prieto and Conget, 2010, Klein et al., 2017). MSCs from multiple sclerosis patients are deficient in SOD1 and have reduced neuroprotective capacity (Redondo et al., 2018, Sarkar et al., 2018). Considering that SOD1 is integral to detoxifying mitochondrial derived $O_2^{\cdot -}$, its role in BM-MSC-mediated neuroprotection was evaluated. Our results indicated that inhibition of SOD1 prevents BM-MSCs from rescuing neuropathy in a paracrine manner which suggests that SOD1 is a major part of their neuroprotective mechanism of action. In other models of neuronal damage, SOD1 has also been demonstrated to confer a neuroprotective effect in cerebral ischemic injury, traumatic brain injury, excitotoxic injury and in *in vitro* models of neurotoxicity (Mikawa et al., 1996, Chan et al., 1998, Peluffo et al., 2006, Davis et al., 2007, Polazzi et al., 2013). Distinct changes in the expression of SODs are observed in CD and UC, with an increase in SOD2 and a decrease in SOD1 in the mucosa (Kruidenier et al., 2003). Comparatively, SOD3 expression was low in the gut; nonetheless a decrease was also observed in IBD patients (Kruidenier et al., 2003). The therapeutic value of SODs has been demonstrated in experimental colitis with the application of SOD and SOD mimetics reducing the severity of colitis in rats (Keshavarzian et al., 1990, Cuzzocrea et al., 2001).

5.8. Conclusion

The presence of oxidative stress in IBD has been established; however, the cause of ROS generation and its role in driving intestinal inflammation requires further exploration. We identified several genes that are either redox sensitive or are involved in ROS production and antioxidant defences that were altered in IBD and *Winnie* mice with chronic inflammation. BM-MSC treatments in *Winnie* mice remedied the dysfunction in expression for many of these genes, suggesting that they can promote a microenvironment that favours the aversion of oxidative insult. This was further supported by a reduction in DNA/RNA adducts throughout the colon. The myenteric ganglia appeared to be particularly sensitive to oxidative stress with a strong accumulation of DNA/RNA adducts and $O_2^{\cdot -}$ generation from the mitochondria. In *in vitro* studies, stimuli that promote an oxidative redox status

caused neuronal loss. This demonstrated that oxidative stress can directly damage myenteric neurons. BM-MSC treatments attenuated oxidative stress in myenteric neurons *in vivo* and myenteric neuropathy induced by oxidative stimuli *in vitro.* This demonstrates that BM-MSCs can protect neurons and promote a microenvironment that is better equipped to alleviate oxidative burden. The neuroprotective effects of BM-MSCs were of paracrine origin which is mediated, at least in part, by SOD1.

CHAPTER SIX

Mesenchymal Stem Cell Treatments Ameliorate HMGB1 Translocation Associated with Myenteric Neuronal Loss

6.1. Summary

High-mobility group box 1 (HMGB1) is a damage associated molecular pattern (DAMP) that is released by dying cells to stimulate the immune response. During necrotic-like mechanisms of cell death, HMGB1 is translocated from the nucleus to the cytoplasm and passively released. High levels of secreted HMGB1 are observed in the faeces of inflammatory bowel disease (IBD) patients, which indicates its potential contribution to the pathophysiology of IBD and has been promising as a non-invasive biomarker for paediatric and adult cases. Inhibition of HMGB1 can be effective as a treatment against acute, experimental, intestinal inflammation. HMGB1 is important in regulating neuronal damage in the central nervous system and its pathological activity is intertwined with oxidative stress and inflammation. Expression of HMGB1 has also been recently identified in enteric neurons. Previously, we demonstrated that oxidative stress and leukocyte infiltration are evident in the myenteric plexus which contributes to neuronal loss in colitis. These were attenuated by bone marrow-derived mesenchymal stem cell (BM-MSC) treatments. Therefore, the potential role of HMGB1 in mediating enteric neuronal loss and the neuroprotective effects of BM-MSCs warrants elucidation. This was examined in organotypic cultures of the myenteric plexus exposed to oxidative stimuli *in vitro* and *Winnie* mice with spontaneous chronic colitis *in vivo. Winnie* mice underwent a treatment regimen over two weeks of four BM-MSC injections delivered by enema or twice-daily intraperitoneal injections of the HMGB1 inhibitor, glycyrrhizic acid (GA). Mice were culled 24h after the final treatment and distal colons were collected for RNA isolation and immunohistochemistry. High-throughput RNA sequencing and bioinformatics were performed to analyse genes associated with cell-death. The effects of oxidative stimuli on HMGB1 expression in myenteric neurons were explored in *in vitro* organotypic cultures. Oxidative stimulus directly resulted in HMGB1 translocation from the nucleus into cytoplasm in myenteric neurons. Likewise, HMGB1 translocation was evident in myenteric neurons of *Winnie* mice with chronic inflammation. Application of BM-MSCs attenuated HMGB1 translocation in both models, which was mediated, in part, by SOD1. HMGB1 translocation

correlated with enteric neuronal loss suggesting that these events were linked. Inhibition of HMGB1 by GA in *Winnie* mice completely ameliorated myenteric neuronal loss which exemplifies that this molecule contributes to neuronal damage. Oxidative stress and leukocyte infiltration appeared to be upstream of HMGB1 translocation-mediated neuronal loss. Thus, the antioxidative and anti-inflammatory properties of BM-MSC treatments are likely to be responsible for their attenuation of HMGB1 translocation and subsequent neuroprotection.

6.2. Abbreviations

BM-MSC	bone marrow-derived mesenchymal stem cell
CNS	central nervous system
CXCL12	C-X-C chemokine ligand 12
CXCR4	C-X-C chemokine receptor 4
DAMP	damage-associated molecular pattern
DMSO	dimethyl sulfoxide
DRG	dorsal root ganglion
DSS	dextran sodium sulphate
ENS	enteric nervous system
ER	endoplasmic reticulum
FBS	foetal bovine serum
GA	glycyrrhizic acid
GEO	Gene Expression Omnibus
GO	gene ontology
HMGB1	high-mobility group box 1
HO-1	haem oxygenase 1
IBD	inflammatory bowel disease
IL	interleukin
LMMP	longitudinal muscle and myenteric plexus
MAP-2	microtubule associated protein 2
mPTP	mitochondrial permeability transition pore
$O_2^{\cdot -}$	superoxide anion
OCT	optimal cutting temperature
RAGE	receptor for advanced glycation end-products
RIP	receptor-interacting protein
ROS	reactive oxygen species
SOD1	superoxide dismutase 1
TLR	toll-like receptors
TNBS	2,4,6-trinitrobenzenesulfonic acid
TNF	tumour necrosis factor
TRAIL	TNF-related apoptosis-inducing ligand

6.3. Gene symbols

Bcl2a1a	B cell leukemia/lymphoma 2 related protein A1a
Bcl2a1b	B cell leukemia/lymphoma 2 related protein A1b
Bcl2a1d	B cell leukemia/lymphoma 2 related protein A1d
Bcl2l15	BCLl2-like 15
Bik	BCL2-interacting killer
Bnip3	BCL2/adenovirus E1B interacting protein 3
Capn6	calpain 6
Cidec	cell death-inducing DFFA-like effector c
Defb1	defensin beta 1
Dlc1	deleted in liver cancer 1
Dpysl4	dihydropyrimidinase-like 4
Ern2	endoplasmic reticulum to nucleus signalling 2
Fas	Fas (TNF receptor superfamily member 6)
Fzd3	frizzled class receptor 3
Galnt5	UDP-N-acetyl-alpha-D-galactosamine:polypeptide N-acetylgalactosaminyltransferase 5
Gcg	glucagon
Glul	glutamate-ammonia ligase (glutamine synthetase)
Hk3	hexokinase 3
Igfbp3	insulin-like growth factor binding protein 3
Jph3	junctophilin 3
Mag	myelin-associated glycoprotein
Mmp3	matrix metallopeptidase 3
Nme5	NME/NM23 family member 5
Nox1	NADPH oxidase 1
Reg3b	regenerating islet-derived 3 beta
Ripk3	receptor-interacting serine-threonine kinase 3
S100a7a	S100 calcium binding protein A7A
Slc7a11	solute carrier family 7 (cationic amino acid transporter, y+ system), member 11

Sycp2	synaptonemal complex protein 2
Tbc1d24	TBC1 domain family, member 24
Tnf	tumor necrosis factor
Tnfrsf1b	tumor necrosis factor receptor superfamily, member 1b
Tnfrsf4	tumor necrosis factor receptor superfamily, member 4
Tnfrsf11b	tumor necrosis factor receptor superfamily, member 11b (osteoprotegerin)
Tnfrsf17	tumor necrosis factor receptor superfamily, member 17
Trp63	transformation related protein 63
Trp73	transformation related protein 73
Tspo	translocator protein

6.4. Introduction

High-mobility group box 1 (HMGB1) is a highly-conserved nuclear protein that binds DNA to stabilise the nucleosome and regulate transcription in physiological conditions (Park et al., 2004, Lotze and Tracey, 2005). Nevertheless, HMGB1 has emerged as an important alarmin to cellular stress involved in the pathophysiology of several diseases (Andersson et al., 2018). In conditions of cellular stress, the two HMGB1 nuclear localization sites are hyperacetylated and HMGB1 translocates to the cellular cytoplasm where is it released actively, by leukocytes, or passively, by necrotic and necroptotic cells (Yiting et al., 2016). Here, HMGB1 functions as a damage-associated molecular pattern (DAMP), acting as a direct chemoattractant via the C-X-C chemokine ligand 12 (CXCL12) and C-X-C chemokine receptor 4 (CXCR4) axis, as well as stimulating the release of pro-inflammatory mediators via toll-like receptors (TLR)-2 and TLR-4 expressed on nearby immune cells (Park et al., 2004). These functions are mutually exclusive and depend on post-translational modifications to HMGB1 that are regulated by the local redox environment.

The role of HMGB1 in mediating the immune response has been established in several inflammatory and autoimmune diseases (Andersson and Tracey, 2011, Magna and Pisetsky, 2014). Likewise, high levels of HMGB1 are observed in animal models of experimental colitis and inflammatory bowel disease (IBD) patients (Davé et al., 2009, Yamasaki et al., 2009, Vitali et al., 2011, Vitali et al., 2013, Palone et al., 2014). The link between HMGB1 and intestinal inflammation is validated by its accuracy as a non-invasive biomarker for paediatric and adult cases of IBD (Vitali et al., 2011, Palone et al., 2014). Thus, pharmacological inhibition of HMGB1 is being considered as a potential therapeutic option for the treatment of IBD (Andersson and Tracey, 2011). Studies in dextran sodium sulphate (DSS) chemically-induced colitis have demonstrated that inhibition of HMGB1 can be effective as a preventative treatment against intestinal inflammation (Yamasaki et al., 2009, Vitali et al., 2013). Nonetheless, the efficacy of HMGB1 inhibition in established chronic intestinal inflammation has not yet been studied. Of interest is the compound glycyrrhizic acid (GA), a specific HMGB1 inhibitor that directly

binds to the molecule; thus, inhibiting its pro-inflammatory and chemoattractant properties (Mollica et al., 2007). Furthermore, the effects of GA on the vital nuclear binding properties of HMGB1 is weak; therefore, its use has already been approved for many diseases in the clinic (Veldt et al., 2006, Mollica et al., 2007).

Although HMGB1 is ubiquitously expressed by virtually all cells, its function in the pathophysiology of nervous system damage, including ischemia, reperfusion, haemorrhage and physical trauma, has gathered much attention (Gong et al., 2011, Ohnishi et al., 2011, Kim et al., 2012, Okuma et al., 2014). In the central nervous system (CNS), HMGB1 appears to be translocated and released almost exclusively from neurons and not the glia (Okuma et al., 2014, Sun et al., 2014). Therefore, HMGB1 signalling may be a specific neuronal mechanism to activate the inflammatory response. Likewise, HMGB1 was recently discovered in the enteric nervous system (ENS); changes in its expression were associated with the neurotoxic effects of chemotherapeutic agents (Nurgali et al., unpublished). The effects of chronic inflammatory conditions on the expression of HMGB1 in the ENS is currently unknown. Although extracellularly released HMGB1 can activate leukocytes, enteric neurons also express the major receptors for HMGB1 including TLR-2 and TLR-4 (Venereau et al., 2012, Chen et al., 2015, Burgueño et al., 2016). Activation of TLRs are known to cause neurotoxicity (Okun et al., 2009, Voss and Ekblad, 2014, Stavely et al., 2015a); thus, HMGB1 could potentially contribute to neuronal death if translocated and released. While enteric neuronal loss is common in inflammatory conditions, the mechanisms of cell death remains unclear. Cytoplasmic accumulation of HMGB1 is a feature of necrotic cell death pathways, conversely, HMGB1 irreversibly binds to nuclear DNA during apoptosis (Janko et al., 2014, Andersson et al., 2018). Therefore, investigating HMGB1 expression may also help to elucidate the pathophysiological mechanism of cell death pathways in enteric neurons during chronic inflammation.

Oxidative stress and changes in the redox status are critical to the alarmin and DAMP activity of HMGB1. While the functions of HMGB1 are dependent on the redox environment, oxidative stress and reactive oxygen species (ROS) also

regulate the translocation of HMGB1 to the cytoplasm and its subsequent release (Tang et al., 2011). Previously, we demonstrated that high levels of mitochondrial superoxide ($O_2^{\cdot -}$) and markers of oxidative stress are present in myenteric neurons in conditions of chronic inflammation (**Chapter 5, Figure 5.6 & 5.10**). Oxidative stress was determined to induce enteric neuronal loss (**Chapter 5, Figure 5.8 & 5.9**). Moreover, it was demonstrated that neuronal loss, oxidative stress and leukocyte infiltration could be attenuated by bone marrow-derived mesenchymal stem cell (BM-MSC) treatment. HMGB1 is important in regulating neuronal damage and its pathological activity is intertwined with oxidative stress and inflammation; both are evident in chronic colitis. Therefore, in this study we test the hypothesis that HMGB1 may play a role in the neuroprotective effects of BM-MSC therapy and the pathophysiology of myenteric neuronal death in chronic colitis.

6.5. Methods

6.5.1. Animals

For organotypic immunohistochemical studies, male C57BL/6 mice aged 14 weeks (total n=22) were obtained from the Animal Resource Centre (Perth, Western Australia, Australia). For *in vivo* studies, male *Winnie* mice aged 14 weeks (total n=26) were obtained from Victoria University (Melbourne, Victoria, Australia). *Winnie* mice were compared to age-matched male C57BL/6 mice (total n=10) obtained from the Animal Resource Centre (Perth, Western Australia, Australia). All mice had *ad libitum* access to food and water and were housed in a temperature-controlled environment with a 12-h day/night cycle. Mice were acclimatised for one week at the Western Centre for Health, Research and Education (Melbourne, Victoria, Australia). All mice were culled by cervical dislocation and the distal portion of the colon was collected for subsequent experiments. All animal experiments in this study complied with the guidelines of the Australian Code of Practice for the Care and Use of Animals for Scientific Purposes and were approved by the Victoria University Animal Experimentation Ethics Committee.

6.5.2. Cell culture and passaging

The MSCs used in this study were derived from human bone marrow (BM-MSC) and were obtained from Tulane University, USA. These BM-MSCs were extensively characterised for cell surface markers, differentiation potential, proliferation, colony formation, morphology and adherence to plastic (Stavely et al., 2015b) (**Chapter 2, Figures 2.1 & 2.2**) and conform to the guidelines set by the International Society for Cell Therapy (Dominici et al., 2006). BM-MSCs were cultured as previously described to generate the required numbers for animal treatments and cell culture experiments (**Chapter 3, Section 3.5.2**). Cells prepared for *in vivo* and *in vitro* experiments had a viability of over 95% after trypsinisation and were used only at the fourth passage to minimise the chance of acquiring genetic abnormalities (Ueyama et al., 2012).

6.5.3. Organotypic culture of myenteric ganglia

Organotypic culture of the myenteric ganglia was performed as previously described (**Chapter 5, Section 5.5.3**). Briefly, the distal colon was collected and pinned in a silicon-lined Petri dishes containing Hank's balanced salt solution (Sigma-Aldrich, Sydney, Australia) to remove the mucosa and submucosa layers before being cut into 1.5cm^2 sheets. The organotypic sheet preparations were loosely pinned into 24-well cell culture plates that were modified to contain a silicon elastomer (Sylgard; Dow Corning, USA) that covered the bottom of the wells with a depth of ~5mm. Preparations were incubated (37°C, 5% CO_2) for 24h in α-MEM supplemented with 100 U/mL penicillin/streptomycin, 1% glutaMAX and 5% (v/v) foetal bovine serum (FBS) (Gibco®, Life Technologies, Melbourne, Australia, for all), unless stated otherwise. Hyperoxic oxygen tension, and the chemical H_2O_2, were utilised as oxidative stimuli in organotypic preparations. A hyperoxic environment (95% O_2 and 5% CO_2) was formed using a self-contained modular incubator (Billups-Rothenberg, Inc., San Diego, CA, USA). Organotypic cultures were exposed to H_2O_2 diluted in α-MEM at a final concentration of 100µM.

An equal volume of the α-MEM vehicle was applied to control cultures. Organotypic preparations were co-cultured with BM-MSCs at a concentration of 1×10^5 cells per well in a transwell semipermeable insert (0.4µm pore size; Sigma-Aldrich) that contained the same media as organotypic cultures. To assess the role of SOD1, the antagonist LCS-1 (Sigma-Aldrich), was applied to organotypic cultures at a final concentration of 10µM. For these experiments, the dimethyl sulfoxide (DMSO) vehicle for LCS-1 was present in all cultures at a concentration of 0.05% (v/v). Organotypic preparations were cultured for 24h before being fixed overnight at 4°C in Zamboni's fixative (2% formaldehyde and 0.2% picric acid). Preparations were subsequently washed in DMSO (Sigma-Aldrich) (3x10min), to permeabilise the tissue, and phosphate buffered saline (PBS) (3x10min), to remove DMSO and the fixative for immunohistochemical experiments.

6.5.4. Treatment administration

BM-MSCs were administered into *Winnie* mice with chronic colitis by enema. A lubricated silicone catheter was inserted 3cm proximal to the anus of mice anesthetised with 2% isoflurane. *Winnie* mice were treated with two doses of $4x10^6$ BM-MSCs in 100µL of sterile PBS and subsequently received two replenishment doses of $2x10^6$ BM-MSCs in the same volume of sterile PBS (*Winnie*-sham). All treatments were administered 4 days apart. Sham-treated *Winnie* mice underwent the same procedure on the same days with an injection of sterile PBS at the same volume. In a sperate group of mice, HMGB1 was inhibited by glycyrrhizic acid (GA) (Sigma-Aldrich) (10 mg/kg) which was dissolved in 2% cremophor (Sigma-Aldrich): 2% EtOH and 96% sterile water and given to mice via i.p. injections twice daily for 14 days with no less than 8h between injections. The dose of GA used in our study was effective in reducing oxidative stress, inflammation and neuronal apoptosis in a rat model of ischemic brain injury (Gong et al., 2014). The vehicle group received 2% cremophor: 2% EtOH and 96% sterile water via i.p. injections twice daily for 14 days with no less than 8h between injections. The volumes for all injections were calculated to each animal's body weight with less than 200µL per injection. Mice were culled 24h after the final treatment for tissue collection.

6.5.5. Evaluation of colitis

Clinical signs of colonic inflammation in *Winnie* mice are characterised by changes to body weight, colon weight and length, diarrhoea, rectal prolapses and rectal bleeding (Heazlewood et al., 2008, Eri et al., 2011). These were assessed as previously described (**Chapter 3, Section 3.5.4**). Animals were closely monitored for clinical symptoms throughout the experimental procedures. Daily body weights were recorded to calculate weight loss. Directly after culling, the entire colon was weighed and photographed for measuring their length to calculate the colon weight:length ratio. To analyse faecal water content, faecal pellets were collected from mice and were weighed immediately to determine their wet weight. Faecal pellets were dried in a fan forced oven at 60ºC for 24h to remove all moisture and weighed again to determine their dry weight. Faecal water content was calculated as the difference expressed as a percentage between the wet and dry weight. Colitis was confirmed by a disease activity index (DAI) which included symptoms of chronic diarrhoea (faecal water content: 60-64%=1, 65-69%=2, 70-74%=3, 75-79%=4, ≥80%=5), rectal manifestations (bleeding=1, prolapse=2), weight loss (weight before treatment to weight after treatment prior to culling: -1 to -4%=1, -5 to -9%=2, ≥-10%=3), and ratios of colon weight:length from the caecum to the anus (0.0110-0.0140=1, 0.0141-0.0160=2, 0.0161-0.0180=3, 0.0181-0.0200=4, ≥0.0200=5) (Stavely et al., 2018a).

6.5.6. Immunohistochemistry

Antibody labelling of fixed longitudinal muscle and myenteric plexus (LMMP) wholemounts and organotypic preparations was performed using the methodology previously described (**Chapter 4, Section 4.5.4**). Wholemounts and organotypic preparations were labelled with the primary antibodies chicken anti-microtubule associated protein (MAP)-2 (1:5000; Abcam, Melbourne, Australia), rabbit anti-HMGB1 (1:2000) (Abcam) and rat anti-CD45 (1:200) (BioLegend, San Diego, USA). Tissues were washed with PBS (3x10min) and then labelled with the

secondary antibodies Alexa Fluor 594 donkey anti-chicken (1:500), Alexa Fluor 647 donkey anti-rabbit (1:500) and Alexa Fluor 488 donkey anti-rat (1:500) (all from Jackson Immunoresearch, West Grove, USA). Tissues were stained with nuclear marker 4',6-diamidino-2-phenylindole (DAPI) for 2min at room temperature prior to being washed with PBS (3x10min) and mounted for imaging. Cross sections of the distal colon from *in vivo* experiments were prepared and immunolabeled using the methodology previously described (**Chapter 3, Section 3.5.6**). Tissue cross sections were labelled with the primary antibodies chicken anti-MAP-2 (1:5000) and rabbit anti-HMGB1 (1:2000) prior to being washed and labelled with the secondary antibodies Alexa Fluor 594 donkey anti-chicken (1:500) and Alexa Fluor 647 donkey anti-rabbit (1:500). Tissues were then stained with DAPI for 2min at room temperature prior to being washed with PBS (3x10min) and mounted for imaging.

6.5.7. MitoSOX Red fluorescent staining

The production of $O_2^{\cdot -}$ in the myenteric plexus was assessed in freshly excised colon segments as previously described (**Chapter 4, Section 5.5.6**). Tissues were collected in physiological saline (composition in mmol L−1: NaCl, 117; NaH2PO4, 1.2; MgSO4, 1.2; CaCl2, 2.5; KCl, 4.7; NaHCO3, 25; and glucose, 11) which was gently bubbled with carbogen (95%O_2–5%CO_2) throughout the entire procedure. Tissues were viewed under a dissection microscope, cut along the mesenteric border and pinned in a silicon-lined Petri dish containing physiological saline. The mucosa, submucosa and circular smooth muscle was immediately removed to expose the LMMP. Tissues were incubated for 40min at 37°C in physiological saline containing MitoSOX Red (1:1000) (Molecular Probes®, Thermofisher, Melbourne, Australia). Tissues were then washed in physiological saline (3×10min) prior to being fixed in 4% paraformaldehyde overnight at 4°C. Paraformaldehyde was removed by washing the tissues with PBS (3×10min) before they were mounted onto glass slides with DAKO fluorescence mounting medium (Agilent Technologies, Melbourne, Australia) and visualised by confocal microscopy.

6.5.8. Imaging and analysis

An Eclipse Ti confocal laser scanning system (Nikon, Tokyo, Japan) was used to visualise MAP-2, HMGB1, CD45 immunofluorescence or the MitoSOX red fluorogenic probe. Identical acquisition settings were used between samples in all experiments. Images were collected as .ND2 files which contained all metadata including fluorescence signals at all Z levels. Images were visualised using Image J v1.50b open source software (National Institute of Health, Bethesda, USA) (Schneider et al., 2012, Rueden et al., 2017) with the Image J ND2 Reader plugin and were converted into maximum intensity projections in 16-bit .TIFF format. All subsequent analysis was performed using Image J. For all analyses, average mean values were calculated from eight individual images per sample.

For HMGB1 and MAP-2 quantification in wholemount LMMPs and organotypic preparations, Z-series images were randomly acquired using the 40X objective at a thickness of 1µm. The average MAP-2 immunoreactive neuronal density was calculated within a 0.1mm^2 (316.23µm x 316.23µm = 100,000µm^2) field of view per image as previously described (Gulbransen et al., 2012) (**Chapter 4, Section 4.5.5**). In the same images, HMGB1 expression in the ganglia was quantified using the cell counter plugin of ImageJ software. HMGB1 was determined to be expressed by MAP-2 immunoreactive neurons or other non-neuronal cells. The intracellular location of HMGB1 in these cells was determined as localised in the nucleus, absent in the nucleus or translocated to the cytoplasm with the aid of the nuclear marker DAPI. HMGB1 expression in cells was reported as the number of cells per 0.01mm^2 (100µm x 100µm = 10,000µm^2) of ganglionated area or expressed as a percentage of total neurons. To quantify HMGB1 expression in cross sections of the distal colon, Z-series images were randomly acquired using the 60X objective at a thickness of 1µm. Eight 16-bit images were analysed in a field of view of 0.04mm^2 (200µm x 200µm = 40,000µm^2) per individual image. The number of MAP-2 immunoreactive neurons was quantified as described previously (**Chapter 4, Section 4.5.5**). The number of neurons expressing HMGB1 in the nucleus weas determined using the cell counter plugin of ImageJ software. Values

were expressed as the percentage of neurons with or without nuclear HMGB1 expression. HMGB1 expression was pseudo-coloured green for all imaging in wholemounts and cross sections for greater visual distinction.

Leukocytes immunoreactive for CD-45 were quantified in images of wholemount LMMP preparations as previously described (**Chapter 4, Section 4.5.5**). Briefly, Z-series images were randomly acquired using the 40X objective at a thickness of 1µm. CD-45 immunoreactive cells were enumerated within a $0.1mm^2$ (316.23µm x 316.23µm = $100,000\mu m^2$) field of view using the cell counter plugin of ImageJ software. Leukocytes were further classified by their location in relation to the MAP-2 immunoreactive ganglia (intra-ganglionic, periphery of ganglia, extra-ganglionic). Values were expressed as the average number of CD45-IR cells per $0.1mm^2$ area from eight images per mouse.

Mitochondria-derived $O_2^{\cdot -}$ was visualised using the MitoSOX fluorogenic probe in wholemount LMMP preparations as previously described (**Chapter 2, Section 2.4.12**). Eight Z-series images were randomly acquired using the 40X objective at a thickness of 1µm; 16-bit images with a field of view of $0.1mm^2$ (316.23µm x 316.23µm = $100,000\mu m^2$) per individual image were analysed. Regions of interest were set to determine MitoSOX fluorescence within the myenteric ganglia. The fluorescence intensity of $O_2^{\cdot -}$ in the ganglia was measured as the mean grey value (mean fluorescence intensity) of the pixels within the regions of interest.

6.5.9. Statistical analysis

Data analysis was performed using GraphPad Prism v7 (GraphPad Software Inc., San Diego, USA). A one-way ANOVA was performed with a post hoc Holm-Sidak test for multiple comparisons. X, Y correlations were determined using a linear regression analysis with *P* values for significant slope relationships recorded. For all analyses $P \leq 0.05$ was considered significant. All data were presented as mean ± standard error of the mean (SEM).

6.5.10. RNA extraction and quality control

Total RNA was extracted from segments of the distal colon as previously described (**Chapter 3, Section 3.5.9**). Briefly, snap frozen colon was homogenised with a bead beater (TissueLyser LT, Qiagen, Melbourne, Australia) and RNA was extracted from the tissue homogenate using TRIzol® reagent (Thermo Fisher Scientific, Melbourne, Australia) and spin columns from the RNeasy Mini Kit (Qiagen, Melbourne, Australia). The concentration of RNA in each sample was quantified by a Qubit 1.0 fluorometer (Invitrogen, Thermosphere, Australia) using the Qubit® RNA Broad Range Assay Kit (Life Technologies, Thermofisher, Australia) as of manufacturers protocol. Contaminates were evaluated in RNA samples using a DeNovix DS-11 spectrophotometer (Gene Target Solutions, Sydney, Australia). Absorbance (A) scores for all samples were between 1.8 – 2.0 for A260/A280 ratios. and 2.0-2.2 for A260/A230 ratios, suggesting that nucleotide purity was high. The quality of RNA was assessed using an 2100 Bioanalyzer (Agilent Technologies, Australia) microfluidics platform with the RNA 6000 Nano Kit (Agilent Technologies) according to the manufacturer's protocol. All sample were free from contamination of genomic DNA and 16S ribosomal RNA from bacteria. All samples were of very high quality and had minimal degradation with RNA integrity number (RIN) values between 9.9-10/10.

6.5.11. High-throughput RNA-Sequencing and bioinformatics

High-throughput sequencing of Poly-A tail purified mRNA was performed as described previously (**Chapter 3, Section 3.5.11**) with an experimental design similar to Seaman et al. (2015). Samples of RNA (n=7/group) from C57BL/6 and *Winnie* mice treated with either sham or BM-MSC enemas were submitted to the Australian Genome Research Facility (AGRF, Melbourne, Australia) and met all quality control criteria. High-throughput sequencing was performed using a 100bp single-end read protocol on the Illumina HiSeq 2500 System. Raw data were processed, and gene reads were mapped as previously described (**Chapter 3, Section 3.5.11**). Gene expression from raw mapped reads were calculated by the R

package DEGseq v 1.34.0 (Wang et al., 2009). Resulting datasets were additionally cleaned by cut-offs for lowly expressed genes with <10 counts and a log fold change (FC) value between ±0.5. Gene expression data on the transcriptome of human IBD patients were obtained from the National Centre for Biotechnology Information (NCBI) Gene Expression Omnibus (GEO) public data repository as previously described (**Chapter 3, Section 3.5.11**) (Edgar et al., 2002, Barrett et al., 2012). Data were uploaded by Peters et al. (2017); similar to our methods RNA was extracted by TRIzol, purified for mRNA and used the same sequencing platform. These data are accessible through GEO series accession number GSE83687 at https://www.ncbi.nlm.nih.gov/geo/. Gene expression of colon samples were used from this dataset including: male (n=14) and female (n=20) controls, male (n=19) and female (n=11) patients with ulcerative colitis (UC) and male (n=7) and female (n=4) patients with Crohn's disease (CD) (total n=75). Gene sets that were representative cell death were collated from the gene ontology (GO) database (Ashburner et al., 2000), including *programmed necrotic cell death* (GO:0097300), *cell death in response to oxidative stress* (GO:0036473), *necrotic cell death* (GO:0070265), *neuron death in response to oxidative stress* (GO:0036475) and *execution phase of apoptosis* (GO:0097194) The fold regulation of genes were visualised as heat maps using the gplots R package (Warnes et al., 2009).

6.6. Results

6.6.1. Translocation of neuronal HMGB1 in the myenteric ganglia is associated with oxidative stress-induced neuropathy

Previously, we demonstrated that high levels of $O_2^{\cdot -}$ is present in the myenteric ganglia in acute and chronic inflammation (**Chapter 2, Figure 2.11 & Chapter 5, Figure 5.5**). Furthermore, oxidative stimuli directly resulted in neuronal loss (**Chapter 5, Figures 5.8 & 5.9**). Cytoplasmic HMGB1 translocation and release has previously been associated with oxidative stress in neurons of the CNS (Sun et al., 2014); therefore, this relationship was evaluated in myenteric neurons. To

determine the effects of oxidative stress on HMGB1 expression in the myenteric ganglia, *in vitro* organotypic cultures were subjected to hyperoxic (**Figure 6.1A-C′′′**) and chemical insult via the application of H_2O_2 (**Figure 6.2 A-C′′′**). Culturing organotypic preparations under hyperoxic conditions (n=7 independent cultures) decreased the total number of neurons with HMGB1 expressed inside the nucleus (**Figure 6.1 B-B′′′**) and increased the total number of neurons with cytoplasmic HMGB1 translocation (**Figure 6.1 C-C′′′**) compared to controls (n=8 independent cultures) ($P<0.05$, for both) (**Figure 6.1D-D′, Table 6.1**). Punctate immunoreactivity of HMGB1 was observed throughout tissues with high levels of neuronal HMGB1 translocation. A negative correlation was found between the latter and the neuronal density of the myenteric ganglia ($F(1,10) = 13.78$, $P<0.01$) with an R^2 of 0.5794 (**Figure 6.1E, Table 6.2**). To account for the decrease in neuronal density caused by hyperoxia (**Chapter 5, Figures 5.8 & 5.9**), the proportions of neurons with HMGB1 expression were also investigated (**Figure 6.1F-F′′**). Similar to total counts, the proportion of neurons with HMGB1 expression in the nucleus decreased ($P<0.05$) and proportions without nuclear HMGB1 ($P<0.05$) or with cytoplasmic translocation increased ($P<0.01$) (**Figure 6.1F-F′′, Table 6.1**). Furthermore, a negative correlation was observed between the proportion of neurons with HMGB1 translocation and neuronal density ($F(1,10) = 17.5$, $P<0.01$) with an R^2 of 0.6364 (**Figure 6.1G, Table 6.2**). No changes were observed in the total number of non-neuronal cells in the myenteric ganglia that expressed HMGB1 in the nucleus or the cytoplasm after hyperoxia (**Figure 6.1H-H′, Table 6.1**).

Comparable results were observed in organotypic cultures exposed to H_2O_2. Application of H_2O_2 (n=9 independent cultures) decreased the total number of neurons with nuclear HMGB1 expression (**Figure 6.2 B-B′′′**) and increased the total number of neurons with cytoplasmic HMGB1 translocation (**Figure 6.1 C-C′′′**) compared to controls ($P<0.05$, for both) (**Figure 6.2D-D′, Table 6.1**).

Figure 6.1 ***Effects of hyperoxia on HMGB1 expression in myenteric neurons after organotypic culture***

A-C‴′) HMGB1 expression within the myenteric ganglia in distal colon organotypic cultures. Myenteric neurons observed by immunofluorescence of the neuronal marker MAP-2 **(A-C)**, nuclear stain with DAPI **(A′-C′)**, HMGB1 **(A″-C″)**, merged images **(A‴-C‴)** and ratio representations of HMGB1:DAPI **(A⁗-C⁗)** for visual distinction. Tissues were cultured for 24h in 5% CO_2 and ambient O_2 conditions (control) **(A)** or hyperoxic (↑O_2) conditions (5% CO_2, 95% O_2) **(B-C)**. Neurons without nuclear HMGB1 expression denoted by arrows **(B-B⁗)** and neurons with HMGB1 translocation into the cytoplasm denoted by stars **(C-C⁗)** (scale bar = 20μm). **D-D′)** Quantification of neurons with HMGB1 expressed in the nucleus **(D)** and translocated to the cytoplasm **(D′)** presented as neurons per ganglionated area. **E)** Linear correlation between neuronal density and neurons with translocation of HMGB1 per area. **F-F″)** Percentage of neurons with HMGB1 expressed in the nucleus (nuclear $HMGB1^{+ve}$) **(F)**, absent in the nucleus (nuclear $HMGB1^{-ve}$) **(F′)** and translocated to the cytoplasm **(F″)**. **E)** Linear correlation between neuronal density and the percentage of neurons with HMGB1 translocation. **H-H′)** Quantification of non-neuronal cells with HMGB1 expressed in the nucleus **(H)** and translocated to the cytoplasm **(H′)** presented as cells per ganglionated area. **P*<0.05, ***P*<0.01; control: n=8 independent samples, ↑O_2: n=7 independent samples.

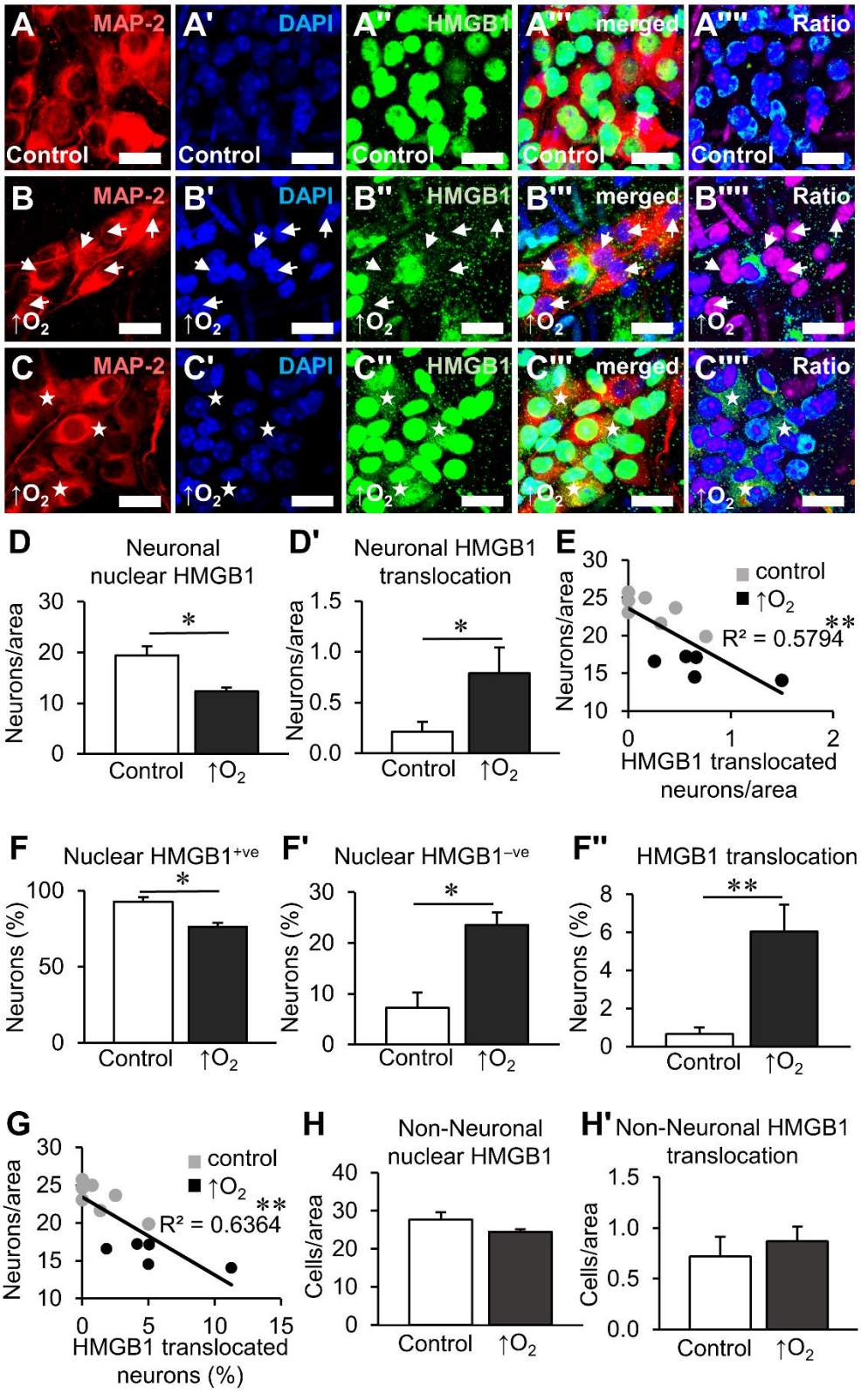
A MAP-2
A' DAPI
A'' HMGB1
A''' merged
A'''' Ratio
Control
B MAP-2
B' DAPI
B'' HMGB1
B''' merged
B'''' Ratio
↑O2
C MAP-2
C' DAPI
C'' HMGB1
C''' merged
C'''' Ratio
D Neuronal nuclear HMGB1
Neurons/area
Control
↑O2
D' Neuronal HMGB1 translocation
Cells/area
E
control
↑O2
R² = 0.5794
HMGB1 translocated neurons/area
F Nuclear HMGB1+ve
Neurons (%)
F' Nuclear HMGB1−ve
F'' HMGB1 translocation
G
R² = 0.6364
HMGB1 translocated neurons (%)
H Non-Neuronal nuclear HMGB1
H' Non-Neuronal HMGB1 translocation

Table 6.1 ***HMGB1 counts in the myenteric plexus of organotypic cultures***

HMGB1 expression	Control	↑O_2	H_2O_2
HMGB1^{+ve} cells/area			
neurons	19.5±1.8	12.4±0.7*	11.5±1.9*
non-neuronal	27.7±2.0	24.5±1.7	23.5±2.1
HMGB1^{-ve} cells/area			
neurons	2.7±1.3	6.6±2.1*	4.8±1.1*
HMGB1-translocated cells/area			
neurons	0.21±0.01	0.92±0.26*	0.71±0.17*
non-neuronal	0.72±0.19	0.87±0.14	1.09±0.29
Neurons %			
HMGB1^{+ve}	92.8±3.0	76.4±2.5*	69.0±8.3*
HMGB1^{-ve}	7.2±3.0	23.6±2.5*	31.1±8.3*
HMGB1-translocated	0.65±0.37	6.05±1.41**	3.76±0.95*

↑O_2 – hyperoxia, H_2O_2, hydrogen peroxide, HMGB1 - High mobility group box-1, HMGB1^{+ve} – HMGB1 expressed in the nucleus, HMGB1^{-ve} – HMGB1 absent from the nucleus. *P<0.05, **P<0.01 significantly different to control. Control: n=8 independent samples, ↑O_2: n=7 independent samples, H_2O_2: n=9 independent samples.

Table 6.2 ***Correlation between HMGB1 counts and neuronal density in hyperoxia-treated organotypic cultures***

HMGB1 expression	R^2	Relationship to neuronal density	*P* value
HMGB1^{+ve} cells/area			
Neurons	0.5874	Increase	**0.0022**
non-neuronal	0.337	Increase	**0.0375**
HMGB1^{-ve} cells/area			
Neurons	0.4404	Decrease	**0.026**
HMGB1-translocated cells/area			
neurons	0.5794	Decrease	**0.004**
non-neuronal	0.01006	-	0.7444
Neurons %			
HMGB1^{-ve}	0.6063	Decrease	**0.0047**
HMGB1-translocated	0.6364	Decrease	**0.0019**

HMGB1 - High mobility group box-1, HMGB1^{+ve} – HMGB1 expressed in the nucleus, HMGB1^{-ve} – HMGB1 absent from the nucleus. Control: n=8 independent samples, ↑O_2: n=7 independent samples.

A negative correlation was observed between the number of neurons with cytoplasmic HMBG1 and neuronal density ($F(1,13) = 38.12$, $P<0.0001$, $R^2 = 0.7457$) (**Figure 6.2E, Table 6.3**). Similarly, the proportion of neurons with HMGB1 expression in the nucleus decreased ($P<0.05$) and the proportion of neurons without nuclear HMGB1 ($P<0.05$) or those with cytoplasmic HMBG1 increased ($P<0.01$) (**Figure 6.2F-F′′, Table 6.1**). The proportion of neurons with HMGB1 translocation was negatively correlated to neuronal density ($F(1,13) = 26.21$, $P<0.001$) with an R^2 of 0.6684 (**Figure 6.2G, Table 6.3**). Similar to organotypic cultures under hyperoxia, no difference was observed in the number of non-neuronal cells with nuclear or translocated HMGB1 in the myenteric ganglia after treatment with H_2O_2 (**Figure 6.2H-H′, Table 6.1**). All together these data demonstrate that HMGB1 translocation is regulated by oxidative stress in myenteric neurons and highlights the relationship between HMGB1 and neuronal loss under oxidative conditions.

6.6.2. BM-MSC treatments attenuate translocation of neuronal HMGB1 in chronic inflammation

HMGB1 expression was associated with oxidative stress-induced myenteric neuronal loss *in vitro*. Previously, it was determined that *Winnie* mice with spontaneous chronic colitis exhibit oxidative stress and neuronal loss which are attenuated by BM-MSC treatments (**Chapter 4, Figure 4.8 & Chapter 5, Figure 5.6**). Therefore, HMGB1 expression was determined in *Winnie* mice treated with BM-MSCs to determine its relationship with myenteric neuronal loss *in vivo* (**Figure 6.3A-C′′′′**). In *Winnie* mice, HMGB1 translocation in myenteric neurons was often observed in clusters, as opposed to sporadically throughout the ganglia (**Figure 6.3B-B′′′′**). The number of neurons expressing HMGB1 in the nucleus was decreased in *Winnie*-sham mice compared to C57BL/6 controls ($P<0.01$) (**Figure 6.3D, Table 6.4**, n=5 animals/group). Loss of nuclear HMGB1 expression appeared to be specific to the neuronal population with no effects observed in non-neuronal cells within the myenteric ganglia in conditions of chronic inflammation (**Figure 6.3D, Table 6.4**).

Figure 6.2 ***Effects of hydrogen peroxide on HMGB1 expression in myenteric neurons after organotypic culture***

A-C‴′) HMGB1 expression within the myenteric ganglia in distal colon organotypic cultures. Myenteric neurons observed by immunofluorescence of the neuronal marker MAP-2 **(A-C)**, nuclear stain with DAPI **(A′-C′)**, HMGB1 **(A″-C″)**, merged images **(A‴-C‴)** and ratio representations of HMGB1:DAPI **(A⁗-C⁗)** for visual distinction. Tissues were cultured for 24h in standard culture medium **(A)** or medium with 100µM H_2O_2 **(B-C)**. Neurons without nuclear HMGB1 expression denoted by arrows **(B-B‴′)** and neurons with HMGB1 translocation into the cytoplasm denoted by stars **(C-C‴′)** (scale bar = 20µm). **D-D′)** Quantification of neurons with HMGB1 expressed in the nucleus **(D)** and translocated to the cytoplasm **(D′)** presented as neurons per ganglionated area. **E)** Linear correlation between neuronal density and neurons with translocation of HMGB1 per area. **F-F″)** Percentage of neurons with HMGB1 expressed in the nucleus **(F)**, absent in the nucleus **(F′)** and translocated to the cytoplasm **(F″)**. **E)** Linear correlation between neuronal density and the percentage of neurons with HMGB1translocation. **H-H′)** Quantification of non-neuronal cells with HMGB1 expressed in the nucleus **(H)** and translocated to the cytoplasm **(H′)** presented as cells per ganglionated area. $*P<0.05$, $***P<0.001$; control: n=8 independent samples, H_2O_2: n=9 independent samples.

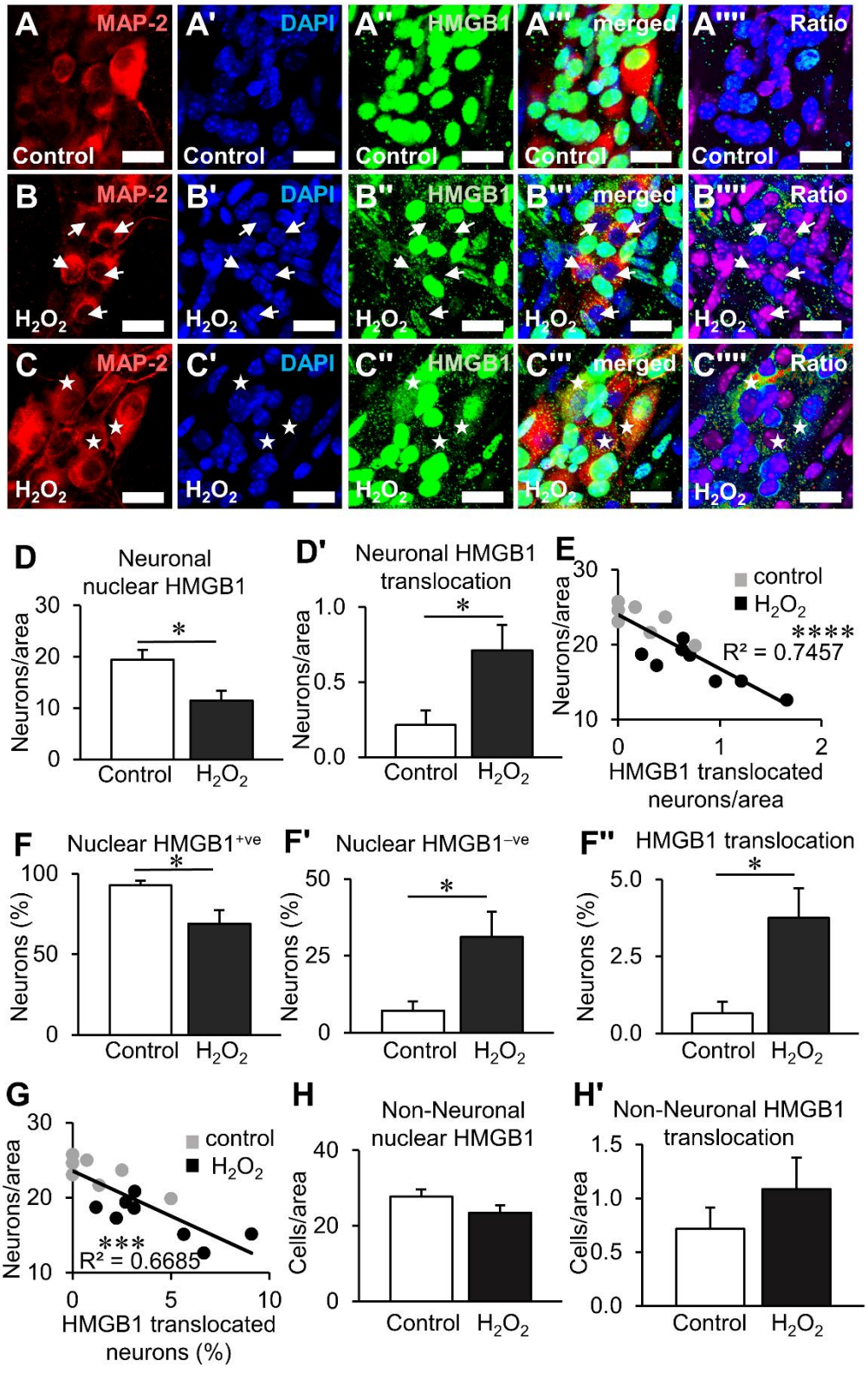
A MAP-2
A' DAPI
A'' HMGB1
A''' merged
A'''' Ratio
Control
B MAP-2
B' DAPI
B'' HMGB1
B''' merged
B'''' Ratio
H2O2
C MAP-2
C' DAPI
C'' HMGB1
C''' merged
C'''' Ratio
H2O2
D Neuronal nuclear HMGB1
Neurons/area
Control
H2O2
D' Neuronal HMGB1 translocation
Neurons/area
Control
H2O2
E
control
H2O2
****
R² = 0.7457
Neurons/area
HMGB1 translocated neurons/area
F Nuclear HMGB1+ve
Neurons (%)
Control
H2O2
F' Nuclear HMGB1−ve
Neurons (%)
Control
H2O2
F'' HMGB1 translocation
Neurons (%)
Control
H2O2
G
control
H2O2
***
R² = 0.6685
Neurons/area
HMGB1 translocated neurons (%)
H Non-Neuronal nuclear HMGB1
Cells/area
Control
H2O2
H' Non-Neuronal HMGB1 translocation
Cells/area
Control
H2O2

Table 6.3 ***Correlation between HMGB1 counts and neuronal density in H_2O_2-treated organotypic cultures***

HMGB1 expression	R^2	Relationship to neuronal density	*P* value
HMGB1^{+ve} cells/area			
neurons	0.6546	Increase	**0.0003**
non-neuronal	0.1768	-	0.1187
HMGB1^{-ve} cells/area			
neurons	0.5551	Decrease	**0.0022**
HMGB1-translocated cells/area			
neurons	0.7457	Decrease	**<0.0001**
non-neuronal	0.054	-	0.424
Neurons %			
HMGB1^{-ve}	0.5029	Decrease	**0.0045**
HMGB1-translocated	0.6684	Decrease	**0.0002**

H_2O_2, hydrogen peroxide, HMGB1 - High mobility group box-1, HMGB1^{+ve} – HMGB1 expressed in the nucleus, HMGB1^{-ve} – HMGB1 absent from the nucleus. Control: n=8 independent samples, H_2O_2: n=9 independent samples.

The total number of cells expressing HMGB1 in the nucleus was increased in BM-MSC treated *Winnie* mice compared to *Winnie*-sham ($P<0.05$) (**Figure 6.3D, Table 6.4**, n=5 animals/group). This was driven by an increase in nuclear HMGB1 expression in the neuronal population ($P<0.01$) after MSC treatment which returned to near control levels (**Figure 6.3D, Table 6.4**). Similarly, BM-MSC treatments had no effect on nuclear HMGB1 expression in the non-neuronal population within the myenteric plexus of *Winnie* mice (**Figure 6.3D, Table 6.4**). Nevertheless, these results were potentially affected by alterations in the neuronal density as previously reported in *Winnie* mice (**Chapter 4, Figure 4.8**). To account for this, the expression patterns of HMGB1 was further investigated as a percentage of neurons within each sample (**Figure 6.3E-H, Tables 6.4 & 6.5**). The percentage of neurons without nuclear expression of HMGB1 was increased in sham-treated *Winnie* mice compared to C57BL/6 mice ($P<0.01$) (**Figure 6.3E, Table 6.4**, n=5 animals/group). BM-MSC treatments reduced the percentage of neurons without nuclear HMGB1 in *Winnie* mice ($P<0.01$) (**Figure 6.3E, Table 6.4**, n=5 animals/group). The effect of nuclear HMGB1 expression on neuronal density was explored by linear regression analysis (**Table 6.5**). A negative correlation was observed between the proportion of neurons without nuclear HMGB1 and the neuronal density of the myenteric ganglia *in vivo* ($F(1,13) = 14.07$, $P<0.01$) (**Figure 6.3F, Table 6.5**). Similar to these results, the percentage of neurons with HMGB1 translocation into the cytoplasm was increased in *Winnie*-sham mice compared to C57BL/6 mice ($P<0.05$) (**Figure 6.3G, Table 6.4**, n=5 animals/group). BM-MSC treatments attenuated these changes in *Winnie* mice ($P<0.05$) (**Figure 6.3G, Table 6.4**, n=5 animals/group). The percentage of neurons with cytoplasmic HMGB1 expression negatively correlated with neuronal density ($F(1,13) = 9.437$, $P<0.01$) (**Figure 6.3H, Table 6.5**). A similar negative correlation was also observed between neuronal density and an increase in the total number of neurons, without nuclear HMGB1 expression ($F(1,13) = 13.43$, $P<0.01$), or those with cytoplasmic HMGB1 expression ($F(1,13) = 9.421$, $P<0.01$). Notably, neuronal density did not correlate with HMGB1 expression patterns in non-neuronal cells ($F(1,13) = 0.06467$, $P=0.8$) (**Table 6.5**).

Figure 6.3 ***Effects of BM-MSC treatments on neuronal HMGB1 expression in wholemount LMMP preparations from the distal colon of Winnie mice***

A-C′′′′) HMGB1 in neurons within the myenteric ganglia were observed by immunofluorescence of the neuronal marker MAP-2 **A-C)** and the nuclear stain DAPI **(A′-C′)**, HMGB1 **(A′′-C′′)**, merged images **(A′′′-C′′′)** and merged magnified images **(A′′′′-C′′′′)** in fresh fixed LMMP wholemount preparations from the distal colon of C57BL/6 mice **(A-A′′′′)**, sham-treated *Winnie* mice **(B-B′′′′)** and *Winnie* mice treated with BM-MSCs **(C-C′′′′)** (scale bar = 50µm). **D)** Quantification of the total number of cells, neurons and non-neuronal cells with nuclear HMGB1 in the myenteric plexus expressed as cells per ganglionated area. **E)** Percentage of neurons without HMGB1 in the nucleus. **F)** Linear correlation between neuronal density and the percentage of neurons without nuclear HMGB1 expression. **G)** Percentage of neurons with HMGB1 translocated to the cytoplasm. **H)** Linear correlation between neuronal density and the percentage of neurons with cytoplasmic HMGB1 translocation. **P*<0.05, ***P*<0.01; C57BL/6: n=5 animals, *Winnie*-sham: n=8 animals, *Winnie*+MSC: n=5 animals.

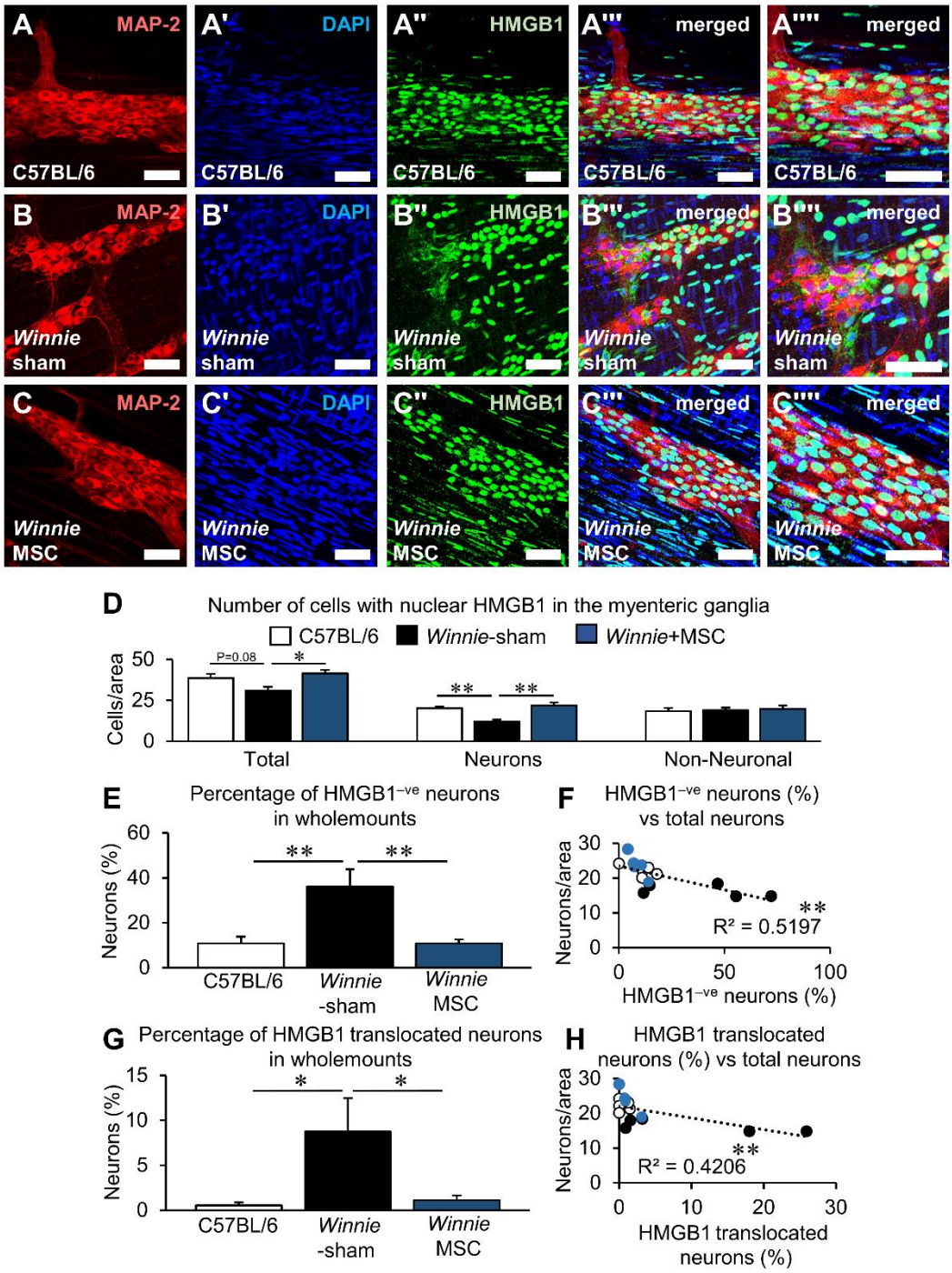
A MAP-2
C57BL/6
A' DAPI
C57BL/6
A'' HMGB1
C57BL/6
A''' merged
C57BL/6
A'''' merged
C57BL/6
B MAP-2
Winnie sham
B' DAPI
Winnie sham
B'' HMGB1
Winnie sham
B''' merged
Winnie sham
B'''' merged
Winnie sham
C MAP-2
Winnie MSC
C' DAPI
Winnie MSC
C'' HMGB1
Winnie MSC
C''' merged
Winnie MSC
C'''' merged
Winnie MSC
D
Number of cells with nuclear HMGB1 in the myenteric ganglia
C57BL/6
Winnie-sham
Winnie+MSC
Cells/area
P=0.08
*
**
**
Total
Neurons
Non-Neuronal
E
Percentage of HMGB1−ve neurons in wholemounts
Neurons (%)
**
**
C57BL/6
Winnie -sham
Winnie MSC
F
HMGB1−ve neurons (%) vs total neurons
Neurons/area
R² = 0.5197
**
HMGB1−ve neurons (%)
G
Percentage of HMGB1 translocated neurons in wholemounts
Neurons (%)
*
*
C57BL/6
Winnie -sham
Winnie MSC
H
HMGB1 translocated neurons (%) vs total neurons
Neurons/area
R² = 0.4206
**
HMGB1 translocated neurons (%)

Table 6.4 ***HMGB1 counts in the myenteric ganglia of Winnie mice***

HMGB1 expression	C57BL/6	*Winnie*-Sham	*Winnie* BM-MSC
HMGB1^{+ve} cells/area			
total	38.5±2.6	31.0±2.3	41.5±2.1†
neurons	20.1±1.1**	12.0±1.2	21.8±1.9††
non-neuronal	18.4±1.8	19.0±1.6	19.7±2.1
HMGB1^{-ve} cells/area			
neurons	2.3±0.6**	7.7±1.3	2.0±0.3††
HMGB1-translocated cells/area			
total	1.1±0.8	5.5±2.1	0.9±0.3
neurons	0.12±0.1*	2.66±0.1	0.24±0.1†
non-neuronal	1.0±0.9	2.8±1.4	0.6±0.2
Neurons %			
HMGB1^{-ve}	10.8±3**	37.1±7.8	8.7±1.7††
HMGB1-translocated	0.5±0.3*	13.5±4.9	1.1±0.5†

BM – bone marrow, MSC – mesenchymal stem cell, HMGB1 - High mobility group box-1, HMGB1^{+ve} – HMGB1 expressed in the nucleus, HMGB1^{-ve} – HMGB1 absent from the nucleus. *P<0.05, **P<0.01 significantly different to C57BL/6. †P<0.05, ††P<0.01 significantly different to *Winnie*-sham; n=5 animals/group.

Table 6.5 ***Correlations between HMGB1 counts and neuronal density in Winnie mice***

HMGB1 expression	R^2	Relationship to neuronal density	*P* value
HMGB1^{+ve} cells/area			
neurons	0.8783	Increase	**<0.0001**
non-neuronal	0.00495	-	0.8032
HMGB1^{-ve} cells/area			
neurons	0.5081	Decrease	**0.0029**
HMGB1-translocated cells/area			
neurons	0.4202	Decrease	**0.009**
non-neuronal	0.07052	-	0.3388
Neurons %			
HMGB1^{-ve}	0.5197	Decrease	**0.0024**
HMGB1-translocated	0.4206	Decrease	**0.0089**

HMGB1 - High mobility group box-1, HMGB1^{+ve} – HMGB1 expressed in the nucleus, HMGB1^{-ve} – HMGB1 absent from the nucleus. C57BL/6, *Winnie*-sham, *Winnie*+MSC n=5 animals/group.

These results were replicated in cross sections of the distal colon from a separate group of mice. An increased percentage of neurons did not express nuclear HMGB1 in the myenteric ganglia of *Winnie*-sham mice (40.5±4.8%) compared to C57BL/6 controls (15.1±2.5%. $P<0.01$) (**Figure 6.4A-D**; n=5 animals/group). This was attenuated by BM-MSC treatments in *Winnie* mice (23.5±3.3%, $P<0.05$) (**Figure 6.4A-D**; n=5 animals/group). A negative correlation was observed between the proportion of neurons without nuclear HMGB1 and neuronal density ($F(1,12) = 16.75$, $P<0.01$) with an R^2 of 0.5826 (**Figure 6.4E**). Together, these data reflect the notion that the absence of nuclear HMGB1 and cytoplasmic translocation are indicative of a necrotic-like mechanism of cell death (Janko et al., 2014).

6.6.3. BM-MSC treatments correct dysregulation of cell death-associated genes in chronic colitis

The loss of nuclear HMGB1 expression in myenteric neurons suggests that these cells were undergoing a necrotic or necroptotic process of cell death in stimulated *in vitro* cultures and in chronic colitis *in vivo* (Janko et al., 2014). To further explore this concept, the expression of cell-death associated genes was determined in *Winnie* mice treated with BM-MSCs compared to *Winnie*-sham mice, as well as, *Winnie*-sham compared to C57BL/6 mice or IBD patients compared to their uninflamed controls (**Figure 6.5, Table 6.6**). A list of genes associated with cell death was compiled using the GO database. The top genes upregulated by BM-MSCs in *Winnie* mice included multiple pro-survival genes. This included: anti-apoptotic genes, *Capn6, Nme5* and *Gcg* (Rho et al., 2008, Vogler, 2012); *Tnfrsf17*, survival of B-cells (O'Connor et al., 2004); and *Tbc1d24*, prevents oxidative stress-induced cell death in neurons (Finelli et al., 2016). Conversely, *Cidec* and *Dlc1* were upregulated which promote apoptosis (Zhou et al., 2004, He et al., 2018). The gene *Jph3* was also upregulated by BM-MSC treatments which has links to necrosis (Hitomi et al., 2008), however this gene is also a likely nervous system marker; thus it may be increased by improvement to neuronal architecture as previously observed (**Chapter 4, Figure 4.8**).

Figure 6.4 ***Effects of BM-MSC treatments on neuronal HMGB1 expression in cross sections of the distal colon from Winnie mice***

A-C‴) HMGB1 in neurons within the myenteric ganglia were observed by immunofluorescence of the neuronal marker MAP-2 **(A-C)**, the nuclear stain DAPI **(A′-C′)**, HMGB1 **(A″-C″)** and merged images **(A‴-C‴)** in cross sections from the distal colon of C57BL/6 mice **(A-A‴)**, sham-treated *Winnie* mice **(B-B‴)** and *Winnie* mice treated with BM-MSCs **(C-C‴)** (scale bar = 50µm). **D)** Percentage of myenteric neurons without nuclear HMGB1 expression. **E**) Linear correlation between neuronal counts and the percentage of neurons without nuclear HMGB1 expression. **P*<0.05, ***P*<0.01; n=5 animals/group.

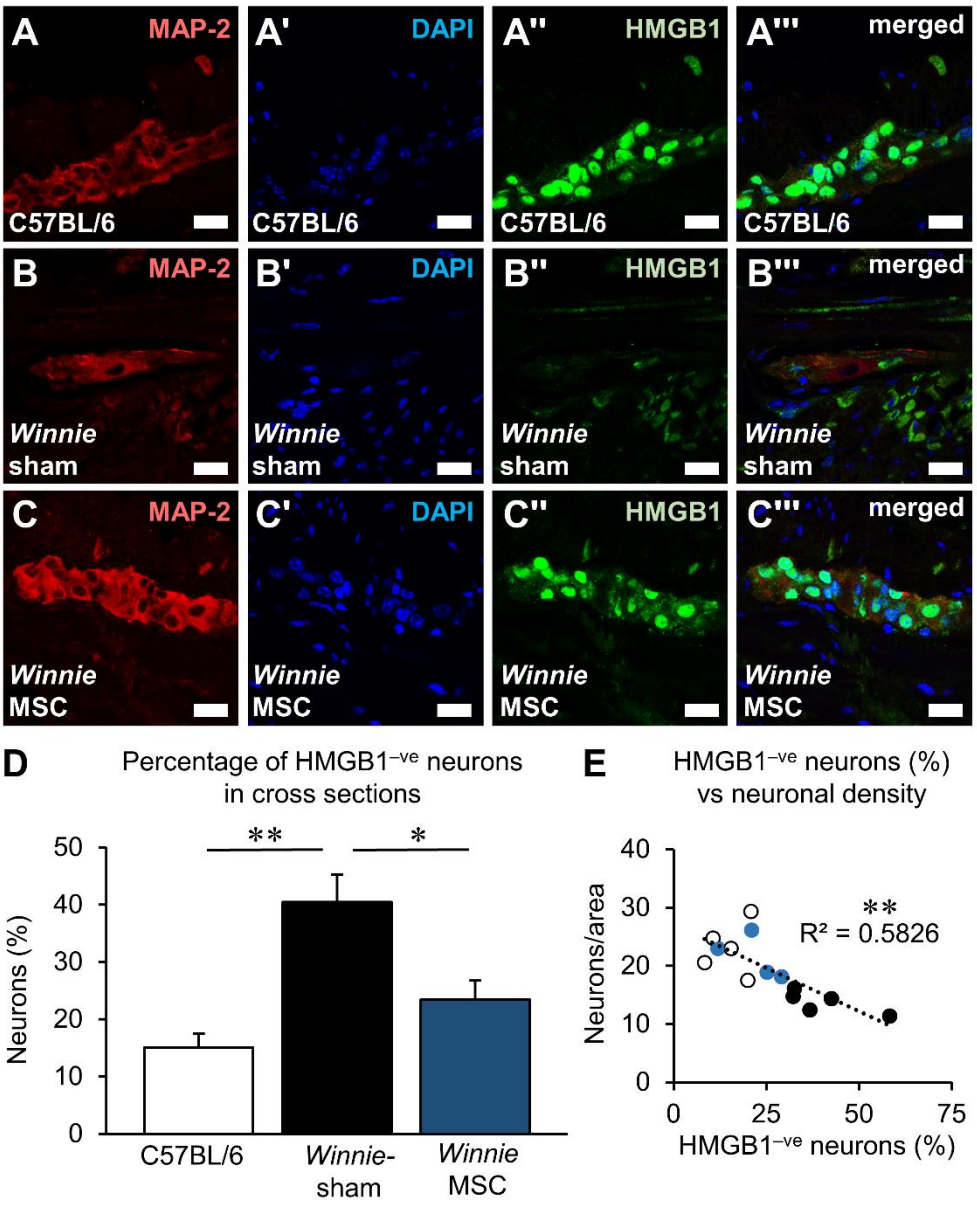
A
MAP-2
C57BL/6
A'
DAPI
C57BL/6
A''
HMGB1
C57BL/6
A'''
merged
C57BL/6
B
MAP-2
Winnie
sham
B'
DAPI
Winnie
sham
B''
HMGB1
Winnie
sham
B'''
merged
Winnie
sham
C
MAP-2
Winnie
MSC
C'
DAPI
Winnie
MSC
C''
HMGB1
Winnie
MSC
C'''
merged
Winnie
MSC
D
Percentage of HMGB1−ve neurons
in cross sections
**
*
Neurons (%)
50
40
30
20
10
0
C57BL/6
Winnie-
sham
Winnie
MSC
E
HMGB1−ve neurons (%)
vs neuronal density
Neurons/area
40
30
20
10
0
**
R² = 0.5826
0
25
50
75
HMGB1−ve neurons (%)

The endoplasmic reticulum (ER) stress response gene, *Ern2*, was also upregulated in BM-MSC treated *Winnie* mice compared to *Winnie*-sham. This gene was also upregulated in IBD patients compared to uninflamed controls (Wang et al., 1998).

The expression of genes associated with the promotion of cell death were observed in the top genes downregulated in *Winnie* mice treated with BM-MSCs compared to *Winnie*-sham. This included: necrosis associated genes, *Mag* and *S100a7a* (Hitomi et al., 2008); the weak apoptotic gene, *Bcl2l15* which is highly expressed in the colon (Coultas et al., 2003); *Tnf*, increased levels in IBD and regulates various cell death pathways (Sedger and McDermott, 2014); *Trp63* and *Trp73*, apoptotic or non-canonical cell death (Flores et al., 2002, Ranjan and Iwakuma, 2016); *Defb1*, associated with necrosis and apoptosis (Bullard et al., 2008, Bose et al., 2009); and *Reg3b*, associated with oxidative stress-induced cell death (Lim et al., 2009). In addition, the inhibitor of cell death *Tnfrsf11b* was downregulated in *Winnie* mice treated with BM-MSC compared to *Winnie*-sham. *Tnfrsf11b* is was upregulated in IBD patients and is a cell death ligand decoy against tumour necrosis factor (TNF)-related apoptosis-inducing ligand (TRAIL) (Emery et al., 1998, Lee et al., 2017).

BM-MSC treatments downregulated several genes compared to *Winnie*-sham mice that were upregulated in *Winnie* mice and IBD patients compared to their uninflamed controls. This included the TNF receptor super family genes *Tnfrsf4* and *Tnfrsf1b* which promote the survival of T lymphocytes and regulate receptor-interacting protein (RIP) kinase dependent cell death, respectively (MacEwan, 2002). Likewise, oxidative stress-associated genes were upregulated including: *Hk3*, regulation of mitochondrial biogenesis (Wyatt et al., 2010); *Slc7a11*, associated with neuronal death (Conrad and Sato, 2012); and *Bnip3*, non-canonical cell death be opening the mitochondrial permeability transition pore (mPTP) (Gustafsson, 2011, Graham et al., 2015).

Figure 6.5 ***Changes in the expression of genes associated with cellular death***

Heat map of the fold regulation of genes identified by RNA-Seq that selectively represent cell death pathways. Fold regulation was determined between *Winnie* and C57BL/6 mice, *Winnie* mice treated with BM-MSCs and sham-treated *Winnie* mice, males and female patients with ulcerative colitis, as well as, male and female patients with Crohn's disease compared to the colon of uninflamed sex-matched controls (left to right columns). Upregulated genes and downregulated genes were visualised as red and green gradients between >5 and <-5 folds, respectively. Genes failing the initial cut off between ±0.5logFC are represented as black (no change).

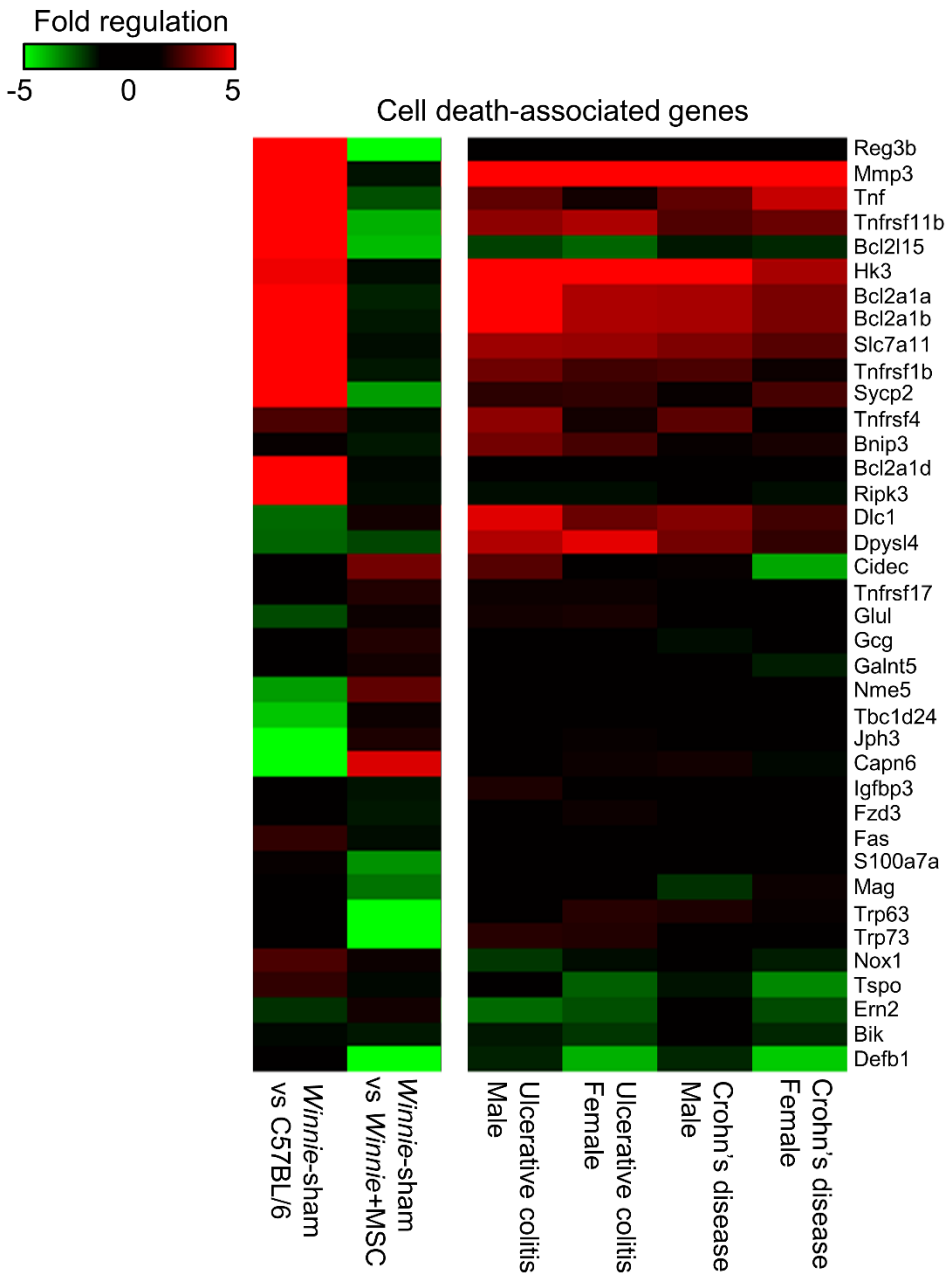
Fold regulation
-5
0
5
Cell death-associated genes
Reg3b
Mmp3
Tnf
Tnfrsf11b
Bcl2l15
Hk3
Bcl2a1a
Bcl2a1b
Slc7a11
Tnfrsf1b
Sycp2
Tnfrsf4
Bnip3
Bcl2a1d
Ripk3
Dlc1
Dpysl4
Cidec
Tnfrsf17
Glul
Gcg
Galnt5
Nme5
Tbc1d24
Jph3
Capn6
Igfbp3
Fzd3
Fas
S100a7a
Mag
Trp63
Trp73
Nox1
Tspo
Ern2
Bik
Defb1
Winnie-sham vs C57BL/6
Winnie-sham vs Winnie+MSC
Ulcerative colitis Male
Ulcerative colitis Female
Crohn's disease Male
Crohn's disease Female

Table 6.6 ***Fold regulation of cell death-associated genes***

Gene	*Winnie* MSC vs *Winnie*-sham	*Winnie*-sham vs C57BL/6	UC male vs control male	UC female vs control female	CD male vs control male	CD female vs control female
Capn6	4.5	-11.1	-1.1	1.5	1.6	-1.4
Cidec	3.0	-1.1	2.6	-1.1	1.5	-3.7
Nme5	2.7	-3.6	1.1	1.1	-1.1	1.2
Tnfrsf17	1.8	1.3	1.5	1.5	-1.4	-1.0
Gcg	1.8	-1.1	-1.3	-1.3	-1.5	1.1
Jph3	1.8	-5.4	-1.2	1.4	-1.2	1.1
Dlc1	1.6	-2.9	4.5	2.8	3.2	2.3
Ern2	1.6	-2.1	-2.8	-2.5	-1.3	-2.4
Galnt5	1.6	-1.2	-1.2	-1.1	1.4	-1.7
Tbc1d24	1.5	-4.2	1.0	1.0	-1.1	-1.0
Glul	1.5	-2.4	1.6	1.7	1.3	1.3
Nox1	1.5	2.4	-2.1	-1.5	1.1	-1.7
Tspo	-1.4	2.0	-1.3	-2.7	-1.6	-3.3
Bcl2a1d	-1.4	6.3	0.0	0.0	0.0	0.0
Tnfrsf4	-1.5	2.4	3.4	1.6	2.6	-1.1
Ripk3	-1.5	7.1	-1.5	-1.5	-1.2	-1.5
Fas	-1.5	2.0	-1.2	1.3	1.1	-1.2
Hk3	-1.5	4.7	10.8	5.1	5.3	3.7
Slc7a11	-1.6	6.5	3.6	3.5	3.1	2.5
Igfbp3	-1.6	-1.3	1.7	1.2	1.1	1.1
Mmp3	-1.6	5.0	270.6	34.9	49.4	6.7
Fzd3	-1.6	-1.4	1.4	1.5	1.2	1.1
Bcl2a1b	-1.6	5.6	7.5	3.8	3.7	3.0
Bnip3	-1.7	1.4	3.0	2.3	1.4	1.7
Tnfrsf1b	-1.7	5.7	2.9	2.3	2.4	1.5
Bik	-1.7	-1.4	-1.7	-2.1	-1.2	-1.9
Bcl2a1a	-1.8	6.5	7.5	3.8	3.7	3.0
Dpysl4	-2.3	-2.8	3.8	4.6	3.0	2.0
Tnf	-2.5	19.5	2.7	1.6	2.7	4.2
Mag	-3.0	-1.3	1.0	-1.0	-2.1	1.5
S100a7a	-3.5	1.4	0.0	0.0	0.0	0.0
Sycp2	-3.6	5.6	1.9	2.0	1.5	2.4
Tnfrsf11b	-3.9	12.1	3.4	3.8	2.5	2.9
Bcl2l15	-4.0	25.1	-2.3	-2.7	-1.7	-1.9
Defb1	-5.6	1.4	-1.8	-3.9	-1.9	-4.3
Trp63	-6.9	1.1	1.3	1.9	1.7	1.4
Trp73	-7.2	-1.1	1.9	1.8	1.3	1.3
Reg3b	-37.7	2245.1	0.0	0.0	0.0	0.0

UC - Ulcerative colitis, CD – Crohn's disease.

Furthermore, BM-MSC treatments downregulated the antiapoptotic genes *Bcl2a1b*, *Bcl2a1a* and *Bcl2a1d* in *Winnie* mice. The homologue for these genes is upregulated in IBD patients (Vogler, 2012). Notably, BM-MSC treatments downregulated *Rip3* which is a principal regulator of necrotic cell death (Zhang et al., 2009a). Expression of *RIP3* was not increased in IBD patients compared to uninflamed controls, albeit expression of its downstream mediator *MLKL* was (Murphy and Vince, 2015). Together these data demonstrate that cell death signalling is dysregulated in chronic inflammation, an unsurprising event given the suppression of apoptosis by intestinal inflammation and the association of IBD with colorectal cancer (Rhodes and Campbell, 2002). The imbalance of cell death genes appears to suggest that the microenvironment in chronic inflammation may favour non-canonical cell death rather than regulated apoptotic pathways that maintain gut homeostasis.

6.6.4. BM-MSC treatments inhibit neuronal HMGB1 translocation associated with oxidative stress-induced myenteric neuropathy by SOD1

Considering that BM-MSCs were previously demonstrated to reduce oxidative stress in the myenteric neurons of *Winnie* mice, *in vitro* cultures were used to investigate the effect of BM-MSCs on oxidative stress-induced HMGB1 translocation. This was performed by exposing myenteric neurons to hyperoxia or H_2O_2 to induce oxidative stress and co-culturing them with BM-MSCs in semi-permeable transwell inserts (**Figure 6.6A-E‴**). In H_2O_2 treated cultures, application of BM-MSCs reduced the proportion of neurons with HMGB1 translocation into the cytoplasm (0.83±0.37%, n=8 independent cultures) compared H_2O_2 alone (3.83±1.08%, $P<0.05$, n=9 independent cultures) to levels similarly observed in controls (0.64±0.43%, n=7 independent cultures) (**Figure 6.6F**).

Figure 6.6 ***Effects of BM-MSCs on oxidative stress-induced HMGB1 translocation in organotypic cultures of myenteric neurons***

A-E′′′′) HMGB1 translocation in organotypic cultures of myenteric neurons was observed by immunofluorescence of the neuronal marker MAP-2 **(A-E)**, nuclear stain **(A′-E′)**, HMGB1 **(A′′-E′′)**, merged images **(A′′′-E′′′)** and merged magnified images **(A′′′′-E′′′′)**. Tissues were cultured for 24h in standard culture medium in 5% CO_2 and ambient O_2 conditions **(A)** and exposed to either 100µM H_2O_2 **(B)**, 100µM H_2O_2 with $1x10^5$ BM-MSCs **(C)**, hyperoxic (↑O_2) conditions (5% CO_2, 95% O_2) **(D)** or hyperoxia with $1x10^5$ BM-MSCs **(E)** (scale bar = 50µm). **F-G)** Quantification of the percentage of neurons with HMGB1 translocated to the cytoplasm in co-cultures with BM-MSCs treated with 100µM H_2O_2 **(F)** or under hyperoxic conditions **(G)**. **P*<0.05, ***P*<0.01; control: n=7 independent samples, H_2O_2: n=9 independent samples, H_2O_2+MSC: n=8 independent samples, ↑O_2: n=7 independent samples, ↑O_2+MSC: n=5 independent samples.

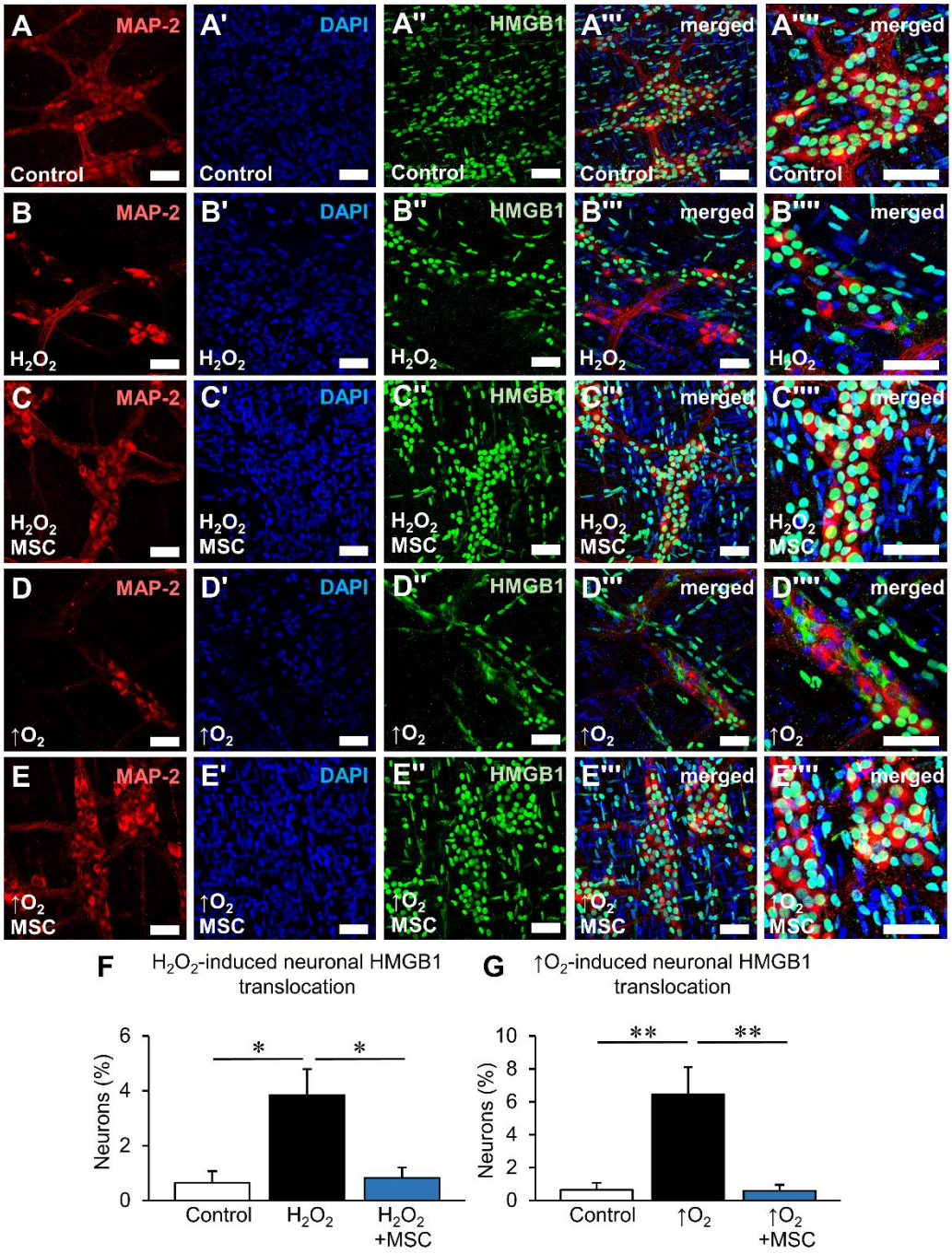
A MAP-2 Control
A' DAPI Control
A'' HMGB1 Control
A''' merged Control
A'''' merged Control
B MAP-2 H2O2
B' DAPI H2O2
B'' HMGB1 H2O2
B''' merged H2O2
B'''' merged H2O2
C MAP-2 H2O2 MSC
C' DAPI H2O2 MSC
C'' HMGB1 H2O2 MSC
C''' merged H2O2 MSC
C'''' merged H2O2 MSC
D MAP-2 ↑O2
D' DAPI ↑O2
D'' HMGB1 ↑O2
D''' merged ↑O2
D'''' merged ↑O2
E MAP-2 ↑O2 MSC
E' DAPI ↑O2 MSC
E'' HMGB1 ↑O2 MSC
E''' merged ↑O2 MSC
E'''' merged ↑O2 MSC
F H2O2-induced neuronal HMGB1 translocation
Neurons (%)
0
2
4
6
*
*
Control
H2O2
H2O2 +MSC
G ↑O2-induced neuronal HMGB1 translocation
Neurons (%)
0
2
4
6
8
10
**
**
Control
↑O2
↑O2 +MSC

Likewise, BM-MSCs inhibited HMGB1 translocation when cultured under hypoxic insult (0.95±0.27%, n=5 independent cultures) compared to cultures without BM-MSCs (6.44±1.7%, $P<0.01$, n=7 independent cultures) (**Figure 6.6G**). These data indicated that BM-MSCs can inhibit neuronal HMGB1 translocation in oxidative conditions. The direct effects of BM-MSCs in protecting myenteric neurons from oxidative insult by H_2O_2 are mediated, at least in part, by SOD1 (**Chapter 5, Figure 5.11**). The expression of HMGB1 in this process was determined by pharmacological inhibition of SOD1 with LCS-1 (**Figure 6.7A-F‴**). Similar levels of HMGB1 translocation were observed in cultures exposed to the DMSO vehicle of LCS-1 compared to naïve cultures. In the presence of DMSO, H_2O_2 increased neuronal HMGB1 translocation (4.2±0.9%, n=9 independent samples) compared to controls (1.2±0.6%, $P<0.01$, n=8 independent samples) which, furthermore, was rescued by the application of BM-MSCs (1.2±0.5%, $P<0.01$, n=9 independent samples) (**Figure 6.7G**). When SOD1 was inhibited in cultures with LCS-1, a similar degree of HMGB1 translocation was induced by H_2O_2 (5.3±0.1%, n=4 independent samples) as vehicle controls compared to cultures with LCS-1 alone (1.4±1.1%, $P<0.05$, n=4 independent samples) (**Figure 6.7G**). No differences in HMGB1 translocation were observed between LCS-1 and vehicle controls, with, or without, exposure to H_2O_2. Inhibition of SOD1 negated the effects of BM-MSCs on H_2O_2-induced HMGB1 translocation (5.7±1.0%, n=6 independent samples); levels were elevated compared to BM-MSC co-cultures exposed to H_2O_2 ($P<0.01$) and the controls, LCS-1 alone ($P<0.05$) and vehicle alone ($P<0.01$) (**Figure 6.7G**). These data further support that BM-MSCs reduce HMGB1 translocation associated with neuropathy and identify the attenuation of oxidative insult as a mechanism of their neuroprotective action. Nonetheless, it remained equivocal whether BM-MSCs attenuated neuronal death by reducing HMGB1 translocation, or contrariwise, HMGB1 was merely a marker of neuronal loss.

Figure 6.7 ***Role of superoxide dismutase [Cu-Zn] (SOD1) in the inhibition of HMGB1 translocation by BM-MSCs in myenteric neurons***

A-F‴) HMGB1 translocation in myenteric neurons was observed by immunofluorescence of the neuronal marker MAP-2 **(A-F)**, nuclear stain DAPI **(A′-F′)**, HMGB1 **(A″-F″)** and merged images **(A‴-F‴)** and merged magnified images **(A⁗-F⁗)**. Tissues were cultured for 24h in standard culture medium **(A)** and exposed to either 100µM H_2O_2 **(B)**, 100µM H_2O_2 with $1x10^5$ BM-MSCs **(C)**, 10µM LCS-1 **(D)**, 100µM H_2O_2 with 10µM LCS-1 **(E)** or 100µM H_2O_2 with 10µM LCS-1 and $1x10^5$ BM-MSCs **(F)** (scale bar = 50µm). DMSO was used as a solvent for LCS-1. Each group contained a total concentration of 0.05% (v/v) DMSO. **G)** Quantification of the percentage of myenteric neurons with cytoplasmic HMGB1 translocation. $*P<0.05$, $**P<0.01$; control: n=8 independent samples, H_2O_2: n=9 independent samples, H_2O_2+MSC n=9 independent samples, LCS-1: n=4 independent samples, H_2O_2+LCS-1: n=4 independent samples, H_2O_2+MSC+LCS-1: n=6 independent samples.

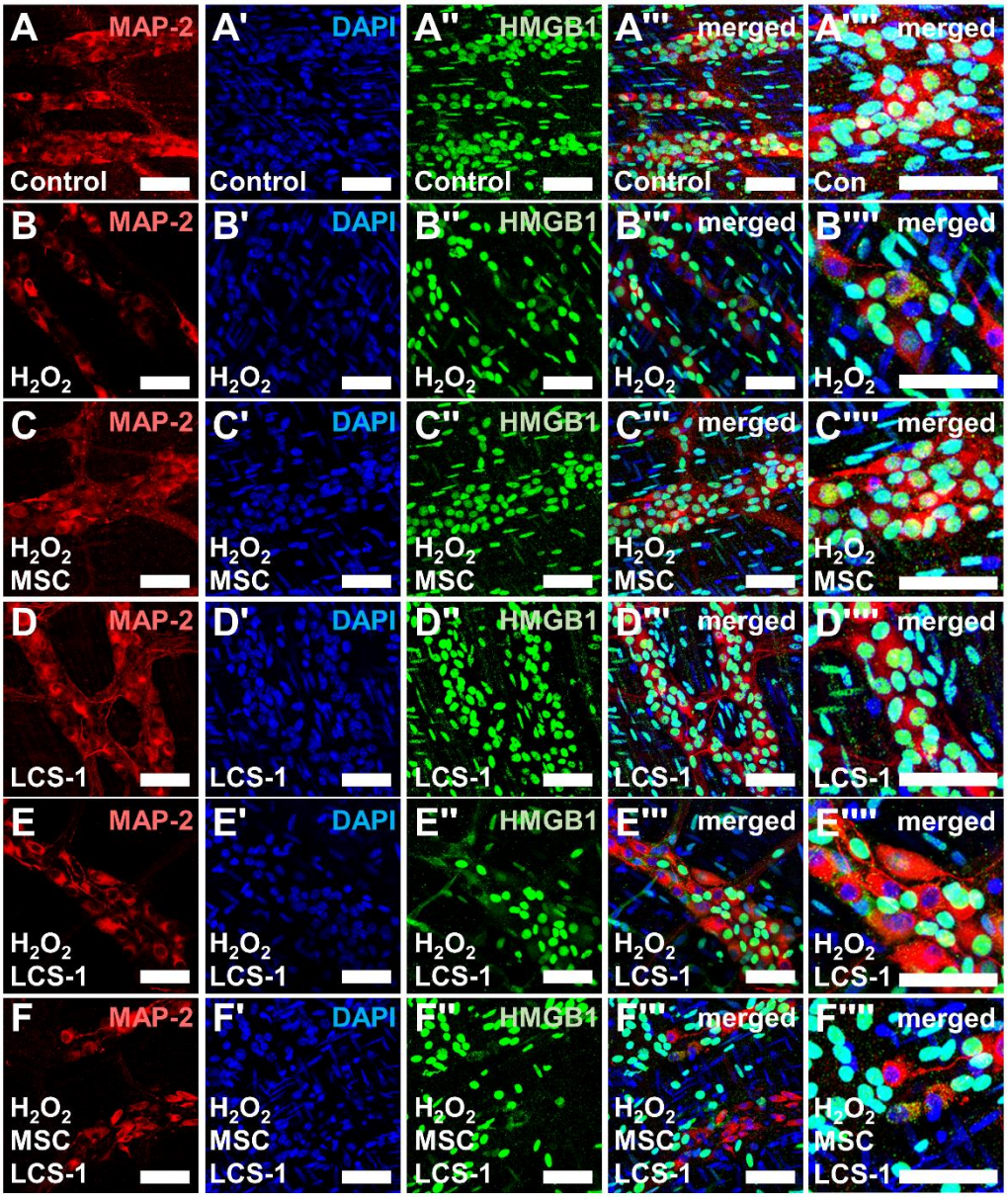
A MAP-2
A' DAPI
A'' HMGB1
A''' merged
A'''' merged
Control
Con
B MAP-2
B' DAPI
B'' HMGB1
B''' merged
B'''' merged
H2O2
C MAP-2
C' DAPI
C'' HMGB1
C''' merged
C'''' merged
H2O2 MSC
D MAP-2
D' DAPI
D'' HMGB1
D''' merged
D'''' merged
LCS-1
E MAP-2
E' DAPI
E'' HMGB1
E''' merged
E'''' merged
H2O2 LCS-1
F MAP-2
F' DAPI
F'' HMGB1
F''' merged
F'''' merged
H2O2 MSC LCS-1

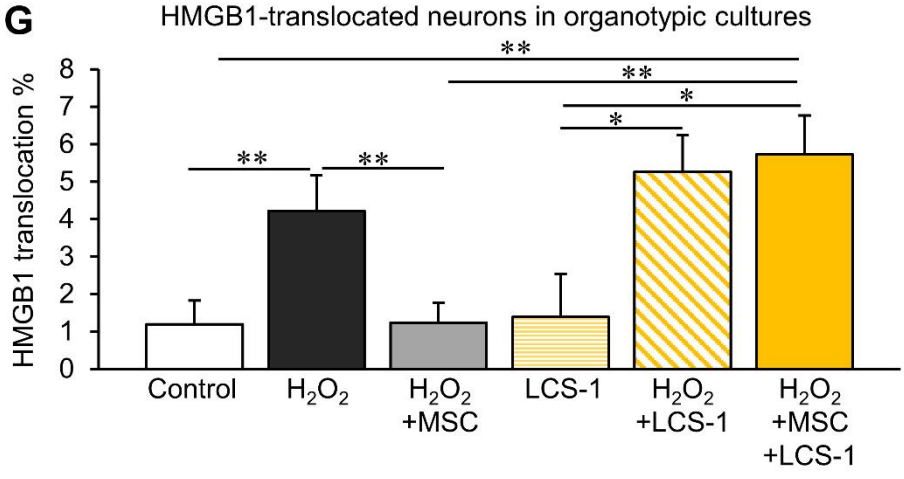
G
HMGB1-translocated neurons in organotypic cultures
HMGB1 translocation %
0
1
2
3
4
5
6
7
8
**
**
**
*
*
Control
H2O2
H2O2 +MSC
LCS-1
H2O2 +LCS-1
H2O2 +MSC +LCS-1

6.6.5. Inhibition of HMGB1 reduces the disease activity and ameliorates stool consistency, but not gross structure of the colon, in chronic colitis

To determine the role of HMGB1 in chronic colitis, *Winnie* mice were treated with the HMGB1 specific inhibitor GA. Body weight loss was observed in GA-treated *Winnie* mice (-3.4±1.1%) compared to C57BL/6 controls which did not lose weight ($P<0.05$) (**Figure 6.8A**; n=6 animals/group). Furthermore, no differences were observed between *Winnie*-sham mice (-1.7±0.4%) and the other groups (**Figure 6.8A**; n=6 animals). Stool consistency was measured by the faecal water content of pellets collected from mice prior to culling. Contrary to colon weight, treatment of *Winnie* mice with GA (66.5±4.0%) reduced the faecal water content of stools compared *Winnie*-sham mice (77.4±2.1%, $P<0.05$) (**Figure 6.8B**; n=6 animals/group). The faecal water content of stools from GA-treated *Winnie* mice remained higher than C57BL/6 control mice (57.3±0.7%, $P<0.05$), but was not as elevated as in sham-treated *Winnie* mice compared to controls ($P<0.001$) (**Figure 6.8B**; n=6 animals/group). Murine colitis is also often evaluated by weight loss (Wirtz et al., 2007, Chassaing et al., 2014).

Colons collected from sham-treated and GA-treated *Winnie* mice appeared morphologically distinct from C57BL/6 mice and exhibited signs of tissue thickening (**Figure 6.9A**). Disease activity scores for colitis were evaluated in C57BL/6 and *Winnie* mice treated with sham or GA and consisted of prolapse and bleeding, changes in colon morphology, diarrhoea and weight loss (**Figure 6.9B**). The disease activity index was higher in sham-treated *Winnie* mice (9.0±0.4) compared to C57BL/6 mice (0.1±0.1, $P<0.0001$) (**Figure 6.9B**; n=6 animals/group). Nonetheless, when *Winnie* mice were treated with GA a reduction in DAI (7.3±0.6) was observed compared to *Winnie*-sham ($P<0.01$) (**Figure 6.9B**).

Figure 6.8 ***Effects of glycyrrhizic acid treatments on stool consistency and weight loss in Winnie mice***

A) Body weight loss was expressed as the percentage of weight loss recorded on the day of culling compared the body weight prior to treatment. **B)** Faecal water content determined by comparing the wet weight to the dry weight of faecal pellets after incubation in an oven at 60ºC for 24h. C57BL/6 mice, *Winnie* mice treated with vehicle sham and *Winnie* mice treated with glycyrrhizic acid (GA). *$P<0.05$, ***$P<0.001$; n=6 animals/group.

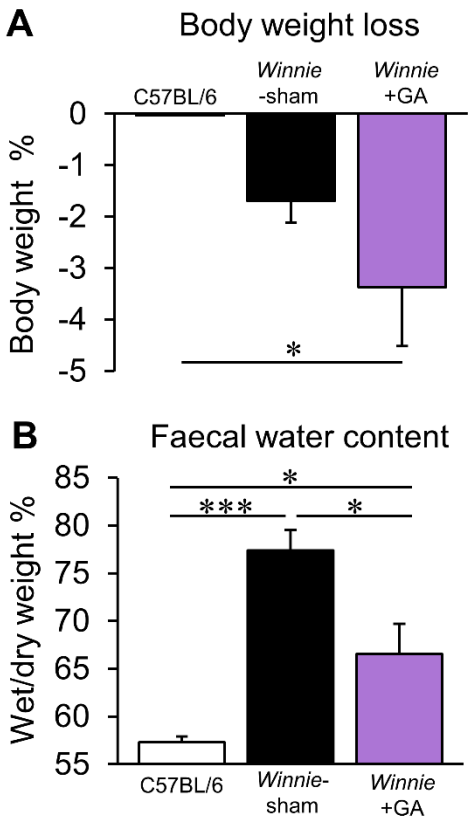
A
Body weight loss
C57BL/6
Winnie -sham
Winnie +GA
Body weight %
0
-1
-2
-3
-4
-5
*
B
Faecal water content
Wet/dry weight %
85
80
75
70
65
60
55
*
***
*
C57BL/6
Winnie-sham
Winnie +GA

Figure 6.9 ***Effects of HMGB1 blocker, glycyrrhizic acid, treatments on colon morphology and the disease activity in Winnie mice***

A) Photographs of the colons obtained from C57BL/6 mice, sham-treated *Winnie* mice and *Winnie* mice treated with glycyrrhizic acid (GA). **B)** Disease activity Index (DAI) of colitis consisting of rectal bleeding, prolapse, colon morphology, diarrhoea and weight loss in C57BL/6 mice, *Winnie* mice treated with vehicle sham and *Winnie* mice treated with glycyrrhizic acid. ***P*<0.01 between *Winnie*-sham and *Winnie*+GA, ††††*P*<0.0001 between C57BL/6 and both *Winnie*-sham and *Winnie*+GA; n=6 animals/group.

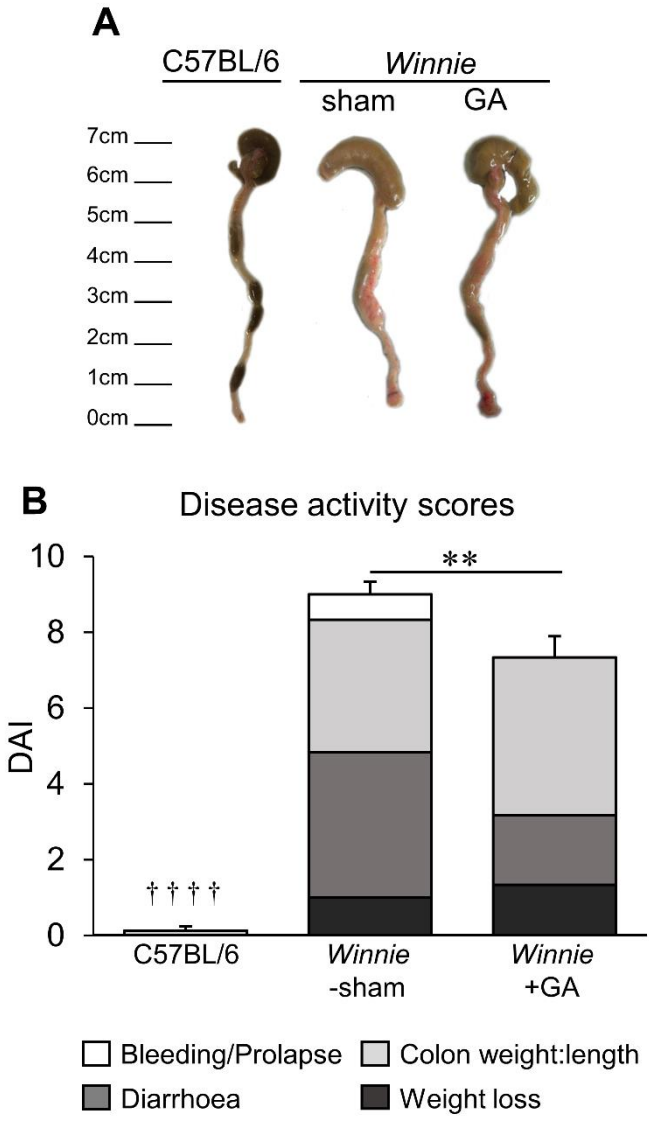
A
C57BL/6
Winnie
sham
GA
7cm
6cm
5cm
4cm
3cm
2cm
1cm
0cm
B
Disease activity scores
DAI
10
8
6
4
2
0
**
††††
C57BL/6
Winnie
-sham
Winnie
+GA
Bleeding/Prolapse
Colon weight:length
Diarrhoea
Weight loss

The length and weight of the colons were evaluated which was previously used as one of the gross morphological indications of colitis (**Chapter 3, Figure 3.2**). The colon weight was increased in both sham (1.78±0.13g) and GA-treated *Winnie* mice (2.11±0.14g) compared to C57BL/6 (0.74±0.03g, $P<0.0001$ for both) controls (**Figure 6.10A**: n=6 animals/group). No differences were observed in between *Winnie*-sham and GA-treated *Winnie* mice. In *Winnie* mice, no differences were observed in colon length compared to C57BL/6 mice (93.1±6.6mm) for sham-treated (95.8±3.7mm) or GA-treated *Winnie* mice (103.7±2.7mm) (**Figure 6.10B**; n=6 animals/group). No difference was observed between the colon weight:length ratios between sham (0.019±0.001) and GA-treated *Winnie* mice (0.020±0.001), which were both higher than C57BL/6 mice (0.008±0.001, $P<0.0001$ for both) (**Figure 6.10C**; n=6 animals/group). Within the disease activity index, only of stool consistency was improved by inhibition of HMGB1 in chronic inflammation. Given the regulatory role of myenteric neurons in this process the effects of HMGB1 inhibition on myenteric neurons were further investigated (Willard et al., 1988, Jodal et al., 1993, Törnblom et al., 2002).

6.6.6. Glycyrrhizic acid inhibits HMGB1-translocation in myenteric neurons and rescues myenteric neurons

The effects of HMGB1 inhibition on myenteric neurons was investigated in wholemount LMMP preparations of the distal colon using the neuronal marker MAP2 (**Figure 6.11A-C**). Enumeration of the neuronal density within the ganglia revealed neuronal loss in sham-treated *Winnie* mice (17.0±1.0 neurons/area) compared to C57BL/6 (22.5±0.7 neurons/area, $P<0.01$) similar to that previously reported (**Chapter 4, Figure 4.8**) (**Figure 6.11D**; n=6 animals/group). Treatment of *Winnie* mice with GA attenuated the observed loss of neurons (22.7±1.0 neurons/area, $P<0.01$) (**Figure 6.11D**; n=6 animals/group). This suggests that HMGB1 is directly implicated in neuronal loss in chronic colitis. To verify this, the pattern of HMGB1 expression in the myenteric ganglia was determined (**Figure 6.11A-C‴**).

Figure 6.10 ***Effects of glycyrrhizic acid treatments on the size of the colon in Winnie mice***

Alterations in colon size measured by the colon weight (grams) **(A)**, length (mm) of the colon from caecum to rectum **(B)** and the colon weight:length ratio **(C)** in C57BL/6 mice, sham-treated *Winnie* mice and *Winnie* mice treated with glycyrrhizic acid (GA). ****$P<0.0001$ between C57BL/6 and both *Winnie*-sham and *Winnie*+GA: n=6 animals/group.

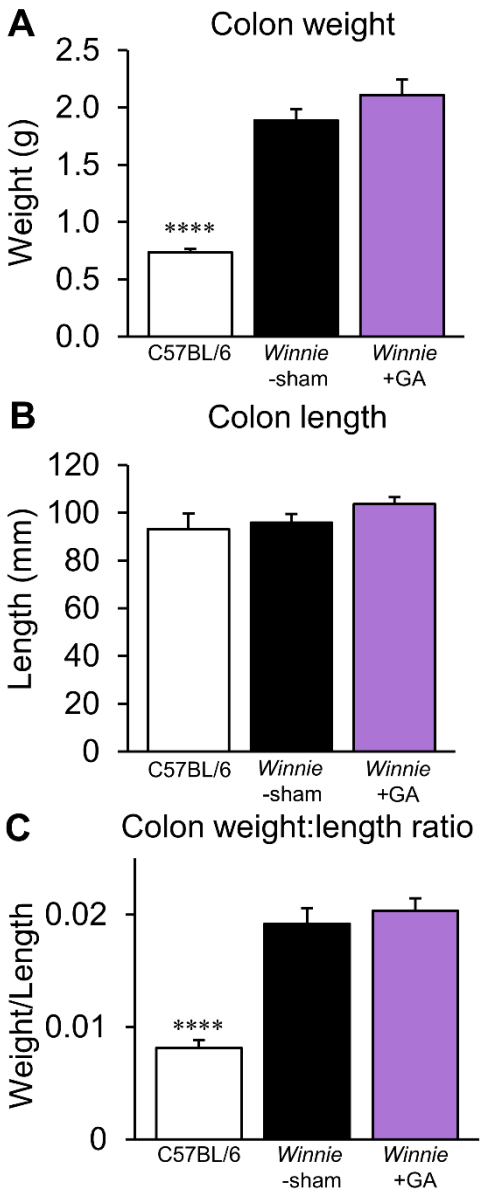
A
Colon weight
Weight (g)
2.5
2.0
1.5
1.0
0.5
0.0
****
C57BL/6
Winnie -sham
Winnie +GA
B
Colon length
Length (mm)
120
100
80
60
40
20
0
C57BL/6
Winnie -sham
Winnie +GA
C
Colon weight:length ratio
Weight/Length
0.02
0.01
0
****
C57BL/6
Winnie -sham
Winnie +GA

Figure 6.11 ***Effects of glycyrrhizic acid treatment on neuronal HMGB1 expression in wholemount LMMP preparations from the distal colon of Winnie mice***

A-C′′′′) HMGB1 in neurons within the myenteric ganglia were observed by immunofluorescence of the neuronal marker MAP-2 **(A-C)**, the nuclear stain DAPI **(A′-C′)**, HMGB1 **(A′′-C′′)** and merged images **(A′′′-C′′′)** and merged magnified images **(A′′′′-C′′′′)** in LMMP wholemount preparations from the distal colon of C57BL/6 mice **(A-A′′′′)**, sham-treated *Winnie* mice **(B-B′′′′)** and *Winnie* mice treated with glycyrrhizic acid (GA) **(C-C′′′′)** (scale bar = 50μm). **D)** Quantification of myenteric neuronal density expressed as the number of neurons per ganglionated area. ***P*<0.01; n=6 animals/group. **E)** The total number of cells, neurons and non-neuronal cells with nuclear HMGB1 within the ganglia expressed as cells per ganglionated area. **F)** Percentage of neurons without HMGB1 in the nucleus. **G)** Percentage of neurons with HMGB1 translocated to the cytoplasm. **P*<0.05, ***P*<0.01, ****P*<0.001; n=5 animals/group.

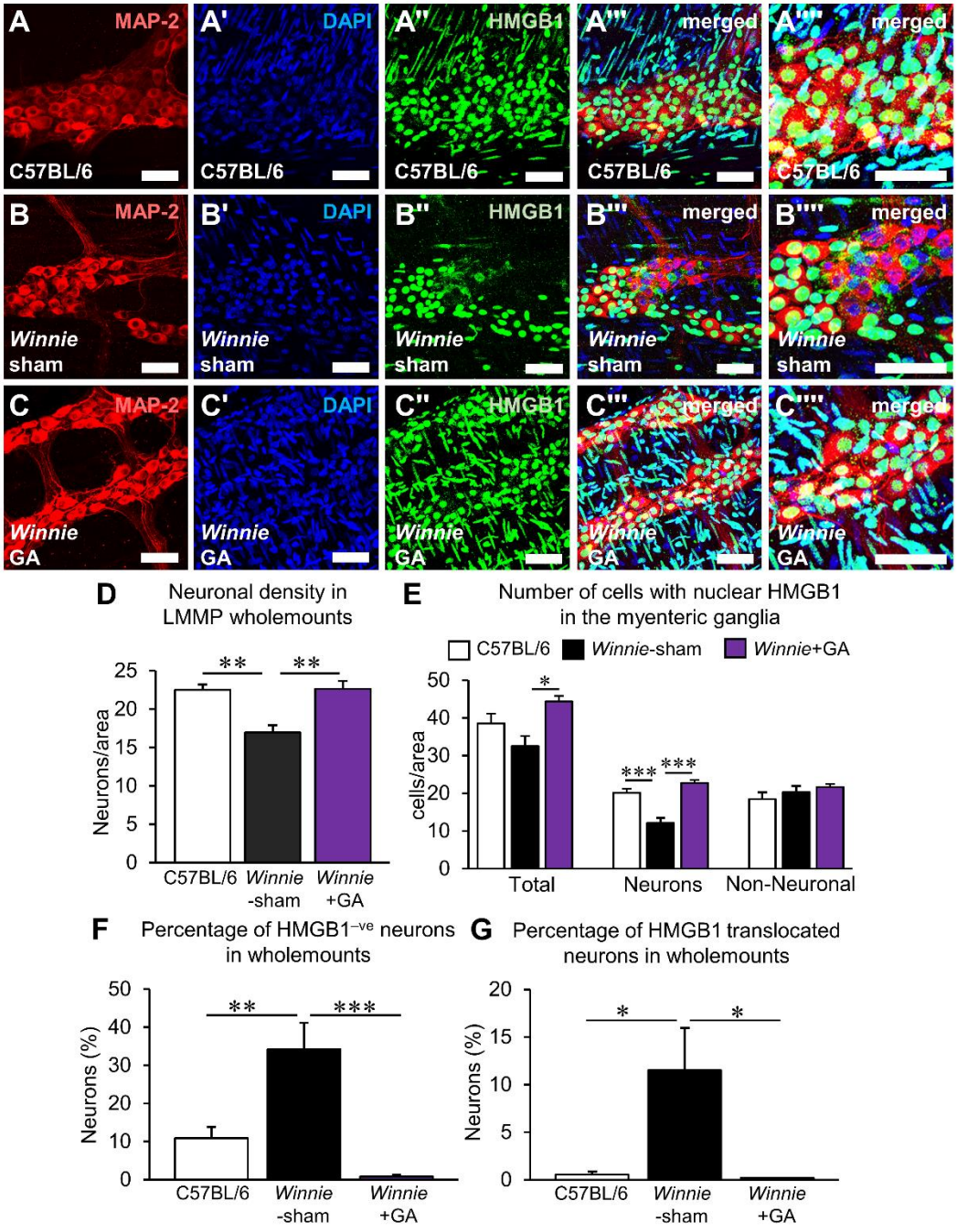
A
MAP-2
C57BL/6
A'
DAPI
C57BL/6
A''
HMGB1
C57BL/6
A'''
merged
C57BL/6
A''''
merged
C57BL/6
B
MAP-2
Winnie sham
B'
DAPI
Winnie sham
B''
HMGB1
Winnie sham
B'''
merged
Winnie sham
B''''
merged
Winnie sham
C
MAP-2
Winnie GA
C'
DAPI
Winnie GA
C''
HMGB1
Winnie GA
C'''
merged
Winnie GA
C''''
merged
Winnie GA
D
Neuronal density in LMMP wholemounts
Neurons/area
25
20
15
10
5
0
**
**
C57BL/6
Winnie -sham
Winnie +GA
E
Number of cells with nuclear HMGB1 in the myenteric ganglia
C57BL/6
Winnie-sham
Winnie+GA
cells/area
50
40
30
20
10
0
*
***
***
Total
Neurons
Non-Neuronal
F
Percentage of HMGB1−ve neurons in wholemounts
Neurons (%)
50
40
30
20
10
0
**
***
C57BL/6
Winnie -sham
Winnie +GA
G
Percentage of HMGB1 translocated neurons in wholemounts
Neurons (%)
20
15
10
5
0
*
*
C57BL/6
Winnie -sham
Winnie +GA

The total number of cells in the myenteric ganglia with nuclear HMGB1 was increased in GA-treated *Winnie* mice (44.4±1.4 cells/area) compared to those treated with sham (32.5±2.7 cells/area, $P<0.05$) (**Figure 6.11E**; n=5 animals/group). No differences were observed compared to control C57BL/6 mice (38.5±2.6 cells/area) and GA-treated *Winnie* mice (**Figure 6.11E**; n=5 animals/group). The increase in cells with nuclear HMGB1 expression in GA-treated *Winnie* mice was correlated with changes in the neuronal population. A reduction in neurons with nuclear HMGB1 was observed in *Winnie*-sham mice (12.2±1.3 neurons/area) compared to C57BL/6 mice (20.1±1.1 neurons/area, $P<0.001$); furthermore, this was attenuated by GA treatments in *Winnie* mice (22.7±0.8 neurons/area, $P<0.001$) (**Figure 6.11E**; n=5 animals/group). No differences were observed between the number of non-neuronal cells expressing nuclear HMGB1 between C57BL/6 mice (18.4±1.8 cells/area) and *Winnie* mice treated with sham (20.3±1.6 cells/area) or GA (21.7±0.8 cells/area) (**Figure 6.11E**; n=5 animals/group). Compared to control C57BL/6 mice, the percentage of neurons without nuclear HMGB1 (10.8±3.0%) was elevated in *Winnie* mice (34.2±7.0%, $P<0.01$). GA treatment greatly reduced the percentage of neurons without nuclear HMGB1 expression in *Winnie* mice to very low levels (0.8±0.5%, $P<0.001$) (**Figure 6.11F**; n=5 animals/group). Likewise, the percentage of neurons with translocation of HMGB1 from the nucleus to the cytoplasm in *Winnie* mice (11.5±4.5%) was elevated compared to control C57BL/6 mice (0.5±0.3%, $P<0.05$); this was ameliorated by GA treatment where virtually no cytoplasmic HMGB1 translocation was observed in neurons ($P<0.05$) (**Figure 6.11G**; n=5 animals/group).

6.6.7. Inhibition of HMGB1 does not attenuate plexitis or elevated neuronal superoxide production

In *Winnie* mice, BM-MSC treatments reduced the number of leukocytes in proximity to the myenteric ganglia and mitochondrial $O_2^{\cdot -}$ levels in myenteric neurons which were associated with their neuroprotective properties (**Chapter 4, Figure 4.10 & Chapter 5, Figure 5.10**).

Figure 6.12 ***Effects of glycyrrhizic acid treatments on leukocyte numbers in proximity to myenteric neurons in the distal colon of Winnie mice***

A-C‴) Leukocytes in proximity to the myenteric ganglia were observed by immunofluorescence of the neuronal marker MAP-2 **(A-C)**, nuclear stain DAPI **(A′-C′)**, the pan-leukocyte marker CD-45 **(A″-C″)** and merged images **(A‴-C‴)** in LMMP wholemount preparations from the distal colon of C57BL/6 mice **(A-A‴)**, sham-treated *Winnie* mice **(B-B‴)** and *Winnie* mice treated with glycyrrhizic acid (GA) **(C-C‴)** (scale bar = 50µm). **D)** Quantification of CD-45 immunoreactive (IR) cells per area. Leukocytes were categorised as residing in the intra-ganglionic region, periphery of the ganglia or extra-ganglionic region. ***P*<0.01, ****P*<0.001, *****P*<0.0001; n=6 animals/group.

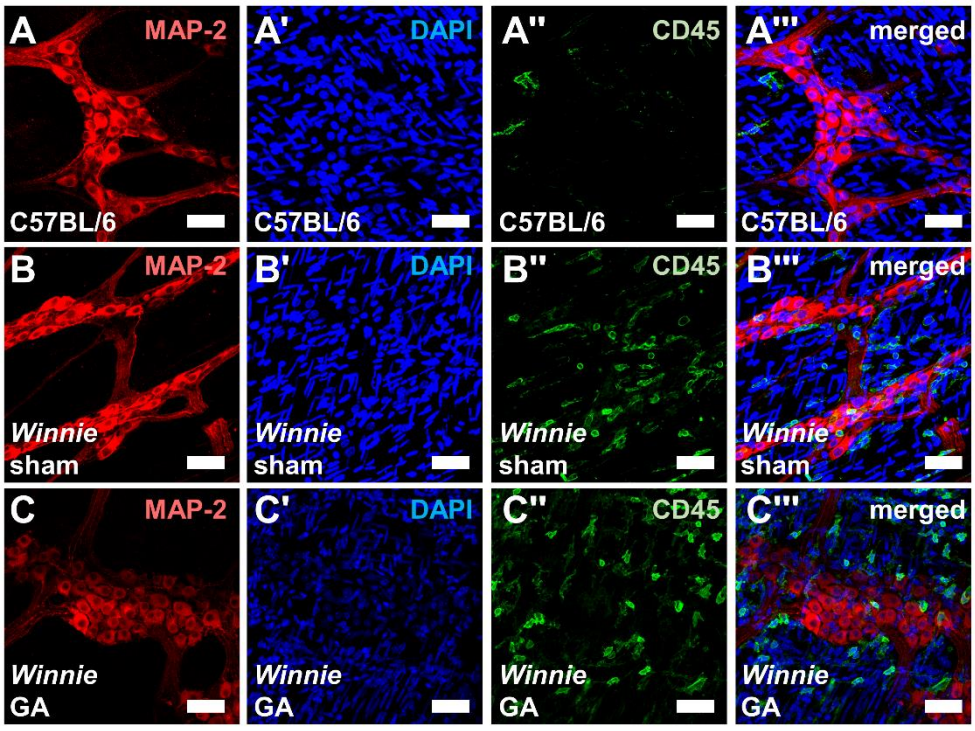
A
MAP-2
C57BL/6
A'
DAPI
C57BL/6
A''
CD45
C57BL/6
A'''
merged
C57BL/6
B
MAP-2
Winnie
sham
B'
DAPI
Winnie
sham
B''
CD45
Winnie
sham
B'''
merged
Winnie
sham
C
MAP-2
Winnie
GA
C'
DAPI
Winnie
GA
C''
CD45
Winnie
GA
C'''
merged
Winnie
GA

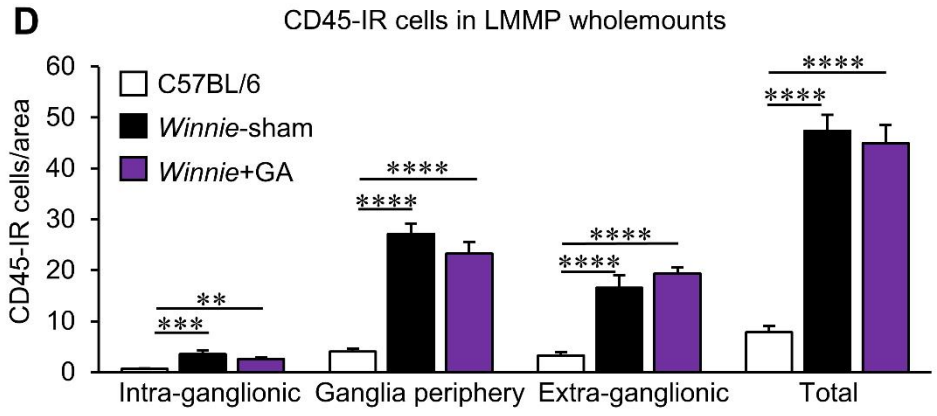
D
CD45-IR cells in LMMP wholemounts
CD45-IR cells/area
60
50
40
30
20
10
0
C57BL/6
Winnie-sham
Winnie+GA
**
***
****
****
****
****
****
****
Intra-ganglionic
Ganglia periphery
Extra-ganglionic
Total

Table 6.7 ***Effects of glycyrrhizic acid treatments on the number of leukocytes in proximity to the myenteric ganglia***

Location	**CD45-IR cells/area**		
	C57BL/6	***Winnie*-Sham**	***Winnie* GA**
In ganglia	0.6±0.2	3.5±0.7***	2.6±0.3**
Edge of the ganglia	4.0±0.6	27.1±2.1****	23.2±2.3****
Outside the ganglia	3.3±0.7	16.6±2.5****	19.3±1.3****
Total	7.8±1.2	47.3±3.2****	44.9±3.6****

GA – glycyrrhizic acid, IR – immunoreactive. ***P*<0.01, ****P*<0.001, *****P*<0.0001 significantly different to C57BL/6; n=6 animals/group.

The effects of HMGB1 inhibition on plexitis and mitochondrial $O_2^{\cdot -}$ production in the myenteric ganglia of *Winnie* mice were evaluated. Leukocytes visualised by CD45 in LMMP wholemount preparations were observed in proximity to the myenteric ganglia using the pan-neuronal marker MAP-2 (**Figure 6.12A-C‴**). Compared to C57BL/6 mice, both *Winnie*-sham and GA-treated *Winnie* mice exhibited higher numbers of leukocytes in the intra-ganglionic region (*Winnie*-sham, $P<0.001$ and *Winnie*+GA, $P<0.01$), periphery of the ganglia ($P<0.0001$, for both), extra-ganglionic region ($P<0.0001$, for both) and in total ($P<0.0001$, for both) (**Figure 6.12D, Table 6.7**; n=6 animas/group). No differences were observed between sham and GA-treated *Winnie* mice (**Figure 6.12D, Table 6.7**; n=6 animas/group). Mitochondrial $O_2^{\cdot -}$ levels were determined by measuring the mean fluorescence intensity of the fluorescent probe, MitoSOX, in fresh LMMP preparations (**Figure 6.13A-C**). Increased $O_2^{\cdot -}$ levels were observed in the myenteric ganglia of sham-treated *Winnie* mice (126.8±22.9 arb. units, n=6 animals) compared to C57BL/6 controls (49.9±2.9 arb. units, $P<0.05$, n=5 animals). No differences were observed for GA-treated *Winnie* mice (80.1±18.8 arb. units, n=6 animals) compared to any other group (**Figure 6.13D**). These results demonstrate that the neuroprotective properties of HMGB1 inhibition were not mediated by attenuation of plexitis or $O_2^{\cdot -}$ production as observed in BM-MSC-treated *Winnie* mice.

6.7. Discussion

This is the first study investigating the effects of chronic inflammation and oxidative stress on HMGB1 expression in the ENS. HMGB1 was constitutively expressed in the nucleus of myenteric neurons. Using organotypic cultures, it was demonstrated that oxidative insult induces the translocation of HMGB1 in myenteric neurons which correlates with neuronal loss. Similarly, a high number of HMGB1 translocation events were observed in the myenteric neurons of *Winnie* mice with chronic inflammation that correlated with the degree of neuronal loss. Notably, high levels of oxidative stress were previously observed in the myenteric ganglia of *Winnie* mice (**Chapter 5, Figure 5.6**).

Figure 6.13 ***Effects of glycyrrhizic acid treatments on mitochondrial superoxide levels in myenteric neurons in the distal colon of Winnie mice***

A-C) Mitochondria-derived superoxide ($O_2^{\cdot -}$) in the myenteric ganglia was visualised by the fluorescent probe MitoSOX in LMMP wholemount preparations from the distal colon of C57BL/6 mice **(A)**, sham-treated *Winnie* mice **(B)** and *Winnie* mice treated with glycyrrhizic acid **(C)** (scale bar = 50µm). All images were taken using the same acquisition settings and are pseudo-coloured (LUT: 'heat', ImageJ) for greater visual distinction in this figure. **D)** The mean fluorescence intensity of the myenteric ganglia in single channel 16-bit images were quantified to determine the intensity of MitoSOX fluorescence. **P*<0.05; C57BL/6: n=5 animals, *Winnie*-sham: n=6 animals, *Winnie*+GA: n=6 animals.

.

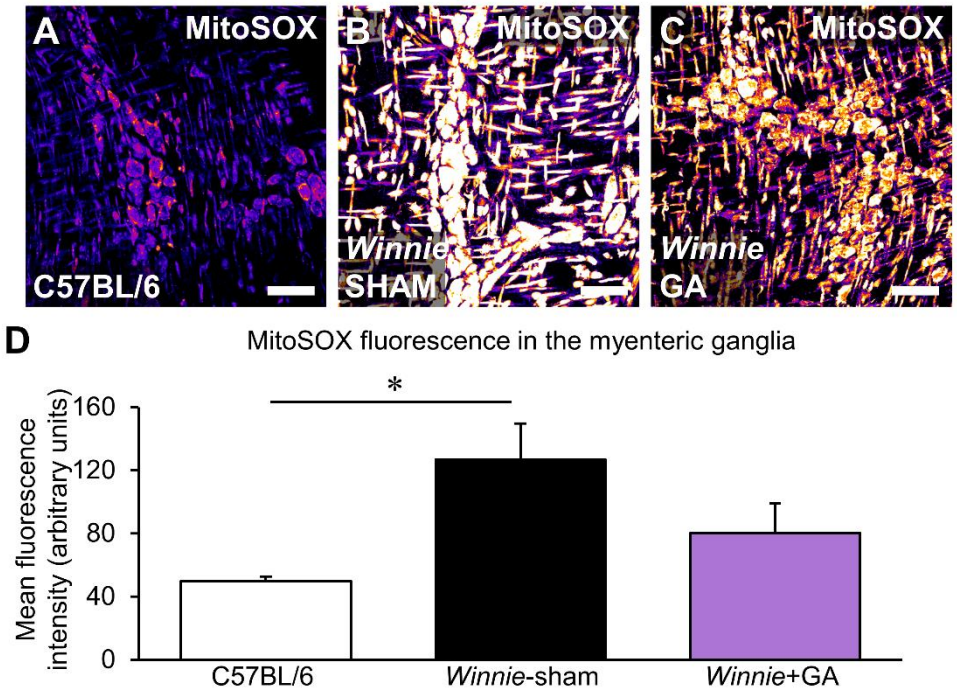
A
MitoSOX
C57BL/6
B
MitoSOX
Winnie
SHAM
C
MitoSOX
Winnie
GA
D
MitoSOX fluorescence in the myenteric ganglia
*
Mean fluorescence intensity (arbitrary units)
160
120
80
40
0
C57BL/6
Winnie-sham
Winnie+GA

In *Winnie* mice and organotypic models of oxidative injury, neurons had a high specificity for HMGB1 translocation in the myenteric ganglia. Treatment with BM-MSCs reduced HMGB1 translocation in myenteric neurons of *Winnie* mice *in vivo*. Furthermore, inhibition of HMGB1 translocation by BM-MSCs was dependent on their antioxidative properties and was mediated by SOD1, as demonstrated in organotypic cultures. Inhibition of HMGB1 by GA in *Winnie* mice completely ameliorated myenteric neuronal loss independently of attenuating $O_{2}^{\cdot -}$ generation and plexitis; thus, implying that these events occur upstream of HMGB1 translocation. Our results suggest that HMGB1 directly mediates myenteric neuronal death in conditions of chronic inflammation and oxidative stress. BM-MSCs appear to attenuate neuronal loss translocation by reducing oxidative stress upstream of HMGB1 translocation.

HMGB1 has important physiological functions in the nucleus of cells, binding DNA and regulating transcription; however, it is also an alarmin to cellular stress that can be released extracellularly eliciting an array of responses depending on the biological context (Andersson et al., 2018). HMGB1 responds to changes in the redox environment and oxidative stress (Janko et al., 2014). These processes are evident in cell death which is closely associated with the pattern of HMGB1 expression (Raucci et al., 2007, Janko et al., 2014, Andersson et al., 2018). In our study, HMGB1 was either absent in the nucleus or translocated into the cytoplasm of myenteric neurons. The cellular compartmentalisation of HMGB1 is redox sensitive and translocation is induced by intracellular ROS (Tang et al., 2011). Hyperacetylation of lysines in the two HMGB1 nuclear localisation sites inhibits HMGB1 entry into the nucleus and results in its accumulation into the cytoplasm (Yiting et al., 2016). This is a feature of necrotic and necroptotic cell death pathways but not apoptosis, where conversely, HMGB1 irreversibly binds to nuclear DNA (Janko et al., 2014, Andersson et al., 2018). Considering the negative association between HMGB1 translocation and neuronal density, myenteric neuronal loss in chronic inflammation and oxidative stress is likely mediated by a necrotic-like pathway of cell death. The strong relationship observed between HMGB1 expression and neuronal density suggests that HMGB1 is a good marker of cell death, or at least myenteric neuropathy in these conditions. However,

HMGB1 has also been demonstrated to contribute directly to the pathophysiological process of cell death in a broad range of cells types including renal cells, hepatocytes and neurons of the CNS (Ohnishi et al., 2011, Gwak et al., 2012, Kim et al., 2012, Lau et al., 2014). Inhibition of HMGB1 by GA dramatically attenuated myenteric neuronal loss which suggests that HMGB1 also had direct role in the mechanism of myenteric neuropathy and did not serve simply as a marker of cell death. GA binds directly to extracellularly released HMGB1 and can inhibit its pro-inflammatory and chemoattractant properties (Mollica et al., 2007). The effect of GA on the intranuclear binding function of HMGB1 is weak, which may explain why inhibition of HMGB1 by this compound has a low chance of causing deleterious effects; GA is already approved for clinical use (Veldt et al., 2006, Mollica et al., 2007). In our study, GA inhibited the translocation of HMGB1 into the cytoplasm. Similarly, studies in the CNS have observed that GA inhibits HMGB1 translocation and secretion under conditions of cellular stress (Gong et al., 2011, Ohnishi et al., 2011, Kim et al., 2012, Okuma et al., 2014). However, it is uncertain whether GA inhibited translocation by binding HMGB1 within the cell or by another mechanism. Considering that GA can weakly effect HMGB1 activity in the nucleus there may be a degree of affinity for GA to bind HMGB1 intracellularly (Mollica et al., 2007). Alternatively, it has been postulated that released HMGB1 can induce HMGB1 translocation and further release in cells that are receptive to extracellular HMGB1 including neurons (Gauley and Pisetsky, 2009, Okuma et al., 2014). In this model, GA could inhibit HMGB1 translocation even if it was only extracellularly active. ROS and oxidative insult are key mediators of HMGB1 translocation and release which can be active or passive (Tang et al., 2007, Tsung et al., 2007). Passive HMGB1 release at high levels is concomitant with necrosis (Lee et al., 2010, Andersson et al., 2018); therefore it is likely that HMGB1 was released from myenteric neurons during cell death in our study. A punctate immunoreactivity of HMGB1 was observed throughout LMMPs in conditions of chronic inflammation or oxidative stress and may reflect this release. Furthermore, myenteric neurons expressing translocated HMGB1 were often observed in clusters, rather than sporadically throughout the ganglia. The proximity of neighbouring myenteric neurons with HMGB1 translocation may support the notion that released HMGB1 induces further translocation. Nevertheless, the mechanism of HMGB1-induced

translocation in myenteric neurons requires further investigation. Myenteric neurons express the major receptors for HMGB1 including the receptor for advanced glycation end-products (RAGE), TLR-2 and TLR-4 (Venereau et al., 2012, Chen et al., 2015, Burgueño et al., 2016). Activation of TLR-4 is known to induce HMGB1 translocation (Gauley and Pisetsky, 2009). Thus, it could be predicted that TLR-4-induced HMGB1 translocation can lead to enteric neuronal death; albeit, HMGB1 can only bind to this receptor in its semi-oxidised state (Janko et al., 2014).

Although HMGB1 is ubiquitously expressed, the CNS has been a focus for the role of HMGB1 in pathophysiological conditions including ischemia, reperfusion, haemorrhage and physical trauma (Gong et al., 2011, Ohnishi et al., 2011, Kim et al., 2012, Okuma et al., 2014). HMGB1 has been observed in the myenteric plexus of the colon and is implicated in damage to the ENS in chemotherapy-induced neurotoxicity (Nurgali et al., 2018, unpublished, Stojanovska et al., 2018). In the nervous system, alterations to HMGB1 expression and its release appear to be specific to neurons (Okuma et al., 2014, Sun et al., 2014). In *in vitro* and *in vivo* models of experimental subarachnoid haemorrhage, HMGB1 translocation was observed primarily in neurons whilst HMGB1 translocation events were rare in the glia (Sun et al., 2014). Similarly, in a model of traumatic brain injury only MAP-2 positive neurons exhibited HMGB1 translocation which was not observed in astrocytes or microglia (Okuma et al., 2014). This suggest that HMGB1 translocation in nervous system pathologies is relatively specific to neurons. In our study, changes in the number of HMGB1 translocation events was increased in neurons and not in other cell types of the myenteric ganglia in conditions of inflammation and oxidative stress. Therefore, like in the CNS, only neuronal HMGB1 appears to be involved in the pathology of damage to the ENS, particularly driving neuronal loss. The exact mechanism of HMGB1-induced neuronal loss in the myenteric plexus is unclear.

HMGB1 has been implicated in many pathologies with concomitant oxidative injury (Gong et al., 2011, Kim et al., 2012, Lau et al., 2014). The translocation and secretion of HMGB1 is regulated by oxidative stress and the redox state, however this relationship may be bilateral as some studies have reported that HMGB1 can promote the generation

of ROS in pathological conditions (Kim et al., 2012). In *Winnie* mice, increased HMGB1 translocation in myenteric neurons paralleled an increase in oxidative stress, as determined by oxidised DNA/RNA adducts, and mitochondria-derived $O_2^{\cdot -}$ production (**Chapter 5, Figures 5.6 & 5.10**). Nevertheless, when HMGB1 translocation was inhibited by GA, high levels of $O_2^{\cdot -}$ were still evident in myenteric neurons. This suggest that HMGB1 did not yield an antioxidative effect in chronic colitis. Additionally, this supports that excessive free radical generation may be upstream of HMGB1 translocation in myenteric neurons. The upstream nature of oxidative stress in this process is also supported by the organotypic models of oxidative insult that promoted HMGB1 translocation in our study. Furthermore, BM-MSCs, which do not act on HMGB1 directly, attenuated its translocation while ameliorating oxidative stress and $O_2^{\cdot -}$ production *in vivo* (**Chapter 5, Figures 5.6 & 5.10**). H_2O_2, which was used as an oxidative stimulus in our cultures, and $O_2^{\cdot -}$, which often parallels H_2O_2 levels, regulate HMGB1 translocation and release (Gauley and Pisetsky, 2009, Aon et al., 2010, Tang et al., 2011). BM-MSCs reduced H_2O_2-induced HMGB1 translocation in *in vitro* cultures in a paracrine manner that was dependent on SOD1, a potent antioxidant via $O_2^{\cdot -}$ scavenging. Therefore, $O_2^{\cdot -}$ and H_2O_2 may have contributed to HMGB1 translocation in myenteric neurons. In support of this, SOD1 and SOD2 can ameliorate HMGB1 release and cellular necrosis in conditions of metabolic stress (Lee et al., 2010). Additionally, SOD mimetics have also demonstrated an ability to reduce HMGB1 secretion and are being considered for use in pathologies associated with aberrant HMGB1 signalling (Janko et al., 2014). Together with these studies, our results suggest that $O_2^{\cdot -}$ production is upstream of HMGB1 translocation in triggering neuronal death; however, HMGB1 translocation appears to still be necessary in this process.

While oxidative stress and the redox status unequivocally have a role in HMGB1 translocation and secretion, the redox environment also regulates the activity and function of HMGB1 by conformational changes to the molecule itself (Janko et al., 2014). In the nucleus HMGB1 is primarily in its fully reduced form (all-thiol HMGB1), however once HMGB1 is translocated or secreted it is subjected to local redox conditions (Janko et al., 2014). HMGB1 can be reversibly partially-oxidised (Disulphide HMGB1) or irreversibly

fully-oxidised (sulfonyl HMGB1) (Janko et al., 2014). These post-translational modifications to HMGB1 result in mutually exclusive functions when HMGB1 is released extracellularly (Janko et al., 2014, Andersson et al., 2018). Fully reduced HMGB1 can bind with CXCL12 and signal through CXCR4 resulting in chemotaxis and leukocyte recruitment (Janko et al., 2014, Andersson et al., 2018). Semi-oxidised HMGB1 signals through TLR-4 and promotes the secretion of pro-inflammatory cytokines and chemokines (Janko et al., 2014, Andersson et al., 2018). Fully oxidised HMGB1 has no known direct role; however, it is predicted that its inactivation by ROS inhibits an over exuberant immune response and promotes the resolution of inflammation (Janko et al., 2014, Andersson et al., 2018). High levels of ROS are observed during apoptosis and necrosis (Simon et al., 2000, Zong and Thompson, 2006, Choi et al., 2009). It has been established that a limited amount of HMGB1 is released by apoptotic cells which is mostly oxidised or bound to DNA (Janko et al., 2014, Andersson et al., 2018). Contrarily, necrosis is considered a pro-inflammatory process and studies in necrotic cells have suggested that HMGB1 is released in its fully-reduced and partially-oxidised forms that can cause localised, sterile inflammation (Venereau et al., 2012). It has also been suggested that passive release of HMGB1 from necrotic cells is predominantly reversibly oxidised which represents 90% of the total pool of HMGB1 (Urbonaviciute et al., 2009). This would suggest that HMGB1 released from necrotic cells is primarily an immuno-stimulator and not a direct chemoattractant. Further studies are required to determine the state of HMGB1 in necrosis and whether this can be disease or tissue specific. Furthermore, it is unknown what the oxidation state of HMGB1 is in cells undergoing necroptosis or other forms of programmed necrotic-like forms of cell death (Tang et al., 2016). All forms of HMGB1 can signal through RAGE which is expressed in myenteric neurons and the idea that fully-oxidised HMGB1 can signal through undiscovered mechanisms has been widely considered (Andersson et al., 2018). It has been demonstrated that application of only oxidised HMGB1 increases cytotoxicity in cancer cells; therefore it may have a role in promoting cell death (Tang et al., 2010)

.

HMGB1 has a well-established role in driving inflammatory and autoimmune diseases (Lotze and Tracey, 2005, Andersson and Tracey, 2011). In IBD, HMGB1 is implicated

in the pathophysiology of intestinal inflammation and has become of interest as a useful faecal biomarker of paediatric and adult IBD (Vitali et al., 2011, Palone et al., 2014). In animal models of colitis, increased HMGB1 expression in colon tissues have been observed in mouse models of 2,4,6-trinitrobenzenesulfonic acid (TNBS), DSS chemically-induced colitis and in interleukin (IL)-10 deficient mice (Davé et al., 2009, Yamasaki et al., 2009, Vitali et al., 2013). In TNBS-induced colitis and IL-10 $^{-/-}$ mice, administration of ethyl pyruvate attenuated colitis and reduced HMGB1 expression (Davé et al., 2009). Concomitantly, the antioxidant enzyme haem oxygenase 1 (HO-1) was upregulated which may indicate that inhibition of oxidative stress contributed to the decrease in HMGB1 (Davé et al., 2009). In DSS-induced colitis, the efficacy of direct HMGB1 inhibitors has been evaluated. Daily treatment with dipotassium glycyrrhizate reduced HMGB1 release and attenuated colitis (Vitali et al., 2013). In a similar model, treatment with an anti-HMGB1 antibody before administration of DSS improved histological scores but had modest effects on clinical scores (Yamasaki et al., 2009). Similar results were observed using GA in our study, with a significant but modest reduction in disease activity. However, in our study, GA was applied after chronic inflammation was established; thus, GA was not investigated as a preventative treatment like previous studies and may offer higher efficacy if employed before the onset of inflammation. In studies of colitis, HMGB1 release was associated with a pro-inflammatory role. Nevertheless, in our study GA treatments did not appear to yield an anti-inflammatory effect on the level of the myenteric ganglia with high levels of leukocytes observed in all regions proximal to myenteric neurons despite the inhibition of neuronal HMGB1 translocation. This may suggest that plexitis is upstream of HMGB1 translocation in myenteric neurons. This is supported by our previous finding that plexitis negatively correlates with neuronal loss which, in addition, parallels neuronal HMGB1 translocation (**Chapter 4, Figure 4.11**). Therefore, BM-MSC treatments may attenuate HMGB1 translocation, as well as neuronal loss, by reducing plexitis. Particularly in myenteric neurons, this may suggest that released HMGB1 is not involved in leukocyte chemotaxis but may more likely function as regulator of cell death.

Mechanisms of neuronal death are highly diverse and can be interrelated. These include traditional caspase-dependent apoptosis pathways and various forms of programmed necrosis or necroptosis (Yakovlev and Faden, 2004). In response to oxidative stress and chronic colitis, myenteric neurons lost expression of HMGB1 in the nucleus or HMGB1 was located in the cytoplasm. This suggest that myenteric neurons might undergo necrotic or necroptotic cell death in these conditions. This is further supported by the correlation between the degree of HMGB1 translocation and neuronal loss, in addition to the neuroprotective effects of GA treatments. High levels of ROS are observed in necrosis (Janko et al., 2014, Negroni et al., 2015). Likewise, high levels of oxidised DNA/RNA adducts, a marker of oxidative stress, were observed specifically in myenteric neurons; this further supports that myenteric neurons underwent either programmed or spontaneous necrosis. This may explain our previously unsuccessful attempts to identify significant levels of the apoptotic marker, cleaved-caspase 3, in myenteric neurons in the *Winnie* model of chronic inflammation (data not shown). HMGB1 expression was studied to help determine the efficacy and mechanisms of BM-MSC treatment in myenteric neuroprotection. However, by studying this molecule, valuable insight has also been gained in the understanding the pathophysiology of cell death in myenteric neurons in chronic inflammation and oxidative insult. Previously, it was observed in a model of dinitrobenzene sulfonic acid (DNBS)-induced colitis that cleaved caspase-3 can be present in 1.4% of neurons at 1.5h after installation (Boyer et al., 2005). Comparatively, there was a 42% loss in myenteric neurons (Boyer et al., 2005). This suggests that a small number of myenteric neurons can undergo apoptosis in the acute stages of chemically-induced colitis; however, other non-caspase 3 dependent cell death pathways appear to be involved. It should also be noted that in the CNS and dorsal root ganglion (DRG) neurons can survive long-term despite expressing activated caspase-3 which can execute physiological processes other than apoptosis such as neuroplasticity and synapse formation (Cheng and Zochodne, 2003, D'Amelio et al., 2010). Therefore, neurons appear to be uniquely robust to this traditional pathway of apoptosis. In physiological conditions, apoptosis is generally reserved for regulating the turnover of highly proliferative cells, or those damaged by chemical insult (Elmore, 2007). This may explain the susceptibility for

myenteric neurons to undergo apoptosis after exposure to chemotherapy (McQuade et al., 2016).

To identify general mechanisms of cell death in chronic inflammation of *Winnie* mice and IBD patients, the expression of cell death-associated genes was identified in the transcriptome. BM-MSC treatments in *Winnie* mice corrected the expression of several genes that were dysregulated in *Winnie*-sham mice compared to C57BL/6 mice. Furthermore, many of these cell death genes were similarly dysregulated in *Winnie* mice and IBD patients. Contrary to our initial predictions, the majority of genes associated with cell survival were upregulated in chronic inflammation including TNF receptor super family members *Tnfrsf11b, Tnfrsf4, Tnfrsf1b,* as well as large changes in the inhibitor of apoptosis, murine *Bcl2a1b, Bcl2a1a, Bcl2a1d* and its human homologue *BCL2A1* (Vogler, 2012). In IBD apoptosis is inhibited; this is expected to contribute to the susceptibility of CRC development in these patients (Wang and Fang, 2014). Our gene expression data appear to support this. Conversely, genes associated with inducing non-canonical pathways of cell death were upregulated in chronic inflammation including *Slc7a11* which can cause neuronal death (Conrad and Sato, 2012) and *Bnip3* which regulates an atypical cell death program characterised by increased mitochondrial ROS and opening of the mPTP (Chinnadurai et al., 2009, Gustafsson, 2011, Graham et al., 2015). Furthermore, *Rip3* the key regulator of necroptosis was upregulated in *Winnie* mice and its direct downstream executioner, *MLKL,* was upregulated in IBD patients (Zhang et al., 2009a, Murphy and Vince, 2015). MSCs have previously been determined to attenuate necroptosis in neurons by downregulating RIP3 (Kong et al., 2017). Together this suggest that cell death pathways may become atypical in chronic inflammation and necrotic types of cell death may be more prominent. These pathways are associated with driving inflammation by damage associated molecular patterns, like HMGB1, and fit the chronic model of inflammation (Rock and Kono, 2008). Nevertheless, future studies should clarify the role of these pathways in the pathophysiology of intestinal inflammation and identify the affected cell types. Further investigation into these pathways of cell death in the ENS are warranted considering they involve rises in cytosolic Ca^{2+} and dysregulation in ionic balance, increased ROS, intracellular

acidification and depletion of ATP which enteric neurons appear to be susceptible to due to their excitable nature and high energy demand (Golstein and Kroemer, 2007, Friedman, 2011). BM-MSCs may be an efficacious cytoprotective treatment as they upregulated a plethora of genes that regulate these processes and attenuated oxidative stress (**Chapter 4, Section 4.6**).

In *Winnie* mice, administration of GA attenuated neuronal loss but appeared to have a limited effect on inflammation. Signs of active inflammation including colon weight and weight loss remained high and levels of myenteric immune cell infiltrate were not attenuated despite appearing to be key drivers of neuronal loss. The neuroprotective effects of GA treatments paralleled the attenuation of diarrhoea. Secretion and motility are neurally-regulated processes that affect stool consistency. Dysfunction in the ENS, is associated with altered stool consistencies in human pathologies and experimental models (Willard et al., 1988, Jodal et al., 1993, Törnblom et al., 2002). Taken together, these results appear to demonstrate that attenuating neuronal loss alone can partially alleviate the disease activity or the presentation of this sequela. However, it should be considered that high levels of ROS and pro-inflammatory cytokines modify the electrochemical properties and promote dysfunction in enteric neurons (Gaginella et al., 1992, Downen et al., 1999, Xia et al., 1999, Kelles et al., 2000, Wada-Takahashi and Tamura, 2000, Roberts et al., 2013). Therefore, despite GA promoting neuronal survival, perturbations in their function are still likely. Conversely, BM-MSCs reduced neuronal loss by ameliorating plexitis and oxidative stress; therefore, these neurons are more likely to function closer to physiological conditions (**Chapter 4, Figure 4.10 & Chapter 5, Figure 5.10**). Application of BM-MSCs had an obvious advantage over GA treatments as they can target several multi-faceted mechanisms to alleviate intestinal inflammation including oxidative stress and leukocyte recruitment (**Chapter 1, Section 1.2.9**). Albeit, these results suggest that HMGB1 inhibitors could be a viable therapeutic option when used in conjunction with current treatments targeting the inflammatory component of the disease.

6.8. Conclusion

Translocation of the HMGB1 protein in myenteric neurons was associated directly with neuronal loss in chronic colitis. HMGB1 is ubiquitously expressed by most nucleated cells, however, the specificity for HMGB1 translocation in neurons is a feature of CNS pathologies associated with inflammation and oxidative stress. Likewise, translocation of HMGB1 within cells of the myenteric ganglia was only increased in neurons with conditions of chronic inflammation. The expression pattern of HMGB1 in myenteric neurons suggests that neuronal loss was caused by programmed or non-programmed mechanisms of necrosis. Colitis in *Winnie* mice and IBD patients resulted in dysregulation of the gene expression of several cell death-associated genes that could favour the execution of non-apoptotic cell death programs in chronic inflammation. High levels of oxidative stress and ROS production are observed in myenteric neurons in chronic colitis. Oxidative stimuli were demonstrated to directly induce HMGB1 translocation in myenteric neurons, therefore oxidative stress appeared to instigate HMGB1 translocation and neuronal loss. Treatment using BM-MSCs inhibited HMGB1 translocation *in vivo* and *in vitro* which was concomitant with increased neuronal density. Thus, HMGB1 was implicated in the neuroprotective effects of BM-MSC therapy. These effects appeared to be mediated by soluble paracrine factors which included the antioxidant enzyme SOD1. Inhibition of HMGB1 by GA validated its importance as a key regulator of neuronal loss *in vivo.* Unlike BM-MSC treatments, GA did not reduce the generation of $O_2^{\cdot -}$ and plexitis in the myenteric ganglia, therefore, these appear to be upstream events of HMGB1 translocation and neuronal loss. BM-MSCs unequivocally attenuated HMGB1 translocation and neuronal loss; this is likely to be mediated by their antioxidative properties and ability to reduce leukocyte recruitment to the ganglia.

CHAPTER SEVEN

General Discussion and Conclusions

7.1. General Comments

The therapeutic application of mesenchymal stem cells (MSCs) have yielded promising results for inflammatory bowel disease (IBD) which may lead to the treatment becoming accessible in the clinic. Understanding the therapeutic mechanisms of MSCs are paramount to improving their efficacy. The enteric nervous system (ENS) has emerged as a novel therapeutic target for IBD; however, investigations into neuroprotective treatments have been limited. This thesis provides evidence that bone marrow derived MSCs (BM-MSCs) as a multi-faceted treatment capable of attenuating the inflammatory and neurological changes in acute and chronic intestinal inflammation (**Chapters 2-4**). After over 80 original research articles, these are the first studies to explore the mechanisms of BM-MSC treatments in a spontaneous chronic model of intestinal inflammation. Moreover, this is the first time that high-throughput sequencing of the transcriptome has been used to explore the many mechanisms of MSC therapy in colitis. Previously, chemically-induced models of acute colitis have been used to elucidate the role of MSC therapy (**Chapter 1**). Discrepancies are beginning to emerge between mechanisms identified in these models and data from clinical trials (Gregoire et al., 2018). The *Winnie* mouse model of spontaneous chronic colitis replicated the inflammatory transcription profile of IBD to a far greater degree of accuracy than models of chemically-induced colitis (**Chapter 3, Section 3.7**). BM-MSC therapies had a large influence on the transcriptome of *Winnie* mice. Using bioinformatics, we identified many pathways that were altered by BM-MSCs in chronic inflammation which may be useful for providing direction for our group, and others, in the field (**Chapter 3**). Genes specifically associated with the ENS, oxidate stress and cell death were profiled in chronic experimental inflammation and after BM-MSC treatments (**Chapter 4-6**). BM-MSC treatments attenuated neuropathy and plexitis which was associated with reduced disease activity (**Chapter 4**); this supports previous observations that plexitis and loss of neuronal density can contribute to the severity of intestinal inflammation in humans and animal models. The mechanisms of BM-MSC-mediated neuroprotection in the myenteric ganglia were elucidated in chronic intestinal inflammation (**Chapter 4-6**). In the following section, key

findings from this thesis will be integrated to propose the mechanisms of neuronal loss and BM-MSC-mediated neuroprotection in chronic colitis.

7.2. Models of Inflammation

The guinea-pig model of 2,4,6-trinitrobenzenesulfonic acid (TNBS)-induced colitis was initially utilised to explore the neuroprotective effects of MSC therapy (**Chapter 2**). This model is the most extensively investigated for ENS damage in intestinal inflammation; thus, providing a solid foundation to determine the neuroprotective value of MSC treatments (Galligan, 2002, Linden et al., 2005a, Furness, 2006, Lomax et al., 2007a, Nurgali et al., 2007, Nurgali, 2009, Nurgali et al., 2009, Nurgali et al., 2011, Furness, 2012, Linden, 2013). In this study, MSCs were observed to avert neuropathy and damage to nerve fibres. MSCs increased the number of cholinergic neurons and the density of cholinergic, sympathetic and sensory fibres. MSCs could migrate to the ENS, however, this number was relatively low. Therefore, the neuroprotective effects of MSCs appeared to be produced by intermediate cells, or by the paracrine secretion of MSCs. The latter is plausible given that the MSC secretome is neuroprotective in *in vitro* models of enteric neuronal damage (**Chapter 5**) (Stavely et al., 2015a).

These results demonstrated that MSCs could protect the ENS from acute inflammation; however, models of chemically-induced colitis do not replicate all the features of IBD. This is a severe limitation for the fields of MSC and ENS research in intestinal inflammation. Using gene expression profiling, concordance rates for these models and the human pathology vary between 6.25%-46.9% depending on species and the chemical used (te Velde et al., 2007, Fang et al., 2010, Brenna et al., 2013). Therefore, it is questionable whether results can be accurately translated to the human pathology. Unlike IBD, the TNBS model provides acute inflammation; thus, a chronic model may be more suitable. In Chapters 3 to 6 we tested the effects of BM-MSC treatments in the *Winnie* mouse model of spontaneous chronic colitis. Using high-throughput transcriptome sequencing, the gene expression profile of BM-MSC-treated and untreated mice was characterised and compared to IBD patients (**Chapter 3**). For inflammation-associated

genes that were altered by BM-MSC treatments (**Chapter 3**), a high degree of concordance was observed between untreated *Winnie* mice and males and females with ulcerative colitis (UC) (90.7%, for both) or males with Crohn's disease (CD) (87.7%). The lowest concordance rate was observed between the male *Winnie* mice used in these studies and females with CD (63.1%). This was higher than models of chemically-induced colitis; however, it should be determined if this can be improved further by utilising female *Winnie* mice. Together, these data provide evidence that BM-MSC treatments in *Winnie* mice are more clinically relevant than those in chemically-induced colitis.

We collated data on the effects of MSCs on the transcriptional or inflammatory signalling milieu from all previous studies in chemically-induced colitis (**Chapter 1, Table 1.3**). These were compared to the effects of BM-MSC treatments in *Winnie* mice. Of these, 20 genes that were altered by MSCs in acute colitis were also differentially expressed by BM-MSC treatments in chronic colitis (**Chapter 3, Figure 3.11, Table 3.4**). However, half those genes were oppositely regulated. This demonstrated a significant variance in the processes elicited by MSCs in acute models and *Winnie* mice. To explore this further, we quantified the number of leukocytes expressing the regulatory T-lymphocyte (Treg) marker, forkhead box P3 (FOXP3), which was previously reported as the key immunosuppressive mechanism of MSCs in chemically-induced colitis in several studies (**Chapter 1, Table 1.2**). Unlike in models of chemically-induced colitis, BM-MSCs did not increase the number of FOXP3 expressing leukocytes in chronic inflammation; rather the proportion increased slightly due to a reduction in the total leukocyte population (**Chapter 3, Figure 3.5**). Similarly, Treg populations were recently demonstrated to not be enhanced by MSC treatments in CD (Gregoire et al., 2018). Together, this reaffirmed our hypothesis that the differences between acute and chronic inflammation would results in different mechanisms of action for MSC treatments. The transcriptional milieu identified in our study can be used to provide the foundation for the exploration of the immunomodulatory activities of BM-MSCs in chronic colitis.

7.3. Mechanisms of MSC-mediated Neuroprotection in Intestinal Inflammation

Several genes that synthesise pan-neuronal proteins including Hu antigen (embryonic lethal abnormal vision-like, ELAVL) family proteins, protein gene product 9.5 (PGP9.5) and microtubule-associated protein 2 (MAP2) were upregulated by MSC treatments in *Winnie* mice (**Chapter 4, Figure 4.1, Table 4.1**). This coincided with the ability of BM-MSCs to attenuate myenteric neuronal loss in acute and chronic inflammation. In chemically-induced colitis, BM-MSCs had a greater neuroprotective efficacy than adipose tissue-derived MSCs (AT-MSCs) (**Chapter 2, Figure 2.5, Table 2.2**); thus, rationalising the use of these cells in chronic colitis to explore their mechanisms of action in neuroprotection. The studies in this thesis have elucidated some of these basic physiological processes involved in neuronal loss and the mechanisms of BM-MSC-mediated neuroprotection in intestinal inflammation. These results are summarised in **Figure 7.1** and are discussed below.

7.3.1. Effects on neuronal signalling pathways

BM-MSC treatments normalised the expression of many genes associated with neurotransmission, physical structure and neurogenic inflammation (**Chapter 4**). Transcriptome analysis revealed that many genes associated with the ENS or neurotransmitter receptors were dysregulated in chronic intestinal inflammation in *Winnie* mice and IBD patients (**Chapter 4, Figures 4.1-4.4, Tables 4.1-4.3**). This is indicative of substantial alterations to the ENS and neuronal signalling in the disease. Male mice were used in this study which did not greatly affect the concordance of the inflammatory profile between males and females with UC. However, it was apparent that changes of the neural transcriptomic milieu in UC patients could be sexually dysmorphic. This adds a layer of complexity to identifying key neural components in the pathophysiology of the disease and designing neuroactive treatments. Our data suggest that the serotonergic system was one of the neuronal signalling pathways affected by gender in IBD patients The impact of sexual dimorphisms on neuroactive treatments have been illustrated in irritable bowel syndrome and current serotonergic treatments are only

therapeutic in females (Crowell, 2004, Katsumata et al., 2017). The number of pathways affected, combined with sexual dimorphisms, suggest that pharmacological intervention on a single receptor or transporter may be an ineffective treatment for IBD. Treatments with BM-MSCs acted on a number of neurotransmission pathways and may provide a solution to remedy dysfunction in multiple neural signalling processes with a single treatment. This was exemplified by the ability of BM-MSCs to attenuate transcriptomic dysregulation in the nicotinic, purinergic, adrenergic, glutaminergic, serotonergic and NPY-ergic systems in *Winnie* mice (**Chapter 4, Table 4.3**). These data should be used as a foundation to identify and explore the specifics of neural dysregulation in the pathophysiology of IBD and the effects of BM-MSC treatments.

Our data support the cholinergic system as a modulator of intestinal inflammation with changes observed in an acute and chronic setting. BM-MSCs attenuated the loss of cholinergic neurons and nerve fibres identified by choline acetyltransferase (ChAT) and the vesicular acetylcholine transporter (VAChT) in acute colitis (**Chapter 2, Figures 2.7 & 2.10, Tables 2.2 & 2.3**). Likewise, their gene expression was upregulated in chronic colitis (**Chapter 4, Figure 4.1, Table 4.1**). In acute colitis, MSCs promoted the density of sensory and sympathetic nerve fibres, identified by calcitonin gene-related peptide (CGRP) and tyrosine hydroxylase (Th), which were initially reduced by acute inflammation (**Chapter 2, Figures 2.8 & 2.9, Table 2.3**). However, these were reduced by BM-MSCs on the level of gene expression in *Winnie* mice and may represent differences between acute and chronic colitis (**Chapter 4, Figure 4.1, Table 4.1**). Moreover, BM-MSCs were identified to upregulate gene expression for neuropeptide Y (NPY) and downregulate substance P; these neuropeptides have been associated with anti and pro-inflammatory immunomodulation, respectively. The effect of BM-MSC treatments on all of these neurotransmitters in chronic colitis requires elucidation on the protein level in both the myenteric and submucosal plexus; this is an ongoing project by our group separate to this thesis. Unpublished data from this project have confirmed that BM-MSCs increase the number of cholinergic neurons and nerve fibres in *Winnie* mice (Robinson, Stavely & Nurgali, unpublished).

7.3.2. Plexitis

Plexitis was linked with disease activity and neuronal cell loss in acute and chronic colitis which supports previous observations in IBD and experimental models of intestinal inflammation (**Chapter 2, Figure 2.4 & Chapter 4, Figures 4.10 & 4.11, Tables 4.6 & 4.7**) (Sanovic et al., 1999, Boyer et al., 2005, Ferrante et al., 2006, Sokol et al., 2009, Bressenot et al., 2013, Filippone et al., 2018a). When leukocyte populations were characterised by morphology in *Winnie* mice, there was an increase in stellate-shaped leukocytes, as well as, a population of leukocytes infiltrating the plexus with a rounded morphology. In physiological conditions, muscularis macrophages exhibiting a stellate morphology are virtually the exclusive leukocyte population around the myenteric plexus. Neuronal density was more dependent on infiltration of the rounded population (**Chapter 4, Figure 4.10, Table 4.7**). Previously it was demonstrated that neutrophils and eosinophils are predominantly responsible for neuronal loss in dinitrobenzenesulfonic acid (DNBS) and TNBS-induced colitis (Sanovic et al., 1999, Sayani et al., 2004, Boyer et al., 2005, Filippone et al., 2018a). Pro-inflammatory cytokines have previously been demonstrated to contribute to enteric neuronal loss and dysfunction *in vitro* (Downen et al., 1999, Xia et al., 1999, Kelles et al., 2000, Sharkey and Kroese, 2001, Schemann et al., 2005). Therefore, local pro-inflammatory mediators may have contributed to neuronal loss *in vivo*. Our gene expression data may be useful to identify specific inflammatory factors contributing to ENS damage in the inflamed colon (**Chapter 3, Figure 3.10, Table 3.3**). The phagocytic role of muscularis macrophages is emerging as a crucial regulator of ganglionic remodelling via the clearance of enteric neurons; however, this has not been explored in intestinal inflammation (De Schepper et al., 2018). Therefore, the contribution of these cells to neuronal loss cannot be dismissed. Moreover, reverse causality of the relationship between plexitis and neuronal loss must be considered. Many leukocyte populations express cholinergic receptors; muscularis macrophages have been confirmed to be under immunomodulatory control by cholinergic myenteric neurons which promote an anti-inflammatory phenotype (Tsuchida et al., 2010, Matteoli et al., 2014).

Figure 7.1 *Mechanisms of BM-MSC-mediated neuroprotection in intestinal inflammation*

A) Mesenchymal stem cells (MSCs) restore myenteric neuronal density and the gene expression of pan-neuronal markers (microtubule-associated protein 2, MAP-2; Hu antigen; protein gene product 9.5, PGP 9.5) in intestinal inflammation. Subsequently, they increase the number of cholinergic neurons and fibres as well as normalise the gene expression of multiple neural signalling pathways. **B)** Various immunomodulatory factors are secreted by MSCs and multiple pathways in the inflammatory response are suppressed by MSC treatments. **(C)** The immunosuppressive properties of MSC treatments attenuate plexitis (leukocyte infiltration to the myenteric plexus) and associated enteric neuronal loss. **D)** MSCs upregulate endogenous antioxidant defences in the host tissue and secrete superoxide dismutase 1 (SOD1). **E)** In chronic intestinal inflammation the mitochondria of myenteric neurons produce excessive levels of superoxide ($O_2^{\cdot -}$) and the subsequent oxidative stress initiates cell death. Oxidative stress and the consequential neuronal loss is averted by antioxidant enzymes including SOD1. **F)** Genes associated with necrotic-like cell death are downregulated by MSCs indicating a transition to a microenvironment that favours cell survival. **G)** During necrotic/necroptotic cell death, nuclear high-mobility group box 1 (HMGB1) translocates to the cytoplasm and is passively released by neurons. The actions of extracellularly released HMGB1 are unknown in the ENS, however both local leukocytes and myenteric neurons are receptive to its signalling which might cause inflammation in the absence of exogenous pathogens or antigens (sterile inflammation). **H)** Consequences of neuronal loss include an increased activity of colitis, dysfunction of neurally-controlled processes and a lack of neuromodulation of the immune system leading to the reoccurrence of inflammation. The neuroprotective, immunomodulatory and antioxidative properties of MSCs alleviate the predisposition to reoccurring intestinal inflammation.

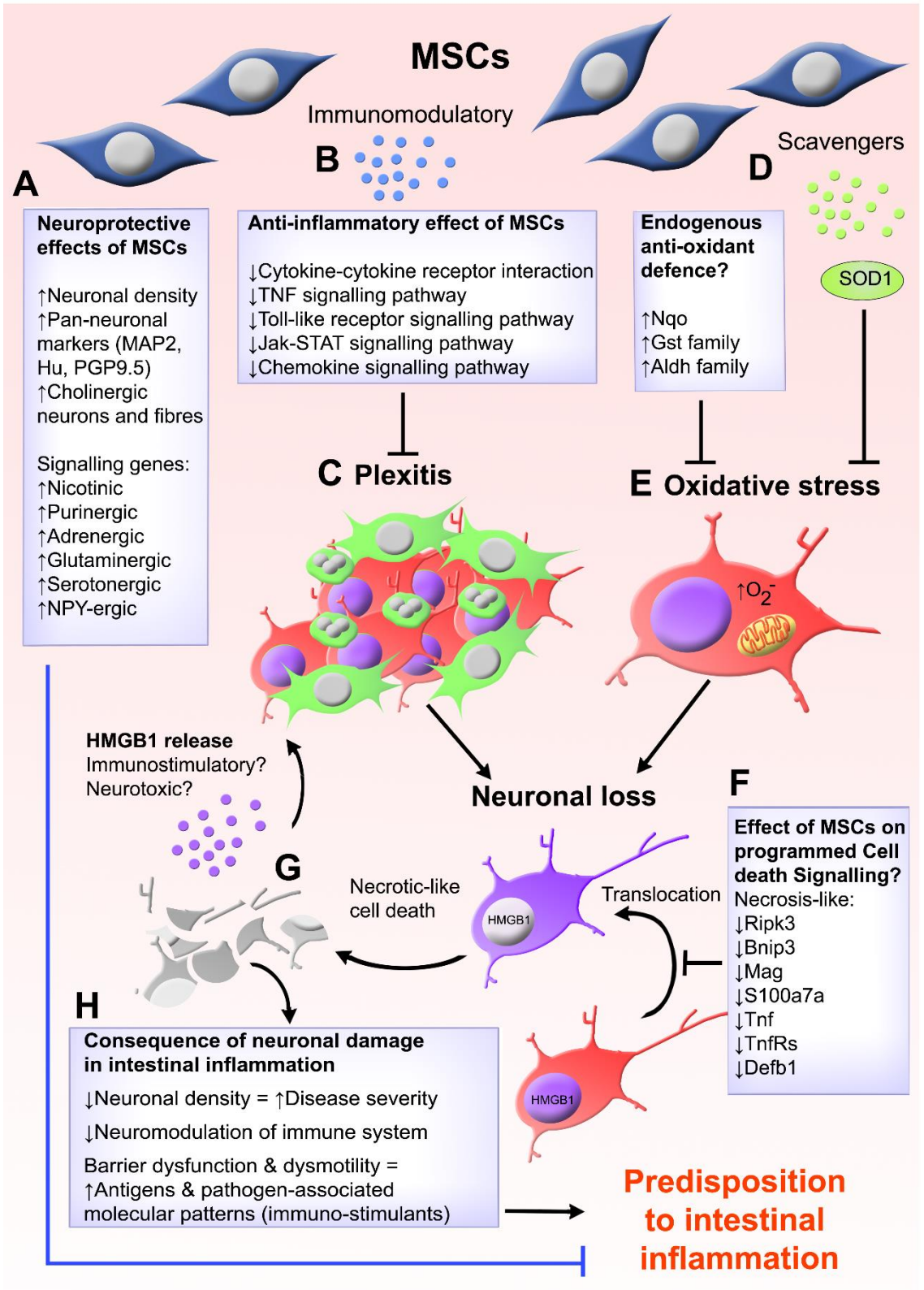
MSCs
Immunomodulatory
A
B
D
Scavengers
Neuroprotective effects of MSCs
↑Neuronal density
↑Pan-neuronal markers (MAP2, Hu, PGP9.5)
↑Cholinergic neurons and fibres
Signalling genes:
↑Nicotinic
↑Purinergic
↑Adrenergic
↑Glutaminergic
↑Serotonergic
↑NPY-ergic
Anti-inflammatory effect of MSCs
↓Cytokine-cytokine receptor interaction
↓TNF signalling pathway
↓Toll-like receptor signalling pathway
↓Jak-STAT signalling pathway
↓Chemokine signalling pathway
Endogenous anti-oxidant defence?
↑Nqo
↑Gst family
↑Aldh family
SOD1
C Plexitis
E Oxidative stress
↑O2-
HMGB1 release
Immunostimulatory?
Neurotoxic?
Neuronal loss
F
Effect of MSCs on programmed Cell death Signalling?
Necrosis-like:
↓Ripk3
↓Bnip3
↓Mag
↓S100a7a
↓Tnf
↓TnfRs
↓Defb1
G
Necrotic-like cell death
HMGB1
Translocation
H
Consequence of neuronal damage in intestinal inflammation
↓Neuronal density = ↑Disease severity
↓Neuromodulation of immune system
Barrier dysfunction & dysmotility = ↑Antigens & pathogen-associated molecular patterns (immuno-stimulants)
Predisposition to intestinal inflammation

Cholinergic neurons, nerve fibres and acetylcholine (ACh) manufacturing enzymes were reduced by intestinal inflammation which paralleled the reduction in neuronal density. Reduced neuronal density is a predisposing factor for severe intestinal inflammation (Margolis et al., 2011). Thus, plexitis and local inflammation could have been promoted by a lack of neural regulation. BM-MSCs attenuated plexitis which coincides with their extensively described ability to switch the pro-inflammatory signalling milieu to an anti-inflammatory profile and reduce leukocyte recruitment in chemically-induced colitis, and in spontaneous chronic colitis (**Chapter 1, Table 1.3 & Chapter 3, Figures 3.6-3.10, Tables 3.1-3.3**). Therefore, the neuroprotective effects of BM-MSC treatments could be explained by their immunosuppressive function (**Figure 7.1**). However, BM-MSCs can avert enteric neuronal loss to stimuli in the absence of chemotactic leukocytes *in vitro* (**Chapter 5, Figure 5.8 & 5.9**) (Stavely et al., 2015a). Thus, BM-MSCs can also offer direct neuroprotective value independent of reducing plexitis.

7.3.3. Oxidative stress

Oxidative stress is prominent in IBD patients; markers for oxidative DNA damage can be used as biomarkers for the disease (D'Inca et al., 2004, Pereira et al., 2016). Likewise, high levels of DNA/RNA oxidation were detected throughout the colon in *Winnie* mice with chronic inflammation (**Chapter 5, Figure 5.5**). High levels of DNA/RNA oxidation were observed in myenteric neurons of the inflamed colon (**Chapter 5, Figure 5.6**). The immune system and oxidative stress are intrinsically linked via bidirectional stimulation; thus, plexitis may have contributed to oxidative stress in myenteric neurons (Biswas, 2016). However, it has been demonstrated that myenteric neurons produce high levels of the free radical superoxide in chemically-induced colitis (Brown et al., 2016). We identified that this was endogenously derived from the mitochondria of myenteric neurons in both acute and chronic colitis (**Chapter 2, Figure 2.11 & Chapter 5, Figure 5.10**). BM-MSC treatments elicited an antioxidative effect and reduced levels of superoxide and DNA oxidation in the myenteric plexus (**Chapter 5, Figures 5.6 & 5.10**). The concomitant attenuation of neuronal loss suggested that these events are linked. Pro-oxidative stimuli were used to model the effects of oxidative stress on myenteric neurons

in vitro (**Chapter 5, Figure 5.7**). These stimuli caused neuronal loss which illustrates that oxidative stress is upstream of neuronal death. The paracrine secretion of BM-MSCs reduced neuronal loss from oxidative stimuli. Thus, BM-MSCs can directly attenuate oxidative stress-induced neuropathy. This was dependent, at least in part, on the secretion of superoxide dismutase 1 (SOD1) (**Chapter 5, Figure 5.11**). The secretion of this enzyme by BM-MSCs is novel and was only recently defined in the literature (Klein et al., 2017). The importance of SOD1 has been highlighted by recent works that demonstrate SOD1-deficient MSCs provide limited protection to central nervous system (CNS) neurons (Redondo et al., 2018, Sarkar et al., 2018). Moreover, BM-MSCs were found to increase the endogenous tissue expression of enzymes with antioxidant roles which may have contributed to the reduction of oxidative stress (**Chapter 5, Figure 5.4, Table 5.4**). This included NAD(P)H:quinone acceptor oxidoreductase, as well as several glutathione S-transferases and aldehyde dehydrogenase family genes. All of these are downregulated in IBD patients and may be associated with disease progression (Mittal et al., 2007, Kosaka et al., 2009).

7.3.4. Necroptosis/necrotic-like cell death

Gene expression profiling suggested a switch from apoptotic mechanism of cell death to more necrotic mechanism in chronic colitis (**Chapter 6, Figure 6.5, Table 6.6**). This is plausible considering that necrosis is induced by, and promotes, inflammation (Rock and Kono, 2008). Studies into the mechanism of cell death in enteric neurons are limited. Apoptosis has previously been illustrated to contribute to myenteric neuropathy after chemotherapy (McQuade et al., 2016). This is highly likely as apoptosis is often associated with xenobiotics and chemical insult (Elmore, 2007). Similarly, myenteric neurons have also been demonstrated to undergo apoptosis in acute experimental inflammation (Boyer et al., 2005). However, during this study, only a maximum of 1.4% of neurons were detected to undergo apoptosis via cleaved-caspase 3 despite a total loss of 42%. Thus, it is apparent that enteric neurons can undergo other mechanisms of cell death. Mechanism of neuronal death in chronic colitis were elucidated by investigating the novel cell death marker and damage associated molecular pattern (DAMP), high-

mobility group box 1 (HMGB1). During apoptosis HMGB1 binds tightly to DNA with minimal release; conversely, necrotic and necroptotic mechanisms of cell death exclusively result in its translocation from the nucleus to the cytoplasm and passive release extracellularly (Janko et al., 2014, Andersson et al., 2018). Loss of HMGB1 expression in the nucleus, an indication of translocation, was observed in 37.1% of myenteric neurons and active translocation into the cytoplasm was detected in 13.5% of neurons (**Chapter 6, Figure 6.3, Table 6.4**). This paralleled the reduction in neuronal density. The relationship between HMGB1 and neuronal loss was explored by linear regression analysis which confirmed negative correlations between HMGB1 translocation and neuronal density (**Chapter 6, Figure 6.3, Table 6.5**). This was observed when HMGB1, or lack thereof, was expressed as a percentage or as a density. Gene expression studies identified novel pathways that may mediate programmed necrosis-like cell death which could be explored further. Within the identified genes, MSCs have previously been determined to attenuate necroptosis in neurons by downregulating receptor interacting protein kinase 3 (RIP3), the major executioner of the process (Kong et al., 2017). Considering that BM-MSC treatments reduced its expression in colitis, examination of this protein may be warranted specifically in enteric neurons in the pathophysiology of intestinal inflammation.

7.3.5. Functional role of HMGB1 in neuronal loss

Oxidative stress appeared to play a large role in HMGB1 translocation. Various oxidative stimuli induced HMGB1 translocation and neuronal death *in vitro* (**Chapter 6, Figures 6.1 & 6.2, Tables 6.1-6.3**). Likewise, high levels of neuronal oxidative stress were concomitant with HMGB1 translocation in chronic intestinal inflammation (**Chapter 5, Figures 5.6 & Chapter 6, Figure 6.3, Table 6.4**). Inhibition of HMGB1 averted neuronal loss *in vivo* with a limited effect on mitochondrial superoxide production (**Chapter 6, Figures 6.11 & 6.13**). This suggests that oxidative stress is upstream of HMGB1 translocation and subsequent neuronal loss. Moreover, this implies that HMGB1 can directly contribute to neuronal loss rather than acting merely as a marker. In the CNS, inhibition of HMGB1 supresses its translocation and release; additionally, it is theorised

that neighbouring neurons are receptive to HMGB1 signalling which promotes further HMGB1 release (Gong et al., 2011, Ohnishi et al., 2011, Kim et al., 2012, Okuma et al., 2014). This is supported in our study by the clustered pattern of myenteric neurons expressing HMGB1 in the cytoplasm. This may be reflective of the role of HMGB1 as an alarmin and mediator of sterile tissue injury (Andersson et al., 2018). Myenteric neurons express receptors for HMGB1 including the receptor for advanced glycation end-products (RAGE), toll-like receptor (TLR)-2 and TLR-4 and thus, are likely to be affected by locally released HMGB1 (Venereau et al., 2012, Chen et al., 2015, Burgueño et al., 2016). Stimulation of TLR-4 by HMGB1 may explain its direct role in myenteric neuronal loss. Inhibition of HMGB1 protected neurons, but did not ameliorate plexitis (**Chapter 6, Figure 6.12, Table 6.7**). However, only the presence of leukocytes as marker of inflammation was examined in this particular study. HMGB1 could potentially stimulate the release of pro-inflammatory mediators and chemotaxis of muscularis macrophages or other local leukocytes that express TLR-4 or C-X-C chemokine receptor type 4 (CXCR4) (Hori et al., 2008). In physiological conditions this could represent a mechanism of immuno-stimulation to clear damaged enteric neurons. In pathophysiology this could lead to an exuberant, 'sterile', inflammatory response. This warrants elucidation in further studies.

7.4. General Conclusions

The inefficacy and toxicity of treatments for IBD necessitates investigations into alternative therapies. The administration of MSCs into IBD patients has demonstrated efficacy in reducing disease activity and produces less severe side effects. While current treatments target the immune system, MSC therapy is multi-faceted which may explain their therapeutic efficacy in patients. Therefore, investigations into their therapeutic mechanisms are crucial. The ENS is beginning to be appreciated as a major contributor to intestinal inflammation. In these studies, we have defined potent neuroprotective properties elicited by BM-MSCs which ameliorate damage to the myenteric ganglia. This signifies the outset of restoring neural regulation that can attenuate the pathophysiology and symptoms of the disease. Furthermore, novel mechanisms of neuronal damage in

intestinal inflammation are reported. The use of high-throughput transcriptome sequencing illustrates the complex alterations to the nervous system in chronic experimental colitis and IBD patients. Likewise, the use of screening technology is a meticulous method in identifying pathways that require exploration to understand the therapeutic mechanisms of MSC therapy. The results of this thesis may be utilised as a reference to provide future direction in the fields of MSC therapies and ENS pathophysiology in intestinal inflammation.

CHAPTER EIGHT

References

ABAIS, J. M., XIA, M., ZHANG, Y., BOINI, K. M. & LI, P.-L. 2015. Redox Regulation of NLRP3 Inflammasomes: ROS as Trigger or Effector? *Antioxid Redox Signal*, 22, 1111-1129.

ABDO, H., DERKINDEREN, P., GOMES, P., CHEVALIER, J., AUBERT, P., MASSON, D., GALMICHE, J.-P., BERGHE, P. V., NEUNLIST, M. & LARDEUX, B. 2010. Enteric Glial Cells Protect Neurons from Oxidative Stress in Part Via Reduced Glutathione. *FASEB J*, 24, 1082-1094.

ABRAHAM, C. & MEDZHITOV, R. 2011. Interactions between the Host Innate Immune System and Microbes in Inflammatory Bowel Disease. *Gastroenterology*, 140, 1729-1737.

ALLOCCA, M., JOVANI, M., FIORINO, G., SCHREIBER, S. & DANESE, S. 2013. Anti-IL-6 Treatment for Inflammatory Bowel Diseases: Next Cytokine, Next Target. *Curr Drug Targets*, 14, 1508-1521.

AMABLE, P. R., TELLES TEIXEIRA, M. V., CARIAS, V., BIZON, R., GRANJEIRO, J. M. & BOROJEVIC, R. 2014. Protein Synthesis and Secretion in Human Mesenchymal Cells Derived from Bone Marrow, Adipose Tissue and Wharton's Jelly. *Stem Cell Res Ther*, 5, 53.

AMIRI, F., JAHANIAN-NAJAFABADI, A. & ROUDKENAR, M. H. 2015. *In vitro* Augmentation of Mesenchymal Stem Cells Viability in Stressful Microenvironments: *In vitro* Augmentation of Mesenchymal Stem Cells Viability. *Cell Stress Chaperones*, 20, 237-251.

ANANTHAKRISHNAN, A. N. 2015. Epidemiology and Risk Factors for IBD. *Nat Rev Gastroenterol Hepatol*, 12, 205.

ANDERSEN, Y. S., GILLIN, F. D. & ECKMANN, L. 2006. Adaptive Immunity-Dependent Intestinal Hypermotility Contributes to Host Defense against Giardia Spp. *Infect Immun*, 74, 2473-2476.

ANDERSON, J. A., LITTLE, D., TOTH, A. P., MOORMAN, C. T., TUCKER, B. S., CICCOTTI, M. G. & GUILAK, F. 2013a. Stem Cell Therapies for Knee Cartilage Repair the Current Status of Preclinical and Clinical Studies. *Am J Sports Med*, 0363546513508744.

ANDERSON, P., SOUZA-MOREIRA, L., MORELL, M., CARO, M., O'VALLE, F., GONZALEZ-REY, E. & DELGADO, M. 2013b. Adipose-Derived Mesenchymal Stromal Cells Induce Immunomodulatory Macrophages Which Protect from Experimental Colitis and Sepsis. *Gut*, 62, 1131-1141.

ANDERSSON, U. & TRACEY, K. J. 2011. HMGB1 Is a Therapeutic Target for Sterile Inflammation and Infection. *Annu Rev Immunol*, 29, 139-162.

ANDERSSON, U., YANG, H. & HARRIS, H. 2018. High-Mobility Group Box 1 Protein (HMGB1) Operates as an Alarmin Outside as Well as inside Cells. *Semin Immunol* [Ahead of print], doi: 10.1016/j.smim.2018.02.011.

ANDO, Y., INABA, M., SAKAGUCHI, Y., TSUDA, M., QUAN, G. K., OMAE, M., OKAZAKI, K. & IKEHARA, S. 2008. Subcutaneous Adipose Tissue–Derived Stem Cells Facilitate Colonic Mucosal Recovery from 2, 4, 6-Trinitrobenzene Sulfonic Acid (TNBS)–Induced Colitis in Rats. *Inflamm Bowel Dis*, 14, 826-838.

ANDRESEN, L., JØRGENSEN, V. L., PERNER, A., HANSEN, A., EUGEN-OLSEN, J. & RASK-MADSEN, J. 2005. Activation of Nuclear Factor Kb in Colonic Mucosa from Patients with Collagenous and Ulcerative Colitis. *Gut*, 54, 503-509.

ANDREWS, S. 2010. Fastqc a Quality Control Tool for High Throughput Sequence Data. https://www.bioinformatics.babraham.ac.uk/projects/fastqc/.

ANITHA, M., GONDHA, C., SUTLIFF, R., PARSADANIAN, A., MWANGI, S., SITARAMAN, S. V. & SRINIVASAN, S. 2006. Gdnf Rescues Hyperglycemia-Induced Diabetic Enteric Neuropathy through Activation of the Pi3k/Akt Pathway. *J Clin Invest*, 116, 344-356.

ANKRUM, J. A., ONG, J. F. & KARP, J. M. 2014. Mesenchymal Stem Cells: Immune Evasive, Not Immune Privileged. *Nat Biotechnol*, 32, 252-260.

ANLAUF, M., SCHÄFER, M. K.-H., EIDEN, L. & WEIHE, E. 2003. Chemical Coding of the Human Gastrointestinal Nervous System: Cholinergic, Vipergic, and Catecholaminergic Phenotypes. *J Comp Neurol*, 459, 90-111.

ANTUNES, M., BRANCO, V., DIAZ, B., MORALES, M., XISTO, D., ROCCO, P. & ABREU, S. 2014a. Mesenchymal Stem Cells Derived from Bone Marrow Present Better Effects on Lung Inflammation and Remodeling Compared with Other Sources in Experimental Asthma. *Am J Respir Crit Care Med*, 189, A5291.

ANTUNES, M. A., ABREU, S. C., CRUZ, F. F., TEIXEIRA, A. C., LOPES-PACHECO, M., BANDEIRA, E., OLSEN, P. C., DIAZ, B. L., TAKYIA, C. M., FREITAS, I. P. R. G., ROCHA, N. N., CAPELOZZI, V. L., XISTO, D. G., WEISS, D. J., MORALES, M. M. & ROCCO, P. R. M. 2014b. Effects of Different Mesenchymal Stromal Cell Sources and Delivery Routes in Experimental Emphysema. *Respir Res*, 15, 118.

AON, M. A., CORTASSA, S. & O'ROURKE, B. 2010. Redox-Optimized Ros Balance: A Unifying Hypothesis. *Biochim Biophys Acta*, 1797, 865-77.

ARNOLD, S. J., FACER, P., YIANGOU, Y., CHEN, M. X., PLUMPTON, C., TATE, S. N., BOUNTRA, C., CHAN, C. L. H., WILLIAMS, N. S. & ANAND, P. 2003. Decreased Potassium Channel Iki and Its Regulator Neurotrophin-3 (NT-3) in Inflamed Human Bowel. *Neuroreport*, 14, 191-195.

ARSLAN, F., LAI, R. C., SMEETS, M. B., AKEROYD, L., CHOO, A., AGUOR, E. N., TIMMERS, L., VAN RIJEN, H. V., DOEVENDANS, P. A. & PASTERKAMP, G. 2013. Mesenchymal Stem Cell-Derived Exosomes Increase ATP Levels, Decrease Oxidative Stress and Activate PI3K/AKT Pathway to Enhance Myocardial Viability and Prevent Adverse Remodeling after Myocardial Ischemia/Reperfusion Injury. *Stem Cell Res*, 10, 301-312.

ASHBURNER, M., BALL, C. A., BLAKE, J. A., BOTSTEIN, D., BUTLER, H., CHERRY, J. M., DAVIS, A. P., DOLINSKI, K., DWIGHT, S. S. & EPPIG, J. T. 2000. Gene Ontology: Tool for the Unification of Biology. *Nat Genet*, 25, 25.

ASHOUR, R. H., SAAD, M.-A., SOBH, M.-A., AL-HUSSEINY, F., ABOUELKHEIR, M., AWAD, A., ELGHANNAM, D., ABDEL-GHAFFAR, H. & SOBH, M. 2016. Comparative Study of Allogenic and Xenogeneic Mesenchymal Stem Cells on Cisplatin-Induced Acute Kidney Injury in Sprague-Dawley Rats. *Stem Cell Res Ther*, 7, 126.

ASSAS, B., PENNOCK, J. & MIYAN, J. 2014. Calcitonin Gene-Related Peptide Is a Key Neurotransmitter in the Neuro-Immune Axis. *Front Neurosci*, 8, 23.

AURON, P. E., ROSENWASSER, L. J., MATSUSHIMA, K., COPELAND, T., DINARELLO, C. A., OPPENHEIM, J. J. & WEBB, A. C. 1985. Human and Murine Interleukin 1 Possess Sequence and Structural Similarities. *J Mol Cell Immunol*, 2, 169-77.

AUST, L., DEVLIN, B., FOSTER, S. J., HALVORSEN, Y. D. C., HICOK, K., DU LANEY, T., SEN, A., WILLINGMYRE, G. D. & GIMBLE, J. M. 2004. Yield of Human Adipose-Derived Adult Stem Cells from Liposuction Aspirates. *Cytotherapy*, 6, 7-14.

AYATOLLAHI, M., SALMANI, M. K., GERAMIZADEH, B., TABEI, S. Z., SOLEIMANI, M. & SANATI, M. H. 2012. Conditions to Improve Expansion of Human Mesenchymal Stem Cells Based on Rat Samples. *World J Stem Cells*, 4, 1-8.

AZIZ, M. T. A., WASSEF, M. A. A., AHMED, H. H., RASHED, L., MAHFOUZ, S., ALY, M. I., HUSSEIN, R. E. & ABDELAZIZ, M. 2014. The Role of Bone Marrow Derived-Mesenchymal Stem Cells in Attenuation of Kidney Function in Rats with Diabetic Nephropathy. *Diabetol Metab Syndr*, 6, 1.

BAH, T. 2009. Inkscape: Guide to a Vector Drawing Program (Digital Short Cut), Pearson education.

BALASUBRAMANIAN, S., VENUGOPAL, P., SUNDARRAJ, S., ZAKARIA, Z., MAJUMDAR, A. S. & TA, M. 2012. Comparison of Chemokine and Receptor Gene Expression between Wharton's Jelly and Bone Marrow-Derived Mesenchymal Stromal Cells. *Cytotherapy*, 14, 26-33.

BANERJEE, A., BIZZARO, D., BURRA, P., DI LIDDO, R., PATHAK, S., ARCIDIACONO, D., CAPPON, A., BO, P., CONCONI, M. T., CRESCENZI, M., PINNA, C. M., PARNIGOTTO, P. P., ALISON, M. R., STURNIOLO, G. C., D'INCA, R. & RUSSO, F. P. 2015. Umbilical Cord Mesenchymal Stem Cells Modulate Dextran Sulfate Sodium Induced Acute Colitis in Immunodeficient Mice. *Stem Cell Res Ther*, 6, 79.

BANKS, C., BATEMAN, A., PAYNE, R., JOHNSON, P. & SHERON, N. 2003. Chemokine Expression in IBD. Mucosal Chemokine Expression Is Unselectively Increased in Both Ulcerative Colitis and Crohn's Disease. *J Pathol*, 199, 28-35.

BARNHOORN, M., DE JONGE-MULLER, E., MOLENDIJK, I., VAN GULIJK, M., LEBBINK, O., JANSON, S., SCHOONDERWOERD, M., VAN DER HELM, D., VAN DER MEULEN-DE JONG, A., HAWINKELS, L. & VERSPAGET, H. 2018. Endoscopic Administration of Mesenchymal Stromal Cells Reduces Inflammation in Experimental Colitis. *Inflamm Bowel Dis*, 24, 1755-1767.

BARRETT, T., WILHITE, S. E., LEDOUX, P., EVANGELISTA, C., KIM, I. F., TOMASHEVSKY, M., MARSHALL, K. A., PHILLIPPY, K. H., SHERMAN, P. M. & HOLKO, M. 2012. NCBI GEO: Archive for Functional Genomics Data Sets—Update. *Nucleic Acids Res*, 41, 991-995.

BASSOTTI, G., VILLANACCI, V., FISOGNI, S., CADEI, M., DI FABIO, F. & SALERNI, B. 2007. Apoptotic Phenomena Are Not a Major Cause of Enteric Neuronal Loss in Constipated Patients with Dementia. *Neuropathology*, 27, 67-72.

BASSOTTI, G., VILLANACCI, V., NASCIMBENI, R., CADEI, M., FISOGNI, S., ANTONELLI, E., CORAZZI, N. & SALERNI, B. 2009. Enteric Neuroglial Apoptosis in Inflammatory Bowel Diseases. *J Crohn's Colitis*, 3, 264-270.

BASTIAN, M., HEYMANN, S. & JACOMY, M. 2009. Gephi: An Open Source Software for Exploring and Manipulating Networks. Proceedings of the Third International ICWSM Conference of the Association for the Advancement of Artificial Intelligence, 8, 361-362.

BAUMGART, D. C. & SANDBORN, W. J. 2012. Crohn's Disease. The Lancet, 380, 1590-1605.

BECK, P. L. & PODOLSKY, D. K. 1999. Growth Factors in Inflammatory Bowel Disease. *Inflamm Bowel Dis*, 5, 44-60.

BEDARD, M., SALIO, M. & CERUNDOLO, V. 2017. Harnessing the Power of Invariant Natural Killer T Cells in Cancer Immunotherapy. *Front Immunol*, 8, 1829-1829.

BELAI, A., BOULOS, P. B., ROBSON, T. & BURNSTOCK, G. 1997. Neurochemical Coding in the Small Intestine of Patients with Crohn's Disease. *Gut*, 40, 767-74.

BELKIND-GERSON, J., HOTTA, R., NAGY, N., THOMAS, A. R., GRAHAM, H., CHENG, L., SOLORZANO, J., NGUYEN, D., KAMIONEK, M., DIETRICH, J., CHERAYIL, B. J. & GOLDSTEIN, A. M. 2015. Colitis Induces Enteric Neurogenesis through a 5-HT4–Dependent Mechanism. *Inflamm Bowel Dis*, 21, 870-878.

BEN-AMI, E., BERRIH-AKNIN, S. & MILLER, A. 2011. Mesenchymal Stem Cells as an Immunomodulatory Therapeutic Strategy for Autoimmune Diseases. *Autoimmun Rev*, 10, 410-415.

BENDERRO, G. F., SUN, X., KUANG, Y. & LAMANNA, J. C. 2012. Decreased Vegf Expression and Microvascular Density, but Increased HIF-1 and 2alpha Accumulation and Epo Expression in Chronic Moderate Hyperoxia in the Mouse Brain. *Brain Res*, 1471, 46-55.

BENJAMINI, Y. & HOCHBERG, Y. 1995. Controlling the False Discovery Rate: A Practical and Powerful Approach to Multiple Testing. *J R Stat Soc Series B Stat Methodol*, 289-300.

BERGFELD, S. A., BLAVIER, L. & DECLERCK, Y. A. 2014. Bone Marrow–Derived Mesenchymal Stromal Cells Promote Survival and Drug Resistance in Tumor Cells. *Mol Cancer Ther*, 13, 962-975.

BERGHE, P. V., KENYON, J. L. & SMITH, T. K. 2002. Mitochondrial Ca2+ Uptake Regulates the Excitability of Myenteric Neurons. *J Neurosci*, 22, 6962-6971.

BERGLUND, A. K., FORTIER, L. A., ANTCZAK, D. F. & SCHNABEL, L. V. 2017. Immunoprivileged No More: Measuring the Immunogenicity of Allogeneic Adult Mesenchymal Stem Cells. *Stem Cell Res Ther*, 8, 288-288.

BERNARDAZZI, C., PÊGO, B. & DE SOUZA, H. S. P. 2016. Neuroimmunomodulation in the Gut: Focus on Inflammatory Bowel Disease. *Mediators Inflamm*, 2016.

BERNARDINI, N., SEGNANI, C., IPPOLITO, C., DE GIORGIO, R., COLUCCI, R., FAUSSONE-PELLEGRINI, M. S., CHIARUGI, M., CAMPANI, D., CASTAGNA, M., MATTII, L., BLANDIZZI, C. & DOLFI, A. 2012. Immunohistochemical Analysis of Myenteric Ganglia and Interstitial Cells of Cajal in Ulcerative Colitis. *J Cell Mol Med*, 16, 318-327.

BERNSTEIN, C. N., FRIED, M., KRABSHUIS, J., COHEN, H., ELIAKIM, R., FEDAIL, S., GEARRY, R., GOH, K., HAMID, S. & KHAN, A. G. 2010. World Gastroenterology Organization Practice Guidelines for the Diagnosis and Management of IBD in 2010. *Inflamm Bowel Dis*, 16, 112-124.

BERTRAND, P. P., BARAJAS-ESPINOSA, A., NESHAT, S., BERTRAND, R. L. & LOMAX, A. E. 2010. Analysis of Real-Time Serotonin (5-HT) Availability During Experimental Colitis in Mouse. *Am J Physiol Gastrointest Liver Physiol*, 298, G446-G455.

BHAT, N. R., ZHANG, P. & BHAT, A. N. 1999. Cytokine Induction of Inducible Nitric Oxide Synthase in an Oligodendrocyte Cell Line: Role of P38 Mitogen-Activated Protein Kinase Activation. *J Neurochem*, 72, 472-8.

BIANCO, F., BONORA, E., NATARAJAN, D., VARGIOLU, M., THAPAR, N., TORRESAN, F., GIANCOLA, F., BOSCHETTI, E., VOLTA, U., BAZZOLI, F., MAZZONI, M., SERI, M., CLAVENZANI, P., STANGHELLINI, V., STERNINI, C. & GIORGIO, R. D. 2016. Prucalopride Exerts Neuroprotection in Human Enteric Neurons. *Am J Physiol Gastrointest Liver Physiol*, 310, 768-775.

BIANCO, P., ROBEY, P. G. & SIMMONS, P. J. 2008. Mesenchymal Stem Cells: Revisiting History, Concepts, and Assays. *Cell stem cell*, 2, 313-319.

BIENERT, G. P., SCHJOERRING, J. K. & JAHN, T. P. 2006. Membrane Transport of Hydrogen Peroxide. *Biophys. Acta Rev. Biomembr*, 1758, 994-1003.

BIRBEN, E., SAHINER, U. M., SACKESEN, C., ERZURUM, S. & KALAYCI, O. 2012. Oxidative Stress and Antioxidant Defense. *World Allergy Organ J*, 5, 9-19.

BISHOP, A. E., POLAK, J. M., BRYANT, M., BLOOM, S. & HAMILTON, S. 1980. Abnormalities of Vasoactive Intestinal Polypeptide-Containing Nerves in Crohn's Disease. *Gastroenterology*, 79, 853-860.

BISWAS, S. K. 2016. Does the Interdependence between Oxidative Stress and Inflammation Explain the Antioxidant Paradox? *Oxid Med Cell Longev*, Article ID 5698931.

BODEN, E. K. & SNAPPER, S. B. 2008. Regulatory T Cells in Inflammatory Bowel Disease. *Curr Opin Gastroenterol*, 24, 733-41.

BOESMANS, W., GOMES, P., JANSSENS, J., TACK, J. & VANDEN BERGHE, P. 2008. Brain-Derived Neurotrophic Factor Amplifies Neurotransmitter Responses and Promotes Synaptic Communication in the Enteric Nervous System. *Gut*, 57, 314-22.

BOLTIN, D., PERETS, T. T., VILKIN, A. & NIV, Y. 2013. Mucin Function in Inflammatory Bowel Disease: An Update. *J Clin Gastroenterol*, 47, 106-11.

BONAB, M. M., ALIMOGHADDAM, K., TALEBIAN, F., GHAFFARI, S. H., GHAVAMZADEH, A. & NIKBIN, B. 2006. Aging of Mesenchymal Stem Cell *in vitro*. *BMC Cell Biol*, 7, 14.

BOSE, S. K., GIBSON, W., BULLARD, R. S. & DONALD, C. D. 2009. Pax2 Oncogene Negatively Regulates the Expression of the Host Defense Peptide Human Beta Defensin-1 in Prostate Cancer. *Mol Immunol*, 46, 1140-1148.

BOUCHEZ, G., SENSEBÉ, L., VOURC'H, P., GARREAU, L., BODARD, S., RICO, A., GUILLOTEAU, D., CHARBORD, P., BESNARD, J.-C. & CHALON, S. 2008. Partial Recovery of Dopaminergic Pathway after Graft of Adult Mesenchymal Stem Cells in a Rat Model of Parkinson's Disease. *Neurochem Int*, 52, 1332-1342.

BOURIN, P., BUNNELL, B. A., CASTEILLA, L., DOMINICI, M., KATZ, A. J., MARCH, K. L., REDL, H., RUBIN, J. P., YOSHIMURA, K. & GIMBLE, J. M. 2013. Stromal Cells from the Adipose Tissue-Derived Stromal Vascular Fraction and Culture Expanded Adipose Tissue-Derived Stromal/Stem Cells: A Joint Statement of the International Federation for Adipose Therapeutics and Science (IFATS) and the International Society for Cellular Therapy (ISCT). *Cytotherapy*, 15, 641-648.

BOUTET, E., LIEBERHERR, D., TOGNOLLI, M., SCHNEIDER, M. & BAIROCH, A. 2007. Uniprotkb/Swiss-Prot. In: EDWARDS, D. (ed.) Plant Bioinformatics: Methods and Protocols. Totowa, NJ: Humana Press.

BOYER, L., GHOREISHI, M., TEMPLEMAN, V., VALLANCE, B. A., BUCHAN, A. M., JEVON, G. & JACOBSON, K. 2005. Myenteric Plexus Injury and Apoptosis in Experimental Colitis. *Auton Neurosci*, 117, 41-53.

BOYER, L., SIDPRA, D., JEVON, G., BUCHAN, A. M. & JACOBSON, K. 2007. Differential Responses of Vipergic and Nitrergic Neurons in Paediatric Patients with Crohn's Disease. *Auton Neurosci*, 134, 106-114.

BRAMLAGE, C. P., HÄUPL, T., KAPS, C., UNGETHÜM, U., KRENN, V., PRUSS, A., MÜLLER, G. A., STRUTZ, F. & BURMESTER, G.-R. 2006. Decrease in Expression of Bone Morphogenetic Proteins 4 and 5 in Synovial Tissue of Patients with Osteoarthritis and Rheumatoid Arthritis. *Arthritis Res Ther*, 8, 3: R58.

BRENNA, Ø., FURNES, M. W., DROZDOV, I., VAN BEELEN GRANLUND, A., FLATBERG, A., SANDVIK, A. K., ZWIGGELAAR, R. T., MÅRVIK, R., NORDRUM, I. S. & KIDD, M. 2013. Relevance of TNBS-Colitis in Rats: A Methodological Study with Endoscopic, Histologic and Transcriptomic Characterization and Correlation to IBD. *PLoS One*, 8, e54543.

BRESSENOT, A., CHEVAUX, J. B., WILLIET, N., OUSSALAH, A., GERMAIN, A., GAUCHOTTE, G., WISSLER, M. P., VIGNAUD, J. M., BRESLER, L., BIGARD, M. A., PLENAT, F., GUEANT, J. L. & PEYRIN-BIROULET, L. 2013. Submucosal Plexitis as a Predictor of Postoperative Surgical Recurrence in Crohn's Disease. *Inflamm Bowel Dis*, 19, 1654-61.

BROWN, I. A. M., MCCLAIN, J. L., WATSON, R. E., PATEL, B. A. & GULBRANSEN, B. D. 2016. Enteric Glia Mediate Neuron Death in Colitis through Purinergic Pathways That Require Connexin-43 and Nitric Oxide. *Cell Mol Gastroenterol Hepatol*, 2, 77-91.

BUBENHEIMER, R. K., BROWN, I. A. M., FRIED, D. E., MCCLAIN, J. L. & GULBRANSEN, B. D. 2016. Sirtuin-3 Is Expressed by Enteric Neurons but It Does Not Play a Major Role in Their Regulation of Oxidative Stress. *Front Cell Neurosci*, 10, 73.

BUISSON, A., VAZEILLE, E., MINET-QUINARD, R., GOUTTE, M., BOUVIER, D., GOUTORBE, F., PEREIRA, B., BARNICH, N. & BOMMELAER, G. 2018. Fecal Matrix Metalloprotease-9 and Lipocalin-2 as Biomarkers in Detecting Endoscopic Activity in Patients with Inflammatory Bowel Diseases. *J Clin Gastroenterol*, 52, e53-e62.

BULLARD, R. S., GIBSON, W., BOSE, S. K., BELGRAVE, J. K., EADDY, A. C., WRIGHT, C. J., HAZEN-MARTIN, D. J., LAGE, J. M., KEANE, T. E. & GANZ, T. A. 2008. Functional Analysis of the Host Defense Peptide Human Beta Defensin-1: New Insight into Its Potential Role in Cancer. *Mol Immunol*, 45, 839-848.

BURGUEÑO, J. F., BARBA, A., EYRE, E., ROMERO, C., NEUNLIST, M. & FERNÁNDEZ, E. 2016. TLR2 and TLR9 Modulate Enteric Nervous System Inflammatory Responses to Lipopolysaccharide. *J Neuroinflammation*, 13, 187.

BUSCH, R. A., HENEGHAN, A. F., PIERRE, J. F., WANG, X. & KUDSK, K. A. 2014. The Enteric Nervous System Neuropeptide, Bombesin, Reverses Innate Immune Impairments During Parenteral Nutrition. *Ann Surg*, 260, 432-444.

CAI, Y., ZOU, Z., LIU, L., CHEN, S., CHEN, Y., LIN, Z., SHI, K., XU, L. & CHEN, Y. 2015. Bone Marrow-Derived Mesenchymal Stem Cells Inhibits Hepatocyte Apoptosis after Acute Liver Injury. *Int J Clin Exp Pathol*, 8, 107-16.

CAILOTTO, C., COSTES, L., VAN DER VLIET, J., VAN BREE, S., VAN HEERIKHUIZE, J., BUIJS, R. & BOECKXSTAENS, G. 2012. Neuroanatomical Evidence Demonstrating the Existence of the Vagal Anti-Inflammatory Reflex in the Intestine. *Neurogastroenterol Motil*, 24, 191-200.

CALIÓ, M. L., MARINHO, D. S., KO, G. M., RIBEIRO, R. R., CARBONEL, A. F., OYAMA, L. M., ORMANJI, M., GUIRAO, T. P., CALIÓ, P. L. & REIS, L. A. 2014. Transplantation of Bone Marrow Mesenchymal Stem Cells Decreases Oxidative Stress, Apoptosis, and Hippocampal Damage in Brain of a Spontaneous Stroke Model. *Free Radic Biol Med*, 70, 141-154.

CAMACHO, C., COULOURIS, G., AVAGYAN, V., MA, N., PAPADOPOULOS, J., BEALER, K. & MADDEN, T. L. 2009. Blast+: Architecture and Applications. *BMC Bioinformatics*, 10, 421.

CAMPBELL, E. L., BRUYNINCKX, W. J., KELLY, C. J., GLOVER, L. E., MCNAMEE, E. N., BOWERS, B. E., BAYLESS, A. J., SCULLY, M., SAEEDI, B. J., GOLDEN-MASON, L., EHRENTRAUT, S. F., CURTIS, V. F., BURGESS, A., GARVEY, J. F., SORENSEN, A., NEMENOFF, R., JEDLICKA, P., TAYLOR, C. T., KOMINSKY, D. J. & COLGAN, S. P. 2014. Transmigrating Neutrophils Shape the Mucosal Microenvironment through Localized Oxygen Depletion to Influence Resolution of Inflammation. *Immunity*, 40, 66-77.

CAO, S. S. 2015. Endoplasmic Reticulum Stress and Unfolded Protein Response in Inflammatory Bowel Disease. *Inflamm Bowel Dis*, 21, 636-44.

CAO, Y., ZHANG, X., SHANG, W., XU, J., WANG, X., HU, X., AO, Y. & CHENG, H. 2013. Proinflammatory Cytokines Stimulate Mitochondrial Superoxide Flashes in Articular Chondrocytes *in vitro* and in Situ. *PLoS One*, 8, e66444.

CAPLAN, A. I. 1991. Mesenchymal Stem Cells. *J Orthop Res*, 9, 641-50.

CAPOCCIA, E., CIRILLO, C., GIGLI, S., PESCE, M., D'ALESSANDRO, A., CUOMO, R., SARNELLI, G., STEARDO, L. & ESPOSITO, G. 2015. Enteric Glia: A New Player in Inflammatory Bowel Diseases. *Int J Immunopathol Pharmacol*, 28, 443-51.

CARDINALE, C. J., WEI, Z., LI, J., ZHU, J., GU, M., BALDASSANO, R. N., GRANT, S. F. A. & HAKONARSON, H. 2014. Transcriptome Profiling of Human Ulcerative Colitis Mucosa Reveals Altered Expression of Pathways Enriched in Genetic Susceptibility Loci. *PLoS One*, 9, e96153.

CASHMAN, J. R. & ZHANG, J. 2006. Human Flavin-Containing Monooxygenases. *Annu Rev Pharmacol Toxicol*, 46, 65-100.

CASTELO-BRANCO, M. T., SOARES, I. D., LOPES, D. V., BUONGUSTO, F., MARTINUSSO, C. A., DO ROSARIO JR, A., SOUZA, S. A., GUTFILEN, B., FONSECA, L. M. B. & ELIA, C. 2012. Intraperitoneal but Not Intravenous Cryopreserved Mesenchymal Stromal Cells Home to the Inflamed Colon and Ameliorate Experimental Colitis. *PLoS One*, 7, e33360.

CHAMBERLAIN, G., FOX, J., ASHTON, B. & MIDDLETON, J. 2007. Concise Review: Mesenchymal Stem Cells: Their Phenotype, Differentiation Capacity, Immunological Features, and Potential for Homing. *Stem Cells*, 25, 2739-2749.

CHAN, P. H., KAWASE, M., MURAKAMI, K., CHEN, S. F., LI, Y., CALAGUI, B., REOLA, L., CARLSON, E. & EPSTEIN, C. J. 1998. Overexpression of Sod1 in Transgenic Rats Protects Vulnerable Neurons against Ischemic Damage after Global Cerebral Ischemia and Reperfusion. *J Neurosci*, 18, 8292-8299.

CHANDRASEKHARAN, B., ANITHA, M., BLATT, R., SHAHNAVAZ, N., KOOBY, D., STALEY, C., MWANGI, S., JONES, D. P., SITARAMAN, S. V. & SRINIVASAN, S. 2011. Colonic Motor Dysfunction in Human Diabetes Is Associated with Enteric Neuronal Loss and Increased Oxidative Stress. *Neurogastroenterol Motil*, 23, 131-138.

CHANDRASEKHARAN, B., BALA, V., KOLACHALA, V. L., VIJAY-KUMAR, M., JONES, D., GEWIRTZ, A. T., SITARAMAN, S. V. & SRINIVASAN, S. 2008. Targeted Deletion of Neuropeptide Y (NPY) Modulates Experimental Colitis. *PLoS One*, 3, e3304.

CHANG, E., HORNICK, K., FRITZ, K. I., MISHRA, O. P. & DELIVORIA-PAPADOPOULOS, M. 2007. Effect of Hyperoxia on Cortical Neuronal Nuclear Function and Programmed Cell Death Mechanisms. *Neurochem Res*, 32, 1142-9.

CHAO, K., ZHANG, S., QIU, Y., CHEN, X., ZHANG, X., CAI, C., PENG, Y., MAO, R., PEVSNER-FISCHER, M., BEN-HORIN, S., ELINAV, E., ZENG, Z., CHEN, B., HE, Y., XIANG, A. P. & CHEN, M. 2016. Human Umbilical Cord-Derived Mesenchymal Stem Cells Protect against Experimental Colitis Via CD5(+) B Regulatory Cells. *Stem Cell Res Ther*, 7, 109.

CHASSAING, B., AITKEN, J. D., MALLESHAPPA, M. & VIJAY-KUMAR, M. 2014. Dextran Sulfate Sodium (DSS)-Induced Colitis in Mice. *Curr Protoc Immunol*, 104, 15.25. 1-15.25. 14.

CHAVAN, S. S., PAVLOV, V. A. & TRACEY, K. J. 2017. Mechanisms and Therapeutic Relevance of Neuro-Immune Communication. *Immunity*, 46, 927-942.

CHEN, L., TREDGET, E. E., WU, P. Y. & WU, Y. 2008. Paracrine Factors of Mesenchymal Stem Cells Recruit Macrophages and Endothelial Lineage Cells and Enhance Wound Healing. *PLoS One*, 3, e1886.

CHEN, L., YOU, Q., HU, L., GAO, J., MENG, Q., LIU, W., WU, X. & XU, Q. 2018a. The Antioxidant Procyanidin Reduces Reactive Oxygen Species Signalling in Macrophages and Ameliorates Experimental Colitis in Mice. *Front Immunol*, 8, 1910.

CHEN, M.-F., LIN, C.-T., CHEN, W.-C., YANG, C.-T., CHEN, C.-C., LIAO, S.-K., LIU, J. M., LU, C.-H. & LEE, K.-D. 2006. The Sensitivity of Human Mesenchymal Stem Cells to Ionizing Radiation. *Int J Radiat Oncol Biol Phys*, 66, 244-253.

CHEN, P.-M., GREGERSEN, H. & ZHAO, J.-B. 2015. Advanced Glycation End-Product Expression Is Upregulated in the Gastrointestinal Tract of Type 2 Diabetic Rats. *World J Diabetes*, 6, 662-672.

CHEN, Q.-Q., YAN, L., WANG, C.-Z., WANG, W.-H., SHI, H., SU, B.-B., ZENG, Q.-H., DU, H.-T. & WAN, J. 2013. Mesenchymal Stem Cells Alleviate TNBS-Induced Colitis by Modulating Inflammatory and Autoimmune Responses. *World J Gastroenterol*, 19, 4702-4717.

CHEN, Y., AZAD, M. B. & GIBSON, S. B. 2009. Superoxide Is the Major Reactive Oxygen Species Regulating Autophagy. *Cell Death Differ*, 16, 1040-52.

CHEN, Z., CHEN, Q., DU, H., XU, L. & WAN, J. 2018b. Mesenchymal Stem Cells and Cxc Chemokine Receptor 4 Overexpression Improved the Therapeutic Effect on Colitis Via Mucosa Repair. *Exp Ther Med*, 16, 821-829.

CHENG, C. & ZOCHODNE, D. W. 2003. Sensory Neurons with Activated Caspase-3 Survive Long-Term Experimental Diabetes. *Diabetes*, 52, 2363-2371.

CHENG, W., SU, J., HU, Y., HUANG, Q., SHI, H., WANG, L. & REN, J. 2017. Interleukin-25 Primed Mesenchymal Stem Cells Achieve Better Therapeutic Effects on Dextran Sulfate Sodium-Induced Colitis Via Inhibiting Th17 Immune Response and Inducing T Regulatory Cell Phenotype. *Am J Transl Res*, 9, 4149-4160.

CHERNAJOVSKY, Y. & ROBBINS, P. D. 2011. Gene Therapy for Autoimmune and Inflammatory Diseases, Birkhäuser.

CHINNADURAI, G., VIJAYALINGAM, S. & GIBSON, S. B. 2009. BNIP3 Subfamily BH3-Only Proteins: Mitochondrial Stress Sensors in Normal and Pathological Functions. *Oncogene*, 27, Suppl 1:114-127.

CHO, Y. B., LEE, W. Y., PARK, K. J., KIM, M., YOO, H.-W. & YU, C. S. 2013. Autologous Adipose Tissue-Derived Stem Cells for the Treatment of Crohns Fistula: A Phase I Clinical Study. *Cell Transplant*, 22, 279-285.

CHO, Y. B., PARK, K. J., YOON, S. N., SONG, K. H., KIM, D. S., JUNG, S. H., KIM, M., JEONG, H. Y. & YU, C. S. 2015. Long-Term Results of Adipose-Derived Stem Cell Therapy for the Treatment of Crohn's Fistula. *Stem Cells Transl Med*, 4, 532-537.

CHOI, D. W. 1995. Calcium: Still Center-Stage in Hypoxic-Ischemic Neuronal Death. *Trends Neurosci*, 18, 58-60.

CHOI, K., KIM, J., KIM, G. W. & CHOI, C. 2009. Oxidative Stress-Induced Necrotic Cell Death via Mitochondira-Dependent Burst of Reactive Oxygen Species. *Curr Neurovasc Res*, 6, 213-22.

CHOI, K. M., GIBBONS, S. J., NGUYEN, T. V., STOLTZ, G. J., LURKEN, M. S., ORDOG, T., SZURSZEWSKI, J. H. & FARRUGIA, G. 2008. Heme Oxygenase-1 Protects Interstitial Cells of Cajal from Oxidative Stress and Reverses Diabetic Gastroparesis. *Gastroenterology*, 135, 2055-2064.

CHONG, P. P., SELVARATNAM, L., ABBAS, A. A. & KAMARUL, T. 2012. Human Peripheral Blood Derived Mesenchymal Stem Cells Demonstrate Similar Characteristics and Chondrogenic Differentiation Potential to Bone Marrow Derived Mesenchymal Stem Cells. *J Orthop Res*, 30, 634-42.

CHONG, W. C., SHASTRI, M. D. & ERI, R. 2017. Endoplasmic Reticulum Stress and Oxidative Stress: A Vicious Nexus Implicated in Bowel Disease Pathophysiology. *Int J Mol Sci*, 18, 771.

CHOUDHERY, M. S., BADOWSKI, M., MUISE, A., PIERCE, J. & HARRIS, D. T. 2014. Donor Age Negatively Impacts Adipose Tissue-Derived Mesenchymal Stem Cell Expansion and Differentiation. *J Transl Med*, 12, 8.

CICCOCIOPPO, R., BERNARDO, M. E., SGARELLA, A., MACCARIO, R., AVANZINI, M. A., UBEZIO, C., MINELLI, A., ALVISI, C., VANOLI, A. & CALLIADA, F. 2011. Autologous Bone

Marrow-Derived Mesenchymal Stromal Cells in the Treatment of Fistulising Crohn's Disease. *Gut*, 60, 788-798.

CIORBA, M. A. 2013. Indoleamine 2, 3 Dioxygenase (IDO) in Intestinal Disease. *Curr Opin Gastroenterol*, 29, 146-152.

CIRILLO, C., SARNELLI, G., ESPOSITO, G., GROSSO, M., PETRUZZELLI, R., IZZO, P., CALI, G., D'ARMIENTO, F. P., ROCCO, A., NARDONE, G., IUVONE, T., STEARDO, L. & CUOMO, R. 2009. Increased Mucosal Nitric Oxide Production in Ulcerative Colitis Is Mediated in Part by the Enteroglial-Derived S100B Protein. *Neurogastroenterol Motil*, 21, 1209.

CIRILLO, C., SARNELLI, G., ESPOSITO, G., TURCO, F., STEARDO, L. & CUOMO, R. 2011. S100b Protein in the Gut: The Evidence for Enteroglial-Sustained Intestinal Inflammation. *World J Gastroenterol*, 17, 1261-1266.

COHEN-CORY, S., KIDANE, A. H., SHIRKEY, N. J. & MARSHAK, S. 2010. Brain-Derived Neurotrophic Factor and the Development of Structural Neuronal Connectivity. *Dev Neurobiol*, 70, 271-288.

COLOMBEL, J. F., SANDBORN, W. J., REINISCH, W., MANTZARIS, G. J., KORNBLUTH, A., RACHMILEWITZ, D., LICHTIGER, S., D'HAENS, G., DIAMOND, R. H., BROUSSARD, D. L., TANG, K. L., VAN DER WOUDE, C. J. & RUTGEERTS, P. 2010. Infliximab, Azathioprine, or Combination Therapy for Crohn's Disease. *N Engl J Med*, 362, 1383-1395.

CONRAD, M. & SATO, H. 2012. The Oxidative Stress-Inducible Cystine/Glutamate Antiporter, System X C−: Cystine Supplier and Beyond. *Amino Acids*, 42, 231-246.

COQUENLORGE, S., DUCHALAIS, E., CHEVALIER, J., COSSAIS, F., ROLLI-DERKINDEREN, M. & NEUNLIST, M. 2014. Modulation of Lipopolysaccharide-Induced Neuronal Response by Activation of the Enteric Nervous System. *J Neuroinflammation*, 11, 202.

CORAZZIARI, E. S. 2009. Intestinal Mucus Barrier in Normal and Inflamed Colon. *J Pediatr Gastroenterol Nutr*, 48, Suppl 2, 54-55.

COSTA, M. & BROOKES, S. 2008. Architecture of Enteric Neural Circuits Involved in Intestinal Motility. *Eur Rev Med Pharmacol Sci*, 12, 3-19.

COSTA, M., BROOKES, S. J. H. & HENNIG, G. W. 2000. Anatomy and Physiology of the Enteric Nervous System. *Gut*, 47, Suppl 4, 15-19.

COTTONE, M. & CRISCUOLI, V. 2010. Infliximab to Treat Crohn's Disease: An Update. *Clin Exp Gastroenterol*, 4, 227-238.

COULTAS, L., PELLEGRINI, M., VISVADER, J., LINDEMAN, G., CHEN, L., ADAMS, J., HUANG, D. & STRASSER, A. 2003. Bfk: A Novel Weakly Proapoptotic Member of the Bcl-2 Protein Family with a BH3 and a BH2 Region. *Cell Death Differ*, 10, 185-192.

CRISTOFALO, V. J., ALLEN, R. G., PIGNOLO, R. J., MARTIN, B. G. & BECK, J. C. 1998. Relationship between Donor Age and the Replicative Lifespan of Human Cells in Culture: A Reevaluation. *Proc Natl Acad Sci U S A*, 95, 10614-10619.

CROHN'S AND COLITIS AUSTRALIA. 2013. PricewaterhouseCoopers (PwC) Australia report: Improving Inflammatory Bowel Disease Care across Australia [Online]. Available https://www.crohnsandcolitis.com.au/site/wp-content/uploads/PwC-report-2013.pdf [Viewed 7/12/2018] [Accessed].

CROWELL, M. D. 2004. Role of Serotonin in the Pathophysiology of the Irritable Bowel Syndrome. *Br J Pharmacol*, 141, 1285-1293.

CUI, Y., XU, N., XU, W. & XU, G. 2017. Mesenchymal Stem Cells Attenuate Hydrogen Peroxide-Induced Oxidative Stress and Enhance Neuroprotective Effects in Retinal Ganglion Cells. *In vitro Cell Dev Biol-Animal*, 53, 328-335.

CURKOVIC, I., EGBRING, M. & KULLAK-UBLICK, G. A. 2013. Risks of Inflammatory Bowel Disease Treatment with Glucocorticosteroids and Aminosalicylates. *Dig Dis*, 31, 368-373.

CURY, D. B., DE OLIVEIRA, R. A., DALBONI, M. A., REIS, L. A., VESOLATO, C., PEREIRA, E. & SCHOR, N. 2016. Comparative Study of Intravenous and Topical Administration of Mesenchymal Stem Cells in Experimental Colitis. *Transl Res*, 1, 79-82.

CUZZOCREA, S., MAZZON, E., DUGO, L., CAPUTI, A. P., RILEY, D. P. & SALVEMINI, D. 2001. Protective Effects of M40403, a Superoxide Dismutase Mimetic, in a Rodent Model of Colitis. *Eur J Pharmacol*, 432, 79-89.

D'AGOSTINO, D. P., PUTNAM, R. W. & DEAN, J. B. 2007. Superoxide (*O2-) Production in Ca1 Neurons of Rat Hippocampal Slices Exposed to Graded Levels of Oxygen. *J Neurophysiol*, 98, 1030-1041

D'AMELIO, M., CAVALLUCCI, V. & CECCONI, F. 2010. Neuronal Caspase-3 Signalling: Not Only Cell Death. *Cell Death Differ*, 17, 1104-14.

D'INCA, R., CARDIN, R., BENAZZATO, L., ANGRIMAN, I., MARTINES, D. & STURNIOLO, G. C. 2004. Oxidative DNA Damage in the Mucosa of Ulcerative Colitis Increases with Disease Duration and Dysplasia. *Inflamm Bowel Dis*, 10, 23-7.

DA COSTA GONÇALVES, F., GRINGS, M., NUNES, N. S., PINTO, F. O., GARCEZ, T. N. A., VISIOLI, F., LEIPNITZ, G. & PAZ, A. H. 2017. Antioxidant Properties of Mesenchymal Stem Cells against Oxidative Stress in a Murine Model of Colitis. *Biotechnol Lett*, 39, 613-622.

DA SILVA MEIRELLES, L., CHAGASTELLES, P. C. & NARDI, N. B. 2006. Mesenchymal Stem Cells Reside in Virtually All Post-Natal Organs and Tissues. *J Cell Sci*, 119, 2204-2213.

DELGADO, M. 2003. VIP: A Very Important Peptide in T Helper Differentiation. *Trends Immunol*, 24, 221-224.

DAN DUNN, J., ALVAREZ, L. A. J., ZHANG, X. & SOLDATI, T. 2015. Reactive Oxygen Species and Mitochondria: A Nexus of Cellular Homeostasis. *Redox Biol*, 6, 472-485.

DASHDORJ, A., KR, J., LIM, S., JO, A., NGUYEN, M. N., HA, J., YOON, K.-S., KIM, H. J., PARK, J.-H., MURPHY, M. P. & KIM, S. S. 2013. Mitochondria-Targeted Antioxidant Mitoq Ameliorates Experimental Mouse Colitis by Suppressing NLRP3 Inflammasome-Mediated Inflammatory Cytokines. *BMC Med*, 11, 178-178.

DAVÉ, S. H., TILSTRA, J. S., MATSUOKA, K., LI, F., DEMARCO, R. A., BEER-STOLZ, D., SEPULVEDA, A. R., FINK, M. P., LOTZE, M. T. & PLEVY, S. E. 2009. Ethyl Pyruvate Decreases HMGB1 Release and Ameliorates Murine Colitis. *J Leukoc Biol*, 86, 633-643.

DAVIS, A. S., ZHAO, H., SUN, G. H., SAPOLSKY, R. M. & STEINBERG, G. K. 2007. Gene Therapy Using Sod1 Protects Striatal Neurons from Experimental Stroke. *Neurosci Lett*, 411, 32-36.

DE AGUIAR, C. F., CASTOLDI, A., ANDRADE-OLIVEIRA, V., IGNACIO, A., DA CUNHA, F. F., FELIZARDO, R. J. F., BASSI, Ê. J., CÂMARA, N. O. S. & DE ALMEIDA, D. C. 2018. Mesenchymal Stromal Cells Modulate Gut Inflammation in Experimental Colitis. *Inflammopharmacology*, 26, 251-260.

DE DEKEN, X., CORVILAIN, B., DUMONT, J. E. & MIOT, F. 2014. Roles of Duox-Mediated Hydrogen Peroxide in Metabolism, Host Defense, and Signalling. *Antioxid Redox Signal*, 20, 2776-2793.

DE FONTGALLAND, D., BROOKES, S. J., GIBBINS, I., SIA, T. C. & WATTCHOW, D. A. 2014. The Neurochemical Changes in the Innervation of Human Colonic Mesenteric and Submucosal Blood Vessels in Ulcerative Colitis and Crohn's Disease. *Neurogastroenterol Motil*, 26, 731-744.

DE GIORGIO, R., BARBARA, G., FURNESS, J. B. & TONINI, M. 2007. Novel Therapeutic Targets for Enteric Nervous System Disorders. *Trends Pharmacol Sci*, 28, 473-481.

DE GODOY, M. A., SARAIVA, L. M., DE CARVALHO, L. R., VASCONCELOS-DOS-SANTOS, A., BEIRAL, H. J., RAMOS, A. B., DE PAULA SILVA, L. R., LEAL, R. B., MONTEIRO, V. H. & BRAGA, C. V. 2018. Mesenchymal Stem Cells and Cell-Derived Extracellular Vesicles Protect Hippocampal Neurons from Oxidative Stress and Synapse Damage Induced by Amyloid-B Oligomers. *J Biol Chem*, 293, 1957-1975.

DE JONG, E. C., VIEIRA, P. L., KALINSKI, P., SCHUITEMAKER, J. H., TANAKA, Y., WIERENGA, E. A., YAZDANBAKHSH, M. & KAPSENBERG, M. L. 2002. Microbial Compounds Selectively Induce Th1 Cell-Promoting or Th2 Cell-Promoting Dendritic Cells *in vitro* with Diverse Th Cell-Polarizing Signals. *J Immunol*, 168, 1704-9.

DE JONGE, W. J. 2013. The Gut's Little Brain in Control of Intestinal Immunity. *ISRN gastroenterol*, 630159. doi: 10.1155/2013/630159.

DE LA PORTILLA, F., ALBA, F., GARCÍA-OLMO, D., HERRERÍAS, J., GONZÁLEZ, F. & GALINDO, A. 2013. Expanded Allogeneic Adipose-Derived Stem Cells (Eascs) for the Treatment of Complex Perianal Fistula in Crohn's Disease: Results from a Multicenter Phase I/IIa Clinical Trial. *Int J Colorectal Dis*, 28, 313-323.

DE LA PORTILLA, F., YUSTE, Y., PEREIRA, S., OLANO, C., MAESTRE, M. V. & PADILLO, F. J. 2018. Local Mesenchymal Stem Cell Therapy in Experimentally Induced Colitis in the Rat. *Int J Stem Cells*, 11, 39-47.

DE LISLE, R. C. & BOROWITZ, D. 2013. The Cystic Fibrosis Intestine. *Cold Spring Harb Perspect Med*, 3, a009753.

DE RIDDER, L., TURNER, D., WILSON, D. C., KOLETZKO, S., MARTIN-DE-CARPI, J., FAGERBERG, U. L., SPRAY, C., SLADEK, M., SHAOUL, R. & ROMA-GIANNIKOU, E. 2014. Malignancy and Mortality in Pediatric Patients with Inflammatory Bowel Disease: A Multinational Study from the Porto Pediatric IBD Group. *Inflamm Bowel Dis*, 20, 291-300.

DE SCHEPPER, S., STAKENBORG, N., MATTEOLI, G., VERHEIJDEN, S. & BOECKXSTAENS, G. E. 2018. Muscularis Macrophages: Key Players in Intestinal Homeostasis and Disease. *Cell Immunol*, 330, 142-150.

DE VADDER, F., GRASSET, E., HOLM, L. M., KARSENTY, G., MACPHERSON, A. J., OLOFSSON, L. E. & BÄCKHED, F. 2018. Gut Microbiota Regulates Maturation of the Adult Enteric Nervous System Via Enteric Serotonin Networks. *Proc Natl Acad Sci U S A*, 25, 6458-6463.

DE VOOGD, F. A., GEARRY, R. B., MULDER, C. J. & DAY, A. S. 2016. Osteoprotegerin: A Novel Biomarker for Inflammatory Bowel Disease and Gastrointestinal Carcinoma. *J Gastroenterol Hepatol*, 31, 1386-92.

DEGRAVE, W., SIMONS, G., DEVOS, R., PLAETINCK, G., REMAUT, E., TAVERNIER, J. & FIERS, W. 1986. Cloning and Structure of a Mouse Interleukin-2 Chromosomal Gene. *Mol Biol Rep*, 11, 57-61.

DEL PILAR MARTÍNEZ-MONTIEL, M., GÓMEZ-GÓMEZ, G. J. & FLORES, A. I. 2014. Therapy with Stem Cells in Inflammatory Bowel Disease. *World J Gastroenterol*, 20, 1211-1227.

DENNIS, G., SHERMAN, B. T., HOSACK, D. A., YANG, J., GAO, W., LANE, H. C. & LEMPICKI, R. A. 2003. DAVID: Database for Annotation, Visualization, and Integrated Discovery. *Genome Biol*, 4, R60.

DESANTIAGO, J., BARE, D. J. & BANACH, K. 2013. Ischemia/Reperfusion Injury Protection by Mesenchymal Stem Cell Derived Antioxidant Capacity. *Stem Cells Dev*, 22, 2497-2507.

DHERE, T., COPLAND, I., GARCIA, M., CHIANG, K., CHINNADURAI, R., PRASAD, M., GALIPEAU, J. & KUGATHASAN, S. 2016. The Safety of Autologous and Metabolically Fit Bone

Marrow Mesenchymal Stromal Cells in Medically Refractory Crohn's Disease–a Phase 1 Trial with Three Doses. *Aliment Pharmacol Ther*, 44, 471-481.

DHILLON, S. S., MASTROPAOLO, L. A., MURCHIE, R., GRIFFITHS, C., THONI, C., ELKADRI, A., XU, W., MACK, A., WALTERS, T., GUO, C., MACK, D., HUYNH, H., BAKSH, S., SILVERBERG, M. S., BRUMELL, J. H., SNAPPER, S. B. & MUISE, A. M. 2014. Higher Activity of the Inducible Nitric Oxide Synthase Contributes to Very Early Onset Inflammatory Bowel Disease. *Clin Transl Gastroenterol*, 5, e46.

DI GIROLAMO, G., FARINA, M., RIBERIO, M. L., OGANDO, D., AISEMBERG, J., DE LOS SANTOS, A. R., MARTI, M. L. & FRANCHI, A. M. 2003. Effects of Cyclooxygenase Inhibitor Pretreatment on Nitric Oxide Production, nNOS and iNOS Expression in Rat Cerebellum. *Br J Pharmacol*, 139, 1164-70.

DIETZ, A. B., DOZOIS, E. J., FLETCHER, J. G., BUTLER, G. W., RADEL, D., LIGHTNER, A. L., DAVE, M., FRITON, J., NAIR, A., CAMILLERI, E. T., DUDAKOVIC, A., VAN WIJNEN, A. J. & FAUBION, W. A. 2017. Autologous Mesenchymal Stem Cells, Applied in a Bioabsorbable Matrix, for Treatment of Perianal Fistulas in Patients with Crohn's Disease. *Gastroenterology*, 153, 59-62.

DIJKSTRA, G., MOSHAGE, H., VAN DULLEMEN, H. M., DE JAGER-KRIKKEN, A., TIEBOSCH, A., KLEIBEUKER, J. H., JANSEN, P. L. & VAN GOOR, H. 1998. Expression of Nitric Oxide Synthases and Formation of Nitrotyrosine and Reactive Oxygen Species in Inflammatory Bowel Disease. *J Pathol*, 186, 416-421.

DMITRIEVA, R. I., MINULLINA, I. R., BILIBINA, A. A., TARASOVA, O. V., ANISIMOV, S. V. & ZARITSKEY, A. Y. 2012. Bone Marrow-and Subcutaneous Adipose Tissue-Derived Mesenchymal Stem Cells: Differences and Similarities. *Cell Cycle*, 11, 377-383.

DOBIN, A., DAVIS, C. A., SCHLESINGER, F., DRENKOW, J., ZALESKI, C., JHA, S., BATUT, P., CHAISSON, M. & GINGERAS, T. R. 2013. Star: Ultrafast Universal RNA-Seq Aligner. *Bioinformatics*, 29, 15-21.

DOBOLYI, A., VINCZE, C., PAL, G. & LOVAS, G. 2012. The Neuroprotective Functions of Transforming Growth Factor Beta Proteins. *Int J Mol Sci*, 13, 8219-8258.

DOMINICI, M., LE BLANC, K., MUELLER, I., SLAPER-CORTENBACH, I., MARINI, F., KRAUSE, D., DEANS, R., KEATING, A., PROCKOP, D. & HORWITZ, E. 2006. Minimal Criteria for Defining Multipotent Mesenchymal Stromal Cells. The International Society for Cellular Therapy Position Statement. *Cytotherapy*, 8, 315-317.

DONNELLY, J. M., ENGEVIK, A., FENG, R., XIAO, C., BOIVIN, G. P., LI, J., HOUGHTON, J., ZAVROS, Y. & ZAVROS, Y. 2014. Mesenchymal Stem Cells Induce Epithelial Proliferation within the Inflamed Stomach. *Am J Physiol Gastrointest Liver Physiol*, 12, 1075-1088.

DOROFEYEV, A. E., VASILENKO, I. V., RASSOKHINA, O. A. & KONDRATIUK, R. B. 2013. Mucosal Barrier in Ulcerative Colitis and Crohn's Disease. *Gastroenterol Res Pract*, 431231.

DOWNEN, M., AMARAL, T. D., HUA, L. L., ZHAO, M. L. & LEE, S. C. 1999. Neuronal Death in Cytokine-Activated Primary Human Brain Cell Culture: Role of Tumor Necrosis Factor-Alpha. *Glia*, 28, 114-127.

DUIJVESTEIN, M., VOS, A. C. W., ROELOFS, H., WILDENBERG, M. E., WENDRICH, B. B., VERSPAGET, H. W., KOOY-WINKELAAR, E. M., KONING, F., ZWAGINGA, J. J. & FIDDER, H. H. 2010. Autologous Bone Marrow-Derived Mesenchymal Stromal Cell Treatment for Refractory Luminal Crohn's Disease: Results of a Phase I Study. *Gut*, 59, 1662-1669.

DUIJVESTEIN, M., WILDENBERG, M. E., WELLING, M. M., HENNINK, S., MOLENDIJK, I., VAN ZUYLEN, V. L., BOSSE, T., VOS, A. C. W., DE JONGE-MULLER, E. S. & ROELOFS, H. 2011. Pretreatment with Interferon-Γ Enhances the Therapeutic Activity of Mesenchymal Stromal Cells in Animal Models of Colitis. *Stem Cells*, 29, 1549-1558.

DVORAKOVA, J., HRUBA, A., VELEBNY, V. & KUBALA, L. 2008. Isolation and Characterization of Mesenchymal Stem Cell Population Entrapped in Bone Marrow Collection Sets. *Cell Biol Int*, 32, 1116-1125.

EDEN, E., NAVON, R., STEINFELD, I., LIPSON, D. & YAKHINI, Z. 2009. GOrilla: A Tool for Discovery and Visualization of Enriched GO Terms in Ranked Gene Lists. *BMC Bioinformatics*, 10, 48.

EDGAR, R., DOMRACHEV, M. & LASH, A. E. 2002. Gene Expression Omnibus: Ncbi Gene Expression and Hybridization Array Data Repository. *Nucleic Acids Res*, 30, 207-210.

EL-ATTAR, S., ELSAYED, L. & RASHED, L. 2012. Role of Stem Cells and Antioxidant on Modulation of Body Defense Mechanism in Lipopolysaccharide-Induced Acute Lung Injury in Rats. *Med J Cairo Univ*, 80, 559-573.

ELMAN, J. S., LI, M., WANG, F., GIMBLE, J. M. & PAREKKADAN, B. 2014. A Comparison of Adipose and Bone Marrow-Derived Mesenchymal Stromal Cell Secreted Factors in the Treatment of Systemic Inflammation. *J Inflamm (Lond)*, 11, 1.

ELMORE, S. 2007. Apoptosis: A Review of Programmed Cell Death. *Toxicol Pathol*, 35, 495-516.

EMERY, J. G., MCDONNELL, P., BURKE, M. B., DEEN, K. C., LYN, S., SILVERMAN, C., DUL, E., APPELBAUM, E. R., EICHMAN, C. & DIPRINZIO, R. 1998. Osteoprotegerin Is a Receptor for the Cytotoxic Ligand Trail. *J Biol Chem*, 273, 14363-14367.

ENGEL, M. A., KHALIL, M., SIKLOSI, N., MUELLER-TRIBBENSEE, S. M., NEUHUBER, W. L., NEURATH, M. F., BECKER, C. & REEH, P. W. 2012. Opposite Effects of Substance P and Calcitonin Gene-Related Peptide in Oxazolone Colitis. *Dig Liver Dis*, 44, 24-29.

ENGEL, M. A., LEFFLER, A., NIEDERMIRTL, F., BABES, A., ZIMMERMANN, K., FILIPOVIĆ, M. R., IZYDORCZYK, I., EBERHARDT, M., KICHKO, T. I., MUELLER–TRIBBENSEE, S. M., KHALIL, M., SIKLOSI, N., NAU, C., IVANOVIĆ–BURMAZOVIĆ, I., NEUHUBER, W. L., BECKER, C., NEURATH, M. F. & REEH, P. W. 2011. TRPA1 and Substance P Mediate Colitis in Mice. *Gastroenterology*, 141, 1346-1358.

ENGLISH, K., BARRY, F. P., FIELD-CORBETT, C. P. & MAHON, B. P. 2007. Ifn-γ and Tnf-α Differentially Regulate Immunomodulation by Murine Mesenchymal Stem Cells. *Immunol Lett*, 110, 91-100.

EPSTEIN, F. H., GOYAL, R. K. & HIRANO, I. 1996. The Enteric Nervous System. *N Engl J Med*, 334, 1106-1115.

ERI, R. D., ADAMS, R. J., TRAN, T. V., TONG, H., DAS, I., ROCHE, D. K., OANCEA, I., PNG, C. W., JEFFERY, P. L., RADFORD-SMITH, G. L., COOK, M. C., FLORIN, T. H. & MCGUCKIN, M. A. 2011. An Intestinal Epithelial Defect Conferring ER Stress Results in Inflammation Involving Both Innate and Adaptive Immunity. *Mucosal Immunol*, 4, 354-364.

EUROPEAN MEDICINES AGENCY 2008. Guideline on Human Cell-Based Medicinal Products [online]. Available: https://www.ema.europa.eu/documents/scientific-guideline/guideline-human-cell-based-medicinal-products_en.pdf [viewed 7/12/18].

EUROPEAN MEDICINES AGENCY 2010. Reflection Paper on Stem Cell-Based Medicinal Products [online]. Available: https://www.ema.europa.eu/documents/scientific-guideline/reflection-paper-stem-cell-based-medicinal-products_en.pdf [viewed 7/12/18].

FANG, K., BRUCE, M., PATTILLO, C. B., ZHANG, S., STONE, R., CLIFFORD, J. & KEVIL, C. G. 2010. Temporal Genomewide Expression Profiling of Dss Colitis Reveals Novel Inflammatory and Angiogenesis Genes Similar to Ulcerative Colitis. *Physiol Genomics*, 43, 43-56.

FAWZY, S. A., EL-DIN ABO-ELNOU, R., ABD-EL-MAKSOUD EL-DEEB, D. & YOUSRY ABD-ELKADER, M. 2013. The Possible Role of Mesenchymal Stem Cells Therapy in the Repair of Experimentally Induced Colitis in Male Albino Rats. *Int J Stem Cells*, 6, 92-103.

FENG, Y., LIAO, Y., HUANG, W., LAI, X., LUO, J., DU, C., LIN, J., ZHANG, Z., QIU, D., LIU, Q., SHEN, H., XIANG, A. P. & ZHANG, Q. 2018. Mesenchymal Stromal Cells-Derived Matrix Gla Protein Contribute to the Alleviation of Experimental Colitis. *Cell Death Dis*, 9, 691.

FERRAND, J., NOËL, D., LEHOURS, P., PROCHAZKOVA-CARLOTTI, M., CHAMBONNIER, L., MÉNARD, A., MÉGRAUD, F. & VARON, C. 2011. Human Bone Marrow-Derived Stem Cells Acquire Epithelial Characteristics through Fusion with Gastrointestinal Epithelial Cells. *PLoS One*, 6, e19569.

FERRANTE, M., DE HERTOGH, G., HLAVATY, T., D'HAENS, G., PENNINCKX, F., D'HOORE, A., VERMEIRE, S., RUTGEERTS, P., GEBOES, K. & VAN ASSCHE, G. 2006. The Value of Myenteric Plexitis to Predict Early Postoperative Crohn's Disease Recurrence. *Gastroenterology*, 130, 1595-606.

FERRER, L., KIMBREL, E. A., LAM, A., FALK, E. B., ZEWE, C., JUOPPERI, T., LANZA, R. & HOFFMAN, A. 2016. Treatment of Perianal Fistulas with Human Embryonic Stem Cell-Derived Mesenchymal Stem Cells: A Canine Model of Human Fistulizing Crohn's Disease. *Regen Med*, 11, 33-43.

FILIPPONE, R., ROBINSON, A. M., JOVANOVSKA, V., STAVELY, R., APOSTOLOPOULOS, V., BORNSTEIN, J. C. & NURGALI, K. 2018a. Targeting Eotaxin-1 and CCR3 Receptor Alleviates Enteric Neuropathy and Colonic Dysfunction in TNBS-Induced Colitis in Guinea Pigs. *Neurogastroenterol Motil*. 11, e13391

FILIPPONE, R., STAVELY, R., APOSTOLOPOULOS, V. & NURGALI, K. 2018b. Targeting CCR3-Eotaxin Axis Alleviates Gastrointestinal Dysfunction in the *Winnie* Murine Model of Spontaneous Chronic Colitis. Poster session presented at FNM 2018 – 3rd Meeting of the Federation of Neurogastroenterology and Motility, Amsterdam, The Netherlands.

FINELLI, M. J., SANCHEZ-PULIDO, L., LIU, K. X., DAVIES, K. E. & OLIVER, P. L. 2016. The Evolutionarily Conserved Tre2/Bub2/Cdc16 (TBC), Lysin Motif (LysM), Domain Catalytic (TLDc) Domain Is Neuroprotective against Oxidative Stress. *J Biol Chem*, 291, 2751-2763.

FINN, R. D., ATTWOOD, T. K., BABBITT, P. C., BATEMAN, A., BORK, P., BRIDGE, A. J., CHANG, H.-Y., DOSZTÁNYI, Z., EL-GEBALI, S., FRASER, M., GOUGH, J., HAFT, D., HOLLIDAY, G. L., HUANG, H., HUANG, X., LETUNIC, I., LOPEZ, R., LU, S., MARCHLER-BAUER, A., MI, H., MISTRY, J., NATALE, D. A., NECCI, M., NUKA, G., ORENGO, C. A., PARK, Y., PESSEAT, S., PIOVESAN, D., POTTER, S. C., RAWLINGS, N. D., REDASCHI, N., RICHARDSON, L., RIVOIRE, C., SANGRADOR-VEGAS, A., SIGRIST, C., SILLITOE, I., SMITHERS, B., SQUIZZATO, S., SUTTON, G., THANKI, N., THOMAS, P. D., TOSATTO, SILVIO C E., WU, C. H., XENARIOS, I., YEH, L.-S., YOUNG, S.-Y. & MITCHELL, A. L. 2017. Interpro in 2017—Beyond Protein Family and Domain Annotations. *Nucleic Acids Res*, 45, 190-199.

FIOCCHI, C. 2018. Inflammatory Bowel Disease: Complexity and Variability Need Integration. *Front Med (Lausanne)*, 5, 75.

FIORINO, G., DANESE, S., PARIENTE, B. & ALLEZ, M. 2014. Paradoxical Immune-Mediated Inflammation in Inflammatory Bowel Disease Patients Receiving Anti-Tnf-α Agents. *Autoimmun Rev*, 13, 15-19.

FISHER, A. B. 2009. Redox Signalling across Cell Membranes. *Antioxid Redox Signal*, 11, 1349-1356.

FLORES, E. R., TSAI, K. Y., CROWLEY, D., SENGUPTA, S., YANG, A., MCKEON, F. & JACKS, T. 2002. P63 and P73 Are Required for P53-Dependent Apoptosis in Response to DNA Damage. *Nature*, 416, 560-564.

FOLSTED, A. C. B., KRISTIAN, S., LINDHARDT, S. K., ANNE, K., STEFAN, R., H., G. J. & KRAGH, M. S. 2017. Haptoglobin. *Antioxid Redox Signal*, 26, 814-831.

FORBES, G. M., STURM, M. J., LEONG, R. W., SPARROW, M. P., SEGARAJASINGAM, D., CUMMINS, A. G., PHILLIPS, M. & HERRMANN, R. P. 2014. A Phase 2 Study of Allogeneic

Mesenchymal Stromal Cells for Luminal Crohn's Disease Refractory to Biologic Therapy. *Clin Gastroenterol Hepatol*, 12, 64-71.

FORTE, D., CICIARELLO, M., VALERII, M. C., DE FAZIO, L., CAVAZZA, E., GIORDANO, R., PARAZZI, V., LAZZARI, L., LAURETI, S., RIZZELLO, F., CAVO, M., CURTI, A., LEMOLI, R. M., SPISNI, E. & CATANI, L. 2015. Human Cord Blood-Derived Platelet Lysate Enhances the Therapeutic Activity of Adipose-Derived Mesenchymal Stromal Cells Isolated from Crohn's Disease Patients in a Mouse Model of Colitis. *Stem Cell Res Ther*, 6, 170.

FRANSEN, M., NORDGREN, M., WANG, B. & APANASETS, O. 2012. Role of Peroxisomes in ROS/RNS-Metabolism: Implications for Human Disease. *Biochim Biophys Acta - Mol Basis Dis* 1822, 1363-1373.

FRASER, J. K., WULUR, I., ALFONSO, Z. & HEDRICK, M. H. 2006. Fat Tissue: An Underappreciated Source of Stem Cells for Biotechnology. *Trends Biotechnol*, 24, 150-154.

FREEMAN, H. J. 2007. Granuloma-Positive Crohn's Disease. *Can J Gastroenterol*, 21, 583–587.

FREEMAN, H. J. 2012. Medical Management of Ulcerative Colitis with a Specific Focus on 5-Aminosalicylates. Clin Med Insights *Gastroenterol*, 5, 77–83.

FRIEDENSTEIN, A., CHAILAKHJAN, R. & LALYKINA, K. 1970. The Development of Fibroblast Colonies in Monolayer Cultures of Guinea-Pig Bone Marrow and Spleen Cells. *Cell Prolif*, 3, 393-403.

FRIEDENSTEIN, A., PIATETZKY-SHAPIRO, I. & PETRAKOVA, K. 1966. Osteogenesis in Transplants of Bone Marrow Cells. *J Embryol Exp Morphol*, 16, 381-390.

FRIEDMAN, J. 2011. Why Is the Nervous System Vulnerable to Oxidative Stress? In: Gadoth N., Göbel H. (eds) Oxidative Stress and Free Radical Damage in Neurology. Oxidative Stress in Applied Basic Research and Clinical Practice. *Humana Press*. 19-27.

FRIES, W., BELVEDERE, A. & VETRANO, S. 2013. Sealing the Broken Barrier in IBD: Intestinal Permeability, Epithelial Cells and Junctions. *Curr Drug Targets*, 14, 1460-1470.

FU, Z. W., ZHANG, Z. Y. & GE, H. Y. 2018. Mesenteric Injection of Adipose-Derived Mesenchymal Stem Cells Relieves Experimentally-Induced Colitis in Rats by Regulating Th17/Treg Cell Balance. *Am J Transl Res*, 10, 54-66.

FUENZALIDA, P., KURTE, M., FERNANDEZ-O'RYAN, C., IBANEZ, C., GAUTHIER-ABELIUK, M., VEGA-LETTER, A. M., GONZALEZ, P., IRARRAZABAL, C., QUEZADA, N., FIGUEROA, F. & CARRION, F. 2016. Toll-Like Receptor 3 Pre-Conditioning Increases the Therapeutic Efficacy of Umbilical Cord Mesenchymal Stromal Cells in a Dextran Sulfate Sodium-Induced Colitis Model. *Cytotherapy*, 18, 630-41.

FUJII, T., MASHIMO, M., MORIWAKI, Y., MISAWA, H., ONO, S., HORIGUCHI, K. & KAWASHIMA, K. 2017. Expression and Function of the Cholinergic System in Immune Cells. *Front Immunol*, 8.

FURNESS, J. 2000. Types of Neurons in the Enteric Nervous System. *J Auton Nerv Syst*, 81, 87-96.

FURNESS, J. B. 2006. The Enteric Nervous System. Blackwell Publishing, Oxford.

FURNESS, J. B. 2012. The Enteric Nervous System and Neurogastroenterology. *Nat Rev Gastroenterol Hepatol*, 9, 286-294.

GABANYI, I., MULLER, PAUL A., FEIGHERY, L., OLIVEIRA, THIAGO Y., COSTA-PINTO, FREDERICO A. & MUCIDA, D. 2016. Neuro-Immune Interactions Drive Tissue Programming in Intestinal Macrophages. *Cell*, 164, 378-391.

GAGINELLA, T. S., GRISHAM, M. B., THOMAS, D. B., WALSH, R. & MOUMMI, C. 1992. Oxidant-Evoked Release of Acetylcholine from Enteric Neurons of the Rat Colon. *J Pharmacol Exp Ther*, 263, 1068-1073.

GALIPEAU, J., KRAMPERA, M., BARRETT, J., DAZZI, F., DEANS, R. J., DEBRUIJN, J., DOMINICI, M., FIBBE, W. E., GEE, A. P., GIMBLE, J. M., HEMATTI, P., KOH, M. B. C., LEBLANC, K., MARTIN, I., MCNIECE, I. K., MENDICINO, M., OH, S., ORTIZ, L., PHINNEY, D. G., PLANAT, V., SHI, Y., STRONCEK, D. F., VISWANATHAN, S., WEISS, D. J. & SENSEBE, L. 2016. International Society for Cellular Therapy Perspective on Immune Functional Assays for Mesenchymal Stromal Cells as Potency Release Criterion for Advanced Phase Clinical Trials. *Cytotherapy*, 18, 151-159.

GALLIGAN, J. 2002. Ligand-Gated Ion Channels in the Enteric Nervous System. *Neurogastroenterol Motil*, 14, 611-623.

GALMES-PASCUAL, B. M., NADAL-CASELLAS, A., BAUZA-THORBRUGGE, M., SBERT-ROIG, M., GARCIA-PALMER, F. J., PROENZA, A. M., GIANOTTI, M. & LLADO, I. 2017. 17beta-Estradiol Improves Hepatic Mitochondrial Biogenesis and Function through PGC1B. *J Endocrinol*, 232, 297-308.

GALVAO, J., DAVIS, B., TILLEY, M., NORMANDO, E., DUCHEN, M. R. & CORDEIRO, M. F. 2014. Unexpected Low-Dose Toxicity of the Universal Solvent DMSO. *FASEB J*, 28, 1317-1330.

GANG, E. J., BOSNAKOVSKI, D., FIGUEIREDO, C. A., VISSER, J. W. & PERLINGEIRO, R. C. R. 2007. Ssea-4 Identifies Mesenchymal Stem Cells from Bone Marrow. *Blood*, 109, 1743-1751.

GANG, E. J., JEONG, J. A., HONG, S. H., HWANG, S. H., KIM, S. W., YANG, I. H., AHN, C., HAN, H. & KIM, H. 2004. Skeletal Myogenic Differentiation of Mesenchymal Stem Cells Isolated from Human Umbilical Cord Blood. *Stem Cells*, 22, 617-624.

GARCÍA-ARRANZ, M., HERREROS, M. D., GONZALEZ-GOMEZ, C., DE LA QUINTANA, P., GUADALAJARA, H., GEORGIEV-HRISTOV, T., TREBOL, J. & GARCÍA-OLMO, D. 2016. Treatment of Crohn's-Related Rectovaginal Fistula with Allogeneic Expanded-Adipose Derived Stem Cells: A Phase I-IIa Clinical Trial. Stem Cells *Transl Med*, 5, 1441-1446.

GARCÍA-OLMO, D., GARCÍA-ARRANZ, M., HERREROS, D., PASCUAL, I., PEIRO, C. & RODRÍGUEZ-MONTES, J. A. 2005. A Phase I Clinical Trial of the Treatment of Crohn's Fistula by Adipose Mesenchymal Stem Cell Transplantation. *Dis Colon Rectum*, 48, 1416-1423.

GARCÍA-OLMO, D., GUADALAJARA, H., RUBIO-PEREZ, I., HERREROS, M. D., DE-LA-QUINTANA, P. & GARCIA-ARRANZ, M. 2015. Recurrent Anal Fistulae: Limited Surgery Supported by Stem Cells. *World J Gastroenterol*, 21, 3330–3336.

GARCÍA-OLMO, D., HERREROS, D., DE-LA-QUINTANA, P., GUADALAJARA, H., TRÉ, J., GEORGIEV-HRISTOV, T. & GARCÍ, M. 2010. Adipose-Derived Stem Cells in Crohn's Rectovaginal Fistula. *Case Report Med*, Article ID 961758.

GARCÍA-OLMO, D., HERREROS, D., PASCUAL, I., PASCUAL, J. A., DEL-VALLE, E., ZORRILLA, J., DE-LA-QUINTANA, P., GARCIA-ARRANZ, M. & PASCUAL, M. 2009b. Expanded Adipose-Derived Stem Cells for the Treatment of Complex Perianal Fistula: A Phase II Clinical Trial. *Dis Colon Rectum*, 52, 79-86.

GARCIA-OLMO, D., HERREROS, D., PASCUAL, M., PASCUAL, I., DE-LA-QUINTANA, P., TREBOL, J. & GARCIA-ARRANZ, M. 2009c. Treatment of Enterocutaneous Fistula in Crohn's Disease with Adipose-Derived Stem Cells: A Comparison of Protocols with and without Cell Expansion. *Int J Colorectal Dis*, 24, 27-30.

GAULEY, J. & PISETSKY, D. S. 2009. The Translocation of HMGB1 During Cell Activation and Cell Death. Autoimmunity, 42, 299-301.

GEARRY, R. B. & LEONG, R. W. 2013. Inflammatory Bowel Disease in Asia: The Start of the Epidemic? *J Gastroenterol Hepatol*, 28, 899-900.

GERAMIZADEH, B., AKBARZADEH, E., IZADI, B., FOROUTAN, H. R. & HEIDARI, T. 2013. Immunohistochemical Study of Enteric Nervous System in Hirschsprung's Disease and Intestinal Neuronal Dysplasia. *Histol Histopathol*, 28, 345-351.

GERSEMANN, M., BECKER, S., NUDING, S., ANTONI, L., OTT, G., FRITZ, P., OUE, N., YASUI, W., WEHKAMP, J. & STANGE, E. F. 2012. Olfactomedin-4 Is a Glycoprotein Secreted into Mucus in Active IBD. *J Crohns Colitis*, 6, 425-434.

GHANNAM, S., BOUFFI, C., DJOUAD, F., JORGENSEN, C. & NOËL, D. 2010. Immunosuppression by Mesenchymal Stem Cells: Mechanisms and Clinical Applications. *Stem Cell Res Ther*, 1, 2.

GIULIANI, N., LISIGNOLI, G., MAGNANI, M., RACANO, C., BOLZONI, M., DALLA PALMA, B., SPOLZINO, A., MANFERDINI, C., ABATI, C. & TOSCANI, D. 2013. New Insights into Osteogenic and Chondrogenic Differentiation of Human Bone Marrow Mesenchymal Stem Cells and Their Potential Clinical Applications for Bone Regeneration in Pediatric Orthopaedics. *Stem Cells Int*, Article ID 312501.

GNECCHI, M. & MELO, L. G. 2009. Bone Marrow-Derived Mesenchymal Stem Cells: Isolation, Expansion, Characterization, Viral Transduction, and Production of Conditioned Medium. *Methods Mol Biol*, 482, 281-294.

GOLDIN, E., KARMELI, F., SELINGER, Z. & RACHMILEWITZ, D. 1989. Colonic Substance P Levels Are Increased in Ulcerative Colitis and Decreased in Chronic Severe Constipation. *Dig Dis Sci*, 34, 754-757.

GOLSTEIN, P. & KROEMER, G. 2007. Cell Death by Necrosis: Towards a Molecular Definition. *Trends Biochem Sci*, 32, 37-43.

GONG, G., XIANG, L., YUAN, L., HU, L., WU, W., CAI, L., YIN, L. & DONG, H. 2014. Protective Effect of Glycyrrhizin, a Direct HMGB1 Inhibitor, on Focal Cerebral Ischemia/Reperfusion-Induced Inflammation, Oxidative Stress, and Apoptosis in Rats. *PLoS One*, 9, e89450.

GONG, G., YUAN, L.-B., HU, L., WU, W., YIN, L., HOU, J.-L., LIU, Y.-H. & ZHOU, L.-S. 2011. Glycyrrhizin Attenuates Rat Ischemic Spinal Cord Injury by Suppressing Inflammatory Cytokines and HMGB1. *Acta Pharmacol Sin*, 33, 11–18.

GONZALEZ-REY, E., ANDERSON, P., GONZÁLEZ, M. A., RICO, L., BÜSCHER, D. & DELGADO, M. 2009. Human Adult Stem Cells Derived from Adipose Tissue Protect against Experimental Colitis and Sepsis. *Gut*, 58, 929-939.

GONZÁLEZ, M. A., GONZALEZ–REY, E., RICO, L., BÜSCHER, D. & DELGADO, M. 2009. Adipose-Derived Mesenchymal Stem Cells Alleviate Experimental Colitis by Inhibiting Inflammatory and Autoimmune Responses. *Gastroenterology*, 136, 978-989.

GORBUNOV, N. V., GARRISON, B. R., MCDANIEL, D. P., ZHAI, M., LIAO, P.-J., NURMEMET, D. & KIANG, J. G. 2013. Adaptive Redox Response of Mesenchymal Stromal Cells to Stimulation with Lipopolysaccharide Inflammagen: Mechanisms of Remodeling of Tissue Barriers in Sepsis. *Oxid Med Cell Longev*, 186795.

GÖRLACH, A., BERTRAM, K., HUDECOVA, S. & KRIZANOVA, O. 2015. Calcium and Ros: A Mutual Interplay. *Redox Biol*, 6, 260-271.

GRAHAM, R. M., THOMPSON, J. W. & WEBSTER, K. A. 2015. BNIP3 Promotes Calcium and Calpain-Dependent Cell Death. *Life Sci*, 142, 26-35.

GRAY, L. R., TOMPKINS, S. C. & TAYLOR, E. B. 2014. Regulation of Pyruvate Metabolism and Human Disease. *Cell Mol Life Sci*, 71, 2577-2604.

GREGOIRE, C., BRIQUET, A., PIRENNE, C., LECHANTEUR, C., LOUIS, E. & BEGUIN, Y. 2018. Allogeneic Mesenchymal Stromal Cells for Refractory Luminal Crohn's Disease: A Phase I–Ii Study. *Dig Liver Dis*, 50, 1251-1255.

GRUNDMANN, D., KLOTZ, M., RABE, H., GLANEMANN, M. & SCHÄFER, K.-H. 2015. Isolation of High-Purity Myenteric Plexus from Adult Human and Mouse Gastrointestinal Tract. *Sci Rep*, 5, 9226.

GSTRAUNTHALER, G. 2003. Alternatives to the Use of Fetal Bovine Serum: Serum-Free Cell Culture. *ALTEX*, 20, 275-281.

GU, Y., HE, M., ZHOU, X., LIU, J., HOU, N., BIN, T., ZHANG, Y., LI, T. & CHEN, J. 2016. Endogenous IL-6 of Mesenchymal Stem Cell Improves Behavioral Outcome of Hypoxic-Ischemic Brain Damage Neonatal Rats by Supressing Apoptosis in Astrocyte. *Sci Rep*, 6, 18587.

GU, Y., ZHANG, Y., BI, Y., LIU, J., TAN, B., GONG, M., LI, T. & CHEN, J. 2015. Mesenchymal Stem Cells Suppress Neuronal Apoptosis and Decrease IL-10 Release Via the TLR2/NFκB Pathway in Rats with Hypoxic-Ischemic Brain Damage. *Mol Brain*, 8, 1-14.

GUADALAJARA, H., HERREROS, D., DE-LA-QUINTANA, P., TREBOL, J., GARCIA-ARRANZ, M. & GARCIA-OLMO, D. 2012. Long-Term Follow-up of Patients Undergoing Adipose-Derived Adult Stem Cell Administration to Treat Complex Perianal Fistulas. *Int J Colorectal Dis*, 27, 595-600.

GUAN, J., WANG, F., LI, Z., CHEN, J., GUO, X., LIAO, J. & MOLDOVAN, N. I. 2011. The Stimulation of the Cardiac Differentiation of Mesenchymal Stem Cells in Tissue Constructs That Mimic Myocardium Structure and Biomechanics. *Biomaterials*, 32, 5568-5580.

GUAN, Y., DONG, J., TACKETT, L., MEYER, J. W., SHULL, G. E. & MONTROSE, M. H. 2006. NHE2 Is the Main Apical NHE in Mouse Colonic Crypts but an Alternative Na+-Dependent Acid Extrusion Mechanism Is Upregulated in NHE2-Null Mice. *Am J Physiol Gastrointest Liver Physiol*, 291, 689-699.

GULBRANSEN, B. D., BASHASHATI, M., HIROTA, S. A., GUI, X., ROBERTS, J. A., MACDONALD, J. A., MURUVE, D. A., MCKAY, D. M., BECK, P. L., MAWE, G. M., THOMPSON, R. J. & SHARKEY, K. A. 2012. Activation of Neuronal P2X7 Receptor-Pannexin-1 Mediates Death of Enteric Neurons During Colitis. *Nat Med*, 18, 600-604.

GUSTAFSSON, Å. B. 2011. BNIP3 as a Dual Regulator of Mitochondrial Turnover and Cell Death in the Myocardium. *Pediatr Cardiol*, 32, 267-274.

GWAK, G.-Y., MOON, T. G., LEE, D. H. & YOO, B. C. 2012. Glycyrrhizin Attenuates HMGB1-Induced Hepatocyte Apoptosis by Inhibiting the P38-Dependent Mitochondrial Pathway. *World J Gastroenterol*, 18, 679-684.

HAN, B., ZHANG, X., LIU, H., DENG, X., CAI, Q., JIA, X., YANG, X., WEI, Y. & LI, G. 2014a. Improved Bioactivity of Pan-Based Carbon Nanofibers Decorated with Bioglass Nanoparticles. *J Biomater Sci Polym Ed*, 25, 341-353.

HAN, X., GAO, W., CHEN, L., YANG, H. & SHI, Q. 2014. Promotion of Neurological Recovery in Rat Spinal Hemisection Injury by Collagen Scaffold Loaded with Mesenchymal Stem Cells. *Bone Jt J Orthopaedic Proceedings Supplement*, 96, 246-246.

HANSEN, M. B. 2003. The Enteric Nervous System III: A Target for Pharmacological Treatment. *Pharmacol Toxicol*, 93, 1-13.

HARTING, M. T., JIMENEZ, F., XUE, H., FISCHER, U. M., BAUMGARTNER, J., DASH, P. K. & COX, C. S. 2009. Intravenous Mesenchymal Stem Cell Therapy for Traumatic Brain Injury. *J Neurosurg*, 110, 1189-1197.

HARUSATO, A., ABO, H., NGO, V., YI, S., MITSUTAKE, K., OSUKA, S., KOHLMEIER, J. E., LI, J.-D., GEWIRTZ, A. T. & NUSRAT, A. 2017. Il-36γ Signalling Controls the Induced Regulatory T Cell–Th9 Cell Balance Via NFκB Activation and Stat Transcription Factors. *Mucosal Immunol*, 10, 1455-1467.

HASSANI, H., LUCAS, G., ROZELL, B., ERNFORS, P. 2005. Attenuation of acute experimental colitis by preventing NPY Y1 receptor signaling. *Am J Physiol Gastrointest Liver Physiol* 288, 550-556.

HAUSER, C. J., LOCKE, R. R., KAO, H. W., PATTERSON, J. & ZIPSER, R. D. 1988. Visceral Surface Oxygen Tension in Experimental Colitis in the Rabbit. *J Lab Clin Med*, 112, 68-71.

HAYASHI, Y., TSUJI, S., TSUJII, M., NISHIDA, T., ISHII, S., IIJIMA, H., NAKAMURA, T., EGUCHI, H., MIYOSHI, E. & HAYASHI, N. 2008. Topical Implantation of Mesenchymal Stem Cells Has Beneficial Effects on Healing of Experimental Colitis in Rats. *J Pharmacol Exp Ther*, 326, 523-531.

HE, J., ZHANG, B. & GAN, H. 2018. Cidec Is Involved in Lps-Induced Inflammation and Apoptosis in Renal Tubular Epithelial Cells. *Inflammation*, 41, 1912-1921.

HE, X.-W., HE, X.-S., LIAN, L., WU, X.-J. & LAN, P. 2012. Systemic Infusion of Bone Marrow-Derived Mesenchymal Stem Cells for Treatment of Experimental Colitis in Mice. *Dig Dis Sci*, 57, 3136-3144.

HEANUE, T. A. & PACHNIS, V. 2006. Expression Profiling the Developing Mammalian Enteric Nervous System Identifies Marker and Candidate Hirschsprung Disease Genes. *Proc Natl Acad Sci U S A*, 103, 6919-6924.

HEAZLEWOOD, C. K., COOK, M. C., ERI, R., PRICE, G. R., TAURO, S. B., TAUPIN, D., THORNTON, D. J., PNG, C. W., CROCKFORD, T. L. & CORNALL, R. J. 2008. Aberrant Mucin Assembly in Mice Causes Endoplasmic Reticulum Stress and Spontaneous Inflammation Resembling Ulcerative Colitis. *PLoS Med*, 5, e54.

HEIDARI, M., POUYA, S., BAGHAEI, K., AGHDAEI, H. A., NAMAKI, S., ZALI, M. R. & HASHEMI, S. M. 2018. The Immunomodulatory Effects of Adipose-Derived Mesenchymal Stem Cells and Mesenchymal Stem Cells-Conditioned Medium in Chronic Colitis. *J Cell Physiol*, 233, 8754-8766.

HERFARTH, H. H., KAPPELMAN, M. D., LONG, M. D. & ISAACS, K. L. 2016. Use of Methotrexate in the Treatment of Inflammatory Bowel Diseases. *Inflamm Bowel Dis*, 22, 224-233.

HIGASHIMORI, H., WHETZEL, T. P. & CARLSEN, R. C. 2008. Inhibition of Inducible Nitric Oxide Synthase Reduces an Acute Peripheral Motor Neuropathy Produced by Dermal Burn Injury in Mice. *J Peripher Nerv Syst*, 13, 289-98.

HIRTEN, R., SULTAN, K., THOMAS, A. & BERNSTEIN, D. E. 2015. Hepatic Manifestations of Non-Steroidal Inflammatory Bowel Disease Therapy. *World J Hepatol*, 7, 2716-2728.

HITOMI, J., CHRISTOFFERSON, D. E., NG, A., YAO, J., DEGTEREV, A., XAVIER, R. J. & YUAN, J. 2008. Identification of a Molecular Signalling Network That Regulates a Cellular Necrotic Cell Death Pathway. *Cell*, 135, 1311-1323.

HOFFMAN, J. M., SIDERI, A., RUIZ, J. J., STAVRAKIS, D., SHIH, D. Q., TURNER, J. R., POTHOULAKIS, C. & KARAGIANNIDES, I. 2018. Mesenteric Adipose-Derived Stromal Cells from Crohn's Disease Patients Induce Protective Effects in Colonic Epithelial Cells and Mice with Colitis. *Cell Mol Gastroenterol Hepatol*, 6, 1-16.

HÖFIG, I., INGAWALE, Y., ATKINSON, M. J., HERTLEIN, H., NELSON, P. J. & ROSEMANN, M. 2016. P53-Dependent Senescence in Mesenchymal Stem Cells under Chronic Normoxia Is Potentiated by Low-Dose Γ-Irradiation. *Stem Cells Int*, Article ID 6429853.

HOGABOAM, C. M., JACOBSON, K., COLLINS, S. M. & BLENNERHASSETT, M. G. 1995. The Selective Beneficial Effects of Nitric Oxide Inhibition in Experimental Colitis. *Am J Physiol*, 268, 673-684.

HOLGERSEN, K., KUTLU, B., FOX, B., SERIKAWA, K., LORD, J., HANSEN, A. K. & HOLM, T. L. 2015. High-Resolution Gene Expression Profiling Using RNA Sequencing in Patients with Inflammatory Bowel Disease and in Mouse Models of Colitis. *J Crohns Colitis*, 9, 492-506.

HONG, G., ZHANG, W., LI, H., SHEN, X. & GUO, Z. 2014. Separate Enrichment Analysis of Pathways for up-and Downregulated Genes. *J Royal Soc Interface*, 11, 20130950.

HONS, I. M., BURDA, J. E., GRIDER, J. R., MAWE, G. M. & SHARKEY, K. A. 2009. Alterations to Enteric Neural Signalling Underlie Secretory Abnormalities of the Ileum in Experimental Colitis in the Guinea Pig. *Am J Physiol Gastrointest Liver Physiol*, 296, 717-726.

HORI, M., NOBE, H., HORIGUCHI, K. & OZAKI, H. 2008. Mcp-1 Targeting Inhibits Muscularis Macrophage Recruitment and Intestinal Smooth Muscle Dysfunction in Colonic Inflammation. *Am J Physiol Cell Physiol*, 294, 391-401.

HSIAO, C.-H., JI, A. T.-Q., CHANG, C.-C., CHENG, C.-J., LEE, L.-M. & HO, J. H.-C. 2015. Local Injection of Mesenchymal Stem Cells Protects Testicular Torsion-Induced Germ Cell Injury. *Stem Cell Res Ther*, 6, 113.

HU, J., ZHAO, G., ZHANG, L., QIAO, C., DI, A., GAO, H. & XU, H. 2016. Safety and Therapeutic Effect of Mesenchymal Stem Cell Infusion on Moderate to Severe Ulcerative Colitis. *Exp Ther Med*, 12, 2983-2989.

HUANG, D. W., SHERMAN, B. T. & LEMPICKI, R. A. 2008a. Bioinformatics Enrichment Tools: Paths toward the Comprehensive Functional Analysis of Large Gene Lists. *Nucleic Acids Res*, 37, 1-13.

HUANG, D. W., SHERMAN, B. T. & LEMPICKI, R. A. 2008b. Systematic and Integrative Analysis of Large Gene Lists Using David Bioinformatics Resources. *Nat Protoc*, 4, 44.

HUANG, L. E., GU, J., SCHAU, M. & BUNN, H. F. 1998. Regulation of Hypoxia-Inducible Factor 1alpha is Mediated by an O2-Dependent Degradation Domain via the Ubiquitin-Proteasome Pathway. *Proc Natl Acad Sci U S A*, 95, 7987-7992.

HUANG, P., GEBHART, N., RICHELSON, E., BROTT, T. G., MESCHIA, J. F. & ZUBAIR, A. C. 2014. Mechanism of Mesenchymal Stem Cell–Induced Neuron Recovery and Anti-Inflammation. *Cytotherapy*, 16, 1336-1344.

HULTÉN, L., LINDHAGEN, J., LUNDGREN, O., FASTH, S. & ÅHREN, C. 1977. Regional Intestinal Blood Flow in Ulcerative Colitis and Crohn's Disease. *Gastroenterology*, 72, 388-396.

HWANG, J. H., SHIM, S. S., SEOK, O. S., LEE, H. Y., WOO, S. K., KIM, B. H., SONG, H. R., LEE, J. K. & PARK, Y. K. 2009. Comparison of Cytokine Expression in Mesenchymal Stem Cells from Human Placenta, Cord Blood, and Bone Marrow. *J Korean Med Sci*, 24, 547-554.

IINO, S., HORIGUCHI, K. & NOJYO, Y. 2008. Interstitial Cells of Cajal Are Innervated by Nitrergic Nerves and Express Nitric Oxide-Sensitive Guanylate Cyclase in the Guinea-Pig Gastrointestinal Tract. *Neuroscience*, 152, 437-448.

IINO, S., WARD, S. M. & SANDERS, K. M. 2004. Interstitial Cells of Cajal Are Functionally Innervated by Excitatory Motor Neurones in the Murine Intestine. *J Physiol*, 556, 521-530.

IKEGAME, Y., YAMASHITA, K., HAYASHI, S., MIZUNO, H., TAWADA, M., YOU, F., YAMADA, K., TANAKA, Y., EGASHIRA, Y., NAKASHIMA, S., YOSHIMURA, S. & IWAMA, T. 2011. Comparison of Mesenchymal Stem Cells from Adipose Tissue and Bone Marrow for Ischemic Stroke Therapy. *Cytotherapy*, 13, 675-685.

INOUE, A., IKOMA, K., MORIOKA, N., KUMAGAI, K., HASHIMOTO, T., HIDE, I. & NAKATA, Y. 1999. Interleukin-1beta Induces Substance P Release from Primary Afferent Neurons through the Cyclooxygenase-2 System. *J Neurochem*, 73, 2206-2213.

ISLAM, M. N., DAS, S. R., EMIN, M. T., WEI, M., SUN, L., WESTPHALEN, K., ROWLANDS, D. J., QUADRI, S. K., BHATTACHARYA, S. & BHATTACHARYA, J. 2012. Mitochondrial Transfer from Bone-Marrow-Derived Stromal Cells to Pulmonary Alveoli Protects against Acute Lung Injury. *Nat Med*, 18, 759-765.

IWAZAWA, R., KOZAKAI, S., KITAHASHI, T., NAKAMURA, K. & HATA, K. I. 2018. The Therapeutic Effects of Adipose-Derived Stem Cells and Recombinant Peptide Pieces on Mouse Model of DSS Colitis. *Cell Transplant*, 27, 1390-1400.

IYER, S. S., TORRES-GONZALEZ, E., NEUJAHR, D. C., KWON, M., BRIGHAM, K. L., JONES, D. P., MORA, A. L. & ROJAS, M. 2010. Effect of Bone Marrow-Derived Mesenchymal Stem Cells on Endotoxin-Induced Oxidation of Plasma Cysteine and Glutathione in Mice. *Stem Cells Int*, 868076.

JANKO, C., FILIPOVIĆ, M., MUNOZ, L. E., SCHORN, C., SCHETT, G., IVANOVIĆ-BURMAZOVIĆ, I. & HERRMANN, M. 2014. Redox Modulation of HMGB1-Related Signalling. *Antioxid Redox Signal*, 20, 1075-1085.

JANUSZ, G. 2010. Morphological Changes in the Enteric Nervous System Caused by Carcinoma of the Human Large Intestine. *Folia Histochem Cytobiol*, 48, 157-162.

JIANG, D., MUSCHHAMMER, J., QI, Y., KÜGLER, A., DE VRIES, J. C., SAFFARZADEH, M., SINDRILARU, A., BEKEN, S. V., WLASCHEK, M., KLUTH, M. A., GANSS, C., FRANK, N. Y., FRANK, M. H., PREISSNER, K. T. & SCHARFFETTER-KOCHANEK, K. 2016. Suppression of Neutrophil-Mediated Tissue Damage—a Novel Skill of Mesenchymal Stem Cells. *Stem Cells*, 34, 2393-2406.

JO, H., EOM, Y. W., KIM, H. S., PARK, H. J., KIM, H. M. & CHO, M. Y. 2018. Regulatory Dendritic Cells Induced by Mesenchymal Stem Cells Ameliorate Dextran Sodium Sulfate-Induced Chronic Colitis in Mice. *Gut Liver*, 12, 664-673.

JODAL, M., HOLMGREN, S., LUNDGREN, O. & SJOQVIST, A. 1993. Involvement of the Myenteric Plexus in the Cholera Toxin-Induced Net Fluid Secretion in the Rat Small Intestine. *Gastroenterology*, 105, 1286-1293.

JOYCE, N., ANNETT, G., WIRTHLIN, L., OLSON, S., BAUER, G. & NOLTA, J. A. 2010. Mesenchymal Stem Cells for the Treatment of Neurodegenerative Disease. *Regen Med*, 5, 933-946.

JUSSILA, A., VIRTA, L. J., PUKKALA, E. & FÄRKKILÄ, M. A. 2014. Mortality and Causes of Death in Patients with Inflammatory Bowel Disease: A Nationwide Register Study in Finland. *J Crohn's Colitis*, 8, 1088-1096.

KANEHISA, M. & GOTO, S. 2000. KEGG: Kyoto Encyclopedia of Genes and Genomes. *Nucleic Acids Res*, 28, 27-30.

KARHAUSEN, J., FURUTA, G. T., TOMASZEWSKI, J. E., JOHNSON, R. S., COLGAN, S. P. & HAASE, V. H. 2004. Epithelial Hypoxia-Inducible Factor-1 Is Protective in Murine Experimental Colitis. *J Clin Invest*, 114, 1098-1106.

KARNOUB, A. E., DASH, A. B., VO, A. P., SULLIVAN, A., BROOKS, M. W., BELL, G. W., RICHARDSON, A. L., POLYAK, K., TUBO, R. & WEINBERG, R. A. 2007. Mesenchymal Stem Cells within Tumour Stroma Promote Breast Cancer Metastasis. *Nature*, 449, 557-563.

KARP, J. M. & LENG TEO, G. S. 2009. Mesenchymal Stem Cell Homing: The Devil Is in the Details. *Cell Stem Cell*, 4, 206-216.

KARUSSIS, D., KASSIS, I., KURKALLI, B. G. S. & SLAVIN, S. 2008. Immunomodulation and Neuroprotection with Mesenchymal Bone Marrow Stem Cells (Mscs): A Proposed Treatment for Multiple Sclerosis and Other Neuroimmunological/Neurodegenerative Diseases. *J Neurol Sci*, 265, 131-135.

KATSUMATA, R., SHIOTANI, A., MURAO, T., ISHII, M., FUJITA, M., MATSUMOTO, H. & HARUMA, K. 2017. Gender Differences in Serotonin Signalling in Patients with Diarrhea-Predominant Irritable Bowel Syndrome. *Intern Med*, 56, 993-999.

KAY, A. G., LONG, G., TYLER, G., STEFAN, A., BROADFOOT, S. J., PICCININI, A. M., MIDDLETON, J. & KEHOE, O. 2017. Mesenchymal Stem Cell-Conditioned Medium Reduces Disease Severity and Immune Responses in Inflammatory Arthritis. *Sci Rep*, 7, 18019.

KEBRIAEI, P. & ROBINSON, S. 2011. Treatment of Graft-Versus-Host-Disease with Mesenchymal Stromal Cells. *Cytotherapy*, 13, 262-268.

KELLES, A., JANSSENS, J. & TACK, J. 2000. Il-1β and Il-6 Excite Neurones and Suppress Cholinergic Neurotransmission in the Myenteric Plexus of the Guinea Pig. *Neurogastroenterol Motil*, 12, 531-538.

KEMP, K., GRAY, E., MALLAM, E., SCOLDING, N. & WILKINS, A. 2010. Inflammatory Cytokine Induced Regulation of Superoxide Dismutase 3 Expression by Human Mesenchymal Stem Cells. *Stem Cell Rev*, 6, 548-559.

KERN, S., EICHLER, H., STOEVE, J., KLUTER, H. & BIEBACK, K. 2006. Comparative Analysis of Mesenchymal Stem Cells from Bone Marrow, Umbilical Cord Blood, or Adipose Tissue. *Stem Cells*, 24, 1294-1301.

KESHAVARZIAN, A., MORGAN, G., SEDGHI, S., GORDON, J. & DORIA, M. 1990. Role of Reactive Oxygen Metabolites in Experimental Colitis. *Gut*, 31, 786-790.

KHOR, B., GARDET, A. & XAVIER, R. J. 2011. Genetics and Pathogenesis of Inflammatory Bowel Disease. *Nature*, 474, 307-317.

KIM, H. S., SHIN, T. H., LEE, B. C., YU, K. R., SEO, Y., LEE, S., SEO, M. S., HONG, I. S., CHOI, S. W. & SEO, K. W. 2013a. Human Umbilical Cord Blood Mesenchymal Stem Cells Reduce Colitis in Mice by Activating NOD2 Signalling to COX2. *Gastroenterology*, 145, 1392-1403.

KIM, S.-W., JIN, Y., SHIN, J.-H., KIM, I.-D., LEE, H.-K., PARK, S., HAN, P.-L. & LEE, J.-K. 2012. Glycyrrhizic Acid Affords Robust Neuroprotection in the Postischemic Brain Via Anti-Inflammatory Effect by Inhibiting HMGB1 Phosphorylation and Secretion. *Neurobiol Dis*, 46, 147-156.

KIM, W.-S., PARK, B.-S., KIM, H.-K., PARK, J.-S., KIM, K.-J., CHOI, J.-S., CHUNG, S.-J., KIM, D.-D. & SUNG, J.-H. 2008. Evidence Supporting Antioxidant Action of Adipose-Derived Stem Cells: Protection of Human Dermal Fibroblasts from Oxidative Stress. *J Dermatol Sci*, 49, 133-142.

KIM, Y., JO, S.-H., KIM, W. H. & KWEON, O.-K. 2015. Antioxidant and Anti-Inflammatory Effects of Intravenously Injected Adipose Derived Mesenchymal Stem Cells in Dogs with Acute Spinal Cord Injury. *Stem Cell Res Ther*, 6, 229.

KIM, Y. W., WEST, X. Z. & BYZOVA, T. V. 2013b. Inflammation and Oxidative Stress in Angiogenesis and Vascular Disease. *J Mol Med (Berl)*, 91, 323-328.

KINOSHITA, K., HORIGUCHI, K., FUJISAWA, M., KOBIRUMAKI, F., YAMATO, S., HORI, M. & OZAKI, H. 2007. Possible Involvement of Muscularis Resident Macrophages in Impairment of Interstitial Cells of Cajal and Myenteric Nerve Systems in Rat Models of TNBS-Induced Colitis. *Histochem Cell Biol*, 127, 41-53.

KLEIN, D., STEENS, J., WIESEMANN, A., SCHULZ, F., KASCHANI, F., RÖCK, K., YAMAGUCHI, M., WIRSDÖRFER, F., KAISER, M. & FISCHER, J. W. 2017. Mesenchymal Stem Cell Therapy Protects Lungs from Radiation-Induced Endothelial Cell Loss by Restoring Superoxide Dismutase 1 Expression. *Antioxid Redox Signal*, 26, 563-582.

KO, I. K., KIM, B.-G., AWADALLAH, A., MIKULAN, J., LIN, P., LETTERIO, J. J. & DENNIS, J. E. 2010. Targeting Improves Msc Treatment of Inflammatory Bowel Disease. *Mol Ther*, 18, 1365-1372.

KONG, D., ZHU, J., LIU, Q., JIANG, Y., XU, L., LUO, N., ZHAO, Z., ZHAI, Q., ZHANG, H., ZHU, M. & LIU, X. 2017. Mesenchymal Stem Cells Protect Neurons against Hypoxic-Ischemic Injury Via Inhibiting Parthanatos, Necroptosis, and Apoptosis, but Not Autophagy. *Cell Mol Neurobiol*, 37, 303-313.

KORDJAZY, N., HAJ-MIRZAIAN, A., HAJ-MIRZAIAN, A., ROHANI, M. M., GELFAND, E. W., REZAEI, N. & ABDOLGHAFFARI, A. H. 2018. Role of Toll-Like Receptors in Inflammatory Bowel Disease. *Pharmacol Res*, 129, 204-215.

KORSAK, K., SILVA, A. T. & SAFFREY, M. J. 2012. Differing Effects of NT-3 and GDNF on Dissociated Enteric Ganglion Cells Exposed to Hydrogen Peroxide *in vitro*. *Neurosci Lett*, 517, 102-106.

KOSAKA, T., YOSHINO, J., INUI, K., WAKABAYASHI, T., KOBAYASHI, T., WATANABE, S., HAYASHI, S., HIROKAWA, Y., SHIRAISHI, T., YAMAMOTO, T., TSUJI, M., KATOH, T. & WATANABE, M. 2009. Involvement of NAD(P)H:Quinone Oxidoreductase 1 and Superoxide Dismutase Polymorphisms in Ulcerative Colitis. *DNA Cell Biol*, 28, 625-631.

KOURIE, J. I. 1998. Interaction of Reactive Oxygen Species with Ion Transport Mechanisms. *Am J Physiol Cell Physiol*, 275, 1-24.

KOUTROUBAKIS, I. E., MALLIARAKI, N., DIMOULIOS, P. D., KARMIRIS, K., CASTANAS, E. & KOUROUMALIS, E. A. 2004. Decreased Total and Corrected Antioxidant Capacity in Patients with Inflammatory Bowel Disease. *Dig Dis Sci*, 49, 1433-1437.

KRAMMER, H. J., KARAHAN, S. T., SIGGE, W. & KUHNEL, W. 1994. Immunohistochemistry of Markers of the Enteric Nervous System in Whole-Mount Preparations of the Human Colon. *Eur J Pediatr Surg*, 4, 274-278.

KRAUTER, E. M., STRONG, D. S., BROOKS, E. M., LINDEN, D. R., SHARKEY, K. A. & MAWE, G. M. 2007. Changes in Colonic Motility and the Electrophysiological Properties of Myenteric Neurons Persist Following Recovery from Trinitrobenzene Sulfonic Acid Colitis in the Guinea Pig. *Neurogastroenterol Motil*, 19, 990-1000.

KRISHNAREDDY, S. & SWAMINATH, A. 2014. When Combination Therapy Isn't Working: Emerging Therapies for the Management of Inflammatory Bowel Disease. *World J Gastroenterol*, 20, 1139-1146.

KRONENBERG, M. 2005. Toward an Understanding of NKT Cell Biology: Progress and Paradoxes. *Annu Rev Immunol*, 23, 877-900.

KRUIDENIER, L., KUIPER, I., VAN DUIJN, W., MARKLUND, S. L., VAN HOGEZAND, R. A., LAMERS, C. B. & VERSPAGET, H. W. 2003. Differential Mucosal Expression of Three Superoxide Dismutase Isoforms in Inflammatory Bowel Disease. *J Pathol*, 201, 7-16.

KRUIDENIER, L., MACDONALD, T. T., COLLINS, J. E., PENDER, S. L. & SANDERSON, I. R. 2006. Myofibroblast Matrix Metalloproteinases Activate the Neutrophil Chemoattractant CXCL7 from Intestinal Epithelial Cells. *Gastroenterology*, 130, 127-136.

KUBLI, D. A., QUINSAY, M. N., HUANG, C., LEE, Y. & GUSTAFSSON, Å. B. 2008. BNIP3 Functions as a Mitochondrial Sensor of Oxidative Stress During Myocardial Ischemia and Reperfusion. *Am J Physiol Heart Circ Physiol*, 295, 2025-2031.

KUCI, Z., BONIG, H., KREYENBERG, H., BUNOS, M., JAUCH, A., JANSSEN, J. W., SKIFIC, M., MICHEL, K., EISING, B., LUCCHINI, G., BAKHTIAR, S., GREIL, J., LANG, P., BASU, O., VON LUETTICHAU, I., SCHULZ, A., SYKORA, K. W., JARISCH, A., SOERENSEN, J., SALZMANN-MANRIQUE, E., SEIFRIED, E., KLINGEBIEL, T., BADER, P. & KUCI, S. 2016. Mesenchymal Stromal Cells from Pooled Mononuclear Cells of Multiple Bone Marrow Donors as Rescue Therapy in Pediatric Severe Steroid-Refractory Graft-Versus-Host Disease: A Multicenter Survey. *Haematologica*, 101, 985-994.

KULKARNI, S., MICCI, M.-A., LESER, J., SHIN, C., TANG, S.-C., FU, Y.-Y., LIU, L., LI, Q., SAHA, M. & LI, C. 2017. Adult Enteric Nervous System in Health Is Maintained by a Dynamic Balance between Neuronal Apoptosis and Neurogenesis. *Proc Natl Acad Sci U S A*, 114, 3709-3718.

KUNDA, P., RODRIGUES, NELIO T. L., MOEENDARBARY, E., LIU, T., IVETIC, A., CHARRAS, G. & BAUM, B. 2012. Pp1-Mediated Moesin Dephosphorylation Couples Polar Relaxation to Mitotic Exit. *Curr Biol*, 22, 231-236.

KUWANO, Y., TOMINAGA, K., KAWAHARA, T., SASAKI, H., TAKEO, K., NISHIDA, K., MASUDA, K., KAWAI, T., TESHIMA-KONDO, S. & ROKUTAN, K. 2008. Tumor Necrosis Factor Alpha Activates Transcription of the Nadph Oxidase Organizer 1 (NOXO1) Gene and Upregulates Superoxide Production in Colon Epithelial Cells. *Free Radic Biol Med*, 45, 1642-52.

KWAK, D. J., KWAK, S. D. & GAUDA, E. B. 2006. The Effect of Hyperoxia on Reactive Oxygen Species (ROS) in Rat Petrosal Ganglion Neurons During Development Using Organotypic Slices. *Pediatr Res*, 60, 371-376.

LAKHAN, S. E. & KIRCHGESSNER, A. 2010. Neuroinflammation in Inflammatory Bowel Disease. *J Neuroinflammation*, 7, 37.

LANDGREN, A. M., LANDGREN, O., GRIDLEY, G., DORES, G. M., LINET, M. S. & MORTON, L. M. 2011. Autoimmune Disease and Subsequent Risk of Developing Alimentary Tract Cancers among 4.5 Million US Male Veterans. *Cancer*, 117, 1163-1171.

LANZA, C., MORANDO, S., VOCI, A., CANESI, L., PRINCIPATO, M. C., SERPERO, L. D., MANCARDI, G., UCCELLI, A. & VERGANI, L. 2009. Neuroprotective Mesenchymal Stem Cells Are Endowed with a Potent Antioxidant Effect *in vivo*. *J Neurochem*, 110, 1674-1684.

LAU, A., WANG, S., LIU, W., HAIG, A., ZHANG, Z.-X. & JEVNIKAR, A. M. 2014. Glycyrrhizic Acid Ameliorates HMGB1-Mediated Cell Death and Inflammation after Renal Ischemia Reperfusion Injury. *Am J Nephrol*, 40, 84-95.

LAZARIDIS, L.-D., PISTIKI, A., GIAMARELLOS-BOURBOULIS, E. J., GEORGITSI, M., DAMORAKI, G., POLYMEROS, D., DIMITRIADIS, G. D. & TRIANTAFYLLOU, K. 2017. Activation of NLRP3 Inflammasome in Inflammatory Bowel Disease: Differences between Crohn's Disease and Ulcerative Colitis. *Dig Dis Sci*, 62, 2348-2356.

LAZEBNIK, L., KNIAZEV, O., KONOPLIANNIKOV, A., PARFENOV, A., RUCHKINA, I., MIKHAĬLOVA, Z., TSAREGORODTSEVA, T., KHOMERIKI, S., ROGOZINA, V. & GUDKOVA, R. 2010a. Allogeneic Mesenchymal Stromal Cells in Patients with Ulcerative Colitis: Two Years of Observation. *Experimental & clinical gastroenterology*, 11, 3-15. Article in Russian.

LAZEBNIK, L., KONOPLIANNIKOV, A., KNIAZEV, O., PARFENOV, A., TSAREGORODTSEVA, T., RUCHKINA, I., KHOMERIKI, S., ROGOZINA, V. & KONOPLIANNIKOVA, O. 2010b. Use of Allogeneic Mesenchymal Stem Cells in the Treatment of Intestinal Inflammatory Diseases. *Ter Arkh*, 82, 38-43. Article in Russian.

LAZEBNIK, L. B., KNYAZEV, O. V., PARFENOV, A. I., RUCHKINA, I. N., SHCHERBAKOV, P. L., KHOMERIKI, S. G. & KONOPLYANNIKOV, A. G. 2012. Optimization of Cell Therapy in Patients with Inflammatory Bowel Diseases. *Ter Arkh*, 84, 10-7. Article in Russian.

LEE, B. C., SHIN, N., LEE, J. Y., KANG, I., KIM, J. J., LEE, S. E., CHOI, S. W., WEBSTER, G. A. & KANG, K. S. 2018. MIS416 Enhances Therapeutic Functions of Human Umbilical Cord Blood-Derived Mesenchymal Stem Cells against Experimental Colitis by Modulating Systemic Immune Milieu. *Front Immunol*, 9, 1078.

LEE, H.-Y. & HONG, I.-S. 2017. Double-Edged Sword of Mesenchymal Stem Cells: Cancer-Promoting Versus Therapeutic Potential. *Cancer Sci*, 108, 1939-1946.

LEE, H. J., OH, S. H., JANG, H. W., KWON, J. H., LEE, K. J., KIM, C. H., PARK, S. J., HONG, S. P., CHEON, J. H., KIM, T. I. & KIM, W. H. 2016. Long-Term Effects of Bone Marrow-Derived Mesenchymal Stem Cells in Dextran Sulfate Sodium-Induced Murine Chronic Colitis. *Gut Liver*, 10, 412-9.

LEE, J., LEE, S., LEE, C. Y., SEO, H.-H., SHIN, S., CHOI, J.-W., KIM, S. W., PARK, J.-C., LIM, S. & HWANG, K.-C. 2017. Adipose-Derived Stem Cell-Released Osteoprotegerin Protects Cardiomyocytes from Reactive Oxygen Species-Induced Cell Death. *Stem Cell Res Ther*, 8, 195.

LEE, R. H., KIM, B., CHOI, I., KIM, H., CHOI, H. S., SUH, K., BAE, Y. C. & JUNG, J. S. 2004. Characterization and Expression Analysis of Mesenchymal Stem Cells from Human Bone Marrow and Adipose Tissue. *Cell Physiol Biochem*, 14, 311-24.

LEE, S. Y., JEON, H. M., KIM, C. H., JEONG, E. K., JU, M. K., PARK, S. Y., JUNG, S. Y., KIM, Y. J., LIM, S. C., HAN, S. I. & KANG, H. S. 2010. Cuznsod and Mnsod Inhibit Metabolic Stress-Induced Necrosis and Multicellular Tumour Spheroid Growth. *Int J Oncol*, 37, 195-202.

LEE, W. Y., PARK, K. J., CHO, Y. B., YOON, S. N., SONG, K. H., KIM, D. S., JUNG, S. H., KIM, M., YOO, H. W. & KIM, I. 2013. Autologous Adipose Tissue-Derived Stem Cells Treatment Demonstrated Favorable and Sustainable Therapeutic Effect for Crohn's Fistula. *Stem Cells*, 31, 2575-2581.

LEGAKI, E., ROUBELAKIS, M. G., THEODOROPOULOS, G. E., LAZARIS, A., KOLLIA, A., KARAMANOLIS, G., MARINOS, E. & GAZOULI, M. 2016. Therapeutic Potential of Secreted Molecules Derived from Human Amniotic Fluid Mesenchymal Stem/Stroma Cells in a Mice Model of Colitis. *Stem Cell Rev*, 12, 604-612.

LEMMENS, B., DE BUCK VAN OVERSTRAETEN, A., ARIJS, I., SAGAERT, X., VAN ASSCHE, G., VERMEIRE, S., TERTYCHNYY, A., GEBOES, K., WOLTHUIS, A., D'HOORE, A., DE HERTOGH, G., FERRANTE, M. 2017. Submucosal Plexitis as a Predictive Factor for Postoperative Endoscopic Recurrence in Patients with Crohn's Disease Undergoing a Resection with Ileocolonic Anastomosis: Results from a Prospective Single-centre Study. *J. Crohns Colitis*. 11(2):212-220.

LEWIS, R. T. & MARON, D. J. 2010. Efficacy and Complications of Surgery for Crohn's Disease. *Gastroenterol Hepatol (N Y)*, 6, 587-596.

LI, F.-J., ZOU, Y.-Y., CUI, Y., YIN, Y., GUO, G. & LU, F.-G. 2013a. Calcitonin Gene-Related Peptide Is a Promising Marker in Ulcerative Colitis. *Dig Dis Sci*, 58, 686-693.

LI, H., HANDSAKER, B., WYSOKER, A., FENNELL, T., RUAN, J., HOMER, N., MARTH, G., ABECASIS, G. & DURBIN, R. 2009. The Sequence Alignment/Map Format and Samtools. *Bioinformatics*, 25, 2078-2079.

LI, J., EZZELARAB, M. B. & COOPER, D. K. 2012. Do Mesenchymal Stem Cells Function across Species Barriers? Relevance for Xenotransplantation. *Xenotransplantation*, 19, 273-285.

LI, J., WONG, W. H., CHAN, S., SAN CHIM, J. C., CHEUNG, K. M., LEE, T. L., AU, W. Y., HA, S. Y., LIE, A. K., LAU, Y. L., LIANG, R. H. & CHAN, G. C. 2011. Factors Affecting Mesenchymal Stromal Cells Yield from Bone Marrow Aspiration. *Chin J Cancer Res*, 23, 43-48.

LI, J. H., ZHANG, N. & WANG, J. A. 2008. Improved Anti-Apoptotic and Anti-Remodeling Potency of Bone Marrow Mesenchymal Stem Cells by Anoxic Pre-Conditioning in Diabetic Cardiomyopathy. *J Endocrinol Invest*, 31, 103-110.

LI, L., LIU, S., XU, Y., ZHANG, A., JIANG, J., TAN, W., XING, J., FENG, G., LIU, H. & HUO, F. 2013b. Human Umbilical Cord-Derived Mesenchymal Stem Cells Downregulate Inflammatory Responses by Shifting the Treg/Th17 Profile in Experimental Colitis. *Pharmacology*, 92, 257-264.

LI, S.-Y., QI, Y., HU, S.-H., PIAO, F.-Y., GUAN, H., WANG, Z.-M., CHEN, R.-L. & LIU, S. 2015. Mesenchymal Stem Cells-Conditioned Medium Protects PC12 Cells against 2, 5-Hexanedione-Induced Apoptosis Via Inhibiting Mitochondria-Dependent Caspase 3 Pathway. *Toxicol Ind Health*, 33, 107-118.

LI, X., MICHAELOUDES, C., ZHANG, Y., WIEGMAN, C. H., ADCOCK, I. M., LIAN, Q., MAK, J. C. W., BHAVSAR, P. K. & CHUNG, K. F. 2018. Mesenchymal Stem Cells Alleviate Oxidative Stress–Induced Mitochondrial Dysfunction in the Airways. *J Allergy Clin Immunol*, 141, 1634-1645.

LIANG, L., DONG, C., CHEN, X., FANG, Z., XU, J., LIU, M., ZHANG, X., GU, D. S., WANG, D. & DU, W. 2011. Human Umbilical Cord Mesenchymal Stem Cells Ameliorate Mice Trinitrobenzene Sulfonic Acid (TNBS)-Induced Colitis. *Cell Transplant*, 20, 1395-1408.

LIAO, Y., SMYTH, G. K. & SHI, W. 2014. Featurecounts: An Efficient General Purpose Program for Assigning Sequence Reads to Genomic Features. *Bioinformatics*, 30, 923-930.

LIH-BRODY, L., POWELL, S. R., COLLIER, K. P., REDDY, G. M., CERCHIA, R., KAHN, E., WEISSMAN, G. S., KATZ, S., FLOYD, R. A., MCKINLEY, M. J., FISHER, S. E. & MULLIN, G. E. 1996. Increased Oxidative Stress and Decreased Antioxidant Defenses in Mucosa of Inflammatory Bowel Disease. *Dig Dis Sci*, 41, 2078-2086.

LIM, J. W., SONG, J. Y., SEO, J. Y., KIM, H. & KIM, K. H. 2009. Role of Pancreatitis-Associated Protein 1 on Oxidative Stress-Induced Cell Death of Pancreatic Acinar Cells. *Ann N Y Acad Sci*, 1171, 545-548.

LIN, A., LOURENSSEN, S., STANZEL, R. D. P. & BLENNERHASSETT, M. G. 2005. Selective Loss of NGF-Sensitive Neurons Following Experimental Colitis. *Exp Neurol*, 191, 337-343.

LIN, C.-S., LIN, G. & LUE, T. F. 2012a. Allogeneic and Xenogeneic Transplantation of Adipose-Derived Stem Cells in Immunocompetent Recipients without Immunosuppressants. *Stem Cells Dev*, 21, 2770-2778.

LIN, C. S., NING, H., LIN, G. & LUE, T. F. 2012. Is CD34 Truly a Negative Marker for Mesenchymal Stromal Cells? *Cytotherapy*, 14, 1159-1163.

LIN, Y.-T., CHERN, Y., SHEN, C.-K. J., WEN, H.-L., CHANG, Y.-C., LI, H., CHENG, T.-H. & HSIEH-LI, H. M. 2011a. Human Mesenchymal Stem Cells Prolong Survival and Ameliorate Motor Deficit through Trophic Support in Huntington's Disease Mouse Models. *PLoS One*, 6, e22924.

LIN, Y., LIN, L., WANG, Q., JIN, Y., ZHANG, Y., CAO, Y. & ZHENG, C. 2015. Transplantation of Human Umbilical Mesenchymal Stem Cells Attenuates Dextran Sulfate Sodium-Induced Colitis in Mice. *Clin Exp Pharmacol Physiol*, 42, 76-86.

LIN, Z., LIU, Y., ZHENG, Q. & HU, Q. 2011b. Increased Proportion of Nitric Oxide Synthase Immunoreactive Neurons in Rat Ileal Myenteric Ganglia after Severe Acute Pancreatitis. *BMC Gastroenterol*, 11, 127-127.

LINDBERG, G., TÖRNBLOM, H., IWARZON, M., NYBERG, B., MARTIN, J. E. & VERESS, B. 2009. Full-Thickness Biopsy Findings in Chronic Intestinal Pseudo-Obstruction and Enteric Dysmotility. *Gut*, 58, 1084-1090.

LINDEN, D., COUVRETTE, J., CIOLINO, A., MCQUOID, C., BLASZYK, H., SHARKEY, K. & MAWE, G. 2005. Indiscriminate Loss of Myenteric Neurones in the TNBS-Inflamed Guinea-Pig Distal Colon. *Neurogastroenterol Motil*, 17, 751-760.

LINDEN, D. R. 2013. Enhanced Excitability of Guinea Pig Ileum Myenteric Ah Neurons During and Following Recovery from Chemical Colitis. *Neurosci Lett*, 545, 91-95.

LINDEN, D. R., FOLEY, K., MCQUOID, C., SIMPSON, J., SHARKEY, K. & MAWE, G. M. 2005b. Serotonin Transporter Function and Expression Are Reduced in Mice with TNBS-Induced Colitis. *Neurogastroenterol Motil*, 17, 565-574.

LINDEN, D. R., SHARKEY, K. A. & MAWE, G. M. 2003. Enhanced Excitability of Myenteric Ah Neurones in the Inflamed Guinea-Pig Distal Colon. *J Physiol*, 547, 589-601.

LIU, D., LIU, L., HU, Z., SONG, Z., WANG, Y. & CHEN, Z. 2018. Evaluation of the Oxidative Stress-Related Genes Alox5, Alox5ap, Gpx1, Gpx3 and Mpo for Contribution to the Risk of Type 2 Diabetes Mellitus in the Han Chinese Population. *Diab Vasc Dis Res*, 15, 336-339.

LIU, H., MCTAGGART, S. J., JOHNSON, D. W. & GOBE, G. C. 2012. Original Article Anti-Oxidant Pathways Are Stimulated by Mesenchymal Stromal Cells in Renal Repair after Ischemic Injury. *Cytotherapy*, 14, 162-172.

LIU, L., DONG, Y., YE, M., JIN, S., YANG, J., JOOSSE, M. E., SUN, Y., ZHANG, J., LAZAREV, M. & BRANT, S. R. 2017. The Pathogenic Role of NLRP3 Inflammasome Activation in Inflammatory Bowel Diseases of Both Mice and Humans. *J Crohn's Colitis*, 11, 737-750.

LIU, S.-H., HUANG, J.-P., LEE, R. K.-K., HUANG, M.-C., WU, Y.-H., CHEN, C.-Y. & CHEN, C.-P. 2010. Paracrine Factors from Human Placental Multipotent Mesenchymal Stromal Cells Protect Endothelium from Oxidative Injury Via STAT3 and Manganese Superoxide Dismutase Activation. *Biol Reprod*, 82, 905-913.

LIU, W., ZHANG, S., GU, S., SANG, L. & DAI, C. 2015. Mesenchymal Stem Cells Recruit Macrophages to Alleviate Experimental Colitis through TGFβ1. *Cell Physiol Biochem*, 35, 858-865.

LIU, X., ZUO, D., FAN, H., TANG, Q., SHOU, Z., CAO, D. & ZOU, Z. 2013. Over-Expression of Cxcr4 on Mesenchymal Stem Cells Protect against Experimental Colitis Via Immunomodulatory Functions in Impaired Tissue. *J Mol Histol*, 45, 181-193.

LOHAN, P., TREACY, O., GRIFFIN, M. D., RITTER, T. & RYAN, A. E. 2017. Anti-Donor Immune Responses Elicited by Allogeneic Mesenchymal Stem Cells and Their Extracellular Vesicles: Are We Still Learning? *Front Immunol*, 8, 1626-1626.

LOHI, H., MAKELA, S., PULKKINEN, K., HOGLUND, P., KARJALAINEN-LINDSBERG, M.-L., PUOLAKKAINEN, P. & KERE, J. 2002. Upregulation of CFTR Expression but Not SLC26A3 and SLC9A3 in Ulcerative Colitis. *Am J Physiol Gastrointest Liver Physiol*, 283, 567-575.

LOMAX, A. E., FERNÁNDEZ, E. & SHARKEY, K. A. 2005. Plasticity of the Enteric Nervous System During Intestinal Inflammation. *Neurogastroenterol Motil*, 17, 4-15.

LOMAX, A. E. & FURNESS, J. B. 2000. Neurochemical Classification of Enteric Neurons in the Guinea-Pig Distal Colon. *Cell Tissue Res*, 302, 59-72.

LOMAX, A. E., O'HARA, J. R., HYLAND, N. P., MAWE, G. M. & SHARKEY, K. A. 2007a. Persistent Alterations to Enteric Neural Signalling in the Guinea Pig Colon Following the Resolution of Colitis. *Am J Physiol Gastrointest Liver Physiol*, 292, 482-491.

LOMAX, A. E., O'REILLY, M., NESHAT, S. & VANNER, S. J. 2007b. Sympathetic Vasoconstrictor Regulation of Mouse Colonic Submucosal Arterioles Is Altered in Experimental Colitis. *J Physiol*, 583, 719-730.

LÖNNFORS, S., VERMEIRE, S., GRECO, M., HOMMES, D., BELL, C. & AVEDANO, L. 2014. IBD and Health-Related Quality of Life—Discovering the True Impact. *J Crohn's Colitis*, 8, 1281-1286.

LOPEZ-SANTALLA, M., MANCHENO-CORVO, P., ESCOLANO, A., MENTA, R., DELAROSA, O., ABAD, J. L., BUSCHER, D., REDONDO, J. M., BUEREN, J. A., DALEMANS, W., LOMBARDO, E. & GARIN, M. I. 2017. Biodistribution and Efficacy of Human Adipose-Derived Mesenchymal Stem Cells Following Intranodal Administration in Experimental Colitis. *Front Immunol*, 8, 638.

LOPEZ-SANTALLA, M., MANCHEÑO-CORVO, P., ESCOLANO, A., MENTA, R., DELAROSA, O., REDONDO, J. M., BUEREN, J. A., DALEMANS, W., LOMBARDO, E. & GARIN, M. I. 2018. Comparative Analysis between the *in vivo* Biodistribution and Therapeutic Efficacy of Adipose-Derived Mesenchymal Stromal Cells Administered Intraperitoneally in Experimental Colitis. *Int J Mol Sci*, 19, E1853.

LOTZE, M. T. & TRACEY, K. J. 2005. High-Mobility Group Box 1 Protein (HMGB1): Nuclear Weapon in the Immune Arsenal. *Nat Rev Immunol*, 5, 331-342.

LOURENSSEN, S., MILLER, K. G. & BLENNERHASSETT, M. G. 2009. Discrete Responses of Myenteric Neurons to Structural and Functional Damage by Neurotoxins *in vitro*. *Am J Physiol Gastrointest Liver Physiol*, 297, 228-239.

LU, P., JONES, L. & TUSZYNSKI, M. 2005. BDNF-Expressing Marrow Stromal Cells Support Extensive Axonal Growth at Sites of Spinal Cord Injury. *Exp Neurol*, 191, 344-360.

LU, Q. L. & PARTRIDGE, T. A. 1998. A New Blocking Method for Application of Murine Monoclonal Antibody to Mouse Tissue Sections. *J Histochem Cytochem*, 46, 977-983.

MA, S., XIE, N., LI, W., YUAN, B., SHI, Y. & WANG, Y. 2013. Immunobiology of Mesenchymal Stem Cells. *Cell Death Differ*, 21, 216-225.

MACDONALD, T. T., MONTELEONE, G. & PENDER, S. L. 2000. Recent Developments in the Immunology of Inflammatory Bowel Disease. *Scand J Immunol*, 51, 2-9.

MACEWAN, D. J. 2002. TNF Ligands and Receptors – a Matter of Life and Death. *Br J Pharmacol*, 135, 855-875.

MAGNA, M. & PISETSKY, D. S. 2014. The Role of HMGB1 in the Pathogenesis of Inflammatory and Autoimmune Diseases. *Mol Med*, 20, 138-146.

MÄKELÄ, S., KERE, J., HOLMBERG, C. & HÖGLUND, P. 2002. SLC26A3 Mutations in Congenital Chloride Diarrhea. *Hum Mutat*, 20, 425-438.

MANICHANH, C., BORRUEL, N., CASELLAS, F. & GUARNER, F. 2012. The Gut Microbiota in IBD. *Nat Rev Gastroenterol Hepatol*, 9, 599-608.

MANOCHANTR, S., KHEOLAMAI, P., ROJPHISAN, S., CHAYOSUMRIT, M., TANTRAWATPAN, C., SUPOKAWEJ, A. & ISSARAGRISIL, S. 2013. Immunosuppressive Properties of Mesenchymal Stromal Cells Derived from Amnion, Placenta, Wharton's Jelly and Umbilical Cord. *Intern Med J*, 43, 430-439.

MAO, F., WU, Y., TANG, X., KANG, J., ZHANG, B., YAN, Y., QIAN, H., ZHANG, X. & XU, W. 2017a. Exosomes Derived from Human Umbilical Cord Mesenchymal Stem Cells Relieve Inflammatory Bowel Disease in Mice. *Biomed Res Int*, 5356760.

MAO, F., WU, Y., TANG, X., WANG, J., PAN, Z., ZHANG, P., ZHANG, B., YAN, Y., ZHANG, X., QIAN, H. & XU, W. 2017b. Human Umbilical Cord Mesenchymal Stem Cells Alleviate Inflammatory Bowel Disease through the Regulation of 15-LOX-1 in Macrophages. *Biotechnol Lett*, 39, 929-938.

MARGOLIS, K. G. & GERSHON, M. D. 2016. Enteric Neuronal Regulation of Intestinal Inflammation. *Trends Neurosci*, 39, 614-624.

MARGOLIS, K. G., STEVANOVIC, K., KARAMOOZ, N., LI, Z. S., AHUJA, A., D'AUTRÉAUX, F., SAURMAN, V., CHALAZONITIS, A. & GERSHON, M. D. 2011. Enteric Neuronal Density Contributes to the Severity of Intestinal Inflammation. *Gastroenterology*, 141, 588-598. e2.

MARTIN ARRANZ, E., MARTIN ARRANZ, M. D., ROBREDO, T., MANCHENO-CORVO, P., MENTA, R., ALVES, F. J., SUAREZ DE PARGA, J. M., MORA SANZ, P., DE LA ROSA, O., BUSCHER, D., LOMBARDO, E. & DE MIGUEL, F. 2018. Endoscopic Submucosal Injection of Adipose-Derived Mesenchymal Stem Cells Ameliorates TNBS-Induced Colitis in Rats and Prevents Stenosis. *Stem Cell Res Ther*, 9, 95.

MARTINEZ, E. C. & KOFIDIS, T. 2011. Adult Stem Cells for Cardiac Tissue Engineering. *J Mol Cell Cardiol*, 50, 312-319.

MASHAGHI, A., MARMALIDOU, A., TEHRANI, M., GRACE, P. M., POTHOULAKIS, C. & DANA, R. 2016. Neuropeptide Substance P and the Immune Response. *Cell Mol Life Sci*, 73, 4249-4264.

MASUDA, H., TAKAHASHI, Y., ASAI, S. & TAKAYAMA, T. 2003. Distinct Gene Expression of Osteopontin in Patients with Ulcerative Colitis. *J Surg Res*, 111, 85-90.

MATOTT, M. P., CIARLONE, G. E., PUTNAM, R. W. & DEAN, J. B. 2014. Normobaric Hyperoxia (95% O(2)) Stimulates CO(2)-Sensitive and CO(2)-Insensitive Neurons in the Caudal Solitary Complex of Rat Medullary Tissue Slices Maintained in 40% O(2). *Neuroscience*, 270, 98-122

MATSUOKA, K. & KANAI, T. The Gut Microbiota and Inflammatory Bowel Disease. 2015. *Semin Immunopathol*, 37, 47-55.

MATTEOLI, G., GOMEZ-PINILLA, P. J., NEMETHOVA, A., DI GIOVANGIULIO, M., CAILOTTO, C., VAN BREE, S. H., MICHEL, K., TRACEY, K. J., SCHEMANN, M., BOESMANS, W., VANDEN BERGHE, P. & BOECKXSTAENS, G. E. 2014. A Distinct Vagal Anti-Inflammatory Pathway Modulates Intestinal Muscularis Resident Macrophages Independent of the Spleen. *Gut*, 63, 938-48.

MATTHES, S. M., REIMERS, K., JANSSEN, I., LIEBSCH, C., KOCSIS, J. D., VOGT, P. M. & RADTKE, C. 2013. Intravenous Transplantation of Mesenchymal Stromal Cells to Enhance Peripheral Nerve Regeneration. *BioMed Res* Int, Article ID 573169.

MAWE, G. M., STRONG, D. S. & SHARKEY, K. A. 2009. Plasticity of Enteric Nerve Functions in the Inflamed and Postinflamed Gut. *Neurogastroenterol Motil*, 21, 481-491.

MAYER, L. 2010. Evolving Paradigms in the Pathogenesis of IBD. J Gastroenterol, 45, 9-16.

MCGRATH, J., MCDONALD, J. W. & MACDONALD, J. K. 2004. Transdermal Nicotine for Induction of Remission in Ulcerative Colitis. *Cochrane Database Syst Rev*, CD004722.

MCQUADE, R. M., CARBONE, S. E., STOJANOVSKA, V., RAHMAN, A., GWYNNE, R. M., ROBINSON, A. M., GOODMAN, C. A., BORNSTEIN, J. C. & NURGALI, K. 2016. Role of Oxidative Stress in Oxaliplatin-Induced Enteric Neuropathy and Colonic Dysmotility in Mice. *Br J Pharmacol*, 173, 3502-3521.

MCQUADE, R. M., STOJANOVSKA, V., STAVELY, R., TIMPANI, C., PETERSEN, A. C., ABALO, R., BORNSTEIN, J. C., RYBALKA, E. & NURGALI, K. 2018. Oxaliplatin-Induced Enteric Neuronal Loss and Intestinal Dysfunction Is Prevented by Co-Treatment with BGP-15. *Br J Pharmacol*, 175, 656-677.

MELIEF, S. M., GEUTSKENS, S. B., FIBBE, W. E. & ROELOFS, H. 2013. Multipotent Stromal Cells Skew Monocytes Towards an Anti-Inflammatory Interleukin-10-Producing Phenotype by Production of Interleukin-6. Haematologica, 98, 888-895.

MIKAWA, S., KINOUCHI, H., KAMII, H., GOBBEL, G. T., CHEN, S. F., CARLSON, E., EPSTEIN, C. J. & CHAN, P. H. 1996. Attenuation of Acute and Chronic Damage Following Traumatic Brain Injury in Copper, Zinc—Superoxide Dismutase Transgenic Mice. *J Neurosurg*, 85, 885-891.

MILASSIN, Á., SEJBEN, A., TISZLAVICZ, L., REISZ, Z., LÁZÁR, G., SZŰCS, M., BOR, R., BÁLINT, A., RUTKA, M., SZEPES, Z., NAGY, F., FARKAS, K., MOLNÁR, T. 2017. Analysis of risk factors - Especially Different Types of Plexitis - For Postoperative Relapse in Crohn's Disease. *World J Gastrointest Surg* 9, 167–173.

MISTELI, H., KOH, C. E., WANG, L. M., MORTENSEN, N. J., GEORGE, B., GUY, R. 2015. Myenteric Plexitis at the Proximal Resection Margin is a Predictive Marker for Surgical Recurrence of Ileocaecal Crohn's Disease. *Colorectal Dis Off J Assoc Coloproctology G B Irel* 17: 304–310.

MITTAL, R. D., MANCHANDA, P. K., BID, H. K. & GHOSHAL, U. C. 2007. Analysis of Polymorphisms of Tumor Necrosis Factor-Alpha and Polymorphic Xenobiotic Metabolizing Enzymes in Inflammatory Bowel Disease: Study from Northern India. *J Gastroenterol Hepatol*, 22, 920-924.

MIYAMOTO, S., OHNISHI, S., ONISHI, R., TSUCHIYA, I., HOSONO, H., KATSURADA, T., YAMAHARA, K., TAKEDA, H. & SAKAMOTO, N. 2017. Therapeutic Effects of Human Amnion-Derived Mesenchymal Stem Cell Transplantation and Conditioned Medium Enema in Rats with Trinitrobenzene Sulfonic Acid-Induced Colitis. *Am J Transl Res*, 9, 940-952.

MIZUNO, H., TOBITA, M. & UYSAL, A. C. 2012. Concise Review: Adipose-Derived Stem Cells as a Novel Tool for Future Regenerative Medicine. *Stem Cells*, 30, 804-810.

MOLENDIJK, I., BARNHOORN, M. C., DE JONGE-MULLER, E. S., MIEREMET-OOMS, M. A., VAN DER REIJDEN, J. J., VAN DER HELM, D., HOMMES, D. W., VAN DER MEULEN-DE JONG, A. E. & VERSPAGET, H. W. 2016. Intraluminal Injection of Mesenchymal Stromal Cells in Spheroids Attenuates Experimental Colitis. *J Crohns Colitis*, 10, 953-64.

MOLENDIJK, I., BONSING, B. A., ROELOFS, H., PEETERS, K. C. M. J., WASSER, M. N. J. M., DIJKSTRA, G., VAN DER WOUDE, C. J., DUIJVESTEIN, M., VEENENDAAL, R. A., ZWAGINGA, J.-J., VERSPAGET, H. W., FIBBE, W. E., VAN DER MEULEN-DE JONG, A. E. & HOMMES, D. W. 2015. Allogeneic Bone Marrow–Derived Mesenchymal Stromal Cells Promote Healing of Refractory Perianal Fistulas in Patients with Crohn's Disease. *Gastroenterology*, 149, 918-927.

MOLL, G., ALM, J. J., DAVIES, L. C., VON BAHR, L., HELDRING, N., STENBECK-FUNKE, L., HAMAD, O. A., HINSCH, R., IGNATOWICZ, L., LOCKE, M., LÖNNIES, H., LAMBRIS, J. D.,

TERAMURA, Y., NILSSON-EKDAHL, K., NILSSON, B. & LE BLANC, K. 2014. Do Cryopreserved Mesenchymal Stromal Cells Display Impaired Immunomodulatory and Therapeutic Properties? *Stem cells*, 32, 2430-2442.

MOLLICA, L., DE MARCHIS, F., SPITALERI, A., DALLACOSTA, C., PENNACCHINI, D., ZAMAI, M., AGRESTI, A., TRISCIUOGLIO, L., MUSCO, G. & BIANCHI, M. E. 2007. Glycyrrhizin Binds to High-Mobility Group Box 1 Protein and Inhibits Its Cytokine Activities. *Chem Biol*, 14, 431-41.

MORAMPUDI, V., DALWADI, U., BHINDER, G., SHAM, H. P., GILL, S. K., CHAN, J., BERGSTROM, K. S. B., HUANG, T., MA, C., JACOBSON, K., GIBSON, D. L. & VALLANCE, B. A. 2016. The Goblet Cell-Derived Mediator RELM-β Drives Spontaneous Colitis in Muc2-Deficient Mice by Promoting Commensal Microbial Dysbiosis. *Mucosal Immunol*, 9, 1218-1233.

MORCUENDE, S., MUÑOZ-HERNÁNDEZ, R., BENÍTEZ-TEMIÑO, B., PASTOR, A. & DE LA CRUZ, R. 2013. Neuroprotective Effects of NGF, BDNF, NT-3 and GDNF on Axotomized Extraocular Motoneurons in Neonatal Rats. *Neuroscience*, 250, 31-48.

MOSNA, F., SENSEBE, L. & KRAMPERA, M. 2010. Human Bone Marrow and Adipose Tissue Mesenchymal Stem Cells: A User's Guide. *Stem Cells Dev*, 19, 1449-1470.

MOTAVALLIAN-NAEINI, A., ANDALIB, S., RABBANI, M., MAHZOUNI, P., AFSHARIPOUR, M. & MINAIYAN, M. 2012. Validation and Optimization of Experimental Colitis Induction in Rats Using 2, 4, 6-Trinitrobenzene Sulfonic Acid. *Res Pharm Sci*, 7, 159-169.

MOVAFAGH, S., CROOK, S. & VO, K. 2015. Regulation of Hypoxia-Inducible Factor-1a by Reactive Oxygen Species: New Developments in an Old Debate. *J Cell Biochem*, 116, 696-703.

MUDDHRRY, P. K., GHATKI, M. A., SPOKKS, R. A., JONHS, P. M., PIERSON, A. M., HAMID, Q. A., KANSE, S., AMARA, S. G., BURRIK, J. M., LEGON, S., POLAK, J. M. & BLOOM, S. R. 1988. Differential Expression of α-CGRP and β-CGRP by Primary Sensory Neurons and Enteric Autonomic Neurons of the Rat. *Neuroscience*, 25, 195-205.

MULLER, PAUL A., KOSCSÓ, B., RAJANI, GAURAV M., STEVANOVIC, K., BERRES, M.-L., HASHIMOTO, D., MORTHA, A., LEBOEUF, M., LI, X.-M., MUCIDA, D., STANLEY, E. R., DAHAN, S., MARGOLIS, KARA G., GERSHON, MICHAEL D., MERAD, M. & BOGUNOVIC, M. 2014. Crosstalk between Muscularis Macrophages and Enteric Neurons Regulates Gastrointestinal Motility. *Cell*, 158, 300-313.

MURPHY, J. M. & VINCE, J. E. 2015. Post-Translational Control of RIPK3 and MLKL Mediated Necroptotic Cell Death. *F1000Res*, 4, 1297.

MURPHY, MICHAEL P. 2009. How Mitochondria Produce Reactive Oxygen Species. *Biochem J*, 417, 1-13.

NAIK, E. & DIXIT, V. M. 2011. Mitochondrial Reactive Oxygen Species Drive Proinflammatory Cytokine Production. *J Exp Med*, 208, 417-420.

NAM, Y. S., KIM, N., IM, K. I., LIM, J. Y., LEE, E. S. & CHO, S. G. 2015. Negative Impact of Bone-Marrow-Derived Mesenchymal Stem Cells on Dextran Sulfate Sodium-Induced Colitis. *World J Gastroenterol*, 21, 2030-2039.

NAN, Z., FAN, H., TANG, Q., ZHANG, M., XU, M., CHEN, Q., LIU, Y., DONG, Y., WU, H. & DENG, S. 2018. Dual Expression of CXCR4 and IL-35 Enhances the Therapeutic Effects of BMSCs on TNBS-Induced Colitis in Rats through Expansion of Tregs and Suppression of Th17cells. *Biochem Biophys Res Commun*, 499, 727-734.

NEBERT, D. W. & RUSSELL, D. W. 2002. Clinical Importance of the Cytochromes P450. *The Lancet*, 360, 1155-1162.

NEGRONI, A., CUCCHIARA, S. & STRONATI, L. 2015. Apoptosis, Necrosis, and Necroptosis in the Gut and Intestinal Homeostasis. *Mediators Inflamm*, Article ID 250762.

NEUHUBER, B., SWANGER, S. A., HOWARD, L., MACKAY, A. & FISCHER, I. 2008. Effects of Plating Density and Culture Time on Bone Marrow Stromal Cell Characteristics. *Exp Hematol*, 36, 1176-1185.

NEUNLIST, M., AUBERT, P., TOQUET, C., ORESHKOVA, T., BAROUK, J., LEHUR, P., SCHEMANN, M. & GALMICHE, J. 2003a. Changes in Chemical Coding of Myenteric Neurones in Ulcerative Colitis. *Gut*, 52, 84-90.

NEUNLIST, M., TOUMI, F., ORESCHKOVA, T., DENIS, M., LEBORGNE, J., LABOISSE, C. L., GALMICHE, J. P. & JARRY, A. 2003b. Human ENS Regulates the Intestinal Epithelial Barrier Permeability and a Tight Junction-Associated Protein ZO-1 via Vipergic Pathways. *Am J Physiol Gastrointest Liver Physiol*, 285, 1028-1036.

NG, S. C. 2014. Epidemiology of Inflammatory Bowel Disease: Focus on Asia. *Best Pract Res Clin Gastroenterol*, 28, 363-372.

NIKOLIC, A., SIMOVIC MARKOVIC, B., GAZDIC, M., RANDALL HARRELL, C., FELLABAUM, C., JOVICIC, N., DJONOV, V., ARSENIJEVIC, N., M, L. L., STOJKOVIC, M. & VOLAREVIC, V. 2018. Intraperitoneal Administration of Mesenchymal Stem Cells Ameliorates Acute Dextran Sulfate Sodium-Induced Colitis by Suppressing Dendritic Cells. *Biomed Pharmacother*, 100, 426-432.

NISHIDA, A., HIDAKA, K., KANDA, T., IMAEDA, H., SHIOYA, M., INATOMI, O., BAMBA, S., KITOH, K., SUGIMOTO, M. & ANDOH, A. 2016. Increased Expression of Interleukin-36, a Member of the Interleukin-1 Cytokine Family, in Inflammatory Bowel Disease. *Inflamm Bowel Dis*, 22, 303-314.

NOVAK, E. A. & MOLLEN, K. P. 2015. Mitochondrial Dysfunction in Inflammatory Bowel Disease. *Front Cell Dev Biol*, 3, 62-62.

NURGALI, K. 2009. Plasticity and Ambiguity of the Electrophysiological Phenotypes of Enteric Neurons. *Neurogastroenterol Motil*, 21, 903-913.

NURGALI, K., NGUYEN, T. V., MATSUYAMA, H., THACKER, M., ROBBINS, H. L. & FURNESS, J. B. 2007. Phenotypic Changes of Morphologically Identified Guinea-Pig Myenteric Neurons Following Intestinal Inflammation. *J Physiol*, 583, 593-609.

NURGALI, K., NGUYEN, T. V., THACKER, M., PONTELL, L. & FURNESS, J. B. 2009. Slow Synaptic Transmission in Myenteric Ah Neurons from the Inflamed Guinea Pig Ileum. *Am J Physiol Gastrointest Liver Physiol*, 297, 582-593.

NURGALI, K., QU, Z., HUNNE, B., THACKER, M., PONTELL, L. & FURNESS, J. B. 2011. Morphological and Functional Changes in Guinea-Pig Neurons Projecting to the Ileal Mucosa at Early Stages after Inflammatory Damage. *J Physiol*, 589, 325-339.

NURGALI, K., STOJANOVSKA, V., MCQUADE, R., RAHMAN, A., DONALD, E., ROBINSON, A., MYERS, D. & BORNSTEIN, J. 2018. Enteric Nervous System as a Therapeutic Target to Alleviate Gastrointestinal Side-Effects of Chemotherapy. Oral session presented at FNM 2018 – 3rd Meeting of the Federation of Neurogastroenterology and Motility, Amsterdam, The Netherlands.

O'CONNOR, B. P., RAMAN, V. S., ERICKSON, L. D., COOK, W. J., WEAVER, L. K., AHONEN, C., LIN, L.-L., MANTCHEV, G. T., BRAM, R. J. & NOELLE, R. J. 2004. BCMA Is Essential for the Survival of Long-Lived Bone Marrow Plasma Cells. *J Exp Med*, 199, 91-98.

OEHMICHEN, M. & REIFFERSCHEID, P. 1977. Intramural Ganglion Cell Degeneration in Inflammatory Bowel Disease. *Digestion*, 15, 482-496.

OH, J. Y., KO, J. H., LEE, H. J., YU, J. M., CHOI, H., KIM, M. K., WEE, W. R. & PROCKOP, D. J. 2014. Mesenchymal Stem/Stromal Cells Inhibit the NLRP3 Inflammasome by Decreasing Mitochondrial Reactive Oxygen Species. *Stem Cells*, 32, 1553-1563.

OHKOUCHI, S., BLOCK, G. J., KATSHA, A. M., KANEHIRA, M., EBINA, M., KIKUCHI, T., SAIJO, Y., NUKIWA, T. & PROCKOP, D. J. 2012. Mesenchymal Stromal Cells Protect Cancer Cells from ROS-Induced Apoptosis and Enhance the Warburg Effect by Secreting STC1. *Mol Ther*, 20, 417-423.

OHNISHI, M., KATSUKI, H., FUKUTOMI, C., TAKAHASHI, M., MOTOMURA, M., FUKUNAGA, M., MATSUOKA, Y., ISOHAMA, Y., IZUMI, Y., KUME, T., INOUE, A. & AKAIKE, A. 2011. HMGB1 Inhibitor Glycyrrhizin Attenuates Intracerebral Hemorrhage-Induced Injury in Rats. *Neuropharmacology*, 61, 975-980.

OHSAWA, I., NISHIMAKI, K., YASUDA, C., KAMINO, K. & OHTA, S. 2003. Deficiency in a Mitochondrial Aldehyde Dehydrogenase Increases Vulnerability to Oxidative Stress in PC12 Cells. *J Neurochem*, 84, 1110-1117.

OIKONOMOPOULOS, A., VAN DEEN, W. K., MANANSALA, A.-R., LACEY, P. N., TOMAKILI, T. A., ZIMAN, A. & HOMMES, D. W. 2015. Optimization of Human Mesenchymal Stem Cell Manufacturing: The Effects of Animal/Xeno-Free Media. *Sci Rep*, 5, 16570-16570.

OKAMOTO, R. 2011. Epithelial Regeneration in Inflammatory Bowel Diseases. *Inflamm Regen*, 31, 275-281.

OKUMA, Y., LIU, K., WAKE, H., LIU, R., NISHIMURA, Y., HUI, Z., TESHIGAWARA, K., HARUMA, J., YAMAMOTO, Y., YAMAMOTO, H., DATE, I., TAKAHASHI, H. K., MORI, S. & NISHIBORI, M. 2014. Glycyrrhizin Inhibits Traumatic Brain Injury by Reducing HMGB1–RAGE Interaction. *Neuropharmacology*, 85, 18-26.

OKUN, E., GRIFFIOEN, K. J., LATHIA, J. D., TANG, S.-C., MATTSON, M. P. & ARUMUGAM, T. V. 2009. Toll-Like Receptors in Neurodegeneration. *Brain Res*, 59, 278-292.

ONISHI, R., OHNISHI, S., HIGASHI, R., WATARI, M., YAMAHARA, K., OKUBO, N., NAKAGAWA, K., KATSURADA, T., SUDA, G., NATSUIZAKA, M., TAKEDA, H. & SAKAMOTO, N. 2015. Human Amnion-Derived Mesenchymal Stem Cell Transplantation Ameliorates Dextran Sulfate Sodium-Induced Severe Colitis in Rats. *Cell Transplant*, 24, 2601-2614.

ONKEN, J., GALLUP, D., HANSON, J., PANDAK, M. & CUSTER, L. 2006. Successful Outpatient Treatment of Refractory Crohn's Disease Using Adult Mesenchymal Stem Cells. Presented at the American College of Gastroenterology annual meeting - 2006.

ONYIAH, J. C., SCHAEFER, R. E. M. & COLGAN, S. P. 2018. A Central Role for Heme Oxygenase-1 in the Control of Intestinal Epithelial Chemokine Expression. *J Innate Immun*, 10, 228-238.

OTAGIRI, S., OHNISHI, S., MIURA, A., HAYASHI, H., KUMAGAI, I., ITO, Y. M., KATSURADA, T., NAKAMURA, S., OKAMOTO, R. & YAMAHARA, K. 2018. Evaluation of Amnion-Derived Mesenchymal Stem Cells for Treatment-Resistant Moderate Crohn's Disease: Study Protocol for a Phase I/Ii, Dual-Centre, Open-Label, Uncontrolled, Dose–Response Trial. *BMJ open gastroenterol*, 5, e000206.

OZ, H. S., ZHONG, J. & DE VILLIERS, W. J. 2009. Pattern Recognition Scavenger Receptors, Sr-a and Cd36, Have an Additive Role in the Development of Colitis in Mice. *Dig Dis Sci*, 54, 2561–2567.

OZSOLAK, F. & MILOS, P. M. 2011. RNA Sequencing: Advances, Challenges and Opportunities. *Nat Rev Genet*, 12, 87-98.

PACHECO, R., RIQUELME, E. & KALERGIS, A. M. 2010. Emerging Evidence for the Role of Neurotransmitters in the Modulation of T Cell Responses to Cognate Ligands. *Cent Nerv Syst Agents Med Chem*, 10, 65-83.

PACHER, P., BECKMAN, J. S. & LIAUDET, L. 2007. Nitric Oxide and Peroxynitrite in Health and Disease. *Physiol Rev*, 87, 315-424.

PAK, S., HWANG, S. W., SHIM, I. K., BAE, S. M., RYU, Y.-M., KIM, H.-B., DO, E.-J., SON, H.-N., CHOI, E.-J., PARK, S.-H., KIM, S.-Y., PARK, S. H., YE, B. D., YANG, S.-K., KANAI, N., MAEDA, M.,

OKANO, T., YANG, D.-H., BYEON, J.-S. & MYUNG, S.-J. 2018. Endoscopic Transplantation of Mesenchymal Stem Cell Sheets in Experimental Colitis in Rats. *Sci Rep*, 8, 11314.

PALONE, F., VITALI, R., CUCCHIARA, S., PIERDOMENICO, M., NEGRONI, A., ALOI, M., NUTI, F., FELICE, C., ARMUZZI, A. & STRONATI, L. 2014. Role of HMGB1 as a Suitable Biomarker of Subclinical Intestinal Inflammation and Mucosal Healing in Patients with Inflammatory Bowel Disease. *Inflamm Bowel Dis*, 20, 1448-1457.

PANES, J., GARCIA-OLMO, D., VAN ASSCHE, G., COLOMBEL, J. F., REINISCH, W., BAUMGART, D. C., DIGNASS, A., NACHURY, M., FERRANTE, M., KAZEMI-SHIRAZI, L., GRIMAUD, J. C., DE LA PORTILLA, F., GOLDIN, E., RICHARD, M. P., LESELBAUM, A. & DANESE, S. 2016. Expanded Allogeneic Adipose-Derived Mesenchymal Stem Cells (Cx601) for Complex Perianal Fistulas in Crohn's Disease: A Phase 3 Randomised, Double-Blind Controlled Trial. *Lancet*, 388, 1281-90.

PANFOLI, I., RAVERA, S., PODESTA, M., COSSU, C., SANTUCCI, L., BARTOLUCCI, M., BRUSCHI, M., CALZIA, D., SABATINI, F., BRUSCHETTINI, M., RAMENGHI, L. A., ROMANTSIK, O., MARIMPIETRI, D., PISTOIA, V., GHIGGERI, G., FRASSONI, F. & CANDIANO, G. 2016. Exosomes from Human Mesenchymal Stem Cells Conduct Aerobic Metabolism in Term and Preterm Newborn Infants. *FASEB J*, 30, 1416-1424.

PARK, J. S., SVETKAUSKAITE, D., HE, Q., KIM, J. Y., STRASSHEIM, D., ISHIZAKA, A. & ABRAHAM, E. 2004. Involvement of Toll-Like Receptors 2 and 4 in Cellular Activation by High Mobility Group Box 1 Protein. *J Biol Chem*, 279, 7370-7377.

PATTISON, D. I. & DAVIES, M. J. 2006. Reactions of Myeloperoxidase-Derived Oxidants with Biological Substrates: Gaining Chemical Insight into Human Inflammatory Diseases. *Curr Med Chem*, 13, 3271-3290.

PAYNE, N. L., SUN, G., MCDONALD, C., LAYTON, D., MOUSSA, L., EMERSON-WEBBER, A., VERON, N., SIATSKAS, C., HERSZFELD, D. & PRICE, J. 2013a. Distinct Immunomodulatory and Migratory Mechanisms Underpin the Therapeutic Potential of Human Mesenchymal Stem Cells in Autoimmune Demyelination. *Cell Transplant*, 22, 1409-1425.

PAYNE, N. L., SUN, G., MCDONALD, C., MOUSSA, L., EMERSON-WEBBER, A., LOISEL-MEYER, S., MEDIN, J. A., SIATSKAS, C. & BERNARD, C. C. 2013b. Human Adipose-Derived Mesenchymal Stem Cells Engineered to Secrete IL-10 Inhibit APC Function and Limit CNS Autoimmunity. *Brain Behav Immun*, 30, 103-114.

PELUFFO, H., ACARIN, L., ARÍS, A., GONZÁLEZ, P., VILLAVERDE, A., CASTELLANO, B. & GONZÁLEZ, B. 2006. Neuroprotection from NMDA Excitotoxic Lesion by Cu/Zn Superoxide Dismutase Gene Delivery to the Postnatal Rat Brain by a Modular Protein Vector. *BMC Neurosci*, 7, 35.

PEREIRA, C., COELHO, R., GRÁCIO, D., DIAS, C., SILVA, M., PEIXOTO, A., LOPES, P., COSTA, C., TEIXEIRA, J. P., MACEDO, G. & MAGRO, F. 2016. DNA Damage and Oxidative DNA Damage in Inflammatory Bowel Disease. *J Crohn's Colitis*, 10, 1316-1323.

PEREZ-MERINO, E. M., USON-CASAUS, J. M., DUQUE-CARRASCO, J., ZARAGOZA-BAYLE, C., MARINAS-PARDO, L., HERMIDA-PRIETO, M., VILAFRANCA-COMPTE, M., BARRERA-CHACON, R. & GUALTIERI, M. 2015. Safety and Efficacy of Allogeneic Adipose Tissue-Derived Mesenchymal Stem Cells for Treatment of Dogs with Inflammatory Bowel Disease: Endoscopic and Histological Outcomes. *Vet J*, 206, 391-397.

PEROTTI, C., FANTE, C. D., VIARENGO, G., PARISI, C., MARCHESI, A., BERGAMASCHI, P. & SALVANESCHI, L. 2006. An Alternative Technique to Wash out DMSO from Thawed PBSC for Autotransplant. Blood, 108, 5213-5213.

PERRIER, E., RONZIÈRE, M.-C., BAREILLE, R., PINZANO, A., MALLEIN-GERIN, F. & FREYRIA, A.-M. 2011. Analysis of Collagen Expression During Chondrogenic Induction of Human Bone Marrow Mesenchymal Stem Cells. *Biotechnol Lett*, 33, 2091-2101.

PETERS, L. A., PERRIGOUE, J., MORTHA, A., IUGA, A., SONG, W. M., NEIMAN, E. M., LLEWELLYN, S. R., DI NARZO, A., KIDD, B. A., TELESCO, S. E., ZHAO, Y., STOJMIROVIC, A., SENDECKI, J., SHAMEER, K., MIOTTO, R., LOSIC, B., SHAH, H., LEE, E., WANG, M., FAITH, J. J., KASARSKIS, A., BRODMERKEL, C., CURRAN, M., DAS, A., FRIEDMAN, J. R., FUKUI, Y., HUMPHREY, M. B., IRITANI, B. M., SIBINGA, N., TARRANT, T. K., ARGMANN, C., HAO, K., ROUSSOS, P., ZHU, J., ZHANG, B., DOBRIN, R., MAYER, L. F. & SCHADT, E. E. 2017. A Functional Genomics Predictive Network Model Identifies Regulators of Inflammatory Bowel Disease. *Nat Genet*, 49, 1437-1449.

PHILLIPS, R. J. & POWLEY, T. L. 2007. Innervation of the Gastrointestinal Tract: Patterns of Aging. *Auton Neurosci*, 136, 1-19.

PHILLIPS, T. E., PHILLIPS, T. H. & NEUTRA, M. R. 1984. Regulation of Intestinal Goblet Cell Secretion. Iv. Electrical Field Stimulation *in vitro*. *Am J Physiol Cell Physiol*, 247, 682-687.

PHINNEY, D. G., DI GIUSEPPE, M., NJAH, J., SALA, E., SHIVA, S., ST CROIX, C. M., STOLZ, D. B., WATKINS, S. C., DI, Y. P., LEIKAUF, G. D., KOLLS, J., RICHES, D. W. H., DEIULIIS, G., KAMINSKI, N., BOREGOWDA, S. V., MCKENNA, D. H. & ORTIZ, L. A. 2015. Mesenchymal Stem Cells Use Extracellular Vesicles to Outsource Mitophagy and Shuttle Micrornas. *Nat Commun*, 6, 8472.

PIECHOTA-POLANCZYK, A. & FICHNA, J. 2014. Review Article: The Role of Oxidative Stress in Pathogenesis and Treatment of Inflammatory Bowel Diseases. *Naunyn Schmiedebergs Arch Pharmacol*, 387, 605-620.

PIERDOMENICO, L., BONSI, L., CALVITTI, M., RONDELLI, D., ARPINATI, M., CHIRUMBOLO, G., BECCHETTI, E., MARCHIONNI, C., ALVIANO, F., FOSSATI, V., STAFFOLANI, N., FRANCHINA, M., GROSSI, A. & BAGNARA, G. P. 2005. Multipotent Mesenchymal Stem Cells with Immunosuppressive Activity Can Be Easily Isolated from Dental Pulp. *Transplantation*, 80, 836-842.

PIRYAEI, A., VALOJERDI, M. R., SHAHSAVANI, M. & BAHARVAND, H. 2011. Differentiation of Bone Marrow-Derived Mesenchymal Stem Cells into Hepatocyte-Like Cells on Nanofibers and Their Transplantation into a Carbon Tetrachloride-Induced Liver Fibrosis Model. *Stem Cell Rev*, 7, 103-118.

PITHADIA, A. B. & JAIN, S. 2011. Treatment of Inflammatory Bowel Disease (IBD). *Pharmacol Rep*, 63, 629-642.

PLANELL, N., LOZANO, J. J., MORA-BUCH, R., MASAMUNT, M. C., JIMENO, M., ORDÁS, I., ESTELLER, M., RICART, E., PIQUÉ, J. M., PANÉS, J. & SALAS, A. 2013. Transcriptional Analysis of the Intestinal Mucosa of Patients with Ulcerative Colitis in Remission Reveals Lasting Epithelial Cell Alterations. *Gut*, 62, 967-976.

POCHARD, C., COQUENLORGE, S., FREYSSINET, M., NAVEILHAN, P., BOURREILLE, A., NEUNLIST, M. & ROLLI-DERKINDEREN, M. 2018. The Multiple Faces of Inflammatory Enteric Glial Cells: Is Crohn's Disease a Gliopathy? *Am J Physiol Gastrointest Liver Physiol*, 315, 1-11.

POLAZZI, E., MENGONI, I., CAPRINI, M., PEÑA-ALTAMIRA, E., KURTYS, E. & MONTI, B. 2013. Copper-Zinc Superoxide Dismutase (Sod1) Is Released by Microglial Cells and Confers Neuroprotection against 6-Ohda Neurotoxicity. *Neurosignals*, 21, 112-128.

POLI, E., LAZZARETTI, M., GRANDI, D., POZZOLI, C. & CORUZZI, G. 2001. Morphological and Functional Alterations of the Myenteric Plexus in Rats with TNBS-Induced Colitis. *Neurochem Res*, 26, 1085-1093.

PONTELL, L., CASTELUCCI, P., BAGYÁNSZKI, M., JOVIC, T., THACKER, M., NURGALI, K., BRON, R. & FURNESS, J. 2009. Structural Changes in the Epithelium of the Small Intestine and Immune Cell Infiltration of Enteric Ganglia Following Acute Mucosal Damage and Local Inflammation. *Virchows Arch*, 455, 55-65.

PORADA, C. D. & ALMEIDA-PORADA, G. 2010. Mesenchymal Stem Cells as Therapeutics and Vehicles for Gene and Drug Delivery. *Adv Drug Deliv Rev*, 62, 1156-1166.

POUOKAM, E., REHN, M. & DIENER, M. 2009. Effects of H2O2 at Rat Myenteric Neurones in Culture. *Eur J Pharmacol*, 615, 40-49.

POUYA, S., HEIDARI, M., BAGHAEI, K., ASADZADEH AGHDAEI, H., MORADI, A., NAMAKI, S., ZALI, M. R. & HASHEMI, S. M. 2018. Study the Effects of Mesenchymal Stem Cell Conditioned Medium Injection in Mouse Model of Acute Colitis. *Int Immunopharmacol*, 54, 86-94.

PROCKOP, D. J., BRENNER, M., FIBBE, W. E., HORWITZ, E., LE BLANC, K., PHINNEY, D. G., SIMMONS, P. J., SENSEBE, L. & KEATING, A. 2010. Defining the Risks of Mesenchymal Stromal Cell Therapy. *Cytotherapy*, 12, 576-578.

PULAVENDRAN, S., VIGNESH, J. & ROSE, C. 2010. Differential Anti-Inflammatory and Anti-Fibrotic Activity of Transplanted Mesenchymal Vs. Hematopoietic Stem Cells in Carbon Tetrachloride-Induced Liver Injury in Mice. *Int Immunopharmacol*, 10, 513-519.

PUZAN, M., HOSIC, S., GHIO, C. & KOPPES, A. 2018. Enteric Nervous System Regulation of Intestinal Stem Cell Differentiation and Epithelial Monolayer Function. *Sci Rep*, 8, 6313.

QI, S. & WU, D. 2013. Bone Marrow-Derived Mesenchymal Stem Cells Protect against Cisplatin-Induced Acute Kidney Injury in Rats by Inhibiting Cell Apoptosis. *Int J Mol Med*, 32, 1262-1272.

QIAN, S.-W., LI, X., ZHANG, Y.-Y., HUANG, H.-Y., LIU, Y., SUN, X. & TANG, Q.-Q. 2010. Characterization of Adipocyte Differentiation from Human Mesenchymal Stem Cells in Bone Marrow. *BMC Dev Biol*, 10, 47.

QIN, H. H., FILIPPI, C., SUN, S., LEHEC, S., DHAWAN, A. & HUGHES, R. D. 2015. Hypoxic Preconditioning Potentiates the Trophic Effects of Mesenchymal Stem Cells on Co-Cultured Human Primary Hepatocytes. *Stem Cell Res Ther*, 6, 237.

QIU, Y., GUO, J., MAO, R., CHAO, K., CHEN, B. L., HE, Y., ZENG, Z. R., ZHANG, S. H. & CHEN, M. H. 2016. TLR3 Preconditioning Enhances the Therapeutic Efficacy of Umbilical Cord Mesenchymal Stem Cells in TNBS-Induced Colitis Via the TLR3-Jagged-1-Notch-1 Pathway. *Mucosal Immunol*, 10, 727-742.

RAFFAGHELLO, L., BIANCHI, G., BERTOLOTTO, M., MONTECUCCO, F., BUSCA, A., DALLEGRI, F., OTTONELLO, L. & PISTOIA, V. 2008. Human Mesenchymal Stem Cells Inhibit Neutrophil Apoptosis: A Model for Neutrophil Preservation in the Bone Marrow Niche. *Stem Cells*, 26, 151-162.

RAHMAN, A. A., ROBINSON, A. M., BROOKES, S. J., ERI, R. & NURGALI, K. 2016. Rectal Prolapse in *Winnie* Mice with Spontaneous Chronic Colitis: Changes in Intrinsic and Extrinsic Innervation of the Rectum. *Cell Tissue Res*, 366, 285-299.

RAHMAN, A. A., ROBINSON, A. M., JOVANOVSKA, V., ERI, R. & NURGALI, K. 2015. Alterations in the Distal Colon Innervation in *Winnie* Mouse Model of Spontaneous Chronic Colitis. *Cell Tissue Res*, 362, 497-512.

RANA, S. V., SHARMA, S., PRASAD, K. K., SINHA, S. K. & SINGH, K. 2014. Role of Oxidative Stress & Antioxidant Defence in Ulcerative Colitis Patients from North India. *Indian J Med Res*, 139, 568-571.

RANJAN, A. & IWAKUMA, T. 2016. Non-Canonical Cell Death Induced by P53. Int J Mol Sci, 17, 2068.

RATSIMANDRESY, R. A., INDRAMOHAN, M., DORFLEUTNER, A. & STEHLIK, C. 2016. The AIM2 Inflammasome Is a Central Regulator of Intestinal Homeostasis through the IL-18/IL-22/STAT3 Pathway. *Cell Mol Immunol*, 14, 127-142.

RAUCCI, A., PALUMBO, R. & BIANCHI, M. E. 2007. HMGB1: A Signal of Necrosis. *Autoimmunity*, 40, 285-289.

RAY-GALLET, D., WOOLFE, A., VASSIAS, I., PELLENTZ, C., LACOSTE, N., PURI, A., SCHULTZ, DAVID C., PCHELINTSEV, NIKOLAY A., ADAMS, PETER D., JANSEN, LARS E. T. & ALMOUZNI, G. 2011. Dynamics of Histone H3 Deposition *In vivo* Reveal a Nucleosome Gap-Filling Mechanism for H3.3 to Maintain Chromatin Integrity. *Mol Cell*, 44, 928-941.

REDONDO, J., SARKAR, P., KEMP, K., HEESOM, K. J., WILKINS, A., SCOLDING, N. J. & RICE, C. M. 2018. Dysregulation of Mesenchymal Stromal Cell Antioxidant Responses in Progressive Multiple Sclerosis. *Stem Cells Transl Med*, 7, 748-758.

REINSHAGEN, M., FLAMIG, G., ERNST, S., GEERLING, I., WONG, H., WALSH, J. H., EYSSELEIN, V. E. & ADLER, G. 1998. Calcitonin Gene-Related Peptide Mediates the Protective Effect of Sensory Nerves in a Model of Colonic Injury. *J Pharmacol Exp Ther*, 286, 657-661.

REN, G., SU, J., ZHANG, L., ZHAO, X., LING, W., L'HUILLIE, A., ZHANG, J., LU, Y., ROBERTS, A. I. & JI, W. 2009. Species Variation in the Mechanisms of Mesenchymal Stem Cell-Mediated Immunosuppression. *Stem Cells*, 27, 1954-1962.

REN, Y., LI, Y., YAN, J., MA, M., ZHOU, D., XUE, Z., ZHANG, Z., LIU, H., YANG, H., JIA, L., ZHANG, L., ZHANG, Q., MU, S., ZHANG, R. & DA, Y. 2017. Adiponectin Modulates Oxidative Stress-Induced Mitophagy and Protects C2C12 Myoblasts against *Apoptosis*. Sci Rep, 7, 3209.

REZAIE, A., PARKER, R. D. & ABDOLLAHI, M. 2007. Oxidative Stress and Pathogenesis of Inflammatory Bowel Disease: An Epiphenomenon or the Cause? *Dig Dis Sci*, 52, 2015-2021.

RHEE, H. J., KIM, G. Y., HUH, J. W., KIM, S. W. & NA, D. S. 2000. Annexin I Is a Stress Protein Induced by Heat, Oxidative Stress and a Sulfhydryl-Reactive Agent. *Eur J Biochem*, 267, 3220-3225.

RHO, S. B., BYUN, H. J., PARK, S. Y. & CHUN, T. 2008. Calpain 6 Supports Tumorigenesis by Inhibiting Apoptosis and Facilitating Angiogenesis. *Cancer Lett*, 271, 306-313.

RHODES, J. M. & CAMPBELL, B. J. 2002. Inflammation and Colorectal Cancer: IBD-Associated and Sporadic Cancer Compared. *Trends Mol Med*, 8, 10-16.

RIEKSTINA, U., MUCENIECE, R., CAKSTINA, I., MUIZNIEKS, I. & ANCANS, J. 2008. Characterization of Human Skin-Derived Mesenchymal Stem Cell Proliferation Rate in Different Growth Conditions. *Cytotechnology*, 58, 153-162.

RIEMANN, J. & SCHMIDT, H. 1982. Ultrastructural Changes in the Gut Autonomic Nervous System Following Laxative Abuse and in Other Conditions. *Scand J Gastroenterol Suppl*, 71, 111-124.

RIVERA, L. R., POOLE, D. P., THACKER, M. & FURNESS, J. B. 2011a. The Involvement of Nitric Oxide Synthase Neurons in Enteric Neuropathies. *Neurogastroenterol Motil*, 23, 980-988.

RIVERA, L. R., THACKER, M., PONTELL, L., CHO, H.-J. & FURNESS, J. B. 2011b. Deleterious Effects of Intestinal Ischemia/Reperfusion Injury in the Mouse Enteric Nervous System Are Associated with Protein Nitrosylation. *Cell Tissue Res*, 344, 111-123.

ROBERTS, J. A., DURNIN, L., SHARKEY, K. A., MUTAFOVA-YAMBOLIEVA, V. N. & MAWE, G. M. 2013. Oxidative Stress Disrupts Purinergic Neuromuscular Transmission in the Inflamed Colon. *J Physiol*, 591, 3725-3737.

ROBINSON, A. M., GONDALIA, S. V., KARPE, A. V., ERI, R., BEALE, D. J., MORRISON, P. D., PALOMBO, E. A. & NURGALI, K. 2016. Fecal Microbiota and Metabolome in a Mouse Model of Spontaneous Chronic Colitis: Relevance to Human Inflammatory Bowel Disease. *Inflamm Bowel Dis*, 22, 2767-2787.

ROBINSON, A. M., MILLER, S., PAYNE, N., BOYD, R., SAKKAL, S. & NURGALI, K. 2015. Neuroprotective Potential of Mesenchymal Stem Cell-Based Therapy in Acute Stages of TNBS-Induced Colitis in Guinea-Pigs. *PLoS One*, 10, e0139023.

ROBINSON, A. M., RAHMAN, A. A., CARBONE, S. E., RANDALL-DEMLLO, S., FILIPPONE, R., BORNSTEIN, J. C., ERI, R. & NURGALI, K. 2017a. Alterations of Colonic Function in the *Winnie* Mouse Model of Spontaneous Chronic Colitis. *Am J Physiol Gastrointest Liver Physiol*, 312, 85-102.

ROBINSON, A. M., RAHMAN, A. A., MILLER, S., STAVELY, R., SAKKAL, S. & NURGALI, K. 2017b. The Neuroprotective Effects of Human Bone Marrow Mesenchymal Stem Cells Are Dose-Dependent in TNBS Colitis. *Stem Cell Res Ther*, 8, 87.

ROBINSON, A. M., SAKKAL, S., PARK, A., JOVANOVSKA, V., PAYNE, N., CARBONE, S. E., MILLER, S., BORNSTEIN, J. C., BERNARD, C., BOYD, R. & NURGALI, K. 2014. Mesenchymal Stem Cells and Conditioned Medium Avert Enteric Neuropathy and Colon Dysfunction in Guinea Pig TNBS-Induced Colitis. *Am J Physiol Gastrointest Liver Physiol*, 307, 1115-1129.

ROCK, K. L. & KONO, H. 2008. The Inflammatory Response to Cell Death. *Annu Rev pathmechdis Mech Dis*, 3, 99-126.

ROEMELING-VAN RHIJN, M., KHAIROUN, M., KOREVAAR, S.S., LIEVERS, E., LEUNING, D.G., IJZERMANS, J.N., BETJES, M.G., GENEVER, P.G., VAN KOOTEN, C., DE FIJTER, H.J. AND RABELINK, T.J., 2013. Human bone marrow-and adipose tissue-derived mesenchymal stromal cells are immunosuppressive *in vitro* and in a humanized allograft rejection model. *J Stem Cell Res Ther*, 6, 20780.

ROLIG, A. S., MITTGE, E. K., GANZ, J., TROLL, J. V., MELANCON, E., WILES, T. J., ALLIGOOD, K., STEPHENS, W. Z., EISEN, J. S. & GUILLEMIN, K. 2017. The Enteric Nervous System Promotes Intestinal Health by Constraining Microbiota Composition. *PLoS Biol*, 15, e2000689.

ROSS, I., THOMPSON, R., MONTGOMERY, R. & ASQUITH, P. 1979. Significance of Serum Complement Levels in Patients with Gastrointestinal Disease. *J Clin Pathol*, 32, 798-801.

ROUDKENAR, M. H., KUWAHARA, Y., BABA, T., ROUSHANDEH, A. M., EBISHIMA, S., ABE, S., OHKUBO, Y. & FUKUMOTO, M. 2007. Oxidative Stress Induced Lipocalin 2 Gene Expression: Addressing Its Expression under the Harmful Conditions. *J Radiat Res*, 48, 39-44.

RUBIO, D., GARCIA-CASTRO, J., MARTÍN, M. C., DE LA FUENTE, R., CIGUDOSA, J. C., LLOYD, A. C. & BERNAD, A. 2005. Spontaneous Human Adult Stem Cell Transformation. *Cancer Res*, 65, 3035-3039.

RUEDEN, C. T., SCHINDELIN, J., HINER, M. C., DEZONIA, B. E., WALTER, A. E., ARENA, E. T. & ELICEIRI, K. W. 2017. Imagej2: Imagej for the Next Generation of Scientific Image Data. *BMC Bioinformatics*, 18, 529.

RUNGOE, C., BASIT, S., RANTHE, M. F., WOHLFAHRT, J., LANGHOLZ, E. & JESS, T. 2013. Risk of Ischaemic Heart Disease in Patients with Inflammatory Bowel Disease: A Nationwide Danish Cohort Study. *Gut*, 62, 689-694.

RUSSELL, A. L., LEFAVOR, R. C. & ZUBAIR, A. C. 2018. Characterization and Cost-Benefit Analysis of Automated Bioreactor-Expanded Mesenchymal Stem Cells for Clinical Applications. *Transfusion (Paris)*, 58, 2374-2382.

RUSSELL, K. A., GIBSON, T. W. G., CHONG, A., CO, C. & KOCH, T. G. 2015. Canine Platelet Lysate Is Inferior to Fetal Bovine Serum for the Isolation and Propagation of Canine Adipose Tissue- and Bone Marrow-Derived Mesenchymal Stromal Cells. *PLoS One*, 10, e0136621.

RYTER, S. W., KIM, H. P., HOETZEL, A., PARK, J. W., NAKAHIRA, K., WANG, X. & CHOI, A. M. 2007. Mechanisms of Cell Death in Oxidative Stress. *Antioxid Redox Signal*, 9, 49-89.

S. PINTO, M. A., SOARES-MOTA S. LOPES, M., T.O. BASTOS, S., L.L. REIGADA, C., F. DANTAS, R., C.B. NETO, J., S. LUNA, A., MADI, K., NUNES, T. & ZALTMAN, C. 2013. Does Active Crohn's Disease Have Decreased Intestinal Antioxidant Capacity? *J Crohn's Colitis*, 7, 358-366.

SALA, E., GENUA, M., PETTI, L., ANSELMO, A., ARENA, V., CIBELLA, J., ZANOTTI, L., D'ALESSIO, S., SCALDAFERRI, F. & LUCA, G. 2015. Mesenchymal Stem Cells Reduce Colitis in Mice

Via Release of TSG6, Independently of Their Localization to the Intestine. *Gastroenterology*, 149, 163-176.

SANNA, B., BRANDT, E. B., KAISER, R. A., PFLUGER, P., WITT, S. A., KIMBALL, T. R., VAN ROOIJ, E., DE WINDT, L. J., ROTHENBERG, M. E., TSCHOP, M. H., BENOIT, S. C. & MOLKENTIN, J. D. 2006. Modulatory Calcineurin-Interacting Proteins 1 and 2 Function as Calcineurin Facilitators *in vivo*. *Proc Natl Acad Sci U S A*, 103, 7327-7332.

SANOVIC, S., LAMB, D. P. & BLENNERHASSETT, M. G. 1999. Damage to the Enteric Nervous System in Experimental Colitis. *Am J Pathol*, 155, 1051-1057.

SARKAR, P., REDONDO, J., KEMP, K., GINTY, M., WILKINS, A., SCOLDING, N. J. & RICE, C. M. 2018. Reduced Neuroprotective Potential of the Mesenchymal Stromal Cell Secretome with *Ex Vivo* Expansion, Age and Progressive Multiple Sclerosis. *Cytotherapy*, 20, 21-28.

SARNELLI, G., DE GIORGIO, R., GENTILE, F., CALÌ, G., GRANDONE, I., ROCCO, A., COSENZA, V., CUOMO, R. & D'ARGENIO, G. 2009. Myenteric Neuronal Loss in Rats with Experimental Colitis: Role of Tissue Transglutaminase-Induced Apoptosis. *Dig Liver Dis*, 41, 185-193.

SAYANI, F. A., KEENAN, C. M., VAN SICKLE, M. D., AMUNDSON, K. R., PARR, E. J., MATHISON, R. D., MACNAUGHTON, W. K., BRAUN, J. E. A. & SHARKEY, K. A. 2004. The Expression and Role of FAS Ligand in Intestinal Inflammation. *Neurogastroenterol Motil*, 16, 61-74.

SCARFE, L., TAYLOR, A., SHARKEY, J., HARWOOD, R., BARROW, M., COMENGE, J., BEEKEN, L., ASTLEY, C., SANTERAMO, I., HUTCHINSON, C., RESSEL, L., SMYTHE, J., AUSTIN, E., LEVY, R., ROSSEINSKY, M. J., ADAMS, D. J., POPTANI, H., PARK, B. K., MURRAY, P. & WILM, B. 2018. Non-Invasive Imaging Reveals Conditions That Impact Distribution and Persistence of Cells after *in vivo* Administration. *Stem Cell Res Ther*. 9, 332.

SCHELLENBERG, A., LIN, Q., SCHÜLER, H., KOCH, C. M., JOUSSEN, S., DENECKE, B., WALENDA, G., PALLUA, N., SUSCHEK, C. V. & ZENKE, M. 2011. Replicative Senescence of Mesenchymal Stem Cells Causes DNA-Methylation Changes Which Correlate with Repressive Histone Marks. *Aging*, 3, 873-888.

SCHELLENBERG, A., STIEHL, T., HORN, P., JOUSSEN, S., PALLUA, N., HO, A. D. & WAGNER, W. 2012. Population Dynamics of Mesenchymal Stromal Cells During Culture Expansion. *Cytotherapy*, 14, 401-411.

SCHEMANN, M., MICHEL, K., CEREGRZYN, M., ZELLER, F., SEIDL, S. & BISCHOFF, S. C. 2005. Human Mast Cell Mediator Cocktail Excites Neurons in Human and Guinea-Pig Enteric Nervous System. *Neurogastroenterol Motil*, 17, 281-289.

SCHIEBER, M. & CHANDEL, NAVDEEP S. 2014. Ros Function in Redox Signalling and Oxidative Stress. *Curr Biol*, 24, 453-462.

SCHNEIDER, C. A., RASBAND, W. S. & ELICEIRI, K. W. 2012. NIH Image to Imagej: 25 Years of Image Analysis. *Nature methods*, 9, 671–675.

SCHNEIDER, J., JEHLE, E. C., STARLINGER, M. J., NEUNLIST, M., MICHEL, K., HOPPE, S. & SCHEMANN, M. 2001. Neurotransmitter Coding of Enteric Neurones in the Submucous Plexus Is Changed in Non-Inflamed Rectum of Patients with Crohn's Disease. *Neurogastroenterol Motil*, 13, 255-264.

SCHNEIDER, P. R., BUHRMANN, C., MOBASHERI, A., MATIS, U. & SHAKIBAEI, M. 2011. Three-Dimensional High-Density Co-Culture with Primary Tenocytes Induces Tenogenic Differentiation in Mesenchymal Stem Cells. *J Orthop Res*, 29, 1351-1360.

SCHOULTZ, I., SODERHOLM, J. D. & MCKAY, D. M. 2011. Is Metabolic Stress a Common Denominator in Inflammatory Bowel Disease? *Inflamm Bowel Dis*, 17, 2008-2018.

SCHRADER, J. W., ZILTENER, H. J. & LESLIE, K. B. 1986. Structural Homologies among the Hemopoietins. *Proc Natl Acad Sci U S A*, 83, 2458-2462.

SCHWAB, M., SCHAFFELER, E., MARX, C., FISCHER, C., LANG, T., BEHRENS, C., GREGOR, M., EICHELBAUM, M., ZANGER, U. M. & KASKAS, B. A. 2002. Azathioprine Therapy and Adverse Drug Reactions in Patients with Inflammatory Bowel Disease: Impact of Thiopurine S-Methyltransferase Polymorphism. *Pharmacogenetics*, 12, 429-36.

SCUTERI, A., MILOSO, M., FOUDAH, D., ORCIANI, M., CAVALETTI, G. & TREDICI, G. 2011. Mesenchymal Stem Cells Neuronal Differentiation Ability: A Real Perspective for Nervous System Repair? *Curr Stem Cell Res Ther*, 6, 82-92.

SEAMAN, J. A., ALOUT, H., MEYERS, J. I., STENGLEIN, M. D., DABIRÉ, R. K., LOZANO-FUENTES, S., BURTON, T. A., KUKLINSKI, W. S., BLACK, W. C. & FOY, B. D. 2015. Age and Prior Blood Feeding of Anopheles Gambiae Influences Their Susceptibility and Gene Expression Patterns to Ivermectin-Containing Blood Meals. *BMC Genomics*, 16, 797.

SEBASTIÁN, V. P., SALAZAR, G. A., CORONADO-ARRÁZOLA, I., SCHULTZ, B. M., VALLEJOS, O. P., BERKOWITZ, L., ÁLVAREZ-LOBOS, M. M., RIEDEL, C. A., KALERGIS, A. M. & BUENO, S. M. 2018. Heme Oxygenase-1 as a Modulator of Intestinal Inflammation Development and Progression. *Front Immunol*, 9, 1956.

SEDGER, L. M. & MCDERMOTT, M. F. 2014. TNF and TNF-Receptors: From Mediators of Cell Death and Inflammation to Therapeutic Giants – Past, Present and Future. *Cytokine Growth Factor Rev*, 25, 453-472.

SEMENOV, O. V., KOESTENBAUER, S., RIEGEL, M., ZECH, N., ZIMMERMANN, R., ZISCH, A. H. & MALEK, A. 2010. Multipotent Mesenchymal Stem Cells from Human Placenta: Critical Parameters for Isolation and Maintenance of Stemness after Isolation. *Am J Obstet Gynecol*, 202, 193.

SÉMONT, A., DEMARQUAY, C., BESSOUT, R., DURAND, C., BENDERITTER, M. & MATHIEU, N. 2013. Mesenchymal Stem Cell Therapy Stimulates Endogenous Host Progenitor Cells to Improve Colonic Epithelial Regeneration. *PLoS One*, 8, e70170.

SEROR, R., RICHEZ, C., SORDET, C., RIST, S., GOSSEC, L., DIREZ, G., HOUVENAGEL, E., BERTHELOT, J.-M., PAGNOUX, C. & DERNIS, E. 2013. Pattern of Demyelination Occurring During Anti-TNF-α Therapy: A French National Survey. *Rheumatology*, 52, 868-874.

SHAH, Y. M. 2016. The Role of Hypoxia in Intestinal Inflammation. *Molecular and Cellular Pediatrics*, 3, 1.

SHALABY, S. M., AMAL, S., ABD-ALLAH, S. H., SELIM, A. O., SELIM, S. A., GOUDA, Z. A., EL MOTTELEB, D. M. A., ZANFALY, H. E., EL-ASSAR, H. M. & ABDELAZIM, S. 2014. Mesenchymal Stromal Cell Injection Protects against Oxidative Stress in Escherichia Coli–Induced Acute Lung Injury in Mice. *Cytotherapy*, 16, 764-775.

SHAMAS-DIN, A., KALE, J., LEBER, B. & ANDREWS, D. W. 2013. Mechanisms of Action of Bcl-2 Family Proteins. *Cold Spring Harb Perspect Biol*, 5, a008714.

SHARKEY, K. A. & KROESE, A. 2001. Consequences of Intestinal Inflammation on the Enteric Nervous System: Neuronal Activation Induced by Inflammatory Mediators. *The Anatomical Record*, 262, 79-90.

SHARKEY, K. A. & MAWE, G. M. 2002. Neuroimmune and Epithelial Interactions in Intestinal Inflammation. *Curr Opin Pharmacol*, 2, 669-677.

SHARMA, R., YANG, Y., SHARMA, A., AWASTHI, S. & AWASTHI, Y. C. 2004. Antioxidant Role of Glutathione S-Transferases: Protection against Oxidant Toxicity and Regulation of Stress-Mediated Apoptosis. *Antioxid Redox Signal*, 6, 289-300.

SHAW, K. A., CUTLER, D. J., OKOU, D., DODD, A., ARONOW, B. J., HABERMAN, Y., STEVENS, C., WALTERS, T. D., GRIFFITHS, A., BALDASSANO, R. N., NOE, J. D., HYAMS, J. S., CRANDALL,

W. V., KIRSCHNER, B. S., HEYMAN, M. B., SNAPPER, S., GUTHERY, S., DUBINSKY, M. C., SHAPIRO, J. M., OTLEY, A. R., DALY, M., DENSON, L. A., KUGATHASAN, S. & ZWICK, M. E. 2018. Genetic Variants and Pathways Implicated in a Pediatric Inflammatory Bowel Disease Cohort. *Genes Immun* [ahead of print]. doi: 10.1038/s41435-018-0015-2.

SHEIKH, M. H. & SOLITO, E. 2018. Annexin A1: Uncovering the Many Talents of an Old Protein. *Int J Mol Sci*, 19, 1045.

SHI, X.-Z., WINSTON, J. H. & SARNA, S. K. 2010. Differential Immune and Genetic Responses in Rat Models of Crohn's Colitis and Ulcerative Colitis. *Am J Physiol Gastrointest Liver Physiol*, 300, 41-51.

SHIBATA, T., NARUSE, K., KAMIYA, H., KOZAKAE, M., KONDO, M., YASUDA, Y., NAKAMURA, N., OTA, K., TOSAKI, T. & MATSUKI, T. 2008. Transplantation of Bone Marrow–Derived Mesenchymal Stem Cells Improves Diabetic Polyneuropathy in Rats. *Diabetes*, 57, 3099-3107.

SIES, H. 2015. Oxidative Stress: A Concept in Redox Biology and Medicine. *Redox Biol*, 4, 180-183.

SILAGI, E. S., BATISTA, P., SHAPIRO, I. M. & RISBUD, M. V. 2018. Expression of Carbonic Anhydrase Iii, a Nucleus Pulposus Phenotypic Marker, Is Hypoxia-Responsive and Confers Protection from Oxidative Stress-Induced Cell Death. *Sci Rep*, 8, 4856.

SIMARD, J.-C., CESARO, A., CHAPETON-MONTES, J., TARDIF, M., ANTOINE, F., GIRARD, D. & TESSIER, P. A. 2013. S100A8 and S100A9 Induce Cytokine Expression and Regulate the Nlrp3 Inflammasome Via Ros-Dependent Activation of NF-KB1. *PLoS One*, 8, e72138.

SIMON, H.-U., HAJ-YEHIA, A. & LEVI-SCHAFFER, F. 2000. Role of Reactive Oxygen Species (Ros) in Apoptosis Induction. *Apoptosis*, 5, 415-418.

SIMOVIC MARKOVIC, B., NIKOLIC, A., GAZDIC, M., NURKOVIC, J., DJORDJEVIC, I., ARSENIJEVIC, N., STOJKOVIC, M., LUKIC, M. L. & VOLAREVIC, V. 2016. Pharmacological Inhibition of Gal-3 in Mesenchymal Stem Cells Enhances Their Capacity to Promote Alternative Activation of Macrophages in Dextran Sulphate Sodium-Induced Colitis. *Stem Cells Int*, Article ID 2640746.

SINGH, S., BROCKER, C., KOPPAKA, V., YING, C., JACKSON, B., MATSUMOTO, A., THOMPSON, D. C. & VASILIOU, V. 2013. Aldehyde Dehydrogenases in Cellular Responses to Oxidative/Electrophilic Stress. *Free Radic Biol Med*, 56, 89-101.

SINGH, U. P., SINGH, N. P., SINGH, B., MISHRA, M. K., NAGARKATTI, M., NAGARKATTI, P. S. & SINGH, S. R. 2010. Stem Cells as Potential Therapeutic Targets for Inflammatory Bowel Disease. *Front Biosci (Schol Ed)*, 2, 993-1008.

SOHNI, A. & VERFAILLIE, C. M. 2013. Mesenchymal Stem Cells Migration Homing and Tracking. *Stem Cells Int*, Article ID 130763.

SOKOL, H., POLIN, V., LAVERGNE-SLOVE, A., PANIS, Y., TRETON, X., DRAY, X., BOUHNIK, Y., VALLEUR, P. & MARTEAU, P. 2009. Plexitis as a Predictive Factor of Early Postoperative Clinical Recurrence in Crohn's Disease. *Gut*, 58, 1218-1225.

SONG, E. M., JUNG, S. A., LEE, K. E., JANG, J. Y., LEE, K. H., TAE, C. H., MOON, C. M., JOO, Y. H., KIM, S. E., JUNG, H. K. & SHIM, K. N. 2017a. The Therapeutic Efficacy of Tonsil-Derived Mesenchymal Stem Cells in Dextran Sulfate Sodium-Induced Acute Murine Colitis Model. *Korean J Gastroenterol*, 69, 119-128.

SONG, J. Y., KANG, H. J., HONG, J. S., KIM, C. J., SHIM, J. Y., LEE, C. W. & CHOI, J. 2017b. Umbilical Cord-Derived Mesenchymal Stem Cell Extracts Reduce Colitis in Mice by Re-Polarizing Intestinal Macrophages. *Sci Rep*, 7, 9412.

SONG, W. J., LI, Q., RYU, M. O., AHN, J. O., BHANG, D. H., JUNG, Y. C. & YOUN, H. Y. 2018. TSG-6 Released from Intraperitoneally Injected Canine Adipose Tissue-Derived Mesenchymal Stem Cells Ameliorate Inflammatory Bowel Disease by Inducing M2 Macrophage Switch in Mice. *Stem Cell Res Ther*, 9, 91.

SONG, W. J., LI, Q., RYU, M. O., AHN, J. O., HA BHANG, D., CHAN JUNG, Y. & YOUN, H. Y. 2017c. TSG-6 Secreted by Human Adipose Tissue-Derived Mesenchymal Stem Cells Ameliorates Dss-Induced Colitis by Inducing M2 Macrophage Polarization in Mice. *Sci Rep*, 7, 5187.

SOONTARARAK, S., CHOW, L., JOHNSON, V., COY, J., WHEAT, W., REGAN, D. & DOW, S. 2018. Mesenchymal Stem Cells (MSC) Derived from Induced Pluripotent Stem Cells (IPSC) Equivalent to Adipose-Derived MSC in Promoting Intestinal Healing and Microbiome Normalization in Mouse Inflammatory Bowel Disease Model. *Stem Cells Transl Med*, 7, 456-467.

SOUSA, A. M. M., MEYER, K. A., SANTPERE, G., GULDEN, F. O. & SESTAN, N. 2017. Evolution of the Human Nervous System Function, Structure, and Development. *Cell*, 170, 226-247.

STADNICKI, A. 2011. Intestinal Tissue Kallikrein-Kinin System in Inflammatory Bowel Disease. *Inflamm Bowel Dis*, 17, 645-654.

STANISZ, A. M. 2001. Neurogenic Inflammation: Role of Substance P. In: BERCZI, I. & GORCZYNSKI, R. M. (eds.) Neuroimmune Biology. Elsevier.

STAVELY, R., FRASER, S., SHARMA, S., RAHMAN, A. A., STOJANOVSKA, V., SAKKAL, S., APOSTOLOPOULOS, V., BERTRAND, P. & NURGALI, K. 2018a. The Onset and Progression of Chronic Colitis Parallels Increased Mucosal Serotonin Release Via Enterochromaffin Cell Hyperplasia and Downregulation of the Serotonin Reuptake Transporter. *Inflamm Bowel Dis*, 24, 1021-1034.

STAVELY, R., ROBINSON, A., FILIPPONE, R., RAHMAN, A., SAKKAL, S. & NURGALI, K. 2018. Mesenchymal Stem Cell Therapy in Chronic Colitis: Potential Therapeutic Mechanisms in Alleviating Oxidative Stress and Enteric Neuropathy. Poster session presented at FNM 2018 – 3rd Meeting of the Federation of Neurogastroenterology and Motility, Amsterdam, The Netherlands.

STAVELY, R., ROBINSON, A. M., MILLER, S., BOYD, R., SAKKAL, S. & NURGALI, K. 2015a. Allogeneic Guinea Pig Mesenchymal Stem Cells Ameliorate Neurological Changes in Experimental Colitis. *Stem Cell Res Ther*, 6, 263.

STAVELY, R., ROBINSON, A. M., MILLER, S., BOYD, R., SAKKAL, S. & NURGALI, K. 2015b. Human Adult Stem Cells Derived from Adipose Tissue and Bone Marrow Attenuate Enteric Neuropathy in the Guinea-Pig Model of Acute Colitis. *Stem Cell Res Ther*, 6, 244.

STAVELY, R., SAKKAL, S., STOJANOVSKA, V. & NURGALI, K. 2014. Mesenchymal Stem Cells for the Treatment of Inflammatory Bowel Disease: From Experimental Models to Clinical Application. *Inflamm Regen*, 34, 184-197.

STEBBING, M., JOHNSON, P., VREMEC, M. & BORNSTEIN, J. 2001. Role of A2-Adrenoceptors in the Sympathetic Inhibition of Motility Reflexes of Guinea-Pig Ileum. *J Physiol*, 534, 465-478.

STOJANOVSKA, V., MCQUADE, R. M., FRASER, S., PRAKASH, M., GONDALIA, S., STAVELY, R., PALOMBO, E., APOSTOLOPOULOS, V., SAKKAL, S. & NURGALI, K. 2018. Oxaliplatin-Induced Changes in Microbiota, TLR4+ Cells and Enhanced HMGB1 Expression in the Murine Colon. *PLoS One*, 13, e0198359.

STORSTEEN, K. A. 1953. The Myenteric Plexus in Ulcerative Colitis. Surg Gynae Obstets, 97, 335-343.

STRAUB, R. H., GRUM, F., STRAUCH, U., CAPELLINO, S., BATAILLE, F., BLEICH, A., FALK, W., SCHÖLMERICH, J. & OBERMEIER, F. 2008. Anti-Inflammatory Role of Sympathetic Nerves in Chronic Intestinal Inflammation. *Gut*, 57, 911-921.

STRAUB, R. H., WIEST, R., STRAUCH, U. G., HÄRLE, P. & SCHÖLMERICH, J. 2006. The Role of the Sympathetic Nervous System in Intestinal Inflammation. *Gut*, 55, 1640-1649.

STRIOGA, M., VISWANATHAN, S., DARINSKAS, A., SLABY, O. & MICHALEK, J. 2012. Same or Not the Same? Comparison of Adipose Tissue-Derived Versus Bone Marrow-Derived Mesenchymal Stem and Stromal Cells. *Stem Cells Dev*, 21, 2724-2752.

STROBER, W., FUSS, I. & MANNON, P. 2007. The Fundamental Basis of Inflammatory Bowel Disease. *J Clin Invest*, 117, 514-521.

SUEMATSU, N., TSUTSUI, H., WEN, J., KANG, D., IKEUCHI, M., IDE, T., HAYASHIDANI, S., SHIOMI, T., KUBOTA, T., HAMASAKI, N. & TAKESHITA, A. 2003. Oxidative Stress Mediates Tumor Necrosis Factor-Alpha-Induced Mitochondrial DNA Damage and Dysfunction in Cardiac Myocytes. *Circulation*, 107, 1418-23.

SUN, Q., WU, W., HU, Y.-C., LI, H., ZHANG, D., LI, S., LI, W., LI, W.-D., MA, B., ZHU, J.-H., ZHOU, M.-L. & HANG, C.-H. 2014. Early Release of High-Mobility Group Box 1 (HMGB1) from Neurons in Experimental Subarachnoid Hemorrhage *in vivo* and *in vitro*. *J Neuroinflammation*, 11, 106.

SUN, T., GAO, G. Z., LI, R. F., LI, X., LI, D. W., WU, S. S., YEO, A. E. & JIN, B. 2015. Bone Marrow-Derived Mesenchymal Stem Cell Transplantation Ameliorates Oxidative Stress and Restores Intestinal Mucosal Permeability in Chemically Induced Colitis in Mice. *Am J Transl Res*, 7, 891-901.

SUNDARAM, U., HASSANAIN, H., SUNTRES, Z., YU, J. G., COOKE, H. J., GUZMAN, J. & CHRISTOFI, F. L. 2003. Rabbit Chronic Ileitis Leads to up-Regulation of Adenosine A1/A3 Gene Products, Oxidative Stress, and Immune Modulation. *Biochem Pharmacol*, 65, 1529-1538.

SUNG, J., YANG, H.-M., PARK, J., CHOI, G.-S., JOH, J.-W., KWON, C., CHUN, J., LEE, S.-K. & KIM, S.-J. Isolation and Characterization of Mouse Mesenchymal Stem Cells. *Transplant Proc*, 40, 2649-2654.

SUPLY, E., DE VRIES, P., SORET, R., COSSAIS, F. & NEUNLIST, M. 2012. Butyrate Enemas Enhance Both Cholinergic and Nitrergic Phenotype of Myenteric Neurons and Neuromuscular Transmission in Newborn Rat Colon. *Am J Physiol Gastrointest Liver Physiol*, 302, 1373-1380.

TADDIO, A., TOMMASINI, A., VALENCIC, E., BIAGI, E., DECORTI, G., DE IUDICIBUS, S., CUZZONI, E., GAIPA, G., BADOLATO, R., PRANDINI, A., BIONDI, A. & VENTURA, A. 2015. Failure of Interferon-γ Pre-Treated Mesenchymal Stem Cell Treatment in a Patient with Crohn's Disease. *World J Gastroenterol*, 21, 4379-4384.

TAGHI, G. M., MARYAM, G. K., TAGHI, L., LEILI, H. & LEYLA, M. 2012. Characterization of *in vitro* Cultured Bone Marrow and Adipose Tissue-Derived Mesenchymal Stem Cells and Their Ability to Express Neurotrophic Factors. *Cell Biol Int*, 36, 1239-1249.

TAKEYAMA, H., MIZUSHIMA, T., UEMURA, M., HARAGUCHI, N., NISHIMURA, J., HATA, T., MATSUDA, C., TAKEMASA, I., IKENAGA, M., MURATA, K., YAMAMOTO, H., DOKI, Y. & MORI, M. 2017. Adipose-Derived Stem Cells Ameliorate Experimental Murine Colitis Via Tsp-1-Dependent Activation of Latent TGF-β. *Dig Dis Sci*, 62, 1963-1974.

TAMAN, H., FENTON, C. G., HENSEL, I. V., ANDERSSEN, E., FLORHOLMEN, J. & PAULSSEN, R. H. 2018. Transcriptomic Landscape of Treatment—Naïve Ulcerative Colitis. *J Crohn's Colitis*, 12, 327-336.

TAMMA, G., VALENTI, G., GROSSINI, E., DONNINI, S., MARINO, A., MARINELLI, R. A. & CALAMITA, G. 2018. Aquaporin Membrane Channels in Oxidative Stress, Cell Signalling, and Aging: Recent Advances and Research Trends. *Oxid Med Cell Longev*, 1501847.

TANAKA, F., TOMINAGA, K., OCHI, M., TANIGAWA, T., WATANABE, T., FUJIWARA, Y., OHTA, K., OSHITANI, N., HIGUCHI, K. & ARAKAWA, T. 2008. Exogenous Administration of Mesenchymal Stem Cells Ameliorates Dextran Sulfate Sodium-Induced Colitis Via Anti-Inflammatory Action in Damaged Tissue in Rats. *Life Sci*, 83, 771-779.

TANAKA, H., ARIMURA, Y., YABANA, T., GOTO, A., HOSOKAWA, M., NAGAISHI, K., YAMASHITA, K., YAMAMOTO, H., SASAKI, Y. & FUJIMIYA, M. 2011. Myogenic Lineage Differentiated Mesenchymal Stem Cells Enhance Recovery from Dextran Sulfate Sodium-Induced Colitis in the Rat. *J Gastroenterol*, 46, 143-152.

TANG, D., KANG, R., CHEH, C.-W., LIVESEY, K. M., LIANG, X., SCHAPIRO, N. E., BENSCHOP, R., SPARVERO, L. J., AMOSCATO, A. A., TRACEY, K. J., ZEH, H. J. & LOTZE, M. T. 2010. HMGB1 Release and Redox Regulates Autophagy and Apoptosis in Cancer Cells. *Oncogene*, 29, 5299-5310.

TANG, D., KANG, R., LIVESEY, K. M., ZEH, H. J. & LOTZE, M. T. 2011. High Mobility Group Box 1 (HMGB1) Activates an Autophagic Response to Oxidative Stress. *Antioxid Redox Signal*, 15, 2185-2195.

TANG, D., SHI, Y., KANG, R., LI, T., XIAO, W., WANG, H. & XIAO, X. 2007. Hydrogen Peroxide Stimulates Macrophages and Monocytes to Actively Release HMGB1. *J Leukoc Biol*, 81, 741-747.

TANG, R. J., SHEN, S. N., ZHAO, X. Y., NIE, Y. Z., XU, Y. J., REN, J., LV, M. M., HOU, Y. Y. & WANG, T. T. 2015a. Mesenchymal Stem Cells-Regulated Treg Cells Suppress Colitis-Associated Colorectal Cancer. *Stem Cell Res Ther*, 6, 71.

TANG, X. Q., TANELIAN, D. L. & SMITH, G. M. 2004. Semaphorin3a Inhibits Nerve Growth Factor-Induced Sprouting of Nociceptive Afferents in Adult Rat Spinal Cord. *J Neurosci*, 24, 819-827.

TANG, Y., CHEN, Y., WANG, X., SONG, G., LI, Y. & SHI, L. 2015b. Combinatorial Intervention with Mesenchymal Stem Cells and Granulocyte Colony-Stimulating Factor in a Rat Model of Ulcerative Colitis. *Dig Dis Sci*, 60, 1948-1957.

TANG, Y., ZHAO, X., ANTOINE, D., XIAO, X., WANG, H., ANDERSSON, U., BILLIAR, T. R., TRACEY, K. J. & LU, B. 2016. Regulation of Posttranslational Modifications of HMGB1 During Immune Responses. *Antioxid Redox Signal*, 24, 620-634.

TAVANO, F., DI MOLA, F. F., LATIANO, A., PALMIERI, O., BOSSA, F., VALVANO, M. R., LATIANO, T., ANNESE, V., ANDRIULLI, A. & DI SEBASTIANO, P. 2012. Neuroimmune Interactions in Patients with Inflammatory Bowel Diseases: Disease Activity and Clinical Behavior Based on Substance P Serum Levels. *J Crohn's Colitis*, 6, 563-570.

TE VELDE, A. A., DE KORT, F., STERRENBURG, E., PRONK, I., TEN KATE, F. J. W., HOMMES, D. W. & VAN DEVENTER, S. J. H. 2007. Comparative Analysis of Colonic Gene Expression of Three Experimental Colitis Models Mimicking Inflammatory Bowel Disease. *Inflamm Bowel Dis*, 13, 325-330.

TEIXEIRA, F. G., CARVALHO, M. M., SOUSA, N. & SALGADO, A. J. 2013. Mesenchymal Stem Cells Secretome: A New Paradigm for Central Nervous System Regeneration? *Cell Mol Life Sci*, 70, 3871-3882.

TERRANEO, L., VIRGILI, E., CARETTI, A., BIANCIARDI, P. & SAMAJA, M. 2014. *In vivo* Hyperoxia Induces Hypoxia-Inducible Factor-1alpha Overexpression in LNCaP Tumors without Affecting the Tumor Growth Rate. *Int J Biochem Cell Biol*, 51, 65-74.

THIN LUU, N., MCGETTRICK, H. M., BUCKLEY, C. D., NEWSOME, P. N., ED RAINGER, G., FRAMPTON, J. & NASH, G. B. 2013. Crosstalk between Mesenchymal Stem Cells and Endothelial Cells Leads to Downregulation of Cytokine-Induced Leukocyte Recruitment. *Stem Cells*, 31, 2690-2702.

THOMAS, G. A. O., RHODES, J. & INGRAM, J. R. 2005. Mechanisms of Disease: Nicotine—a Review of Its Actions in the Context of Gastrointestinal Disease. *Nat Clin Pract Gastroenterol Hepatol*, 2, 536-544.

THORPE, D., STRINGER, A. & BUTLER, R. 2013. Chemotherapy-Induced Mucositis: The Role of Mucin Secretion and Regulation, and the Enteric Nervous System. *Neurotoxicology*, 38, 101-105.

THRASIVOULOU, C., SOUBEYRE, V., RIDHA, H., GIULIANI, D., GIARONI, C., MICHAEL, G. J., SAFFREY, M. J. & COWEN, T. 2006. Reactive Oxygen Species, Dietary Restriction and Neurotrophic Factors in Age-Related Loss of Myenteric Neurons. *Aging Cell*, 5, 247-257.

TIAN, T., WANG, Z. & ZHANG, J. 2017. Pathomechanisms of Oxidative Stress in Inflammatory Bowel Disease and Potential Antioxidant Therapies. *Oxid Med Cell Longev*, Article ID 4535194.

TIXIER, E., GALMICHE, J. P. & NEUNLIST, M. 2006. Intestinal Neuro-Epithelial Interactions Modulate Neuronal Chemokines Production. *Biochem Biophys Res Commun*, 344, 554-561.

TOLAR, J., NAUTA, A. J., OSBORN, M. J., PANOSKALTSIS MORTARI, A., MCELMURRY, R. T., BELL, S., XIA, L., ZHOU, N., RIDDLE, M. & SCHROEDER, T. M. 2007. Sarcoma Derived from Cultured Mesenchymal Stem Cells. *Stem Cells*, 25, 371-379.

TONG, C. K., VELLASAMY, S., TAN, B. C., ABDULLAH, M., VIDYADARAN, S., SEOW, H. F. & RAMASAMY, R. 2011. Generation of Mesenchymal Stem Cell from Human Umbilical Cord Tissue Using a Combination Enzymatic and Mechanical Disassociation Method. *Cell Biol Int*, 35, 221-226.

TÖRNBLOM, H., LINDBERG, G., NYBERG, B. & VERESS, B. 2002. Full-Thickness Biopsy of the Jejunum Reveals Inflammation and Enteric Neuropathy in Irritable Bowel Syndrome. *Gastroenterology*, 123, 1972-1979.

TOUBOUL, C., LIS, R., AL FARSI, H., RAYNAUD, C. M., WARFA, M., ALTHAWADI, H., MERY, E., MIRSHAHI, M. & RAFII, A. 2013. Mesenchymal Stem Cells Enhance Ovarian Cancer Cell Infiltration through Il6 Secretion in an Amniochorionic Membrane Based 3D Model. *J Transl Med*, 11, 28.

TRACEY, K. J. 2002. The Inflammatory Reflex. *Nature*, 420, 853-859.

TREMAINE, W. 2012. Is Indeterminate Colitis Determinable? *Curr Gastroenterol Rep*, 14, 162-165.

TSUCHIDA, Y., HATAO, F., FUJISAWA, M., MURATA, T., KAMINISHI, M., SETO, Y., HORI, M. & OZAKI, H. 2010. Neuronal Stimulation with 5-Hydroxytryptamine 4 Receptor Induces Anti-Inflammatory Actions Via α7nACh Receptors on Muscularis Macrophages Associated with Postoperative Ileus. *Gut*, 60, 638–647.

TSUNADA, S., IWAKIRI, R., OOTANI, H., AW, T. & FUJIMOTO, K. 2003. Redox Imbalance in the Colonic Mucosa of Ulcerative Colitis. *Scand J Gastroenterol*, 38, 1002-1003.

TSUNG, A., KLUNE, J. R., ZHANG, X., JEYABALAN, G., CAO, Z., PENG, X., STOLZ, D. B., GELLER, D. A., ROSENGART, M. R. & BILLIAR, T. R. 2007. HMGB1 Release Induced by Liver Ischemia Involves Toll-Like Receptor 4–Dependent Reactive Oxygen Species Production and Calcium-Mediated Signalling. *J Exp Med*, 204, 2913-2923.

UCCELLI, A., BENVENUTO, F., LARONI, A. & GIUNTI, D. 2011. Neuroprotective Features of Mesenchymal Stem Cells. *Best Pract Res Clin Haematol*, 24, 59-64.

UEYAMA, H., HORIBE, T., HINOTSU, S., TANAKA, T., INOUE, T., URUSHIHARA, H., KITAGAWA, A. & KAWAKAMI, K. 2012. Chromosomal Variability of Human Mesenchymal Stem Cells Cultured under Hypoxic Conditions. *J Cell Mol Med*, 16, 72-82.

URBONAVICIUTE, V., MEISTER, S., FURNROHR, B. G., FREY, B., GUCKEL, E., SCHETT, G., HERRMANN, M. & VOLL, R. E. 2009. Oxidation of the Alarmin High-Mobility Group Box 1 Protein (HMGB1) During Apoptosis. *Autoimmunity*, 42, 305-307.

VALLE-PRIETO, A. & CONGET, P. A. 2010. Human Mesenchymal Stem Cells Efficiently Manage Oxidative Stress. *Stem Cells Dev*, 19, 1885-1893.

VAN BEELEN GRANLUND, A., ØSTVIK, A. E., BRENNA, Ø., TORP, S. H., GUSTAFSSON, B. I. & SANDVIK, A. K. 2013. Reg Gene Expression in Inflamed and Healthy Colon Mucosa Explored by in Situ Hybridisation. *Cell Tissue Res*, 352, 639-646.

VARAS, A., VALENCIA, J., LAVOCAT, F., MARTÍNEZ, V. G., THIAM, N. N., HIDALGO, L., FERNÁNDEZ-SEVILLA, L. M., SACEDÓN, R., VICENTE, A. & MIOSSEC, P. 2015. Blockade of Bone Morphogenetic Protein Signalling Potentiates the Pro-Inflammatory Phenotype Induced by Interleukin-17 and Tumor Necrosis Factor-α Combination in Rheumatoid Synoviocytes. *Arthritis Res Ther*, 17, 192.

VELDT, B. J., HANSEN, B. E., IKEDA, K., VERHEY, E., SUZUKI, H. & SCHALM, S. W. 2006. Long-Term Clinical Outcome and Effect of Glycyrrhizin in 1093 Chronic Hepatitis C Patients with Non-Response or Relapse to Interferon. *Scand J Gastroenterol*, 41, 1087-1094.

VENEREAU, E., CASALGRANDI, M., SCHIRALDI, M., ANTOINE, D. J., CATTANEO, A., DE MARCHIS, F., LIU, J., ANTONELLI, A., PRETI, A., RAELI, L., SHAMS, S. S., YANG, H., VARANI, L., ANDERSSON, U., TRACEY, K. J., BACHI, A., UGUCCIONI, M. & BIANCHI, M. E. 2012. Mutually Exclusive Redox Forms of HMGB1 Promote Cell Recruitment or Proinflammatory Cytokine Release. *J Exp Med*, 209, 1519-1528.

VERCELLI, A., MEREUTA, O., GARBOSSA, D., MURACA, G., MARESCHI, K., RUSTICHELLI, D., FERRERO, I., MAZZINI, L., MADON, E. & FAGIOLI, F. 2008. Human Mesenchymal Stem Cell Transplantation Extends Survival, Improves Motor Performance and Decreases Neuroinflammation in Mouse Model of Amyotrophic Lateral Sclerosis. *Neurobiol Dis*, 31, 395-405.

VICENTINI, G. E., FRACARO, L., DE SOUZA, S. R. G., MARTINS, H. A., GUARNIER, F. A. & ZANONI, J. N. 2016. Experimental Cancer Cachexia Changes Neuron Numbers and Peptide Levels in the Intestine: Partial Protective Effects after Dietary Supplementation with L-Glutamine. *PLoS One*, 11, e0162998.

VILLADANGOS, J. A., HEATH, W. R. & CARBONE, F. R. 2007. Outside Looking In: The Inner Workings of the Cross-Presentation Pathway within Dendritic Cells. *Trends Immunol*, 28, 45-7.

VILLANACCI, V., BASSOTTI, G., NASCIMBENI, R., ANTONELLI, E., CADEI, M., FISOGNI, S., SALERNI, B. & GEBOES, K. 2008. Enteric Nervous System Abnormalities in Inflammatory Bowel Diseases. *Neurogastroenterol Motil*, 20, 1009-1016.

VITALI, R., PALONE, F., CUCCHIARA, S., NEGRONI, A., CAVONE, L., COSTANZO, M., ALOI, M., DILILLO, A. & STRONATI, L. 2013. Dipotassium Glycyrrhizate Inhibits HMGB1-Dependent Inflammation and Ameliorates Colitis in Mice. *PLoS One*, 8, e66527.

VITALI, R., STRONATI, L., NEGRONI, A., DI NARDO, G., PIERDOMENICO, M., DEL GIUDICE, E., ROSSI, P. & CUCCHIARA, S. 2011. Fecal HMGB1 Is a Novel Marker of Intestinal Mucosal Inflammation in Pediatric Inflammatory Bowel Disease. *Am J Gastroenterol*, 106, 2029-2040.

VOGLER, M. 2012. Bcl2a1: The Underdog in the Bcl2 Family. *Cell Death Differ*, 19, 67-74.

VON BAHR, L., SUNDBERG, B., LONNIES, L., SANDER, B., KARBACH, H., HAGGLUND, H., LJUNGMAN, P., GUSTAFSSON, B., KARLSSON, H., LE BLANC, K. & RINGDEN, O. 2012. Long-Term Complications, Immunologic Effects, and Role of Passage for Outcome in Mesenchymal Stromal Cell Therapy. *Biol Blood Marrow Transplant*, 18, 557-564.

VOSS, U. & EKBLAD, E. 2014. Lipopolysaccharide-Induced Loss of Cultured Rat Myenteric Neurons - Role of Amp-Activated Protein Kinase. *PLoS One*, 9, e114044.

VOUKALI, E., SHOTTON, H. & LINCOLN, J. 2011. Selective Responses of Myenteric Neurons to Oxidative Stress and Diabetic Stimuli. *Neurogastroenterol Motil*, 23, 964.

WADA-TAKAHASHI, S. & TAMURA, K. 2000. Actions of Reactive Oxygen Species on AH/Type 2 Myenteric Neurons in Guinea Pig Distal Colon. *Am J Physiol Gastrointest Liver Physiol*, 279, 893-902.

WAGNER, W., WEIN, F., SECKINGER, A., FRANKHAUSER, M., WIRKNER, U., KRAUSE, U., BLAKE, J., SCHWAGER, C., ECKSTEIN, V. & ANSORGE, W. 2005. Comparative Characteristics of Mesenchymal Stem Cells from Human Bone Marrow, Adipose Tissue, and Umbilical Cord Blood. *Exp Hematol*, 33, 1402-1416.

WANG, C.-H., WANG, T.-M., YOUNG, T.-H., LAI, Y.-K. & YEN, M.-L. 2013a. The Critical Role of ECM Proteins within the Human MSC Niche in Endothelial Differentiation. *Biomaterials*, 34, 4223-4234.

WANG, C., CHEN, J., SUN, L. & LIU, Y. 2014. Tgf-Beta Signalling-Dependent Alleviation of Dextran Sulfate Sodium-Induced Colitis by Mesenchymal Stem Cell Transplantation. *Mol Biol Rep*, 41, 4977-4983.

WANG, H. S., HUNG, S. C., PENG, S. T., HUANG, C. C., WEI, H. M., GUO, Y. J., FU, Y. S., LAI, M. C. & CHEN, C. C. 2004. Mesenchymal Stem Cells in the Wharton's Jelly of the Human Umbilical Cord. *Stem Cells*, 22, 1330-1337.

WANG, L., FENG, Z., WANG, X., WANG, X. & ZHANG, X. 2009. Degseq: An R Package for Identifying Differentially Expressed Genes from RNA-Seq Data. *Bioinformatics*, 26, 136-138.

WANG, M., LIANG, C., HU, H., ZHOU, L., XU, B., WANG, X., HAN, Y., NIE, Y., JIA, S., LIANG, J. & WU, K. 2016. Intraperitoneal Injection (Ip), Intravenous Injection (Iv) or Anal Injection (AI)? Best Way for Mesenchymal Stem Cells Transplantation for Colitis. *Sci Rep*, 6, 30696.

WANG, S., QU, X. & ZHAO, R. C. 2012. Clinical Applications of Mesenchymal Stem Cells. *J Hematol Oncol*, 30, 19. doi: 10.1186/1756-8722-5-19.

WANG, W., LV, X., LI, M., SUN, Z., WANG, F., ZHANG, L., LUO, X., LIU, V., ZHAO, G., CAO, W., ZHANG, X. & WANG, R. 2017. Efficacy and Biodistribution of Autologous, Allogeneic, and Xenogeneic Adipose Mesenchymal Stem Cells on Osteoarthritis. *Osteoarthritis Cartilage*, 25, 422-423.

WANG, W. Q., DONG, K., ZHOU, L., JIAO, G. H., ZHU, C. Z., LI, W. W., YU, G., WU, W. T., CHEN, S., SUN, Z. N., WANG, Y. M., LIU, W. T., ZHANG, J., WANG, B. M. & FENG, X. M. 2015. Il-37b Gene Transfer Enhances the Therapeutic Efficacy of Mesenchymal Stromal Cells in DSS-Induced Colitis Mice. *Acta Pharmacol Sin*, 36, 1377-1387.

WANG, X. Z., HARDING, H. P., ZHANG, Y., JOLICOEUR, E. M., KURODA, M. & RON, D. 1998. Cloning of Mammalian IRE1 Reveals Diversity in the ET Stress Responses. *EMBO J*, 17, 5708-5717.

WANG, Y., XUE, M., XUAN, Y.-L., HU, H.-S., CHENG, W.-J., SUO, F., LI, X.-R., YAN, S.-H. & WANG, L.-X. 2013b. Mesenchymal Stem Cell Therapy Improves Diabetic Cardiac Autonomic Neuropathy and Decreases the Inducibility of Ventricular Arrhythmias. *Heart Lung Circ*, 22, 1018-1025.

WANG, Z.-H. & FANG, J.-Y. 2014. Colorectal Cancer in Inflammatory Bowel Disease: Epidemiology, Pathogenesis and Surveillance. *Gastrointestinal tumors*, 1, 146-154.

WAPENAAR, M. C., MONSUUR, A. J., POELL, J., VAN 'T SLOT, R., MEIJER, J. W. R., MEIJER, G. A., MULDER, C. J., MEARIN, M. L. & WIJMENGA, C. 2007. The SPINK Gene Family and Celiac Disease Susceptibility. *Immunogenetics*, 59, 349–357.

WARNES, G. R., BOLKER, B., BONEBAKKER, L., GENTLEMAN, R., HUBER, W., LIAW, A., LUMLEY, T., MAECHLER, M., MAGNUSSON, A. & MOELLER, S. 2009. Gplots: Various R Programming Tools for Plotting Data. R package version, 2, 1.

WASZAK, P., ALPHONSE, R., VADIVEL, A., IONESCU, L., EATON, F. & THÉBAUD, B. 2012. Preconditioning Enhances the Paracrine Effect of Mesenchymal Stem Cells in Preventing Oxygen-Induced Neonatal Lung Injury in Rats. *Stem Cells Dev*, 21, 2789-2797.

WATANABE, S., ARIMURA, Y., NAGAISHI, K., ISSHIKI, H., ONODERA, K., NASUNO, M., YAMASHITA, K., IDOGAWA, M., NAISHIRO, Y. & MURATA, M. 2013. Conditioned Mesenchymal Stem Cells Produce Pleiotropic Gut Trophic Factors. *J Gastroenterol*, 49, 270-282.

WATERMAN, R. S., TOMCHUCK, S. L., HENKLE, S. L. & BETANCOURT, A. M. 2010. A New Mesenchymal Stem Cell (MSC) Paradigm: Polarization into a Pro-Inflammatory MSC1 or an Immunosuppressive MSC2 Phenotype. *PLoS One*, 5, e10088.

WATTCHOW, D., BROOKES, S., MURPHY, E., CARBONE, S., DE FONTGALLAND, D. & COSTA, M. 2008. Regional Variation in the Neurochemical Coding of the Myenteric Plexus of the Human Colon and Changes in Patients with Slow Transit Constipation. *Neurogastroenterol Motil*, 20, 1298-1305.

WEI, X., YANG, X., HAN, Z. P., QU, F. F., SHAO, L. & SHI, Y. F. 2013. Mesenchymal Stem Cells: A New Trend for Cell Therapy. *Acta Pharmacol Sin*, 34, 747-754.

WESSLER, I. & KIRKPATRICK, C. J. 2008. Acetylcholine Beyond Neurons: The Non-Neuronal Cholinergic System in Humans. *Br J Pharmacol*, 154, 1558-1571.

WHONE, A. L., KEMP, K., SUN, M., WILKINS, A. & SCOLDING, N. J. 2012. Human Bone Marrow Mesenchymal Stem Cells Protect Catecholaminergic and Serotonergic Neuronal Perikarya and Transporter

Function from Oxidative Stress by the Secretion of Glial-Derived Neurotrophic Factor. *Brain Res*, 1431, 86-96.

WILKINS, A., KEMP, K., GINTY, M., HARES, K., MALLAM, E. & SCOLDING, N. 2009. Human Bone Marrow-Derived Mesenchymal Stem Cells Secrete Brain-Derived Neurotrophic Factor Which Promotes Neuronal Survival *in vitro*. *Stem Cell Res*, 3, 63-70.

WILLARD, M. D., MULLANEY, T., KARASEK, S. & YAMINI, B. 1988. Diarrhea Associated with Myenteric Ganglionitis in a Dog. *J Am Vet Med Assoc*, 193, 346-8.

WILSON, J., HAIR, C., KNIGHT, R., CATTO-SMITH, A., BELL, S., KAMM, M., DESMOND, P., MCNEIL, J. & CONNELL, W. 2010. High Incidence of Inflammatory Bowel Disease in Australia: A Prospective Population-Based Australian Incidence Study. *Inflamm Bowel Dis*, 16, 1550-1556.

WINSTON, J. H., LI, Q. & SARNA, S. K. 2013. Paradoxical Regulation of Chat and Nnos Expression in Animal Models of Crohn's Colitis and Ulcerative Colitis. *Am J Physiol Gastrointest Liver Physiol*, 305, 295-302.

WINTERBOURN, C. C. 1995. Toxicity of Iron and Hydrogen Peroxide: The Fenton Reaction. *Toxicol Lett*, 82, 969-974.

WIRTZ, S., NEUFERT, C., WEIGMANN, B. & NEURATH, M. F. 2007. Chemically Induced Mouse Models of Intestinal Inflammation. Nat Protoc, 2, 541–546.

WOOD, J. D. 2007. Effects of Bacteria on the Enteric Nervous System: Implications for the Irritable Bowel Syndrome. *J Clin Gastroenterol*, 41, 7-19.

WU, J., LIN, Q., LU, Y., WILLIS, W. D. & WESTLUND, K. N. 1998. Changes in Nitric Oxide Synthase Isoforms in the Spinal Cord of Rat Following Induction of Chronic Arthritis. *Exp Brain Res*, 118, 457-65.

WU, T., LIU, Y., FAN, Z., XU, J., JIN, L., GAO, Z., WU, Z., HU, L., WANG, J., ZHANG, C., CHEN, W. & WANG, S. 2015. MiR-21 Modulates the Immunoregulatory Function of Bone Marrow Mesenchymal Stem Cells through the PTEN/AKT/TGF-Beta1 Pathway. *Stem Cells*, 33, 3281-3290.

WU, W. & LI, L. 1993. Inhibition of Nitric Oxide Synthase Reduces Motoneuron Death Due to Spinal Root Avulsion. *Neurosci Lett*, 153, 121-124.

WU, Y., CHEN, L., SCOTT, P. G. & TREDGET, E. E. 2007. Mesenchymal Stem Cells Enhance Wound Healing through Differentiation and Angiogenesis. *Stem Cells*, 25, 2648-2659.

WULLAERT, A., BONNET, M. C. & PASPARAKIS, M. 2010. NF-KB in the Regulation of Epithelial Homeostasis and Inflammation. *Cell Res*, 21, 146-158.

WYATT, E., WU, R., RABEH, W., PARK, H.-W., GHANEFAR, M. & ARDEHALI, H. 2010. Regulation and Cytoprotective Role of Hexokinase III. *PLoS On*e, 5, e13823.

XIA, Y., HU, H.-Z., LIU, S., REN, J., ZAFIROV, D. H. & WOOD, J. D. 1999. IL-1β and IL-6 Excite Neurons and Suppress Nicotinic and Noradrenergic Neurotransmission in Guinea Pig Enteric Nervous System. *J Clin Invest*, 103, 1309-1316.

XIANG, M.-X., HE, A.-N., WANG, J.-A. & GUI, C. 2009. Protective Paracrine Effect of Mesenchymal Stem Cells on Cardiomyocytes. *J Zhejiang Univ Sci B*, 10, 619-624.

XIE, M., QIN, H., LUO, Q., HE, X., HE, X., LAN, P. & LIAN, L. 2017. Comparison of Adipose-Derived and Bone Marrow Mesenchymal Stromal Cells in a Murine Model of Crohn's Disease. *Dig Dis Sci*, 62, 115-123.

XU, H., GHISHAN, F. K. & KIELA, P. R. 2011. SLC9 Gene Family: Function, Expression, and Regulation. *Compr Physiol*, 8, 555-583.

XUE, X., RAMAKRISHNAN, S., ANDERSON, E., TAYLOR, M., ZIMMERMANN, E. M., SPENCE, J. R., HUANG, S., GREENSON, J. K. & SHAH, Y. M. 2013. Endothelial Pas Domain Protein 1 Activates

the Inflammatory Response in the Intestinal Epithelium to Promote Colitis in Mice. *Gastroenterology*, 145, 831-841.

YABANA, T., ARIMURA, Y., TANAKA, H., GOTO, A., HOSOKAWA, M., NAGAISHI, K., YAMASHITA, K., YAMAMOTO, H., ADACHI, Y. & SASAKI, Y. 2009. Enhancing Epithelial Engraftment of Rat Mesenchymal Stem Cells Restores Epithelial Barrier Integrity. *J Pathol*, 218, 350-359.

YADAV, P. K., CHEN, C. & LIU, Z. 2011. Potential Role of NK Cells in the Pathogenesis of Inflammatory Bowel Disease. *J Biomed Biotechnol*, 348530.

YAKOVLEV, A. G. & FADEN, A. I. 2004. Mechanisms of Neural Cell Death: Implications for Development of Neuroprotective Treatment Strategies. *NeuroRx*, 1, 5-16.

YAMADA, H., UEDA, T. & YANO, A. 2011. Water-Soluble Extract of Pacific Krill Prevents Triglyceride Accumulation in Adipocytes by Suppressing PPARγ and C/EBPα Expression. *PloS One*, 6, e21952.

YAMASAKI, H., MITSUYAMA, K., MASUDA, J., KUWAKI, K., TAKEDATSU, H., SUGIYAMA, G., YAMADA, S. & SATA, M. 2009. Roles of High-Mobility Group Box 1 in Murine Experimental Colitis. *Mol Med Rep*, 2, 23-27.

YAN, Y., ZHAO, N., HE, X., GUO, H., ZHANG, Z. & LIU, T. 2018. Mesenchymal Stem Cell Expression of Interleukin-35 Protects against Ulcerative Colitis by Suppressing Mucosal Immune Responses. *Cytotherapy*, 20, 911-918.

YANG, D., ELNER, S. G., BIAN, Z.-M., TILL, G. O., PETTY, H. R. & ELNER, V. M. 2007. Pro-Inflammatory Cytokines Increase Reactive Oxygen Species through Mitochondria and NADPH Oxidase in Cultured RPE Cells. *Exp Eye Res*, 85, 462-472.

YANG, J., LIU, X.-X., FAN, H., TANG, Q., SHOU, Z.-X., ZUO, D.-M., ZOU, Z., XU, M., CHEN, Q.-Y. & PENG, Y. 2015. Extracellular Vesicles Derived from Bone Marrow Mesenchymal Stem Cells Protect against Experimental Colitis Via Attenuating Colon Inflammation, Oxidative Stress and Apoptosis. *PLoS One*, 10, e0140551.

YANG, Y.-H. K., OGANDO, C. R., WANG SEE, C., CHANG, T.-Y. & BARABINO, G. A. 2018. Changes in Phenotype and Differentiation Potential of Human Mesenchymal Stem Cells Aging *in vitro*. *Stem Cell Res Ther*, 9, 131.

YITING, T., XIN, Z., DANIEL, A., XIANZHONG, X., HAICHAO, W., ULF, A., R., B. T., J., T. K. & BEN, L. 2016. Regulation of Posttranslational Modifications of HMGB1 During Immune Responses. *Antioxid Redox Signal*, 24, 620-634.

YOO, K. H., JANG, I. K., LEE, M. W., KIM, H. E., YANG, M. S., EOM, Y., LEE, J. E., KIM, Y. J., YANG, S. K., JUNG, H. L., SUNG, K. W., KIM, C. W. & KOO, H. H. 2009. Comparison of Immunomodulatory Properties of Mesenchymal Stem Cells Derived from Adult Human Tissues. *Cell Immunol*, 259, 150-156.

YU, G., WANG, L.-G., HAN, Y. & HE, Q.-Y. 2012. Clusterprofiler: An R Package for Comparing Biological Themes among Gene Clusters. *OMICS*, 16, 284-287.

ZENLEA, T. & PEPPERCORN, M. A. 2014. Immunosuppressive Therapies for Inflammatory Bowel Disease. *World J Gastroenterol*, 20, 3146-3152.

ZHANG, D.-W., SHAO, J., LIN, J., ZHANG, N., LU, B.-J., LIN, S.-C., DONG, M.-Q. & HAN, J. 2009a. Rip3, an Energy Metabolism Regulator That Switches TNF-Induced Cell Death from Apoptosis to Necrosis. *Science*, 325, 332-336.

ZHANG, J., LV, S., LIU, X., SONG, B. & SHI, L. 2018. Umbilical Cord Mesenchymal Stem Cell Treatment for Crohn's Disease: A Randomized Controlled Clinical Trial. *Gut Liver*, 12, 73-78.

ZHANG, J., SHI, Q., YANG, P., XU, X., CHEN, X., QI, C., LU, H., ZHAO, B., ZHENG, P. & ZHANG, P. 2012. Neuroprotection of Neurotrophin-3 against Focal Cerebral Ischemia/Reperfusion Injury Is Regulated by Hypoxia-Responsive Element in Rats. *Neuroscience*, 222, 1-9.

ZHANG, J., ZHOU, S., ZHOU, Y., FENG, F., WANG, Q., ZHU, X., ZHAO, J., FU, H., LV, M., AI, H., HUANG, X. & ZHANG, X. 2016. Adipose-Derived Mesenchymal Stem Cells (Adscs) with the Potential to Ameliorate Platelet Recovery, Enhance Megakaryopoiesis, and Inhibit Apoptosis of Bone Marrow Cells in a Mouse Model of Radiation-Induced Thrombocytopenia. *Cell Transplant*, 25, 261-273.

ZHANG, Q., SHI, S., LIU, Y., UYANNE, J., SHI, Y., SHI, S. & LE, A. D. 2009b. Mesenchymal Stem Cells Derived from Human Gingiva Are Capable of Immunomodulatory Functions and Ameliorate Inflammation-Related Tissue Destruction in Experimental Colitis. *J Immunol*, 183, 7787-7798.

ZHANG, R., BRENNAN, M.-L., SHEN, Z., MACPHERSON, J. C., SCHMITT, D., MOLENDA, C. E. & HAZEN, S. L. 2002. Myeloperoxidase Functions as a Major Enzymatic Catalyst for Initiation of Lipid Peroxidation at Sites of Inflammation. *J Biol Chem*, 277, 46116-46122.

ZHANG, S., ZHANG, Z., SANDHU, G., MA, X., YANG, X., GEIGER, J. D. & KONG, J. 2007. Evidence of Oxidative Stress-Induced BNIP3 Expression in Amyloid Beta Neurotoxicity. *Brain Res*, 1138, 221-230.

ZHANG, Y., JIN, Y., LIN, Y., LIN, L. J., CAO, Y., WANG, D. X. & ZHENG, C. Q. 2015. Adipose-Derived Mesenchymal Stem Cells Ameliorate Ulcerative Colitis through Mir-1236 Negatively Regulating the Expression of Retinoid-Related Orphan Receptor Gamma. *DNA Cell Biol*, 34, 618-625.

ZHAO, M., TANG, S., XIN, J., WEI, Y. & LIU, D. 2018. Reactive Oxygen Species Induce Injury of the Intestinal Epithelium During Hyperoxia. *Int J Mol Med*, 41, 322-330.

ZHOU, X., THORGEIRSSON, S. S. & POPESCU, N. C. 2004. Restoration of DLC-1 Gene Expression Induces Apoptosis and Inhibits Both Cell Growth and Tumorigenicity in Human Hepatocellular Carcinoma Cells. *Oncogene*, 23, 1308-1313.

ZHOU, Y., XU, H., XU, W., WANG, B., WU, H., TAO, Y., ZHANG, B., WANG, M., MAO, F., YAN, Y., GAO, S., GU, H., ZHU, W. & QIAN, H. 2013. Exosomes Released by Human Umbilical Cord Mesenchymal Stem Cells Protect against Cisplatin-Induced Renal Oxidative Stress and Apoptosis *in vivo* and *in vitro*. *Stem Cell Res Ther*, 4, 34.

ZHU, X., SHI, W., TAI, W. & LIU, F. 2012. The Comparition of Biological Characteristics and Multilineage Differentiation of Bone Marrow and Adipose Derived Mesenchymal Stem Cells. *Cell Tissue Res*, 350, 277-287.

ZONG, W.-X. & THOMPSON, C. B. 2006. Necrotic Death as a Cell Fate. *Genes Dev*, 20, 1-15.

ZUK, P. A., ZHU, M., ASHJIAN, P., DE UGARTE, D. A., HUANG, J. I., MIZUNO, H., ALFONSO, Z. C., FRASER, J. K., BENHAIM, P. & HEDRICK, M. H. 2002. Human Adipose Tissue Is a Source of Multipotent Stem Cells. *Mol Biol Cell*, 13, 4279-4295.

ZUO, D., LIU, X., SHOU, Z., FAN, H., TANG, Q., DUAN, X., CAO, D., ZOU, Z. & ZHANG, L. 2013. Study on the Interactions between Transplanted Bone Marrow-Derived Mesenchymal Stem Cells and Regulatory T Cells for the Treatment of Experimental Colitis. *Int J Mol Med*, 32, 1337-1344.

ZUO, D., TANG, Q., FAN, H., SHOU, Z., LIU, X., CAO, D. & ZOU, Z. 2015. Modulation of Nuclear Factor-Kappab-Mediated Pro-Inflammatory Response Is Associated with Exogenous Administration of Bone Marrow-Derived Mesenchymal Stem Cells for Treatment of Experimental Colitis. *Mol Med Rep*, 11, 2741-2748.

APPENDIX A

Supplementary Data

Figure S1 ***Volcano plot representation of differential expressed genes between Winnie-sham and C57BL/6 mice***

Differentially expressed genes (DEGs) from raw mapped reads were evaluated between *Winnie*-sham and C57BL/6 mice by the R package DEGseq v 1.34.0 (Wang et al., 2009). **A)** Data followed a normal distribution when the LogFC values were plotted against -Log10 of the *P* values. Out of the 26609 genes screened in the mouse transcriptome expression was detected for 18699 genes. **B)** Resulting datasets were cleaned by cut-offs for a *P* value of <0.001 (4, -*P* value^{Log10}), <10 counts for the gene (low expression) and low changes in expression between ±0.5LogFC. The remaining gene set contained 5619 differentially expressed genes which were used for further analysis (blue), while the remaining genes were disregarded (red).

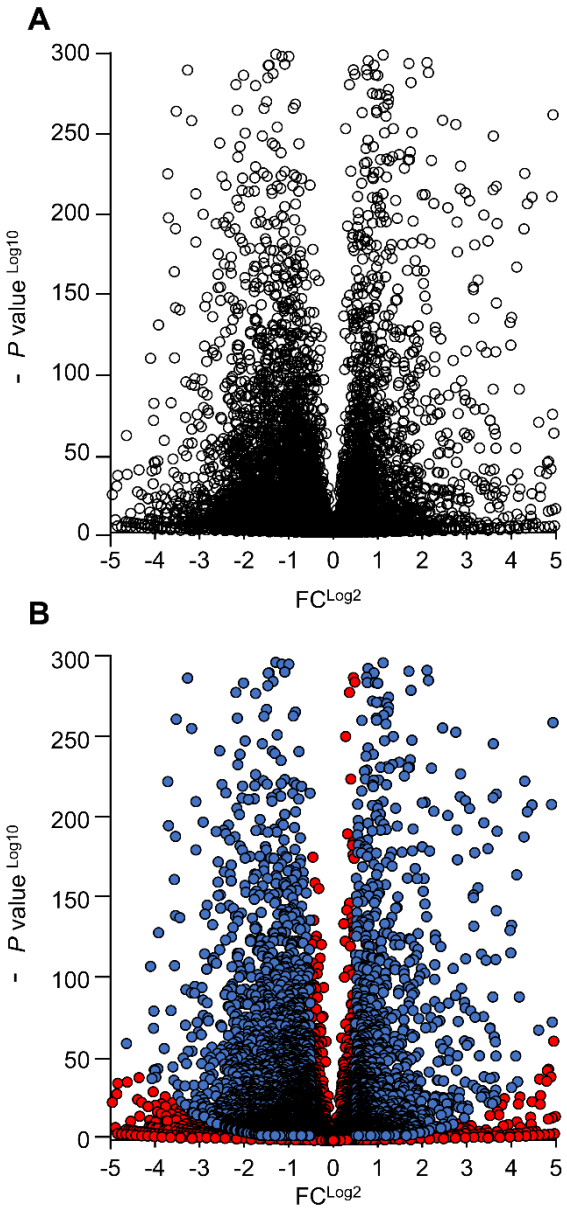
A
300
250
200
150
100
50
0
- P value Log10
-5 -4 -3 -2 -1 0 1 2 3 4 5
FC Log2
B
300
250
200
150
100
50
0
- P value Log10
-5 -4 -3 -2 -1 0 1 2 3 4 5
FC Log2

Figure S2 ***Volcano plot representation of differential expressed genes between Winnie treated with BM-MSCs and Winnie-sham***

Differentially expressed genes (DEGs) from raw mapped reads were evaluated between *Winnie* mice treated with BM-MSCs and *Winnie*-sham mice by the R package DEGseq v 1.34.0 (Wang et al., 2009). **A)** Data followed a normal distribution with a slight skew in gene downregulation when the LogFC values were plotted against - Log10 of the *P* values. Out of the 26609 genes screened in the mouse transcriptome expression was detected for 18399 genes. **B)** Resulting datasets were cleaned by cut-offs for a *P* value of <0.001 (4, -*P* value^{Log10}), <10 counts for the gene (low expression) and low changes in expression between ±0.5LogFC. The remaining gene set contained 1171 differentially expressed genes which were used for further analysis (blue), while the remaining genes were disregarded (red).

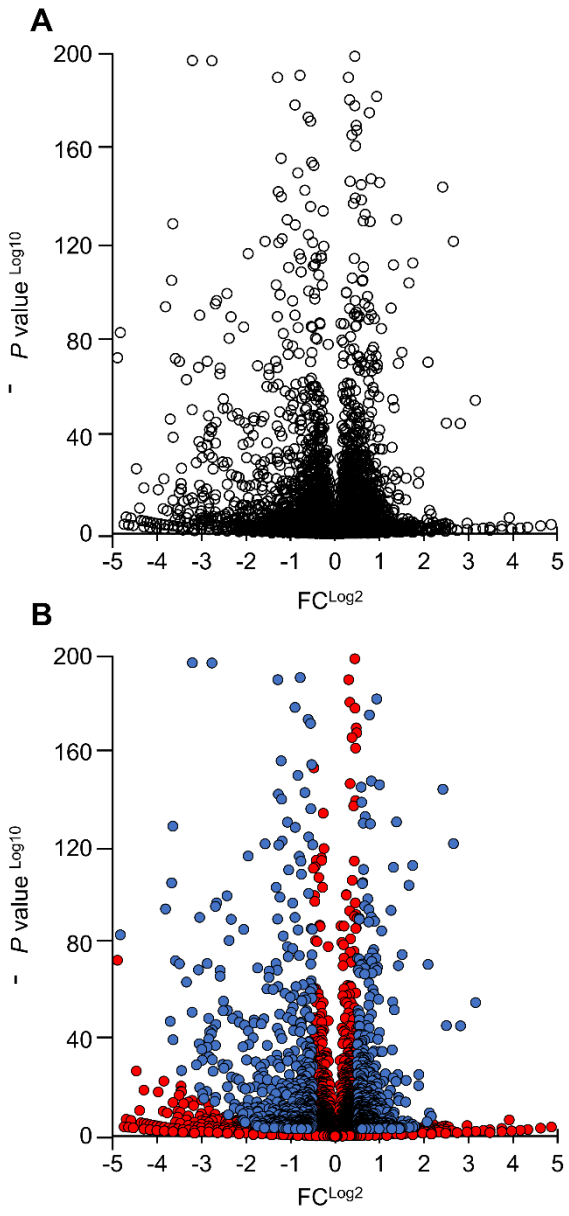
A
200
160
120
80
40
0
- P value Log10
-5 -4 -3 -2 -1 0 1 2 3 4 5
FC Log2
B
200
160
120
80
40
0
- P value Log10
-5 -4 -3 -2 -1 0 1 2 3 4 5
FC Log2

Figure S3 ***Comparison between gene expression by RT-PCR and RNA-Seq***

The expression pattern of genes observed by RNA-Seq were validated using RT-qPCR. Genes with a known expression pattern in *Winnie* mice were chosen (Stavely et al., 2018a). This included *Slc6a4* (downregulated), *Ido1* (upregulated) and *Tph1* (unchanged). Gene expression was determined by qRT-PCR as previously described (Stavely et al., 2018a). Gene expression was normalised to the geometric mean of reference genes *Gapdh* and *Vil1* for all samples. LogFC values were calculated between *Winnie* mice treated with BM-MSC and *Winnie* sham, as well as, between *Winnie* sham and C57BL/6 mice. LogFC obtained from RT-PCR results (X axis) were plotted against hose derived from RNA-Seq (Y axis) and a linear regression analysis was performed.

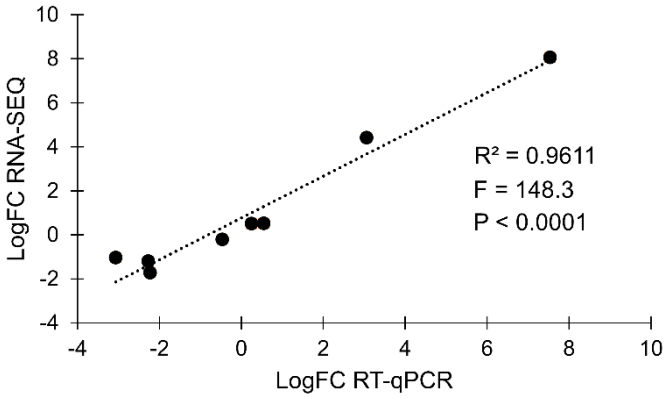
LogFC RNA-SEQ
LogFC RT-qPCR
R² = 0.9611
F = 148.3
P < 0.0001
10
8
6
4
2
0
-2
-4
-4
-2
0
2
4
6
8
10

Figure S4 ***Linear correlation between disease activity index and neuronal density in BM-MSC and sham-treated Winnie mice***

Linear regression analysis between the disease activity index (DAI) (X axis) and myenteric neuronal density (Y axis) expressed as the number of neurons per $0.01mm^2$ area. Analysis performed in BM-MSC (blue) and sham-treated *Winnie* mice (black). A significant correlation between DAI and neuronal density was only observed in *Winnie* mice and not C57BL/6 mice.

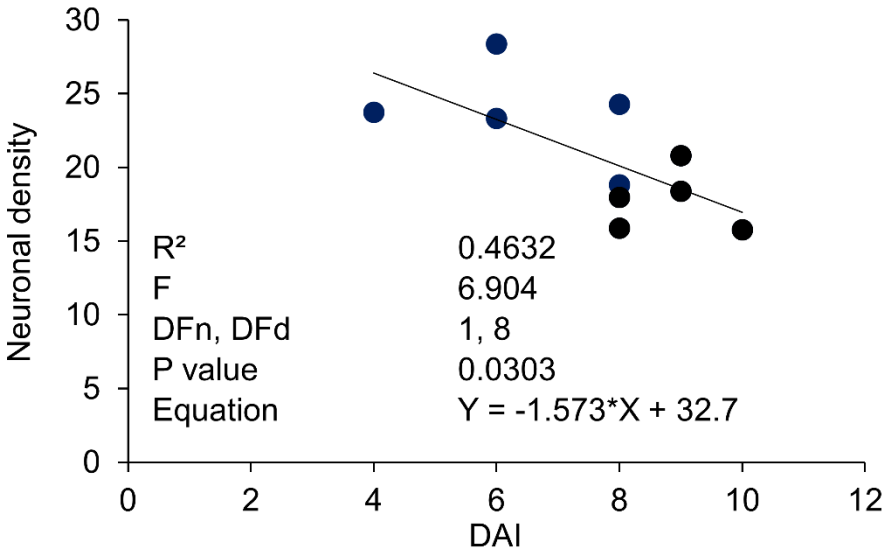
Neuronal density
DAI
R²
0.4632
F
6.904
DFn, DFd
1, 8
P value
0.0303
Equation
Y = -1.573*X + 32.7
0
5
10
15
20
25
30
0
2
4
6
8
10
12

Table S1 ***Gene ontology term enrichment in downregulated differential expressed genes between Winnie mice treated with BM-MSCs and Winnie-sham mice***

GO Term	Description	*P*-value	FDR q-value	Enrichment	N	B	n	b
Biological Process								
GO:0006952	defence response	4.07E-19	2.82E-15	1.72	1138	132	582	116
GO:0002376	immune system process	2.77E-13	9.62E-10	1.56	1138	150	582	120
GO:0006955	immune response	1.37E-12	3.17E-09	1.69	1138	96	582	83
GO:0098542	defence response to other organism	2.32E-11	4.02E-08	1.85	1138	55	582	52
GO:0043207	response to external biotic stimulus	3.42E-11	4.74E-08	1.61	1138	109	582	90
GO:0031347	regulation of defence response	5.46E-11	6.31E-08	1.71	1138	82	577	71
GO:0009607	response to biotic stimulus	9.87E-11	9.78E-08	1.6	1138	110	582	90
GO:0051707	response to other organism	2.54E-10	2.20E-07	1.65	1138	90	582	76
GO:0051704	multi-organism process	4.00E-10	3.08E-07	1.58	1138	107	593	88
GO:0006954	inflammatory response	6.38E-10	4.42E-07	2.2	1138	59	394	45
GO:0006950	response to stress	1.70E-09	1.07E-06	1.39	1138	215	582	153
GO:0002682	regulation of immune system process	2.10E-09	1.21E-06	1.53	1138	136	558	102
GO:0080134	regulation of response to stress	2.44E-09	1.30E-06	1.51	1138	132	582	102
GO:0050727	regulation of inflammatory response	2.50E-09	1.24E-06	2.23	1138	53	395	41
GO:0045087	innate immune response	6.31E-09	2.92E-06	1.82	1138	49	573	45
GO:0050900	leukocyte migration	1.05E-08	4.54E-06	2.03	1138	36	529	34
GO:0002684	positive regulation of immune system process	1.12E-08	4.56E-06	1.63	1138	90	558	72
GO:0031424	keratinization	2.51E-08	9.68E-06	4.06	1138	16	263	15
GO:0034341	response to interferon-gamma	9.10E-08	3.32E-05	2.05	1138	26	556	26
GO:0034097	response to cytokine	1.14E-07	3.97E-05	1.63	1138	76	568	62
GO:0050776	regulation of immune response	1.38E-07	4.56E-05	1.65	1138	74	558	60
GO:0032101	regulation of response to external stimulus	3.00E-07	9.44E-05	1.54	1138	94	582	74
GO:0001817	regulation of cytokine production	4.01E-07	1.21E-04	1.64	1138	70	564	57
GO:0002694	regulation of leukocyte activation	5.39E-07	1.56E-04	1.74	1138	53	554	45
GO:0031349	positive regulation of defence response	6.13E-07	1.70E-04	1.84	1138	40	558	36
GO:0050865	regulation of cell activation	9.66E-07	2.58E-04	1.7	1138	64	534	51
GO:0050778	positive regulation of immune response	1.16E-06	2.98E-04	1.75	1138	49	558	42
GO:0030595	leukocyte chemotaxis	2.91E-06	7.20E-04	2	1138	28	529	26
GO:0002697	regulation of immune effector process	3.67E-06	8.78E-04	1.75	1138	42	573	37
GO:0045109	intermediate filament organization	3.74E-06	8.64E-04	9.42	1138	9	94	7
GO:0006959	humoral immune response	4.10E-06	9.17E-04	3.99	1138	21	190	14
GO:0002252	immune effector process	4.40E-06	9.53E-04	1.7	1138	46	582	40

GO:0044278	cell wall disruption in other organism	4.64E-06	9.74E-04	379.33	1138	2	3	2
GO:0071346	cellular response to interferon-gamma	6.01E-06	1.22E-03	2.05	1138	20	556	20
GO:0071621	granulocyte chemotaxis	6.30E-06	1.25E-03	2.06	1138	23	529	22
GO:0097530	granulocyte migration	6.30E-06	1.21E-03	2.06	1138	23	529	22
GO:0009615	response to virus	6.56E-06	1.23E-03	1.89	1138	26	578	25
GO:0051607	defence response to virus	6.79E-06	1.24E-03	1.97	1138	21	578	21
GO:0061844	antimicrobial humoral immune response mediated by antimicrobial peptide	8.42E-06	1.50E-03	5.93	1138	12	144	9
GO:0019730	antimicrobial humoral response	8.42E-06	1.46E-03	5.93	1138	12	144	9
GO:0042742	defence response to bacterium	9.72E-06	1.64E-03	1.82	1138	30	582	28
GO:0022407	regulation of cell-cell adhesion	1.03E-05	1.70E-03	1.67	1138	43	601	38
GO:0009605	response to external stimulus	1.03E-05	1.66E-03	1.38	1138	146	582	103
GO:0071345	cellular response to cytokine stimulus	1.15E-05	1.81E-03	1.6	1138	64	568	51
GO:0030162	regulation of proteolysis	1.23E-05	1.89E-03	1.66	1138	54	559	44
GO:0030216	keratinocyte differentiation	1.23E-05	1.85E-03	3.3	1138	11	345	11
GO:0045103	intermediate filament-based process	1.26E-05	1.85E-03	7.45	1138	13	94	8
GO:0045104	intermediate filament cytoskeleton organization	1.26E-05	1.81E-03	7.45	1138	13	94	8
GO:0030593	neutrophil chemotaxis	1.29E-05	1.82E-03	2.05	1138	22	529	21
GO:1990266	neutrophil migration	1.29E-05	1.78E-03	2.05	1138	22	529	21
GO:1903037	regulation of leukocyte cell-cell adhesion	1.29E-05	1.75E-03	1.77	1138	31	601	29
GO:0035456	response to interferon-beta	1.42E-05	1.89E-03	2.02	1138	19	562	19
GO:0061436	establishment of skin barrier	1.56E-05	2.04E-03	4.08	1138	9	279	9
GO:0033561	regulation of water loss via skin	1.56E-05	2.00E-03	4.08	1138	9	279	9
GO:0009617	response to bacterium	1.96E-05	2.48E-03	1.58	1138	62	582	50
GO:0050729	positive regulation of inflammatory response	2.08E-05	2.57E-03	2.19	1138	26	439	22
GO:0097529	myeloid leukocyte migration	2.29E-05	2.79E-03	1.98	1138	25	529	23
GO:0050867	positive regulation of cell activation	2.37E-05	2.84E-03	1.78	1138	37	554	32
GO:0048584	positive regulation of response to stimulus	2.39E-05	2.81E-03	1.35	1138	174	558	115
GO:0001819	positive regulation of cytokine production	2.72E-05	3.14E-03	1.7	1138	46	554	38
GO:0006935	chemotaxis	3.62E-05	4.11E-03	1.58	1138	47	628	41
GO:0042330	taxis	3.62E-05	4.05E-03	1.58	1138	47	628	41
GO:0050777	negative regulation of immune response	4.75E-05	5.23E-03	1.97	1138	18	577	18
GO:0050863	regulation of T cell activation	4.84E-05	5.24E-03	1.84	1138	29	554	26
GO:0019221	cytokine-mediated signalling pathway	5.46E-05	5.83E-03	1.75	1138	36	560	31
GO:0035458	cellular response to interferon-beta	5.66E-05	5.94E-03	2.02	1138	17	562	17
GO:0032103	positive regulation of response to external stimulus	6.80E-05	7.04E-03	2.05	1138	38	395	27

GO:0002683	negative regulation of immune system process	7.24E-05	7.38E-03	1.61	1138	46	601	39
GO:0048583	regulation of response to stimulus	7.49E-05	7.52E-03	1.24	1138	291	558	177
GO:0051249	regulation of lymphocyte activation	7.96E-05	7.88E-03	1.7	1138	41	554	34
GO:0042129	regulation of T cell proliferation	1.15E-04	1.12E-02	2.03	1138	19	532	18
GO:0002687	positive regulation of leukocyte migration	1.16E-04	1.12E-02	2.43	1138	19	394	16
GO:0002703	regulation of leukocyte mediated immunity	1.19E-04	1.13E-02	1.88	1138	24	554	22
GO:1903039	positive regulation of leukocyte cell-cell adhesion	1.19E-04	1.11E-02	1.88	1138	24	554	22
GO:0002696	positive regulation of leukocyte activation	1.25E-04	1.16E-02	1.75	1138	34	554	29
GO:0043900	regulation of multi-organism process	1.40E-04	1.28E-02	1.63	1138	45	575	37
GO:0050891	multicellular organismal water homeostasis	1.42E-04	1.27E-02	3.67	1138	10	279	9
GO:0060326	cell chemotaxis	1.47E-04	1.31E-02	2.16	1138	37	341	24
GO:0022409	positive regulation of cell-cell adhesion	1.57E-04	1.38E-02	1.83	1138	27	554	24
GO:0050670	regulation of lymphocyte proliferation	1.83E-04	1.58E-02	1.94	1138	22	532	20
GO:0016477	cell migration	1.95E-04	1.66E-02	1.28	1138	86	796	77
GO:0002237	response to molecule of bacterial origin	1.96E-04	1.65E-02	1.67	1138	38	574	32
GO:0048522	positive regulation of cellular process	2.17E-04	1.81E-02	1.11	1138	353	868	298
GO:0043901	negative regulation of multi-organism process	2.18E-04	1.80E-02	1.82	1138	24	572	22
GO:0042176	regulation of protein catabolic process	2.46E-04	2.01E-02	1.66	1138	25	658	24
GO:0050794	regulation of cellular process	2.65E-04	2.14E-02	1.07	1138	604	857	486
GO:0001818	negative regulation of cytokine production	3.01E-04	2.40E-02	1.75	1138	30	564	26
GO:0030855	epithelial cell differentiation	3.49E-04	2.75E-02	4.71	1138	39	62	10
GO:0002831	regulation of response to biotic stimulus	4.02E-04	3.13E-02	1.88	1138	19	573	18
GO:0032496	response to lipopolysaccharide	4.22E-04	3.25E-02	1.7	1138	35	556	29
GO:0031348	negative regulation of defence response	4.58E-04	3.49E-02	1.8	1138	23	577	21
GO:0030155	regulation of cell adhesion	4.63E-04	3.49E-02	1.49	1138	79	533	55
GO:0045089	positive regulation of innate immune response	4.85E-04	3.62E-02	1.93	1138	18	558	17
GO:0006953	acute-phase response	5.05E-04	3.72E-02	108.38	1138	7	3	2
GO:0002699	positive regulation of immune effector process	5.27E-04	3.84E-02	1.81	1138	25	554	22
GO:0052548	regulation of endopeptidase activity	5.50E-04	3.97E-02	2.65	1138	29	237	16
GO:0051130	positive regulation of cellular component organization	6.14E-04	4.39E-02	1.29	1138	96	737	80
GO:0051171	regulation of nitrogen compound metabolic process	6.58E-04	4.65E-02	1.11	1138	307	868	260
GO:0030104	water homeostasis	6.72E-04	4.71E-02	4.1	1138	11	202	8
GO:0009913	epidermal cell differentiation	6.82E-04	4.73E-02	7.44	1138	17	54	6
GO:0052547	regulation of peptidase activity	7.36E-04	5.05E-02	2.37	1138	36	253	19

GO:0045682	regulation of epidermis development	7.40E-04	5.03E-02	2.77	1138	16	308	12
GO:0032944	regulation of mononuclear cell proliferation	7.75E-04	5.22E-02	1.86	1138	23	532	20
GO:0051240	positive regulation of multicellular organismal process	8.16E-04	5.44E-02	1.31	1138	153	569	100
GO:0050878	regulation of body fluid levels	8.50E-04	5.61E-02	1.6	1138	37	596	31
GO:1903207	regulation of hydrogen peroxide-induced neuron death	8.79E-04	5.75E-02	1,138.00	1138	1	1	1
GO:1903208	negative regulation of hydrogen peroxide-induced neuron death	8.79E-04	5.69E-02	1,138.00	1138	1	1	1
GO:0071347	cellular response to interleukin-1	9.63E-04	6.18E-02	2.4	1138	10	474	10
GO:0070555	response to interleukin-1	9.63E-04	6.12E-02	2.4	1138	10	474	10
GO:0070098	chemokine-mediated signalling pathway	9.87E-04	6.22E-02	2.23	1138	11	510	11
Molecular Function								
GO:0005198	structural molecule activity	1.86E-09	3.07E-06	8.34	1138	49	39	14
GO:0005126	cytokine receptor binding	7.01E-06	5.78E-03	1.78	1138	32	601	30
GO:0005125	cytokine activity	9.08E-05	4.99E-02	1.81	1138	33	534	28
GO:0070492	oligosaccharide binding	1.71E-04	7.04E-02	151.73	1138	5	3	2
GO:0042834	peptidoglycan binding	1.71E-04	5.63E-02	151.73	1138	5	3	2
GO:0030280	structural constituent of epidermis	2.14E-04	5.89E-02	33.47	1138	6	17	3
GO:0030414	peptidase inhibitor activity	2.66E-04	6.27E-02	2.81	1138	24	253	15
GO:0061134	peptidase regulator activity	2.66E-04	5.48E-02	2.81	1138	24	253	15
GO:0042379	chemokine receptor binding	3.18E-04	5.83E-02	1.89	1138	16	601	16
GO:0004252	serine-type endopeptidase activity	3.40E-04	5.60E-02	2.92	1138	23	237	14
GO:0004175	endopeptidase activity	3.70E-04	5.55E-02	2.33	1138	45	239	22
GO:0008236	serine-type peptidase activity	6.70E-04	9.21E-02	2.8	1138	24	237	14
Cellular Component								
GO:0005882	intermediate filament	2.83E-09	2.07E-06	8.87	1138	19	81	12
GO:0045095	keratin filament	3.72E-08	1.36E-05	10.54	1138	12	81	9
GO:0001533	cornified envelope	9.13E-07	2.22E-04	20.2	1138	13	26	6
GO:0005615	extracellular space	1.79E-06	3.28E-04	1.39	1138	186	534	121
GO:0005576	extracellular region	5.29E-06	7.72E-04	1.67	1138	205	239	72
GO:0044421	extracellular region part	1.11E-05	1.35E-03	1.32	1138	222	534	138
GO:0099513	polymeric cytoskeletal fibre	2.19E-05	2.29E-03	7.29	1138	36	39	9
GO:0099081	supramolecular polymer	9.28E-05	8.47E-03	6.25	1138	42	39	9
GO:0099080	supramolecular complex	9.28E-05	7.53E-03	6.25	1138	42	39	9
GO:0099512	supramolecular fibre	9.28E-05	6.77E-03	6.25	1138	42	39	9
GO:0030141	secretory granule	3.38E-04	2.24E-02	19.13	1138	34	7	4
GO:0042599	lamellar body	8.16E-04	4.96E-02	34.48	1138	2	33	2

Analysis performed by *GOrilla*. Enrichment = (b/n) / (B/N). N - the total number of genes, B - the total number of genes associated with a specific GO term, n - the number of genes in the top of the user's input list, b - the number of genes in the intersection

Table S5 Gene ontology term enrichment *in upregulated differential expressed genes between Winnie-sham and C57BL/6 mice*

GO Term	Description	P-value	FDR q-value	Enrichment	N	B	n	b
Biological Process								
GO:0002376	immune system process	1.24E-95	1.46E-91	3.24	5461	539	893	286
GO:0006952	defence response	4.55E-76	2.68E-72	3.43	5461	384	899	217
GO:0006955	immune response	5.66E-71	2.22E-67	3.67	5461	312	893	187
GO:0043207	response to external biotic stimulus	8.94E-63	2.63E-59	3.48	5461	311	904	179
GO:0009607	response to biotic stimulus	2.85E-61	6.71E-58	3.41	5461	319	904	180
GO:0051707	response to other organism	1.62E-57	3.19E-54	3.75	5461	247	885	150
GO:0002682	regulation of immune system process	2.18E-56	3.67E-53	2.9	5461	471	857	214
GO:0002684	positive regulation of immune system process	2.88E-50	4.24E-47	3	5461	324	996	177
GO:0050776	regulation of immune response	5.87E-49	7.69E-46	3.49	5461	263	857	144
GO:0009605	response to external stimulus	1.78E-46	2.10E-43	2.63	5461	475	909	208
GO:0051704	multi-organism process	3.77E-46	4.04E-43	3.6	5461	326	647	139
GO:0098542	defence response to other organism	1.99E-41	1.95E-38	4.22	5461	167	768	99
GO:0009617	response to bacterium	1.11E-39	1.01E-36	4.36	5461	155	743	92
GO:0050778	positive regulation of immune response	1.40E-39	1.18E-36	3.48	5461	187	956	114
GO:0006950	response to stress	1.53E-39	1.20E-36	2.03	5461	860	909	291
GO:0031347	regulation of defence response	4.61E-38	3.39E-35	3.27	5461	227	904	123
GO:0050896	response to stimulus	5.68E-38	3.93E-35	1.69	5461	1504	909	422
GO:0002697	regulation of immune effector process	2.90E-36	1.90E-33	3.82	5461	155	877	95
GO:0001817	regulation of cytokine production	1.31E-35	8.13E-33	3.26	5461	250	803	120
GO:0045087	innate immune response	1.05E-33	6.19E-31	3.49	5461	151	996	96
GO:0002252	immune effector process	3.10E-32	1.74E-29	3.58	5461	162	875	93
GO:0006954	inflammatory response	8.67E-32	4.64E-29	3.48	5461	166	899	95
GO:0002694	regulation of leukocyte activation	2.24E-31	1.15E-28	3.4	5461	188	846	99
GO:0050865	regulation of cell activation	1.89E-30	9.28E-28	3.23	5461	208	846	104
GO:0001819	positive regulation of cytokine production	2.12E-30	1.00E-27	3.52	5461	159	877	90
GO:0002699	positive regulation of immune effector process	3.24E-30	1.47E-27	4.28	5461	99	877	68
GO:0002703	regulation of leukocyte mediated immunity	8.04E-30	3.51E-27	4.43	5461	90	877	64
GO:0034097	response to cytokine	4.22E-29	1.78E-26	4.68	5461	220	382	72
GO:0080134	regulation of response to stress	8.13E-28	3.30E-25	2.3	5461	441	910	169

GO:0002822	regulation of adaptive immune response based on somatic recombination of immune receptors built from immunoglobulin superfamily domains	3.52E-27	1.38E-24	4.63	5461	74	877	55
GO:0002819	regulation of adaptive immune response	9.32E-27	3.54E-24	4.4	5461	82	877	58
GO:0034341	response to interferon-gamma	2.04E-26	7.52E-24	7.29	5461	59	508	40
GO:0050867	positive regulation of cell activation	2.71E-26	9.66E-24	3.95	5461	127	762	70
GO:0002696	positive regulation of leukocyte activation	2.88E-26	9.99E-24	3.81	5461	121	841	71
GO:0031349	positive regulation of defence response	3.50E-24	1.18E-21	3.68	5461	110	904	67
GO:0042742	defence response to bacterium	8.05E-24	2.63E-21	4.44	5461	91	743	55
GO:0035458	cellular response to interferon-beta	1.28E-23	4.08E-21	12.86	5461	28	364	24
GO:0035456	response to interferon-beta	4.21E-23	1.30E-20	11.47	5461	34	364	26
GO:0051249	regulation of lymphocyte activation	5.24E-23	1.58E-20	3.25	5461	157	846	79
GO:0002824	positive regulation of adaptive immune response based on somatic recombination of immune receptors built from immunoglobulin superfamily domains	9.91E-23	2.92E-20	4.87	5461	55	877	43
GO:0045088	regulation of innate immune response	1.36E-22	3.91E-20	3.71	5461	101	904	62
GO:0002706	regulation of lymphocyte mediated immunity	1.83E-22	5.13E-20	4.46	5461	67	877	48
GO:0002237	response to molecule of bacterial origin	2.35E-22	6.45E-20	3.76	5461	114	803	63
GO:0002705	positive regulation of leukocyte mediated immunity	2.69E-22	7.19E-20	4.72	5461	58	877	44
GO:0048584	positive regulation of response to stimulus	4.70E-22	1.23E-19	1.85	5461	722	914	224
GO:0050727	regulation of inflammatory response	1.37E-21	3.50E-19	3.74	5461	125	735	63
GO:0071345	cellular response to cytokine stimulus	1.74E-21	4.36E-19	4.63	5461	170	382	55
GO:0050900	leukocyte migration	1.99E-21	4.89E-19	3.85	5461	89	892	56
GO:0032101	regulation of response to external stimulus	2.51E-21	6.02E-19	2.65	5461	295	740	106
GO:0002821	positive regulation of adaptive immune response	2.96E-21	6.97E-19	4.57	5461	60	877	44
GO:0001775	cell activation	5.30E-21	1.22E-18	2.95	5461	189	833	85
GO:0045321	leukocyte activation	5.42E-21	1.23E-18	3.08	5461	168	833	79
GO:1903039	positive regulation of leukocyte cell-cell adhesion	7.62E-21	1.69E-18	3.85	5461	89	877	55

GO:0051251	positive regulation of lymphocyte activation	1.26E-20	2.74E-18	3.64	5461	107	841	60
GO:0050870	positive regulation of T cell activation	2.45E-20	5.25E-18	3.88	5461	85	877	53
GO:0031341	regulation of cell killing	2.49E-20	5.24E-18	5.01	5461	46	877	37
GO:0050863	regulation of T cell activation	9.50E-20	1.96E-17	3.39	5461	122	846	64
GO:0009615	response to virus	4.67E-19	9.49E-17	3.38	5461	94	996	58
GO:0032944	regulation of mononuclear cell proliferation	7.15E-19	1.43E-16	3.94	5461	93	760	51
GO:0050670	regulation of lymphocyte proliferation	7.15E-19	1.40E-16	3.94	5461	93	760	51
GO:1903037	regulation of leukocyte cell-cell adhesion	9.62E-19	1.86E-16	3.39	5461	117	841	61
GO:0010033	response to organic substance	1.17E-18	2.23E-16	2.15	5461	705	511	142
GO:0030595	leukocyte chemotaxis	1.43E-18	2.67E-16	4.24	5461	64	865	43
GO:0070663	regulation of leukocyte proliferation	2.61E-18	4.81E-16	3.86	5461	95	760	51
GO:0022409	positive regulation of cell-cell adhesion	2.95E-18	5.35E-16	3.45	5461	103	877	57
GO:0001910	regulation of leukocyte mediated cytotoxicity	3.19E-18	5.69E-16	4.92	5461	43	877	34
GO:0071216	cellular response to biotic stimulus	4.00E-18	7.03E-16	4.11	5461	79	774	46
GO:0048583	regulation of response to stimulus	4.67E-18	8.10E-16	1.61	5461	1267	744	278
GO:0071346	cellular response to interferon-gamma	5.74E-18	9.80E-16	8.45	5461	44	382	26
GO:0032496	response to lipopolysaccharide	5.81E-18	9.77E-16	3.61	5461	102	800	54
GO:0071219	cellular response to molecule of bacterial origin	7.87E-18	1.31E-15	4.2	5461	74	774	44
GO:0002708	positive regulation of lymphocyte mediated immunity	2.12E-17	3.47E-15	4.57	5461	49	877	36
GO:0060326	cell chemotaxis	3.39E-17	5.47E-15	4.35	5461	92	601	44
GO:0002250	adaptive immune response	5.20E-17	8.28E-15	3.34	5461	87	996	53
GO:0071222	cellular response to lipopolysaccharide	6.46E-17	1.02E-14	4.25	5461	68	774	41
GO:0042221	response to chemical	6.59E-17	1.02E-14	1.96	5461	857	517	159
GO:0019221	cytokine-mediated signalling pathway	8.31E-17	1.27E-14	3.36	5461	97	904	54
GO:0002831	regulation of response to biotic stimulus	9.86E-17	1.49E-14	6.5	5461	59	427	30
GO:0045089	positive regulation of innate immune response	1.04E-16	1.55E-14	3.71	5461	65	996	44
GO:0031343	positive regulation of cell killing	1.38E-16	2.03E-14	5.28	5461	33	877	28
GO:0019882	antigen processing and presentation	2.06E-16	2.99E-14	4.67	5461	44	877	33
GO:0002683	negative regulation of immune system process	3.66E-16	5.26E-14	2.76	5461	173	846	74
GO:0050777	negative regulation of immune response	4.41E-16	6.26E-14	4.77	5461	64	644	36
GO:0051607	defence response to virus	4.59E-16	6.43E-14	4.04	5461	74	768	42

GO:0002764	immune response-regulating signalling pathway	9.96E-16	1.38E-13	3.3	5461	83	996	50
GO:0032103	positive regulation of response to external stimulus	1.26E-15	1.72E-13	2.85	5461	123	996	64
GO:0022407	regulation of cell-cell adhesion	1.76E-15	2.39E-13	2.75	5461	161	877	71
GO:0097530	granulocyte migration	1.85E-15	2.48E-13	6.51	5461	48	472	27
GO:0042129	regulation of T cell proliferation	2.71E-15	3.59E-13	4.05	5461	71	760	40
GO:0071621	granulocyte chemotaxis	2.73E-15	3.57E-13	6.68	5461	45	472	26
GO:1990266	neutrophil migration	2.73E-15	3.53E-13	6.68	5461	45	472	26
GO:0070665	positive regulation of leukocyte proliferation	3.28E-15	4.20E-13	4.01	5461	59	877	38
GO:0048002	antigen processing and presentation of peptide antigen	3.50E-15	4.43E-13	5.09	5461	33	877	27
GO:0030593	neutrophil chemotaxis	3.81E-15	4.77E-13	6.89	5461	42	472	25
GO:0032946	positive regulation of mononuclear cell proliferation	5.61E-15	6.96E-13	4.04	5461	57	877	37
GO:0050671	positive regulation of lymphocyte proliferation	5.61E-15	6.88E-13	4.04	5461	57	877	37
GO:0032649	regulation of interferon-gamma production	6.74E-15	8.19E-13	4.84	5461	47	744	31
GO:0002253	activation of immune response	1.15E-14	1.38E-12	3.1	5461	92	996	52
GO:0002709	regulation of T cell mediated immunity	1.18E-14	1.40E-12	4.84	5461	36	877	28
GO:0001912	positive regulation of leukocyte mediated cytotoxicity	1.97E-14	2.32E-12	5.19	5461	30	877	25
GO:0050830	defence response to Gram-positive bacterium	3.01E-14	3.52E-12	4.63	5461	39	877	29
GO:0002757	immune response-activating signal transduction	3.04E-14	3.51E-12	3.28	5461	77	996	46
GO:0097529	myeloid leukocyte migration	3.25E-14	3.72E-12	4.98	5461	57	596	31
GO:1903708	positive regulation of hemopoiesis	5.56E-14	6.30E-12	3.45	5461	81	841	43
GO:1902105	regulation of leukocyte differentiation	7.93E-14	8.89E-12	3.1	5461	104	846	50
GO:0043900	regulation of multi-organism process	8.04E-14	8.93E-12	2.55	5461	144	996	67
GO:0042035	regulation of cytokine biosynthetic process	1.10E-13	1.21E-11	4.11	5461	40	996	30
GO:0006935	chemotaxis	1.10E-13	1.20E-11	2.61	5461	137	978	64
GO:0042102	positive regulation of T cell proliferation	1.29E-13	1.39E-11	4.4	5461	41	877	29
GO:1903706	regulation of hemopoiesis	1.40E-13	1.50E-11	2.78	5461	144	846	62
GO:0042330	taxis	1.69E-13	1.80E-11	2.59	5461	138	978	64
GO:0002521	leukocyte differentiation	2.25E-13	2.36E-11	3.06	5461	110	811	50
GO:0071310	cellular response to organic substance	2.30E-13	2.40E-11	2.48	5461	477	383	83
GO:0001562	response to protozoan	3.57E-13	3.69E-11	6.63	5461	20	741	18
GO:0050707	regulation of cytokine secretion	6.20E-13	6.35E-11	3.47	5461	88	733	41

GO:0046649	lymphocyte activation	6.68E-13	6.79E-11	2.82	5461	128	833	55
GO:0001914	regulation of T cell mediated cytotoxicity	1.23E-12	1.23E-10	5.63	5461	21	877	19
GO:0051250	negative regulation of lymphocyte activation	1.29E-12	1.29E-10	5.16	5461	59	484	27
GO:0050729	positive regulation of inflammatory response	1.31E-12	1.29E-10	3.58	5461	52	996	34
GO:0042832	defence response to protozoan	1.97E-12	1.94E-10	6.94	5461	17	741	16
GO:0070887	cellular response to chemical stimulus	2.80E-12	2.72E-10	2.19	5461	573	383	88
GO:1902107	positive regulation of leukocyte differentiation	3.22E-12	3.11E-10	3.54	5461	66	841	36
GO:0045582	positive regulation of T cell differentiation	3.27E-12	3.13E-10	4.23	5461	43	841	28
GO:0019884	antigen processing and presentation of exogenous antigen	3.64E-12	3.46E-10	5.81	5461	20	846	18
GO:0002695	negative regulation of leukocyte activation	3.70E-12	3.49E-10	4.67	5461	70	484	29
GO:0001818	negative regulation of cytokine production	4.49E-12	4.20E-10	2.92	5461	97	905	47
GO:0002274	myeloid leukocyte activation	6.02E-12	5.59E-10	4.22	5461	52	721	29
GO:0051240	positive regulation of multicellular organismal process	7.77E-12	7.15E-10	1.6	5461	696	916	187
GO:0002685	regulation of leukocyte migration	8.74E-12	7.98E-10	2.83	5461	91	996	47
GO:0006959	humoral immune response	1.17E-11	1.06E-09	13.04	5461	41	143	14
GO:0061844	antimicrobial humoral immune response mediated by antimicrobial peptide	1.21E-11	1.08E-09	29.75	5461	14	118	9
GO:0045619	regulation of lymphocyte differentiation	1.25E-11	1.11E-09	3.42	5461	68	846	36
GO:0045785	positive regulation of cell adhesion	1.26E-11	1.11E-09	2.31	5461	186	877	69
GO:0042108	positive regulation of cytokine biosynthetic process	1.86E-11	1.64E-09	4.47	5461	27	996	22
GO:0045621	positive regulation of lymphocyte differentiation	1.92E-11	1.67E-09	3.92	5461	48	841	29
GO:0002768	immune response-regulating cell surface receptor signalling pathway	1.96E-11	1.69E-09	3.65	5461	56	855	32
GO:0031348	negative regulation of defence response	2.55E-11	2.19E-09	3.6	5461	81	655	35
GO:0002711	positive regulation of T cell mediated immunity	2.55E-11	2.18E-09	4.84	5461	27	877	21
GO:0042110	T cell activation	2.64E-11	2.24E-09	3.25	5461	86	762	39
GO:1903555	regulation of tumor necrosis factor superfamily cytokine production	2.64E-11	2.22E-09	3.17	5461	64	996	37
GO:0045580	regulation of T cell differentiation	2.72E-11	2.28E-09	3.55	5461	60	846	33
GO:0050866	negative regulation of cell activation	4.74E-11	3.93E-09	4.18	5461	81	484	30

GO:0002478	antigen processing and presentation of exogenous peptide antigen	5.78E-11	4.76E-09	8.49	5461	18	500	14
GO:0050715	positive regulation of cytokine secretion	7.35E-11	6.01E-09	3.73	5461	62	733	31
GO:0019730	antimicrobial humoral response	9.36E-11	7.61E-09	21.04	5461	22	118	10
GO:0070098	chemokine-mediated signalling pathway	9.66E-11	7.79E-09	8.32	5461	24	410	15
GO:0002460	adaptive immune response based on somatic recombination of immune receptors built from immunoglobulin superfamily domains	1.09E-10	8.73E-09	3.92	5461	35	996	25
GO:0043901	negative regulation of multi-organism process	1.14E-10	9.05E-09	2.97	5461	72	996	39
GO:0030155	regulation of cell adhesion	1.35E-10	1.06E-08	1.96	5461	296	877	93
GO:0033993	response to lipid	1.71E-10	1.34E-08	2.64	5461	225	487	53
GO:0001916	positive regulation of T cell mediated cytotoxicity	1.97E-10	1.54E-08	5.54	5461	18	877	16
GO:0002449	lymphocyte mediated immunity	1.97E-10	1.53E-08	4.07	5461	31	996	23
GO:1903038	negative regulation of leukocyte cell-cell adhesion	1.99E-10	1.54E-08	4.99	5461	52	484	23
GO:0032729	positive regulation of interferon-gamma production	2.11E-10	1.61E-08	4.82	5461	32	744	21
GO:0050868	negative regulation of T cell activation	2.30E-10	1.75E-08	5.17	5461	48	484	22
GO:0032680	regulation of tumor necrosis factor production	2.72E-10	2.05E-08	3.1	5461	62	996	35
GO:0002366	leukocyte activation involved in immune response	3.03E-10	2.27E-08	3.73	5461	50	819	28
GO:0002886	regulation of myeloid leukocyte mediated immunity	3.84E-10	2.87E-08	4.84	5461	25	857	19
GO:0048518	positive regulation of biological process	4.77E-10	3.53E-08	1.26	5461	1913	993	440
GO:0002443	leukocyte mediated immunity	4.98E-10	3.67E-08	3.66	5461	39	996	26
GO:2000106	regulation of leukocyte apoptotic process	5.69E-10	4.16E-08	3.73	5461	47	841	27
GO:0002263	cell activation involved in immune response	5.74E-10	4.17E-08	3.66	5461	51	819	28
GO:0002474	antigen processing and presentation of peptide antigen via MHC class I	7.47E-10	5.40E-08	4.87	5461	23	877	18
GO:0002428	antigen processing and presentation of peptide antigen via MHC class Ib	7.95E-10	5.71E-08	5.81	5461	15	877	14
GO:0002475	antigen processing and presentation via MHC class Ib	7.95E-10	5.68E-08	5.81	5461	15	877	14
GO:0002429	immune response-activating cell surface receptor signalling pathway	8.63E-10	6.13E-08	3.58	5461	50	855	28

GO:0046634	regulation of alpha-beta T cell activation	1.39E-09	9.80E-08	3.68	5461	44	877	26
GO:0002700	regulation of production of molecular mediator of immune response	1.59E-09	1.11E-07	3.34	5461	56	877	30
GO:0050688	regulation of defence response to virus	1.97E-09	1.37E-07	6.6	5461	31	427	16
GO:0002688	regulation of leukocyte chemotaxis	2.40E-09	1.67E-07	3.15	5461	55	978	31
GO:0045824	negative regulation of innate immune response	2.52E-09	1.74E-07	4.67	5461	24	877	18
GO:0002687	positive regulation of leukocyte migration	2.82E-09	1.93E-07	2.92	5461	67	978	35
GO:0071396	cellular response to lipid	3.78E-09	2.57E-07	5.1	5461	141	167	22
GO:0051716	cellular response to stimulus	3.97E-09	2.69E-07	1.8	5461	824	383	104
GO:0032479	regulation of type I interferon production	4.16E-09	2.80E-07	4.06	5461	27	996	20
GO:0032945	negative regulation of mononuclear cell proliferation	4.32E-09	2.89E-07	5.49	5461	37	484	18
GO:0050672	negative regulation of lymphocyte proliferation	4.32E-09	2.87E-07	5.49	5461	37	484	18
GO:0002476	antigen processing and presentation of endogenous peptide antigen via MHC class Ib	4.48E-09	2.96E-07	5.78	5461	14	877	13
GO:0002483	antigen processing and presentation of endogenous peptide antigen	5.53E-09	3.64E-07	5.19	5461	18	877	15
GO:0019883	antigen processing and presentation of endogenous antigen	5.53E-09	3.62E-07	5.19	5461	18	877	15
GO:0071347	cellular response to interleukin-1	6.16E-09	4.01E-07	7.68	5461	21	440	13
GO:0030217	T cell differentiation	6.78E-09	4.39E-07	3.52	5461	55	762	27
GO:0070664	negative regulation of leukocyte proliferation	7.23E-09	4.66E-07	5.34	5461	38	484	18
GO:0032652	regulation of interleukin-1 production	8.06E-09	5.16E-07	4.78	5461	28	735	18
GO:0002702	positive regulation of production of molecular mediator of immune response	9.23E-09	5.88E-07	3.65	5461	41	877	24
GO:0002698	negative regulation of immune effector process	9.46E-09	5.99E-07	3.67	5461	49	760	25
GO:0008284	positive regulation of cell proliferation	1.12E-08	7.06E-07	1.79	5461	360	841	99
GO:0072676	lymphocyte migration	1.26E-08	7.92E-07	6.27	5461	21	581	14
GO:0043903	regulation of symbiosis, encompassing mutualism through parasitism	1.31E-08	8.15E-07	2.74	5461	72	996	36
GO:0001816	cytokine production	1.36E-08	8.44E-07	3.64	5461	43	838	24
GO:0002825	regulation of T-helper 1 type immune response	1.40E-08	8.61E-07	6.05	5461	16	733	13
GO:0030098	lymphocyte differentiation	1.44E-08	8.83E-07	2.94	5461	78	811	34

GO:0022408	negative regulation of cell-cell adhesion	1.55E-08	9.48E-07	4.08	5461	73	440	24
GO:0046635	positive regulation of alpha-beta T cell activation	1.99E-08	1.21E-06	4.02	5461	31	877	20
GO:0002833	positive regulation of response to biotic stimulus	2.00E-08	1.21E-06	8.15	5461	21	383	12
GO:0002793	positive regulation of peptide secretion	2.03E-08	1.22E-06	2.58	5461	124	733	43
GO:0002791	regulation of peptide secretion	2.11E-08	1.26E-06	2.17	5461	203	733	59
GO:0002820	negative regulation of adaptive immune response	2.27E-08	1.35E-06	5.84	5461	16	760	13
GO:0043300	regulation of leukocyte degranulation	2.35E-08	1.39E-06	5.42	5461	18	783	14
GO:1902533	positive regulation of intracellular signal transduction	2.36E-08	1.39E-06	1.93	5461	358	623	79
GO:0002707	negative regulation of lymphocyte mediated immunity	2.67E-08	1.56E-06	5.13	5461	17	877	14
GO:0002526	acute inflammatory response	2.70E-08	1.58E-06	8.23	5461	23	346	12
GO:0007159	leukocyte cell-cell adhesion	2.97E-08	1.73E-06	4.46	5461	29	760	18
GO:0019724	B cell mediated immunity	3.21E-08	1.86E-06	4.8	5461	16	996	14
GO:1903557	positive regulation of tumor necrosis factor superfamily cytokine production	3.88E-08	2.23E-06	3.26	5461	42	996	25
GO:0002285	lymphocyte activation involved in immune response	3.89E-08	2.22E-06	4.33	5461	28	811	18
GO:0050764	regulation of phagocytosis	4.12E-08	2.34E-06	4.27	5461	41	624	20
GO:1901700	response to oxygen-containing compound	4.25E-08	2.41E-06	1.84	5461	415	630	88
GO:0050714	positive regulation of protein secretion	5.04E-08	2.84E-06	2.61	5461	114	733	40
GO:0002888	positive regulation of myeloid leukocyte mediated immunity	5.18E-08	2.91E-06	7.2	5461	14	596	11
GO:0048522	positive regulation of cellular process	6.70E-08	3.74E-06	1.27	5461	1720	918	366
GO:0051246	regulation of protein metabolic process	6.85E-08	3.81E-06	1.41	5461	867	972	217
GO:0051247	positive regulation of protein metabolic process	7.39E-08	4.09E-06	1.71	5461	549	617	106
GO:0060334	regulation of interferon-gamma-mediated signalling pathway	8.05E-08	4.43E-06	15.07	5461	8	317	7
GO:0060330	regulation of response to interferon-gamma	8.05E-08	4.41E-06	15.07	5461	8	317	7
GO:0051709	regulation of killing of cells of other organism	8.71E-08	4.75E-06	18.26	5461	6	299	6
GO:0017014	protein nitrosylation	1.05E-07	5.69E-06	82.43	5461	5	53	4
GO:0050851	antigen receptor-mediated signalling pathway	1.08E-07	5.86E-06	3.76	5461	40	762	21
GO:0002827	positive regulation of T-helper 1 type immune response	1.21E-07	6.50E-06	6.77	5461	11	733	10

GO:0002823	negative regulation of adaptive immune response based on somatic recombination of immune receptors built from immunoglobulin superfamily domains	1.25E-07	6.68E-06	5.75	5461	15	760	12
GO:0032760	positive regulation of tumor necrosis factor production	1.25E-07	6.66E-06	3.21	5461	41	996	24
GO:0042534	regulation of tumor necrosis factor biosynthetic process	1.31E-07	6.97E-06	6.7	5461	11	741	10
GO:0002704	negative regulation of leukocyte mediated immunity	1.42E-07	7.49E-06	4.33	5461	23	877	16
GO:0002718	regulation of cytokine production involved in immune response	1.43E-07	7.51E-06	5.72	5461	38	377	15
GO:0033003	regulation of mast cell activation	1.43E-07	7.48E-06	4.91	5461	19	819	14
GO:0032481	positive regulation of type I interferon production	1.47E-07	7.64E-06	4.52	5461	17	996	14
GO:0070228	regulation of lymphocyte apoptotic process	1.51E-07	7.84E-06	4.03	5461	29	841	18
GO:0002690	positive regulation of leukocyte chemotaxis	1.61E-07	8.31E-06	3.19	5461	42	978	24
GO:0009967	positive regulation of signal transduction	1.68E-07	8.67E-06	1.55	5461	523	914	136
GO:0050864	regulation of B cell activation	1.70E-07	8.73E-06	3.39	5461	44	841	23
GO:0051222	positive regulation of protein transport	1.83E-07	9.35E-06	2.27	5461	160	736	49
GO:0050708	regulation of protein secretion	1.91E-07	9.68E-06	2.13	5461	189	733	54
GO:0002828	regulation of type 2 immune response	1.92E-07	9.68E-06	8.75	5461	17	367	10
GO:0032675	regulation of interleukin-6 production	1.93E-07	9.73E-06	2.84	5461	56	996	29
GO:0010942	positive regulation of cell death	1.99E-07	9.96E-06	1.85	5461	244	909	75
GO:0050728	negative regulation of inflammatory response	2.00E-07	9.96E-06	3.55	5461	54	655	23
GO:0002673	regulation of acute inflammatory response	2.02E-07	1.01E-05	3.96	5461	29	857	18
GO:0045058	T cell selection	2.10E-07	1.04E-05	4.69	5461	23	760	15
GO:0050852	T cell receptor signalling pathway	2.10E-07	1.04E-05	4.69	5461	23	760	15
GO:0023056	positive regulation of signalling	2.13E-07	1.05E-05	1.51	5461	603	914	152
GO:0070555	response to interleukin-1	2.18E-07	1.07E-05	6.21	5461	26	440	13
GO:0051239	regulation of multicellular organismal process	2.40E-07	1.17E-05	1.35	5461	1166	865	249
GO:0002675	positive regulation of acute inflammatory response	2.41E-07	1.17E-05	4.7	5461	19	857	14
GO:0090087	regulation of peptide transport	2.52E-07	1.22E-05	1.91	5461	272	736	70
GO:0002758	innate immune response-activating signal transduction	2.88E-07	1.38E-05	3.59	5461	29	996	19

GO:1904951	positive regulation of establishment of protein localization	2.91E-07	1.39E-05	2.24	5461	162	736	49
GO:0048247	lymphocyte chemotaxis	3.00E-07	1.43E-05	5.59	5461	16	733	12
GO:0051046	regulation of secretion	3.00E-07	1.43E-05	1.72	5461	324	903	92
GO:0010647	positive regulation of cell communication	3.32E-07	1.57E-05	1.57	5461	598	737	127
GO:0002286	T cell activation involved in immune response	3.53E-07	1.67E-05	5.51	5461	16	743	12
GO:0042130	negative regulation of T cell proliferation	3.58E-07	1.68E-05	5.13	5461	33	484	15
GO:2000377	regulation of reactive oxygen species metabolic process	3.68E-07	1.72E-05	2.84	5461	74	779	30
GO:0046641	positive regulation of alpha-beta T cell proliferation	4.40E-07	2.05E-05	6.23	5461	9	877	9
GO:1903532	positive regulation of secretion by cell	4.51E-07	2.09E-05	2.22	5461	169	685	47
GO:2000379	positive regulation of reactive oxygen species metabolic process	4.74E-07	2.19E-05	3.51	5461	42	779	21
GO:0035821	modification of morphology or physiology of other organism	5.29E-07	2.43E-05	4.32	5461	28	722	16
GO:0051047	positive regulation of secretion	6.08E-07	2.79E-05	2.16	5461	181	685	49
GO:0002504	antigen processing and presentation of peptide or polysaccharide antigen via MHC class II	6.55E-07	2.99E-05	9.42	5461	10	464	8
GO:0002495	antigen processing and presentation of peptide antigen via MHC class II	6.55E-07	2.98E-05	9.42	5461	10	464	8
GO:0019886	antigen processing and presentation of exogenous peptide antigen via MHC class II	6.55E-07	2.97E-05	9.42	5461	10	464	8
GO:0031663	lipopolysaccharide-mediated signalling pathway	6.74E-07	3.04E-05	4.7	5461	14	996	12
GO:0016064	immunoglobulin mediated immune response	6.75E-07	3.03E-05	4.7	5461	14	996	12
GO:0032642	regulation of chemokine production	6.80E-07	3.05E-05	4.67	5461	39	480	16
GO:0060760	positive regulation of response to cytokine stimulus	7.34E-07	3.28E-05	8.2	5461	21	317	10
GO:0032689	negative regulation of interferon-gamma production	7.69E-07	3.42E-05	8.88	5461	15	369	9
GO:1901701	cellular response to oxygen-containing compound	8.36E-07	3.70E-05	2.02	5461	278	565	58
GO:0002523	leukocyte migration involved in inflammatory response	8.46E-07	3.73E-05	8.48	5461	14	414	9
GO:1903556	negative regulation of tumor necrosis factor superfamily cytokine production	8.56E-07	3.76E-05	4.38	5461	25	748	15

GO:0007166	cell surface receptor signalling pathway	9.04E-07	3.96E-05	1.63	5461	644	550	106
GO:0002221	pattern recognition receptor signalling pathway	9.57E-07	4.17E-05	3.52	5461	28	996	18
GO:0002715	regulation of natural killer cell mediated immunity	9.64E-07	4.19E-05	4.36	5461	20	877	14
GO:0042269	regulation of natural killer cell mediated cytotoxicity	9.64E-07	4.17E-05	4.36	5461	20	877	14
GO:0032270	positive regulation of cellular protein metabolic process	1.21E-06	5.24E-05	1.67	5461	508	617	96
GO:0001961	positive regulation of cytokine-mediated signalling pathway	1.23E-06	5.29E-05	15.5	5461	18	137	7
GO:0006953	acute-phase response	1.27E-06	5.45E-05	33.96	5461	12	67	5
GO:0042535	positive regulation of tumor necrosis factor biosynthetic process	1.29E-06	5.50E-05	7.87	5461	9	617	8
GO:0051712	positive regulation of killing of cells of other organism	1.32E-06	5.60E-05	18.26	5461	5	299	5
GO:0071674	mononuclear cell migration	1.45E-06	6.15E-05	9.53	5461	12	382	8
GO:0002548	monocyte chemotaxis	1.45E-06	6.13E-05	9.53	5461	12	382	8
GO:1903901	negative regulation of viral life cycle	1.45E-06	6.12E-05	3.25	5461	34	989	20
GO:0051223	regulation of protein transport	1.57E-06	6.59E-05	1.88	5461	257	736	65
GO:0050704	regulation of interleukin-1 secretion	1.60E-06	6.68E-05	5.46	5461	15	733	11
GO:0048525	negative regulation of viral process	1.71E-06	7.10E-05	3.13	5461	37	989	21
GO:0097190	apoptotic signalling pathway	1.76E-06	7.32E-05	2.37	5461	95	899	37
GO:0090026	positive regulation of monocyte chemotaxis	1.90E-06	7.86E-05	5.12	5461	11	969	10
GO:0051050	positive regulation of transport	2.10E-06	8.66E-05	1.92	5461	398	450	63
GO:0071675	regulation of mononuclear cell migration	2.18E-06	8.96E-05	4.08	5461	25	803	15
GO:0032722	positive regulation of chemokine production	2.33E-06	9.52E-05	5.99	5461	31	353	12
GO:0010574	regulation of vascular endothelial growth factor production	2.35E-06	9.57E-05	5.01	5461	14	857	11
GO:0045123	cellular extravasation	2.48E-06	1.01E-04	10.26	5461	9	414	7
GO:0050706	regulation of interleukin-1 beta secretion	2.55E-06	1.03E-04	5.73	5461	13	733	10
GO:0008219	cell death	2.56E-06	1.03E-04	1.92	5461	228	737	59
GO:0002720	positive regulation of cytokine production involved in immune response	2.66E-06	1.07E-04	6.37	5461	25	377	11
GO:0002920	regulation of humoral immune response	2.83E-06	1.13E-04	5.31	5461	12	857	10
GO:0032651	regulation of interleukin-1 beta production	2.87E-06	1.15E-04	4.6	5461	21	735	13
GO:0042127	regulation of cell proliferation	3.02E-06	1.20E-04	1.66	5461	616	497	93

GO:1903530	regulation of secretion by cell	3.03E-06	1.20E-04	1.82	5461	303	685	69
GO:0050766	positive regulation of phagocytosis	3.31E-06	1.31E-04	4.7	5461	32	508	14
GO:0050691	regulation of defence response to virus by host	3.35E-06	1.32E-04	6.73	5461	19	427	10
GO:0045061	thymic T cell selection	3.47E-06	1.36E-04	4.79	5461	18	760	12
GO:0002507	tolerance induction	3.58E-06	1.40E-04	7.43	5461	7	735	7
GO:0032720	negative regulation of tumor necrosis factor production	3.71E-06	1.45E-04	4.26	5461	24	748	14
GO:0012501	programmed cell death	3.78E-06	1.47E-04	1.93	5461	215	737	56
GO:0052547	regulation of peptidase activity	3.84E-06	1.49E-04	3.76	5461	122	238	20
GO:0002437	inflammatory response to antigenic stimulus	3.86E-06	1.49E-04	5.49	5461	18	608	11
GO:0070201	regulation of establishment of protein localization	4.01E-06	1.54E-04	1.83	5461	263	736	65
GO:0044406	adhesion of symbiont to host	4.07E-06	1.56E-04	9.5	5461	9	447	7
GO:0032655	regulation of interleukin-12 production	4.11E-06	1.57E-04	3.76	5461	23	948	15
GO:0050663	cytokine secretion	4.26E-06	1.63E-04	4.43	5461	28	617	14
GO:2000107	negative regulation of leukocyte apoptotic process	4.27E-06	1.62E-04	3.44	5461	34	841	18
GO:0043065	positive regulation of apoptotic process	4.31E-06	1.63E-04	1.79	5461	221	909	66
GO:0090025	regulation of monocyte chemotaxis	4.31E-06	1.63E-04	5.13	5461	16	732	11
GO:0030162	regulation of proteolysis	4.34E-06	1.64E-04	2.21	5461	199	522	42
GO:0002710	negative regulation of T cell mediated immunity	4.48E-06	1.68E-04	7.19	5461	7	760	7
GO:0018119	peptidyl-cysteine S-nitrosylation	4.50E-06	1.68E-04	97.52	5461	4	42	3
GO:0097191	extrinsic apoptotic signalling pathway	4.65E-06	1.73E-04	3.82	5461	31	737	16
GO:0043068	positive regulation of programmed cell death	4.86E-06	1.81E-04	1.79	5461	222	909	66
GO:0002712	regulation of B cell mediated immunity	4.89E-06	1.81E-04	4.5	5461	17	857	12
GO:0002889	regulation of immunoglobulin mediated immune response	4.89E-06	1.81E-04	4.5	5461	17	857	12
GO:0002218	activation of innate immune response	5.21E-06	1.92E-04	3.16	5461	33	996	19
GO:0032663	regulation of interleukin-2 production	5.49E-06	2.01E-04	4.69	5461	19	735	12
GO:0002837	regulation of immune response to tumor cell	5.64E-06	2.06E-04	14.07	5461	5	388	5
GO:0002834	regulation of response to tumor cell	5.64E-06	2.06E-04	14.07	5461	5	388	5
GO:0043067	regulation of programmed cell death	5.74E-06	2.09E-04	1.49	5461	516	909	128
GO:0010941	regulation of cell death	5.84E-06	2.12E-04	1.46	5461	571	909	139

GO:0046640	regulation of alpha-beta T cell proliferation	6.06E-06	2.19E-04	4.4	5461	17	877	12
GO:0007162	negative regulation of cell adhesion	6.11E-06	2.20E-04	2.86	5461	117	440	27
GO:0032653	regulation of interleukin-10 production	6.24E-06	2.24E-04	4.65	5461	19	741	12
GO:0052548	regulation of endopeptidase activity	6.43E-06	2.30E-04	3.97	5461	104	238	18
GO:0045071	negative regulation of viral genome replication	6.46E-06	2.31E-04	3.35	5461	28	989	17
GO:0043304	regulation of mast cell degranulation	6.49E-06	2.31E-04	5.71	5461	11	783	9
GO:0042981	regulation of apoptotic process	6.52E-06	2.31E-04	1.49	5461	512	909	127
GO:0042119	neutrophil activation	6.68E-06	2.36E-04	5.41	5461	14	721	10
GO:0043302	positive regulation of leukocyte degranulation	6.87E-06	2.42E-04	8.02	5461	8	596	7
GO:0002714	positive regulation of B cell mediated immunity	7.48E-06	2.63E-04	4.67	5461	15	857	11
GO:0002891	positive regulation of immunoglobulin mediated immune response	7.48E-06	2.62E-04	4.67	5461	15	857	11
GO:0001934	positive regulation of protein phosphorylation	7.63E-06	2.67E-04	1.74	5461	377	617	74
GO:0046637	regulation of alpha-beta T cell differentiation	8.26E-06	2.88E-04	3.58	5461	29	841	16
GO:0034612	response to tumor necrosis factor	8.32E-06	2.89E-04	4.21	5461	40	487	15
GO:0032268	regulation of cellular protein metabolic process	9.16E-06	3.17E-04	1.47	5461	799	617	133
GO:0050854	regulation of antigen receptor-mediated signalling pathway	9.40E-06	3.25E-04	4.97	5461	13	845	10
GO:0071622	regulation of granulocyte chemotaxis	9.71E-06	3.35E-04	3.5	5461	28	892	16
GO:0032102	negative regulation of response to external stimulus	1.03E-05	3.55E-04	2.24	5461	125	740	38
GO:0048585	negative regulation of response to stimulus	1.04E-05	3.56E-04	1.54	5461	579	674	110
GO:0060759	regulation of response to cytokine stimulus	1.07E-05	3.67E-04	2.89	5461	48	865	22
GO:1902531	regulation of intracellular signal transduction	1.09E-05	3.71E-04	1.5	5461	588	741	120
GO:0002922	positive regulation of humoral immune response	1.19E-05	4.05E-04	6.37	5461	7	857	7
GO:0070232	regulation of T cell apoptotic process	1.31E-05	4.44E-04	4.02	5461	21	841	13
GO:0030099	myeloid cell differentiation	1.36E-05	4.58E-04	2.69	5461	63	805	25
GO:0031622	positive regulation of fever generation	1.40E-05	4.70E-04	16.6	5461	7	235	5
GO:0032735	positive regulation of interleukin-12 production	1.41E-05	4.75E-04	4.07	5461	17	948	12
GO:1903900	regulation of viral life cycle	1.52E-05	5.10E-04	2.76	5461	51	893	23

GO:0002577	regulation of antigen processing and presentation	1.59E-05	5.30E-04	5.74	5461	9	846	8
GO:0036230	granulocyte activation	1.74E-05	5.80E-04	5.05	5461	15	721	10
GO:0001776	leukocyte homeostasis	1.74E-05	5.79E-04	3.7	5461	30	737	15
GO:0002230	positive regulation of defence response to virus by host	1.76E-05	5.83E-04	7.31	5461	14	427	8
GO:0042327	positive regulation of phosphorylation	1.87E-05	6.17E-04	1.69	5461	392	617	75
GO:0043030	regulation of macrophage activation	1.87E-05	6.16E-04	5.6	5461	13	675	9
GO:0010562	positive regulation of phosphorus metabolic process	1.91E-05	6.27E-04	1.67	5461	419	617	79
GO:0045937	positive regulation of phosphate metabolic process	1.91E-05	6.25E-04	1.67	5461	419	617	79
GO:0046903	secretion	1.94E-05	6.32E-04	2	5461	203	618	46
GO:0043902	positive regulation of multi-organism process	1.94E-05	6.31E-04	3.91	5461	59	379	16
GO:0002374	cytokine secretion involved in immune response	2.03E-05	6.58E-04	19.03	5461	4	287	4
GO:0031401	positive regulation of protein modification process	2.09E-05	6.77E-04	1.66	5461	420	617	79
GO:0002861	regulation of inflammatory response to antigenic stimulus	2.10E-05	6.77E-04	3.92	5461	17	984	12
GO:0016477	cell migration	2.11E-05	6.80E-04	1.91	5461	336	450	53
GO:0038034	signal transduction in absence of ligand	2.15E-05	6.90E-04	4.94	5461	15	737	10
GO:0097192	extrinsic apoptotic signalling pathway in absence of ligand	2.15E-05	6.88E-04	4.94	5461	15	737	10
GO:0002573	myeloid leukocyte differentiation	2.15E-05	6.87E-04	3.3	5461	35	805	17
GO:0033006	regulation of mast cell activation involved in immune response	2.18E-05	6.96E-04	5.23	5461	12	783	9
GO:0048872	homeostasis of number of cells	2.25E-05	7.14E-04	2.79	5461	61	737	23
GO:0001906	cell killing	2.31E-05	7.32E-04	5.87	5461	15	558	9
GO:0032732	positive regulation of interleukin-1 production	2.34E-05	7.39E-04	4.55	5461	18	733	11
GO:0035455	response to interferon-alpha	2.53E-05	7.96E-04	5.8	5461	15	565	9
GO:0072678	T cell migration	2.56E-05	8.04E-04	7.31	5461	9	581	7
GO:0006915	apoptotic process	2.65E-05	8.30E-04	1.95	5461	202	651	47
GO:0048870	cell motility	2.66E-05	8.30E-04	1.87	5461	356	450	55
GO:0050921	positive regulation of chemotaxis	2.97E-05	9.25E-04	2.43	5461	62	978	27
GO:0060335	positive regulation of interferon-gamma-mediated signalling pathway	2.98E-05	9.26E-04	17.23	5461	4	317	4
GO:0060332	positive regulation of response to interferon-gamma	2.98E-05	9.23E-04	17.23	5461	4	317	4

GO:0001932	regulation of protein phosphorylation	3.10E-05	9.59E-04	1.57	5461	523	617	93
GO:0007165	signal transduction	3.27E-05	1.01E-03	1.29	5461	1275	762	230
GO:0071677	positive regulation of mononuclear cell migration	3.28E-05	1.01E-03	4.34	5461	13	969	10
GO:0050920	regulation of chemotaxis	3.29E-05	1.01E-03	2.11	5461	98	978	37
GO:1901222	regulation of NIK/NF-kappaB signalling	3.48E-05	1.06E-03	4.65	5461	33	427	12
GO:0001959	regulation of cytokine-mediated signalling pathway	3.51E-05	1.07E-03	2.87	5461	44	865	20
GO:0032753	positive regulation of interleukin-4 production	3.77E-05	1.15E-03	4.45	5461	14	877	10
GO:0031620	regulation of fever generation	3.77E-05	1.14E-03	14.52	5461	8	235	5
GO:0050792	regulation of viral process	3.79E-05	1.15E-03	6.26	5461	57	153	10
GO:0033032	regulation of myeloid cell apoptotic process	3.96E-05	1.20E-03	5.88	5461	18	464	9
GO:0045637	regulation of myeloid cell differentiation	4.05E-05	1.22E-03	2.48	5461	76	783	27
GO:0002830	positive regulation of type 2 immune response	4.12E-05	1.24E-03	10.08	5461	10	325	6
GO:0007204	positive regulation of cytosolic calcium ion concentration	4.23E-05	1.27E-03	2.17	5461	119	762	36
GO:1902622	regulation of neutrophil migration	4.25E-05	1.27E-03	3.13	5461	28	996	16
GO:0030730	sequestering of triglyceride	4.47E-05	1.33E-03	147.59	5461	2	37	2
GO:0046136	positive regulation of vitamin metabolic process	4.47E-05	1.33E-03	147.59	5461	2	37	2
GO:0060559	positive regulation of calcidiol 1-monooxygenase activity	4.47E-05	1.33E-03	147.59	5461	2	37	2
GO:0060557	positive regulation of vitamin D biosynthetic process	4.47E-05	1.32E-03	147.59	5461	2	37	2
GO:0043410	positive regulation of MAPK cascade	4.51E-05	1.33E-03	1.91	5461	223	617	48
GO:0033033	negative regulation of myeloid cell apoptotic process	4.70E-05	1.38E-03	7.49	5461	11	464	7
GO:0046006	regulation of activated T cell proliferation	4.88E-05	1.43E-03	6.45	5461	14	484	8
GO:0042325	regulation of phosphorylation	5.04E-05	1.48E-03	1.41	5461	563	957	139
GO:0033005	positive regulation of mast cell activation	5.17E-05	1.51E-03	7.85	5461	7	596	6
GO:0002724	regulation of T cell cytokine production	5.19E-05	1.51E-03	7.97	5461	13	369	7
GO:2000514	regulation of CD4-positive, alpha-beta T cell activation	5.21E-05	1.51E-03	3.68	5461	23	838	13
GO:0050710	negative regulation of cytokine secretion	5.24E-05	1.52E-03	4.85	5461	29	427	11
GO:1900015	regulation of cytokine production involved in inflammatory response	5.25E-05	1.52E-03	5.9	5461	12	617	8
GO:0055082	cellular chemical homeostasis	5.45E-05	1.57E-03	1.82	5461	243	668	54
GO:0002224	toll-like receptor signalling pathway	5.49E-05	1.58E-03	3.34	5461	23	996	14

GO:0070488	neutrophil aggregation	5.78E-05	1.66E-03	130.02	5461	2	42	2
GO:0001911	negative regulation of leukocyte mediated cytotoxicity	5.91E-05	1.69E-03	4.67	5461	12	877	9
GO:0031342	negative regulation of cell killing	5.91E-05	1.69E-03	4.67	5461	12	877	9
GO:0043032	positive regulation of macrophage activation	5.99E-05	1.71E-03	7.59	5461	7	617	6
GO:0032490	detection of molecule of bacterial origin	6.00E-05	1.71E-03	7.59	5461	7	617	6
GO:0030888	regulation of B cell proliferation	6.13E-05	1.74E-03	3.49	5461	27	811	14
GO:0051241	negative regulation of multicellular organismal process	6.29E-05	1.78E-03	1.67	5461	485	486	72
GO:0044419	interspecies interaction between organisms	6.78E-05	1.92E-03	3.73	5461	56	392	15
GO:0055080	cation homeostasis	6.91E-05	1.95E-03	1.8	5461	251	651	54
GO:0010575	positive regulation of vascular endothelial growth factor production	6.99E-05	1.97E-03	5.1	5461	10	857	8
GO:0030003	cellular cation homeostasis	7.09E-05	1.99E-03	1.78	5461	217	762	54
GO:0050829	defence response to Gram-negative bacterium	7.16E-05	2.00E-03	3.95	5461	23	722	12
GO:0070486	leukocyte aggregation	7.17E-05	2.00E-03	55.72	5461	7	42	3
GO:0035634	response to stilbenoid	7.21E-05	2.01E-03	6.21	5461	9	684	7
GO:0042116	macrophage activation	7.30E-05	2.03E-03	4.6	5461	17	698	10
GO:0055065	metal ion homeostasis	7.35E-05	2.04E-03	1.83	5461	228	668	51
GO:0050716	positive regulation of interleukin-1 secretion	7.42E-05	2.05E-03	5.42	5461	11	733	8
GO:0050718	positive regulation of interleukin-1 beta secretion	7.42E-05	2.05E-03	5.42	5461	11	733	8
GO:0030335	positive regulation of cell migration	7.49E-05	2.06E-03	1.74	5461	239	760	58
GO:0045766	positive regulation of angiogenesis	7.56E-05	2.08E-03	3	5461	83	438	20
GO:0045807	positive regulation of endocytosis	7.64E-05	2.09E-03	3.05	5461	67	508	19
GO:0051049	regulation of transport	7.66E-05	2.09E-03	1.56	5461	691	450	89
GO:0006968	cellular defence response	7.70E-05	2.10E-03	6.58	5461	10	581	7
GO:0072503	cellular divalent inorganic cation homeostasis	7.80E-05	2.12E-03	1.87	5461	176	762	46
GO:2000116	regulation of cysteine-type endopeptidase activity	8.02E-05	2.18E-03	4.32	5461	69	238	13
GO:0002643	regulation of tolerance induction	8.06E-05	2.18E-03	5.35	5461	11	743	8
GO:0002883	regulation of hypersensitivity	8.09E-05	2.19E-03	5.58	5461	8	857	7
GO:0050871	positive regulation of B cell activation	8.40E-05	2.26E-03	3.25	5461	30	841	15
GO:0042590	antigen processing and presentation of exogenous peptide antigen via MHC class I	9.00E-05	2.42E-03	10.11	5461	6	450	5

GO:2000401	regulation of lymphocyte migration	9.06E-05	2.43E-03	3.85	5461	23	740	12
GO:0043383	negative T cell selection	9.16E-05	2.45E-03	5.23	5461	11	760	8
GO:0045060	negative thymic T cell selection	9.16E-05	2.45E-03	5.23	5461	11	760	8
GO:0042592	homeostatic process	9.17E-05	2.45E-03	1.48	5461	517	773	108
GO:0071356	cellular response to tumor necrosis factor	9.25E-05	2.46E-03	5.11	5461	28	382	10
GO:0006875	cellular metal ion homeostasis	9.34E-05	2.48E-03	1.78	5461	198	805	52
GO:0006691	leukotriene metabolic process	9.36E-05	2.48E-03	4.88	5461	10	896	8
GO:0051092	positive regulation of NF-kappaB transcription factor activity	9.38E-05	2.48E-03	4.04	5461	44	399	13
GO:0046638	positive regulation of alpha-beta T cell differentiation	9.61E-05	2.53E-03	3.52	5461	24	841	13
GO:0072507	divalent inorganic cation homeostasis	1.00E-04	2.64E-03	1.84	5461	183	762	47
GO:0045076	regulation of interleukin-2 biosynthetic process	1.01E-04	2.64E-03	8.14	5461	5	671	5
GO:0032673	regulation of interleukin-4 production	1.01E-04	2.64E-03	4.15	5461	15	877	10
GO:0031294	lymphocyte costimulation	1.01E-04	2.64E-03	5.43	5461	12	671	8
GO:0031295	T cell costimulation	1.01E-04	2.63E-03	5.43	5461	12	671	8
GO:0043122	regulation of I-kappaB kinase/NF-kappaB signalling	1.01E-04	2.63E-03	5.57	5461	53	185	10
GO:2000403	positive regulation of lymphocyte migration	1.06E-04	2.76E-03	4.38	5461	17	733	10
GO:0055074	calcium ion homeostasis	1.07E-04	2.78E-03	1.86	5461	173	762	45
GO:0032635	interleukin-6 production	1.11E-04	2.86E-03	94.16	5461	2	58	2
GO:0097028	dendritic cell differentiation	1.13E-04	2.91E-03	5.79	5461	9	733	7
GO:0032757	positive regulation of interleukin-8 production	1.16E-04	2.99E-03	7.57	5461	17	297	7
GO:2000147	positive regulation of cell motility	1.17E-04	3.00E-03	1.63	5461	246	910	67
GO:0032647	regulation of interferon-alpha production	1.18E-04	3.02E-03	4.32	5461	12	948	9
GO:0098581	detection of external biotic stimulus	1.19E-04	3.03E-03	6.2	5461	10	617	7
GO:0098771	inorganic ion homeostasis	1.20E-04	3.05E-03	1.77	5461	256	651	54
GO:0046636	negative regulation of alpha-beta T cell activation	1.20E-04	3.05E-03	6.27	5461	19	367	8
GO:0070304	positive regulation of stress-activated protein kinase signalling cascade	1.21E-04	3.07E-03	2.21	5461	72	996	29
GO:0006874	cellular calcium ion homeostasis	1.26E-04	3.19E-03	1.87	5461	169	762	44
GO:0032940	secretion by cell	1.28E-04	3.23E-03	2.06	5461	163	618	38
GO:0040011	locomotion	1.32E-04	3.34E-03	1.79	5461	385	428	54
GO:0032755	positive regulation of interleukin-6 production	1.34E-04	3.38E-03	2.82	5461	33	996	17

GO:0010758	regulation of macrophage chemotaxis	1.40E-04	3.51E-03	4.95	5461	11	803	8
GO:0060340	positive regulation of type I interferon-mediated signalling pathway	1.45E-04	3.63E-03	37.23	5461	5	88	3
GO:0032880	regulation of protein localization	1.45E-04	3.63E-03	1.59	5461	355	736	76
GO:0045589	regulation of regulatory T cell differentiation	1.48E-04	3.70E-03	5.57	5461	9	762	7
GO:0006873	cellular ion homeostasis	1.49E-04	3.71E-03	1.74	5461	222	762	54
GO:0043281	regulation of cysteine-type endopeptidase activity involved in apoptotic process	1.52E-04	3.79E-03	4.37	5461	63	238	12
GO:0040017	positive regulation of locomotion	1.53E-04	3.79E-03	1.61	5461	253	910	68
GO:1901224	positive regulation of NIK/NF-kappaB signalling	1.54E-04	3.81E-03	5.34	5461	23	400	9
GO:0032691	negative regulation of interleukin-1 beta production	1.56E-04	3.85E-03	7.43	5461	5	735	5
GO:0002579	positive regulation of antigen processing and presentation	1.59E-04	3.91E-03	6.39	5461	7	733	6
GO:0032879	regulation of localization	1.62E-04	3.98E-03	1.42	5461	1023	450	120
GO:0031652	positive regulation of heat generation	1.66E-04	4.07E-03	11.62	5461	10	235	5
GO:2000427	positive regulation of apoptotic cell clearance	1.68E-04	4.10E-03	29.9	5461	4	137	3
GO:2000425	regulation of apoptotic cell clearance	1.68E-04	4.09E-03	29.9	5461	4	137	3
GO:0043370	regulation of CD4-positive, alpha-beta T cell differentiation	1.80E-04	4.40E-03	3.77	5461	19	838	11
GO:0045620	negative regulation of lymphocyte differentiation	1.82E-04	4.44E-03	5.95	5461	20	367	8
GO:0044278	cell wall disruption in other organism	1.83E-04	4.45E-03	5,461.00	5461	1	1	1
GO:0030316	osteoclast differentiation	2.00E-04	4.86E-03	4.36	5461	14	805	9
GO:1904407	positive regulation of nitric oxide metabolic process	2.01E-04	4.87E-03	3.85	5461	21	743	11
GO:0045429	positive regulation of nitric oxide biosynthetic process	2.01E-04	4.86E-03	3.85	5461	21	743	11
GO:0002369	T cell cytokine production	2.06E-04	4.97E-03	10.75	5461	4	508	4
GO:2001186	negative regulation of CD8-positive, alpha-beta T cell activation	2.07E-04	4.97E-03	69.13	5461	2	79	2
GO:0002790	peptide secretion	2.09E-04	5.01E-03	2.72	5461	65	617	20
GO:0034121	regulation of toll-like receptor signalling pathway	2.35E-04	5.63E-03	3.38	5461	27	779	13
GO:0032695	negative regulation of interleukin-12 production	2.39E-04	5.72E-03	9.09	5461	7	429	5
GO:2000866	positive regulation of estradiol secretion	2.39E-04	5.71E-03	64.25	5461	2	85	2

GO:0045069	regulation of viral genome replication	2.48E-04	5.89E-03	2.79	5461	38	875	17
GO:0002717	positive regulation of natural killer cell mediated immunity	2.55E-04	6.06E-03	4.53	5461	11	877	8
GO:0032874	positive regulation of stress-activated MAPK cascade	2.57E-04	6.09E-03	2.16	5461	71	996	28
GO:0034116	positive regulation of heterotypic cell-cell adhesion	2.61E-04	6.17E-03	98.4	5461	3	37	2
GO:0002678	positive regulation of chronic inflammatory response	2.61E-04	6.15E-03	98.4	5461	3	37	2
GO:0060558	regulation of calcidiol 1-monooxygenase activity	2.61E-04	6.14E-03	98.4	5461	3	37	2
GO:0060556	regulation of vitamin D biosynthetic process	2.61E-04	6.13E-03	98.4	5461	3	37	2
GO:0009306	protein secretion	2.62E-04	6.14E-03	2.76	5461	61	617	19
GO:2000110	negative regulation of macrophage apoptotic process	2.64E-04	6.18E-03	25.92	5461	4	158	3
GO:0032693	negative regulation of interleukin-10 production	2.66E-04	6.22E-03	15.22	5461	7	205	4
GO:0015682	ferric iron transport	2.67E-04	6.23E-03	5.81	5461	7	805	6
GO:0072512	trivalent inorganic cation transport	2.67E-04	6.22E-03	5.81	5461	7	805	6
GO:0002260	lymphocyte homeostasis	2.70E-04	6.27E-03	3.56	5461	25	737	12
GO:1904892	regulation of STAT cascade	2.71E-04	6.28E-03	2.94	5461	39	762	16
GO:0071224	cellular response to peptidoglycan	2.76E-04	6.40E-03	19.03	5461	3	287	3
GO:0009595	detection of biotic stimulus	2.80E-04	6.47E-03	5.63	5461	11	617	7
GO:0002637	regulation of immunoglobulin production	2.81E-04	6.48E-03	3.61	5461	19	877	11
GO:0031399	regulation of protein modification process	2.86E-04	6.57E-03	1.35	5461	607	963	145
GO:0010950	positive regulation of endopeptidase activity	2.87E-04	6.59E-03	2.67	5461	51	762	19
GO:0050857	positive regulation of antigen receptor-mediated signalling pathway	2.88E-04	6.61E-03	5.77	5461	7	811	6
GO:0031650	regulation of heat generation	2.90E-04	6.64E-03	10.56	5461	11	235	5
GO:0002829	negative regulation of type 2 immune response	2.91E-04	6.65E-03	7.83	5461	6	581	5
GO:0060142	regulation of syncytium formation by plasma membrane fusion	2.92E-04	6.65E-03	5.83	5461	12	546	7
GO:0050801	ion homeostasis	2.98E-04	6.78E-03	1.7	5461	277	651	56
GO:0002438	acute inflammatory response to antigenic stimulus	2.99E-04	6.79E-03	8.67	5461	7	450	5
GO:0051272	positive regulation of cellular component movement	3.02E-04	6.84E-03	1.59	5461	253	910	67
GO:0045919	positive regulation of cytolysis	3.06E-04	6.92E-03	18.39	5461	3	297	3
GO:0042268	regulation of cytolysis	3.06E-04	6.91E-03	18.39	5461	3	297	3

GO:0002863	positive regulation of inflammatory response to antigenic stimulus	3.07E-04	6.92E-03	4.96	5461	9	857	7
GO:0070374	positive regulation of ERK1 and ERK2 cascade	3.09E-04	6.95E-03	2.4	5461	109	521	25
GO:0070949	regulation of neutrophil mediated killing of symbiont cell	3.09E-04	6.94E-03	18.26	5461	3	299	3
GO:0060338	regulation of type I interferon-mediated signalling pathway	3.13E-04	7.01E-03	31.03	5461	6	88	3
GO:1901739	regulation of myoblast fusion	3.14E-04	7.02E-03	6.67	5461	9	546	6
GO:0008630	intrinsic apoptotic signalling pathway in response to DNA damage	3.17E-04	7.07E-03	2.94	5461	31	899	15
GO:0051341	regulation of oxidoreductase activity	3.18E-04	7.09E-03	7.33	5461	32	163	7
GO:0071624	positive regulation of granulocyte chemotaxis	3.19E-04	7.09E-03	3.54	5461	19	892	11
GO:0090022	regulation of neutrophil chemotaxis	3.23E-04	7.16E-03	3.34	5461	22	892	12
GO:1902624	positive regulation of neutrophil migration	3.23E-04	7.15E-03	3.34	5461	22	892	12
GO:0001909	leukocyte mediated cytotoxicity	3.26E-04	7.22E-03	5.71	5461	12	558	7
GO:2000515	negative regulation of CD4-positive, alpha-beta T cell activation	3.32E-04	7.33E-03	7.44	5461	12	367	6
GO:0051090	regulation of DNA-binding transcription factor activity	3.38E-04	7.44E-03	2.49	5461	132	399	24
GO:1905521	regulation of macrophage migration	3.41E-04	7.50E-03	4.53	5461	12	803	8
GO:0032943	mononuclear cell proliferation	3.44E-04	7.55E-03	3.45	5461	25	760	12
GO:0046651	lymphocyte proliferation	3.44E-04	7.54E-03	3.45	5461	25	760	12
GO:0002292	T cell differentiation involved in immune response	3.45E-04	7.53E-03	9.05	5461	8	377	5
GO:0045624	positive regulation of T-helper cell differentiation	3.46E-04	7.55E-03	5.22	5461	10	733	7
GO:2000108	positive regulation of leukocyte apoptotic process	3.46E-04	7.54E-03	5.95	5461	14	459	7
GO:1904018	positive regulation of vasculature development	3.51E-04	7.64E-03	2.82	5461	92	400	19
GO:1903531	negative regulation of secretion by cell	3.52E-04	7.64E-03	2.93	5461	91	369	18
GO:2001242	regulation of intrinsic apoptotic signalling pathway	3.54E-04	7.67E-03	5.34	5461	50	184	9
GO:0050878	regulation of body fluid levels	3.61E-04	7.80E-03	2.08	5461	95	857	31
GO:0070229	negative regulation of lymphocyte apoptotic process	3.61E-04	7.80E-03	3.57	5461	20	841	11
GO:0002534	cytokine production involved in inflammatory response	3.66E-04	7.89E-03	2,730.50	5461	1	2	1

GO:0034275	kynurenic acid metabolic process	3.66E-04	7.87E-03	2,730.50	5461	1	2	1
GO:0034276	kynurenic acid biosynthetic process	3.66E-04	7.86E-03	2,730.50	5461	1	2	1
GO:0036269	swimming behaviour	3.66E-04	7.84E-03	2,730.50	5461	1	2	1
GO:0019441	tryptophan catabolic process to kynurenine	3.66E-04	7.83E-03	2,730.50	5461	1	2	1
GO:0009966	regulation of signal transduction	3.67E-04	7.83E-03	1.44	5461	956	412	104
GO:2000404	regulation of T cell migration	3.70E-04	7.88E-03	3.92	5461	19	733	10
GO:0010952	positive regulation of peptidase activity	3.74E-04	7.96E-03	2.62	5461	52	762	19
GO:0045428	regulation of nitric oxide biosynthetic process	3.81E-04	8.08E-03	3.27	5461	29	748	13
GO:2001233	regulation of apoptotic signalling pathway	3.82E-04	8.09E-03	1.83	5461	127	985	42
GO:0030216	keratinocyte differentiation	3.84E-04	8.12E-03	3.91	5461	19	736	10
GO:0019220	regulation of phosphate metabolic process	3.93E-04	8.31E-03	1.35	5461	615	957	145
GO:0043306	positive regulation of mast cell degranulation	3.99E-04	8.40E-03	9.16	5461	4	596	4
GO:0033008	positive regulation of mast cell activation involved in immune response	3.99E-04	8.39E-03	9.16	5461	4	596	4
GO:0045059	positive thymic T cell selection	4.12E-04	8.66E-03	5.03	5461	10	760	7
GO:2000406	positive regulation of T cell migration	4.17E-04	8.75E-03	4.19	5461	16	733	9
GO:0051174	regulation of phosphorus metabolic process	4.19E-04	8.77E-03	1.34	5461	616	957	145
GO:0045622	regulation of T-helper cell differentiation	4.24E-04	8.86E-03	4.58	5461	13	733	8
GO:0042532	negative regulation of tyrosine phosphorylation of STAT protein	4.34E-04	9.05E-03	12.34	5461	6	295	4
GO:0009725	response to hormone	4.39E-04	9.14E-03	5.68	5461	171	45	8
GO:2001185	regulation of CD8-positive, alpha-beta T cell activation	4.44E-04	9.22E-03	5.34	5461	7	877	6
GO:0051048	negative regulation of secretion	4.48E-04	9.29E-03	2.61	5461	103	427	21
GO:0032733	positive regulation of interleukin-10 production	4.54E-04	9.40E-03	4.54	5461	13	741	8
GO:0060627	regulation of vesicle-mediated transport	4.55E-04	9.40E-03	1.89	5461	173	636	38
GO:0002275	myeloid cell activation involved in immune response	4.57E-04	9.44E-03	3.33	5461	24	819	12
GO:0045124	regulation of bone resorption	4.67E-04	9.62E-03	3.77	5461	18	805	10
GO:0032743	positive regulation of interleukin-2 production	4.84E-04	9.95E-03	5.18	5461	11	671	7
GO:0018198	peptidyl-cysteine modification	4.91E-04	1.01E-02	32.51	5461	12	42	3
GO:0019885	antigen processing and presentation of endogenous peptide	4.93E-04	1.01E-02	7.8	5461	7	500	5

	antigen via MHC class I							
GO:1903426	regulation of reactive oxygen species biosynthetic process	5.00E-04	1.02E-02	2.92	5461	36	779	15
GO:0072677	eosinophil migration	5.14E-04	1.05E-02	8.69	5461	9	349	5
GO:0048245	eosinophil chemotaxis	5.14E-04	1.05E-02	8.69	5461	9	349	5
GO:0032815	negative regulation of natural killer cell activation	5.15E-04	1.05E-02	15.47	5461	3	353	3
GO:0032677	regulation of interleukin-8 production	5.28E-04	1.07E-02	4.6	5461	25	427	9
GO:0030100	regulation of endocytosis	5.47E-04	1.11E-02	2.25	5461	101	624	26
GO:0050730	regulation of peptidyl-tyrosine phosphorylation	5.49E-04	1.11E-02	2.06	5461	108	762	31
GO:0030334	regulation of cell migration	5.52E-04	1.12E-02	1.7	5461	390	446	54
GO:0032814	regulation of natural killer cell activation	5.55E-04	1.12E-02	5.24	5461	12	608	7
GO:0032480	negative regulation of type I interferon production	5.60E-04	1.13E-02	4.81	5461	10	795	7
GO:0032692	negative regulation of interleukin-1 production	5.77E-04	1.16E-02	5.57	5461	8	735	6
GO:0070233	negative regulation of T cell apoptotic process	5.95E-04	1.20E-02	3.9	5461	15	841	9
GO:0051770	positive regulation of nitric-oxide synthase biosynthetic process	5.96E-04	1.19E-02	5.16	5461	12	617	7
GO:1902884	positive regulation of response to oxidative stress	6.20E-04	1.24E-02	5.9	5461	9	617	6
GO:2001032	regulation of double-strand break repair via nonhomologous end joining	6.28E-04	1.25E-02	14.45	5461	3	378	3
GO:0045086	positive regulation of interleukin-2 biosynthetic process	6.35E-04	1.26E-02	8.14	5461	4	671	4
GO:0009593	detection of chemical stimulus	6.37E-04	1.27E-02	4.19	5461	19	617	9
GO:0045581	negative regulation of T cell differentiation	6.45E-04	1.28E-02	5.79	5461	18	367	7
GO:0030885	regulation of myeloid dendritic cell activation	6.60E-04	1.31E-02	14.26	5461	3	383	3
GO:0002839	positive regulation of immune response to tumor cell	6.60E-04	1.31E-02	14.26	5461	3	383	3
GO:0002836	positive regulation of response to tumor cell	6.60E-04	1.30E-02	14.26	5461	3	383	3
GO:0002858	regulation of natural killer cell mediated cytotoxicity directed against tumor cell target	6.63E-04	1.31E-02	14.26	5461	3	383	3
GO:0002855	regulation of natural killer cell mediated immune response to tumor cell	6.63E-04	1.31E-02	14.26	5461	3	383	3
GO:0009893	positive regulation of metabolic process	6.78E-04	1.33E-02	1.23	5461	1071	996	241

GO:0051480	regulation of cytosolic calcium ion concentration	6.79E-04	1.33E-02	1.93	5461	134	762	36
GO:0002726	positive regulation of T cell cytokine production	7.11E-04	1.39E-02	8.4	5461	10	325	5
GO:1903428	positive regulation of reactive oxygen species biosynthetic process	7.18E-04	1.41E-02	3.24	5461	26	779	12
GO:0031325	positive regulation of cellular metabolic process	7.19E-04	1.40E-02	1.25	5461	983	963	217
GO:1903207	regulation of hydrogen peroxide-induced neuron death	7.25E-04	1.42E-02	2,730.50	5461	2	1	1
GO:1903208	negative regulation of hydrogen peroxide-induced neuron death	7.25E-04	1.41E-02	2,730.50	5461	2	1	1
GO:1900017	positive regulation of cytokine production involved in inflammatory response	7.31E-04	1.42E-02	5.48	5461	5	996	5
GO:0045954	positive regulation of natural killer cell mediated cytotoxicity	7.32E-04	1.42E-02	4.59	5461	10	833	7
GO:0002532	production of molecular mediator involved in inflammatory response	7.41E-04	1.44E-02	6.35	5461	6	717	5
GO:0002544	chronic inflammatory response	7.47E-04	1.45E-02	73.8	5461	4	37	2
GO:0002439	chronic inflammatory response to antigenic stimulus	7.47E-04	1.44E-02	73.8	5461	4	37	2
GO:0002676	regulation of chronic inflammatory response	7.47E-04	1.44E-02	73.8	5461	4	37	2
GO:0030656	regulation of vitamin metabolic process	7.47E-04	1.44E-02	73.8	5461	4	37	2
GO:0060337	type I interferon signalling pathway	7.70E-04	1.48E-02	7.09	5461	7	550	5
GO:0051817	modification of morphology or physiology of other organism involved in symbiotic interaction	7.75E-04	1.49E-02	4.19	5461	21	558	9
GO:0042509	regulation of tyrosine phosphorylation of STAT protein	7.78E-04	1.49E-02	5.1	5461	27	317	8
GO:1903409	reactive oxygen species biosynthetic process	7.78E-04	1.49E-02	5.26	5461	8	779	6
GO:0007249	I-kappaB kinase/NF-kappaB signalling	7.89E-04	1.51E-02	4.03	5461	12	904	8
GO:2000109	regulation of macrophage apoptotic process	7.94E-04	1.51E-02	20.74	5461	5	158	3
GO:0048878	chemical homeostasis	7.99E-04	1.52E-02	1.55	5461	373	651	69
GO:0002761	regulation of myeloid leukocyte differentiation	8.06E-04	1.53E-02	2.73	5461	42	763	16
GO:0038094	Fc-gamma receptor signalling pathway	8.31E-04	1.58E-02	9.42	5461	5	464	4
GO:0050869	negative regulation of B cell activation	8.35E-04	1.58E-02	4.72	5461	11	737	7

GO:2000516	positive regulation of CD4-positive, alpha-beta T cell activation	8.61E-04	1.63E-02	4.26	5461	14	733	8
GO:0043372	positive regulation of CD4-positive, alpha-beta T cell differentiation	8.61E-04	1.63E-02	4.26	5461	14	733	8
GO:0070661	leukocyte proliferation	8.67E-04	1.63E-02	3.19	5461	27	760	12
GO:2001234	negative regulation of apoptotic signalling pathway	8.70E-04	1.64E-02	3.93	5461	65	235	11
GO:0002864	regulation of acute inflammatory response to antigenic stimulus	8.74E-04	1.64E-02	4.46	5461	10	857	7
GO:0002604	regulation of dendritic cell antigen processing and presentation	8.92E-04	1.67E-02	7.45	5461	4	733	4
GO:0002606	positive regulation of dendritic cell antigen processing and presentation	8.92E-04	1.67E-02	7.45	5461	4	733	4
GO:0070234	positive regulation of T cell apoptotic process	8.93E-04	1.67E-02	10.11	5461	6	360	4
GO:0010759	positive regulation of macrophage chemotaxis	9.09E-04	1.70E-02	5.1	5461	8	803	6
GO:1905523	positive regulation of macrophage migration	9.09E-04	1.69E-02	5.1	5461	8	803	6
GO:0072604	interleukin-6 secretion	9.16E-04	1.70E-02	1,092.20	5461	1	5	1
GO:0032494	response to peptidoglycan	9.23E-04	1.72E-02	4.7	5461	7	996	6
GO:0006911	phagocytosis, engulfment	9.52E-04	1.77E-02	3.38	5461	17	951	10
GO:0035743	CD4-positive, alpha-beta T cell cytokine production	9.66E-04	1.79E-02	12.5	5461	3	437	3
GO:0043368	positive T cell selection	9.67E-04	1.79E-02	5.89	5461	11	506	6
GO:0002456	T cell mediated immunity	9.74E-04	1.80E-02	4.03	5461	13	833	8
GO:0050856	regulation of T cell receptor signalling pathway	9.77E-04	1.80E-02	5.05	5461	8	811	6
GO:0051094	positive regulation of developmental process	9.90E-04	1.82E-02	1.36	5461	585	860	125
Molecular Function								
GO:0005125	cytokine activity	7.75E-17	2.35E-13	5.58	5461	67	497	34
GO:0005126	cytokine receptor binding	1.81E-12	2.74E-09	4.18	5461	94	472	34
GO:0042379	chemokine receptor binding	1.92E-12	1.94E-09	8.33	5461	25	446	17
GO:0004896	cytokine receptor activity	2.43E-12	1.84E-09	4.25	5461	48	776	29
GO:0008009	chemokine activity	4.84E-12	2.94E-09	9.18	5461	20	446	15
GO:0005102	signalling receptor binding	5.89E-12	2.98E-09	2.09	5461	552	450	95
GO:0042605	peptide antigen binding	2.47E-11	1.07E-08	5.86	5461	17	877	16
GO:0030545	receptor regulator activity	3.61E-11	1.37E-08	3.19	5461	145	507	43
GO:0048018	receptor ligand activity	3.82E-11	1.29E-08	3.3	5461	134	507	41

GO:0003823	antigen binding	3.86E-11	1.17E-08	5.14	5461	23	877	19
GO:0045236	CXCR chemokine receptor binding	4.21E-08	1.16E-05	30.85	5461	9	118	6
GO:0048020	CCR chemokine receptor binding	7.46E-07	1.89E-04	8.63	5461	14	407	9
GO:0042287	MHC protein binding	1.01E-06	2.36E-04	5.46	5461	11	909	10
GO:0046977	TAP binding	1.13E-06	2.46E-04	8.74	5461	10	500	8
GO:0003924	GTPase activity	1.60E-06	3.25E-04	13.17	5461	107	31	8
GO:0019955	cytokine binding	1.73E-06	3.29E-04	2.9	5461	63	776	26
GO:0038023	signalling receptor activity	2.12E-06	3.79E-04	1.82	5461	345	617	71
GO:0050664	oxidoreductase activity, acting on NAD(P)H, oxygen as acceptor	2.16E-06	3.65E-04	6.28	5461	8	870	8
GO:0042288	MHC class I protein binding	3.04E-06	4.86E-04	6.01	5461	8	909	8
GO:0042834	peptidoglycan binding	3.11E-06	4.72E-04	16.3	5461	5	335	5
GO:0035662	Toll-like receptor 4 binding	4.50E-06	6.51E-04	97.52	5461	4	42	3
GO:0060089	molecular transducer activity	8.51E-06	1.18E-03	1.76	5461	357	617	71
GO:0004950	chemokine receptor activity	1.33E-05	1.75E-03	5.59	5461	12	733	9
GO:0001637	G-protein coupled chemoattractant receptor activity	1.33E-05	1.68E-03	5.59	5461	12	733	9
GO:0016493	C-C chemokine receptor activity	1.33E-05	1.61E-03	5.59	5461	12	733	9
GO:0030881	beta-2-microglobulin binding	1.60E-05	1.87E-03	11.56	5461	9	315	6
GO:0019763	immunoglobulin receptor activity	1.63E-05	1.83E-03	11.77	5461	5	464	5
GO:0042277	peptide binding	1.90E-05	2.06E-03	2.42	5461	119	607	32
GO:0019956	chemokine binding	2.04E-05	2.14E-03	4.97	5461	15	733	10
GO:0070891	lipoteichoic acid binding	2.47E-05	2.50E-03	18.39	5461	4	297	4
GO:0004888	transmembrane signalling receptor activity	2.78E-05	2.73E-03	1.73	5461	278	751	66
GO:0019957	C-C chemokine binding	4.32E-05	4.10E-03	5.16	5461	13	733	9
GO:0033218	amide binding	5.09E-05	4.69E-03	2.47	5461	138	464	29
GO:0051400	BH domain binding	5.73E-05	5.12E-03	21.42	5461	6	170	4
GO:0019864	IgG binding	1.08E-04	9.36E-03	9.81	5461	6	464	5
GO:0019770	IgG receptor activity	1.44E-04	1.22E-02	11.77	5461	4	464	4
GO:0042608	T cell receptor binding	1.47E-04	1.21E-02	8.67	5461	12	315	6
GO:0035325	Toll-like receptor binding	1.75E-04	1.40E-02	43.34	5461	9	42	3
GO:0023026	MHC class II protein complex binding	1.83E-04	1.43E-02	29.26	5461	4	140	3
GO:0023023	MHC protein complex binding	1.83E-04	1.39E-02	29.26	5461	4	140	3
GO:0061134	peptidase regulator activity	1.86E-04	1.38E-02	2.77	5461	71	555	20
GO:0017111	nucleoside-triphosphatase activity	2.40E-04	1.74E-02	6.15	5461	229	31	8
GO:0019865	immunoglobulin binding	3.06E-04	2.16E-02	7.06	5461	10	464	6
GO:0071723	lipopeptide binding	3.06E-04	2.12E-02	18.39	5461	3	297	3

GO:0016175	superoxide-generating NADPH oxidase activity	3.65E-04	2.47E-02	6.28	5461	5	870	5
GO:0004833	tryptophan 2,3-dioxygenase activity	3.66E-04	2.42E-02	2,730.50	5461	1	2	1
GO:0033754	indoleamine 2,3-dioxygenase activity	3.66E-04	2.37E-02	2,730.50	5461	1	2	1
GO:0016817	hydrolase activity, acting on acid anhydrides	3.79E-04	2.40E-02	5.75	5461	245	31	8
GO:0016818	hydrolase activity, acting on acid anhydrides, in phosphorus-containing anhydrides	3.79E-04	2.35E-02	5.75	5461	245	31	8
GO:0016462	pyrophosphatase activity	3.79E-04	2.31E-02	5.75	5461	245	31	8
GO:0001664	G-protein coupled receptor binding	3.95E-04	2.35E-02	2.69	5461	91	446	20
GO:0031406	carboxylic acid binding	6.94E-04	4.05E-02	8.48	5461	69	56	6
GO:0030414	peptidase inhibitor activity	7.20E-04	4.13E-02	2.86	5461	56	545	16
GO:0031727	CCR2 chemokine receptor binding	7.40E-04	4.16E-02	51.04	5461	2	107	2
GO:0016597	amino acid binding	7.68E-04	4.24E-02	114.97	5461	19	5	2
GO:0005515	protein binding	7.72E-04	4.19E-02	1.11	5461	2850	993	575
GO:0098772	molecular function regulator	7.88E-04	4.20E-02	1.44	5461	540	682	97
GO:0070628	proteasome binding	8.67E-04	4.54E-02	23.17	5461	7	101	3
GO:0061135	endopeptidase regulator activity	8.88E-04	4.57E-02	2.81	5461	56	555	16
GO:0050544	arachidonic acid binding	9.45E-04	4.79E-02	65.01	5461	4	42	2
GO:0050542	icosanoid binding	9.45E-04	4.71E-02	65.01	5461	4	42	2
GO:0050543	icosatetraenoic acid binding	9.45E-04	4.63E-02	65.01	5461	4	42	2
GO:0050786	RAGE receptor binding	9.45E-04	4.56E-02	65.01	5461	4	42	2
GO:0043177	organic acid binding	9.69E-04	4.60E-02	8.02	5461	73	56	6
Cellular Component								
GO:0009897	external side of plasma membrane	1.94E-25	2.71E-22	3.43	5461	168	776	82
GO:0098552	side of membrane	3.24E-23	2.27E-20	3.16	5461	189	776	85
GO:0044421	extracellular region part	5.07E-17	2.37E-14	2.19	5461	610	518	127
GO:0005615	extracellular space	1.62E-15	5.67E-13	2.31	5461	494	513	107
GO:0009986	cell surface	1.80E-12	5.04E-10	1.99	5461	291	972	103
GO:0042611	MHC protein complex	4.39E-12	1.02E-09	12.52	5461	18	315	13
GO:0005576	extracellular region	4.55E-12	9.10E-10	1.99	5461	551	534	107
GO:0031224	intrinsic component of membrane	9.13E-11	1.60E-08	1.33	5461	1516	974	360
GO:0001772	immunological synapse	1.15E-10	1.79E-08	6.69	5461	15	762	14
GO:0044425	membrane part	7.33E-10	1.03E-07	1.27	5461	1947	915	415
GO:0016021	integral component of membrane	2.47E-09	3.15E-07	1.32	5461	1452	974	341
GO:0016020	membrane	7.69E-09	8.98E-07	1.2	5461	2525	976	540
GO:0033643	host cell part	3.64E-08	3.92E-06	21.58	5461	11	161	7

GO:0042613	MHC class II protein complex	7.20E-08	7.20E-06	23.17	5461	7	202	6
GO:0020005	symbiont-containing vacuole membrane	8.07E-08	7.54E-06	25.44	5461	8	161	6
GO:0044217	other organism part	9.15E-08	8.01E-06	19.79	5461	12	161	7
GO:0005797	Golgi medial cisterna	1.28E-06	1.06E-04	12.14	5461	10	315	7
GO:0042612	MHC class I protein complex	1.28E-06	9.97E-05	12.14	5461	10	315	7
GO:0044459	plasma membrane part	6.80E-06	5.02E-04	1.42	5461	965	624	157
GO:0042101	T cell receptor complex	6.87E-06	4.82E-04	8.02	5461	8	596	7
GO:0005789	endoplasmic reticulum membrane	2.52E-05	1.68E-03	11.52	5461	107	31	7
GO:0070971	endoplasmic reticulum exit site	8.05E-05	5.12E-03	9.46	5461	11	315	6
GO:0044432	endoplasmic reticulum part	9.28E-05	5.65E-03	7.01	5461	201	31	8
GO:0031985	Golgi cisterna	1.06E-04	6.19E-03	7.58	5461	16	315	7
GO:0042105	alpha-beta T cell receptor complex	2.04E-04	1.14E-02	10.79	5461	4	506	4
GO:1990111	spermatoproteasome complex	5.56E-04	2.99E-02	15.09	5461	3	362	3

Analysis performed by *GOrilla*. Enrichment = (b/n) / (B/N). N - the total number of genes, B - the total number of genes associated with a specific GO term, n - the number of genes in the top of the user's input list, b - the number of genes in the intersection

Table S3 ***Enriched KEGG pathways identified in differentially expressed genes downregulated in Winnie mice treated with BM-MSCs compared to sham-treated Winnie mice (no genes)***

Ref	Term	Fold Enrichment	Count	*P* Value	Benjamini
mmu04060	Cytokine-cytokine receptor interaction	4.29	29	9.68E-11	2.10E-08
mmu04668	TNF signalling pathway	5.32	16	2.41E-07	2.61E-05
mmu04640	Hematopoietic cell lineage	5.61	13	2.67E-06	1.93E-04
mmu05152	Tuberculosis	3.71	18	6.08E-06	3.30E-04
mmu05150	Staphylococcus aureus infection	6.52	9	5.64E-05	2.44E-03
mmu05323	Rheumatoid arthritis	4.86	11	7.51E-05	2.71E-03
mmu05133	Pertussis	4.90	10	1.76E-04	5.44E-03
mmu05143	African trypanosomiasis	7.25	7	3.33E-04	9.00E-03
mmu05140	Leishmaniasis	5.10	9	3.34E-04	8.03E-03
mmu04610	Complement and coagulation cascades	4.29	9	1.07E-03	2.31E-02
mmu05321	Inflammatory bowel disease (IBD)	4.91	8	1.08E-03	2.11E-02
mmu05132	Salmonella infection	4.18	9	1.27E-03	2.28E-02
mmu05146	Amoebiasis	3.41	11	1.36E-03	2.24E-02
mmu04620	Toll-like receptor signalling pathway	3.59	10	1.76E-03	2.69E-02
mmu05144	Malaria	5.29	7	1.87E-03	2.67E-02
mmu04630	Jak-STAT signalling pathway	3.00	12	2.09E-03	2.79E-02
mmu05164	Influenza A	2.76	13	2.56E-03	3.22E-02
mmu04062	Chemokine signalling pathway	2.59	14	2.86E-03	3.39E-02
mmu05134	Legionellosis	4.45	7	4.51E-03	5.03E-02
mmu05202	Transcriptional misregulation in cancer	2.62	12	5.89E-03	6.21E-02
mmu05142	Chagas disease (American trypanosomiasis)	3.17	9	7.22E-03	7.21E-02
mmu04623	Cytosolic DNA-sensing pathway	3.96	7	7.96E-03	7.58E-02
mmu04512	ECM-receptor interaction	3.29	8	1.03E-02	9.33E-02
mmu05168	Herpes simplex infection	2.27	13	1.21E-02	1.04E-01
mmu05145	Toxoplasmosis	2.89	9	1.23E-02	1.02E-01
mmu05332	Graft-versus-host disease	4.18	6	1.36E-02	1.08E-01
mmu04970	Salivary secretion	3.29	7	1.88E-02	1.41E-01
mmu04380	Osteoclast differentiation	2.59	9	2.24E-02	1.61E-01
mmu04066	HIF-1 signalling pathway	2.79	8	2.40E-02	1.66E-01
mmu04650	Natural killer cell mediated cytotoxicity	2.76	8	2.51E-02	1.68E-01
mmu05414	Dilated cardiomyopathy	3.06	7	2.62E-02	1.69E-01

mmu04940	Type I diabetes mellitus	3.51	6	2.72E-02	1.70E-01
mmu04514	Cell adhesion molecules (CAMs)	2.24	10	3.41E-02	2.04E-01
mmu04930	Type II diabetes mellitus	3.62	5	4.77E-02	2.68E-01
mmu04145	Phagosome	2.08	10	5.00E-02	2.72E-01
mmu04064	NF-kappa B signalling pathway	2.62	7	5.02E-02	2.67E-01
mmu05410	Hypertrophic cardiomyopathy (HCM)	2.75	6	6.55E-02	3.28E-01
mmu04621	NOD-like receptor signalling pathway	3.24	5	6.71E-02	3.28E-01
mmu05162	Measles	2.13	8	8.02E-02	3.72E-01
mmu04350	TGF-beta signalling pathway	2.56	6	8.39E-02	3.78E-01
mmu04975	Fat digestion and absorption	3.82	4	8.54E-02	3.77E-01
mmu04014	Ras signalling pathway	1.74	11	9.86E-02	4.15E-01

Analysed using DAVID.

Table S4 ***Enriched KEGG pathways identified in differentially expressed genes downregulated in Winnie mice treated with BM-MSCs compared to sham-treated Winnie mice (genes)***

Ref	Term	Genes
mmu04060	Cytokine-cytokine receptor interaction	*Il1r2, Ccl3, Tnf, Osmr, Tnfrsf12a, Il4ra, Cxcl9, Ccl8, Cxcr2, Ccl5, Ccl4, Ccl7, Lif, Tnfrsf1b, Tnfrsf11b, Ifng, Il1b, Csf3r, Csf2rb, Fas, Il1a, Thpo, Il18rap, Il2ra, Osm, Tnfrsf9, Ppbp, Cxcl14, Cxcl16*
mmu04668	TNF signalling pathway	*Icam1, Tnf, Cebpb, Socs3, Mmp9, Cxcl3, Cxcl2, Ifi47, Ccl5, Mmp3, Lif, Nod2, Tnfrsf1b, Ripk3, Il1b, Fas*
mmu04640	Hematopoietic cell lineage	*Il1r2, Tnf, Il2ra, Il4ra, Itga2, Itgam, Cd55, Gp1bb, Cd33, Il1b, Csf3r, Il1a, Thpo*
mmu05152	Tuberculosis	*Mrc1, Cebpb, Tnf, Sphk1, Tlr2, Fcgr4, Itgam, Nod2, Clec4e, Calml3, Ifng, Calm4, Il1b, Fcer1g, Lbp, Clec7a, Nos2, Il1a*
mmu05150	Staphylococcus aureus infection	*Icam1, Selp, Fpr1, Fcgr4, Cfh, C2, Fpr2, Itgam, Ptafr*
mmu05323	Rheumatoid arthritis	*Icam1, Ctsk, Ccl3, Tnf, Cxcl5, Ifng, Tlr2, Il1b, Ccl5, Mmp3, Il1a*
mmu05133	Pertussis	*Tnf, Cxcl5, Calml3, Calm4, Il1b, Nos2, C2, Nlrp3, Itgam, Il1a*
mmu05143	African trypanosomiasis	*Icam1, Tnf, Ifng, Il1b, Hbb-B1, Fas, Ido1*
mmu05140	Leishmaniasis	*Tnf, Marcksl1, Ifng, Fcgr4, Tlr2, Il1b, Nos2, Itgam, Il1a*
mmu04610	Complement and coagulation cascades	*Plat, Cd55, F10, F13a1, F3, Serpine1, Cfh, C2, Plaur*
mmu05321	Inflammatory bowel disease (IBD)	*Nod2, Tnf, Il18rap, Ifng, Il4ra, Tlr2, Il1b, Il1a*
mmu05132	Salmonella infection	*Ccl3, Cxcl3, Cxcl2, Ifng, Il1b, Lbp, Nos2, Ccl4, Il1a*
mmu05146	Amoebiasis	*Il1r2, Arg1, Lama3, Tnf, Ifng, Tlr2, Il1b, Serpinb3a, Lamc2, Nos2, Itgam*
mmu04620	Toll-like receptor signalling pathway	*Ctsk, Ccl3, Tnf, Cxcl9, Tlr2, Il1b, Lbp, Ccl5, Ccl4, Spp1*
mmu05144	Malaria	*Icam1, Selp, Tnf, Ifng, Tlr2, Il1b, Hbb-B1*
mmu04630	Jak-STAT signalling pathway	*Osm, Lif, Il2ra, Osmr, Socs3, Socs1, Ifng, Il4ra, Pim1, Csf2rb, Csf3r, Thpo*
mmu05164	Influenza A	*Icam1, Tnf, Socs3, Oas3, Oas2, Il33, Ccl5, Nlrp3, Ifng, Il1b, Fas, Dnajb1, Il1a*
mmu04062	Chemokine signalling pathway	*Ccl3, Cxcl14, Cxcl5, Ppbp, Adcy8, Cxcl3, Cxcl16, Cxcl2, Cxcl9, Ccl8, Cxcr2, Ccl5, Ccl4, Ccl7*
mmu05134	Legionellosis	*Tnf, Cxcl3, Cxcl2, Tlr2, Il1b, Bnip3, Itgam*
mmu05202	Transcriptional misregulation in cancer	*Plat, Il1r2, Cebpb, Rel, Bcl2a1b, Mmp9, Igf1, Mmp3, Igfbp3, Runx2, Meis1, Itgam*
mmu05142	Chagas disease (American trypanosomiasis)	*Ccl3, Tnf, Serpine1, Ifng, Tlr2, Il1b, Nos2, Fas, Ccl5*
mmu04623	Cytosolic DNA-sensing pathway	*Tmem173, Ripk3, Il1b, Il33, Ccl5, Ccl4, Zbp1*

mmu04512	ECM-receptor interaction	*Cd47, Lama3, Gp1bb, Itgav, Itgb6, Itga2, Lamc2, Spp1*
mmu05168	Herpes simplex infection	*Ifit1, Tnf, Socs3, Tap1, Ifng, Oas3, Tlr2, Il1b, Oas2, Fas, Ccl5, H2-Q7, Pilra*
mmu05145	Toxoplasmosis	*Irgm1, Igtp, Lama3, Tnf, Socs1, Ifng, Tlr2, Lamc2, Nos2*
mmu05332	Graft-versus-host disease	*Tnf, Ifng, Il1b, Fas, H2-Q7, Il1a*
mmu04970	Salivary secretion	*Adrb2, Adcy8, Calml3, Bst1, Calm4, Trpv6, Dmbt1*
mmu04380	Osteoclast differentiation	*Tnfrsf11b, Ctsk, Tnf, Socs3, Socs1, Ifng, Fcgr4, Il1b, Il1a*
mmu04066	HIF-1 signalling pathway	*Pfkfb3, Hk3, Serpine1, Ifng, Hk2, Igf1, Nos2, Timp1*
mmu04650	Natural killer cell mediated cytotoxicity	*Icam1, Tnf, Rac3, Ifng, Zap70, Fcgr4, Fcer1g, Fas*
mmu05414	Dilated cardiomyopathy	*Tnf, Adcy8, Myl3, Itgav, Itgb6, Itga2, Igf1*
mmu04940	Type I diabetes mellitus	*Tnf, Ifng, Il1b, Fas, H2-Q7, Il1a*
mmu04514	Cell adhesion molecules (CAMs)	*Icam1, Selp, Cldn4, Itgav, Cd274, Cldn1, Cdh3, Cd6, H2-Q7, Itgam*
mmu04930	Type II diabetes mellitus	*Tnf, Socs3, Hk3, Socs1, Hk2*
mmu04145	Phagosome	*Mrc1, Olr1, Itgav, Tap1, Fcgr4, Tlr2, Itga2, Clec7a, H2-Q7, Itgam*
mmu04064	NF-kappa B signalling pathway	*Icam1, Tnf, Bcl2a1b, Zap70, Il1b, Lbp, Ccl4*
mmu05410	Hypertrophic cardiomyopathy (HCM)	*Tnf, Myl3, Itgav, Itgb6, Itga2, Igf1*
mmu04621	NOD-like receptor signalling pathway	*Nod2, Tnf, Il1b, Ccl5, Nlrp3*
mmu05162	Measles	*Il2ra, Ifng, Oas3, Tlr2, Il1b, Oas2, Fas, Il1a*
mmu04350	TGF-beta signalling pathway	*Inhba, Tnf, Fst, Ifng, Chrd, Bmp8b*
mmu04975	Fat digestion and absorption	*Abcg8, Abcg5, Pla2g2a, Pla2g2e*
mmu04014	Ras signalling pathway	*Pak6, Pld2, Rel, Rac3, Calml3, Pla2g2a, Zap70, Calm4, Pla1a, Igf1, Pla2g2e*

Analysed using DAVID.

Table S5 ***Enriched KEGG pathways identified in differentially expressed genes upregulated in Winnie-sham mice compared C57BL/6 mice (without genes)***

Ref	Term	Fold Enrichment	Count	*P* Value	Benjamini
mmu04145	Phagosome	3.17	55	5.55E-15	1.52E-12
mmu04060	Cytokine-cytokine receptor interaction	2.74	67	1.18E-14	1.61E-12
mmu05150	Staphylococcus aureus infection	5.41	27	7.18E-14	6.56E-12
mmu05416	Viral myocarditis	4.31	34	9.86E-14	6.75E-12
mmu04668	TNF signalling pathway	3.59	39	1.19E-12	6.55E-11
mmu05140	Leishmaniasis	4.54	29	1.91E-12	8.71E-11
mmu05164	Influenza A	2.93	50	3.03E-12	1.19E-10
mmu05168	Herpes simplex infection	2.60	54	5.58E-11	1.91E-09
mmu05332	Graft-versus-host disease	4.63	24	1.42E-10	4.32E-09
mmu04640	Hematopoietic cell lineage	3.70	31	1.48E-10	4.04E-09
mmu04514	Cell adhesion molecules (CAMs)	2.78	45	2.77E-10	6.91E-09
mmu04612	Antigen processing and presentation	3.67	30	3.93E-10	8.97E-09
mmu04062	Chemokine signalling pathway	2.56	50	6.20E-10	1.31E-08
mmu05134	Legionellosis	4.22	24	1.31E-09	2.57E-08
mmu05145	Toxoplasmosis	3.11	35	1.70E-09	3.11E-08
mmu05323	Rheumatoid arthritis	3.55	29	1.99E-09	3.41E-08
mmu05152	Tuberculosis	2.56	45	4.77E-09	7.68E-08
mmu05330	Allograft rejection	4.12	23	5.48E-09	8.34E-08
mmu04940	Type I diabetes mellitus	3.88	24	9.08E-09	1.31E-07
mmu04380	Osteoclast differentiation	2.86	36	1.01E-08	1.39E-07
mmu05162	Measles	2.73	37	2.50E-08	3.26E-07
mmu05340	Primary immunodeficiency	5.01	17	3.18E-08	3.96E-07
mmu05133	Pertussis	3.39	25	8.84E-08	1.05E-06
mmu05320	Autoimmune thyroid disease	3.25	23	7.43E-07	8.48E-06
mmu04660	T cell receptor signalling pathway	2.70	28	2.13E-06	2.33E-05
mmu05321	Inflammatory bowel disease (IBD)	3.40	20	2.21E-06	2.33E-05
mmu04650	Natural killer cell mediated cytotoxicity	2.67	28	2.60E-06	2.63E-05
mmu03050	Proteasome	3.79	17	3.25E-06	3.18E-05
mmu04630	Jak-STAT signalling pathway	2.35	34	3.94E-06	3.72E-05
mmu05166	HTLV-I infection	1.91	53	4.58E-06	4.18E-05
mmu04672	Intestinal immune network for IgA production	3.82	16	6.19E-06	5.47E-05
mmu04621	NOD-like receptor signalling pathway	3.22	18	1.83E-05	1.57E-04
mmu04064	NF-kappa B signalling pathway	2.58	25	1.88E-05	1.56E-04
mmu04620	Toll-like receptor signalling pathway	2.48	25	3.85E-05	3.10E-04
mmu04210	Apoptosis	3.01	18	4.93E-05	3.86E-04

mmu04666	Fc gamma R-mediated phagocytosis	2.63	22	5.25E-05	3.99E-04
mmu05132	Salmonella infection	2.70	21	5.34E-05	3.96E-04
mmu05142	Chagas disease (American trypanosomiasis)	2.43	25	5.41E-05	3.90E-04
mmu05161	Hepatitis B	2.13	31	8.47E-05	5.95E-04
mmu04662	B cell receptor signalling pathway	2.72	19	1.20E-04	8.24E-04
mmu04670	Leukocyte transendothelial migration	2.15	26	2.96E-04	1.98E-03
mmu05310	Asthma	4.18	10	3.03E-04	1.98E-03
mmu05222	Small cell lung cancer	2.39	20	4.75E-04	3.02E-03
mmu04141	Protein processing in endoplasmic reticulum	1.91	32	4.95E-04	3.08E-03
mmu05169	Epstein-Barr virus infection	1.77	38	6.08E-04	3.70E-03
mmu05203	Viral carcinogenesis	1.74	40	6.45E-04	3.84E-03
mmu04115	p53 signalling pathway	2.54	17	6.94E-04	4.04E-03
mmu00900	Terpenoid backbone biosynthesis	3.92	9	1.17E-03	6.68E-03
mmu03060	Protein export	3.46	10	1.47E-03	8.20E-03
mmu00100	Steroid biosynthesis	4.22	8	1.63E-03	8.91E-03
mmu05144	Malaria	2.72	13	2.08E-03	1.11E-02
mmu04664	Fc epsilon RI signalling pathway	2.36	16	2.37E-03	1.24E-02
mmu05160	Hepatitis C	1.84	25	3.78E-03	1.94E-02
mmu04810	Regulation of actin cytoskeleton	1.64	35	3.92E-03	1.97E-02
mmu05212	Pancreatic cancer	2.31	15	4.12E-03	2.04E-02
mmu04066	HIF-1 signalling pathway	1.93	20	6.44E-03	3.11E-02
mmu01130	Biosynthesis of antibiotics	1.59	34	7.05E-03	3.35E-02
mmu04610	Complement and coagulation cascades	2.11	16	7.17E-03	3.34E-02
mmu05146	Amoebiasis	1.80	21	1.11E-02	5.04E-02
mmu05211	Renal cell carcinoma	2.09	14	1.37E-02	6.09E-02
mmu04510	Focal adhesion	1.50	31	2.24E-02	9.67E-02
mmu04623	Cytosolic DNA-sensing pathway	2.04	13	2.25E-02	9.57E-02
mmu05202	Transcriptional misregulation in cancer	1.57	26	2.30E-02	9.61E-02
mmu05014	Amyotrophic lateral sclerosis (ALS)	2.16	11	2.68E-02	1.10E-01
mmu00565	Ether lipid metabolism	2.28	10	2.70E-02	1.09E-01
mmu04360	Axon guidance	1.63	21	2.98E-02	1.18E-01
mmu05322	Systemic lupus erythematosus	1.57	23	3.36E-02	1.30E-01
mmu04110	Cell cycle	1.62	20	3.73E-02	1.42E-01
mmu00480	Glutathione metabolism	2.01	11	4.28E-02	1.60E-01
mmu04151	PI3K-Akt signalling pathway	1.31	46	4.43E-02	1.62E-01
mmu05200	Pathways in cancer	1.29	51	4.61E-02	1.67E-01
mmu04978	Mineral absorption	2.20	9	4.63E-02	1.65E-01
mmu00051	Fructose and mannose metabolism	2.36	8	4.69E-02	1.65E-01
mmu05230	Central carbon metabolism in cancer	1.88	12	4.97E-02	1.72E-01
mmu00520	Amino sugar and nucleotide sugar metabolism	2.05	10	5.03E-02	1.72E-01
mmu04014	Ras signalling pathway	1.36	31	7.09E-02	2.33E-01

mmu00030	Pentose phosphate pathway	2.34	7	7.17E-02	2.33E-01
mmu04975	Fat digestion and absorption	2.11	8	7.81E-02	2.49E-01
mmu00564	Glycerophospholipid metabolism	1.60	15	8.12E-02	2.55E-01
mmu04512	ECM-receptor interaction	1.60	14	9.52E-02	2.90E-01
mmu05215	Prostate cancer	1.60	14	9.52E-02	2.90E-01
mmu04920	Adipocytokine signalling pathway	1.67	12	9.88E-02	2.97E-01
mmu05210	Colorectal cancer	1.72	11	9.99E-02	2.97E-01

Analysed using DAVID.

Table S6 ***Enriched KEGG pathways identified in differentially expressed genes upregulated in Winnie-sham mice compared C57BL/6 mice (genes)***

Ref	Term	Genes
mmu04145	Phagosome	*Msr1, Tlr2, H2-D1, Tlr4, C1ra, Tuba1c, H2-K1, Dync1i1, Ncf2, Ncf1, Ncf4, H2-Dmb1, Sec61b, H2-Oa, H2-Aa, Tuba4a, Sec61g, C3, Itgb2, Atp6v1g1, Calr, Itgam, Stx18, Tap2, Itgav, Tap1, Rac1, H2-T10, Sec61a1, Tubb4b, Actb, H2-Q10, H2-M3, H2-M2, Nox1, Fcgr4, Itga2, H2-Ab1, H2-Q6, H2-Q7, Fcgr1, Fcgr3, Cyba, Coro1a, Cybb, Fcgr2b, Tfrc, H2-Eb1, Atp6v0a1, H2-T22, H2-T23, Clec7a, H2-T24, H2-Dma, Cd14*
mmu04060	Cytokine-cytokine receptor interaction	*Osmr, Il21r, Cxcr2, Tnfsf13, Cxcl10, Il11, Tnfrsf11b, Cxcr4, Cxcr6, Csf2rb, Csf3r, Il1b, Fas, Il13ra1, Ltb, Il1a, Egfr, Il18rap, Tnfrsf14, Cd40, Ccr9, Osm, Tnfrsf9, Ccr7, Tnfsf13b, Ppbp, Ccr5, Ccr4, Ccr2, Il1r2, Tnf, Ccl2, Csf2rb2, Tnfrsf12a, Crlf2, Ccr1, Il4ra, Cxcl9, Ccl8, Tnfrsf8, Il7r, Ccl5, Tnfrsf4, Ccl7, Lif, Tnfrsf1a, Tnfrsf1b, Il12rb1, Ccl20, Il10ra, Tnfrsf18, Il2rg, Cd27, Csf1r, Thpo, Il18r1, Il2rb, Il2ra, Met, Hgf, Tnfsf8, Tnfsf10, Cxcl14, Cxcl13, Cxcl16, Il5ra, Il3ra*
mmu05150	Staphylococcus aureus infection	*C3ar1, Itgal, C3, Itgb2, Itgam, C1ra, Cfh, C2, Selplg, Icam1, Selp, C5ar1, C4b, Cfb, Fcgr4, H2-Dmb1, H2-Ab1, Fcgr1, Fcgr3, C1qa, C1qb, H2-Oa, Fcgr2b, H2-Eb1, H2-Aa, H2-Dma, Ptafr*
mmu05416	Viral myocarditis	*Itgal, H2-D1, Itgb2, Casp3, Rac2, Rac3, Casp8, Rac1, H2-T10, Cd28, H2-K1, Actb, Icam1, H2-Q10, H2-M3, H2-M2, Cycs, H2-Dmb1, H2-Ab1, Cd40, H2-Q6, H2-Q7, Ccnd1, Cd55, Cd86, Cd80, H2-Oa, H2-Eb1, H2-Aa, H2-T22, H2-T23, H2-T24, H2-Dma, Abl2*
mmu04668	TNF signalling pathway	*Cxcl1, Tnf, Ccl2, Ptgs2, Mmp9, Cxcl3, Cxcl2, Nfkbia, Gm5431, Ccl5, Mmp3, Cxcl10, Lif, Tnfrsf1a, Tnfrsf1b, Nod2, Casp3, Ccl20, Casp7, Casp8, Il1b, Bcl3, Pik3r5, Mlkl, Creb3l3, Fas, Akt3, Il18r1, Icam1, Cebpb, Creb3, Socs3, Map2k3, Pik3cd, Ifi47, Junb, Rps6ka4, Ripk3, Tnfaip3*
mmu05140	Leishmaniasis	*Tnf, Ptgs2, Marcksl1, C3, Nfkbib, Tlr2, Nfkbia, Tlr4, Itgb2, Itgam, Myd88, Il1b, Nos2, Il1a, Ncf2, Ncf1, Ncf4, Fcgr4, H2-Dmb1, H2-Ab1, Stat1, Fcgr1, Fcgr3, Cyba, H2-Oa, H2-Eb1, H2-Aa, Jak2, H2-Dma*
mmu05164	Influenza A	*Ifih1, Tnf, Ccl2, Agfg1, Nfkbib, Oas3, Nfkbia, Tlr3, Rsad2, Tlr4, Oas2, Ccl5, Cxcl10, Tnfrsf1a, Myd88, Pycard, Il1b, Pik3r5, Fas, Casp1, Dnajc3, Mx2, Akt3, Il1a, Actb, Ciita, Icam1, Socs3, Map2k3, Cycs, Pik3cd, Fdps, H2-Dmb1, H2-Ab1, Stat1, Nlrp3, Furin, Stat2, Irf9, Tnfsf10, H2-Oa, Irf7, H2-Eb1, H2-Aa, Jak2, Dnajb1, Oas1a, H2-Dma, Eif2ak2, Oas1g*
mmu05168	Herpes simplex infection	*H2-D1, Tlr2, Tlr3, Casp3, Myd88, Casp8, Il1b, Fas, Pilra, H2-K1, Cdk1, Sp100, Socs3, Taf4b, Cycs, H2-Dmb1, Tnfrsf14, H2-Oa, H2-Aa, Oas1a, Eif2ak2, Oas1g, Ifih1, Ccl2, Tnf, C3, Nfkbib, Oas3, Nfkbia, Oas2, Ccl5, Cd74, Tnfrsf1a, Tap2, Tap1, H2-T10, H2-Q10, H2-M3, H2-M2, Alyref, H2-Ab1, Stat1, H2-Q6, H2-Q7, Stat2, Irf9, Ifit1, Irf7, H2-Eb1, H2-T22, H2-T23, Jak2, H2-T24, H2-Dma*
mmu05332	Graft-versus-host disease	*H2-K1, H2-Q10, Tnf, H2-M3, H2-M2, H2-D1, H2-Dmb1, H2-Ab1, H2-Q6, H2-Q7, Cd86, Cd80, H2-Oa, H2-Eb1, Il1b, H2-Aa, H2-T22, H2-T23, H2-T10, H2-T24, Fas, H2-Dma, Il1a, Cd28*
mmu04640	Hematopoietic cell lineage	*Il1r2, Tnf, Cd8a, Il4ra, Il7r, Itgam, Il11, Cd44, Gp1bb, Cd2, Il1b, Csf3r, Cd4, Cd5, Il1a, Csf1r, Thpo, Cd3g, Il2ra, Cd3d, Cd3e, Itga2, Itga3, Fcgr1, Cd55, Itga6, Tfrc, H2-Eb1, Il5ra, Cd14, Il3ra*
mmu04514	Cell adhesion molecules (CAMs)	*Itgal, Cldn7, Cldn4, Cd8a, H2-D1, Itgb2, Cldn14, Itgam, Itgb7, Itgav, Icos, Cd2, Cd4, H2-T10, Cd6, Selplg, Spn, Cd28, H2-K1, Ptprc, Icam1, Selp, H2-Q10, H2-M3, H2-M2, Sell, Ctla4, H2-Dmb1, H2-Ab1, Cd40, H2-Q6, H2-Q7, Cldn23, Cd86, Cd80, H2-Oa, Itga6, H2-Eb1, Cd274, H2-T22, H2-Aa, H2-T23, H2-T24, H2-Dma, Cd226*
mmu04612	Antigen processing and presentation	*Tnf, Pdia3, Cd8a, H2-D1, Calr, Cd74, Tapbp, B2m, Tap2, Tap1, Cd4, H2-T10, Ciita, H2-K1, H2-Q10, H2-M3, H2-M2, H2-Dmb1, H2-Ab1, H2-Q6, H2-Q7, Psme1, H2-Oa, Psme2, H2-Eb1, H2-Aa, H2-T22, H2-T23, H2-T24, H2-Dma*
mmu04062	Chemokine signalling pathway	*Cxcl1, Ccl2, Cxcl5, Fgr, Adcy8, Prex1, Cxcl3, Nfkbib, Ccr1, Cxcl2, Ccl9, Cxcl9, Ccl8, Nfkbia, Cxcr2, Ccl5, Ccl7, Cxcl10, Ccl22, Dock2, Rac2, Ccl20, Cxcr4, Rac1, Cxcr6, Pik3r5, Pak1, Akt3, Lyn, Rock2, Ncf1, Hck, Pik3cd, Stat1, Vav1, Ccl17, Stat2, Ccr9, Nras, Ccr7, Cxcl14, Ccr5, Ppbp, Ccr4, Cxcl13, Cxcl16, Ccr2, Rap1b, Jak2, Jak3*
mmu05134	Legionellosis	*Cxcl1, Tnf, C3, Cxcl3, Cxcl2, Cycs, Tlr2, Nfkbia, Bnip3, Tlr4, Itgb2, Itgam, Nlrc4, Casp3, Myd88, Arf1, Naip2, Casp7, Casp8, Pycard, Il1b, Apaf1, Casp1, Cd14*
mmu05145	Toxoplasmosis	*Tnf, Nfkbib, Tlr2, Nfkbia, Tlr4, Bcl2l1, Tnfrsf1a, Casp3, Lamb3, Myd88, Igtp, Il10ra, Casp8, Pik3r5, Nos2, Akt3, Ciita, Irgm1, Map2k3, Socs1, Cycs, Pik3cd, H2-Dmb1, H2-Ab1, Cd40, Stat1, Lama3, H2-Oa, Itga6, Ccr5, H2-Eb1, H2-Aa, Lamc2, Jak2, H2-Dma*

mmu05323	Rheumatoid arthritis	*Itgal, Tnf, Ccl2, Cxcl5, Tlr2, Tnfsf13, Tlr4, Itgb2, Atp6v1g1, Ccl5, Mmp3, Il11, Ccl20, Il1b, Ltb, Il1a, Cd28, Icam1, Ctla4, H2-Dmb1, H2-Ab1, Cd86, Tnfsf13b, Cd80, H2-Oa, H2-Eb1, H2-Aa, Atp6v0a1, H2-Dma*
mmu05152	Tuberculosis	*Tnf, C3, Tirap, Tlr2, Tlr4, Itgb2, Cd74, Itgam, Tnfrsf1a, Casp3, Nod2, Myd88, Clec4e, Itgax, Il10ra, Casp8, Il1b, Fcer1g, Ppp3cc, Lbp, Nos2, Il1a, Akt3, Syk, Ciita, Cebpb, Card9, Cycs, Fcgr4, H2-Dmb1, H2-Ab1, Stat1, Fcgr1, Fcgr3, Coro1a, Fcgr2b, H2-Oa, H2-Eb1, Atp6v0a1, H2-Aa, Jak2, Apaf1, Clec7a, H2-Dma, Cd14*
mmu05330	Allograft rejection	*H2-K1, H2-Q10, Tnf, H2-M3, H2-M2, H2-D1, H2-Dmb1, H2-Ab1, Cd40, H2-Q6, H2-Q7, Cd86, Cd80, H2-Oa, H2-Eb1, H2-Aa, H2-T22, H2-T23, H2-T10, H2-T24, Fas, H2-Dma, Cd28*
mmu04940	Type I diabetes mellitus	*H2-K1, H2-Q10, Tnf, H2-M3, H2-M2, H2-D1, H2-Dmb1, H2-Ab1, H2-Q6, H2-Q7, Cd86, Cd80, H2-Oa, H2-Eb1, Il1b, H2-Aa, H2-T22, H2-T23, H2-T10, H2-T24, Fas, H2-Dma, Il1a, Cd28*
mmu04380	Osteoclast differentiation	*Tnf, Pparg, Nfkbia, Btk, Tnfrsf1a, Tnfrsf11b, Rac1, Il1b, Ppp3cc, Pik3r5, Akt3, Il1a, Csf1r, Tec, Syk, Tyrobp, Ncf2, Ncf1, Socs3, Ncf4, Nox1, Pik3cd, Socs1, Fcgr4, Stat1, Fcgr1, Sirpa, Junb, Fcgr3, Stat2, Irf9, Cyba, Cybb, Fcgr2b, Lck, Lcp2*
mmu05162	Measles	*Ifih1, Nfkbib, Oas3, Tlr2, Nfkbia, Tlr4, Oas2, Ccne1, Myd88, Il1b, Il2rg, Pik3r5, Fas, Mx2, Akt3, Il1a, Cd28, Il2rb, Cd3g, Il2ra, Cd3d, Cd3e, Pik3cd, Stat1, Slamf1, Stat2, Irf9, Ccnd1, Tnfsf10, Fcgr2b, Irf7, Jak2, Oas1a, Jak3, Eif2ak2, Tnfaip3, Oas1g*
mmu05340	Primary immunodeficiency	*Ciita, Ptprc, Cd3d, Cd8a, Cd3e, Cd40, Il7r, Ada, Btk, Tap2, Icos, Tap1, Lck, Zap70, Il2rg, Cd4, Cd79a*
mmu05133	Pertussis	*Tnf, Cxcl5, C4b, C3, Tirap, Tlr4, Itgb2, Nlrp3, Itgam, C1qa, C1ra, C1qb, Casp3, Myd88, Casp7, Irf8, Cfl1, Pycard, Irf1, Il1b, Nos2, C2, Casp1, Cd14, Il1a*
mmu05320	Autoimmune thyroid disease	*H2-K1, H2-Q10, H2-M3, H2-M2, Ctla4, H2-D1, H2-Dmb1, H2-Ab1, Cd40, H2-Q6, H2-Q7, Cd86, Cd80, H2-Oa, H2-Eb1, H2-Aa, H2-T22, H2-T23, H2-T10, H2-T24, Fas, H2-Dma, Cd28*
mmu04660	T cell receptor signalling pathway	*Tnf, Cd8a, Nfkbie, Nfkbib, Cd247, Nfkbia, Pak6, Icos, Rasgrp1, Zap70, Ppp3cc, Pik3r5, Cd4, Pak1, Akt3, Tec, Cd28, Ptprc, Cd3g, Cd3d, Cd3e, Pik3cd, Ctla4, Vav1, Nras, Lat, Lck, Lcp2*
mmu05321	Inflammatory bowel disease (IBD)	*Il18r1, Tnf, Il18rap, Il4ra, Il21r, Tlr2, H2-Dmb1, Tlr4, H2-Ab1, Stat1, Stat4, Nod2, Il12rb1, H2-Oa, H2-Eb1, Il1b, H2-Aa, Il2rg, H2-Dma, Il1a*
mmu04650	Natural killer cell mediated cytotoxicity	*Itgal, Tnf, Cd247, Klrk1, Itgb2, Cd48, Casp3, Rac2, Rac3, Rac1, Zap70, Ppp3cc, Fcer1g, Pik3r5, Pak1, Fas, Syk, Tyrobp, Icam1, Pik3cd, Fcgr4, Vav1, Nras, Lat, Tnfsf10, Lck, Sh3bp2, Lcp2*
mmu03050	Proteasome	*Psmb10, Shfm1, Psma7, Psmb8, Psmb9, Psma2, Psmb4, Psma1, Psmd14, Psme1, Psma5, Psme2, Psma4, Psmb3, Psma3, Psmb2, Pomp*
mmu04630	Jak-STAT signalling pathway	*Csf2rb2, Osmr, Crlf2, Il21r, Il4ra, Bcl2l1, Il7r, Il11, Lif, Stat4, Il12rb1, Il10ra, Csf2rb, Csf3r, Il2rg, Pik3r5, Il13ra1, Akt3, Thpo, Il2rb, Il2ra, Socs3, Pik3cd, Socs1, Pim1, Stat1, Stat2, Irf9, Osm, Ccnd1, Jak2, Il5ra, Jak3, Il3ra*
mmu05166	HTLV-I infection	*E2f2, Tspo, Adcy8, H2-D1, Slc2a1, Ranbp1, Akt3, H2-K1, Icam1, Cd3g, Cd3d, Cd3e, Pik3cd, H2-Dmb1, Cd40, Ccnd1, Mad2l1, H2-Oa, Lck, H2-Aa, Itgal, Il1r2, Tnf, Crem, Nfkbia, Itgb2, Bcl2l1, Calr, Mybl2, Tnfrsf1a, Xbp1, Ppp3cc, Il2rg, Pik3r5, H2-T10, Il2rb, H2-Q10, Il2ra, H2-M3, H2-M2, Fdps, H2-Ab1, H2-Q6, Vdac2, H2-Q7, Nras, H2-Eb1, Pcna, H2-T22, H2-T23, H2-T24, Jak3, H2-Dma*
mmu04672	Intestinal immune network for IgA production	*H2-Dmb1, Tnfsf13, H2-Ab1, Cd40, Ccr9, Cd86, Tnfsf13b, Cd80, H2-Oa, Cxcr4, Itgb7, Icos, H2-Eb1, H2-Aa, H2-Dma, Cd28*
mmu04621	NOD-like receptor signalling pathway	*Card9, Ccl2, Tnf, Nfkbib, Nfkbia, Ccl5, Nlrp3, Hsp90b1, Nod2, Nlrc4, Mefv, Naip2, Casp8, Pstpip1, Pycard, Il1b, Tnfaip3, Casp1*
mmu04064	NF-kappa B signalling pathway	*Icam1, Tnf, Ptgs2, Lyn, Tirap, Nfkbia, Tlr4, Bcl2l1, Cd40, Btk, Lat, Tnfrsf1a, Bcl2a1d, Myd88, Tnfsf13b, Bcl2a1b, Bcl2a1a, Lck, Zap70, Il1b, Lbp, Tnfaip3, Ltb, Cd14, Syk*
mmu04620	Toll-like receptor signalling pathway	*Tnf, Tirap, Cxcl9, Tlr2, Tlr3, Nfkbia, Tlr4, Ccl5, Cxcl10, Myd88, Rac1, Casp8, Il1b, Pik3r5, Lbp, Akt3, Spp1, Map2k3, Pik3cd, Cd40, Stat1, Cd86, Cd80, Irf7, Cd14*
mmu04210	Apoptosis	*Tnf, Csf2rb2, Cycs, Pik3cd, Nfkbia, Bcl2l1, Capn2, Tnfrsf1a, Tnfsf10, Casp3, Casp7, Casp8, Csf2rb, Pik3r5, Apaf1, Fas, Akt3, Il3ra*
mmu04666	Fc gamma R-mediated phagocytosis	*Ptprc, Lyn, Ncf1, Marcksl1, Hck, Pik3cd, Arf6, Arpc5, Vav1, Fcgr1, Arpc1b, Lat, Dock2, Arpc3, Fcgr2b, Rac2, Rac1, Cfl1, Pik3r5, Pak1, Akt3, Syk*
mmu05132	Salmonella infection	*Dync1i1, Cxcl1, Actb, Rock2, Cxcl3, Cxcl2, Tlr4, Arpc5, Flnb, Arpc1b, Nlrc4, Myd88, Arpc3, Rac1, Pycard, Il1b, Lbp, Nos2, Casp1, Cd14, Il1a*
mmu05142	Chagas disease (American trypanosomiasis)	*Gna14, Ccl2, Tnf, C3, Cd247, Tlr2, Nfkbia, Tlr4, Calr, Ccl5, Tnfrsf1a, Myd88, Serpine1, Casp8, Il1b, Pik3r5, Nos2, Fas, Akt3, Cd3g, Cd3d, Cd3e, Pik3cd, C1qa, C1qb*
mmu05161	Hepatitis B	*E2f2, Ywhaz, Ifih1, Tnf, Mmp9, Tirap, Tlr2, Tlr3, Nfkbia, Tlr4, Ccne1, Stat4, Casp3, Myd88, Casp8, Pik3r5, Creb3l3, Fas, Ccna2, Akt3, Creb3, Cycs, Pik3cd, Birc5, Stat1, Stat2, Nras, Ccnd1, Irf7, Pcna, Apaf1*

mmu04662	B cell receptor signalling pathway	*Lyn, Nfkbie, Nfkbib, Pik3cd, Nfkbia, Cd72, Vav1, Btk, Nras, Fcgr2b, Rac2, Rac3, Rac1, Ppp3cc, Cd79b, Pik3r5, Cd79a, Akt3, Syk*
mmu04670	Leukocyte transendothelial migration	*Itgal, Cldn7, Myl7, Cldn4, Mmp9, Itgb2, Cldn14, Itgam, Rac2, Cxcr4, Rac1, Pik3r5, Rhoh, Actb, Icam1, Ncf2, Rock2, Ncf1, Ncf4, Nox1, Pik3cd, Vav1, Cldn23, Cyba, Cybb, Rap1b*
mmu05310	Asthma	*Tnf, H2-Oa, Prg2, H2-Eb1, H2-Dmb1, Fcer1g, H2-Aa, H2-Ab1, Cd40, H2-Dma*
mmu05222	Small cell lung cancer	*E2f2, Cks1b, Ptgs2, Cycs, Pik3cd, Nfkbia, Itga2, Itga3, Bcl2l1, Ccne1, Ccnd1, Lamb3, Lama3, Itga6, Itgav, Pik3r5, Lamc2, Apaf1, Nos2, Akt3*
mmu04141	Protein processing in endoplasmic reticulum	*Pdia3, Dnajc10, Pdia6, Pdia4, Calr, Derl3, Bak1, Dnajb11, Xbp1, Fbxo6, Rpn1, Ero1l, Hspa5, Dnajc3, Tram1, Sec61a1, P4hb, Herpud1, Rrbp1, Ckap4, Capn2, Hyou1, Hsp90b1, Sec61b, Hspa4l, Dnajb1, Ssr4, Eif2ak2, Ssr2, Sec61g, Sec23b, Ssr3*
mmu05169	Epstein-Barr virus infection	*Itgal, Ywhaz, Fgr, Nfkbie, Nfkbib, Shfm1, H2-D1, Nfkbia, Polr2d, Cd44, Il10ra, H2-T10, Pik3r5, Ccna2, Spn, Akt3, Syk, H2-K1, Icam1, Cdk1, H2-Q10, Lyn, H2-M3, H2-M2, Map2k3, Pik3cd, Cd40, H2-Q6, H2-Q7, Cd38, Psmd14, Ywhah, H2-T22, H2-T23, Jak3, H2-T24, Eif2ak2, Tnfaip3*
mmu05203	Viral carcinogenesis	*Ywhaz, C3, H2-D1, Nfkbia, Pmaip1, Ccne1, Bak1, Casp3, Rel, Casp8, Rac1, H2-T10, Pik3r5, Ranbp1, Creb3l3, Ccna2, Syk, H2-K1, Cdk1, H2-Q10, Sp100, Creb3, Lyn, H2-M3, H2-M2, Pik3cd, H2-Q6, H2-Q7, Irf9, Nras, Ccnd1, Ywhah, Ccr5, Ccr4, Irf7, H2-T22, H2-T23, Jak3, H2-T24, Eif2ak2*
mmu04115	p53 signalling pathway	*Cdk1, Cycs, Sfn, Pmaip1, Gtse1, Ccnb1, Ccne1, Casp3, Ccnd1, Ccnb2, Serpinb5, Rrm2, Serpine1, Casp8, Apaf1, Fas, Gadd45a*
mmu00900	Terpenoid backbone biosynthesis	*Nus1, Mvd, Hmgcr, Fdps, Hmgcs1, Acat2, Idi1, Pmvk, Pdss1*
mmu03060	Protein export	*Sec61b, Sec11c, Spcs3, Spcs1, Spcs2, Hspa5, Srp19, Srp9, Sec61a1, Sec61g*
mmu00100	Steroid biosynthesis	*Cyp51, Soat2, Sc5d, Sqle, Lss, Hsd17b7, Nsdhl, Fdft1*
mmu05144	Malaria	*Selp, Icam1, Itgal, Tnf, Ccl2, Met, Tlr2, Itgb2, Tlr4, Hgf, Cd40, Myd88, Il1b*
mmu04664	Fc epsilon RI signalling pathway	*Tnf, Lyn, Map2k3, Pik3cd, Vav1, Btk, Nras, Lat, Rac2, Rac3, Rac1, Fcer1g, Pik3r5, Akt3, Syk, Lcp2*
mmu05160	Hepatitis C	*Egfr, Cldn7, Tnf, Cldn4, Socs3, Pik3cd, Oas3, Nfkbia, Tlr3, Oas2, Stat1, Cldn14, Cldn23, Stat2, Irf9, Nras, Tnfrsf1a, Ifit1, Irf7, Irf1, Pik3r5, Oas1a, Eif2ak2, Oas1g, Akt3*
mmu04810	Regulation of actin cytoskeleton	*Myl7, Itgal, Ssh1, Itgae, Ssh2, Iqgap2, Bdkrb1, Itgb2, Arpc5, Itgam, Pak6, Rac2, Arpc3, Itgax, Rac3, Itgav, Itgb7, Rac1, Itgb6, Pik3r5, Pak1, Fgd3, Egfr, Actb, Rock2, Pik3cd, Nckap1l, Itga2, Itga3, Vav1, Nras, Arpc1b, Itga6, Cfl1, Cd14*
mmu05212	Pancreatic cancer	*Egfr, E2f2, Ccnd1, Rac2, Rac3, Pik3cd, Rac1, Ralb, Rala, Tgfa, Pik3r5, Bcl2l1, Stat1, Akt3, Rad51*
mmu04066	HIF-1 signalling pathway	*Egfr, Pfkfb3, Pik3cd, Nox1, Hk2, Egln3, Tlr4, Trf, Timp1, Cybb, Eif4ebp1, Hif1a, Tfrc, Hk3, Serpine1, Slc2a1, Pik3r5, Nos2, Akt3, Eno1*
mmu01130	Biosynthesis of antibiotics	*Cyp51, Sc5d, Mvd, Hmgcr, Pgd, Hmgcs1, Hk2, Lss, Acat2, Psph, Fdft1, Arg1, Arg2, Hk3, Idh1, Rpia, Hsd17b7, Eno1, Nsdhl, Fdps, Bpgm, Ak4, Tat, Nme6, Rpe, Nme1, Sqle, Pgm1, Phgdh, Pla2g7, Idi1, Pgk1, Psat1, Prps1*
mmu04610	Complement and coagulation cascades	*Plat, C3ar1, C5ar1, Cfb, C3, C4b, Bdkrb1, Plaur, C1qa, C1ra, C1qb, Cd55, F3, Serpine1, Cfh, C2*
mmu05146	Amoebiasis	*Il1r2, Gna14, Tnf, Pik3cd, Tlr2, Serpinb1a, Tlr4, Itgb2, Itgam, Arg1, Serpinb9, Casp3, Lamb3, Lama3, Serpinb6b, Arg2, Il1b, Pik3r5, Lamc2, Nos2, Cd14*
mmu05211	Renal cell carcinoma	*Pik3cd, Met, Egln3, Hgf, Pak6, Nras, Hif1a, Rac1, Slc2a1, Tgfa, Rap1b, Pik3r5, Pak1, Akt3*
mmu04510	Focal adhesion	*Myl7, Pak6, Lamb3, Rac2, Col6a5, Rac3, Itgav, Itgb7, Rac1, Itgb6, Pik3r5, Pak1, Akt3, Spp1, Parvg, Actb, Egfr, Rock2, Met, Pik3cd, Itga2, Itga3, Hgf, Capn2, Flnb, Vav1, Ccnd1, Lama3, Itga6, Lamc2, Rap1b*
mmu04623	Cytosolic DNA-sensing pathway	*Nfkbib, Trex1, Nfkbia, Ccl5, Cxcl10, Ifi202b, Tmem173, Irf7, Pycard, Ripk3, Il1b, Casp1, Zbp1*
mmu05202	Transcriptional misregulation in cancer	*Slc45a3, Il1r2, Mmp9, Pparg, Bcl2l1, Mmp3, Itgam, Rel, Itgb7, Runx2, Csf1r, Plat, Nfkbiz, Il2rb, Cebpb, Met, Cd40, Fcgr1, Prom1, Ccr7, Cd86, Bcl2a1d, Bcl2a1b, Nupr1, Bcl2a1a, Cd14*
mmu05014	Amyotrophic lateral sclerosis (ALS)	*Tnfrsf1a, Casp3, Tnfrsf1b, Tnf, Map2k3, Rac1, Cycs, Ppp3cc, Bcl2l1, Apaf1, Casp1*
mmu00565	Ether lipid metabolism	*Pla2g16, Agps, Pla2g2a, Pla2g7, Ept1, Lpcat2, Pla2g2e, Pla2g2d, Lpcat4, Pla2g5*
mmu04360	Axon guidance	*Plxnc1, Plxna2, Rock2, Met, Fes, Epha2, Ephb2, Pak6, Nras, Ephb6, Sema6b, Rnd1, Rac2, Cxcr4, Rac3, Sema7a, Rac1, Cfl1, Ppp3cc, Robo2, Pak1*

mmu05322	Systemic lupus erythematosus	*Tnf, C4b, C3, Fcgr4, Snrpd1, H2-Dmb1, H2-Ab1, Cd40, Fcgr1, Trim21, C1qa, C1ra, C1qb, Cd86, Cd80, H2-Oa, H2-Eb1, H2afz, H2-Aa, H2afx, C2, H2-Dma, Cd28*
mmu04110	Cell cycle	*Cdc7, Cdk1, E2f2, Ywhaz, Dbf4, Ttk, Sfn, Mcm3, Ccnb1, Ccne1, Ccnd1, Cdc45, Mad2l1, Ccnb2, Ywhah, Pcna, Bub1, Orc6, Ccna2, Gadd45a*
mmu00480	Glutathione metabolism	*Gsta1, Lap3, Gpx2, Gsr, Srm, Rrm2, Pgd, Idh1, Ggt1, Mgst1, Mgst2*
mmu04151	PI3K-Akt signalling pathway	*Ywhaz, Osmr, Il4ra, Tlr2, Tlr4, Bcl2l1, Il7r, Ccne1, Eif4ebp1, Lamb3, Col6a5, Itgb7, Itgav, Rac1, Itgb6, Csf3r, Il2rg, Pik3r5, Creb3l3, Akt3, Csf1r, Spp1, Syk, Egfr, Il2rb, Il2ra, Sgk2, Creb3, Met, Pik3cd, Itga2, Itga3, Hgf, Epha2, Ddit4, Osm, Nras, Ccnd1, Hsp90b1, Ywhah, Lama3, Itga6, Lamc2, Jak2, Jak3, Il3ra*
mmu05200	Pathways in cancer	*Cks1b, E2f2, Ptgs2, Adcy8, Mmp9, Pparg, Egln3, Nfkbia, Bdkrb1, Bcl2l1, Tpm3, Ccne1, Casp3, Lamb3, Rac2, Rac3, Cxcr4, Rasgrp1, Itgav, Casp8, Rac1, Slc2a1, Ralb, Rala, Csf3r, Tgfa, Pik3r5, Nos2, Fas, Akt3, Csf1r, Egfr, Rock2, Met, Cycs, Pik3cd, Itga2, Birc5, Itga3, Hgf, Stat1, Dapk2, Appl1, Rad51, Nras, Ccnd1, Hsp90b1, Lama3, Hif1a, Itga6, Lamc2*
mmu04978	Mineral absorption	*Slc11a1, Slc9a3, Hmox1, Heph, Trpv6, Slc39a4, Steap2, Steap1, Trf*
mmu00051	Fructose and mannose metabolism	*Gmppb, Mpi, Gmds, Pfkfb3, Hk3, Pfkfb1, Hk2, Pmm2*
mmu05230	Central carbon metabolism in cancer	*Egfr, Slc16a3, Nras, Hif1a, Hk3, Slc2a1, Met, Pik3cd, Hk2, Pik3r5, Slc7a5, Akt3*
mmu00520	Amino sugar and nucleotide sugar metabolism	*Gmppb, Mpi, Gmds, Cmas, Hk3, Pgm1, Cmah, Hk2, Gale, Pmm2*
mmu04014	Ras signalling pathway	*Arf6, Bcl2l1, Pak6, Rel, Rac2, Rac3, Rasgrp1, Rac1, Zap70, Ralb, Rala, Pla1a, Pik3r5, Pak1, Akt3, Csf1r, Egfr, Pla2g16, Pik3cd, Met, Hgf, Epha2, Nras, Lat, Htr7, Pla2g2a, Rap1b, Pla2g2e, Pla2g2d, Abl2, Pla2g5*
mmu00030	Pentose phosphate pathway	*Rpe, H6pd, Pgd, Pgm1, Dera, Rpia, Prps1*
mmu04975	Fat digestion and absorption	*Apob, Dgat2, Pla2g2a, Fabp2, Pla2g2e, Pla2g2d, Agpat2, Pla2g5*
mmu00564	Glycerophospholipid metabolism	*Gpd2, Pla2g16, Pgs1, Lpgat1, Ept1, Lpin2, Lpcat2, Lpcat4, Agpat9, Pla2g2a, Pemt, Pla2g2e, Pla2g2d, Agpat2, Pla2g5*
mmu04512	ECM-receptor interaction	*Itga2, Itga3, Cd47, Lamb3, Lama3, Cd44, Itga6, Gp1bb, Col6a5, Itgav, Itgb7, Itgb6, Lamc2, Spp1*
mmu05215	Prostate cancer	*Egfr, E2f2, Creb3, Pik3cd, Nfkbia, Nras, Ccne1, Hsp90b1, Ccnd1, Tgfa, Pik3r5, Srd5a2, Creb3l3, Akt3*
mmu04920	Adipocytokine signalling pathway	*Tnfrsf1a, Tnfrsf1b, Tnf, Nfkbie, Socs3, Nfkbib, Slc2a1, Nfkbia, Jak2, Akt3, Acsl5, Acsbg1*
mmu05210	Colorectal cancer	*Casp3, Ccnd1, Rac2, Rac3, Pik3cd, Rac1, Cycs, Pik3r5, Birc5, Appl1, Akt3*

Analysed using DAVID.

Table S7 *Functional cluster analysis of ENS and neurotransmitter receptor genes: Cholinergic terms*

Cluster #	Term	Fold Enrichment	*P*-value	Genes
***Winnie*+MSC vs *Winnie*-sham upregulated**				
C2	IPR027361:Nicotinic acetylcholine-gated receptor, transmembrane domain	121.71	6.51E-08	Chrna9, Chrnb4, Htr3a, Chrna1, Chrna3
C2	IPR002394:Nicotinic acetylcholine receptor	109.54	5.72E-06	Chrna9, Chrnb4, Chrna1, Chrna3
C2	GO:0004889~acetylcholine-activated cation-selective channel activity	103.11	1.26E-07	Chrna9, Chrnb4, Htr3a, Chrna1, Chrna3
C2	GO:0042166~acetylcholine binding	97.68	1.59E-07	Chrna9, Chrnb4, Slc18a3, Chrna1, Chrna3
C2	GO:0015464~acetylcholine receptor activity	92.80	1.99E-07	Chrna9, Chrnb4, Htr3a, Chrna1, Chrna3
C2	GO:0005892~acetylcholine-gated channel complex	102.81	6.96E-06	Chrna9, Chrnb4, Chrna1, Chrna3
C2	GO:0007271~synaptic transmission, cholinergic	52.41	5.58E-05	Chrna9, Chrnb4, Chrna1, Chrna3
***Winnie*-sham vs C57BL/6 downregulated**				
C3	GO:0042166~acetylcholine binding	88.29	5.33E-16	Ache, Chrm3, Chrna9, Chrnb4, Slc18a3, Chrnb2, Chrna7, Chrnb1, Chrna1, Chrna3
C3	GO:0015464~acetylcholine receptor activity	83.88	9.65E-16	Chrm3, Chrna9, Chrnb4, Chrnb2, Chrna7, Chrnb1, Htr3a, Chrna1, Htr3b, Chrna3
C3	IPR027361:Nicotinic acetylcholine-gated receptor, transmembrane domain	98.07	1.35E-14	Chrna9, Chrnb4, Chrnb2, Chrna7, Chrnb1, Htr3a, Chrna1, Htr3b, Chrna3
C3	GO:0004889~acetylcholine-activated cation-selective channel activity	83.88	4.67E-14	Chrna9, Chrnb4, Chrnb2, Chrna7, Chrnb1, Htr3a, Chrna1, Htr3b, Chrna3
C3	GO:0007271~synaptic transmission, cholinergic	58.52	5.23E-14	Chrm3, Chrna9, Chrm2, Chrm1, Chrnb4, Chrnb2, Chrna7, Chrnb1, Chrna1, Chrna3
C3	IPR002394:Nicotinic acetylcholine receptor	85.81	1.10E-10	Chrna9, Chrnb4, Chrnb2, Chrna7, Chrnb1, Chrna1, Chrna3
C3	GO:0005892~acetylcholine-gated channel complex	78.60	1.98E-10	Chrna9, Chrnb4, Chrnb2, Chrna7, Chrnb1, Chrna1, Chrna3
C3	mmu04725:Cholinergic synapse	10.16	8.67E-08	Ache, Chrm3, Chrm2, Chrm1, Chrnb4, Slc18a3, Chrnb2, Chrna7, Gng3, Chrna3, Chat
C12	IPR000995:Muscarinic acetylcholine receptor family	117.68	2.50E-04	Chrm3, Chrm2, Chrm1
C12	GO:0007197~adenylate cyclase-inhibiting G-protein coupled acetylcholine receptor signalling pathway	75.24	6.50E-04	Chrm3, Chrm2, Chrm1
C12	GO:0007207~phospholipase C-activating G-protein coupled acetylcholine receptor signalling pathway	75.24	6.50E-04	Chrm3, Chrm2, Chrm1
C12	GO:0016907~G-protein coupled acetylcholine receptor activity	71.89	7.11E-04	Chrm3, Chrm2, Chrm1
Ulcerative colitis male vs control male downregulated				
C2	GO:0042166~acetylcholine binding	136.69	8.49E-14	Htr3e, Ache, Chrna4, Chrna1, Htr3b, Htr3c, Chrng, Chrna2
C2	GO:0005892~acetylcholine-gated channel complex	139.88	6.00E-12	Htr3e, Chrna4, Chrna1, Htr3b, Htr3c, Chrng, Chrna2
C2	IPR027361:Nicotinic acetylcholine-gated receptor, transmembrane domain	138.80	6.38E-12	Htr3e, Chrna4, Chrna1, Htr3b, Htr3c, Chrng, Chrna2

C2	GO:0015464~acetylcholine receptor activity	135.20	7.11E-12	Htr3e, Chrna4, Chrna1, Htr3b, Htr3c, Chrng, Chrna2
C2	GO:0004889~acetylcholine-activated cation-selective channel activity	135.20	7.11E-12	Htr3e, Chrna4, Chrna1, Htr3b, Htr3c, Chrng, Chrna2
C2	IPR002394:Nicotinic acetylcholine receptor	105.75	6.33E-06	Chrna4, Chrna1, Chrng, Chrna2
C2	GO:0007271~synaptic transmission, cholinergic	104.73	1.16E-14	Htr3e, Chrm5, Chrm1, Chrna4, Chrna1, Htr3b, Htr3c, Chrng, Chrna2
C5	hsa04725:Cholinergic synapse	11.97	6.15E-04	Ache, Chrm5, Chrm1, Chrna4, Chat
Ulcerative colitis male vs control male upregulated				
C8	GO:0007271~synaptic transmission, cholinergic	37.67	1.53E-04	Chrm4, Chrna9, Chrna6, Chrne
Ulcerative colitis female vs control female downregulated				
C3	IPR027361:Nicotinic acetylcholine-gated receptor, transmembrane domain	162.80	2.32E-14	Htr3e, Chrna4, Chrna7, Chrnd, Chrna1, Htr3b, Htr3c, Chrng
C3	GO:0005892~acetylcholine-gated channel complex	159.86	2.63E-14	Htr3e, Chrna4, Chrna7, Chrnd, Chrna1, Htr3b, Htr3c, Chrng
C3	GO:0015464~acetylcholine receptor activity	154.52	3.18E-14	Htr3e, Chrna4, Chrna7, Chrnd, Chrna1, Htr3b, Htr3c, Chrng
C3	GO:0004889~acetylcholine-activated cation-selective channel activity	154.52	3.18E-14	Htr3e, Chrna4, Chrna7, Chrnd, Chrna1, Htr3b, Htr3c, Chrng
C3	GO:0042166~acetylcholine binding	136.69	8.49E-14	Htr3e, Chrna4, Chrna7, Chrnd, Chrna1, Htr3b, Htr3c, Chrng
C3	IPR002394:Nicotinic acetylcholine receptor	135.67	4.01E-08	Chrna4, Chrna7, Chrnd, Chrna1, Chrng
C3	GO:0007271~synaptic transmission, cholinergic	131.37	2.37E-19	Htr3e, Chrm5, Chrm2, Chrm1, Chrna4, Chrna7, Chrnd, Chrna1, Htr3b, Htr3c, Chrng
C7	IPR000995:Muscarinic acetylcholine receptor family	293.04	3.85E-05	Chrm5, Chrm2, Chrm1
C7	GO:0016907~G-protein coupled acetylcholine receptor activity	190.39	9.75E-05	Chrm5, Chrm2, Chrm1
C7	GO:0007197~adenylate cyclase-inhibiting G-protein coupled acetylcholine receptor signalling pathway	189.38	9.85E-05	Chrm5, Chrm2, Chrm1
C7	hsa04725:Cholinergic synapse	12.05	1.01E-04	Chrm5, Chrm2, Chrm1, Chrna4, Chrna7, Chat
C7	GO:0007207~phospholipase C-activating G-protein coupled acetylcholine receptor signalling pathway	165.71	1.31E-04	Chrm5, Chrm2, Chrm1
C7	GO:0007213~G-protein coupled acetylcholine receptor signalling pathway	88.38	4.87E-04	Chrm5, Chrm2, Chrm1
Ulcerative colitis female vs control female upregulated				
C4	GO:0042166~acetylcholine binding	54.11	2.50E-09	Chrnb4, Slc18a3, Chrnb2, Chrna6, Chrne, Chrna3, Chrna2
C4	IPR002394:Nicotinic acetylcholine receptor	72.78	1.38E-08	Chrnb4, Chrnb2, Chrna6, Chrne, Chrna3, Chrna2
C4	GO:0007271~synaptic transmission, cholinergic	37.37	2.68E-08	Chrm4, Chrnb4, Chrnb2, Chrna6, Chrne, Chrna3, Chrna2
C4	GO:0005892~acetylcholine-gated channel complex	54.89	6.48E-08	Chrnb4, Chrnb2, Chrna6, Chrne, Chrna3, Chrna2
C4	IPR027361:Nicotinic acetylcholine-gated receptor, transmembrane domain	54.59	6.69E-08	Chrnb4, Chrnb2, Chrna6, Chrne, Chrna3, Chrna2
C4	GO:0015464~acetylcholine receptor activity	52.43	7.98E-08	Chrnb4, Chrnb2, Chrna6, Chrne, Chrna3, Chrna2
C4	GO:0004889~acetylcholine-activated cation-selective channel activity	52.43	7.98E-08	Chrnb4, Chrnb2, Chrna6, Chrne, Chrna3, Chrna2
C4	hsa04725:Cholinergic synapse	7.39	3.08E-04	Chrm4, Chrnb4, Slc18a3, Gng2, Chrnb2, Chrna6, Chrna3

Analysed using DAVID.

Table S8 ***Functional cluster analysis of ENS and neurotransmitter receptor genes: Purinergic terms***

Cluster #	Term	Fold Enrichment	*P*-value	Genes
***Winnie*+MSC vs *Winnie*-sham upregulated**				
C6	IPR027309:P2X purinoreceptor extracellular domain	250.38	3.63E-07	P2rx5, P2rx6, P2rx1, P2rx3
C6	IPR001429:P2X purinoreceptor	250.38	3.63E-07	P2rx5, P2rx6, P2rx1, P2rx3
C6	GO:0004931~extracellular ATP-gated cation channel activity	212.11	5.96E-07	P2rx5, P2rx6, P2rx1, P2rx3
C6	GO:0001614~purinergic nucleotide receptor activity	185.60	9.52E-07	P2rx5, P2rx6, P2rx1, P2rx3
C6	GO:0033198~response to ATP	78.62	1.59E-05	P2rx5, P2rx6, P2rx1, P2rx3
***Winnie*-sham vs C57BL/6 downregulated**				
C6	IPR027309:P2X purinoreceptor extracellular domain	140.10	2.12E-08	P2rx5, P2rx6, P2rx1, P2rx3, P2rx2
C6	IPR001429:P2X purinoreceptor	140.10	2.12E-08	P2rx5, P2rx6, P2rx1, P2rx3, P2rx2
C6	GO:0004931~extracellular ATP-gated cation channel activity	119.82	3.96E-08	P2rx5, P2rx6, P2rx1, P2rx3, P2rx2
C6	GO:0001614~purinergic nucleotide receptor activity	104.84	7.88E-08	P2rx5, P2rx6, P2rx1, P2rx3, P2rx2
C6	GO:0033198~response to ATP	43.89	4.31E-06	P2rx5, P2rx6, P2rx1, P2rx3, P2rx2
Ulcerative colitis male vs control male downregulated				
C6	IPR027309:P2X purinoreceptor extracellular domain	203.95	8.52E-05	P2rx4, P2rx6, P2rx2
Ulcerative colitis female vs control female upregulated				
C5	GO:0045028~G-protein coupled purinergic nucleotide receptor activity	86.13	4.92E-09	P2ry8, P2ry12, P2ry13, P2ry6, P2ry10, P2ry14
C5	GO:0035589~G-protein coupled purinergic nucleotide receptor signalling pathway	84.67	5.37E-09	P2ry8, P2ry12, P2ry13, P2ry6, P2ry10, P2ry14
Ulcerative colitis female vs control female downregulated				
C9	IPR027309:P2X purinoreceptor extracellular domain	256.58	5.28E-05	P2rx4, P2rx6, P2rx3
C9	IPR001429:P2X purinoreceptor	224.50	7.03E-05	P2rx4, P2rx6, P2rx3
C9	GO:0004931~extracellular ATP-gated cation channel activity	204.21	8.49E-05	P2rx4, P2rx6, P2rx3
C9	GO:0001614~purinergic nucleotide receptor activity	204.21	8.49E-05	P2rx4, P2rx6, P2rx3
C9	GO:0035590~purinergic nucleotide receptor signalling pathway	203.13	8.58E-05	P2rx4, P2rx6, P2rx3

Analysed using DAVID.

Table S9 ***Functional cluster analysis of ENS and neurotransmitter receptor genes: Adrenergic terms***

Cluster #	Term	Fold Enrichment	*P*-value	Genes
***Winnie*+MSC vs *Winnie*-sham upregulated**				
C9	IPR002233:Adrenergic receptor	194.74	8.68E-07	Adrb3, Adra1b, Adra1a, Adra2b
C9	GO:0004935~adrenergic receptor activity	148.48	2.03E-06	Adrb3, Adra1b, Adra1a, Adra2b
C9	GO:0071880~adenylate cyclase-activating adrenergic receptor signalling pathway	82.76	1.36E-05	Adrb3, Adra1b, Adra1a, Adra2b
***Winnie*-sham vs C57BL/6 downregulated**				
C9	IPR002233:Adrenergic receptor	130.76	3.70E-10	Adrb3, Adrb1, Adra2a, Adra1b, Adra1a, Adra2b
C9	GO:0004935~adrenergic receptor activity	100.65	1.60E-09	Adrb3, Adrb1, Adra2a, Adra1b, Adra1a, Adra2b
C9	GO:0071880~adenylate cyclase-activating adrenergic receptor signalling pathway	55.44	5.65E-08	Adrb3, Adrb1, Adra2a, Adra1b, Adra1a, Adra2b
C9	GO:0051379~epinephrine binding	111.83	3.95E-06	Adrb3, Adrb1, Adra2a, Adra2b
C9	GO:0001996~positive regulation of heart rate by epinephrine-norepinephrine	175.55	9.42E-05	Adrb1, Adra1b, Adra1a
C9	GO:0001997~positive regulation of the force of heart contraction by epinephrine-norepinephrine	175.55	9.42E-05	Adrb1, Adra1b, Adra1a
Ulcerative colitis male vs control male downregulated				
C5	IPR002233:Adrenergic receptor	143.01	2.26E-06	Adrb2, Adra1a, Adra2c, Adra1d
C5	GO:0004935~adrenergic receptor activity	112.55	4.80E-06	Adrb2, Adra1a, Adra2c, Adra1d
C5	GO:0071880~adenylate cyclase-activating adrenergic receptor signalling pathway	59.48	3.75E-05	Adrb2, Adra1a, Adra2c, Adra1d
Ulcerative colitis female vs control female downregulated				
C7	IPR002233:Adrenergic receptor	121.30	4.84E-08	Adrb3, Adrb2, Adra1a, Adra2c, Adra2b
C7	GO:0071880~adenylate cyclase-activating adrenergic receptor signalling pathway	51.99	2.13E-06	Adrb3, Adrb2, Adra1a, Adra2c, Adra2b
C7	GO:0051379~epinephrine binding	133.98	2.27E-06	Adrb3, Adrb2, Adra2c, Adra2b

Analysed using DAVID.

Table S60 *Functional cluster analysis of ENS and neurotransmitter receptor genes: Glutaminergic terms*

Cluster #	Term	Fold Enrichment	*P*-value	Genes
***Winnie*+MSC vs *Winnie*-sham upregulated**				
C4	IPR019594:Glutamate receptor, L-glutamate/glycine-binding	97.37	8.31E-06	Gria2, Grin2d, Grin1, Gria4
C4	IPR001508:NMDA receptor	97.37	8.31E-06	Gria2, Grin2d, Grin1, Gria4
C4	IPR001320:Ionotropic glutamate receptor	97.37	8.31E-06	Gria2, Grin2d, Grin1, Gria4
C4	GO:0005234~extracellular-glutamate-gated ion channel activity	82.49	1.36E-05	Gria2, Grin2d, Grin1, Gria4
C4	GO:0004970~ionotropic glutamate receptor activity	82.49	1.36E-05	Gria2, Grin2d, Grin1, Gria4
***Winnie*-sham vs C57BL/6 downregulated**				
C4	IPR019594:Glutamate receptor, L-glutamate/glycine-binding	87.17	2.07E-12	Gria2, Grin2b, Gria1, Grin2d, Grin1, Gria3, Gria4, Grin3a
C4	IPR001320:Ionotropic glutamate receptor	87.17	2.07E-12	Gria2, Grin2b, Gria1, Grin2d, Grin1, Gria3, Gria4, Grin3a
C4	IPR001508:NMDA receptor	87.17	2.07E-12	Gria2, Grin2b, Gria1, Grin2d, Grin1, Gria3, Gria4, Grin3a
C4	GO:0005234~extracellular-glutamate-gated ion channel activity	74.56	6.13E-12	Gria2, Grin2b, Gria1, Grin2d, Grin1, Gria3, Gria4, Grin3a
C4	GO:0004970~ionotropic glutamate receptor activity	74.56	6.13E-12	Gria2, Grin2b, Gria1, Grin2d, Grin1, Gria3, Gria4, Grin3a
C4	GO:0004971~AMPA glutamate receptor activity	167.75	7.96E-07	Gria2, Gria1, Gria3, Gria4
C4	GO:0004972~NMDA glutamate receptor activity	83.88	1.10E-05	Grin2b, Grin2d, Grin1, Grin3a
C4	mmu04724:Glutamatergic synapse	8.16	1.14E-05	Gria2, Grin2b, Gria1, Grin2d, Grin1, Gria3, Gria4, Gng3, Grin3a
C4	GO:0017146~NMDA selective glutamate receptor complex	63.63	2.88E-05	Grin2b, Grin2d, Grin1, Grin3a
C4	GO:0035235~ionotropic glutamate receptor signalling pathway	50.16	6.06E-05	Gria2, Grin2b, Grin1, Grin3a
C4	GO:0032281~AMPA glutamate receptor complex	25.45	4.97E-04	Gria2, Gria1, Gria3, Gria4
Ulcerative colitis male vs control male downregulated				
C7	GO:0004970~ionotropic glutamate receptor activity	88.85	4.82E-04	Gria2, Grin2a, Gria3
C7	IPR001320:Ionotropic glutamate receptor	79.31	6.12E-04	Gria2, Grin2a, Gria3
C7	IPR001508:NMDA receptor	79.31	6.12E-04	Gria2, Grin2a, Gria3
C7	IPR019594:Glutamate receptor, L-glutamate/glycine-binding	79.31	6.12E-04	Gria2, Grin2a, Gria3
C7	GO:0005234~extracellular-glutamate-gated ion channel activity	74.04	7.00E-04	Gria2, Grin2a, Gria3
Ulcerative colitis female vs control female downregulated				
C5	GO:0004970~ionotropic glutamate receptor activity	118.46	4.33E-06	Grin1, Grin2a, Gria3, Gria4
C5	IPR001320:Ionotropic glutamate receptor	108.53	5.83E-06	Grin1, Grin2a, Gria3, Gria4
C5	IPR001508:NMDA receptor	108.53	5.83E-06	Grin1, Grin2a, Gria3, Gria4
C5	IPR019594:Glutamate receptor, L-glutamate/glycine-binding	108.53	5.83E-06	Grin1, Grin2a, Gria3, Gria4
C5	GO:0005234~extracellular-glutamate-gated ion channel activity	98.72	7.73E-06	Grin1, Grin2a, Gria3, Gria4
C5	GO:0035235~ionotropic glutamate receptor signalling pathway	73.65	1.93E-05	Grin1, Grin2a, Gria3, Gria4
C5	GO:0007215~glutamate receptor signalling pathway	88.38	4.87E-04	Grin2a, Gria3, Gria4

Analysed using DAVID.

Table S71 ***Functional cluster analysis of ENS and neurotransmitter receptor genes: GABA-ergic terms***

Cluster #	Term	Fold Enrichment	*P*-value	Genes
***Winnie*+MSC vs *Winnie*-sham downregulated**				
C1	GO:0004890~GABA-A receptor activity	208.68	5.94E-09	Gabrr2, Gabrd, Gabrg2, Gabra1, Gabrp
C1	IPR006028:Gamma-aminobutyric acid A receptor	194.65	8.53E-09	Gabrr2, Gabrd, Gabrg2, Gabra1, Gabrp
C1	GO:1902711~GABA-A receptor complex	189.97	9.81E-07	Gabrr2, Gabrd, Gabrg2, Gabra1
C1	mmu04727:GABAergic synapse	27.73	1.87E-05	Gabrr2, Gabrd, Gabrg2, Gabra1, Gabrp
C1	GO:0007214~gamma-aminobutyric acid signalling pathway	94.34	4.17E-04	Gabrr2, Gabrg2, Gabra1
***Winnie*-sham vs C57BL/6 downregulated**				
C2	GO:0004890~GABA-A receptor activity	70.63	9.67E-12	Gabrr2, Gabre, Gabrg2, Gabra1, Gabrb3, Gabra3, Gabrb2, Gabrp
C2	IPR006028:Gamma-aminobutyric acid A receptor	68.22	1.57E-11	Gabrr2, Gabre, Gabrg2, Gabra1, Gabrb3, Gabra3, Gabrb2, Gabrp
C2	GO:1902711~GABA-A receptor complex	74.24	2.96E-10	Gabrr2, Gabre, Gabrg2, Gabra1, Gabrb3, Gabra3, Gabrb2
C2	GO:0007214~gamma-aminobutyric acid signalling pathway	49.15	4.51E-09	Gabrr2, Gabre, Gabrg2, Gabra1, Gabrb3, Gabra3, Htr4
C2	mmu04727:GABAergic synapse	10.79	1.39E-06	Gabrr2, Gabre, Gabrg2, Gabra1, Gabrb3, Gabra3, Gabrb2, Gng3, Gabrp
C2	GO:0051932~synaptic transmission, GABAergic	58.52	3.69E-05	Gabrg2, Gabra1, Gabrb3, Gabrb2
C2	GO:1902710~GABA receptor complex	190.89	7.97E-05	Gabrg2, Gabra1, Gabrb2
C2	GO:0016917~GABA receptor activity	125.81	2.06E-04	Gabrg2, Gabra1, Gabrb2
Ulcerative colitis male vs control male upregulated				
C2	GO:0004890~GABA-A receptor activity	118.48	2.18E-13	Gabrr2, Gabrd, Gabre, Gabrg3, Gabra3, Gabrb1, Gabrq, Gabrp
C2	IPR006028:Gamma-aminobutyric acid A receptor	111.92	4.19E-13	Gabrr2, Gabrd, Gabre, Gabrg3, Gabra3, Gabrb1, Gabrq, Gabrp
C2	GO:1902711~GABA-A receptor complex	119.47	1.53E-11	Gabrr2, Gabrd, Gabre, Gabrg3, Gabra3, Gabrb1, Gabrq
C2	mmu04727:GABAergic synapse	18.15	1.97E-08	Gabrr2, Gabrd, Gabre, Gabrg3, Gabra3, Gabrb1, Gng2, Gabrq, Gabrp
C2	GO:0007214~gamma-aminobutyric acid signalling pathway	56.51	1.60E-06	Gabrr2, Gabre, Gabrg3, Gabra3, Gabrq
Ulcerative colitis female vs control female upregulated				
C2	GO:1902711~GABA-A receptor complex	146.38	2.36E-22	Gabrr2, Gabrd, Gabrg1, Gabrg2, Gabra2, Gabrg3, Gabra1, Gabrb3, Gabra4, Gabra3, Gabrb1, Gabrq
C2	GO:0004890~GABA-A receptor activity	126.92	1.49E-21	Gabrr2, Gabrd, Gabrg1, Gabrg2, Gabra2, Gabrg3, Gabra1, Gabrb3, Gabra4, Gabra3, Gabrb1, Gabrq
C2	IPR006028:Gamma-aminobutyric acid A receptor	113.92	1.07E-20	Gabrr2, Gabrd, Gabrg1, Gabrg2, Gabra2, Gabrg3, Gabra1, Gabrb3, Gabra4, Gabra3, Gabrb1, Gabrq
C2	hsa04727:GABAergic synapse	17.91	3.05E-12	Gabrg1, Gabrd, Gabrg2, Gabrg3, Gabra2, Gabra1, Gabra4, Gabrb3,

				Gabra3, Gabrb1, Gabrr2, Gng2, Gabrq
C2	GO:0007214~gamma-aminobutyric acid signalling pathway	71.84	9.75E-12	Gabrr2, Gabrg1, Gabrg2, Gabra2, Gabrg3, Gabra1, Gabra4, Gabra3
C2	IPR001390:Gamma-aminobutyric-acid A receptor, alpha subunit	145.56	1.77E-06	Gabra2, Gabra1, Gabra4, Gabra3
C2	IPR005437:Gamma-aminobutyric-acid A receptor, gamma subunit	218.34	6.05E-05	Gabrg1, Gabrg2, Gabrg3

Analysed using DAVID.

Table S82 ***Functional cluster analysis of ENS and neurotransmitter receptor genes: Serotonergic terms***

Cluster #	Term	Fold Enrichment	*P*-value	Genes
***Winnie*-sham vs C57BL/6 downregulated**				
C8	GO:0007210~serotonin receptor signalling pathway	87.78	1.95E-07	Htr4, Htr3a, Htr2b, Htr3b, Htr2a
C8	mmu04726:Serotonergic synapse	7.11	3.12E-05	Gabrb3, Gabrb2, Slc6a4, Htr4, Gng3, Htr3a, Htr2b, Htr3b, Htr2a
C8	GO:0004993~G-protein coupled serotonin receptor activity	23.96	5.21E-05	Htr4, Htr3a, Htr2b, Htr3b, Htr2a
Ulcerative colitis male vs control male downregulated				
C4	IPR002231:5-Hydroxytryptamine receptor family	128.71	3.22E-06	Htr1b, Htr1d, Htr1f, Htr2a
C4	GO:0051378~serotonin binding	93.80	8.75E-06	Htr1b, Htr1d, Htr1f, Htr2a
C4	GO:0004993~G-protein coupled serotonin receptor activity	32.16	2.46E-04	Htr1b, Htr1d, Htr1f, Htr2a
C4	mmu04726:Serotonergic synapse	7.98	7.74E-04	Htr1b, Gabrb1, Gng2, Htr1d, Htr1f, Htr2a
Ulcerative colitis female vs control female downregulated				
C6	hsa04726:Serotonergic synapse	14.06	6.51E-06	Htr3e, Gabrb2, Htr7, Slc6a4, Htr4, Htr3b, Htr3c
C6	GO:0004993~G-protein coupled serotonin receptor activity	63.46	3.06E-05	Htr3e, Htr7, Htr4, Htr3c
C6	GO:0007210~serotonin receptor signalling pathway	101.98	3.63E-04	Htr3e, Htr4, Htr3c
Ulcerative colitis female vs control female upregulated				
C6	IPR002231:5-Hydroxytryptamine receptor family	97.04	7.37E-06	Htr1b, Htr2b, Htr1f, Htr2a
C6	GO:0051378~serotonin binding	80.39	1.34E-05	Htr1b, Htr2b, Htr1f, Htr2a
C6	hsa04726:Serotonergic synapse	7.39	3.08E-04	Htr1b, Gabrb3, Gabrb1, Gng2, Htr2b, Htr1f, Htr2a
C6	GO:0004993~G-protein coupled serotonin receptor activity	28.71	3.44E-04	Htr1b, Htr2b, Htr1f, Htr2a

Analysed using DAVID.

Table S9 ***Functional cluster analysis of ENS and neurotransmitter receptor genes: NPY-ergic terms***

Cluster #	Term	Fold Enrichment	*P*-value	Genes
***Winnie*-sham vs C57BL/6 downregulated**				
C15	GO:0001601~peptide YY receptor activity	100.65	3.41E-04	Npy2r, Npy6r, Npy1r
C15	GO:0007631~feeding behaviour	20.65	9.18E-04	Npy, Npy2r, Npy6r, Npy1r
Ulcerative colitis male vs control male downregulated				
C4	GO:0004983~neuropeptide Y receptor activity	197.44	8.07E-07	Npy2r, Npy6r, Npy1r, Npy5r
C4	IPR000611:Neuropeptide Y receptor family	173.04	1.29E-06	Npy2r, Npy6r, Npy1r, Npy5r
C4	GO:0001601~peptide YY receptor activity	444.24	1.40E-05	Npy2r, Npy1r, Npy5r

Analysed using DAVID.